JSCSEN 72(12)1171–1554(2007)

UDC 54:66

ISSN 0352–5139

Journal of the Serbian Chemical Society 72, No. 12, 1171–1554 (2007)

Journal of the Serbian Chemical Society

VOLUME 72

NO 12

BELGRADE 2007

Journal of the Serbian Chemical Society
JSCS@tmf.bg.ac.yu • www.shd.org.yu/JSCS

Issue dedicated to Dragutin M. Dražić on the occasion of his retirement as Editor-in-Chief and in recognition of his great effort and success in editing of the *Journal of the Serbian Chemical Society*

Journal of the Serbian Chemical Society
JSCS@tmf.bg.ac.yu • www.shd.org.yu/JSCS

J. Serb. Chem. Soc. *72* (12) 1171 (2007)

EDITORIAL

This issue of the *Journal of the Serbian Chemical Society* was chosen by the members of the Presidency of the Society and of the Editorial Board from Serbia to mark the retirement of Dragutin M. Dražić as Editor-in-Chief of the *Journal*.

Dragutin Dražić succeeded Slobodan V. Ribnikar, who was Editor-in-Chief for 10 years, among others in the 77-year old history of the *Journal* and who introduced many improvements in editing and editing policy, including editing in English since 1985.

Dragutin Dražić was Editor-in Chief for more than 20 years. In addition to his immense impact as a scientist and university teacher to the field of Electrochemistry and Physical Chemistry and to the understanding of the importance of chemistry and of the natural science in general (see *J. Serb. Chem Soc.* **66** (2001) 731), his great effort in the editing of the *Journal* resulted in its pivotal position in the world of scientific journals in Serbia. With no intention to repeat Dragutin Dražić's great contribution to the development of contemporary chemical minds in the former Yugoslavia, and lately in Serbia (see *J. Serb. Chem. Soc.* **72** (2007) 1), we simply say: THANK YOU! Saying this, we are aware that we express the gratitude of the chemistry community not only in Serbia, but also worldwide, where the name Dragutin Dražić is recognized.

The papers in this issue were prepared by the authors from Serbia who aided Dragutin Dražić, *JSCS* Honorary Editor, in his editing efforts, by submitting their manuscripts, through sub-editing and revision of the submitted manuscripts, or some other way, to establish a journal with the reputation which *Journal of the Serbian Chemical Society* holds today on the international scene.

Branislav Ž. Nikolić
Editor-in-Chief

Bogdan Šolaja
President of the Serbian Chemical Society

Journal of the Serbian Chemical Society
JSCS@tmf.bg.ac.yu • www.shd.org.yu/JSCS

J. Serb. Chem. Soc. 72 (12) 1173–1179 (2007)
JSCS–3650

UDC 54.024+542.9:547.815:547.514
Original scientific paper

Radical reactions of xanthates: annulation of the cyclopentene ring

AHMED MOHAMED ELHESHI[1], VESELIN MASLAK[1,2#] and RADOMIR N. SAIČIĆ[1,2*#]

[1]*Faculty of Chemistry, University of Belgrade, Studentski trg 16, P. O. Box 158, 11000 Belgrade, and* [2]*ICTM, Center for Chemistry, Njegoseva 12, Belgrade, Serbia*

(Received 3 July 2007)

Abstract: Homoallylic radicals, generated from the corresponding xanthates, react with terminal alkynes to give cyclopentene derivatives in moderate yields.

Keywords: radicals, annulation, cyclopentene, xanthates, alkynes.

In the rich armamentarium of synthetic free radical reactions, the xanthate based methodology occupies a prominent place.[1] An especially useful feature of the radical chemistry of xanthates is the ability of stabilized radicals to add efficiently to non-activated alkenes – a possibility which has given rise to numerous synthetic applications of this method. However, to the best of our knowledge, no examples are known of reactions of xanthate derived radicals with alkynes, although this latter class of compounds should, at least theoretically, be good acceptor partner for group-transfer radical additions.[2] As represented in Scheme 1, radical addition to an alkyne should produce a vinyl radical **1** – a reactive species capable of abstracting the xanthate group from the radical precursor, thus propagating the chain reaction.

To test this possibility, a mixture of xanthate **2** and propargyl acetate was submitted to the "standard" conditions for a radical addition. Indeed, the expected product **3** was formed under both photolytic and thermal initiation; however, the yield was low (17 %) and the conversion incomplete (Scheme 2). Attempts to optimize the reaction conditions did not meet with success. Thus, a synthetically useful xanthate radical addition to alkynes appeared not to be feasible.

Two mechanistic steps could be responsible for this failure: the addition step or the group transfer step. Unable to envisage any reasons hampering the addition step, we believed that it may be a too high reactivity of the intermediary vinyl ra-

Serbian Chemical Society member.
* Corresponding author. E-mail: rsaicic@chem.bg.ac.yu
doi: 10.2298/JSC0712173E

dical **1,** which leads to side reactions and stops the desired radical chain. If this reasoning were correct, the problem could be circumvented by conferring to the vinyl radical another role, instead of a chain carrier. For example, a vinyl radical possessing a Δ^5-olefinic bond could undergo the well-established, rapid 5-*exo*-cyclization; the alkyl radical thus obtained would then effect the crucial chain carrying step, *i.e.*, xanthate group transfer from the radical precursor. This modified reaction is actually a free radical annulation sequence which would produce cyclopentene derivatives.[3] Somewhat counterintuitively, the yield of the sequential reaction as a whole could be better than the yield of the addition step only.

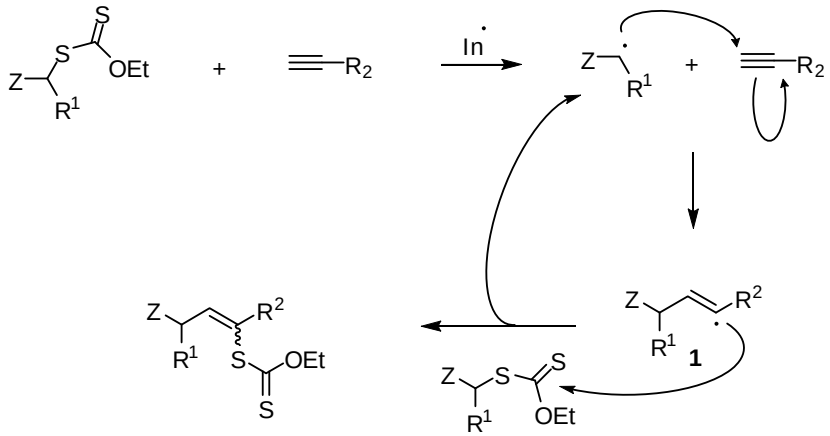

Scheme 1: The proposed mechanism of the intermolecular addition of xanthate derived radicals to alkynes.

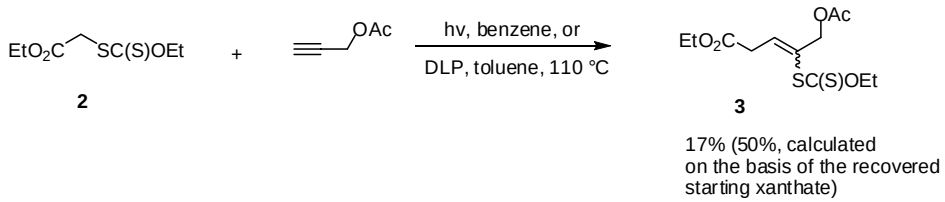

Scheme 2. Addition reaction of a simple xanthate ester to propargyl acetate

To test the correctness of this reasoning and the feasibility of the cyclopentene annulation, suitably substituted xanthate radical precursors **5** and **6**, as shown in Scheme 3, were prepared.[3] Gratifyingly, when a benzene solution of **5** and phenylacetylene was exposed to irradiation with visible light, the desired cyclopentene derivative **7a** was obtained in 33 % yield (42 % yield, calculated on the basis of recovered starting compound **5**). Similarly, other combinations of xanthates and alkynes also gave cyclopentene derivatives **7b**–**g**, in modest to moderate yields, as represented in Scheme 4. Interestingly, with xanthate **5**, the products **7b** and **7c** were obtained stereoselectively, while **7a** was obtained as an equimolar mixture of *cis*/*trans* isomers.

Thus, the intermolecular addition of radicals generated from xanthates to alkynes proved to be possible, provided that the intermediary vinyl radical is trapped by a rapid intramolecular reaction. The described annulation procedure may represent a useful extension of the existing methodology.[4]

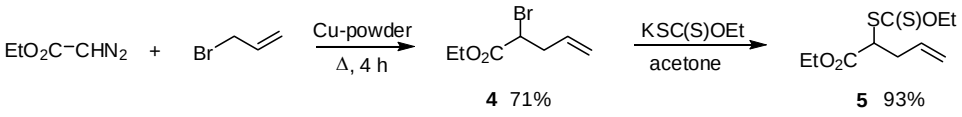

4 71% **5** 93%

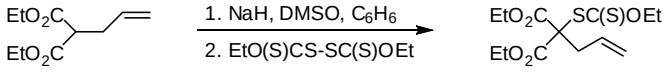

6 50%

Scheme 3. Preparation of the annulation precursors.

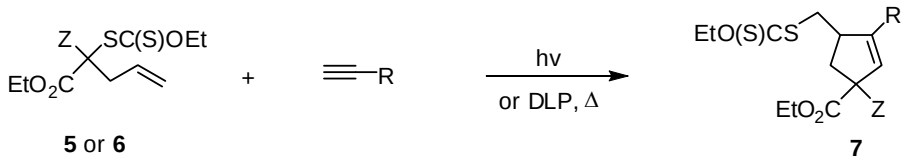

5 or **6** **7**

Entry	Z	R	method	yield (%)[a]
a	H	Ph	hv	33 (42)
b	H	CH_2OAc	hv	46
c	H	$CH_2O_2CCH_2Cl$	hv	30
d	CO_2Et	n-C_4H_9	hv	60
e	CO_2Et	CH_2OAc	hv	21 (27)
	CO_2Et	CH_2OAc	Δ	30
f	CO_2Et	$CH_2O_2CCH_2Cl$	hv or Δ	30
g	CO_2Et	Ph	hv	48 (62)
	CO_2Et	Ph	Δ	35 (43)

a) Yields in the parenthesis are calculated on the basis of the recovered starting xanthate

Scheme 4. Cyclopentene annulation.

EXPERIMENTAL

General

All chromatographic separations were performed on Silica 10-18, 60Å, ICN Biomedicals. Standard techniques were used for the purification of the reagents and solvents. The NMR spectra were recorded on a Varian Gemini 200, ^{1}H-NMR at 200 MHz, ^{13}C-NMR at 50 MHz, for samples in deuterated chloroform. Chemical shifts are expressed in ppm using tetramethylsilane as the internal standard. The IR spectra were recorded on a Nicolet 6700 FT instrument, and are expressed

in cm^{-1}. The mass spectra were obtained on Agilent Technologies 6210 TOF LC/MS instrument (LC, series 1200).

*Intermolecular addition of radicals to alkynes: ethyl 5-acetoxy-4-(ethoxycarbonothioylthio)pent-3-enoate (**3**)*

In a Pyrex, external water-cooled reactor, a deaerated solution of xanthate **2** (210 mg; 1 mmol) and propargyl acetate (980 mg; 10 mmol) in benzene (1 ml) was irradiated 6 h with a 250 W xenophot sun-lamp, under an argon atmosphere. The solvent was removed under reduced pressure and the product purified by column chromatography on SiO_2 (eluent: 10 % ethyl acetate in petroleum ether) to afford 52 mg (17 %) of the title compound **3,** as a light-yellow oil, and 140 mg of recovered starting xanthate **2** (the yield of **3**, calculated on the basis of the recovered **2**, was 50 %). Spectra of the mixture of isomers: IR_{film}: 2961, 2980, 2920, 2851, 1738, 1647, 1444, 1370, 1224, 1180, 1109 and 1038. ^{1}H-NMR (200 MHz, $CDCl_3$, δ / ppm): 6.61 (*dt*, J_1 = 7.0 Hz, J_2 = 1.0 Hz, 1H, major isomer); 6.47 (*t*, *J* = 7.4 Hz, 1H, minor isomer); 4.86 (*s*, 2H, minor isomer); 4.78 (*d*, *J* = 1.0 Hz, 2H, major isomer); 4.62 (*q*, *J* = 7.0 Hz, 2H); 4.19 (*q*, *J* = 7.2 Hz, 2H, minor isomer); 4.16 (*q*, *J* = = 7.2 Hz, 2H, major isomer); 3.39 (*d*, *J* = 7.0 Hz, 2H, minor isomer); 3.38 (*d*, *J* = 7.0 Hz, 2H, major isomer); 2.10 (*s*, 3H, major isomer); 2.07 (*s*, 3H, minor isomer); 1.4 (*t*, *J* = 7.0 Hz); 1.28 (*t*, *J* = 7.2 Hz, 3H, minor isomer); 1.27 (*t*, *J* = 7.2 Hz, 3H, major isomer). ^{13}C-NMR (50 MHz, $CDCl_3$, δ / ppm): 217.0, 170.4, 170.2, 139.8, 136.1, 129.3, 70.6, 70.3, 66.8, 62.0, 61.1, 35.2, 34.7, 20.8, 14.1, 13.6.

*Ethyl 2-bromo-4-pentenoate (**4**)*[3,5]

A suspension of copper powder (50 mg; 0.78 mmol) in allyl bromide (23 g; 0.19 mol) was heated gently to reflux. To this mixture was added dropwise over 4 h a solution of allyl bromide (3 ml) in ethyl diazoacetate (3 g; 26 mmol). When the addition was complete, the mixture was refluxed for a further 60 min, then filtered, concentrated and distilled under reduced pressure, to give 3.83 g (71 %) of the title compound **4**, E_{21} 88–90 °C; the physical data were identical to that previously reported.[5]

S-*(1-Ethoxycarbonyl-3-butenyl)-O-ethyl dithiocarbonate (**5**)*[3]

A solution of **4** (18 mmol) in acetone (2 ml) was added to a suspension of potassium *O*-ethyl xanthate (2.9 g; 18 mmol) in acetone (5 ml), over 10 min, with stirring under an argon atmosphere. Upon completion of the reaction, the acetone was removed under reduced pressure and the residue was partitioned between water and ether. The combined ethereal extract was dried over anh. sodium sulfate and concentrated to give 4.04 g (93 %) of the title compound **5** as a light-yellow oil. ^{1}H-NMR (δ, ppm): 5.89–5.68 (*m*, 1H); 5.21–5.09 (*m*, 2H); 4.64 (*q*, *J* = 7.0, 2H); 4.43 (*t*, *J* = 7.0 Hz, 1H); 4.21 (*q*, *J* = 7.2 Hz, 2H); 2.76–2.60 (*m*, 2H); 1.42 (*t*, *J* = 7.2 Hz, 3H); 1.30 (*t*, *J* = 7.0 Hz, 3H). IR_{film} (ν, cm^{-1}): 3081, 2982, 1737, 1642, 1293.

S-*(1,1-Bisethoxycarbonyl-3-butenyl)*-O-*ethyl dithiocarbonate (**6**)*[3]

Sodium hydride (80 % in mineral oil) was added to a solution of diethyl allylmalonate (2.0 g; 10 mmol) in benzene (90 ml) and DMSO (10 ml), and the mixture was stirred until a clear solution was formed. To this solution, diethyl dithiobis(thioformate) (2.66 g; 11 mmol) was added and the reaction mixture was stirred at r.t. Upon completion of the reaction, the mixture was carefully diluted with water and extracted with benzene. The combined organic extract was washed with water, dried over anh. sodium sulfate and concentrated under reduced pressure. Purification by column chromatography (SiO_2; eluent: petroleum ether/ethyl acetate 95/5) afforded 1.6 g (50 %) of the title compound **6** as a light-yellow oil. ^{1}H-NMR (δ, ppm): 5.95–5.75 (*m*, 1H); 5.20–5.08 (*m*, 2H); 4.60 (*q*, *J* = 7.1 Hz, 2H); 4.24 (*q*, *J* = 7.2 Hz, 4H); 3.14–3.06 (*m*, 2H); 1.39 (*t*, *J* = 7.1 Hz, 3H); 1.27 (*t*, *J* = 7.2 Hz, 6H). ^{13}C-NMR (δ, ppm): 209.2; 166.5; 131.6; 119.8; 70.0; 66.6; 62.5; 39.3; 13.8; 13.0. IR_{film} (ν, cm^{-1}): 3080, 2983, 1736, 1642, 1294, 1228, 1132.

*General procedure for the annulation reaction with photolytic initiation: diethyl 3-butyl-4-((ethoxycarbonothioylthio)methyl)cyclopent-2-ene-1,1-dicarboxylate (**7d**)*

In a Pyrex, external water-cooled reactor, a deaerated solution of xanthate **6** (100 mg; 0.3 mmol) and 1-hexyne (246 mg; 3 mmol) in benzene (0.3 ml) was irradiated 3 h with a 250 W xenophot sun lamp, under an argon atmosphere. The solvent was removed under reduced pressure and the product purified by column chromatography on SiO_2 (eluent: 5 % ethyl acetate in petroleum ether) to afford 75 mg (60 %) of the title compound **7d** as a light-yellow oil. IR_{film} (ν, cm^{-1}): 2959, 2931, 2871, 1732, 1645, 1462, 1367, 1232, 1112, 1050. ^{1}H-NMR (200 MHz, $CDCl_3$) (δ, ppm): 5.55 (*d*, J = 1.4 Hz, 1H); 4.65 (*q*, J = 7.0 Hz, 2H); 4.31–4.11 (*m*, 4H); 3.56 (*dd*, J_1 = 13.2 Hz, J_2 = 3.8 Hz, 1H); 3.18–2.97 (*m*, 1H); 2.90 (*dd*, J_1 = 13.0 Hz, J_2 = 9.6 Hz, 1H); 2.72 (*dd*, J_1 = 13.8 Hz, J_2 = 8.0 Hz, 1H); 2.25–2.04 (*m*, 3H) 1.43 (*t*, J = 7.0 Hz, 3H); 1.36–1.21 (*m*, 10H); 0.92 (*t*, J = 7.0 Hz, 3H). ^{13}C-NMR (50 MHz, $CDCl_3$) (δ, ppm): 214.7 (C); 171.4 (C); 171.2 (C); 151.1 (C); 123.4 (CH); 69.9 (CH_2); 64.8 (C); 61.4 (CH_2); 45.2 (CH); 39.7 (CH_2); 37.3 (CH_2); 29.3 (CH_2); 28.6 (CH_2); 22.3 (CH_2); 13.9 (CH_3); 13,8 (CH_3); 13.7 (CH_3). HRMS (EI): calcd. for $C_{19}H_{31}O_5S_2$ ($M+H^+$) 403.1607; found 403.1591.

*General procedure for the annulation reaction with thermal initiation: diethyl 3-((2-chloroacetoxy)methyl)-4-((ethoxycarbonothioylthio)methyl)cyclopent-2-ene-1,1-dicarboxylate (**7f**)*

A deaerated solution of xanthate **6** (100 mg; 0.3 mmol) and propargyl chloroacetate (400 mg; 3 mmol) in benzene (0.3 ml) was heated to reflux under an argon atmosphere, while dilauroyl peroxide (4 mg) was added every 2 h. After 5 h, the reaction was complete (TLC). The mixture was concentrated under reduced pressure and purified by column chromatography on SiO_2 (eluent: 10 % ethyl acetate in petroleum ether) to afford 43 mg (30 %) of the title compound **7f** as a light-yellow oil. IR_{film} (ν, cm^{-1}): 2982, 2938, 1731, 1446, 1367, 1235, 1163, 1048. ^{1}H-NMR (200 MHz, $CDCl_3$) (δ, ppm): 5.80 (*s*, 1H); 4.84 (*s*, 2H); 4.62 (*q*, J = 7.3 Hz, 2H); 4.29–4.14 (*m*, 4H) 4.13 (*s*, 2H); 3.53 (*dd*, J_1 = 13.5 Hz, J_2 = 4.2 Hz , 1H); 3.33–3,22 (*m*, 2H); 3.02 (*dd*, J_1 = 13.2 Hz, J_2 = 9.0 Hz , 1H); 2,78 (*dd*, J_1 = 14.0 Hz, J_2 = 8.4 Hz , 1H); 2.31 (*dd*, J_1 = 14.0 Hz, J_2 = 5.1 Hz, 1H); 1.43 (*t*, J = 7.0 Hz, 3H); 1.26 (*t*, J = 7.2 Hz, 3H); 1.26 (*t*, J = 7.0 Hz, 3H). ^{13}C-NMR (50 MHz, $CDCl_3$) (δ, ppm): 214.3 (C); 170.5 (C); 170.3 (C); 166.8 (C); 143.9 (C); 128.6 (CH); 70.2 (CH_2); 65.0 (C); 62.6 (CH_2); 61.8 (CH_2); 44.1 (CH); 40.7 (CH_2); 39.4 (CH_2); 37.4 (CH_2); 13.9 (2 x CH_3); 13.7 (CH_3). HRMS (EI): calcd. for $C_{18}H_{26}O_7S_2Cl$ ($M+H^+$) 453.0803; found 453.0804.

Spectral data for the other annulated compounds

Ethyl 4-((ethoxycarbonothioylthio)methyl)-3-phenylcyclopent-2-enecarboxylate (**7a**): IR_{film} (ν, cm^{-1}): 3057, 2957, 2924, 2854, 1730, 1646, 1445, 1215, 1112, and 1049. ^{1}H-NMR (200 MHz, $CDCl_3$) (δ, ppm): 7.57–7.46 (*m*, 2H); 7.41 (*m*, 3H); 6.15–6.14 (*m*, 1H, isomer A); 6.09–6.07 (*m*, 1H, isomer B); 4.71–4.58 (*m*, 2H), 4.65 (*q*, J = 7.0 Hz, 2H, isomer A); 4.64 (*q*, J = 7.0 Hz, 2H isomer B); 3.79–3.55 (*m*, 3H); 2.98–2.80 (*m*, 1H); 2.60–2.45 (*m*, 1H); 2.29–2.14 (*m*, 1H); 1.43 (*t*, J = 7.0 Hz, 3H, isomer A); 1.40 (*t*, J = 7.2 Hz, 3H, isomer B); 1.29 (*t*, J = 7.2 Hz, 3H, isomer A); 1.27 (*t*, J = 7.0 Hz, 3H, isomer B). ^{13}C-NMR (50 MHz, $CDCl_3$) (δ, ppm): 214.0, 174.0, 147.4, 134.5, 128.5, 127.9, 126.7, 126.4, 125.7, 125.5, 70.0, 69.9, 60.8, 49.4, 43.9, 40.4, 39.60, 32.5, 32.1, 14.2, 13.8, 11.4. HRMS (EI): calcd. for $C_{18}H_{23}O_3S_2$ ($M+H^+$) 351.1083; found 351.1083.

Ethyl 3-(acetoxymethyl)-4-((ethoxycarbonothioylthio)methyl)cyclopent-2-enecarboxylate (**7b**): IR_{film} (ν, cm^{-1}): 2981, 2932, 1738, 1652, 1450, 1369, 1227, 1112, and 1050. ^{1}H-NMR (200 MHz, $CDCl_3$) (δ, ppm): 5.81 (*s*, 1H); 4.71 (*s*, 2H); 4.65 (*q*, J = 7.2 Hz, 2H); 4.15 (*q*, J = 7.2 Hz, 2H); 3.64–3.49 (*m*, 2H); 3.15–2.97 (*m*, 2H); 2.54–2.38 (*m*, 1H); 2.11(*s*, 3H); 2.10–1.97 (*m*, 1H); 1.43 (*t*, J = 7.0 Hz, 3H); 1.27 (*t*, J = 7.2 Hz, 3H). ^{13}C-NMR (50 MHz, $CDCl_3$) (δ, ppm): 214.7 (C); 173.8 (C); 170.7 (C); 142.8 (C); 128.6 (CH); 70.0 (CH_2); 61.3 (CH_2); 60.9 (CH_2); 49.0 (CH); 44.3 (CH); 39.9 (CH); 32.9 (CH); 20.9 (CH_3); 14.2 (CH_3); 13.8 (CH_3). HRMS (EI): calcd. for $C_{15}H_{23}O_5S_2$ ($M+H^+$) 347.0981; found 347.0989.

Ethyl 3-((2-chloroacetoxy)methyl)-4-((ethoxycarbonothioylthio)methyl)cyclopent-2-enecarboxylate (**7c**): IR_{film} (ν, cm^{-1}): 2984, 1731, 1448, 1371, 1286, 1216, 1113, and 1050. ^{1}H-NMR (200 MHz, $CDCl_3$) (δ, ppm): 5.86 (*s*, 1H); 4.84 (*s*, 2H); 4.65 (*q*, *J* = 7.0 Hz, 2H); 4.15 (*q*, *J* = 7.1 Hz, 2H); 4.12 (*s*, 2H); 3.59–3.49 (*m*, 2H); 3.11–2.99 (*m*, 2H); 2.55–2.31 (*m*, 1H); 2.17–1.97 (*m*, 1H); 1.43 (*t*, *J* = 7.0 Hz, 3H); 1.26 (*t*, *J* = 7.1 Hz, 3H). ^{13}C-NMR (50 MHz, $CDCl_3$) (δ, ppm): 214.5 (C); 173.5(C); 166.9 (C); 141.8 (C); 129.4 (CH); 70.1 (CH_2); 62.8 (CH_2); 60.9 (CH_2); 48.9 (CH); 44.2 (CH); 40.7 (CH_2); 39.7 (CH_2); 32.9 (CH_2); 14.1 (CH_3); 13.7 (CH_3).

Diethyl 3-(acetoxymethyl)-4-((ethoxycarbonothioylthio)methyl)cyclopent-2-ene-1,1-dicarboxylate (**7e**): IR_{film} (ν, cm^{-1}): 2982, 2936, 1732, 1445, 1367, 1223, 1112, and 1047. ^{1}H- NMR (200 MHz, $CDCl_3$) (δ, ppm): 5.87 (*d*, *J* = 1.6 Hz, 1H); 4.72 (*s*, 2H); 4.65 (*q*, *J* = 7.0 Hz), 4.32–4.11 (*m*, 4H); 3.55 (*dd*, J_1 = 13.2 Hz, J_2 = 4.0 Hz, 1H); 3.29–3.21 (*m*, 1H); 3.00 (*dd*, J_1 = 13.2 Hz, J_2 = 9.2 Hz, 1H); 2.78 (*dd*, J_1 = 14.0 Hz, J_2 = 8.4 Hz, 1H); 2.31 (*dd*, J_1 = 14.0 Hz, J_2 = 5.0 Hz, 1H); 2.12 (*s*, 3H); 1.43 (*t*, *J* = 7.0 Hz, 3H); 1.26 (*t*, *J* = 7.2 Hz, 3H); 1.25 (*t*, *J* = 7.2 Hz, 3H). ^{13}C NMR (50 MHz, $CDCl_3$) (δ, ppm): 214.4 (C); 170.7 (C); 170.5 (C); 144.8 (C); 127.6 (CH); 70.1 (CH_2); 65.0 (C); 61.8 (CH_2); 61.1 (CH_2); 44.1 (CH); 39.4 (CH_2); 37.4 (CH_2); 20.9 (CH_3); 14.0 (CH_3); 13.7 (CH_3). HRMS (EI): calcd. for $C_{18}H_{26}O_7S_2Na$ ($M+Na^+$) 441.1012; found 441.0992.

Ethyl 4-((ethoxycarbonothioylthio)methyl)-3-phenylcyclopent-2-enecarboxylate (**7g**): Spectra of the mixture of isomers: IR_{film} (δ, ppm): 3057, 2957, 2924, 2854, 1730, 1646, 1445, 1215, 1112, 1049. ^{1}H-NMR (200 MHz, $CDCl_3$) (δ, ppm): 7.57–7.46 (*m*, 2H); 7.41 (*m*, 3H); 6.15–6.14 (*m*, 1H, isomer A); 6.09–6.07 (*m*, 1H, isomer B); 4.71–4.58 (*m*, 2H), 4.65 (*q*, *J* = 7.0 Hz, 2H, isomer A); 4.64 (*q*, *J* = 7.0 Hz, 2H, isomer B); 3.79–3.55 (*m*, 3H); 2.98–2.80 (*m*, 1H); 2.60–2.45 (*m*, 1H); 2.29–2.14 (*m*, 1H); 1.43 (*t*, *J* = 7.0 Hz, 3H, isomer A); 1.40 (*t*, *J* = 7.2 Hz, 3H, isomer B); 1.29 (*t*, *J*= = 7.2 Hz, 3H, isomer A); 1.27 (*t*, *J* = 7.0 Hz, 3H, isomer B). ^{13}C-NMR (50 MHz, $CDCl_3$) (δ, ppm): 214.0, 174.0, 147.4, 134.5 128.5, 127.9, 126.7, 126.4, 125.7, 125.5, 70.0, 69.9, 60.83, 49.4, 43.9, 40.4, 39.60, 32.5, 32.1, 14.2, 13.8, 11.4. HRMS (EI): calcd. for $C_{18}H_{23}O_3S_2$ ($M+H^+$) 351.1083; found 351.1083.

Acknowledgments: This research was part of the project No. 142021 supported by the Ministry of Science of the Republic of Serbia.

И З В О Д

РАДИКАЛСКЕ РЕАКЦИЈЕ КСАНТАТА: АНЕЛАЦИЈА ЦИКЛОПЕНТЕНОВОГ ПРСТЕНА

AHMED MOHAMED ELHESHI[1], ВЕСЕЛИН МАСЛАК[1,2] и РАДОМИР Н. САИЧИЋ[1,2]

[1]Хемијски факултет, Универзитет у Београду, Студентски трг 16, п. пр. 158, 11000 Београд и [2]ИХТМ, Центар за хемију, Његошева 12, Београд

Хомоалилни радикали, настали из одговарајућих ксантата, реагују са терминалним алкинима и дају деривате циклопентена у умереним приносима.

(Примљено 3. јула 2007)

REFERENCES

1. For review articles on xanthates, see: a) S. Z. Zard, *Angew. Chem. Int. Ed.* **36** (1997) 672; b) B. Quiclet–Sire, S. Z. Zard, *Topics Curr. Chem.* **264** (2006) 201; c) R. N. Saicic, in *Electronic Encyclopedia of Reagents for Organic Synthesis* (e-EROS), Wiley–InterScience (www3.interscience.wiley.com), 2005, DOI: 10.1002/047084289X.rn00544

2. In reference 1b) (page 207) an example of addition to phenylacetylene is provided. However, no reference to the primary literature was given, and we experienced difficulties in trying to repeat the result reported (64 % yield of the addition product)
3. a) V. Maslak, Z. Cekovic, R. N. Saicic, *Synlett* (1998) 1435; b) V. Maslak, *M.Sc. Thesis*, Faculty of Chemistry, University of Belgrade, Belgrade, 1999
4. A review article on free radical annulations: T. R. Rheault, M. P. Sibi, *Synthesis* (2003) 803
5. D. D. Phillips, *J. Am. Chem. Soc.* **76** (1954) 5385.

Journal of the Serbian Chemical Society
JSCS@tmf.bg.ac.yu • www.shd.org.yu/JSCS

J. Serb. Chem. Soc. 72 (12) 1181–1190 (2007)
JSCS–3651

UDC 541.459:615.28
Original scientific paper

On peroxide antimalarials

IGOR OPSENICA[1#☆], DEJAN OPSENICA[1#], MILKA JADRANIN[1#], KIRSTEN S. SMITH[2], WILBUR K. MILHOUS[2≡], MANOLIS STRATAKIS[3] and BOGDAN ŠOLAJA[4*#]

[1]*Institute of Chemistry, Technology and Metallurgy, Belgrade, Serbia,* [2]*Division of Experimental Therapeutics, Walter Reed Army Institute of Research, Washington, DC 20307-5100,USA,* [3]*Department of Chemistry, University of Crete, Voutes, 71003 Iraklion, Greece and* [4]*Faculty of Chemistry, University of Belgrade, P.O. Box 158, 11001 Belgrade, Serbia*

(Received 6 September 2007)

Abstract: Several dicyclohexylidene tetraoxanes were prepared in order to gain a further insight into structure–activity relationship of this kind of antimalarials. The tetraoxanes **2**–**5**, obtained as a *cis*/*trans* mixture, showed pronounced antimalarial activity against *Plasmodium falciparum* chloroquine susceptible D6, chloroquine resistant W2 and multidrug-resistant TM91C235 (Thailand) strains. They have better than or similar activity to the corresponding desmethyl dicyclohexylidene derivatives. Two chimeric endoperoxides with superior antimalarial activity to the natural product ascaridole were also synthesized.

Keywords: mixed tetraoxanes, endoperoxides, malaria, *P. falciparum*.

INTRODUCTION

Malaria affects more than 500 million people per annum, causing more than one million deaths, mostly in Africa.[1] Infants, young children and pregnant women are particularly at risk; in fact, it has been estimated that a child dies of malaria every 30 seconds. Furthermore, the disease has as an immeasurable negative impact, both personally and socioeconomically, on families and communities in endemic areas. Although malaria is treatable, increased resistance of the protozoan parasite *Plasmodium falciparum* to standard and affordable anti-malarial drugs, such as chloroquine (CQ), complicates the treatment of infected individuals. Peroxide antimalarials of the 1,2,4-trioxacyclohexane class (artemisinin and its derivatives)[2] and drugs of the trioxolane class[3] offer some new possibilities for treating malaria.

Compounds of another peroxide class, the 1,2,4,5-tetraoxacyclohexanes (tetraoxanes), although less investigated, also have been shown to have potent anti-

Serbian Chemical Society member.
☆Current address: Faculty of Chemistry, University of Belgrade, Belgrade, Serbia.
≡ Current address: College of Public Health, University of South Florida, Tampa, USA.
* Corresponding author. E-mail: bsolaja@chem.bg.ac.yu
doi: 10.2298/JSC0712181O

malarial activity.[4] Subsequently, the syntheses of mixed tetraoxanes[5,6] enabled the controlled preparation of a new generation of this promising class of antimalarials.* In addition to the steroidal tetraoxanes, a significant number of dicyclohexylidene tetraoxanes have been synthesized and their anti-malarial activity evaluated both *in vitro* and *in vivo*.[8,9]

Monoterpene ascaridole (Scheme 1), a natural bicyclic [2.2.2] endoperoxide with moderate antimalarial properties, was used as a model for the synthesis of a series of diaryl substituted ascaridole-type endoperoxides, which showed higher activity as compared to ascaridole or dihydroascaridole.[10] More recently, the syntheses of less volatile ascaridole and dihydroascaridole derivatives have been accomplished starting from perillyl and nopol derivatives.[11]

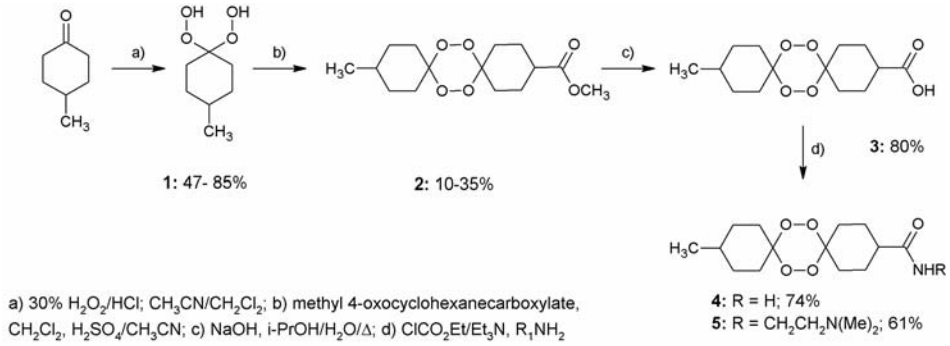

Scheme 1.

Here are reported the synthesis and results of anti-malarial screening of two types of anti-malarial peroxides: mixed tetraoxanes, the derivatives of 12-methyl--7,8,15,16-tetraoxadispiro[5.2.5.2]hexadecane-3-carboxylic acid, and endoperoxides, monoterpene ascaridole derivatives, bound to another anti-malarial pharmacophore, 4-amino-7-chloroquinoline. In addition, the results of *in vivo* screening of some mixed steroidal tetraoxanes are also discussed.

RESULTS AND DISCUSSION

Chemistry

The class of dicyclohexylidene tetraoxanes (**2**–**5**) was designed with varying substituents at the C(4") position in order to obtain further insight into the structure–activity relationship related to spiro-substituents in 1,2,4,5-tetraoxacyclohexane at C(3) and C(6). Gem-dihydroperoxide **1** was prepared from 4-methylcyclohexanone using 30 % hydrogen peroxide and HCl as a catalyst.[5a] Compound **1** was isolated in 47–85 % yield and was pure enough (Scheme 2) to be directly used in the next step.** This gem-dihydroperoxide was coupled to 4-oxocyclohe-

* The structure of the previously evaluated dicyclohexylidene tetraoxanes was limited by a synthetic constraint: only bis compounds could be obtained directly from the corresponding ketones.[7]

** For alternative excellent syntheses of gem-dihydroperoxides, see reference 12.

xanecarboxylate according to a previously developed procedure[5a] to yield the parent mixed tetraoxane, achiral methyl 12-methyl-7,8,15,16-tetraoxadispiro[5.2.5.2]hexadecane-3-carboxylate (**2**; 10–35 %). Further transformations using the ester → → acid → amide sequence (Scheme 2) afforded the desired amides **4** and **5** in 59 % and 49 % yield, respectively.

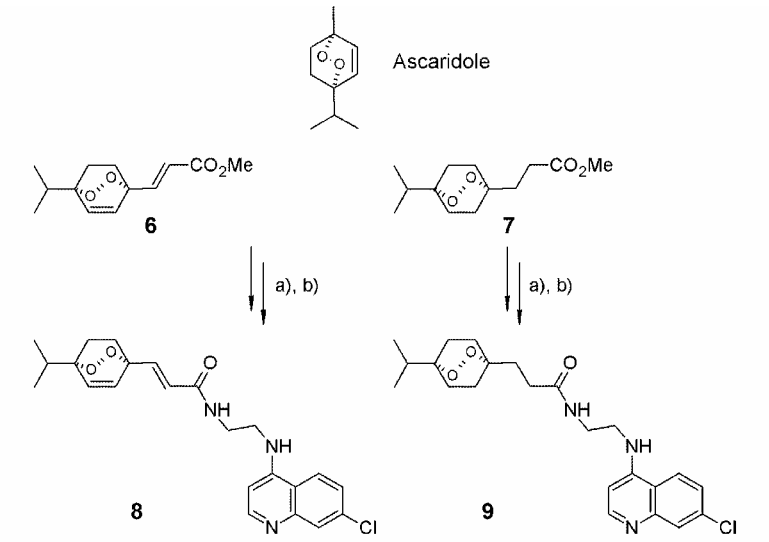

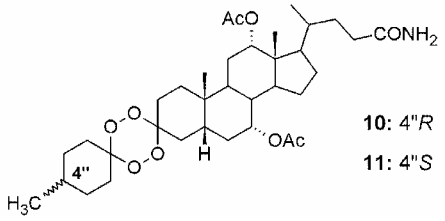

Scheme 2.

Ascaridole derivatives **6** and **7** synthesized earlier[11] were hydrolysed with LiOH into the corresponding acids and further coupled to *N*-(7-chloroquinolin-4--yl)ethane-1,2-diamine to afford the final aminoquinoline products **8** and **9**, respectively (Scheme 1).

Antimalarial activity

The synthesized peroxides were screened *in vitro* against three *Plasmodium falciparum* strains: D6 (chloroquine-susceptible), W2 (chloroquine-resistant, sus-

ceptible to mefloquine), and TM91C235 (Thailand), a multidrug-resistant strain, following the protocol given in the literature.[5a] All the synthesized tetraoxanes exhibited interesting antimalarial activity. In accordance with previous findings,[5a] the acid **3** was less active (in this particular case – practically inactive) than the methyl ester **2** and the corresponding amides **4** and **5** against all parasite strains. One of the current hypotheses regarding the mechanism of antimalarial action of peroxides is that they act in the food vacuole (FV) of *P. falciparum*, which has a pH around 5.5. As such, amide **5** was designed to have an *N,N*-dimethylamino group, expecting that protonation of the basic nitrogen would enhance the flux of the compound through the FV membrane, thereby increasing its concentration at the desired site of action. However, the *in vitro* antimalarial activity data for tetraoxane **5** (Table I) does not support this hypothesis, since amide **4** (which possesses only an acidic hydrogen at the nitrogen) and ester **2** exhibit very similar activity (both IC_{50} and IC_{90}) against all the tested parasites. In addition, the activities of the dicyclohexylidene tetraoxanes presented in this paper are better or equivalent to similar desmethyl compounds.[6d,9]

TABLE I. *In vitro* antimalarial activities of tetraoxanes **2**–**9** against *P. falciparum* D6,[a] W2,[b] and TM91C235[c] strains

Compd.	IC_{50} / nM			IC_{90} / nM		
	D6	W2	TM91C235	D6	W2	TM91C235
2	12.9	6.1	16.0	32.0	20.5	57.5
3	206.6	131.4	300.4	506.9	487.1	1110.1
4	13.6	8.4	18.8	22.1	22.5	41.1
5	14.9	6.1	22.6	23.9	15.8	45.5
6	109.0	42.7	98.2	196.5	68.5	338.9
7	41.4	20.2	47.4	62.5	ND	112.7
8	101.1	58.6	99.7	156.4	140.8	221.4
9	38.3	30.4	60.6	111.6	89.7	200.7
Chloroquine	8.6	354.3	113.7	10.7	653.0	166.0
Mefloquine	17.1	4.7	49.5	36.1	15.5	121.0
Artemisinin[d]	9.0	6.7	13.0	12.8	11.5	17.4

[a]*P. falciparum* African D6 clone; [b]*P. falciparum* Indochina W2 clone; [c]*P. falciparum* multidrug resistant TM91C23 strain (Thailand); [d]average of greater than eight replicates

The antimalarial activity of compounds **6**–**9** appears to be strongly dependent on the degree of saturation: the saturated bicyclic endoperoxides (**7**,**9**) are more potent antimalarials relative to their unsaturated counterparts (Table I), and both unsaturated (**6**,**8**) and saturated (**7**,**9**) endoperoxides are 5–12 times more active than ascaridole and dihydroascaridole themselves. These results indicate that peroxide–aminoquinoline chimeras, in addition to the trioxaquines,[13] might represent a promising addition to the existing antimalarial arsenal.

Finally, the results of an *in vivo* study on the epimeric mixed steroidal tetraoxanes **10** and **11** (Table II) are presented.[5a] The *in vitro* activity of the com-

pounds differs 20- to 30-fold, with the (4"*R*)-epimer **10** being more active; this structure-activity relationship qualitatively holds for other epimeric pairs at the same carbon.[5] Docking calculations of **10** and **11** with heme[14] are consistent with the observation that the proximity of the heme iron to the oxygen atom of the tetraoxane moiety favours potent *in vitro* activity of both compounds. The more potent analogues have much lower energy minimized docked structures. In addition, preliminary metabolic stability assays and metabolite identification were performed using human and mouse liver microsomes to aid the estimation of the first-pass metabolism of the drug candidates in relevant species (Table II).[5c] It is important to note that no scission of peroxide bond was observed (the tetraoxane moiety is stable in this assay); only monohydroxylations occurred. In this assay,[5c] stable compounds were defined as having half-lives > 60 min. Both compounds have similar metabolic half-lives ($t_{1/2}$(mouse) ≅ 30 min). Hence, it would be logical that the observed difference in *in vitro* activity would also be seen in the *in vivo* efficacy test in mice. However, the collective *in vivo* results presented in Table II are not consistent with results from the *in vitro* screening and with the docking calculations: epimers **10** and **11** exert similar *in vivo* activity in mice, regardless of whether they were administered orally or subcutaneously (Table II). Furthermore, at 600 mg/kg total dose p.o. and 480 mg/kg total dose s.c. of tetraoxane **10**, 4/5 and 5/5 mice cured were observed and the respective survival times were 28 and 31 days. At a total dose 150 mg/kg p.o. and 120 mg/kg s.c., very similar survival times were observed.

Analogous results were also seen for epimer **11**. In addition, at comparable total doses of 150 mg/kg p.o. and 120 mg/kg s.c., compounds **10** and **11** both cured more animals orally than subcutaneously. This apparent higher bioavailability by the oral route may have resulted from a lack of absorption due to s.c. depot formation: a subcutaneous sterile pocket of oil and unabsorbed test compound was commonly found in each animal. Alternatively, one of the hydroxylated metabolites formed after oral administration may be more active than the administered parent drug. For both compounds, **10** and **11**, no toxic effects were observed at any tested concentration or applied protocol.

To conclude, several dicyclohexylidene tetraoxanes were prepared and tested in order to gain additional insight into the structure-activity relationship of this structural class of antimalarials. The tetraoxanes **2**–**5** obtained as *cis*/*trans* mixtures exerted better, or similar activity, than the corresponding desmethyl dicyclohexylidene derivatives.[6d,9] The initial work on ascaridole-related compounds[11] enabled the synthesis of two chimeric endoperoxides with superior antimalarial activity to the natural product, ascaridole. The present results indicate that further efforts should be put into research of peroxide–aminoquinoline chimeras as potential antimalarial drug leads. Finally, the results of *in vivo* tests of two epimeric tetraoxanes with a steroidal carrier indicate that subcutaneous testing using an oil vehicle for these compounds may be unsuitable.

TABLE II. *In vivo* activity of tetraoxanes **10** and **11** against *Plasmodium berghei*[a]

Compd.	mg/kg per day	mg/kg total	Admin.	Mice dead/day died	Mice alive day 31/total	Survival time days[b]	Metabolic stability $t_{1/2}$ /min	Metabolite identification	*In vitro* (IC_{50} / nM)[c]	
									D6	W2
10	600	1800	p.o.[d]	1/26	4/5	30	human, 15	hydroxylation (3)	1.17	0.58
	200	600	p.o.[d]	1/16	4/5	28				
	50	150	p.o.[d]	1/12 1/16 1/19	2/5	21.8	mouse, 29	hydroxylation (3)		
	160	480	s.c.		5/5	31				
	40	120	s.c.	1/15, 1/16, 1/18, 1/23	1/5	20.6				
	20	60	s.c.	2/12, 1/17, 2/20	0/5	16.2				
11	600	1800	p.o.[d]		5/5	31	human, 32	hydroxylation (2)	20.03	14.10
	200	600	p.o.[d]	1/15 1/16 1/22 1/26	1/5	22				
	50	150	p.o.[d]	2/13 1/20	2/5	21.6	mouse, 30	hydroxylation (2)		
	160	480	s.c.	1/18	4/5	28.4				
	40	120	s.c.	1/12, 1/16, 1/17, 1/20, 1/24	0/5	17.8				
	20	60	s.c.	1/8, 1/11, 1/16, 2/17	0/5	13.8				

[a]Groups of five *P. berghei* (KBG 173 strain) infected CD-1 mice were treated on days 3, 4, and 5 post infection with tetraoxanes suspended in sesame oil. Mice alive on day 31 with no parasites in a blood film are considered cured; [b]Including cured mice; [c]Taken from ref. 5a; [d]Taken from ref. 5c.

EXPERIMENTAL

General remarks

For details, please see references 5a, 5b, 5c.

ESI MS spectra of the synthesized compounds were recorded on an Agilent Technologies 6210 Time-of-Flight LC/MS instrument in the positive ion mode using CH_3CN/H_2O = 1/1 with 0.2 % HCOOH as the carrying solvent solution. The samples were dissolved in pure acetonitrile (HPLC grade). The selected values were as follows: capillary voltage 4 kV; gas temperature 350 °C; drying gas 12 l min^{-1}; nebuliser pressure 45 psig; fragmentator voltage 70 V.

*1,1-Dihydroperoxy-4-methylcyclohexane (**1**)*

4-Methylcyclohexanone (1.1 ml, 8.9 mmol) was dissolved at r.t. in a CH_2Cl_2/CH_3CN mixture (20 ml, 1:3 v/v), followed by addition of 30 % H_2O_2 (10.4 ml, 0.1 mol) and a few drops of conc. HCl. The reaction mixture was stirred for 2 h at r.t. and then quenched with saturated $NaHCO_3$ and CH_2Cl_2. The organic layer was separated, the water layer was additionally extracted with EtOAc (3×50 ml), and the combined organic layers were dried over anhydrous $MgSO_4$ and evaporated to dryness. The crude product (680 mg, 47 %) was used in the following step without further purification. IR (film, cm^{-1}): 3420*s*, 2935*s*, 2865*s*, 1712*m*, 1637*w*, 1554*m*, 1378*m*, 1357*m*, 1265*m*, 1200*w*, 1158*m*, 1104*m*, 1050*m*, 1017*m*, 980*m*, 910*m*, 861*m* cm^{-1}. IR (CCl_4, cm^{-1}): 3431*m*, 2957*s*, 2930*s*, 2865*m*, 1712*w*, 1551*s*, 1454*m*, 1384*m*, 1357*m*, 1255*s*, 1222*s*, 1162*w*, 1103*m*, 1071*m*, 1012*s*, 980s. ^{1}H-NMR (200 MHz, $CDCl_3$, δ, ppm): 9.40−9.00 (*m*, 2×HOO−C(1)), 2.30−2.00 (*m*), 1.70−1.30 (*m*), 1.30−1.10 (*m*), 0.93 (*d*, H_3C−C(4), J = 6.2 Hz). ^{13}C-NMR (50 MHz, $CDCl_3$, δ, ppm): 110.73, 40.83, 31.59, 30.58, 29.03, 21.38.

*Methyl 12-methyl-7,8,15,16-tetraoxadispiro[5.2.5.2]hexadecane-3-carboxylate (**2**)*

To a cooled solution (ice bath) of dihydroperoxide **1** (1.2 g, 7.4 mmol) in CH_2Cl_2 (20 ml), methyl 4-oxocyclohexanecarboxylate was added and after stirring for 30 min at the same temperature, 1.66 ml of an ice-bath cooled H_2SO_4/CH_3CN mixture (1:10, v/v) was added dropwise. After an additional 50 min stirring, the reaction mixture was worked-up in the usual manner and purified by SiO_2 column chromatography (Lobar B, LichroPrep Si 60, eluent: heptane/EtOAc = 95/5) affording 222 mg (10 %) **2**.* **2**: Colourless foam, softens at 57−59 °C. IR (KBr, cm^{-1}): 3449*w*, 2958*s*, 2938*m*, 2860*m*, 1736*s*, 1442*m*, 1368*m*, 1329*m*, 1265*m*, 1201*s*, 1182*m*, 1133*m*, 1074*s*, 976*m*, 932*m*, 897*m*, 828*w*. ^{1}H-NMR (200 MHz, $CDCl_3$, δ, ppm): 3.68 (*s*, CH_3CO_2−C(1)), 2.98 (*bs*, 2 H), 2.51−2.32 (*m*, 1H), 2.02−1.14 (*m*, 15 H), 0.93 (*d*, CH_3−C(12), J = 6.6 Hz). ^{13}C-NMR (50 MHz, $CDCl_3$, δ, ppm): 175.01, 108.33, 107.22, 51.64, 41.51, 41.30, 31.61, 31.55, 31.26, 30.21, 28.86, 28.09, 24.53, 23.76, 21.30. (+)ESI–MS (*m*/*z* (%)): 304.4 (100), 284.4 (58), 244.3 (25), 164.2 (21), 159.2 (51). Anal. calcd. for $C_{15}H_{24}O_6 \cdot 1/4\ H_2O$: C 59.10, H 8.10; Found: C 59.52, H 8.72.

*12-Methyl-7,8,15,16-tetraoxadispiro[5.2.5.2]hexadecane-3-carboxylic acid (**3**)*

Methyl ester **2** (400 mg, 1.3 mmol) was hydrolyzed at 80 °C with NaOH (72.8 mg, 1.82 mmol) in an *i*-PrOH/H_2O mixture (12 ml, 3:1 v/v). After 15 min, the reaction mixture was cooled and diluted with 20 ml H_2O and 50 ml CH_2Cl_2. The water layer was acidified to pH 2 with dilute HCl, and layers were separated. The water layer was further extracted with CH_2Cl_2 (3×20 ml); the combined organic layers were washed with water and brine, dried over anh. $MgSO_4$, and evaporated to dryness. Triturating with Et_2O afforded 305 mg (80 %) of product. m.p. 134−137 °C. IR (KBr, cm^{-1}): 3449*m*, 2948*s*, 2870*m*, 1707*s*, 1447*m*, 1324*w*, 1270*m*, 1226*m*, 1069*m*, 976*m*, 936*m*. ^{1}H-NMR (200 MHz, $CDCl_3$, δ, ppm): 2.99 (*bs*, 2H), 2.60−2.31 (*m*, 1H), 2.03−1.12 (*m*, 15 H), 0.93 (*d*, CH_3−C(12), J = 6.2 Hz). ^{13}C-NMR (50 MHz, $CDCl_3$, δ, ppm): 180.73, 108.44, 107.19, 41.30, 41.08, 31.65, 31.61, 30.24, 24.29, 21.38. (–)ESI–MS (*m*/*z* (%)): 285.0 ($[M-H]^-$, 89), 104.9 (100). Anal. calcd. for $C_{14}H_{22}O_6 \cdot 1/4\ H_2O$: C 57.52, H 7.82; Found: C 57.99, H 8.39.

* The yields varied within 10–35 %.

General procedure for the preparation of amides

A solution of acid **3** (103 mg, 0.36 mmol) in dry CH_2Cl_2 (20 ml), with added Et_3N (51 µl, 0.36 mmol) and $ClCO_2Et$ (35 µl, 0.36 mmol) was stirred for 90 min at 0 °C. A given amount of amine was added and after 30 min stirring, the reaction mixture was warmed to r.t. After 90 min it was diluted with H_2O, the layers were separated and the organic layer was washed with brine, dried over anh. $MgSO_4$ and evaporated to dryness.

*12-Methyl-7,8,15,16-tetraoxadispiro[5.2.5.2]hexadecane-3-carboxamide (**4**)*

Acid **3** was transformed into amide **4** (75 mg, 74 %), which upon triturating with Et_2O afforded a sample having m.p. 161−165 °C. IR (KBr, cm^{-1}): 3402*s*, 3210*m*, 2949*m*, 2860*w*, 1653*s*, 1441*m*, 1372*w*, 1234*m*, 1077*m*, 978*w*, 940*w*, 904*w*. ^{1}H-NMR (200 MHz, CD_3OD, δ, ppm): 3.40−3.10 (*bs*, 2H), 2.60−2.40 (*m*, 1 H), 2.10−1.20 (*m*, 15 H), 1.12 (*d*, CH_3−C(12), J = 6.3 Hz). ^{13}C-NMR (50 MHz, CD_3OD, δ, ppm): 180.79, 109.27, 108.36, 44.28, 32.92, 32.30, 31.61, 29.99, 29.43, 26.59, 25.69, 21.83, 9.29, 7.58. (+)ESI–MS (*m*/*z* (%)): 327.3 (18), 286.2 ([M+H]$^+$, 15), 152.2 (28), 150.2 (90), 142.2 (25), 102.3 (32), 100.3 (55), 83.3 (100). Anal. calcd. for $C_{14}H_{23}NO_5 \cdot 2/3\ H_2O$: C 56.55, H 8.25, N 4.71; Found: C 56.24, H 8.59, N 5.03.

N-*(2-dimethylamino-ethyl)-12-methyl-7,8,15,16-tetraoxadispiro[5.2.5.2]hexadecane-3-carboxamide (**5**)*

Acid **3** (103 mg, 0.36 mmol) was transformed into amide **5** (79 mg, 61 %) using 10 equivalents of $(CH_3)_2NCH_2CH_2NH_2$ in dry CH_2Cl_2 (25 ml). Upon triturating with Et_2O, a colourless foam was obtained, softness at 140−145 °C. IR (KBr, cm^{-1}): 3443*m*, 3317*s*, 2946*s*, 2873*m*, 2824*m*, 2775*m*, 1649*s*, 1556*s*, 1449*m*, 1371*w*, 1264*w*, 1220*m*, 1069*m*, 976*w*, 927*m*. ^{1}H-NMR (200 MHz, $CDCl_3$, δ, ppm): 6.20 (*bs*, HN−CO), 3.40−3.30 (*m*, $(CH_3)_2NCH_2C\mathbf{H}_2NH$−CO)), 3.10 (*bs*, H–C(1)), 2.45−2.35 (*m*, $(CH_3)_2NC\mathbf{H}_2CH_2NH$−CO)), 2.35−2.10 (*m*, $(C\mathbf{H}_3)_2NCH_2CH_2NH$−CO)), 1.90−1.10 (*m*, 15H), 0.93 (*d*, CH_3−C(12), J = 6.2 Hz). ^{13}C-NMR (50 MHz, $CDCl_3$, δ, ppm): 174.50, 108.39, 107.31, 57.65, 45.01, 43.99, 43.77, 36.45, 31.65, 31.57, 28.42, 24.76, 21.32. (+)ESI–MS (*m*/*z* (%)): 357.3 ([M+H]$^+$, 100). Anal. calc. for $C_{18}H_{32}N_2O_5$ 1/2 H_2O: C 59.16, H 9.10, N 7.67; Found: C 59.39, H 9.61, N 7.75.

*(E)-N-{2-[(7-chloro-4-quinolinyl)amino]ethyl}-3-(4-isopropyl-2,3-dioxabicyclo[2.2.2]oct-5-en-1--yl)-2-propenamide (**8**)*

Employing the above procedure, compound **6** was hydrolysed and the intermediate acid[11] was transformed into amide **8** (31 mg, 91 %), which was then triturated with Et_2O. Oil. **8**: ^{1}H-NMR (200 MHz, $CDCl_3$, δ, ppm): 8.42 (*m*, H−C(2')), 7.90 (*m*, H−C(5')), 7.83 (*m*, H−C(8')), 7.36 (*m*, H−C(6')), 7.03 (*d*, 1H, J = 15.6 Hz), 6.95 (*bs*, NH−Ar), 6.62 (*bs*, NH−CO), 6.58 (*d*, 1H, J = 8.7 Hz), 6.49 (*d*, 1H, J = 8.7 Hz), 6.26 (*m*, H−C(3')), 6.14 (*d*, 1H, J = 15.6 Hz), 3.80−3.70 (*m*, $CONHCH_2C\mathbf{H}_2NHAr$), 3.48−3.36 (*m*, $CONHC\mathbf{H}_2CH_2NHAr$), 2.20−1.95 (*m*, 4H), 1.50−1.70 (*m*, 1H), 1.02 (*m*, 6H). ^{13}C-NMR (50 MHz, $CDCl_3$, δ, ppm): 167.53, 150.90, 150.54, 147.94, 143.44, 141.80, 135.30, 133.77, 127.36, 125.59, 123.83, 122.30, 117.00, 98.08, 80.79, 75.60, 45.43, 38.93, 32.06, 28.91, 24.54, 17.53, 17.08. (+)ESI–HRMS (*m*/*z* (%)): 428.1735 ([M+H]$^+$, 100); calculated 428.1736.

*N-{2-[(7-chloro-4-quinolinyl)amino]ethyl}-3-(4-isopropyl-2,3-dioxabicyclo[2.2.2]oct-1-yl)propanamide (**9**)*

Employing the above procedure, compound **7** was hydrolysed and the intermediate acid[11] was transformed into amide **9** (32 mg, 85 %), which was then triturated with Et_2O. Oil. **9**: ^{1}H-NMR (200 MHz, $CDCl_3$, δ, ppm): 8.45 (*m*, H−C(2')), 7.88 (*m*, H−C(5')), 7.78 (*m*, H−C(8')), 7.33 (*m*, H−C(6')), 6.65 (*bs*, NH−Ar), 6.45 (*bs*, NH−CO), 6.24 (m, H−C(3')), 3.69−3.65 (*m*, $CONHCH_2C\mathbf{H}_2NHAr$), 3.39−3.37 (*m*, $CONHC\mathbf{H}_2CH_2NHAr$), 2.31−2.28 (*t*, 2H, J = 9.0 Hz), 1.94−1.88 (*m*, 4H), 1.84−1.78 (*m*, 2H), 1.67−1.57 (*m*, 5H), 0.86 (*d*, 6H, J = 7.0 Hz). ^{13}C-NMR (50 MHz, $CDCl_3$, δ, ppm): 175.56, 151.80, 150.15, 148.93, 134.91, 128.24, 125.43, 122.07, 117.26, 98.17, 79.70, 76.08, 45.61, 38.79, 34.15, 33.23, 30.25, 28.87, 25.68, 16.85. (+)ESI-HRMS (*m*/*z* (%)): 432.2050 ([M+H]$^+$, 100); calculated 432.2048.

In vitro *antimalarial activity*

The *in vitro* antimalarial drug susceptibility screen was a modification of the procedures first published by Desjardins *et al*.,[15] with modifications developed by Milhous *et al*.,[16] with the details given in ref. 4c.

In vivo *antimalarial activity*

The *P. berghei* mouse efficacy tests were conducted using a modified version of the Thompson test. On day 0, each mouse was inoculated intraperitoneally with 0.1 ml, 1.0×10^6 *P. berghei* P-line infected red blood cells from donor mice. The test drugs at 10, 20, and 80 mg/kg were suspended or dissolved in sesame oil and administered s.c. beginning on day 3 post-infection. Drug administrations were performed twice per day at 12 hours intervals for 3 days. The dose levels are given in Table II. Cure was defined as survival until day 31 post-treatment. Untreated control mice typically died on day 7−9 post-infection.

Acknowledgements: This work was supported by the Ministry of Science of Serbia (Grant No. 142022 and a Serbo-Greek bilateral project) and the Serbian Academy of Sciences and Arts. The material has been reviewed by the Walter Reed Army Institute of Research. There is no objection to its presentation or publication. The opinions or assertions contained herein are the private views of the authors and are not to be construed as official or as reflecting true views of the Department of the Army or the Department of Defence.

ИЗВОД

О ПЕРОКСИДНИМ АНТИМАЛАРИЦИМА

ИГОР ОПСЕНИЦА[1], ДЕЈАН ОПСЕНИЦА[1], МИЛКА ЈАДРАНИН[1], KIRSTEN SMITH[2], WILBUR K. MILHOUS[2], MANOLIS STRATAKIS[3] и БОГДАН ШОЛАЈА[4]

[1]Институт за хемију, технологију и металургију, Београд, [2]Division of Experimental Therapeutics, Walter Reed Army Institute of Research, Washington, DC 20307-5100, USA, [3]Department of Chemistry, University of Crete, Voutes, 71003 Iraklion, Greece и [4]Хемијски факултет Универзитета у Београду, п. пр. 158, Београд

У овом раду приказана је синтеза неколико дицикилохексилиденских тетраоксана у циљу сагледавања односа структура–активност ове врсте антималарика. Једињења **2**–**5** добијена као (cis,trans)-смесе показала су изражену антималаријску активност према D6, W2 и TM91C235 (Thailand) сојевима *P. falciparum*. Она имају бољу или сличну активност од одговарајућих десметил циклохексилиденских деривата. Синтетисана су и два ендопероксида химерне структуре знатно израженије активности од природног производа аскаридола.

(Примљено 6. септембра 2007)

REFERENCES

1. World Health Organization http://www.who.int/mediacentre/factsheets/fs094/en/index.html
2. (a) G. H. Posner, A. J. McRiner, I.–H. Paik, S. Sur, K. Borstnik, S. Xie, A. S. Shapiro, A. Alagbala, B. Foster, *J. Med. Chem.* **47** (2004) 1299; (b) G. H. Posner, I.-H. Paik, W. Chang, K. Borstnik, S. Sinishtaj, A. S. Rosenthal, T. A. Shapiro, *J. Med. Chem.* **50** (2007) 2516; (c) L. Vivas, L. Rattray, L. B. Stewart, B. L. Robinson, B. Fugmann, R. K. Haynes, W. Peters, S. L. Croft, *J. Antimicrob. Chemother.* **59** (2007) 658 and references cited therein
3. (a) J. L. Vennerstrom, Y. Dong, J. Chollet, H. Matile, US patent 6,486,199 (2002); (b) J. L. Vennerstrom, Y. Dong, J. Chollet, H. Matile, M. Padmanilayam, Y. Tang, W. N. Charman, US continuation-in-part based on PCT/US02/19767 (filed 21 June 2002); (c) M. Padmanilayam, B. Scorneaux, Y. Dong, J. Chollet, H. Matile, S. A. Charman, D. J. Creek, W. N. Charman, J.

S. Tomas, C. Scheurer, S. Wittlin, R. Brun, J. L. Vennerstrom, *Bioorg. Med. Chem. Lett.* **16** (2006) 5542

4. (a) J. L. Vennerstrom, H.-N. Fu, W. Y. Ellis, A. L. Ager Jr., J. K. Wood, S. L. Andersen, L. Gerena, W. K. Milhous, *J. Med. Chem.* **35** (1992) 3023; (b) N. M. Todorović, M. Stefanović, B. Tinant, J.-P. Declercq, M. T. Makler, B. A. Šolaja, *Steroids* **61** (1996) 688; (c) D. Opsenica, G. Pocsfalvi, Z. Juranić, B. Tinant, J.-P. Declercq, D. E. Kyle, W. K. Milhous, B. A. Šolaja, *J. Med. Chem.* **43** (2000) 3274; (d) D. Opsenica, G. Angelovski, G. Pocsfalvi, Z. Juranić, Ž. Žižak, D. Kyle, W. K. Milhous, B. A. Šolaja, *Bioorg. Med. Chem.* **11** (2003) 2761
5. (a) B. A. Šolaja, N. Terzić, G. Pocsfalvi, L. Gerena, B. Tinant, D. Opsenica, W. K. Milhous, *J. Med. Chem.* **45** (2002) 3331; (b) D. Opsenica, D. E. Kyle, W. K. Milhous, B. A. Šolaja, *J. Serb. Chem. Soc.* **68** (2003) 291; (c) I. Opsenica, N. Terzić, D. Opsenica, D. Angelovski, M. Lehnig, P. Eilbracht, B. Tinant, Z. Juranić, K. S. Smith, Y. S. Yang, D. S. Diaz, P. L. Smith, W. K. Milhous, D. Doković, B. A. Šolaja *J. Med. Chem.* **49** (2006) 3790
6. (a) H.–S. Kim, K. Tsuchiya, Y. Shibata, Y. Wataya, Y. Ushigoe, A. Masuyama, M. Nojima, K. J. McCullough, *J. Chem. Soc., Perkin Trans 1* (1999) 1867; (b) J. Iskra, D. Bonnet–Delpon, J.––P. Bégue, *Tetrahedron Lett.* **44** (2003) 6309; (c) A. O. Terent'ev, A. V. Kutkin, Z. A. Starikova, M. Yu. Antipin, Yu. N. Ogibin, G. I. Nikishin, *Synthesis* (2004) 2356; (d) R. Amewu, A. V. Stachulski, S. A. Ward, N. G. Berry, P. G. Bray, J. Davies, G. Labat, L. Vivas, P. M. O'Neill, *Org. Biomol. Chem.* **4** (2006) 4431
7. J. L. Vennerstrom, Y. Dong, S. L. Andersen, A. L. Ager Jr., H.-N. Fu, R. E. Miller, D. L. Wesche, D. E. Kyle, L. Gerena, S. M. Walters, J. K. Wood, G. Edwards, A. D. Holme, W. G. McLean, W. K. Milhous, *J. Med. Chem.* **43** (2000) 2753 and references cited therein
8. J. L. Vennerstrom, A. L. Ager, S. L. Andersen, J. M. Grace, V. Wongpanich, C. K. Angerhofer, J. K. Hu, D. L. Wesche, *Am. J. Trop. Med. Hyg.* **62** (2000) 573
9. I. Opsenica, N. Terzić, D. Opsenica, W. K. Milhous, B. Šolaja, *J. Serb. Chem. Soc.* **69** (2004) 919
10. G. H. Posner, X. Tao, J. N. Cumming, D. Klinedinst, T. A. Shapiro, *Tetrahedron Lett.* **37** (1996) 7225
11. E. Hatzakis, I. Opsenica, B. A. Šolaja, M. Stratakis, *Arkivoc* **VIII** (2007) 124
12. (a) J. Iskra, D. Bonnet–Delpon, J.–P. Bégue, *Tetrahedron Lett.* **44** (2003) 6309; (b) K. Žmitek, M. Zupan, S. Stavber, J. Iskra, *Org. Lett.* **8** (2006) 2491
13. O. Dechy, F. Benoit–Vical, C. Loup, A. Robert, H. Gornitzka, A. Bonhour, V. Vial, J. F. Magnaval, J. P. Seguela, B. Meunier, *Chem. Eur. J.* **10** (2004) 1625
14. A. K. Bhattacharjee, K. A. Carvalho, D. Opsenica, B. A. Šolaja, *J. Serb. Chem. Soc.* **70** (2005) 329
15. R. E. Desjardins, C. J. Canfield, D. E. Haynes, J. D. Chulay, *Antimicrob. Agents Chemother.* **16** (1979) 710
16. W. K. Milhous, N. F. Weatherly, J. H. Bowdre, R. E. Desjardins, *Antimicrob. Agents Chemother.* **27** (1985) 525.

Journal of the Serbian Chemical Society
JSCS@tmf.bg.ac.yu • www.shd.org.yu/JSCS

J. Serb. Chem. Soc. 72 (12) 1191–1200 (2007) UDC 530.13:541.124:544.4:547.564.8:66.012
JSCS–3652 *Original scientific paper*

Substituent and structural effects on the kinetics of the reaction of *N*-(substituted phenylmethylene)-*m*- and -*p*-aminobenzoic acids with diazodiphenylmethane

BRATISLAV Ž. JOVANOVIĆ[1#], ALEKSANDAR D. MARINKOVIĆ[1*#], ŽELJKO VITNIK[2] and IVAN O. JURANIĆ[2#]

[1]*Department of Organic Chemistry, Faculty of Technology and Metallurgy, University of Belgrade, Karnegijeva 4, P.O. Box 35-03, 11120 Belgrade and* [2]*Faculty of Chemistry, University of Belgrade, Studentski trg 12–16, 11001 Belgrade, Serbia*

(Received 26 April 2007)

Abstract: The rate constants for the reaction of twenty-two *N*-(substituted phenylmethylene)-*m*- and -*p*-aminobenzoic acids with diazodiphenylmethane were determined in absolute ethanol at 30 °C. The effects of substituents on the reactivity of the investigated compounds were interpreted by correlation of the rate constants with LFER equations. The results of quantum mechanical calculations of the molecular structure together with experimental results gave a better insight into the effects of structure on the transmission of electronic effects of the substituents. New σ constants for substituted benzylideneamino group were calculated.

Keywords: rate constants; substituent and structural effects; geometry optimization.

INTRODUCTION

It has been reported that *N*-benzylidenealdimines are important intermediates for the synthesis of a number of pharmacologically active compounds.[1–4] Numerous former investigations of the molecular structures of *N*-benzylideneanilines[5–9] showed that substituents in the aniline and benzylidene moiety largely influence the deflection of the angles θ_N or θ_C by their electronic and/or steric effects, and, therefore, determine the conformation of the corresponding molecules (Fig. 1, the torsion angle around the C=N double bond is labeled as θ_D).

The aim of the present study was to investigate the effects of substituents at the benzylidene ring on the reactivity of the carboxylic group in *N*-(substituted phenylmethylene)-*m*- and -*p*-aminobenzoic acids with diazodiphenylmethane (DDM). It is a continuation of the investigation of the effects of substituents on the ^{13}C-NMR chemical shifts of the same acids.[10]

Serbian Chemical Society member.
* Corresponding author. E-mail: marinko@tmf.bg.ac.yu
doi: 10.2298/JSC0712191J

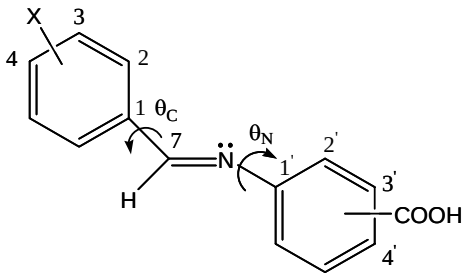

Fig. 1. Structure of *N*-(substituted phenylmethylene)-*m*- and -*p*-aminobenzoic acids with the descriptors of their geometry.

EXPERIMENTAL

All of the *N*-(substituted phenylmethylene)-*m*- and -*p*-aminobenzoic acids were synthesized by heating equimolar amounts of the corresponding *m*- or *p*-aminobenzoic acids and the corresponding substituted aldehydes in appropriate solvents.[10] As an example: 1.37 g (0.01 mol) *p*-aminobenzoic acid and 1.06 g (0.01 mol) benzaldehyde were refluxed in 10 ml absolute ethanol for two hours. After crystallization, the crude product was filtered and recrystallized from absolute ethanol. The structure and purity of the obtained compounds were controlled by melting points, elemental analysis, ^{1}H- and ^{13}C-NMR spectroscopy, which were in agreement with literature data.

Diazodiphenylmethane was prepared by the Smith and Howard method.[11] A stock solution of *ca*. 0.06 mol dm^{-3} was stored in a refrigerator and diluted immediately before use. Kinetic measurements of the reaction rate in absolute ethanol were performed by the spectroscopic method of Roberts and coworkers,[12] using a Shimadzu 160A UV spectrophotometer. Optical density measurements were performed at 525 nm with 1-cm cells at 30±0.05 °C. Three determinations were made for each acid and in every case the individual second order or pseudo-first-order rate constants agreed within 3 % of the mean. All regression analyses in this work were performed with the Microsoft Excel® program package.

Method of calculation

The MNDO-PM3 method has proved to be highly reliable for investigating the molecular properties of molecules, ions[13,14] and zwitterions.[15] The MOPAC program package, Version 7.01, was used. The initial structures of the compounds were generated by PC MODEL, version 4.0,[16] which involves an MMX force field[17] and were saved as MOPAC input files for MNDO-PM3 semi-empirical calculations.[18,19] The geometries of all molecular species, corresponding to the energy minima in vacuum, were optimized by the PM3 method. As the conformers may have different stabilities in vacuum and in the condensed state, the conformational space was also systematically searched for local energy minima, starting from various conformations differing from the most stable one. The simulation of the polar medium, with full geometry optimization, was performed using the COSMO facility in MOPAC.[20]

RESULTS AND DISCUSSION

The reaction of carboxylic acids with DDM has been used by numerous authors for quantitative structure–reactivity studies.[21–23] The mechanism of this reaction, suggested by Roberts and later proved,[12,24] involves proton transfer from the acids to DDM in the rate-determining step.

The values of second-order rate constants for the reaction of *N*-(substituted phenylmethylene)-*m*- and -*p*-aminobenzoic acids with DDM in absolute ethanol at 30 °C are given in Table I, together with corresponding $\sigma_{m/p}$ substituent constants.[25]

TABLE I. The second-order rate constants, k_2, for the reaction of *N*-(substituted phenylmethylene)-*m*- and -*p*-aminobenzoic acids with DDM at 30 °C in absolute ethanol

Substituent (X)	k_2 / dm^{3}mol^{-1}min^{-1}		$\sigma_{m/p}$
	N-(Substituted phenylmethylene)-*m*--aminobenzoic acids	*N*-(Substituted phenylmethylene)-*p*--aminobenzoic acids	
H	1.086	0.386	0
p-$N(CH_3)_2$	0.945	0.284	–0.83
p-OCH_3	1.045	0.354	–0.27
p-CH_3	1.063	0.387	–0.17
p-Br	1.151	0.455	0.23
p-Cl	1.135	0.442	0.23
p-NO_2	1.282	0.571	0.78
p-CN	1.228	0.520	0.66
m-CH_3	1.078	0.384	–0.07
m-OCH_3	1.130	0.425	0.12
m-Cl	1.160	0.470	0.37

For quantitative assessment of the substituent effects on the rate constants, the simple Hammett Equation was used:

$$\log k_2 = \log k_0 + \rho\sigma_{m/p} \quad (1)$$

where ρ is a reaction constant reflecting the sensitivity of the rate constants to substituents effects and k_0 is the rate constant of the parent (unsubstituted) compound of the series. The following correlation parameters were obtained using the data from Table I for *N*-(substituted phenylmethylene)-*m*-aminobenzoic acids:

$$\log k_2 = 0.039 + 0.079\sigma_{m/p} \quad (2)$$
$$(r = 0.995;\ s = 0.004;\ n = 11)$$

while the corresponding correlation for *N*-(substituted phenylmethylene)-*p*-aminobenzoic acids is:

$$\log k_2 = -0.396 + 0.184\sigma_{m/p} \quad (3)$$
$$(r = 0.993;\ s = 0.009;\ n = 11)$$

where r is the correlation coefficient, s the standard deviation and n the number of data included in the correlation.

The low values of the reaction constant ρ for both series of acids indicate a significant attenuation effect of the imino group diminishing the transmission of electronic effects of the substituents through that group. The lower value of ρ for *N*-(substituted phenylmethylene)-*m*-aminobenzoic acids leads to the conclusion that the rate constants of these acids are significantly less sensitive to the substituent effects than is the case of *N*-(substituted phenylmethylene)-*p*-aminobenzoic acids.

Applying the Taft dual substituent–parameter Equation (DSP) in the form:

$$\log k_2 = \log k_0 + \rho_I\sigma_I + \rho_R\sigma_R \quad (4)$$

the overall substituent effect is separated into inductive, σ_I, and resonance, σ_R or σ_R^+, contribution. This approach gives the following results for *N*-(substituted phenylmethylene)-*m*-aminobenzoic acids:

$$\log k_2 = 0.04 + 0.085\sigma_I + 0.074\sigma_R \quad (5)$$

($r = 0.992$; $s = 0.015$; $n = 8$)

$$\log k_2 = 0.04 + 0.085\sigma_I + 0.040\ \sigma_R^+ \quad (6)$$

($r = 0.992$; $s = 0.014$; $n = 8$)

and for *N*-(substituted phenylmethylene)-*p*-aminobenzoic acids:

$$\log k_2 = -0.40 + 0.198\sigma_I + 0.175\sigma_R \quad (7)$$

($r = 0.992$; $s = 0.015$; $n = 8$)

$$\log k_2 = -0.41 + 0.198\sigma_I + 0.093\ \sigma_R^+ \quad (8)$$

($r = 0.993$; $s = 0.013$; $n = 8$)

In these correlations only acids with substituents in the *para* position at the phenylmethylene ring were included and σ_I, σ_R and σ_R^+ were taken from the literature.[25]

The relative contribution of inductive and resonance substituent effects were quantitatively estimated by calculating the parameter λ as the ratio of ρ_R and ρ_I, giving values of $\lambda_m = \rho_{Rm}/\rho_{Im} = 0.872$ and $\lambda_m^+ = \rho_{Rm}^+/\rho_{Im} = 0.471$ for *N*–(substituted phenylmethylene)-*m*-aminobenzoic acids, and $\lambda_p = \rho_{Rp}/\rho_{Ip} = 0.884$ and $\lambda_p^+ = \rho_{Rp}^+/\rho_{Ip} = 0.470$ for *N*-(substituted phenylmethylene)-*p*-aminobenzoic acids. It is evident that the contribution of the resonance substituent effect is less significant compared to the inductive one. The lower values of parameters λ^+ calculated from correlations (6) and (8) indicate that the contribution of direct conjugation (π,π-conjugation) of the substituent, and carboxylic group as the reaction centre, across the investigated molecules, was attenuated because of inadequate molecular geometry for this type of conjugation. A more important resonance interaction all the way through the molecules of *N*-(substituted phenylmethylene)-*p*--aminobenzoic acids, than that in the molecules of *N*-(substituted phenylmethylene)-*m*-aminobenzoic acids, could have been expected, but the values of the parameters λ show that the differences between the two series of acids are negligible. This obvious leveling effect could be explained by the relatively high electronegativity of the nitrogen atom, causing a considerable localization of the π-electrons.

There are two experimental facts which could be inferred from Table I and Eqs. (1)−(8). The rate constants for the *m*-carboxy series are 2.2−3.2 times higher than those for the *p*-carboxy series. On the other hand, the better transmission of the variation in the electronic effects in the *p*-carboxy series results in the higher value of the reaction constant ρ. In the *m*-carboxy series, the absence of direct conjugation with the reaction centre, together with the facts established in a former study[10] about an electron deficiency at the azomethine carbon and, consequently, a limited transmission of the variation in the electron acceptor effect, causes the lower value of the constant ρ.

Specific electronic interactions within the *N*-(substituted phenylmethylene)-*m*- and -*p*-aminobenzoic acid molecules found in both a previous[10] and the present study, prompted us to calculate the σ_m and σ_p substituent constants for the substituted benzylideneamino groups, which have not been previously reported. The kinetic data from Table I were used for the calculation of these new σ(exp) constants on the basis of the Hammett Equation, given by Eq. (1) in the form $\log k_2 = \log k_0 + \rho\sigma$ (for $\log k_0 = 0.039$ and $\rho = 0.937$), for benzoic acids for the same reaction conditions.[12]

All σ_p(exp) constants (Table II) of *p*-substituted benzylideneamino groups are negative, which means that these groups, according to their electronic effects, are electron-donating. This indicates that the *n*,π-conjugation in the aniline part of *N*-(substituted phenylmethylene)-*p*-aminobenzoic acids is the dominant effect, because of the electron-accepting carboxylic group. Electronic effects of substituents from the benzylidene part influence only an increase or decrease of this conjugation. The *n*,π-conjugation in the aniline part of *N*-(substituted phenylmethylene)-*m*-aminobenzoic acids has a weaker effect in comparison to that in the previous *p*-series of acids, as reflected in the σ_m(exp) values of the corresponding substituted benzylideneamino groups (Table II). The electronic effect is negative for electron-donating and positive for electron-accepting substituents. On the basis of the calculated values of the σ constants for *p*- and *m*-substituted benzylideneamino groups, two opposite effects could be identified. One is the electronic effect of the substituents in the benzylidene ring and the other is electronic conjugation interactions in the aniline part of the molecule. Generally, it can be said that the balance of these two effects produces the overall effect of these groups on the reactivity of the investigated acids.

TABLE II. The substituent constants, σ(exp), of *m*- and *p*-substituted benzylideneamino groups

Substituent (X)	σ_m(exp)	σ_p(exp)
H	–0.003	–0.478[a]
p-$N(CH_3)_2$	–0.068	–0.639
p-OCH_3	–0.022	–0.533
p-CH_3	–0.014	–0.492
p-Br	0.024	–0.406
p-Cl	0.017	–0.397
p-NO_2	0.074	–0.312
p-CN	0.054	–0.345
m-CH_3	–0.006	–0.490
m-OCH_3	0.015	–0.444
m-Cl	0.027	–0.391

[a]Value: –0.55[26]

In order to get rationalized the transmission of electronic substituent effects in the investigated acids we searched for a method to determine their geometry,

and as the result semi-empirical calculations were performed using the MOPAC program package. Full optimization of the molecular geometry of the investigated acids was performed by the MNDO-PM3 method.[18,19] As major descriptors of their geometry, the following structural elements were selected (see Fig. 1): a) *Z*/*E* isomerization about the C=N double bond; b) rotation of the carboxylic group by a certain degree about the $C_{carbonyl}$−C_{phenyl} bond; c) rotation of the hydroxyl group around the C−O bond, d) the torsional angle C(2')−C(1')−N−C(7), marked as θ_N; e) torsional angle C(1')−N−C(7)−C(1), marked as θ_D; f) torsional angle N−C(7)−C(1)−C(2), marked as θ_C for the molecular structures with a minimum potential energy.

The calculated energies of the two possible *Z*/*E* geometrical isomers for both series of acids are very similar, indicating that an appropriate equilibrium of isomers of acids may exist in solution. It was assumed that a corresponding contribution of the isomers conforms to the statistical Boltzman distribution, thus the weighted average values of the molecular energies and corresponding angles were calculated. It was assumed that the inductive effect should not be markedly affected by conformational variations of the molecule. The opposite is true for the resonance effect, which is strongly dependent on the conformational arrangement. The resonance effect is proportional to $\cos^2$ of the corresponding torsional angle between the reaction centre and the substituent. Following this procedure and multiplying σ_R substituent constants[25] with the corresponding calculated values of the angle in the form $\cos^2\theta = \cos^2\theta_N \cos^2\theta_D \cos^2\theta_C$, a new resonance constants $\sigma_R\cos^2\theta$ for the *m*- and *p*-substituted benzylideneamino groups were obtained. Finally, the $\sigma_{m/p}$(calcd.) constants of these groups for both series of acids were obtained according to the formula $\sigma_{m/p}(\text{calcd.}) = \sigma_I + \sigma_R\cos^2\theta$, the calculated values of which are given in Tables III and IV. Examples of the most stable conformers of *N*-(substituted phenylmethylene)-*m*- and -*p*-aminobenzoic acids are shown in Figs. 2 and 3, respectively.

TABLE III. The values of angles θ_N, θ_D and θ_C of *N*-(substituted phenylmethylene)-*m*-aminobenzoic acids and σ_m(calcd.) constants of substituted benzylideneamino groups

Substituent	θ_N	θ_D	θ_C	σ_m(calcd.)
H	64.157	0.349	35.253	0.035
p-$N(CH_3)_2$	62.296	0.566	30.061	-0.024
p-OCH_3	62.869	0.740	31.534	0.015
p-CH_3	63.774	0.371	34.144	0.031
p-Br	63.732	0.321	38.125	0.062
p-Cl	62.143	0.501	34.559	0.059
p-NO_2	61.838	0.439	40.400	0.101
p-CN	62.792	0.333	38.838	0.092
m-CH_3	64.661	0.417	36.240	0.030
m-OCH_3	63.426	0.466	38.235	0.050
m-Cl	62.889	0.354	35.938	0.069

TABLE IV. The values of angles θ_N, θ_D and θ_C of *N*-(substituted phenylmethylene)-*p*-aminobenzoic acids and σ_p(calcd.) constants of substituted benzylideneamino groups

Substituent	θ_N	θ_D	θ_C	σ_p(calcd.)
H	66.917	0.353	36.577	-0.402
p-$N(CH_3)_2$	65.910	0.563	31.579	-1.012
p-OCH_3	65.941	0.754	32.623	-0.455
p-CH_3	66.252	0.375	34.075	-0.429
p-Br	66.916	0.327	38.669	-0.342
p-Cl	66.300	0.419	35.636	-0.348
p-NO_2	64.303	0.292	41.033	-0.247
p-CN	64.799	0.550	39.373	-0.272
m-CH_3	67.429	0.705	34.816	-0.420
m-OCH_3	68.356	0.547	39.956	-0.372
m-Cl	67.504	0.391	36.550	-0.325

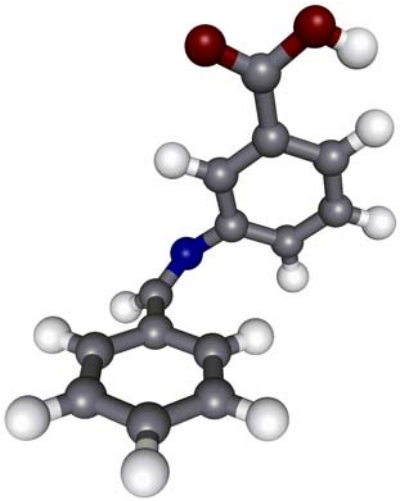

Fig. 2. Structure of the most stable conformer of *N*–(phenylmethylene)-*m*-aminobenzoic acid calculated by the MNDO-PM3 method.

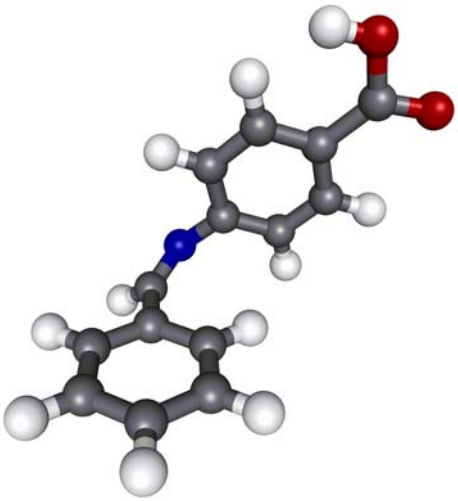

Fig. 3. Structure of the most stable conformer of *N*-(phenylmethylene)–*p*–aminobenzoic acid calculated by the MNDO-PM3 method.

The results from Tables III and IV indicate a large out of plane deviation of the aniline ring, while the deviation of benzylidene ring has a lower value, but the deviations are significant for both series of acids. Regularity can be observed for the values of the angles θ_C, *i.e.*, for electron-donor substituents, these values are lower and for electron-acceptors higher for higher values of the substituent constant. This is in agreement with a previous study,[10] as a good correlation was obtained with σ_I for electron-acceptor and with the electrophilic substituent constant σ_p^+ for electron donors. These results show that electron-donor substituents induce planarity of the benzylidene part of the molecules, while electron-acceptors cause a deviation from planarity. Therefore, only the inductive part of their substituent effect is transmitted to the reaction center. Since no regularity in the va-

riation of the values of angle θ_N were observed, this probably means that complex electronic effects involving both π,π- and *n*,π-conjugation in aniline part influence the values of the angle θ_N.

Intercorrelation of the experimental σ_m(exp) values (Table II) and the calculated σ_m(calcd.) (Table III) for *N*-(substituted phenylmethylene)-*m*-aminobenzoic acids gave the following result:

$$\sigma_m(\text{exp}) = -0.004 + 1.072\sigma_m(\text{calcd.}) \quad (9)$$
$$(r = 0.999;\ s = 0.004;\ n = 11)$$

having the *y*-axis interception close to zero.

Also, intercorrelation of the σ_p(exp) (Table II) and σ_p(calcd.) (Table IV) values for *N*-(substituted phenylmethylene)-*p*-aminobenzoic acids gives the following correlation:

$$\sigma_p(\text{exp}) = -0.034 + 1.099\sigma_p(\text{calcd.}) \quad (10)$$
$$(r = 0.996;\ s = 0.004;\ n = 11)$$

where $\sigma_{m/p}$(exp) (Table II) are the values of the substituent constants calculated on the basis of experimental data and $\sigma_{m/p}$ (calcd.) (Tables III and IV) are data calculated according to the optimization of molecular geometry. It can be seen, on the basis of the correlation results, that the modeling of the geometry of the investigated molecules by quantum mechanical calculation is a reliable method for an estimation of their structure.

CONCLUSIONS

The excellent Hammett correlations obtained with $\sigma_{m/p}$ substituent constants (Eqs. (2) and (3)) and low values of the reaction constants indicate a moderate transmission of electronic effects through the whole system of the investigated acids. The separation of the electronic substituent effect into a resonance and inductive part by the Taft equation shows a smaller contribution of resonance interaction. As a consequence, when electron-donating substituents are present in the benzylidene ring, there is a substantial decrease of the angle θ_C and, consequently, the molecules tend to attain a planar conformation. Thus, a better transmission of the resonance substituent electronic effects through the molecules is achieved.

The above correlations and the results of a previous study[10] show that the effects of substituents on the variations of the angles θ_N and θ_C are a significant feature of the geometry of the investigated molecules. Therefore, it can be concluded that the conformation of the molecules is determined by a balance of *n*,π-conjugation in the aniline part of the molecule and inductive and resonance effects of substituents in the benzylidene ring. Consequently, the carboxylic group in the *para* position causes the values of the angles θ_N and θ_C to have slightly higher values than when that group is in the *meta* position. This is corroborated by a mathematical (quantum-mechanical) optimization of the structure of the investigated

molecules, whereby the changes of the values of the angle follow the above-stated principles. Also, the higher values of the rate constants for the *N*-(substituted phenylmethylene)-*m*-aminobenzoic acids indicate a stronger conjugation in the series of *N*-(substituted phenylmethylene)-*p*-aminobenzoic acids, due to the better electron donating power of the benzylideneamino groups, thus decreasing the acidity of these acids.

It should be pointed out that the excellent intercorrelation of the experimentally determined and calculated $\sigma_{m/p}$ values for the substituted benzylideneamino groups verify the credibility of both approaches.

И З В О Д

ЕФЕКТИ СУПСТИТУЕНАТА И СТРУКТУРЕ НА КИНЕТИКУ РЕАКЦИЈЕ *N*-(СУПСТИТУИСАНИХ)-*m*- И -*p*-АМИНОБЕНЗОЕВИХ КИСЕЛИНА СА ДИАЗОДИФЕНИЛМЕТАНОМ

БРАТИСЛАВ Ж. ЈОВАНОВИЋ[1], АЛЕКСАНДАР Д. МАРИНКОВИЋ[1], ЖЕЉКО ВИТНИК[2] и ИВАН О. ЈУРАНИЋ[2]

[1]Катедра за органску хемију, Технолошко–металуршки факултет, Универзитет у Београду, Карнегијева 4, п. пр. 3503, Београд и [2]Хемијаки факултет, Универзитет у Београду, Студентски трг 12–16, 11001 Београд

Константе брзина реакција између двадесет две *N*-(супституисане фенилметилен)-*m*- и -*p*-аминобензоеве киселине и диазодифенилметана одређене су у апсолутном етанолу на 30 °C. Ефекти супституената на реактивност испитиваних једињења су интерпретирани корелацијом реакционих константи помоћу LFER једначина. Резултати квантно-механичких рачунања молекулске структуре заједно са експерименталним резултатима омогућили су боље разумевање утицаја структуре на пренос електронских ефеката супституената. Израчунате су нове σ константе за супституисане бензилиденамино групе.

(Примљено 26. априла 2007)

REFERENCES

1. J. E. Robertson, H. J. Biel, T. F. Mitchell, *J. Med. Chem.* **6** (1963) 805
2. P. K. Kadaba, *J. Heterocyclic Chem*. **1** (1975) 143
3. P. K. Kadaba, *J. Med. Chem*. **31** (1988) 196
4. S. Huneck, K. Schreiber, H. D.Grimmecke, *J. Plant Growth Reg.* **3** (1984) 75
5. R. Akaba, K. Tokumaru, T. Kobayashi, *Bull. Chem. Soc. Jpn*. **53** (1980) 1993
6. P. Skrabal, J. Steiger, H. Zollinger, *Helv. Chim. Acta*. **58** (1975) 800
7. V. I. Minkin, Yu. A. Zhdanov, E. A. Medyantseva, Yu. A. Ostroumov, *Tetrahedron* **23** (1967) 3651
8. B. Ž. Jovanović, M. Mišić–Vuković, A. D.Marinković, V. Vajs, *J. Mol. Struct*. **482-483** (1999) 375
9. B. Ž. Jovanović, M. Mišić–Vuković, A. D. Marinković, V. Vajs, *J. Mol. Struct.* **642** (2002) 113
10. B. Ž. Jovanović, A. D. Marinković, F. H. Assaleh, J. Csanádi, *J. Mol. Struct*. **744-747** (2005) 411
11. L. I. Smith, K. L. Howard, *Org. Synth. Coll.* **3** (1955) 351
12. J. D. Roberts, E.A. McElhill, R. Armstrong, *J. Am. Chem. Soc*. **71** (1949) 2923
13. J. J. P. Stewart, *J. Comp. Aided Molec. Des*. **4** (1990) 1
14. J. J. P. Stewart, QCPE # 455
15. T. Matsuoka, K. Harano, *Tetrahedron* **51** (1995) 6451
16. Serena Software Box, Bloomington, IN, 45402–3076
17. J. J. Gajevski, K. E. Gilbert, J. McKelvey, *Adv. Mol. Model*. **2** (1990) 65

18. J. J. P. Stewart, *J. Comp. Chem.* **10** (1989) 209
19. J. J. P. Stewart, *J. Comp. Chem.* **10** (1989) 221
20. C. J. Cramer, D. G. Truhlar, *Chem. Rev*. **99** (1999) 2161
21. R. A. More O'Ferrall, W. K. Kwok, S. I. Miller, *J. Am. Chem*. *Soc*. **86** (1964) 5553
22. K. Bowden, N. B. Chapman, J. Shorter, *Can. J. Chem*. **42** (1964) 1979
23. K. Bowden, A. Buckley, N. B. Chapman, J. Shorter, *J. Chem. Soc*. (1964) 3370
24. A. Buckley, N. B. Chapman, N. R. J. Dack, J. Shorter, H. M. Wall, *J. Chem. Soc. B* **6** (1968) 631
25. R. A. Y. Jones, *Physical and Mechanistic Organic Chemistry*, Cambridge University Press, London, 1979, pp. 55, 56
26. O. Exner, J. Lakomy, *Coll. Czech. Chem. Commun.* **25** (1970) 1371.

Journal of the Serbian Chemical Society
JSCS@tmf.bg.ac.yu • www.shd.org.yu/JSCS

J. Serb. Chem. Soc. 72 (12) 1201–1216 (2007) UDC 546–32+547.53.024:541.121+544.35:543.4/.5
JSCS–3653 *Original scientific paper*

An LFER study of the protolytic equilibria of 4-aryl-2,4-dioxobutanoic acids in aqueous solutions

TATJANA Ž. VERBIĆ[1], BRANKO J. DRAKULIĆ[2*#], MIRE F. ZLOH[3], JOVANA R. PECELJ[1], GORDANA V. POPOVIĆ[4#] and IVAN O. JURANIĆ[1#]

[1]Faculty of Chemistry, University of Belgrade, Studentski Trg 12–16, 11000 Belgrade, [2]Department of Chemistry – Institute of Chemistry, Technology and Metallurgy, University of Belgrade, Njegoševa 12, 11000 Belgrade, Serbia, [3]The School of Pharmacy, University of London, 29/39 Brunswick Square, London WC1N 1AX, United Kingdom and [4]Faculty of Pharmacy, University of Belgrade, Vojvode Stepe 450, 11000 Belgrade, Serbia

(Received 29 May 2007)

Abstract: The protolytic equilibria of 13 4-aryl-2,4-dioxobutanoic acids (ADKs) were spectrophotometrically studied in aqueous solutions in the pH range 1–9 at 25±1 °C and an ionic strength of 0.1 mol l^{-1} (NaCl), with the exception of the 4-OH-derivative which was also potentiometrically studied in the pH range 7–10 at 25±1 °C and an ionic strength of 0.1 mol l^{-1} (NaCl). In solution, the compounds simultaneously exist in one diketo and two enolic forms; therefore, the determined acidity constants (pK_{a1} 1.87–2.29, pK_{a2} 6.63–8.13 and pK_{a3}(4-OH-) 9.52) represent system macro constants. The ^{1}H-NMR spectrum of the parent compound (4-phenyl--2,4-dioxobutanoic acid) (25 °C, pD 5.0) proved the existence of all tautomeric forms. Using the extended Hammett relation, the determined pK_a values were correlated with literature σ values. The predicted pK_a values were in fair accordance with the experimentally observed ones. Molecular, monoanionic and dianionic forms of the parent compound were optimized by the semi-empirical molecular orbital PM6 method using the implicit water solvation model (COSMO). The obtained geometries were used to explain the quality of the LFER models.

Keywords: acidity constants, 4-aryl-2,4-dioxobutanoic acids (ADK), linear free energy relationship (LFER).

INTRODUCTION

4-Aryl-2,4-dioxobutanoic acid (Ar-C(O)-CH_2-C(O)-COOH) (ADK) derivatives exert widespread biological activities.[1] The targeting of HIV-1 integrase (IN), the enzyme responsible for the integration of viral DNA in the host genome, is among the most important ones.[2–4] Appropriate structural modifications on the phenyl ring were used to assess the different types of biological activity

* Corresponding author. E-mail: bdrakuli@chem.bg.ac.yu
# Serbian Chemical Society member.
doi: 10.2298/JSC0712201V

(manuscript in preparation). Part of current studies on the physicochemical profiling of these compounds is presented in this manuscript, which describes the protolytic equilibria of 13 alkyl-, alkoxy-, hydroxy-, nitro- and halo-phenyl substituted derivatives (limited set) in aqueous solutions in the pH range 1–10 (Table I). The reported compounds (**1**–**13**) are inactive or exert low activity and are intended to be used to develop a model for a larger set incorporating active congeners. Acidity constants of the studied compounds in aqueous solutions have hitherto not been reported. The only reported pK_a values (pK_{a1} 3.68–4.14 and pK_{a2} 9.52–11.13, substances **1**–**3**, **7**–**10** and **13** (Table I)) were potentiometrically determined in an ethanol–water (3:1, v/v) mixture.[5] As reported by others,[6–8] these compounds simultaneously exist in two enolic forms (conformationally locked by the pseudo-ring) and one diketo form, having two rotatable bonds responsible for the conformational flexibility (Scheme 1).

TABLE I. Concentration equilibrium constants ($\overline{pK_a}\pm\sigma$) in aqueous solution of ADKs with the wavelengths used for the spectrophotometric determinations (I = 0.1 mol l^{-1} (NaCl); t = 25±1 °C)

Comp.	R–	pK_{a1}	λ / nm	pK_{a2}	λ / nm	pK_{a3}
1	H–	2.06±0.03	314.0	7.56±0.02	328.5	–
2	4-Me–	2.22±0.05	319.0	7.99±0.02	329.3	–
3	4-Et–	2.28±0.02	319.9	7.83±0.05	326.8	–
4	4-*i*-Pr–	2.29±0.05	319.9	7.85±0.02	329.3	–
5	4-*tert*-Bu–	2.21±0.03	321.6	7.77±0.06	331.9	–
6	3,4-di-Me–	2.09±0.04	321.6	7.92±0.04	326.8	–
7	4-F–	2.06±0.05	314.8	7.50±0.03	325.9	–
8	4-Cl–	2.09±0.04	316.5	7.30±0.03	334.4	–
9	4-Br–	2.06±0.03	318.2	7.53±0.03	333.6	–
10	4-NO_2–	1.87±0.06	328.5	6.63±0.02	324.2	–
11	3-OH–	2.18±0.04	314.0	7.45±0.04	332.7	–
12	4-OH–	2.29±0.05	331.9	7.73±0.01[a]	–	9.54±0.07[a]
13	4-MeO–	2.28±0.03	316.5	8.13±0.03	326.8	–

[a]Potentiometrically determined values

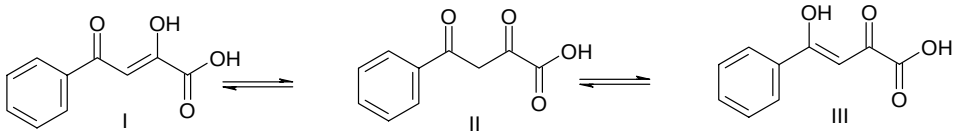

Scheme 1. The diketo (II) and two enolic (I and III) forms of 4-phenyl-2,4-dioxobutanoic acid (**1**).

Aim of this work was to study the protolytic equilibria of a set of 13 ADKs. The determined acidity constants within the studied set are useful to develop a model in which more active and significantly less soluble congeners will be incorporated.

EXPERIMENTAL

Apparatus and reagents

All used chemicals were of analytical reagent grade, purchased from Aldrich, Fluka, or Merck, and were used without further purification. The deuterated compounds had, at least, 99.5 % deuterium.

Melting points were determined in open capillary tubes on a Büchi apparatus and are uncorrected. The infrared spectra (IR) were recorded on an FT Perkin-Elmer 1725X spectrometer, (KBr disc). The ^{1}H- and ^{13}C-NMR spectra were recorded in DMSO-d_6 on a Varian Gemini 200 spectrometer at 200/50 MHz. Tetramethylsilane (TMS) was used as the internal standard for the ^{1}H-NMR spectra. The residual solventsignal of DMSO-d_6 was used as the internal standard at 39.70 ppm for ^{13}C-NMR calibration. The mass spectra (ESI-MS) were recorded on a ThermoQuest Navigator.

The ^{1}H- and ^{13}C-NMR spectra of compound **1** were recorded in deuterated acetate buffer (c^{tot} = = 0.1 mol l^{-1}, pD 5.0 (pD = $pH_{measured}$ + 0.4)[9,10]) on Bruker Avance spectrometer at 500/125 MHz. The ^{1}H-NMR spectrum was referenced to the HOD peak at 4.70 ppm as the internal standard; the TSP (3-(trimethylsilyl)-1-propanesulfonic acid-d_6 sodium salt) was not added to avoid interactions between the salt and the sample. The pH measurements in deuterated solutions were performed using a Corning pH-meter 120 with a Corning Ag/AgCl microelectrode (KCl solution). For determination of acidity constants, a GBC Cintra 6 spectrophotometer with 1 cm silica cells and a PHM240 pH-meter (Radiometer) with a combined GK2401B electrode (Radiometer) were used. The titrations were performed with a TTT-60 titrator with an ABU-12 autoburette (Radiometer).

*Synthesis of compounds **1**–**13***

Examined compounds (**1**–**13**) were synthesized using a previously described procedure.[11] Compounds were obtained by addition of equimolar amounts of aryl ketones and diethyl oxalate (0.05 mol*) to a twofold molar quantity of sodium methoxide (Scheme 2), obtained by dissolution of sodium in dry methanol (2.3 g (0.1 mol) Na in 40 ml), mixed overnight and poured into ice-cold water.

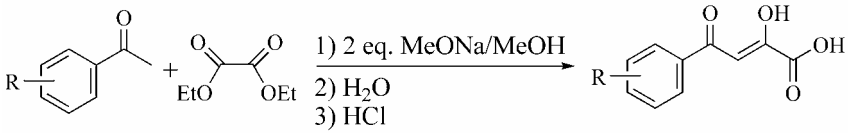

Scheme 2. Synthesis of the examined compounds, R– = **1**) H–; **2**) 4-Me–; **3**) 4-Et–; **4**) 4-*i*-Pr–; **5**) 4-*tert*-Bu–; **6**) 3,4-di-Me–; **7**) 4-F–; **8**) 4-Cl–; **9**) 4-Br–; **10**) 4-NO_2–; **11**) 3-OH–; **12**) 4-OH–; **13**) 4-MeO–.

After 3–4 hours of vigorous stirring at room temperature, the reaction mixture was filtered into water that had been acidified with conc. hydrochloric acid to pH 2–3. The obtained precipitate was collected by filtration and washed with ice-cold water. The filtrates were concentrated under reduced pressure to remove MeOH. Additional amounts of the compounds were harvested from the in this way obtained solutions. The crude products were crystallized from an appropriate solvent. Characterization of synthesized compounds **1**–**13** was performed by melting points, IR, ^{1}H- and ^{13}C- NMR spectroscopy, and ESI-MS (Electrospray Ionization Mass Spectrometry).

*Characterization of compounds **1**–**13***

The NMR integrals belonging to the diketo tautomers are not reported for the ^{1}H-NMR spectra. In the "aromatic" region, the overlaps of low intensity peaks of the diketo form with significantly stronger ones from the enol form were observed. The overlap of the enol aromatic peaks (mainly) was also observed. Thus, for some signals, full multiplicities are not reported and, as a conse-

* Compounds **5** and **7** were prepared starting with 0.025 mol of substituted acetophenones and equivalents of other reagents.

quence, some peak integrals (overlapped) have fractional values. The ESI-MS spectra were recorded in the negative mode.

*4-Phenyl-2,4-dioxobutanoic acid (**1**)*: m.p. 143–144 °C*, decomposition; pale yellow powder (7.90 g, 80 %, AcOEt/PhH); $C_{10}H_8O_4$; M_w 192.17; MS: M^+ 191 (100 %); 119 (60 %). IR ν (cm^{-1}): 1720; 1625; 1276; 1244. ^{1}H-NMR (200 MHz, 29 °C, DMSO-d_6) δ 10.91 (*b*); 8.08 (*d*, *J* = = 7.02 Hz, 2H); 7.95 (*d*, *J* = 9.54 Hz); distinct maxima 7.76, 7.72, 7.69 (triplet-like overlapped peaks, $J_{1,2}$ = = 7.20 Hz, $J_{2,3}$ = 7.30 Hz, "1.04 H"); distinct maxima 7.63, 7.59, 7.56 (triplet-like overlapped peaks, $J_{1,2}$ = 7.58 Hz, $J_{2,3}$ = 7.02 Hz, "2.19 H"); 7.48 (*d*, *J* = 7.30 Hz); 7.15 (*s*, 1H); 4.65 (*s*). ^{13}C-NMR (50 MHz, 29 °C, DMSO-d_6) δ 195.71; 192.04; 190.85; 170.70; 163.58; 161.89; 134.99; 134.22; 129.44; 129.26; 128.85; 128.21; 98.22; 49.46.

*4-(4-Methylphenyl)-2,4-dioxobutanoic acid (**2**)*: m.p. 141–142 °C, light yellow crystals (6.30 g, 61 %, AcOEt/PhMe); $C_{11}H_{10}O_4$; M_w 206.19; M^+ 205 (100 %) 133 (62 %). IR ν (cm^{-1}): 3520; 1603; 1290; 1248; 1142; 700. ^{1}H-NMR (200 MHz, 29 °C, DMSO-d_6) 7.96 (*d*, *J* = 8.08 Hz, 2H); 7.91 (*d*, *J* = 8.11 Hz); 7.38 (*d*, *J* = 8.07 Hz, 2H); 4.57 (*s*); 2.56 (*s*); 2.41 (*s*, 3H). ^{13}C-NMR (50 MHz, 29 °C, DMSO-d_6) δ 190.61; 170.00, 163.42; 145.03; 132.21; 129. 94; 128.21; 97.87; 21.40.

*4-(4-Ethylphenyl)-2,4-dioxobutanoic acid (**3**)*: m.p. 101–102 °C, light yellow crystals (7.30 g, 66 %, AcOEt/PhMe); $C_{12}H_{12}O_4$; M_w 220.22; M^+ 219 (100 %) 147 (82 %) IR ν (cm^{-1}): 3523; 1700; 1607; 1290; 1247. ^{1}H-NMR (200 MHz, 29 °C, DMSO-d_6) δ 7.84 (*b*, overlapped with aromatic signals); 7.96 (*d*, *J* = 8.42 Hz, 2H); 7.89 (*d*, *J* = 8.70 Hz); 7.40 (*d*, *J* = 8.14 Hz, 2H); 7.25 (*d*, *J* = 8.70 Hz); 7.11(*s*, 1H); 4.58 (*s*); 2.70 (*q*, $J_{1,3}$ = 15.16 Hz, $J_{1,2}$ = 7.58 Hz, 2H); 1.22 (*t*, *J* = = 7.58 Hz, 3H). ^{13}C-NMR (50 MHz, 29 °C, DMSO-d_6) δ 190.91; 170.22; 163.65; 151.15; 162.63; 129.08; 128.86; 128.62; 128.44; 98.05; 28.63; 15.28.

*4-(4-*i*-Propylphenyl)-2,4-dioxobutanoic acid (**4**)*: m.p. 96–97 °C, light yellow crystals (4.1 g, 35 %**, PhMe); $C_{13}H_{14}O_4$; M_w 234.25; M^+ 233 (100 %) 161 (71 %); IR ν (cm^{-1}): 3503; 1702; 1606; 1293; 1249. ^{1}H-NMR (200 MHz, 29 °C, DMSO-d_6) δ 8.77 (*b*); 8.01 (*d*, 2H, *J* = 8.43 Hz); 7.93 (*d*, *J* = 8.14 Hz); 7.61 (*d*, *J* = 7.30 Hz); 7.44 (*d*, 2H, *J* = 8.42 Hz); 2.99 (*sp*, $J_{1,2}$ = 6.92 Hz, $J_{1,3}$ = = 13.84 Hz, $J_{1,4}$ = 20.44 Hz, 1H); 1.23 (*d*, *J* = 6.73 Hz, 6H). ^{13}C-NMR (50 MHz, 29 °C, DMSO-d_6) δ 190.66; 170.29; 163.55; 155.50; 132.71; 129.03; 128.43; 127.37; 127.10; 97.97; 33.84; 23.66.

*4-(4-*tert*-Butylphenyl)-2,4-dioxobutanoic acid (**5**)*: m.p. 124–125 °C, pale yellow powder (4.60 g, 75 %, PhMe); $C_{14}H_{16}O_4$; M_w 248;27; M^+ 247 (100 %); 175 (46 %); IR ν (cm^{-1}): 3537.0; 1706.0; 1610.0; 1297.0; 1249.0. ^{1}H-NMR (200 MHz, 29 °C, DMSO-d_6) δ 8.01 (*d*, *J* = 8.71 Hz, 2H); 7.92 (*d*, *J* = 8.42 Hz); 7.60 (*d*, *J* = 8.43 Hz, 2H); 7.09 (*s*, 1H); 4.55 (*s*); 1.32 (*s*, 9H). ^{13}C-NMR (50 MHz, 29 °C, DMSO-d_6) δ 190.64; 170.27; 163.53; 157.71; 132.29; 128.75; 128.17; 128.28; 97.98; 35.22; 30.98.

*4-(3,4-Dimethylphenyl)-2,4-dioxobutanoic acid (**6**)*: m.p. 175–177 °C, decomposition; white powder (6.30 g, 57 %, PhMe); M_w 220.22, $C_{12}H_{12}O_4$; M^+ 219 (100 %); 147 (64.3 %); IR ν (cm^{-1}): 1705; 1612; 1261. ^{1}H-NMR (200 MHz, 29 °C, DMSO-d_6) δ 7.77 (*s*, 1H); 7.71 (*d*, *J* = 7.86 Hz, 1H); 7.28 (*d*, *J* = 7.86 Hz, 1H); 6.64 (*b*); 4.40 (*b*). ^{13}C-NMR (50 MHz, 29 °C, DMSO-d_6) δ 164.42; 142.81; 137.34; 133.28; 130.30; 128.70; 97.93; 19.84; 19.55.

*4-(4-Fluorophenyl)-2,4-dioxobutanoic acid (**7**)*: m.p. 145–147 °C, decomposition; white needles (crystalline) (3.60 g, 69 %, AcOEt/PhMe); M_w 210.16, $C_{10}H_7FO_4$; M^+ 209 (100 %), 137 (33.1 %); IR ν (cm^{-1}): 3522; 1631; 1601; 1240. ^{1}H-NMR (200 MHz, 29 °C, DMSO-d_6) δ 8.17 (*dd*, *J* = 8.71 Hz, 2H); 7.41 (*t*, *J* = 8.70 Hz, 2H); 7.11 (*s*, 1H); 4.58 (*s*). ^{13}C-NMR (50 MHz, 29 °C, DMSO-d_6) δ 189.93; 169.69; 168.38; 163.44; 131.72; 131.41; 131.21; 116.74; 116.30; 98.20; 49.33.

---

* At 143–144 °C the compound turns to a dark red color. This product melts at 155–156 °C. In the literature the latter temperature is reported as the melting point (Ref. 11 from the main text and *Tetrahedron* **60** (2004) 6479).

** Hydrolysis of the Et-ester described in main text is insufficiently efficient for compound **4**.

*4-(4-Chlorophenyl)-2,4-dioxobutanoic acid (**8**)*: m.p. 164–165 °C, decomposition; white crystals (8.30 g, 73 %, AcOEt/PhMe); M_w 226.61, $C_{10}H_7ClO_4$; M^+ 225 (100 %), 153 (51.7 %); IR ν (cm^{-1}): 3504; 1630; 1591; 1323; 1286; 1241; 1142. ^{1}H-NMR (200 MHz, 29 °C, DMSO-d_6) δ 8.08 (*d*, *J* = 8.70 Hz, 2H); 8.01 (*d*, *J* = 8.70 Hz); 7.63 (*d*, *J* = 8.69 Hz, 2H); 7.57 (*d*, *J* = = 8.90 Hz); 7.10 (*s*, 1H); 4.59 (*s*). ^{13}C-NMR (50 MHz, 29 °C, DMSO-d_6) δ 189.50; 170.44; 163.61; 163.63; 139.22; 133.68; 131.43; 130.66; 130.02; 129.50; 129.50; 129.28; 129.00; 98.20; 49.37.

*4-(4-Bromophenyl)-2,4-dioxobutanoic acid (**9**)*: m.p. 163–164 °C, decomposition; white powder (3.95 g, 58 %, PhMe); M_w 271.06, $C_{10}H_7BrO_4$; M^+ 271 (100 %), 269 (82 %), 199 (8.8 %), 197 (8.7 %); IR ν (cm^{-1}): 3534; 1622; 1588; 1291; 1241. ^{1}H-NMR (200 MHz, 29 °C, DMSO-d_6) δ 7.94 (*d*, *J* = 8.70 Hz, 2H); 7.72 (*d*, *J* = 8.70 Hz, 2H); 7.01 (*s*); 4.53 (*s*). ^{13}C-NMR (50 MHz, 29 °C, DMSO-d_6) δ 189.13; 171.05; 163.44; 134.11; 132.43; 130.07; 128.34; 98.18.

*4-(4-Nitrophenyl)-2,4-dioxobutanoic acid (**10**)*: m.p. 158–160 °C, light orange-red powder (9.50 g, 80 %, AcOH/PhMe); $C_{10}H_7NO_6$; M_w 237.17; M^+ 236 (100 %) 164 (60 %); IR ν (cm^{-1}): 3492; 1707; 1603; 1528; 1349; 1288; 1239. ^{1}H-NMR (200 MHz, 29 °C, DMSO-d_6) δ 8.40–8.12 (*m*, "5.7 H"), within distinct strong doublet 8.32 (*J* = 6.70 Hz). Other observable peaks at: 8.38, 8.37, 8.35, 8.27, 8.26, 8.21, 8.20, 8.19, 8.18, 8.15; 7.125 (*s*, 1H); 4.67 (*s*). ^{13}C-NMR (50 MHz, 29 °C, DMSO-d_6) δ 186.86; 172.31; 166.17; 163.26; 152.00; 150.37; 140.10; 130.99; 130.19; 129.48; 124.31; 124.021; 98.88.

*4-(3-Hydroxyphenyl)-2,4-dioxobutanoic acid (**11**)*: m.p. 175 °C, light dull-orange powder (5.60 g, 54 %, AcOEt); $C_{10}H_8O_5$; M_w 208.17; M^+ 207 (100 %) 135 (24.6 %); IR ν (cm^{-1}): 3390; 1628; 1580; 1283; 1199. ^{1}H-NMR (200 MHz, 29 °C, DMSO-d_6) δ 8.97 (*b*); 7.47 (*d*, *J* = 7.65 Hz, 1H); 7.39 (*s*, *b*, "1.38 H"); 7.33 (doublet-like, *J* = 7.88 Hz, "0.9 H"); 7.07 (*d* (peak broadening), *J* = = 8.11 Hz, 1H); 6.99 (*s*, 1H); 4.48 (*s*). ^{13}C-NMR (50 MHz, 29 °C, DMSO-d_6) δ 195.93; 191.98; 190.81; 170.27; 163.53; 158.25; 137. 54; 136.32; 130.59; 130.33; 121.56; 119.88; 119.14; 114.71; 114.15; 98.22; 49.46.

*4-(4-Hydroxyphenyl)-2,4-dioxobutanoic acid (**12**)*: m.p. 202–204 °C, dark yellow-orange powder (4.6 g, 44 %, water); $C_{10}H_8O_5$; M_w 208.17; M^+ 207 (100 %), 135 (10.4 %); IR ν (cm^{-1}): 3233; 1723; 1604; 1270; 1226. ^{1}H-NMR (200 MHz, 29 °C, DMSO-d_6) δ 14.10 (*b*, 1H); 10.74 (*b*, 1H); 7.99 (*d*, *J* = 8.71 Hz, 2H); 7.86 (*d*, *J* = 8.71 Hz); 7.05 (*s*, 1H); 6.93 (*d*, *J* = 8.71 Hz, 2H) broadening in peak basis; 4.47 (*s*). ^{13}C-NMR (50 MHz, 29 °C, DMSO-d_6) δ 190.79; 168.34; 163.70; 163.62; 131.085; 126.06; 116.19; 97.75.

*4-(4-Methoxyphenyl)-2,4-dioxobutanoic acid (**13**)*: m.p. 158–159 °C, decomposition; yellow powder (7.80 g, 70 %, AcOEt/PhH); M_w 222.19, $C_{11}H_{10}O_5$; M^+ 221 (100 %), 149 (70.9 %); IR ν (cm^{-1}): 3468; 1688; 1602; 1295; 1261; 1180. ^{1}H-NMR (200 MHz, 29 °C, DMSO-d_6) δ 8.06 (*d*, *J* = = 8.70 Hz, 2H); 7.11 and 7.07 doublet overlapped with singlet, "3.3 H"; 4.54 (*s*); 3.89 (*s*, 3H). ^{13}C-NMR (50 MHz, 29 °C, DMSO-d_6) δ 190.66; 168.94; 164.46; 163.73; 131.25; 130.76; 127.57; 114.79; 114.42; 97.91; 55.96; 49.15.

Determination of acidity constants

The acidity constants were spectrophotometrically determined (except for pK_{a2} and pK_{a3} of compound **12,** which were potentiometrically determined) at t = 25±1 °C and constant ionic strength 0.1 mol l^{-1} (NaCl). Stock solutions of compounds **1**–**13** were prepared in ethanol ($c = 1.0\times10^{-2}$ mol l^{-1}, except for **5** where $c = 0.5\times10^{-2}$ mol l^{-1} due to its lower solubility). Working solutions ($c = 1.0\times10^{-4}$ mol l^{-1} for all but **5**, $c_5 = 0.5\times10^{-4}$ mol l^{-1}) were prepared in deionized water (the ethanol concentration was up to 1 %, vol) in the pH ranges 1.1–3.5 for pK_{a1} and 5.9–9.1 for pK_{a2} determination. HCl solutions were used for pH 1.1–3.5, phosphate buffers for pH 5.9–8.0 (c^{tot} = 0.01 mol l^{-1}), carbonate buffers for pH 8.1–9.1 (c^{tot} = 0.01 mol l^{-1}). The UV–Vis spectra of compounds **1**–**13** in their monoanionic form (HA^-) were recorded in acetate buffer (c^{tot} = 0.01 mol l^{-1}, pH 5.5*). The

* For 4-NO_2– derivative (**10**) the acetate buffer pH 4.5 was used.

measured pH values were converted to pc_H according to the relation:[12] $pc_H = -\log [H_3O^+] = pH - A$, where A is the correction factor ($A = 0.08$) determined by potentiometric titration of a standard HCl solution with a standard NaOH solution at 25±1 °C and ionic strength 0.1 mol l^{-1} (NaCl). For solutions with pH < 2, the pc_H values were calculated according to the concentration of the standard HCl solution.

The spectra were recorded over the 220–500 nm range at a scanning speed of 500 nm min^{-1} against the corresponding blank. For pK_a determination, the absorbances were measured at the wavelength of the absorption maximum or at the wavelength of the maximal differences in absorbances. Three sets of experiments were performed.

For the potentiometric determination of pK_{a2} and pK_{a3} of the compound **12**, 20.00 ml aliquots of the stock solution of **12** ($c_{\mathbf{12}} = 9.9198\times10^{-4}$ mol l^{-1}) in 0.1 mol l^{-1} NaCl were titrated with 0.020 ml increments of the standard NaOH solution ($c = 0.1298$ mol l^{-1}) until the pH 10 was attained. The values of pK_{a2} and pK_{a3} were found according to the formation function $\bar{n}$ (the mean number of protons bound to the base (**12**)), with the data from three times repeated experiments. The formation function was calculated according to equation:[13]

$$\bar{n} = \frac{3c_{\mathbf{12}} - [H_3O] - [OH^-]}{c_{\mathbf{12}}} \quad (1)$$

where $c_{\mathbf{12}}$ is the concentration of **12**, $[H_3O^+]$ is calculated from pc_H, and $[OH^-]$ is the concentration of NaOH in the solution.

LFER calculations

Linear regressions were obtained using the BILIN program.[14] The coefficients following the terms in Eqs. (5–10) are twofold standard deviations. The statistical parameters are reported as follows: n – number of observations; r – correlation coefficient; F – Fischer test, Q^2 – leave one out cross-validation; s_{PRESS} – standard deviation of Q.

Geometry optimization

The reported conformations of the molecular, monoanionic and dianionic forms of **1** (Figs. 5a–5c, respectively) were obtained by the semi-empirical MO PM6 method[15a] with implicit water solvation (COSMO) (Keywords: EF, PM6, GNORM = 0.01, PRECISE, EPS = 78.4, RSOLV = 1.000, DISEX = 3.000, NSPA = 92) using the MOPAC 2007 package.[15b] The VegaZZ 2.1.0 was used as the graphical user interface (GUI).[16]

RESULTS AND DISCUSSION

The examined set (compounds **1**–**13**), comprised mainly of 4-substituted derivatives (**1**–**5**, **7**–**10**, **12**, **13**) and alkyl-, halo-, hydroxy-, alkoxy- and nitro-phenyl substituents, can be considered as sufficient for the derivation of a linear free energy relationship. Compounds **6** (3,4-di-Me-) and **11** (3-OH-) were included because the majority of the so far reported biologically active ADK derivatives have alkyl- or oxygen-containing substituents in position 3 of the phenyl ring. In this way, the model could be tested for further expansion. Using the extended Hammett correlation, the determined pK_a values were correlated with literature substitutent constants[17] (σ_p and σ_m; σ_R and σ_I; Table II).

ADKs in aqueous solution, in the studied pH range, act as diprotic acids, with the exception of compound **12**, which showed dissociation of carboxyl, α-hydroxyl, and 4-OH-phenyl groups. As mentioned before, ADKs in solution under-

go keto-enol tautomerization. The NMR spectra (Fig. 1), recorded in aqueous solution (pD 5.0), proved the existence of the diketo and both enolic forms, thus the acidity constants represent system macro constants.

TABLE II. Structures, experimentally determined pK_a values of the studied compounds (**1**–**13**) and the used substituent constants

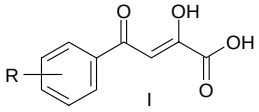

I

Comp.	R–	pK_{a1}	σ_p	σ_m	σ_R	σ_I
1	H–	2.06	0	0	0	0
2	4-Me–	2.22	–0.14	0	–0.10[5)]	–0.03[6)]
3	4-Et–	2.28	–0.32*[1)]	0	–0.10[5)]	–0.05[7)]
4	4-*i*-Pr–	2.29	–0.28*[2)]	0	–0.12[5)]	–0.06[7)]
5	4-*tert*-Bu–	2.21	–0.20	0	–0.13	–0.07[8)]
6	3,4-di-Me–	2.09	–0.14	–0.07	–	–
7	4-F–	2.06	0.21[3)]	0	–0.45[9)]	0.62
8	4-Cl–	2.09	0.23	0	–0.23	0.52
9	4-Br–	2.06	0.23	0	–0.25[10)]	0.50
10	4-NO_2–	1.87	0.78	0	0.27	0.64[11)]
11	3-OH–	2.18	0	0.02[4)]	–0.06	0.18
12	4-OH–	2.29	–0.37	0	–0.43[12)]	0.23[6)]
13	4-MeO–	2.28	–0.27	0	–0.61	0.27
Comp.	R–	pK_{a2}	σ_p	σ_m	σ_R	σ_I
1	H–	7.56	0	0	0	0
2	4-Me–	7.99	–0.14	0	–0.14	–0.04
3	4-Et–	7.83	–0.13[4)]	0	–0.10[5)]	–0.05[7)]
4	4-*i*-Pr–	7.85	–0.13[4)]	0	–0.12[5)]	–0.06[7)]
5	4-*tert*-Bu–	7.72	–0.15[4)]	0	–0.15[9)]	–0.07[8)]
6	3,4-di-Me–	7.92	–0.14	–0.06[4)]	–	–
7	4-F–	7.50	0.21[3)]	0	–0.45[9)]	0.62
8	4-Cl–	7.30	0.28[3)]	0	–0.23	0.52
9	4-Br–	7.53	0.15*[2)]	0	–0.30[#]	0.44
10	4-NO_2–	6.63	0.78	0	0.15	0.64[10)]
11	3-OH–	7.45	0	0.12	–0.06	0.18
12	4-OH–	7.73	–	–	–	–
13	4-MeO–	8.13	–0.27	0	–0.61	0.27

* σ_p^+ ; [#]σ_R^+ ; 1) *J. Org. Chem.* **23** (1958) 1215; 2) *J. Am. Chem. Soc.* **80** (1958) 4979; 3) *Summ. Sci Techn., Ser. Gen. Ques. Org. Chem.* p. 163 (1979); 4) *Chem. Scripta* **9** (1976) 200; 5) *J. Am. Chem. Soc.* **90** (1968) 1757; 6) *Can. J. Chem.* **46** (1968) 2929; 7) *J. Am. Chem. Soc.* **100** (1978) 7765; 8) *J. Org. Chem.* **29** (1964) 1222; 9) *Can. J. Chem.* **61** (1983) 2376; 10) *Prog. Phys. Org. Chem.* **13** (1981) 119; 11) *Prog. Phys. Org. Chem.* **10** (1973) 81; 12) J. Am. Chem. Soc. **85** (1963) 3146; The other σ_p and σ_m values are taken from *J. Org. Chem.* **23** (1958) 420; The other σ_R and σ_I values are taken from *J. Am. Chem. Soc.* **94** (1972) 9113

As the differences in the acidities of the carboxyl and α-hydroxyl groups are sufficiently high (Table I), the pK_{a1} and pK_{a2} of the diprotic acids could be separately determined. The values of pK_{a2} and pK_{a3} of compound **12** are too close to

be determined spectrophotometrically, thus they were potentiometrically determined. Briefly, as this will be reported separately, the 4-OH-phenyl group dissociates at a lower pH than the α-hydroxyl group. The formed phenolate ion is tautomerically equilibrated *via* a quiynoid structure and transfers the negative charge to the former aroyl oxygen. The negative charge on the "aroyl" oxygen, in turn, stabilizes the α-hydroxyl oxygen; this results in the higher pK_a value of the α-hydroxyl.

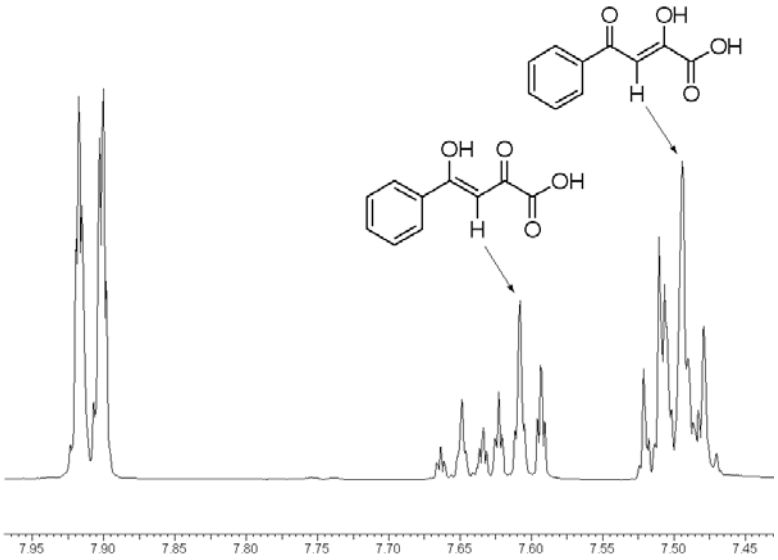

Fig. 1. 1D ^{1}H-NMR spectrum of compound **1** (region 7.4–8.0 ppm)* at pD 5.0 and t = 25 °C in D_2O.

For the spectrophotometric determination of the acidity constants, two transformed forms of the classical spectrophotometric equation[18] were applied:

$$A = A_{H_2A} - K_{a1}\frac{A - A_{HA^-}}{[H_3O^+]} \tag{2}$$

$$A = A_{A^{2-}} - \frac{1}{K_{a2}}[H_3O^+](A_{HA^-} - A) \tag{3}$$

where A_{H_2A}, A_{HA^-}, $A_{A^{2-}}$, and A represent the absorbances of the molecular (H_2A), monoanionic (HA^-) and dianionic (A^{2-}) forms of the ADKs and their mixture at specified wavelengths, respectively. Eqs. 2 and 3 gave linear dependences when the spectrum of only one "pure" form (HA^-) was required for the determination of K_{a1} and K_{a2}. The absorption spectra used for the determination of the acidity constants of compound **1**, as a representative, are shown in Fig. 2a and 2c. The values of K_{a1} and K_{a2} were calculated by linear regression analysis from the slope of the corresponding lines (Fig. 2b and 2d).

* As the singlet of $-CH_2-$ protons from the diketo form, present at 4.50 ppm, is signifycantly weaker, just the region with the signals from the two enolic forms is shown.

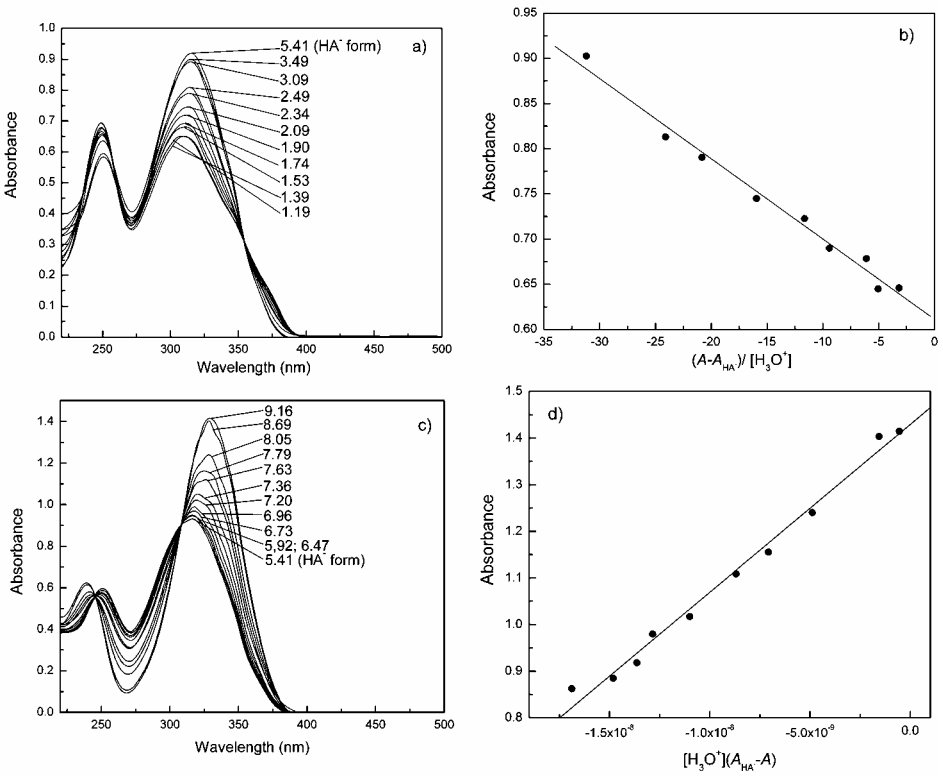

Fig. 2. a) Absorption spectra of compound **1**, used for the determination of K_{a1} in solutions of different acidity, the pH values are indicated on the figure; b) spectrophotometric determination of K_{a1} according to Eq. 2; $c_{\mathbf{1}} = 1.0176\times10^{-4}$ mol l^{-1}; $\lambda = 314.0$ nm; c) absorption spectra of compound **1** used for the determination of K_{a2} in solutions of different acidity, the pH values are indicated on the figure; d) spectrophotometric determination of K_{a2} according to Eq. 3; $c_{\mathbf{1}} = 1.0021\times10^{-4}$ mol l^{-1}; $\lambda = 328.5$ nm.

As mentioned previously, K_{a2} and K_{a3} for the 4-OH-derivative (**12**) were determined potentiometrically according to the formation function. In the pH interval where the H_2A^-, HA^{2-} and A^{3-} forms are present, the formation function gave the following linear dependence:[13]

$$\frac{[H_3O^+]^2(2-\bar{n})}{\bar{n}} = K_{a2}\frac{[H_3O^+](\bar{n}-1)}{\bar{n}} + K_{a2}K_{a3} \qquad (4)$$

K_{a2} (pK_{a2} 7.73±0.01) and K_{a3} (pK_{a3} 9.52±0.07) were determined from the slope and the intercept of the corresponding line from three times repeated experiments (Fig. 3).

Considering the obtained pK_a values (Table I), the distribution of the species at some physiologically important pH values can be calculated. As the pK_{a1} of all the studied compounds lies within the interval 1.87–2.29, at pH 1.5, 30 to 70 %

of the ADKs (depending on the specific pK_{a1} value) are present in the H_2A form (H_3A for compound **12**). The pK_{a2} values of compounds **1**–**11** and **13** lie within the 6.63–8.13 range, thus at pH 7.4, 15 to 85 % of these compounds (depending on the specific pK_{a2} value) is present in the HA^- form, and at pH 9, most of ADKs **1**–**11** and **13** are completely deprotonated (A^{2-} form). The situation for compound **12** is slightly more complicated with H_2A^- and HA^{2-} being the dominant species in the pH range 6.7–8.6 and HA^{2-} and A^{3-} in the pH range 8.6–10.5. Representative distribution diagrams for compounds **1** and **12** are shown in Figs. 4a and 4b, respectively.

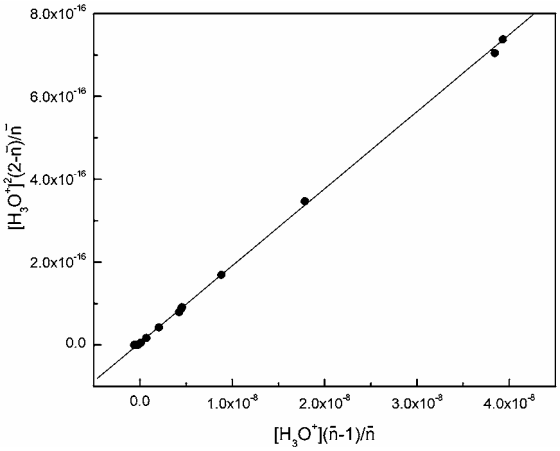

Fig. 3. Potentiometric determination of K_{a2} and K_{a3} for compound **12** according to Eq. (4), $c_{\mathbf{12}} = 9.9198\times10^{-4}$ mol l^{-1}.

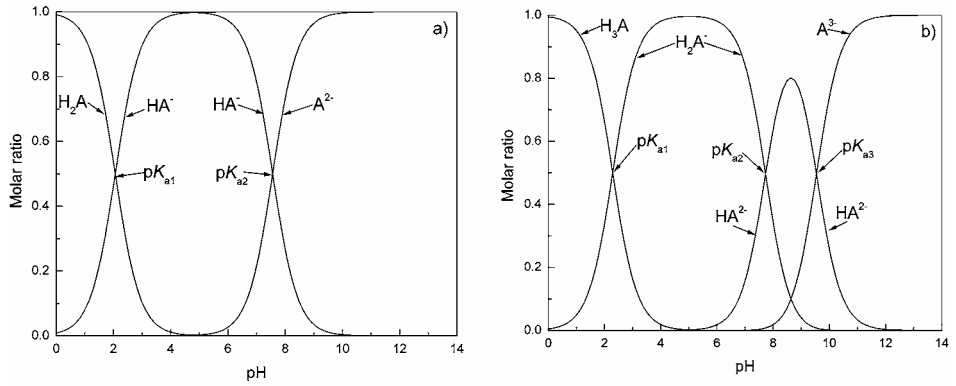

Fig. 4. Distribution diagrams: a) compound **1** and b) compound **12**.

LFER

The determined acidity constants (pK_{a1} and pK_{a2}) were correlated with literature substituent constants in order to build a linear model of the Hammett type. Correlation of the determined pK_{a1}values with the σ_p and σ_m substituent constants has moderate statistics:

$$pK_{a1} = -0.382\ (\pm 0.070)\ \sigma_p + 1.622\ (\pm 1.080)\ \sigma_m + 2.151\ (\pm 0.022) \quad (5)$$

(n = 13; r = 0.969; s = 0.034; F = 76.069; Q^2 = 0.916; s_{PRESS} = 0.040)

The constant term in Eq. (5) is far for the experimentally obtained pK_{a1} of the unsubstituted compound **1**. Exclusion of the parent compound (**1**) results in a statistically better correlation.

$$pK_{a1} = -0.381\ (\pm 0.037)\ \sigma_p + 1.694\ (\pm 0.570)\ \sigma_m + 2.159\ (\pm 0.012) \quad (6)$$

(n = 12; r = 0.992; s = 0.018; F = 280.480; Q^2 = 0.960; s_{PRESS} = 0.029)

Factorization of the influences of the substituent on resonance and inductive ones does not allow the inclusion of the disubstituted derivative (**6**):

$$pK_{a1} = -0.380\ (\pm 0.180)\ \sigma_R - 0.392\ (\pm 0.140)\ \sigma_I + 2.174\ (\pm 0.055) \quad (7)$$

(n = 12; r = 0.925; s = 0.055; F = 26.574; Q^2 = 0.771; s_{PRESS} = 0.069)

Again, exclusion of the parent compound (**1**) results in a statistically better correlation:

$$pK_{a1} = -0.333\ (\pm 0.130)\ \sigma_R - 0.423\ (\pm 0.980)\ \sigma_I + 2.202\ (\pm 0.043) \quad (8)$$

(n = 11; r = 0.968; s = 0.037; F = 59.605; Q^2 = 0.891; s_{PRESS} = 0.049)

Even the terms in Eqs. (7) and (8) are not standardized; the inductive term has a somewhat higher weight. In the pH range 1–5, the diketo form is present in a significantly lower amount compared to the enolic form I in the existing tautomeric mixture (Scheme 1) (this is clearly seen in the NMR spectra, exemplified by the ^{1}H-NMR spectrum of the parent compound (**1**) at pD = 5.0, Fig. 1). Therefore, resonance transmission of the substituent effects to the carboxylic group could be expected to be dominant. However, the optimized structures of the enolate molecular and monoanionic forms with the implicit water solvation model (COSMO) clearly show that the carboxyl group of the molecular form and the carboxylate anion of the monoanionic form of the compounds is torsionally distorted from the rest of the molecule, as exemplified on the parent compound (**1**) (Figs. 5a and 5b). Accordingly, the higher weight of the inductive effect reproduces the real situation in water, which was used as the medium in the present study of protolytic equilibria.

Correlation of the determined pK_{a2} values with the σ_p and σ_m substituent constants has much better statistics than the corresponding equation describing pK_{a1} (Eq. (5)):

$$pK_{a2} = -1.319\ (\pm 0.220)\ \sigma_p - 1.706\ (\pm 1.600)\ \sigma_m + 7.677\ (\pm 0.062) \quad (9)$$

(n = 12; r = 0.977; s = 0.094; F = 93.574; Q^2 = 0.927; s_{PRESS} = 0.118)

The 4-OH-substituted derivative could not be included in Eqs. (9) and (10); the explanation is offered above. Exclusion of the 4-*tert*-Bu- derivative (**5**) gives a superior correlation (r = 0.985, F = 128.15, Q^2 = 0.931). For this, no explana-

tion can be offered. Factorization of the influences of the substituent on resonance and inductive ones, with exclusion of the disubstituted derivative (**6**), gave a good correlation:

$$pK_{a2} = -1.416\ (\pm 0.290)\ \sigma_R - 1.168\ (\pm 0.220)\ \sigma_I + 7.591\ (\pm 0.086) \qquad (10)$$

(n = 11; r = 0.983; s = 0.083; F = 114.494; Q^2 = 0.949; s_{PRESS} = 0.102)

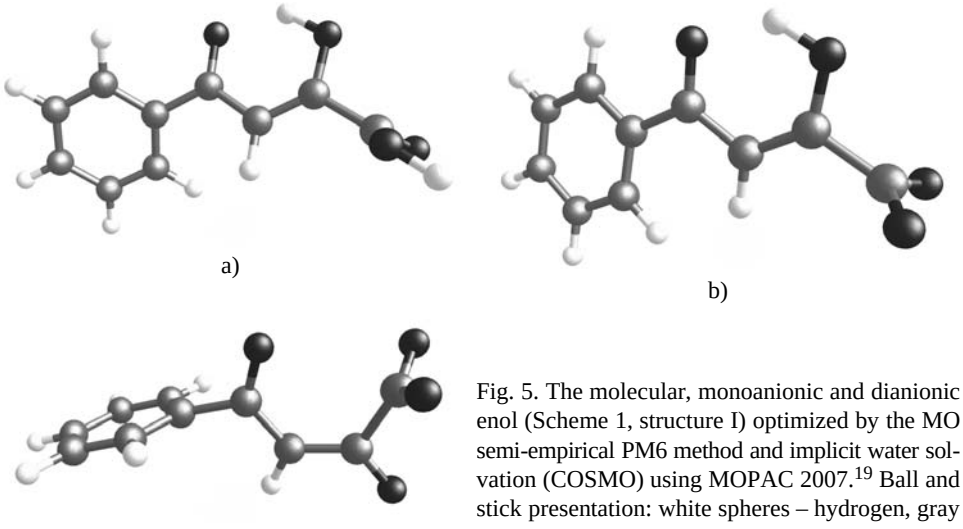

Fig. 5. The molecular, monoanionic and dianionic enol (Scheme 1, structure I) optimized by the MO semi-empirical PM6 method and implicit water solvation (COSMO) using MOPAC 2007.[19] Ball and stick presentation: white spheres – hydrogen, gray spheres – carbon and dark gray spheres – oxygen.

Additional exclusion of the 4-*tert*-Bu- derivative (**5**) gave the best of the in this article reported correlations (r = 0.993, F = 264.285, Q^2 = 0.977).

At this stage, obvious question arises: Why the Hammett correlations of pK_{a2} (Eqs. (9) and (10)) are statistically significantly better than corresponding ones correlating pK_{a1}? The optimized structures[19] of the molecular, monoanionic and dianionic forms of the compounds (exemplified by the parent compound (**1**), Figs. 5a–5c) offer the probable explanation. The molecular form of enol I (Scheme 1) has an almost perfect coplanar > C(O)–CH=C(OH)– (keto-enol) moiety, stabilized by an intramolecular H-bond. In the parent compound, the > C=O···H–O– distance is 1.71 Å, with a H-bond energy of –0.2997 kcal mol^{-1}. The aryl group is twisted from the plain of the keto-enol moiety by 37.61°, while the carboxyl group is twisted by 101.70°. In the monoanionic form, a similar distortion of the carboxylic group exists (91.25° for the parent compound (**1**)), *i.e.*, the carboxylic group is almost perpendicular to the plane of the keto-enol moiety. Transmission of the resonance effect is efficiently suppressed in this manner. Accordingly, the inferior statistics of Eqs. (5)–(8) in respect to Eqs. (9) and (10) could be reasonably explained. On the other hand, in the monoanionic form, the aryl group is twisted in respect to the keto-enol moiety by a minor amount (7.83° for the pa-

rent compound (**1**)), *i.e.*, the aryl ring is almost coplanar with the keto-enol moiety, therefore transmission of resonance and inductive effects is very efficient and could be described by the extended correlation of the Hammett type. As a note, in the dianionic form (exemplified by the parent compound (**1**), Fig. 5c) the keto-enol moiety is again coplanar, but the aroyl keto and ionized vinyl hydroxyl are in the *Z* configuration with respect to each other, because of the repulsion between the charge on the enolate anion and the lone pair of the aroyl keto group. Time scales of the rotation around the aroyl keto-vinyl =CH– and the deprotonation of the –OH group should be examined in the future.

The values of pK_a predicted from Eqs. (5)–(10) are given in Table III and shown in Fig. 6. The substituent constants were taken from different sources and the main criterion was to choose those derived from the ionization of carboxylic acids or solvolysis of the corresponding derivatives. To the best of our knowledge, a set of substituents constants derived from compounds having an enolizable interface between a phenyl ring and the reaction center (carboxylic group in the present case) has not been reported in the literature. For compounds **3** and **4**, σ_p^+ values were used in Eqs. (5) and (6). This could be an indication that hyperconjugation of 4-Et- (**3**) and 4-*i*-Pr- (**4**) substituents could influence the overall structures of these molecules, which is possible, particularly considering the tautomeric form III (Scheme 1). The σ_R of compounds **2**, **7**, **8**, and **13** (π-electron delocalization) are derived from the benzoic acid ionization model, while the others are π-electron delocalizations derived from ^{13}C-NMR shifts.

TABLE III. Experimentally obtained (pK_{a1} and pK_{a2}) and predicted acidity constant values

Comp.	R–	pK_{a1}	Predicted pK_{a1}				pK_{a2}	Predicted pK_{a2}	
			Eq. (5)	Eq. (6)	Eq. (7)	Eq. (8)		Eq. (9)	Eq. (10)
1	H–	2.06	2.15	*[a]	2.17	*	7.56	7.68	7.59
2	4-Me–	2.22	2.20	2.21	2.23	2.25	7.99	7.86	7.84
3	4-Et–	2.28	2.27	2.28	2.23	2.26	7.83	7.85	7.79
4	4-*i*-Pr–	2.29	2.26	2.27	2.24	2.27	7.85	7.85	7.83
5	4-*tert*-Bu–	2.21	2.23	2.24	2.25	2.28	7.72	7.87	7.88
6	3,4-di-Me–	2.09	2.09	2.09	*	*	7.92	7.96	a
7	4-F–	2.06	2.07	2.08	2.10	2.09	7.50	7.40	7.50
8	4-Cl–	2.09	2.06	2.07	2.06	2.06	7.30	7.31	7.31
9	4-Br–	2.06	2.06	2.07	2.07	2.07	7.53	7.48	7.50
10	4-NO_2–	1.87	1.85	1.86	1.87	1.88	6.63	6.65	6.63
11	3-OH–	2.18	2.18	2.19	2.13	2.15	7.45	7.47	7.47
12	4-OH–	2.29	2.29	2.30	2.25	2.25	7.73	*	*
13	4-MeO–	2.28	2.25	2.26	2.30	2.29	8.13	8.03	8.14

[a]Omitted from equation derivation

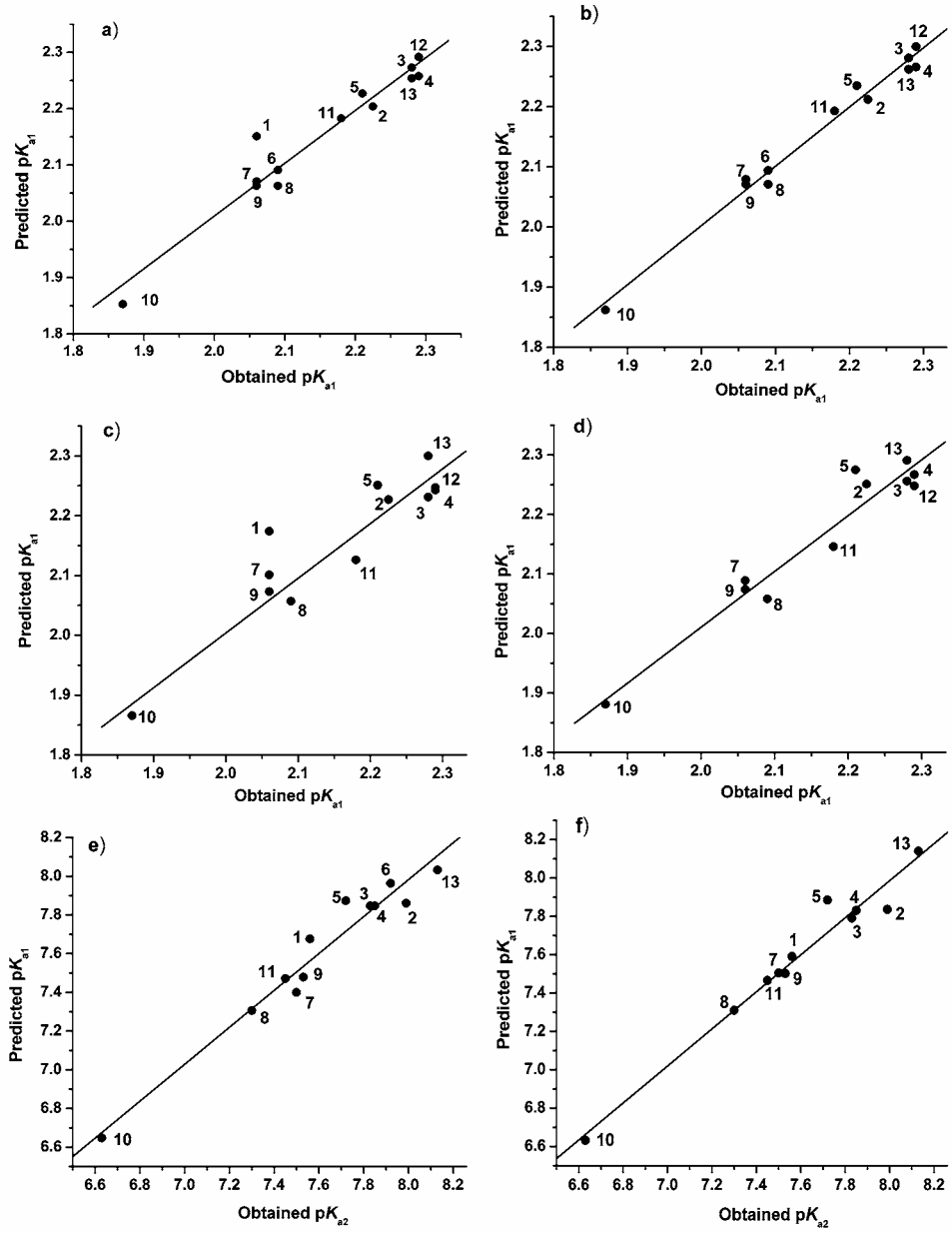

Fig. 6. Experimentally obtained *vs.* calculated pK_a values for compounds **1**–**13**. Graph a) corresponds to Eq. (5), graph b) to Eq. (6), graph c) to Eq. (7), graph d) to Eq. (8), graph e) to Eq. (9) and graph f) to Eq. (10).

The selection of the substituent constants could roughly indicate possible differences between the amounts of all three possible tautomeric forms in aqueous

solution for the molecular or ionized forms of every studied compound, as well as differences in the mode of their solvation. This account offers rationale for the magnitudes of the experimentally obtained pK_a values, which have been discussed in the presented correlations. These partially "empirically" derived models by the classical LFER approach could be extended to a larger set of congeners.

Acknowledgement. The Ministry of Science of Serbia supports this work. Grants 142062 and 142010.

И З В О Д

ЛИНЕАРНЕ КОРЕЛАЦИЈЕ СЛОБОДНЕ ЕНЕРГИЈЕ (LFER) ПРОТОЛИТИЧКИХ РАВНОТЕЖА 4-АРИЛ-2,4-ДИОКСОБУТАНСКИХ КИСЕЛИНА У ВОДЕНИМ РАСТВОРИМА

ТАТЈАНА Ж. ВЕРБИЋ[1], БРАНКО Ј. ДРАКУЛИЋ[2], MIRE F. ZLOH[3], ЈОВАНА Р. ПЕЦЕЉ[1], ГОРДАНА В. ПОПОВИЋ[4] и ИВАН О. ЈУРАНИЋ[1]

[1]Хемијски факултет, Универзитет у Београду, Студентски трг 12–16, 11000 Београд, [2]Центар за хемију – Институт за хемију, технологију и металургију, Универзитет у Београду, Његошева 12, 11000 Београд, [3]The School of Pharmacy, University of London, 29/39 Brunswick Square, London WC1N 1AX, United Kingdom и [4]Фармацеутски факултет, Универзитет у Београду, Војводе Степе 450, 11000 Београд

Протолитичке равнотеже 13 једињења из класе 4-арил-2,4-диоксобутанских киселина (АДК) спектрофотометријски су проучаване у воденим растворима у pH интервалу 1–9 при температури 25±1 °C и јонској јачини раствора 0.1 mol l^{-1} (NaCl), са изузетком 4-OH-деривата који је проучаван и потенциометријски у pH интервалу 7–10 при истим условима. Како АДК у воденом раствору подлежу кето-енолној таутомерији и истовремено постоје у дикето и два енолна облика, то одређене киселинске константе (pK_{a1} 1.87–2.29, pK_{a2} 6.63–8.13 и pK_{a3}(4-OH-) 9.52) представљају макро константе за дати систем. ^{1}H-NMR спектар основне супстанце (4-фенил-2,4-диоксобутанска киселина) (25 °C, pD 5.0) потврђује присуство свих таутомерних облика. Употребом проширене Хаметове корелације, одређене pK_a вредности корелисане су са литературним σ вредностима. Предвиђене pK_a вредности добро се слажу са експериментално добијеним. Молекулски, моноанјонски и дианјонски облици основне супстанце су оптимизовани семиемпиријском молекулско–орбиталном PM6 методом са имплицитним моделом солватације у води (COSMO). Добијене геометрије су употребљене за објашњење квалитета LFER модела.

(Примљено 29. маја 2007)

REFERENCES

1. V. O.Koz'minykh, E. N. Koz'minykh, *Russ. Pharm. Chem. J.* **38** (2004) 67
2. J. S. Wai, M. S. Egbertson, L. S. Payne, T. E. Fisher, M. W. Embrey, L. O. Tran, J. Y. Melamed, H. M. Langford, J. P. Guare Jr., L. Zhuang, V. E. Grey, J. P. Vacca, M. K. Holloway, A. M. Naylor–Olsen, D. J. Hazuda, P. J. Felock, A. L. Wolfe, K. A. Stillmock, W. A. Schleif, L. J. Gabryelski, S. D. Young, *J. Med. Chem.* **43** (2000) 4923
3. R. Di Santo, R. Costi, A. Roux, M. Artico, A. Lavecchia, L. Marinelli, E. Novellino, L. Palmisano, M. Andreotti, R. Amici, C. M. Galluzzo, L. Nencioni, A. T. Palamara, Y. Pommier, C. Marchand, *J. Med. Chem.* **49** (2006) 1939
4. R. Dayam, N. Neamati, *Bioorg. Med. Chem.* **12** (2004) 6371

5. Yu. S. Andreichikov, R. F. Saraeva, Yu. A. Nalimova, S. P. Tendryakova, N. I. Lebedev, *Zh. Org. Khim.* **14** (1978) 371
6. L. Brecker, M. Pogorevc, H. Griengl, W. Steiner, T. Kappe, D. W. Ribbons, *New J. Chem.* **23** (1999) 437
7. M. Sechi, A. Bacchi, M. Carcelli, C. Compari, E. Duce, E. Fisicaro, D. Rogolino, P. Gates, M. Derudas, L. Q. Al–Mawsawi, N. Neamati, *J. Med. Chem.* **49** (2006) 4248
8. M. Huang, W. G. Richards, G. H. Grant, *J. Phys. Chem. A* **109** (2005) 5198
9. K. Popov, H. Rönkkömäki, L. H. J. Lajunen, *Pure Appl. Chem.* **78** (2006) 663
10. P. K. Glasoe, F. A. Long, *J. Phys. Chem.* **64** (1960) 188
11. O. A. Sof'ina, N. M. Igidov, E. N. Koz'minykh, N. N. Trapeznikova, Yu. S. Kasatkina, V. O. Koz'minykh, *Russ. J. Org. Chem.* **37** (2001) 1017
12. L. B. Pfendt, D. M. Sladić, T. J. Janjić, G. V. Popović, *Analyst* **115** (1990) 383A
13. H. Rossoti, *The Study of Ionic Equilibria*, Longman Ltd., New York, 1978, p. 28
14. H. Kubiniyi, *J. Med. Chem.* **20** (1977) 629; BILIN program, BASF A.G. (1998) (http://www.kubinyi.de/bilin.zip)
15. a) J. J. P. Stewart, *J. Mol. Mod.* **13** (2007) 1173; b) J. J. P. Stewart, *J. Comput. Aid. Mol. Des.* **4** (1990) 1
16. A. Pedretti, L. Villa, G. Vistoli, *J. Comput. Aid. Mol. Des.* **18** (2004) 167; VegaZZ 2.1.0 (http://www.ddl.unimi.it)
17. C. Hansch, A. Leo, D. Hoekman, *Exploring QSAR. Hydrophobic, Electronic and Steric Constants.* ACS Professional Reference Book, American Chemical Society, Washington, DC, 1995
18. A. Albert, E. P. Serjeant, *The Determination of Ionization Constants*, 2nd Ed., Chapman and Hall, London, 1971, p. 44
19. B. J. Drakulić, I. O. Juranić, unpublished results.

Journal of the Serbian Chemical Society
JSCS@tmf.bg.ac.yu • www.shd.org.yu/JSCS

J. Serb. Chem. Soc. 72 (12) 1217–1227 (2007)
JSCS–3654

UDC 547.595+66.093.1+66.061:531.61
Original scientific paper

A linear solvation energy relationship study for the reactivity of 2-substituted cyclohex-1-enecarboxylic and 2-substituted benzoic acids with diazodiphenylmethane in aprotic and protic solvents

JASMINA B. NIKOLIĆ*# and GORDANA S. UŠĆUMLIĆ#

Department of Organic Chemistry, Faculty of Technology and Metallurgy, University of Belgrade, Karnegijeva 4, P. O. Box 3505, 11120 Belgrade, Serbia

(Received 17 July 2007)

Abstract: The rate constants for the reaction of 2-substituted cyclohex-1-enecarboxylic acids and the corresponding 2-substituted benzoic acids with diazodiphenylmethane were determined in various aprotic solvents at 30 ºC. In order to explain the kinetic results through solvent effects, the second order rate constants of the reaction of the examined acids were correlated using the Kamlet–Taft solvatochromic equation. The correlations of the kinetic data were carried out by means of multiple linear regression analysis and the solvent effects on the reaction rates were analyzed in terms of the contributions of the initial and transition state. The signs of the equation coefficients support the proposed reaction mechanism. The quantitative relationship between the molecular structure and the chemical reactivity is discussed, as well as the effect of geometry on the reactivity of the examined molecules.

Keywords: carboxylic acids, linear solvation energy relationship, diazodiphenylmethane, aprotic solvents, protic solvents.

INTRODUCTION

Related to the study of the influence of the solvent on the reactivity[1–3] of organic molecules, previous work is extended in this paper towards the reactivity of α,β-unsaturated carboxylic acids in their reaction with diazodiphenylmethane (DDM) in various aprotic and protic solvents. In a previous study, the reactivity of 2-substituted cyclohex-1-enecarboxylic acids with DDM in various alcohols was investigated.[1] The rate data for these acids were correlated with the simple and extended Hammett equations. The results showed that linear free energy relationships (LFER) are applicable to the kinetic data for the 2-substituted cyclohex--1-enylcarboxylic acid system. In a recent paper,[2] hydroxylic solvent effects were examined on the reaction of α,β-unsaturated carboxylic acids with DDM by means

* Corresponding author. E-mail: jasmina@tmf.bg.ac.yu
# Serbian Chemical Society member.
doi: 10.2298/JSC0712217N

of the linear solvation energy relationship (LSER) concept, developed by Kamlet *et al.*[4] The correlation equations obtained by stepwise regression for all the examined acids showed that the most successful approach, which aids the hydroxylic solvent effects in the reaction to be understood, lies in the separate correlations of the kinetic data with the hydrogen bond donating (HBD) and the hydrogen bond accepting (HBA) ability of the solvent. Multiple linear regression analysis (MLRA) is very useful in separating and quantifying such interactions of the examined reactivity. The first comprehensive application of multiple linear regression analysis to kinetic phenomena was that of Koppel and Palm,[5] who listed regression constants for the simple Koppel–Palm equation, for various processes. Aslan *et al.*[6] showed that correlation analysis of second-order rate constants for the reaction of benzoic acid with DDM in hydroxylic solvents did not give satisfactory results with the Koppel–Palm model.[5] They came to the conclusion that the possibility of Koppel–Palm analysis of data related to protic solvents depends on the fitting of data in a regression with the main lines being determined by a much larger number of aprotic solvents. To the best of our knowledge, the influence of aprotic solvents on the reactivity of carboxylic acids with DDM by the Kamlet–Taft treatment has not been systematically presented before, except for benzoic acid.[7]

This paper demonstrates how the linear solvation energy relationship method can be used to explain and present multiple interacting effects of the solvent on the reactivity of 2-substituted cyclohex-1-enecarboxylic and 2-substituted benzoic acids in their reaction with DDM and the influence of the substituents of different nature at the C-2 position for the reactions in a given solvent set.

RESULTS AND DISCUSSION

The second order rate constants for the reaction of various 2-substituted cyclohex-1-enecarboxylic acids and 2-substituted benzoic acids with DDM in eleven aprotic solvents at 30 °C were determined. In order to explain the kinetic results through solvent effects, the second order rate constants of the examined acids in aprotic solvents, together with the previously determined second-order rate constants for the same acids in hydroxylic solvents,[1,2] were correlated using the total solvatochromic equation, of the form:

$$\log k = A_0 + s\pi^* + a\alpha + b\beta \qquad (1)$$

where α and β are solvatochromic parameters, s, a and b are solvatochromic coefficients, and A_0 is the regression value of the examined solute property in the reference solvent, cyclohexane.

In Eq. (1), π^* is an index of the solvent dipolarity/polarizability, which is a measure of the ability of a solvent to stabilize a charge or a dipole by its own dielectric effect. The π^* scale was selected to run from 0.00 for cyclohexanone to 1.00 for dimethyl sulphoxide.

The α parameter represents the scale of solvent hydrogen bond donor (HBD) acidity and has a range from 0.00 for non-HBD solvents (*e.g. n*-hexane, cyclohexane) to 1.00 for methanol. It describes the ability of a solvent to donate a proton, or accept an electron pair in a solvent-to-solute hydrogen bond. The β parameter represents the scale of solvent hydrogen bond acceptor (HBA) basicity, in other words, the ability of a solvent to donate an electron pair, or accept a proton in a solvent-to-solute hydrogen bond. The β scale runs from 0.00 for non-HBA solvents (*e.g. n*-hexane) to about 1.00 for hexamethylphosphoric acid triamide.

The obtained second-order rate constants for the examined cyclohex-1-enecarboxylic and benzoic acids in eleven aprotic solvents, together with the previously determined rate constants for the same acids in the hydroxylic solvents, are given in Tables I and II.

TABLE I. Reaction rate constants for the reaction of 2-substituted cyclohex-1-enecarboxylic acids with diazodiphenylmethane at 30 °C in various solvents

Solvent	k / dm^3 mol^{-1}min^{-1}					
	Cyclohex--1-enecarboxylic acid	2-Methylcyclohex-1-enecarboxylic acid	2-Ethylcyclohex-1-enecarboxylic acid	2-Chlorocyclohex-1-enecarboxylic acid	2-Bromocyclohex-1-enecarboxylic acid	2-Iodocyclohex-1-enecarboxylic acid
Methyl acetate	0.032	0.093	0.095	0.563	0.614	0.642
Cyclohexanone	0.020	0.044	0.099	0.531	0.583	0.603
Diethyl ketone	0.053	0.064	0.110	0.583	0.634	0.653
Carbon tetrachloride	0.329	0.359	0.256	0.795	1.006	1.036
Ethyl acetate	0.025	0.058	0.082	0.501	0.574	0.606
Cyclopentanone	0.025	0.053	0.108	0.569	0.614	0.658
Dioxane	0.065	0.077	0.046	0.554	0.646	0.684
Acetone	0.048	0.106	0.116	0.680	0.831	0.891
Methanol	0.817	0.567	0.583	2.244	2.321	2.614
Ethanol	0.417	0.264	0.278	1.130	1.279	1.470
Dimethyl sulfoxide	0.008	0.013	0.060	0.198	0.210	0.230
Tetrahydrofuran	0.019	0.027	0.055	0.179	0.191	0.204
Acetonitrile	0.318	0.420	0.347	1.580	1.623	1.782
Ethylene glycol	1.962	1.631	1.649	5.222	5.169	5.738

The obtained results show that the rate constants increase with increasing solvent polarity. Comparison of the values of the reaction constants in protic and aprotic solvents indicates that the examined reaction is slower in aprotic solvents, which is in accordance with the proposed reaction mechanism.[8–11] The mechanism of this reaction in both protic and aprotic solvents was found to involve the same rate-determining step: proton transfer from the carboxylic acid to DDM,

forming a diphenylmethanediazonium carboxylate ion pair, which rapidly reacts to give esters, or ethers in the case of hydroxylic solvents:

$$Ph_2CN_2 + RCOOH \rightarrow Ph_2CHN_2^+O_2^-CR$$

TABLE II. Reaction rate constants for the reaction of 2-substituted benzoic acids with diazodiphenylmethane at 30 °C in various solvents

Solvent	k / dm^3 mol^{-1} min^{-1}					
	Benzoic acid	2-Methyl-benzoic acid	2-Ethylben-zoic acid	2-Chloro-benzoic acid	2-Bromoben-zoic acid	2-Iodo-benzoic acid
Methyl acetate	0.260	0.124	0.130	1.543	1.620	1.720
Cyclohexanone	0.220	0.129	0.138	1.393	1.510	1.580
Diethyl ketone	0.265	0.157	0.160	1.510	1.690	1.760
Carbon tetrachloride	0.638	0.389	0.496	1.200	1.380	1.412
Ethyl acetate	0.180	0.094	0.106	1.479	1.480	1.590
Cyclopentanone	0.293	0.145	0.154	1.530	1.620	1.780
Dioxane	0.058	0.035	0.048	0.750	0.758	0.813
Acetone	0.350	0.152	0.170	2.087	2.440	2.680
Methanol	2.470	1.860	2.526	12.71	13.75	15.22
Ethanol	0.995	0.933	0.986	4.388	5.627	5.960
Dimethyl sulfoxide	0.141	0.079	0.072	0.512	0.522	0.586
Tetrahydrofuran	0.105	0.060	0.062	0.454	0.464	0.482
Acetonitrile	3.730	1.590	1.654	5.852	6.023	6.759
Ethylene glycol	4.020	2.590	2.680	10.69	11.08	11.84

The previous investigations of the reactivity of α,β-unsaturated carboxylic acids with DDM in various solvents[1–3] established that the characteristics of a solvent on the reaction rate should be given in terms of the following solvent properties: (*i*) the behaviour of a solvent as a dielectric, facilitating the separation of opposite charges in the transition state; (*ii*) the ability of a solvent to donate a proton in a solvent-to-solute hydrogen bond and thus stabilize the carboxylate anion in the transition state; (*iii*) the ability of a solvent to donate an electron pair and thereby stabilize the initial carboxylic acid, through a hydrogen bond between the carboxylic proton and the solvent electron pair. The parameter π^* is an appropriate measure of the first property, while the second and the third properties are governed by the effects of the solvent acidity and basicity, expressed quantitatively by the parameters α and β, respectively.

Solvent – reactivity relationship

In order to explain the obtained kinetic results through solvent dipolarity/polarizability and basicity or acidity, the rate constants of the examined acids were correlated with the solvent properties using the total solvatochromic Equation (1). The solvent parameters[12] are given in Table III.

TABLE III. Solvent parameters

Solvent	π^*	α	β
Methyl acetate	0.60	0.00	0.42
Cyclohexanone	0.76	0.00	0.53
Diethyl ketone	0.72	0.00	0.45
Carbon tetrachloride	0.28	0.00	0.00
Ethyl acetate	0.55	0.00	0.45
Cyclopentanone	0.76	0.00	0.52
Dioxane	0.55	0.00	0.37
Acetone	0.72	0.08	0.48
Methanol	0.60	0.93	0.62
Ethanol	0.54	0.83	0.77
Dimethyl sulfoxide	1.00	0.00	0.76
Tetrahydrofuran	0.58	0.00	0.55
Acetonitrile	0.85	0.19	0.31
Ethylene glycol	0.92	0.90	0.52

The correlation of the kinetic data was performed by means of multiple linear regression analysis. It was found that the rate constants in the applied set of fourteen solvents show satisfactory correlation with the π^*,α and β solvent parameters together in the same equation. The obtained correlation results are given in Table IV.

TABLE IV. The result of the correlation of the kinetic data with Eq. (1)

Acid	A_0	s[a]	a[a]	b[a]	R[b]	sd[c]	F[d]	N[e]
Cyclohex-1-enecarboxylic acid	–0.58	0.38±0.20	2.07±0.09	–2.48±0.21	0.990	0.11	168	14
2-Methylcyclohex-1-ene-carboxylic acid	–0.49	0.52±0.16	1.66±0.07	–2.35±0.17	0.989.	0.09	162	14
2-Ethylcyclohex-1-ene-carboxylic acid	–0.93	0.87±0.21	1.24±0.10	–1.51±0.22	0.972	0.12	58	14
2-Chlorocyclohex-1-ene-carboxylic acid	–0.18	0.75±0.21	1.07±0.10	–1.42±0.22	0.960	0.12	39	14
2-Bromocyclohex-1-ene-carboxylic acid	–0.05	0.64±0.22	1.04±0.10	–1.42±0.23	0.954	0.13	20	14
2-Iodocyclohex-1-ene-carboxylic acid	–0.05	0.65±0.22	1.07±0.10	–1.40±0.23	0.957	0.13	36	14
Benzoic acid	–0.64	1.34±0.47	1.51±0.22	–1.98±0.49	0.915	0.26	17	14
2-Methylbenzoic acid	–0.83	1.05±0.44	1.64±0.20	–1.75±0.46	0.932	0.25	22	14
2-Ethylbenzoic acid	–0.71	0.92±0.29	1.81±0.13	–1.79±0.31	0.973	0.10	75	14
2-Chlorobenzoic acid	0.15	0.93±0.19	1.28±0.09	–1.33±0.20	0.978	0.10	75	14
2-Bromobenzoic acid	0.29	0.83±0.19	1.28±0.09	–1.25±0.20	0.976	0.11	70	14
2-Iodobenzoic acid	0.20	0.89±0.19	1.31±0.09	–1.27±0.21	0.977	0.11	71	14

[a]Calculated solvatochromic coefficient; [b]correlation coefficient; [c]standard deviation of the estimate; [d]Fisher's test; [e]number of the points used in the calculations

From the results presented in Table IV, the general conclusion can be reached that the solvent effects influence the carboxylic acid–DDM reaction by two opposite contributions. The opposite signs of the electrophilic and the nucleophilic parameters are, as expected, in accordance with the described mechanism of the reaction. The positive signs of the *s* and *a* coefficients prove that the classical solvation and HBD effects increase the reaction rate, supporting the formation of the transition state, and the negative sign of the *b* coefficient indicates that HBA effects decrease the reaction rate and stabilize the state before the reaction begins. From the values of regression coefficients, the contribution of each parameter to reactivity, on a percentage basis, was calculated and is listed in Table V.

TABLE V. The percentage contributions of Kamlet–Taft's solvatochromic parameters to the reactivity

Acid	π^* / %	α / %	β / %
Cyclohex-1-enecarboxylic acid	8	42	50
2-Methylcyclohex-1-enecarboxylic acid	11	37	52
2-Ethylcyclohex-1-enecarboxylic acid	24	34	42
2-Chlorocyclohex-1-enecarboxylic acid	23	33	44
2-Bromocyclohex-1-enecarboxylic acid	21	34	46
2-Iodocyclohex-1-enecarboxylic acid	21	34	45
Benzoic acid	28	31	41
2-Methylbenzoic acid	24	37	39
2-Ethylbenzoic acid	20	40	40
2-Chlorobenzoic acid	26	36	38
2-Bromobenzoic acid	25	38	37
2-Iodobenzoic acid	26	38	36

From these results, it can be noticed that the non-specific interactions (π^*) are less pronounced than the specific ones (α,β) in both carboxylic acid systems. However, the specific interactions have more influence on the cyclohexenyl than on the benzoic system. This probably means that the carboxyl group of the cyclohexenyl acids is more susceptible to the proton-donor and proton-acceptor solvent effects than the carboxyl group of the benzoic acids.

In order to obtain a complete view of the solvent interactions with the molecules of the examined carboxylic acids, the solvent effects are expressed quantitatively for every acid and refer separately to the reactants and the transition state in Table VI.

Higher reaction rates and a more pronounced effect of the HBD solvation and non-specific interactions (polarity/polarizability) can be noticed for halogen-substituted acids in both systems. As the negative inductive effect of the halogen at C-2 stabilizes the carboxylic anion, it supports the transition state, thus accelerating the reaction.

TABLE VI. The solvent effects

Acid	HBA solvation β / %	Sum of HBD solvation (α / %) and non-specific interactions (π^* / %)
Cyclohex-1-enecarboxylic acid	50	50
2-Methylcyclohex-1-enecarboxylic acid	52	48
2-Ethylcyclohex-1-enecarboxylic acid	42	58
2-Chlorocyclohex-1-enecarboxylic acid	44	56
2-Bromocyclohex-1-enecarboxylic acid	46	54
2-Iodocyclohex-1-enecarboxylic acid	45	55
Benzoic acid	41	59
2-Methylbenzoic acid	39	61
2-Ethylbenzoic acid	40	60
2-Chlorobenzoic acid	38	62
2-Bromobenzoic acid	37	63
2-Iodobenzoic acid	36	64

The results presented here show that the proton-acceptor solvent effects are somewhat more pronounced in the ground state for cyclohex-1-enecarboxylic acid and its 2-substituted derivatives than for benzoic acids, supporting the fact that the reaction rates are higher for benzoic acids. For the benzoic acid type, the dominant solvent effects are the proton-donor and non-specific interactions, characteristic for the transition state. This fact is likely to be a consequence of the degree of conjugation of the carboxylic group of the benzoic acids with the ring, in other words, the charge distribution in the carboxylic group, because of conjugation, makes the anion more stable and therefore the reaction faster. However, the more general conclusion arising from these results is that substituents at the C-2 position in both types of carboxylic acid have a secondary influence on the reaction with DDM and do not seem to cause steric hindrance between the reactants and the solvent. The principal influences on the reaction rate are apparently the solvent properties and the general form of the carboxylic acid molecule.

Structure – reactivity relationship

Taking into account the results presented in this work, it can be concluded that the solvation differences of the examined acids in their reaction with DDM derive from the structural differences between the cyclohex-1-enecarboxylic and benzoic acids. Such a conclusion can be drawn from the minimal energy molecular conformations. The geometric layout of the benzoic and cyclohex-1-enecarboxylic acids corresponding to the energy minima in solution were obtained using semi-empirical MNDO-PM3 energy calculations, as reported previously[13] and are shown in Figs. 1 and 2.

In the molecule of benzoic acid, the carboxylic group is almost planar with the ring (Fig. 1), which is the cause of the conjugation of the carbonyl group of the carboxylic group and the benzene ring. In the case of cyclohex-1-enecarboxylic acid (Fig. 2), the carboxylic group is 142° twisted out of the plane of the double bond and is of the opposite orientation compared to benzoic acid. The double bond of cyclohex-1-enecarboxylic acid is much closer to the carboxylic group, which can have consequently an interaction between the carboxylic proton and the π-electrons of the double bond. This is hardly possible for benzoic acid because the position of its carboxylic group is quite different.

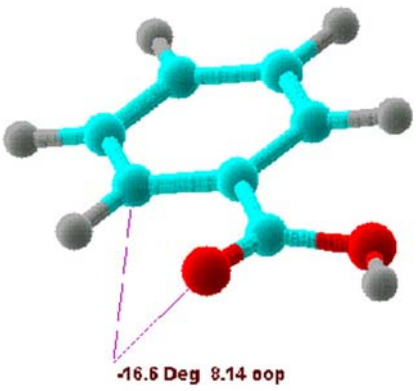

Fig. 1. The most stable conformation of benzoic acid.

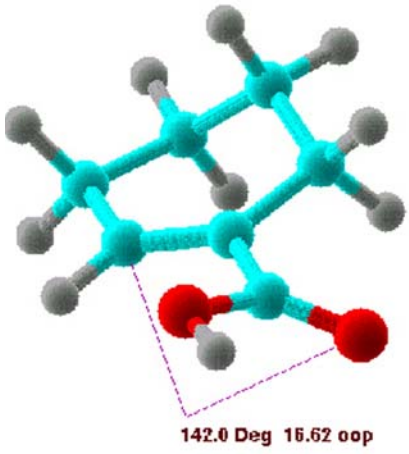

Fig. 2. The most stable conformation of cyclohex-1-enecarboxylic acid.

Additional evidence of the solvent effect on the structure–reactivity relationship in the reaction of 2-subsituted cyclohex-1-enecarboxylic and 2-subsitututed benzoic acids with DDM was also obtained by the correlation of the log *k* values for the examined acids with the Hammett Equation (2):[14]

$$\log k = \log k_0 + \rho\sigma_p \qquad (2)$$

where ρ is the reaction constant, reflecting the sensitivity of log *k* to substituent effects. The substituent constant σ_p[15] is a measure of the electronic effects of a substituent. The results of the correlations are given in Tables VII and VIII.

The difference in the transmission of substituent effects through the benzene ring and the double bond in the cyclohexene ring were ascribed to the different polarizability of the double bonds of the examined compounds and the different solvent effects on the transmission of the substituent proximity effect at the C-2 position.

The poor correlation coefficients for the Hammett equations related to 2-substituted cyclohex-1-enecarboxylic acids, particularly in aprotic solvents, indicate that the cyclohex-1-enecarboxylic acid system is more sensitive to solvent effects

than the benzoic acid system, for which the Hammett equations have rather high, reliable correlation coefficients.

TABLE VII. Hammett reaction constants and correlation parameters for 2-substituted cyclohex-1-ene-carboxylic acids

Solvent	ρ[a]	r[b]	sd[c]	n[d]
Methyl acetate	2.38	0.799	0.37	6
Cyclohexanone	2.77	0.798	0.43	6
Diethyl ketone	2.49	0.883	0.27	6
Carbon tetrachloride	1.33	0.920	0.12	6
Ethyl acetate	2.66	0.820	0.38	6
Cyclopentanone	2.68	0.805	0.41	6
Dioxane	2.80	0.934	0.22	6
Acetone	2.48	0.834	0.34	6
Methanol	1.66	0.975	0.08	6
Ethanol	1.81	0.974	0.09	6
Dimethyl sulfoxide	2.64	0.756	0.47	6
Tetrahydrofuran	2.03	0.819	0.29	6
Acetonitrile	1.78	0.902	0.17	6
Ethylene glycol	1.40	0.964	0.08	6

[a]Reaction constant; [b]correlation coefficient; [c]standard deviation of the estimate; [d]number of the points used in the calculations

TABLE VIII. Hammett reaction constants and correlation parameters for 2-substituted benzoic acids

Solvent	ρ[a]	r[b]	sd[c]	n[d]
Methyl acetate	2.97	0.985	0.10	6
Cyclohexanone	2.84	0.977	0.13	6
Diethyl ketone	2.75	0.977	0.12	6
Carbon tetrachloride	1.28	0.977	0.06	6
Ethyl acetate	3.20	0.979	0.14	6
Cyclopentanone	2.79	0.983	0.10	6
Dioxane	3.50	0.964	0.20	6
Acetone	3.14	0.982	0.12	6
Methanol	2.22	0.949	0.15	6
Ethanol	2.04	0.936	0.16	6
Dimethyl sulfoxide	2.28	0.984	0.08	6
Tetrahydrofuran	2.38	0.973	0.09	6
Acetonitrile	1.50	0.973	0.07	6
Ethylene glycol	1.68	0.984	0.06	6

[a]Reaction constant; [b]correlation coefficient; [c]standard deviation of the estimate; [d]number of the points used in the calculations

Based on the results presented in this paper and previously reported results for more than fifty carboxylic acids, it can be concluded that the solvatochromic concept of Kamlet and Taft is applicable to the kinetic data for the reaction of different carboxylic acids with DDM in various solvents. This means that this model gives a correct interpretation of the solvating effects on the carboxylic group in various solvents. The solvation models for 2-substituted cyclohex-1-enecarboxylic and 2-substituted benzoic acids are suggested. The results show that the 2-substituted cyclohex-1-enecarboxylic acid system is more sensitive to aprotic solvent effects than the 2-substituted benzoic acid system.

EXPERIMENTAL

Cyclohex-1-enecarboxylic, 2-methylcyclohex-1-enecarboxylic, 2-ethylcyclo-hex-1-enecarboxylic, 2-chlorocyclohex-1-enecarboxylic, 2-bromocyclohex-1-enecarboxylic and 2-iodo-cyclohex-1-enecarboxylic acids were prepared by the method of Wheeler and Lerner,[16] from the corresponding cyclohexanone cyanohydrine which was dehydrated to cyanocyclohexene. The nitrile was hydrolyzed with phosphoric acid to the corresponding cyclohex-1-enecarboxylic acid. Benzoic, 2-methylbenzoic, 2-ethylbenzoic, 2-chlorobenzoic, 2-bromobenzoic and 2-iodobenzoic acids were commercial products (Fluka, Germany).

The chemical structure and purity of the obtained compounds were confirmed by melting or boiling points, as well as ^{1}H-NMR, FTIR and UV spectroscopy.

Diazodiphenylmethane was prepared by the method of Smith *et al.*[17] and stock solutions were stored in a refrigerator and diluted before use. Solvents were purified as described in previous papers.[8,18] All the solvents used in the kinetic studies were of analytical grade. Rate constants for the reaction of examined acids with DDM were determined as reported previously, by the spectroscopic method of Roberts and co-workers,[19] using a Shimadzu UV-1700 spectrophotometer. Optical density measurements were performed at 525 nm with 1 cm cells at 30±0.05 ºC. The second order rate constants for all acids were obtained by dividing the pseudo-first order rate constants by the acid concentration (the concentration of acid was 0.06 mol dm^{-3} and of DDM 0.006 mol dm^{-3}). Three to five rate constant determinations were made for each acid in every case and, in particular, the second-order rate constants agreed within 3 % of the mean value. The correlation analyses were performed using Origin and Microsoft Excel computer software. The goodness of fit was discussed using the correlation coefficient (*R*), standard deviation (*s*) and the Fisher's value (*F*).

Acknowledgement. The authors acknowledge the financial support of the Ministry of Science of the Republic of Serbia (Project 142063).

И З В О Д

ПРОУЧАВАЊЕ РЕАКТИВНОСТИ 2-СУПСТИТУИСАНИХ ЦИКЛОХЕКС-1--ЕНКАРБОКСИЛНИХ И 2-СУПСТИТУИСАНИХ БЕНЗОЕВИХ КИСЕЛИНА У АПРОТИЧНИМ И ПРОТИЧНИМ РАСТВАРАЧИМА ПОМОЋУ ЛИНЕАРНЕ КОРЕЛАЦИЈЕ СОЛВАТАЦИОНИХ ЕНЕРГИЈА

ЈАСМИНА Б. НИКОЛИЋ и ГОРДАНА С. УШЋУМЛИЋ

Катедра за органску хемију, Технолошкометалуршки факултет, Универзитет у Београду, п. пр. 3503, Карнегијева 4, 11120 Београд

Константе брзине за реакцију 2-супституисаних циклохекс-1-енкарбоксилних и одговарајућих 2-супституисаних бензоевих киселина са диазодифенилметаном су одређене у низу

различитих апротичних растварача на температури од 30 °C. Да би се кинетички резултати објаснили помоћу ефеката растварача, добијене константе брзине реакције другог реда су корелисане Камлет–Тафтовом солватохромном једначином. Корелације кинетичких података су добијене помоћу методе вишеструке линеарне регресионе анализе и ефекти растварача су посебно анализирани у односу на основно и прелазно стање. Аритметички знаци испред коефицијената солватохромних параметара растварача одговарају претпостављеном механизму испитиване реакције. Такође је проучаван квантитативни однос молекулске структуре и реактивности, као и ефекат геометрије молекула испитиваних једињења на њихову реактивност.

(Примљено 17. јула 2007)

REFERENCES

1. G. S. Ušćumlić, V. V. Krstić, M. D. Muškatirović, *J. Chem. Soc. Perkin Trans. 2* (1993) 999
2. G. S. Ušćumlić, J. B. Nikolić, V. V. Krstić, *Indian J. Chem. B* **44** (2005) 361
3. J. B. Nikolić, G. S. Ušćumlić, V. V. Krstić, *Int. J. Chem. Kin.* **37** (2005) 361
4. M. Kamlet, J. Abboud, R. W. Taft, *Progress in Physical Organic Chemistry*, Vol. 13, Wiley, New York, 1981, p. 485
5. I. A. Koppel, V. A. Palm, in *Advanced Linear Free Energy Relationships;* N. B. Chapman, J. Shorter, Eds., Plenum Press, London, 1972, p. 447
6. M. H. Aslan, G. Collier, J. Shorter, *J. Chem. Soc. Perkin Trans. 2* (1981) 1572
7. C. Reinchart, *Solvents and Solvent Effects in Organic Chemistry*, Wiley-VCH, Weinheim, 2003, p. 447
8. A. Buckley, N. B. Chapman, M. R. Dack, J. Shorter, H. M. Wall , *J. Chem. Soc. B* (1968) 631
9. K. Bowden, A. Buckley, N. B. Chapman, J. Shorter, *J. Chem. Soc.* (1964) 3380
10. R. A. More, R. M. O'Ferral, W. K. Kwok, S. I. Miller, *J. Am. Chem. Soc.* **86** (1964) 5553
11. N. B. Chapman, M. R. Dack, D. Newman, J. Shorter, R. Wilkinson, *J. Chem. Soc. Perkin Trans. 2* (1974) 962
12. M. Kamlet, J. Abboud, R. W. Taft, *J. Org. Chem.* **48** (1983) 287
13. J. B. Nikolić, G. S. Ušćumlić, I. O. Juranić, *Int. J. Chem. Kin.* **39** (2007) 664
14. L. P. Hammett, *J. Am. Chem. Soc.* **59** (1937) 96
15. M. Charton, *Progress in Physical Organic Chemistry*, Vol. 13, Wiley, New York, 1981, p. 178
16. O. H. Wheeler, I. Lerner, *J. Am. Chem. Soc.* **78** (1956) 63
17. L. I. Smith, K. L. Howard, *Org. Synth. Coll. Vol. 3*, Wiley, New York, 1955, p. 351
18. N. B. Chapman, M. R. Dack, J. Shorter, *J. Chem Soc. B.* (1971) 834
19. J. D. Roberts, E. A. McElhill, R. Armstrong, *J. Am. Chem. Soc.* **71** (1949) 2923.

Journal of the Serbian Chemical Society
JSCS@tmf.bg.ac.yu • www.shd.org.yu/JSCS

J. Serb. Chem. Soc. 72 (12) 1229–1236 (2007)
JSCS–3655

UDC 546.17'11+547.53.024:543.422.25
Original scientific paper

A study of substituent effects on the NH bond in alkyl and aryl 4,6-disubstituted-3-cyano-2-pyridones*

MILICA MIŠIĆ–VUKOVIĆ[1]**#, SLOBODANKA JOVANOVIĆ[2], DUŠAN MIJIN[1#], JANOS CSANADI[3#] and DEJAN DJOKOVIĆ[4#]

[1]Faculty of Technology and Metallurgy, University of Belgrade, 11000 Belgrade, [2]Galenika a.d., R&D Institute, Batajnički drum b.b., 11000 Belgrade, [3]Faculty of Science, University of Novi Sad, 21000 Novi Sad and [4]Faculty of Chemistry, University of Belgrade, 11000 Belgrade, Serbia

(Received 8 October 2007)

Abstract: Substituent effects on the IR stretching frequencies and ^{1}H-NMR chemical shifts of the pyridone NH group in 4- and 6-disubstituted alkyl and aryl 3-cyano-2-pyridones were investigated. The bands most sensitive to substituent effects from the broad and multiple IR NH band for each compound were selected by a computer calculation. The selected values of the IR frequencies and the determined ^{1}H-NMR chemical shifts were subjected to LFER analysis, by correlations with the Hamett $\sigma_{m/p}$ and Swain–Lupton *F* and *R* substituent constants.

Keywords: substituted 2-pyridones, LFER analysis, NH bond, IR and ^{1}H-NMR spectra.

INTRODUCTION

In a recent paper,[1] an investigation of the spectral characteristics of the title compounds was reported. The effects of substituents in the 4 and 6 positions of the 2-pyridone nucleus on CN, CO, ring and 5H functions were estimated there, by applying the LFER principles. At that time, it was not possible to report on the effect of substituents on the NH bond, due to the well known controversy of the broad multiple NH band in the IR spectra, which is otherwise the most interesting functional group in 2-pyridones. In the present paper, for the same three series of compounds from the previous work, of the general formulae shown in Scheme 1, the data on the NH IR stretching frequencies and the ^{1}H-NMR chemical shifts were subjected to correlation analysis using the LFER principles, with the intention of gaining information concerning the transmission of substituent effects to the NH bond. It was believed that this is important because of the known potential biological activity of substituted pyridones.[1] It is reasonable to expect, due to the presence of the CONH group in the pyridone molecule and the similarity

* Presented partly at the 15th Lakeland Heterocyclic Symposium, Grasmere, May 10–14, 2001.
** Corresponding author. E-mail: milica@tmf.bg.ac.yu
# Serbian Chemical Society member.
doi: 10.2298/JSC0712229M

of this group to the peptide bond in proteins, that the interactions of 2-pyridone derivatives with natural substrates would occur *via* the hydrogen bond formation between the two complementary functions.

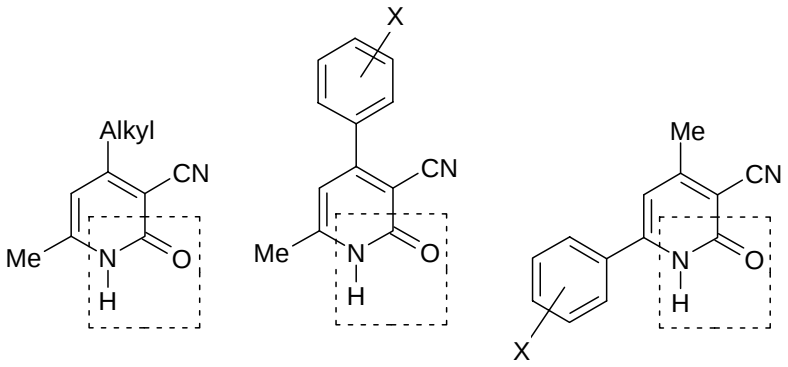

1		**2**		**3**	
Compd.	Substituent	Compd.	Substituent	Compd.	Substituent
1a	Me	**2a**	*p*-OCH_3	**3a**	*p*-OCH_3
1b	Et	**2b**	H	**3b**	H
1c	*n*-Pr	**2c**	*p*-Br	**3c**	*p*-Br
1d	*i*-Pr	**2d**	*p*-Cl	**3d**	*p*-Cl
1e	*n*-Bu	**2e**	*m*-NO_2	**3e**	*m*-NO_2
1f	*i*-Bu	**2f**	*p*-NO_2	**3f**	*p*-NO_2
1g	*t*-Bu				

Scheme 1. General structures of the investigated 4,6-disubstituted-3-cyano-2-pyridones.

In the first investigation of the IR spectra of the NH bond in 2-pyridones,[2] the main peak in the solid state was assigned at 3100 cm^{-1} and at 2850 cm^{-1} in solution. In both forms, broad multiple bands were observed with well resolved subsidiary peaks. Later, it was claimed[3] that 2-pyridones exist as hydrogen bonded spiral dimers both in the solid state and in concentrated solutions, with the NH peaks very broad and strong with many maxima in the region 3200–2800 cm^{-1}. It was also observed that some free ν_{NH} frequencies were found at *ca*. 3400 cm^{-1} in dilute CCl_4 solutions and in the gas phase at 3448 cm^{-1}.[4] Recently, the IR spectra of the 2-pyridone NH bond were used to study 2-pyridone/2-hydroxypyridine tautomerism in the context of water clusters in supersonic jets,[4,5] and as analogues for biological systems,[6,7] or for comparison in a theoretical study of the same phenomenon.[8] In all these studies, broad multiple NH bands were observed, and the main peak was estimated as above. However, it should be pointed out that all these studies refer to unsubstituted 2-pyridone.

EXPERIMENTAL

All substances, the spectral characteristics of which are presented in the present paper and were used for correlations with the LFER parameters, were synthesized by literature methods or by ana-

logy to those, sometimes by modified procedures. Some of these were new compounds, fully characterized by IR, NMR, MS and UV spectroscopy, and were reported in previous communications.[9–11]

The LFER equations and substituent constants employed for the calculations were taken from the standard texts on the subject.[12,13]

A computer calculation based on Fortran 77 was devised and used for the selection of IR frequencies of investigated alkyl and aryl 2-pyridones with the highest sensitivity to substituent effects. Experimental values of frequencies with well-defined peaks from the broad multiple NH band were used. In a stepwise elimination procedure, in the predetermined range of regression coefficients 0.970–0.999, corresponding alkyl and aryl IR frequencies for each investigated compound were obtained. These are given in Tables I and II and were subjected to regression analysis, and the corresponding statistical parameters are presented in Eqs. (1), (2), (4), (5) and (8).

TABLE I. IR stretching frequencies and ^{1}H-NMR chemical shifts for the NH bond in 4-alkyl-6-methyl-3-cyano-2-pyridones

Compd.	Substituent	ν_{NH} (KBr) / cm^{-1}	δ_{NH} (DMSO-d_6) / ppm
1a	Me	2996	12.24
1b	Et	2982	12.40
1c	*n*-Pr	2957	
1d	*i*-Pr	2975	12.26
1e	*n*-Bu	2986	
1f	*i*-Bu	2963	
1g	*t*-Bu	3019	11.53

The instruments used in the investigation were as follows: the IR spectra were recorded on Perkin–Elmer FTIR 1725x and Bomem MB 100 FTIR spectrophotometer. ^{1}H-NMR spectra were determined in DMSO-d_6 on a Varian–Gemini 200 MHz spectrometer using TMS as the internal standard.

TABLE II. IR stretching frequencies and ^{1}H-NMR chemical shifts for the NH bond in 4(6)-aryl--6(4)-methyl-3-cyano-2-pyridones (KBr)

Compd.	Substituent	ν_{NH} (KBr) / cm^{-1}	δ_{NH} (DMSO-d_6) / ppm
	4-Aryl substitution		
2a	p-OCH_3	3134	
2b	H	3054	12.61
2c	*p*-Br	3020	
2d	*p*-Cl	3013	
2e	*m*-NO_2	2899	
2f	*p*-NO_2	2897	12.75
	6-Aryl substitution		
3a	*p*-OCH_3	3131	12.48
3b	H	3066	12.55
3c	*p*-Br	3018	12.60
3d	*p*-Cl	3019	12.62
3e	*m*-NO_2	2928	12.80
3f	*p*-NO_2	2898	

RESULTS AND DISCUSSION

No attempt to resolve the broad multiple NH band in the IR spectra of substituted 2-pyridone, not even for 2-pyridone itself, were found in the literature. In all literature references, the IR NH absorption is described as a broad band of peaks of approximately the same intensity, but usually one is singled out, being called the main peak at 3100 cm^{-1},[2] the bonded NH frequency (the middle-band or peak absorption) at 2700 cm^{-1},[3] or a bound NH stretch as a sharp band at 3140 cm^{-1}.[7] It has been stated that 2-pyridone in the solid state, in KBr and Nujol mull, exists exclusively in the oxo-form.[2,3] In a fairly recent Japanese database, absorption of 2-pyridone in the IR region 3119–2880 cm^{-1} was also assignned to its oxo-form.

In the present investigation, the IR spectra of 4,6-disubstituted-3-cyano-2-pyridones were recorded in the form of KBr pellets on two instruments with very good resolution and the corresponding spectra from both were practically the same. The spectra of the three series of 4,6-disubstituted-3-cyano-2-pyridone shown in Scheme 1 have a broad band in the IR region 3200–2300 cm^{-1}, but the absorption bands which vary with the substituent, and presumably indicate substituent effects on the NH bond, were in a more narrow region 3150–2750 cm^{-1}. The absorption frequencies outside of this region are few and more or less constant, therefore not sensitive to substituent effects. Peaks in the region 3100––3000 cm^{-1} did not show appreciable substituent effects, as the corresponding correlation coefficients with the Hammett $\sigma_{p/m}$ constant were extremely low, which was also true for the region 2850–2750 cm^{-1}. Therefore, it was decided to select by a computer calculation, absorption bands in the mid-region 3140–2880 cm^{-1}, which gave the best fit to the Hammett equation with $\sigma_{p/m}$ constants as a standard test for the existence of an LFER relationship. This method was applied to both alkyl and aryl substituted 3-cyano-2-pyridones. The selected frequencies are presented in the Tables I and II and were used in the calculations presented in the following section. These values expectedly give the best correlations with both 2 and 3 parameter equations.

There was not sufficient data available for correlations of the ^{1}H-NMR chemical shifts, due to the insolubility of the investigated compounds in $CDCl_3$ and DMSO-d_6. Also, some of the compounds did not show visible peaks in the range of the NH bond, probably due to the inadequate sensitivity of the employed instruments.

*4-Alkyl-6-methyl-3-cyano-2-pyridones (compounds **1a**–**f**)*

The IR stretching frequencies of the alkyl substituted series (Table I) selected in the above described manner were correlated with Hammett $\sigma_{m/p}$ constants and the result is presented in Eq. (1).

$$\nu_{NH} = (-772.61 \pm 71.02)\sigma_p + (2863.37 \pm 12.03) \quad (1)$$

$$R = 0.976,\ s = 4.97,\ n = 7,\ F = 100.6$$

Except for the relatively high standard error, the correlation is fairly good, considering the weak electronic effects of the alkyl groups. Similar result was obtained by use of the Swain–Lupton parameters, Eq. (2):

$$\nu_{NH} = (-884.87.18 \pm 102.70)F + (-742.18 \pm 72.18)R + (2868.45 \pm 11.34) \quad (2)$$

$$R = 0.984,\ s = 4.47,\ n = 7,\ F = 63.4$$

Only four compounds from the alkyl series were sufficiently soluble in DMSO-d_6 for the ^{1}H-NMR spectra to be recorded but had sufficiently different and well-defined chemical shifts for the NH group. The corresponding correlation is presented in Eq. (3):

$$\delta_{NH} = (16.07 \pm 3.47)\sigma_p + (14.81 \pm 0.58) \quad (3)$$

$$R = 0.956,\ s = 0.14,\ n = 4,\ F = 21.4$$

It is interesting to note that neither of the above correlations required correction with the steric parameters. Actually, the inclusion of these parameters gave inferior results, which is opposed to that observed in a previous study.[1]

The obtained high standard deviations in the correlations of IR spectra could perhaps be explained by interference with the IR absorption in the same region of methyl and methylene groups and also the aromatic C−H stretching absorption from the 5H C−H bond. These disturbances are probably not very strong but are not constant and, except for the aromatic 5H, could cause dispersion of the data points.

*4(6)-Substituted aryl-6(4) methyl-3-cyano-2-pyridones (compounds **2a-f** and **3a-f**)*

In the previous investigation[1] on the correlation analysis on the same series of compounds as here, the effects from aryl substituents in positions 4 and 6 of the 3-cyano-2-pyridones on the CN, CO, ring and 5H groups was studied separately. In treating the broad multiple peak IR band in the same manner as for alkyl substituted compounds **1a**–**g**, it appeared that the equation which gives the best fit to Hammett $\sigma_{m/p}$ values could include all 12 compounds from **2a**–**f** and **3a**–**f** series. The corresponding correlation is given in Eq. (4):

$$\nu_{NH}^{4,6} = (-219.14 \pm 6.59)\sigma_{m/p} + (3067.00 \pm 3.06) \quad (4)$$

$$R = 0.995,\ s = 8.45,\ n = 12,\ F = 110.48$$

Except for the high standard deviations, the correlation according to Eq. (4) is satisfactory, but the correlation for both **2a**–**f** and **3a**–**f** series with F and R parameters is slightly less good considering the standard deviation (Eq. (5)):

$$\nu_{NH}^{4,6} = (-204.90 \pm 14.47)F + (-3219.45 \pm 12.88)R + (3066.48 \pm 7.33) \quad (5)$$

$$R = 0.994,\ s = 8.87,\ n = 12,\ F = 403.65$$

For the aryl substituted compounds, due to insolubility in DMSO-d_6, only seven data on the chemical shifts of the NH bond from series **2a**–**f** and **3a**–**f** are available, but these gave a very good correlation as can be seen in Eq. (6):

$$\delta_{NH}^{4,6} = (0.277 \pm 0.04)\sigma_{m/p} + (12.56 \pm 0.02) \quad (6)$$
$$R = 0.961,\ s = 0.03,\ n = 7,\ F = 59.9$$

The correlation with F and R was also good (Eq. (7)):

$$\delta_{NH}^{4,6} = (0.245 \pm 0.04)F + (0.305 \pm 0.05)R + (12.57 \pm 0.02) \quad (7)$$
$$R = 0.977,\ s = 0.03,\ n = 7,\ F = 41.5$$

Good fit in the two last correlations, Eqs. (6) and (7), shows that the ^{1}H-NMR chemical shifts for the N–H bond, although the corresponding peaks are somewhat broad, are quite distinctive and seemingly free from any interferences.

The good correlations with the ^{1}H-NMR spectral data, led to the idea to check the validity of the method employed for selecting the IR bands most sensitive to the effect of substituents. Therefore, the values of the IR stretching frequencies and the available ^{1}H-NMR data were intercorrelated and the obtained correlation is presented in Eq. (8):

$$\delta_{NH} = (-0.00131 \pm 0.0001)\nu_{NH} + (15.69 \pm 0.54) \quad (8)$$
$$R = 0.957,\ s = 0.04,\ n = 7,\ F = 54.68$$

Considering that the determination of the ^{1}H-NMR chemical shifts is much more precise than that of the IR stretching frequencies, particularly because of the broad multiple NH band, this fairly good intercorrelation proves that the selection of the IR NH stretching frequencies for use in the correlations presented in this paper was justified.

It was taken for granted that 2-pyridone in the solid state is in the oxo-form and, on the basis of crystallographic data, mostly as a dimer. Hence, the IR spectra in KBr were treated accordingly. In solution, a tautomeric equilibrium exists,[2,3] which has been extensively investigated.[4] It was recently confirmed that 2-pyridone in the gaseous phase also exists as a dimer of both tautomeric forms, 2Py·2HP, resulting from a double proton transfer.[5] However, the IR spectrum of 3-nitro-2-pyridone in KBr published in a Japanese database[14] was declared as belonging to 3-nitro-2-hydroxypyridine, and had a distinctive hydroxy absorption band at 3432 cm^{-1}. In the same database, as mentioned previously, the unsubstituted 2-pyridone is presented as being exclusively in the oxo-form. This example shows that electronic effects drastically influence the existence of tautomeric forms, even in the solid state. This effect is particularly strong in the above-mentioned 3-nitro-2-pyridone,[14] because the electron attracting nitro group in this compound is directly attached to the pyridone nucleus, as opposed to the compounds investigated in this paper, where the phenyl group is interpolated between the substituent and the pyridone ring, weakening the strong-electron accepting effects.

In the light of these data, it is also possible that the high standard errors in the presented calculations, in addition to resulting from the large numerical diffe-

rence between the two correlated values, $\sigma_{m/p}$ and the IR stretching frequencies, could also be due to some contribution of the 2-hydroxypyridine, which might also be the reason for the dispersion of the values of IR stretching frequencies of the nitro-substituted derivatives and the high standard deviations. It is possible that strong electron-attracting groups in the *p*- and *o*-position of the phenyl ring weaken the NH bond and facilitate a proton transfer to the carbonyl oxygen.

CONCLUSION

This paper presents the results of an LFER analysis of substituent effects on the IR stretching frequencies of the NH group and ^{1}H-NMR chemical shifts for three series of 4,6-disubstituted-3-cyano-2-pyridones. It was established that satisfactory correlations could be obtained with simple Hammett type parameters. Correlations with the Swain–Lupton constants yielded equations of similar precision.

It appears that electronic effects of both alkyl and aryl substituents considerably influence the spectral characteristics of the NH bond. It was not necessary to include steric parameters in the calculations to improve the correlations, as was previously necessary.[1] This is probably due to better transmission of substituent effects to the NH bond *via* the direct conjugation from the substituted phenyl group in position 4 and the negligibly small steric interaction of the substituent in position 6 with the practically linear N−H group. The substituent effects are therefore stronger and less affected by non-planarity of the pyridone nucleus and steric hindrance as was the case for CN, CO and 5H in a previous investigation.[1]

The importance of a better knowledge of the effects of substituents on the NH bond, particularly in a view of the potential use of substituted 2-pyridones as therapeutic agents and DNA base mimics should be stressed.

Acknowledgments. The authors acknowledge the financial support of the Ministry of Science of the Republic of Serbia (projects: TR-6719B, 142063, 142052B, 142000/053). We are grateful to Mr. Zoran Pavlović, of TMF, for the computer calculations.

И З В О Д

КОРЕЛАЦИОНА АНАЛИЗА IR И ^{1}H-NMR СПЕКТРАЛНИХ ПОДАТАКА ЗА NH ВЕЗУ У АЛКИЛ И АРИЛ 4,6-ДИСУПСТИТУИСАНИМ 3-ЦИЈАНО-2-ПИРИДОНИМА

МИЛИЦА МИШИЋ–ВУКОВИЋ[1], СЛОБОДАНКА ЈОВАНОВИЋ[2], ДУШАН МИЈИН[1], JANOS CSANADI[3] и ДЕЈАН ЂОКОВИЋ[4]

[1]Технолошко-металуршки факултет, Универзитет у Београду, Карнегијева 4, Београд, [2]Галеника а.д., Институт, Батајнички друм б.б., Београд, [3]Природно–математички факултет, Универзитет у Новом Саду, Нови Сад и [4]Хемијски факултет, Универзитет у Београду, Београд

У раду је разматран утицај супституената на IR фреквенције и ^{1}H-NMR хемијска померања за пиридонску NH групу у 4- и 6-дисупституисаним алкил и арил 3-цијано-2-пиридонима коришћењем принципа линеарне корелације слободне енергије. За израчунавања су примењене Хаметове $\sigma_{m/p}$ константе као и Swain–Lupton константе супституената *F* и *R*. Развијен је компјутерски метод за избор IR NH трака најосетљивијих на утицај супституената.

(Примљено 8. октобра 2007)

REFERENCES

1. S. Jovanović, D. Mijin, M. Mišić–Vuković, *ARKIVOC* **10** (2006) 116
2. L. J. Bellamy, P. E. Roqasch, *Proc. Roy. Soc.* **A257** (1960) 98
3. A. R. Katritzky, A. P. Ambler, in *Physical Methods in Heterocyclic Chemistry*, Vol. II, A. R. Katritzky, Ed., Academic Press, New York, 1963, p. 262
4. Z. Matsuda, T. Ebata, N. Mikami, *J. Chem. Phys.***110** (1999) 8397, and references cited therein
5. G. M. Florio, C. J. Grueriloh, R. C. Quimpo, S. Zwier, *J. Chem. Phys.* **113** (2000) 11143
6. M. Menwlz, A. Müller, S. Leutwyler, *Phys. Chem. Chem. Phys.* **5** (2003) 2663
7. J. A. Frey, A. Müler, H. M. Frez, S. Leutwyler, *J. Chem. Phys.* **121** (2004) 8237
8. M. J. Wójcik, W. Tatara, M. Boczar, A. Apola, S. Ikeda, *J. Mol. Struct*. **596** (2001) 207
9. V. Krstić, M. Mišić–Vuković, M. Radojković–Veličković, *J. Chem. Res. (S)* **4** (1991) 81; (M) 783
10. M. Mišić–Vuković, M. Radojković–Veličković, *J. Chem. Soc. Perkin Trans. 2* (1992) 1965
11. a) D. Mijin, D. Antonović, M. Mišić–Vuković, *Indian J. Chem.* **33B** (1994) 309; b) D. Mijin, M. Mišić–Vuković, *Indian J. Chem.* **34B** (1995) 348; c) D. Mijin, M. Mišić–Vuković, *Indian J. Chem.* **37B** (1998) 988
12. C. Hansch, A. Leo, R. W. Taft, *Chem. Rev.* (1991) 91
13. M. Charton, *Prog. Phys. Org. Chem.* **13** (1981) 119
14. SDBSWeb : http://www.aist.go.jp/RIODB/SDBS/, (05.5.2006).

Journal of the Serbian Chemical Society
JSCS@tmf.bg.ac.yu • www.shd.org.yu/JSCS

J. Serb. Chem. Soc. 72 (12) 1237–1254 (2007)
JSCS–3656

UDC 547.2–035.8+547.52:547.915(497.11)
Original scientific paper

Evaluation of saturated and aromatic hydrocarbons oil–oil maturity correlation parameters (SE Pannonian Basin, Serbia)

KSENIJA STOJANOVIĆ[1,2#], BRANIMIR JOVANČIĆEVIĆ[2,3#], DRAGOMIR VITOROVIĆ[2,3*#], YULIA GOLOVKO[4], GALINA PEVNEVA[4] and ANATOLY GOLOVKO[4]

[1]*Department of Medicine, University of Belgrade, Višegradska 26, 11000 Belgrade,* [2]*ICTM – Center of Chemistry, University of Belgrade, Njegoševa 12, 11000 Belgrade,* [3]*Faculty of Chemistry, University of Belgrade, Studentski trg 12–16, 11000 Belgrade, Serbia and* [4]*Institute of Petroleum Chemistry, 3, Academichesky Ave., 634055 Tomsk, Russia*

(Received 10 May 2007)

Abstract: Twenty three crude oils from the Serbian part of the Pannonian Basin (14 from the Vojvodina Province and 9 from the Drmno Depression) were investigated, aimed at an evaluation of oil–oil maturity correlation parameters based on the distribution and abundance of saturated biomarkers and alkylarene constituents. Factor and cluster analyses were used for this purpose. Factor analyses using varimax rotation were first run separately, *i.e.*, of maturity parameters based on the abundance of (a) *n*-alkanes and isoprenoids, (b) steranes and triterpanes, (c) alkylnaphthalenes, and (d) alkylphenanthrenes. These analyses yielded 9 important "maturity factors". Eight of them, showing higher than 30 % of variance, were further involved in another factor analysis, as well as in cluster analysis using the Ward method. In this way, all maturity parameters based on saturated biomarkers and alkylarenes were evaluated and ranged, considering the fact that the observed factors represented their linear combinations. The results showed that in the correlation of crude oils from the Serbian part of the Pannonian Basin, the most important were maturity parameters based on isomerization reactions involving one methyl group in thermodynamically less stable α-methylnaphthalenes, ethylnaphthalenes, dimethylnaphthalenes and methylphenanthrenes, and their change into more stable isomers with the methyl group in the β-position in the aromatic ring. Processes constituting high loadings factor 2 and factor 3 parameters were also defined. Hierarchy between the "factors" and parameters were controlled, and approved, by cluster analysis using the Ward method. Finally, the investigated crude oils were correlated by factor and cluster analyses, using all the important "maturity factors". Differences in maturity were observed between the Vojvodina and Drmno Depression crude oils, as well as between oils originating from South Banat, North Banat and the Velebit oil field (Vojvodina locality).

Keywords: crude oils, SE Pannonian Basin, saturated biomarkers, alkylarenes, maturity, factor and cluster analyses.

Serbian Chemical Society member.
* Corresponding author. E-mail: vitor@chem.bg.ac.yu
doi: 10.2298/JSC0712237S

INTRODUCTION

Due to the advancement of instrumental methods, such as gas chromatography (GC), gas chromatography–mass spectrometry (GC–MS), and recently GC–MS–MS, very small (ppm) amounts of crude oil components were identified. On the other hand, biosphere → geosphere transformation processes of a large number of petroleum constituents were explained. Evidently, in addition to origin, the chemical composition of crude oils and thus their physical and physicochemical properties depended on the depositional environment, length of migration path, thermal maturation, microbiological degradation, water washing, and lithology, temperature and pressure of the source and reservoir rocks.[1,2]

From the point of view of exploration studies, crude oil thermal maturation may be considered as one of the most important geochemical effects. Maturation processes involve cracking, isomerization and aromatization reactions, as well as alkylation and dealkylation of aromatic rings. They commence in the source rocks; continue during migration and in the reservoir rocks. During a long geological time, they have been affected by heat, pressure and mineral catalysts,[3–5] which resulted in the formation of thermodynamically more stable structural and stereochemical isomers or smaller molecules, as well as in transformation of saturated into aromatic hydrocarbons. The degree of maturity is most often estimated on the basis of parameters calculated from the distribution and abundance of saturated[6–8] and aromatic hydrocarbons,[9–16] *i.e.*, compounds which generally constitute 95−98 % of crude oils.

Isomerization processes at chiral centers or in rings were used in maturity estimation more often compared to cracking reactions, aromatization or alkylation–dealkylation processes.[2] Parameters based on these processes also served for corresponding correlations with vitrinite reflectance and depth of source rocks, as well as with the maximal expulsion temperature of hydrocarbons. Moreover, they also help in obtaining a better evaluation of reservoir potentials and contribute to reducing the number of dry boreholes.[17–20]

A great number of different maturity parameters were hitherto proposed. However, practically all of them were shown to perhaps depend on several of the above-mentioned factors. Moreover, equilibria of a number of isomerization reactions, *e.g.*, moretanes → hopanes; $22R \rightarrow 22S$ hopanes; $14\alpha(\mathrm{H})17\alpha(\mathrm{H}) \rightarrow$ $\rightarrow 14\beta(\mathrm{H})17\beta(\mathrm{H})$ steranes; $20R \rightarrow 20S$ steranes, are attained before the end of catagenetic changes of organic matter of the source rock. Therefore, reliable evaluation of maturity parameters and their applicability in oil–oil and oil–source rock correlations required the simultaneous critical consideration of all known maturity parameters.[2,16]

In this paper, the applicability of almost all the hitherto known maturity parameters, based on the distribution and abundance of saturated and aromatic hydrocarbons, was investigated using as an example 23 crude oil samples origin-

nating from the Serbian part of the Pannonian Basin (14 from Vojvodina localities and 9 from the Drmno Depression). For this purpose, different advanced multivariate statistical methods[18,21–27] were available. A new statistical approach was chosen, based on factor and cluster analyses. The investigated oils were finally correlated according to maturity, using simultaneously all statistically selected crude oil maturity parameters.

EXPERIMENTAL

The most important oil and gas deposits in Serbia were discovered in the Banat Depression (south–eastern part of the Pannonian Basin). The major part of the Banat Depression is located on the territory of Vojvodina (north of the Sava and Danube rivers), while its smaller, southern part, is situated in the vicinity of the city of Požarevac (south of the Sava and Danube), forming the separate, smaller, Drmno Depression (Fig. 1).

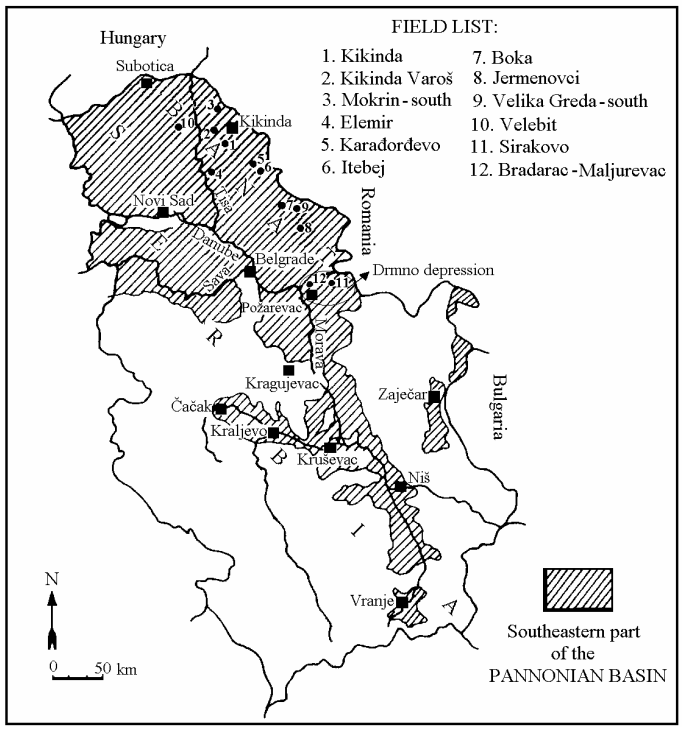

Fig. 1. Serbian Part of the Pannonian Basin with the localities of oil fields indicated.

The Banat Depression, with a surface of approximately 13,500 km^2, is located in the south–eastern part of the Pannonian Basin. Twenty-three samples of crude oils from twelve Banat Depression oil fields were investigated in this study, 14 samples originating from localities in Vojvodina, and 9 samples from Drmno Depression localities. The crude oil samples originated from reservoir rocks located at depths of 752–2572 m. All Drmno depression crude oils were found in reservoir rocks of Miocene age, and the crude oils from the Vojvodina localities in reservoir rocks of Paleozoic, Mesozoic, Miocene and Pliocene ages. The stratigraphy of the Drmno Depression has previously been studied in detail and the source rocks of the corresponding crude oils were identified.[28-34] Crude oils from boreholes Bradarac–Maljurevac 2 and 4 originated from Red Formations. By seis-

mic investigation, a large fault was discovered between these two boreholes (2 and 4). The boreholes Sirakovo 1, 2 and 18 are located in one zone, *i.e.*, in a deeper, faulty zone, whereas the boreholes Sirakovo 19 and 20 are situated in another, shallower zone of the Ottnangian–Carpathian sediments. Badenian oil deposits were found at depths of 1804–1808 and 1985–1989 m.[29,30,35] Detailed stratigraphic relationships between the Vojvodina Banat Depression crude oils have hitherto not been determined. The locations of their source rocks are still unknown.

The list of the investigated samples, including data on depths, temperature, lithology and age of the corresponding reservoir rocks, is given in Table I. The locations of the corresponding oil fields are shown in Fig. 1.

TABLE I. The investigated crude oil samples with the corresponding basic geological characteristics

	Sample	Oil field	Borehole	Depth, m	Reservoir temp., °C	Lithology	Age
VOJVODINA	V1	Kikinda	23	1196–1200	105.0	Sandstone	Pliocene
	V2	Kikinda	49	1730–1781	–	Sand	Pliocene
	V3	Kikinda-Varoš	3	1897–1942	108.0	Shale	Paleozoic
	V4	Velebit	87	753–759	61.4	Sand	Pliocene
	V5	Velebit	98	752–758	–	Sand	Pliocene
	V6	Velebit	120	756–758	–	Sand	Miocene
	V7	Mokrin-south	8	2040–2047	116.0	Conglomerate	Miocene
	V8	Mokrin-south	11	2040–2045	117.0	Sandstone	Miocene
	V9	Jermenovci	1	896–899	61.7	Marly sandstone	Miocene
	V10	Boka	37/2	1196–1206	76.9	Sandstone, limestone	Miocene
	V11	Karađorđevo	10	2557–2572	139.2	Sandstone	Mesozoic
	V12	Itebej	8	2190–2198	126.6	Aleurolite	Mesozoic
	V13	Elemir	19	1657–1668	99.0	Sandstone	Miocene
	V14	Velika Greda-south	20	1006–1010	60.4	Large-grain sandstone, conglomerate	Miocene
DRMNO – POŽAREVAC	PO1	Sirakovo	1	1778–1782	101.9	Sandstone, aleurolite, breccia, conglomerate	Miocene (Ottnangian–Carpathian)
	PO2	Sirakovo	2	1701–1704	98.0	Sandstone, aleurolite, breccia, conglomerate	Miocene (Ottnangian–Carpathian)
	PO3	Sirakovo	18	1544-1548	92.2	Sandstone, marlstone, aleurolite, limestone	Miocene (Ottnangian–Carpathian)
	PO4	Sirakovo	19	1429–1436	85.8	Sandstone, marlstone, aleurolite, limestone	Miocene (Ottnangian–Carpathian)
	PO5	Sirakovo	20	1440–1444	87.8	Sandstone, marlstone, aleurolite, limestone	Miocene (Ottnangian–Carpathian)

TABLE I. Continued

	Sample	Oil field	Borehole	Depth, m	Reservoir temp., °C	Lithology	Age
DRMNO – POŽAREVAC	PO6	Bradarac–Maljurevac	2	2302–2307	121.9	Crystalline rock	Miocene (Red Formations)
	PO7	Bradarac–Maljurevac	4	2156–2170	116.0	Marlstone, sandstone, breccia, conglomerate	Miocene (Red Formations)
	PO8	Bradarac–Maljurevac	5	1985–1989	107.0	Sandstone, aleurolite, breccia, conglomerate	Miocene (Baden)
	PO9	Bradarac–Maljurevac	10	1804–1808	99.0	Sandstone, aleurolite, breccia, conglomerate	Miocene (Baden)

The separation and purification of the saturated and aromatic fractions of the crude oils, as well as the GC and GC–MS techniques, which were used for analyses of *n*-alkanes, isoprenoids, steranes, terpanes, and individual alkylarenes, were explained in detail in previous papers.[34,36,37]

Based on the distribution and abundance of saturated biomarkers and alkylarenes, numerous maturity parameters were calculated. The values of these parameters observed for the examined Banat Depression crude oils are shown in Tables II and III.

RESULTS AND DISCUSSION

Factor analyses using varimax rotation (program SPSS 11.5 for Windows)[21,23,25] of the maturity parameters based on the abundance of (a) *n*-alkanes and isoprenoids, (b) steranes and triterpanes, (c) alkylnaphthalenes, and finally (d) alkylphenanthrenes were first run separately.

Factor analysis of n-*alkane and isoprenoid maturity parameters*

The factor analysis of maturity parameters calculated on the basis of the distribution and abundance of *n*-alkanes and isoprenoids (Table II) resulted in two statistically important "maturity factors":

$$F_{1\text{alkanes+isoprenoids}} = 0.95\text{CPI} + 0.90\text{CPI } 1 + 0.76\text{Phyt}/n\text{-C}_{18} + 0.37\text{Pr}/n\text{-C}_{17} - - 0.09\text{Pr/Phyt} - 0.02\Sigma\text{odd}(n\text{-C}_{21} - n\text{-C}_{33})/\Sigma\text{even}(n\text{-C}_{12} - n\text{-C}_{20})$$

and

$$F_{2\text{alkanes+isoprenoids}} = 0.92\Sigma\text{odd}(n\text{-C}_{21} - n\text{-C}_{33})/\Sigma\text{even}(n\text{-C}_{12} - n\text{-C}_{20}) + 0.89\text{Pr}/n\text{-C}_{17} + + 0.57\text{Phyt}/n\text{-C}_{18} - 0.55\text{Pr/Phyt} + 0.19\text{CPI } 1 - 0.03\text{CPI}$$

characterized by variances of 40.50 % and 38.56 %, respectively. As the cited formulae show, the first factor was defined by high loadings (> 0.70) of the parameters CPI and CPI 1, which represented the ratios of the odd *vs.* the even *n*-alkane homologues (in the C_{14}–C_{35} and C_{15}–C_{17} ranges, respectively), and the phytane/*n*-C_{18} ratio. "Maturity factor" 2 was determined by high loadings (> 0.80) of the ratio of higher odd members (*n*-C_{21}–*n*-C_{33}) *vs.* lower even members (*n*-C_{12}–*n*-C_{20}) of *n*-alkane homologous series, and the pristane/*n*-C_{17} ratio.

TABLE II. Maturation parameters calculated from the distributions and abundances of saturated biomarkers

Sample	CPI	CPI 1	$\Sigma_{odd}(n\text{-}C_{21}–n\text{-}C_{33})/\Sigma_{even}(n\text{-}C_{12}–n\text{-}C_{20})$	Pr/Phyt	Pr/n-C_{17}	Phyt/n-C_{18}	$C_{29}\alpha\alpha(S)/(\alpha\alpha(S)+\alpha\alpha(R))$	$C_{29}\beta\beta(R)/(\beta\beta(R)+\alpha\alpha(R))$	C_{27}dia/dia+ster	$C_{31}(S)/((S)+(R))$	C_{30}M/C_{30}H	C_{29}M/C_{29}H	Ts/(Ts+Tm)	C_{29}Ts/C_{29}H
V1	1.05	0.83	0.69	1.25	0.50	0.46	0.45	0.55	0.26	0.59	0.11	0.09	0.46	0.27
V2	1.05	0.85	0.61	1.19	0.51	0.50	0.44	0.54	0.21	0.58	0.13	0.10	0.46	0.25
V3	1.08	0.92	0.54	1.53	0.46	0.35	0.50	0.57	0.31	0.58	0.10	0.09	0.53	0.33
V4	1.16	1.11	1.72	0.64	9.48	42.77	0.49	0.57	0.27	0.59	0.14	0.09	0.53	0.29
V5	1.31	1.04	1.61	0.70	9.59	44.37	0.49	0.57	0.29	0.59	0.10	0.10	0.56	0.31
V6	1.20	0.97	1.49	0.95	14.65	46.93	0.48	0.57	0.26	0.59	0.11	0.10	0.55	0.32
V7	1.08	0.86	0.51	1.58	0.33	0.25	0.49	0.57	0.33	0.59	0.10	0.08	0.57	0.38
V8	1.11	0.95	0.49	1.73	0.39	0.27	0.51	0.57	0.35	0.60	0.10	0.08	0.59	0.37
V9	0.98	0.86	7.09	0.90	24.04	25.29	0.35	0.39	0.07	0.58	0.14	0.12	0.34	0.21
V10	0.97	0.77	1.26	0.56	0.60	1.17	0.33	0.34	0.03	0.57	0.15	0.14	0.17	0.18
V11	1.02	0.80	0.69	1.05	0.87	0.90	0.47	0.49	0.13	0.60	0.11	0.11	0.32	0.17
V12	1.08	0.92	0.61	1.24	0.84	0.73	0.48	0.56	0.17	0.60	0.10	0.15	0.33	0.18
V13	1.03	0.84	0.75	1.15	0.81	0.70	0.50	0.59	0.23	0.58	0.10	0.15	0.37	0.17
V14	1.04	0.92	2.09	1.72	6.63	3.99	0.39	0.46	0.13	0.60	0.11	0.10	0.44	0.25
PO1	1.06	0.79	0.75	2.41	0.16	0.08	0.57	0.56	0.52	0.60	0.13	0.08	0.46	0.76
PO2	1.01	0.70	0.84	1.45	0.12	0.08	0.53	0.54	0.51	0.61	0.14	0.10	0.48	0.70
PO3	0.93	0.73	0.35	1.35	0.14	0.14	0.46	0.56	0.18	0.61	0.13	0.09	0.39	0.43
PO4	1.00	0.81	0.99	1.09	0.14	0.13	0.50	0.59	0.19	0.60	0.14	0.12	0.41	0.46
PO5	0.99	0.80	0.86	0.87	0.12	0.15	0.47	0.58	0.17	0.61	0.12	0.09	0.41	0.44
PO6	1.00	0.76	0.81	2.09	0.22	0.13	0.55	0.60	0.57	0.62	0.12	0.09	0.54	0.81
PO7	0.98	0.72	1.12	0.76	0.30	0.40	0.45	0.39	0.04	0.61	0.14	0.08	0.24	0.20
PO8	1.01	0.74	1.03	1.19	0.16	0.16	0.48	0.59	0.19	0.61	0.12	0.11	0.43	0.45
PO9	0.81	0.79	0.64	0.87	1.02	0.59	0.45	0.56	0.12	0.60	0.12	0.08	0.11	0.07

CPI = 1/2 $[\Sigma_{odd}(n\text{-}C_{15}–n\text{-}C_{33})/\Sigma_{even}(n\text{-}C_{14}–n\text{-}C_{32}) + \Sigma_{odd}(n\text{-}C_{15}–n\text{-}C_{33})/\Sigma_{even}(n\text{-}C_{16}–n\text{-}C_{34})]$; CPI 1 = 1/2 $[(n\text{-}C_{15}+n\text{-}C_{17})/n\text{-}C_{16}]$; Pr – Pristane; Phyt – Phytane; $C_{29}\alpha\alpha(R)$ – $C_{29}14\alpha$(H)17α(H)20(R)-sterane; $C_{29}\alpha\alpha(S)$ – $C_{29}14\alpha$(H)17α(H)20(S)-sterane; $C_{29}\beta\beta(R)$ – $C_{29}14\beta$(H)17β(H)20(R)-sterane; ster – $C_{27}14\alpha$(H)17α(H)20(R)-sterane; C_{27}dia – $C_{27}13\beta$(H)17α(H)20(S)-diasterane; $C_{31}(S)$ – $C_{31}17\alpha$(H)21β(H)22(S)-hopane; $C_{31}(R)$ – $C_{31}17\alpha$(H)21β(H)22(R)-hopane; C_{30}H – $C_{30}17\alpha$(H)21β(H)--hopane; C_{30}M – $C_{30}17\beta$(H)21α(H)-moretane; C_{29}H – $C_{29}17\alpha$(H)21β(H)-hopane; C_{29}M – $C_{29}17\beta$(H)21α(H)-moretane; Ts – $C_{27}18\alpha$(H)-22,29,30-trisnorneohopane; Tm – $C_{27}17\alpha$(H)-22,29,30-trisnorhopane; C_{29}Ts – $C_{29}18\alpha$(H)-30-norneohopane

TABLE III. Maturation parameters calculated from the distributions and abundances of di- and tricyclic aromatic hydrocarbons (an explanation of the abbreviations is given in the Appendix)

Sample	MNR	ENR	DNR 1	α/βDN 1	DNx	TNR 1	TNR 2	TNR 3	TNy	MPI 1	MPI 3	MPR 1	DMPI 1	DMPI 2	PAI 1	MDR	MTR
V1	1.51	1.87	2.82	0.41	4.25	0.27	0.56	3.11	2.54	0.85	1.17	1.38	1.19	0.36	2.05	1.02	2.94
V2	1.54	1.92	2.97	0.53	4.33	0.37	0.67	2.17	2.63	0.87	1.20	1.41	1.12	0.45	2.04	0.91	3.43
V3	1.57	1.95	2.44	0.47	4.37	0.36	0.61	3.33	2.65	0.86	1.25	1.43	0.99	0.43	1.90	0.94	2.85
V4	1.23	0.85	2.13	0.62	3.23	0.59	0.82	2.83	2.13	0.72	0.83	1.00	1.25	0.57	2.49	0.79	2.29
V5	1.28	0.86	2.62	0.55	3.77	0.23	0.76	2.89	2.28	0.75	0.87	1.02	1.09	0.44	2.50	0.85	2.51
V6	1.25	0.87	1.84	0.66	3.23	0.56	0.84	3.16	2.09	0.71	0.90	1.07	1.07	0.44	2.13	0.78	2.14
V7	1.82	3.80	6.62	0.21	7.19	0.25	0.67	3.22	3.07	0.90	1.41	1.69	0.63	0.39	1.79	1.76	5.68
V8	1.75	3.22	3.84	0.30	7.10	0.77	0.99	2.48	3.04	0.87	1.37	1.64	0.61	0.38	1.73	1.75	3.70
V9	0.80	0.78	1.61	0.94	2.36	0.44	0.76	0.92	1.66	0.65	0.77	0.83	1.20	0.47	2.30	0.74	1.34
V10	0.93	0.82	1.17	0.84	2.48	0.42	0.47	2.63	1.97	0.80	0.80	0.92	0.87	0.25	3.54	0.74	1.62
V11	1.37	1.99	1.53	0.89	4.07	0.74	0.79	1.21	2.51	0.79	1.07	1.31	1.04	0.53	1.99	1.22	3.01
V12	1.63	1.96	1.28	1.09	4.79	0.65	0.76	1.46	2.67	0.88	1.26	1.45	1.35	0.38	1.97	1.14	2.86
V13	1.53	1.91	1.73	0.99	4.31	0.59	0.77	2.70	2.60	0.88	1.19	1.40	1.43	0.64	2.14	1.23	2.79
V14	1.14	0.97	1.62	1.11	2.90	0.21	0.58	2.51	2.03	0.69	0.81	0.97	1.00	0.31	2.39	0.86	2.56
PO1	1.61	1.67	4.34	0.33	4.38	1.18	0.87	1.80	2.61	0.86	1.27	1.48	0.92	0.23	1.87	1.95	7.26
PO2	1.65	2.19	7.11	0.24	6.53	1.23	0.90	1.82	2.73	0.76	1.27	1.23	0.69	0.51	1.52	3.42	5.40
PO3	2.20	4.18	9.50	0.20	7.29	1.47	0.94	5.80	3.07	0.87	1.33	1.61	1.19	0.44	1.80	2.43	5.24
PO4	1.98	2.95	5.82	0.19	7.81	1.50	0.99	3.74	3.08	1.23	1.49	1.88	1.37	0.55	3.02	1.03	3.44
PO5	2.22	3.11	6.32	0.20	10.21	1.55	0.92	4.35	3.07	1.12	1.66	1.91	1.02	0.45	2.17	1.44	6.06
PO6	1.43	2.23	3.74	0.45	2.88	1.18	0.85	1.87	2.33	0.85	0.99	1.11	1.13	0.49	2.67	0.73	1.52
PO7	1.19	2.35	2.31	0.42	3.98	1.15	0.82	1.33	2.20	0.67	0.81	0.99	0.79	0.26	2.21	0.84	1.75
PO8	1.44	1.84	3.17	0.31	5.39	1.48	0.98	3.09	2.90	0.90	1.14	1.28	1.02	0.43	2.39	0.85	2.35
PO9	1.73	5.82	2.33	0.33	7.37	1.06	0.67	5.38	2.96	1.17	1.44	1.70	1.32	0.42	2.91	0.76	1.36

Parameter Pr/Phyt was found to have no importance as a maturity indicator, a fact which could have been expected, since it has often been shown that this ratio, in addition to maturation, significantly depends on depositional environment and origin.[2,38] Moreover, it was shown earlier, with Drmno Depression crude oils only, that this ratio may be used as a maturity parameter only for oils generated during the early stage of catagenesis.[39–43] Due to categorization into Factor 1, parameters CPI, CPI 1 and Phyt/*n*-C_{18} may be supposed to be more reliable as maturity indicators for the Banat Depression crude oils, compared to parameters Σodd(*n*-C_{21} − *n*-C_{33})/Σeven(*n*-C_{12} − *n*-C_{20}) and Pr/*n*-C_{17}, which, based on high loadings, defined Factor 2. Such a presumption is corroborated by the fact that in "maturity Factor" 2, the loadings value of the Pr/Phyt ratio was significantly higher than in Factor 1 (0.57 *vs.* 0.09), indicating that Factor 2 involved alkane parameters which, in addition to maturation, significantly depend on the depositional environment and origin. A better applicability of Phyt/*n*-C_{18} parameters compared to the analogous Pr/*n*-C_{17} in maturity estimation of crude oils and sediments from the Serbian part of the Pannonian Basin was already observed in earlier investigations.[43,44] This observation may be explained by the fact that most of these samples have a relatively high content of pristane, due to genetic factors and depositional environment effects, a fact which certainly limits the application of the Pr/*n*-C_{17} ratio as a maturity indicator.

Factor analysis of sterane and terpane maturity parameters

Factor analysis of maturity parameters calculated based on the distribution and abundance of sterane and terpane biomarkers (Table II) resulted in two statistically important "maturity factors":

$$F_{1\text{steranes+terpanes}} = 0.92C_{29}\text{Ts}/C_{29}\text{H} + 0.77C_{31}(S)/((S)+(R)) + 0.73C_{27}\text{dia}/(\text{dia+ster}) + \\ + 0.69C_{29}\alpha\alpha(S)/(\alpha\alpha(S)+\alpha\alpha(R)) - 0.51C_{29}\text{M}/C_{29}\text{H} + 0.39C_{29}\beta\beta(R)/(\beta\beta(R)+\alpha\alpha(R)) + \\ + 0.38\text{Ts}/\text{Ts+Tm} + 0.30C_{30}\text{M}/C_{30}\text{H}$$

and

$$F_{2\text{steranes+terpanes}} = -0.86C_{30}\text{M}/C_{30}\text{H} + 0.78C_{29}\beta\beta(R)/(\beta\beta(R)+\alpha\alpha(R)) + \\ + 0.72\text{Ts}/(\text{Ts+Tm}) + 0.61C_{29}\alpha\alpha(S)/(\alpha\alpha(S)+\alpha\alpha(R)) + 0.53C_{27}\text{dia}/(\text{dia+ster}) - \\ - 0.20C_{29}\text{M}/C_{29}\text{H} + 0.14C_{29}\text{Ts}/C_{29}\text{H} - 0.08C_{31}(S)/((S)+(R))$$

characterized by variances of 38.54 % and 32.38 %, respectively.

High loadings (> 0.65) in the first "maturity factor" were observed for parameters based on isomerization reactions on chiral carbon atoms in the side chains of C_{29} sterane and C_{31} hopane (20R → 20S; 22R → 22S), as well as for ratios of typical geoisomers, C_{27} diasterane and C_{29}Ts, and the corresponding precursors of C_{27} regular sterane or C_{29} hopane. The second factor was determined, with high loadings values (> |0.70|), by parameters based on higher energy demanding

isomerizations in rings ($\alpha\alpha \rightarrow \beta\beta C_{29}$-steranes and $C_{30}\beta\alpha$-moretanes $\rightarrow C_{30}\alpha\beta$-hopanes) and the Ts/(Ts+Tm) ratio. Separation of the related parameters $C_{29}Ts/C_{29}H$ and Ts/(Ts + Tm) into different factors confirmed that the difference in stability of Ts and Tm (3.8 kJ mol^{-1}) is higher than in the case of C_{29}Ts and C_{29}-hopane.[45] Consequently, the transformation Tm $\rightarrow$ Ts requires more energy, a fact which explains the finding of the Ts/(Ts+Tm) ratio in Factor 2. The ratio of $C_{29}\alpha\alpha$-sterane *S- vs. R*-isomers, in addition to significant loadings in Factor 1, showed a certain degree of significance in Factor 2 as well (loadings of 0.61), confirming a well-known geochemical fact that isomerization reactions in sterane biomarkers side chains, as higher energy demanding, occur during advanced catagenesis, compared to analogous terpane maturation transformations.[15,16,46] Formulae $F_{1steranes+terpanes}$ and $F_{2steranes+terpanes}$ show that the C_{29}-moretane *vs.* C_{29}-hopane ratio has no critical value for a significant loading of 0.60 or 0.70 in either of the two factors. This is not surprising, due to the fact that earlier it was shown that the C_{29}-terpane content in crude oils significantly depends on origin as well, and that it is considerably higher in crude oils originating from calcareous deposits.[47]

Factor analysis of alkylnaphthalene maturity parameters

The factor analysis of diarene maturity parameters (Table III) resulted in two statistically important "maturity factors":

$$F_{1alkylnaphthalenes} = 0.86ENR + 0.84MNR + 0.83TNR\,3 + 0.83TNy + 0.83DNx - - 0.64\alpha/\beta DN\,1 + 0.63DNR\,1 + 0.29TNR\,1 + 0.07TNR\,2$$

and

$$F_{2alkylnaphthalenes} = 0.94TNR\,2 + 0.84TNR\,1 + 0.56DNR\,1 - 0.52\alpha/\beta DN\,1 + 0.44DNx + 0.42MNR + 0.38TNy + 0.16ENR - 0.04TNR\,3$$

characterized by variances of 49.12 % and 30.28 %, respectively. Factor 1 was determined by high loadings of maturity parameters based on isomerization of thermodynamically less stable methyl- (MN), dimethyl- (DMN), trimethyl- (TMN) and ethylnaphthalenes (EN) with alkyl groups in the α-position into the corresponding thermodynamically more stable β-isomers. Specifically, parameters MNR, DNx, TNR 3, TNy and ENR, characterized by the highest loadings in the more significant "maturity factor", comprise isomerization of just one aromatic ring alkyl substituent (α-MN $\rightarrow$ β-MN; $\alpha\alpha$-DMN $\rightarrow$ $\alpha\beta$-DMN; $\alpha\beta\alpha$-TMN $\rightarrow$ $\alpha\beta\beta$-TMN; α-EN $\rightarrow$ β-EN). Parameters α/βDN 1 and DNR 1, also conforming with the loadings limit of 0.60 in Factor 1, though with less significance compared to the above mentioned parameters, comprise isomerization of two methyl groups on the naphthalene ring ($\alpha\alpha$-DMN $\rightarrow$ $\beta\beta$-DMN), a change requiring more energy. Consequently, it is not surprising that the loadings values of α/βDN 1 and DNR 1 parameters are close to the significance limit value in Factor 2 as well. Factor 2 is determined by the parameters TNR 1 and TNR 2, also based on isomerization of

two methyl groups ($\alpha\beta\alpha$-TMN $\rightarrow$ $\beta\beta\beta$-TMN). However, in this case the thermodynamically most stable $\beta\beta\beta$-isomer, *i.e.*, 2,3,6-TMN, the formation of which requires the most energy, is also involved.

Factor analysis of alkylphenanthrene maturity parameters

The factor analysis of the phenanthrene maturity parameters (Table III) resulted in three statistically important "maturity factors":

$F_{1alkylphenanthrenes}$ = 0.96MPI 1 + 0.95MPR 1 + 0.92MPI 3 + 0.47MTR +
+ 0.20MDR + 0.15DMPI 1 + 0.06DMPI 2 + 0.05PAI 1
$F_{2alkylphenanthrenes}$ = −0.90PAI 1 + 0.88MDR + 0.75MTR – 0.48DMPI 1 +
+ 0.35MPI 3 + 0.24MPR 1 − 0.20MPI 1 + 0.11DMPI 2

and

$F_{3alkylphenanthrenes}$ = 0.93DMPI 2 + 0.73DMPI 1 − 0.23MTR + 0.14MPI 1 −
– 0.08MDR + 0.07MPI 3 + 0.07MPR 1 − 0.05PAI 1

characterized by variances of 37.22 %, 32.38 % and 18.62 %, respectively. The most important triarene "maturity factor" was defined by the MPI 1, MPR 1 and MPI 3 ratios, based on the isomerization of one methyl group in the thermodynamically less stable α-methylphenanthrenes (1-MP and 9-MP), into the corresponding more stable isomers with the methyl group in the β-position (2-MP and 3-MP). Factor 2 was determined by high loadings of the MTR and MDR parameters, based on dealkylation reactions of trimethyl- (TMP) and dimethylphenanthrene (DMP) into the corresponding methylphenanthrenes (MP), as well as the PAI 1 ratio, based on the alkylation–dealkylation transformation phenanthrene (P) $\leftrightarrows$ methylphenanthrenes (MP). In a number of investigations, it was shown that dealkylation processes requiring more energy occurred at more advanced thermal maturity, compared to the isomerizations α-MP $\rightarrow$ β-MP.[5,11,36,37,46,48] Hence, generally, factor analysis of maturity parameters calculated on the basis of the distribution of different types of petroleum hydrocarbons clearly indicates the energy changes required for individual maturation processes.

In the last, Factor 3, high loadings values were observed with dimethylphenanthrene indexes DMPI 1 and DMPI 2, also defined by isomerizations ($\alpha \rightarrow \beta$) in dimethylphenanthrene molecules. The low percent of variance (18.62 %) in this case was not surprising, considering the fact that the corresponding parameters involved a large number of isomers of different stability (see Appendix), which co-eluted during the GC and GC–MS analyses.

Re-evaluation of all extracted "maturity factors"

All "maturity factors" observed in individual factor analyses showing higher than 30 % of variance (*i.e.*, all factors extracted from separate analyses, except $F_{3alkylphenanthrenes}$), were involved in another factor analysis, and also in cluster

analysis using the Ward method (Table IV, Fig. 2). In this way, all maturity parameters based on saturated biomarkers and alkylarenes were re-evaluated, considering the fact that the observed "maturity factors" represented their linear combinations. For this purpose, a loadings value of |0.70| was taken as the significance limit, aimed at a more reliable consideration of "maturity factors".

TABLE IV. Results of the final factor analysis of "maturity factors" based on saturated biomarkers and alkylarenes maturity parameters

Varimax rotated component matrix			
Variables	Factor (% of variance)		
	1 (29.07)	2 (26.80)	3 (22.86)
$F_{1alkanes+isoprenoids}$	–0.32	–0.10	0.83
$F_{2alkanes+isoprenoids}$	–0.65	–0.31	–0.37
$F_{1steranes+terpanes}$	0.10	0.90	–0.06
$F_{2steranes+terpanes}$	0.29	0.03	0.89
$F_{1alkylnaphtalenes}$	0.92	–0.02	0.03
$F_{2alkylnaphtalenes}$	0.03	0.88	–0.20
$F_{1alkylphenanthrenes}$	0.92	0.08	–0.14
$F_{2alkylphenanthrenes}$	0.09	0.67	0.36

The most important Factor 1 in the final factor analysis was defined by the $F_{1alkylnaphthalenes}$ and $F_{1alkylphenanthrenes}$ factors (loadings > 0.90), which represented linear combinations of parameters based on isomerization of one alkyl group from the α- into β-positions in the aromatic rings of MN, EN, DMN, TMN and MP (Table IV). Factor 2 was determined by high loadings of factor $F_{1steranes+terpanes}$, based on isomerization reactions in the aliphatic chains of saturated biomarkers, and transformations of steranes into diasteranes and C_{29}-hopane into C_{29}Ts, and factor $F_{2alkylnaphtalenes}$, based on the isomerization of two methyl groups $\alpha \rightarrow \beta$ in the rings of trimethylnaphthalenes, including the most stable $\beta\beta\beta$-isomer, 2,3,6-TMN. In the last significant factor, Factor 3, high loadings were observed with $F_{1alkanes+isoprenoids}$ and $F_{2steranes+terpanes}$, which includes the ratio of odd *vs.* even *n*-alkanes, the parameter Phyt/*n*-C_{18}, as well as parameters based on transformations in the rings of polycyclic saturated biomarkers (steranes and terpanes), and Tm $\rightarrow$ Ts (Table IV). The presumption derived from individual factor analysis of *n*-alkane and isoprenoid maturity ratios that parameters determining the factor $F_{2alkanes+isoprenoids}$ were not reliable maturity indicators was in this way corroborated, since the mentioned factor showed relatively low maximal loadings value (−0.65) compared with other "maturity factors" (Table IV). Also, the relatively low maximal loadings value observed for factor $F_{2alkylphenanthrenes}$ (0.67), defined by alkylation–dealkylation methylphenanthrene processes, compared to other "maturity factors", was not surprising,

since it was often suggested that during catagenesis alkylation reactions occur first on the phenanthrene ring and only later, in the stage of the "oil window", the reaction changes direction into the reverse dealkylation process. Application of dealkylation phenanthrene parameters as maturity indicators is, therefore, limited only to crude oils characterized by higher degrees of thermal maturity,[5,11,36,46] which is in agreement with their smaller significance in the factor analysis.

Hierarchy within the observed factors/parameters was additionally checked by cluster analysis using the Ward method (Fig. 2).

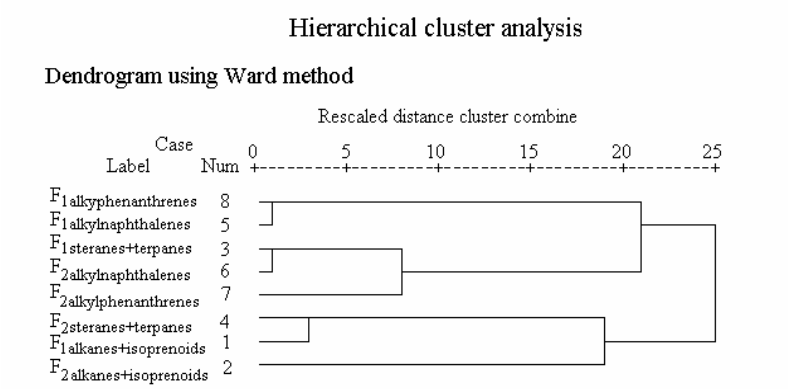

Fig. 2. Dendrogram from cluster analysis using the Ward method of "maturity factors" based on maturity parameters of saturated biomarkers and alkylarenes.

Two groups of "maturity factors" clearly separated in the dendrogram, which are shown in Fig. 2. The first group is composed of "maturity factors" which, showing high loadings values, defined Factors 1 and 2 in the collective factor analysis (Table IV). "maturity factors" which showed significant loadings values in Factor 3 of the collective factor analysis (Table IV), formed the second group. The "maturity factor" $F_{2alkanes+isoprenoids}$ joined the latter group as a special member, confirming that the parameters Pr/*n*-C_{17} and Σodd(*n*-C_{21}−*n*-C_{33})/ /Σeven(*n*-C_{12}−*n*-C_{20}) which define it, are less important in the estimation of the maturity of Banat depression crude oils. Fig. 2 also shows that the factors in the first group are divided into two subgroups, which completely correspond with high loadings "maturity factors" in Factor 1 and 2 from the collective factor analysis (Table IV). Finally, the distance of the "maturity factor" $F_{2alkylphenanthrenes}$, based on dealkylation reactions of TMP, DMP and MP, from factors $F_{1steranes+terpanes}$ and $F_{2alkylnaphthalenes}$ (Fig. 2) is in concordance with the lower loadings value of this "maturity factor" in Factor 2 in the collective factor analysis (Table IV). These observations indicate the full agreement of the results of factor and cluster analyses of "maturity factors" and confirmed the maturity parameters based on the isomerization of one methyl group from *α*- into *β*-positions

in naphthalene and phenanthrene aromatic rings to be most reliable in the investigation of the thermal maturity of crude oils originating from the Serbian part of the Pannonian Basin.

Correlation of the investigated oils based on maturity parameters

The investigated crude oils were classified according to maturity, using for this purpose factor and cluster analyses, and taking into consideration, simultaneously, all eight "maturity factors" from the individual factor analyses showing variances higher than 30 %, *i.e*, all parameters calculated on the basis of the distribution and abundance of constituting saturated and aromatic hydrocarbons (Fig. 3).

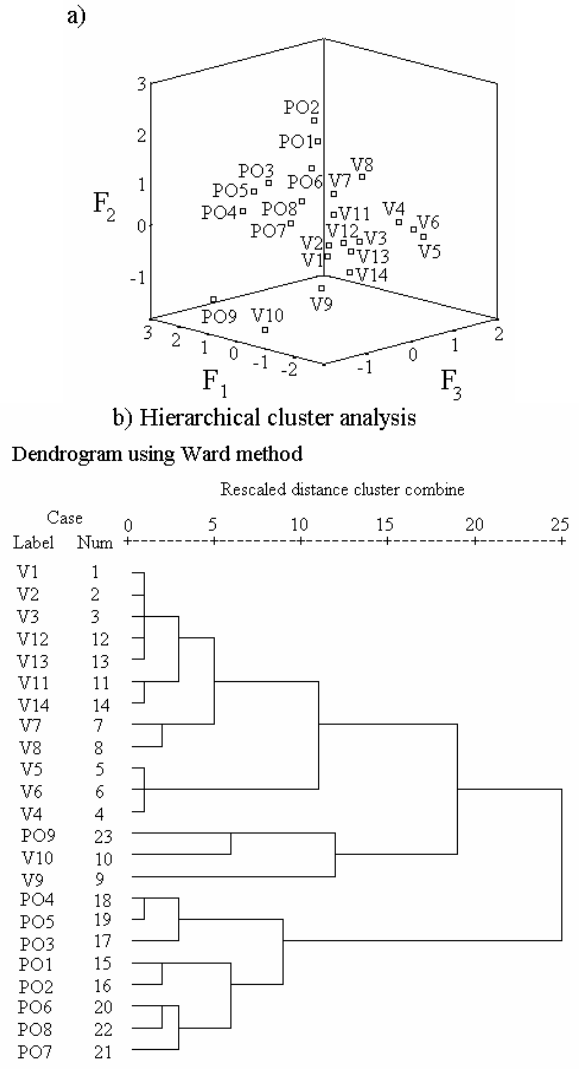

Fig. 3. Correlation of investigated oils according to maturity using factor (a) and cluster (b) analyses of all "maturity factors".

Based on factor analysis, a 3D diagram was constructed, the axes of which represent three factors derived from collective factor analysis (Fig. 3; Table IV). In Fig. 3, three groups of oils are clearly distinguished: the first composed of samples from the Drmno Depression (PO1–PO8); the second composed of samples from the localities Jermenovci (V9), Boka (V10), and one single crude oil from the Drmno Depression (PO9); the third included all the other investigated Vojvodina crude oils. Within the last (third) group, the crude oils V4–V6, from the Velebit locality, are somewhat separated.

The observed categorization showed the Drmno Depression crude oils to differ from the Vojvodina crude oils not only according to their genetic type, but also according to their thermal maturity. Moreover, in this way, the presumption is confirmed that South Banat crude oils, in the first place the oils from Jermenovci and Boka, differ from North Banat and Bačka crude oils.[40,49] The exceptional close relation of sample PO9 from the Drmno Depression with the South Banat crude oils (Fig. 3a) indicates a certain connection of the samples originating from these two localities, a fact also observed in geological investigations (A. Kostić, personal communication). The finding of the Velebit crude oils in a separate subgroup is also in agreement with up-to-date geological and geochemical investigations, which, on the one hand, suggested homogeneity of this oil field, and, on the other, differences from North Banat crude oils.[25,40,50]

The investigated oils were also classified by Ward cluster analysis (Fig. 3b) using all eight "maturity factors", *i.e.*, all constituting parameters. The results observed were in full accordance with the results obtained by factor analysis (Fig. 3a): the Drmno Depression crude oils PO1–PO8 were clearly separated, the exception being the sample PO9. Furthermore, within the "large" second dendrogram branch, a group of oils was observed composed of sample PO9 and South Banat oils Jermenovci and Boka (V9 and V10). A slight separation of Velebit oils was also observed. Hence, factor and cluster analyses were in full agreement in both the evaluation of maturity parameters, as well as in the maturity classification of the crude oils.

CONCLUSIONS

Crude oil maturity parameters based on the distribution and abundance of saturated biomarkers and alkyl arenes were evaluated using a novel approach in factor and cluster analyses. For this purpose, 23 samples of crude oils originating from the Serbian part of the Pannonian Basin were investigated. Furthermore, the investigated crude oils (from localities in Vojvodina and the Drmno Depression) were correlated by simultaneous consideration of a large number of selected "maturity" parameters.

The results of factor and cluster analyses suggested that parameters based on the isomerization of one alkyl group from α- into β-positions on the aromatic ring

of methylnaphthalenes, ethylnaphthalenes, dimethylnaphthalenes, trimethylnaphthalenes and methylphenanthrenes, were the most important parameters in maturity investigations of Banat Depression crude oils. They were followed by maturation indexes based on the isomerization on chiral centers ($R \rightarrow S$) in the side chains of polycyclic saturated sterane and terpane biomarkers, as well as ratios based on the isomerization of two methyl groups from α- into β-positions on the aromatic ring of trimethylnaphthalenes. The last statistically important factor was defined by ratios based on isomerization in the rings of polycyclic sterane and terpane alkanes and parameters CPI, CPI 1 and Phyt/*n*-C_{18}, calculated from the distribution and abundance of *n*-alkanes and isoprenoids.

The factor and cluster analyses indicated a limited applicability of indexes based on P, MP, DMP and TMP alkylation-dealkylation transformations, Pr/Phyt, and Pr/*n*-C_{17} parameters, and ratios of higher odd *vs.* even *n*-alkane members, in the maturity evaluation of crude oils from the Serbian part of the Pannonian Basin.

In individual factor analyses of parameters calculated on the basis of the distribution of individual types of saturated and aromatic hydrocarbons, good agreement was observed between the distribution of the parameters among the factors, and the energy necessary for the corresponding maturation changes.

Correlation of crude oils based on the simultaneous consideration of a large number of selected "maturity" parameters showed the Vojvodina and Drmno Depression crude oils to differ not only according to genetic type, but also according to thermal maturity.

According to maturity, three groups of samples were distinguished among the Vojvodina crude oils: North Banat localities, the Velebit oil field, and South Banat locality. Furthermore, certain similarities were observed in the thermal maturity of South Banat (Jermenovci and Boka) and Drmno Depression (Bradarac–Maljurevac) crude oils. Both conclusions are in agreement with presumptions based on geological investigations.

Acknowledgements. We thank Dr. Hermann Wehner (Federal Institute for Geosciences and Natural Resources) for his help with the GC–MS analyses. This work was supported in part by the Research Fund of the Republic of Serbia.

APPENDIX

MNR = 2-MN/1-MN[9]
ENR = 2-EN/1-EN[10]
DNR 1 = (2,6- + 2,7-DMN)/1,5-DMN[10]
α/βDN 1 = (1,4- + 1,5- + 1,8- + 2,3-DMN)/(2,6- + 2,7-DMN)[51]
DNx = (1,3- + 1,6-DMN)/(1,4- + 1,5-DMN)[43,52]
TNR 1 = 2,3,6-TMN/(1,3,5- + 1,4,6-TMN)[13]
TNR 2 = (1,3,7- + 2,3,6-TMN)/(1,3,5- + 1,3,6- + 1,4,6-TMN)[53]
TNR 3 = 1,3,6-TMN/1,2,5-TMN[12]
TNy = (1,3,6- + 1,3,7-TMN)/(1,3,5- + 1,4,6-TMN)[43,52]
MPI 1 = 1,5(2- + 3-MP)/(P+1- + 9-MP)[9]

MPI 3 = (2- + 3-MP)/(1- + 9-MP)[11]

MPR 1= 2-MP/1-MP[10]

DMPI 1 = 4(2,6- + 2,7- + 3,5- + 3,6-DMP + 1- + 2- + 9-EP)/(P+1,3- + 1,6- + 1,7- + 2,5- + + 2,9- + 2,10- + 3,9- + 3,10-DMP)[9]

DMPI 2 = (2,6- + 2,7- + 3,5-DMP)/(1,3- + 1,6- + 2,5- + 2,9- + 2,10- + 3,9- + 3,10-DMP)[10]

PAI 1 = (1- + 2- + 3- + 9-MP)/P[54]

MDR = ΣMP/ΣDMP[43,52]

MTR = ΣMP/ΣTMP[43,52]

MN – Methylnaphthalene; EN – ethylnaphthalene; DMN – dimethylnaphthalene; TMN – trimethylnaphthalene; P – phenanthrene; MP – methylphenanthrene; DMP – dimethylphenanthrene; EP – ethylphenanthrene.

И З В О Д

ЕВАЛУАЦИЈА МАТУРАЦИОНИХ ПАРАМЕТАРА ЗАСНОВАНИХ НА ЗАСИЋЕНИМ И АРОМАТИЧНИМ УГЉОВОДОНИЦИМА У КОРЕЛАЦИЈИ НАФТА–НАФТА (ЈУГОИСТОЧНИ ДЕО ПАНОНСКОГ БАСЕНА, СРБИЈА)

КСЕНИЈА СТОЈАНОВИЋ[1,2], БРАНИМИР ЈОВАНЧИЋЕВИЋ[2,3], ДРАГОМИР ВИТОРОВИЋ[2,3], YULIA GOLOVKO[4], GALINA PEVNEVA[4] и ANATOLY GOLOVKO[4]

[1]Медицински факултет Универзитета у Београду, Вишеградска 26, 11000 Београд, [2]ИХТМ – Центар за хемију, Његошева 12, 11000 Београд, [3]Хемијски факултет Универзитета у Београду, Студентски трг 12–16, 11000 Београд и [4]Institute of Petroleum Chemistry, 3, Academichesky Ave., 634055 Tomsk, Russia

У овом раду је, применом новог приступа у факторској и кластерској анализи, евалуиран значај матурационих параметара заснованих на расподели и обилности засићених биомаркера и алкиларена у корелацији нафта–нафта на примеру 23 узорка сирове нафте из дела Панонског басена у Србији (14 са локалитета у Војводини и 9 из депресије Дрмно). Факторске анализе су, уз примену varimax ротације, најпре извођене посебно са матурационим параметрима израчунатим из расподеле и обилности (а) *n*-алкана и изопреноидних алифатичних алкана, (б) стерана и тритерпана, (в) алкилнафталена и (г) алкилфенантрена. Ове анализе резултирале су са 9 значајних "матурационих фактора". Осам од њих, који су показивали проценат варијације већи од 30 %, укључени су у нову факторску и кластерску анализу, уз примену Ward методе. На тај начин су сви матурациони параметри засновани на расподели и обилности засићених биомаркера и алкиларена били процењени и рангирани, имајући у виду чињеницу да фактори представљају њихове линеарне комбинације. Резултати су показали да су за корелацију нафти из дела Панонског басена у Србији најзначајанији матурациони параметри засновани на изомеризацији једне алкил-групе из α- у термодинамички стабилније β-положаје на ароматичном прстену метилнафталена, етилнафталена, диметилнафталена, триметилнафталена и метилфенантрена. Такође, одређени су параметри/типови матурационих реакција који су у великој мери дефинисали факторе 2 и 3. Редослед и сагласност између фактора, односно параметара, проверена је и потврђена кластерском анализом уз примену Ward методе. Коначно, испитивани узорци сирове нафте су корелисани помоћу факторске и кластерске анализе, користећи све значајне "матурационе факторе". Разлике у степену термичке зрелости уочене су како између узорака из Војводине и депресије Дрмно, тако и између узорака из Војводине који потичу из лежишта јужног Баната, северног Баната и нафтног поља Велебит.

(Примљено 10. маја 2007)

REFERENCES

1. B. P. Tissot, D. H. Welte, *Petroleum Formation and Occurrence*, 2nd Ed., Springer–Verlag, Heidelberg, 1984, pp. 69 and 291
2. K. E. Peters, C. C. Walters, J. M. Moldowan, *The Biomarker Guide, Vol. 2: Biomarkers and Isotopes in the Petroleum Exploration and Earth History*, Cambridge University Press, Cambridge, 2005, pp. 483, 488, 499, 608, 612, 643, 645 and 964
3. C. S. Sajgó, J. R. Maxwell, A. S. Mackenzie, *Org. Geochem.* **5** (1983) 65
4. D. Waples, *Geochemistry in Petroleum Exploration*, International Human Resources Development Corporation, Boston, 1985, p. 133
5. B. G. K. van Aarssen, T. P. Bastow, R. Alexander, R. I. Kagi, *Org. Geochem.* **30** (1999) 1213
6. P. R. Philp, *Fossil Fuel Biomarkers. Applications and Spectra*, Elsevier, Amsterdam, 1985, pp. 36 and 45
7. W. K. Seifert, J. M. Moldowan, in: *Methods in Geochemistry and Geophysics, Vol. 24*, B. R. Johns, Ed., Pergamon Press, Oxford, 1986, p. 261
8. K. R. Al–Arouri, D. M. McKirdy, C. J. Boreham, in *Advances in Organic Geochemistry 1997, Part 1*, B. Horsfield, Ed., Pergamon Press, Oxford, 1998, p. 713
9. M. Radke, D. H. Welte, H. Willsch, *Geochim. Cosmochim. Acta* **46** (1982) 1
10. M. Radke, H. Willsch, D. Leythaeuser, M. Teichmüller, *Geochim. Cosmochim. Acta* **46** (1982) 1831
11. M. Radke, in *Advances in Petroleum Geochemistry*, M. Radke, Ed., Academic Press, London, 1987, p. 141
12. M. G. Strachan, R. Alexander, R. I. Kagi, *Geochim. Cosmochim. Acta* **52** (1988) 1255
13. R. Alexander, R. I. Kagi, S. J. Rowland, P. N. Sheppard, T. V. Chirila, *Geochim. Cosmochim. Acta* **49** (1985) 385
14. R. Alexander, R. I. Kagi, R. K. Singh, I. B. Sosrowidjojo, *Org. Geochem.* **21** (1994) 115
15. S. C. George, M. Lisk, R. E. Summons, A. R. Quezada, in *Advances in Organic Geochemistry 1997, Part 1*, B. Horsfield, *et al.* Eds., Pergamon Press, Oxford, 1998, p. 631
16. S. C. George, T. E. Ruble, A. Dutkiewicz, P. J. Eadington, *Appl. Geochem.* **16** (2001) 451
17. Z. Sofer, D. R. Regan, D. S. Muller, in *Proceedings of XII Geological Congress, Book of Abstracts*, Buenos Aires, Argentina, 1993, p. 407
18. K. Gürgey, *Mar. Petrol. Geol.* **20** (2003) 1119
19. R. P. Suggate, *J. Petrol. Geol.* **21** (1998) 5
20. C. E. Barker, M. J. Pawlewicz, in *Vitrinite reflectance as a maturity parameter: applications and limitations, ACS Symposium Series 570*, P. K. Mukhopadhyay, W.G. Dow, Eds., 1994, p. 216
21. K. G. Jöreskog, J. E. Klovan, R. A. Reyment, *Methods in Geomathematics I, Geological Factor Analysis*, Elsevier, Oxford, 1976, p. 9
22. W. Odden, O. M. Kvalheim, *Appl. Geochem.* **15** (2000) 611
23. C. Reimann, P. Filmoser, R. G. Garrett, *Appl. Geochem.* **17** (2002) 185
24. N. Pasadakis, M. Obermajer, K. G. Osadetz,. *Org. Geochem.* **35** (2004) 453
25. T. Šolević, K. Stojanović, B. Jovančićević, G. Mandić, J. Schwarzbauer, D. Vitorović, *J. Serb. Chem. Soc.* **71** (2006) 745
26. J. Davis, *Statistics and Data Analysis in Geology, 3rd Ed.*, Wiley, New York, 2002, p. 509
27. http://www.statsoftinc.com/textbook/stfacan.html
28. M. Ercegovac, A. Kostić, *Annales Géologiques de la Péninsule Balkanique* **57** (1993) 331
29. M. Ercegovac, A. Kostić, *J. Serb. Chem. Soc.* **61** (1996) 1063
30. M. Ercegovac, A. Grubić, I. Đoković, B. Kuzeljević, M. Marović, D. Vitorović, M. Branković, S. Grkavac, A. Kostić, B. Prstojević, *Annales Géologiques de la Péninsule Balkanique* **57** (1993) 373

31. M. Ercegovac, M. Jeremić, S. Đajić, *Annales Géologiques de la Péninsule Balkanique* **61** (1997) 143
32. M. Ercegovac, A. Kostić, H. Karg, D. H. Welte, R. Littke, *Petrol. Geol.* **26** (2003) 5
33. B. Jovančićević, H. Wehner, G. Scheeder, K. Stojanović, A. Šainović, O. Cvetković, M. Ercegovac, D. Vitorović, *J. Serb. Chem. Soc.* **67** (2002) 553
34. K. Stojanović, B. Jovančićević, D. Vitorović, J. Golovko, G. Pevneva, A. Golovko, *J. Petrol. Sci. Eng.* **55** (2007) 237
35. B. Jovančićević, H. Wehner, G. Scheeder, D. Plećaš, M. Ercegovac, D. Vitorović, *J. Serb. Chem. Soc.* **66** (2001) 297
36. V. I. Ivanov, O. S. Andrienko, A. K. Golovko, *Geokhimiya* **3** (1991) 91 (in Russian)
37. K. Stojanović, B. Jovančićević, G. S. Pevneva, J. A. Golovko, A. K. Golovko, P. Pfendt, *Org. Geochem.* **32** (2001) 721
38. B. M. Didyk, B. R. T. Simoneit, S. C. Brassell, G. Eglinton, *Nature* **272** (1978) 216
39. B. Jovančićević, P. Polić, M. Šaban, D. Vitorović, *J. Serb. Chem. Soc.* **59** (1994) 983
40. B. Jovančićević, P. Polić, D. Vitorović, *J. Serb. Chem. Soc.* **63** (1998) 397
41. A. G. Borrego, P. Bernard, C. G Blanco, *Appl. Geochem.* **14** (1999) 1049
42. S. Li, X. Pang, M. Li, Z. Jin, *Org. Geochem.* **34** (2003) 389
43. K. Stojanović, *Ph.D. Thesis*, University of Belgrade, 2004, pp. 174, 190 and 226 (in Serbian)
44. A. Šajnović, K. Stojanović, I. Filipović, O. Cvetković, B. Jovančićević, D. Vitorović, *J. Serb. Chem. Soc.* **69** (2004) 611
45. E. Kolaczkowska, N. E. Slougui, D. S. Watt, R. E. Marcura, J. M. Moldowan, *Org. Geochem.* **16** (1990) 1033
46. D.–J. H. Simons, F. Kenig, C. J. Schröder–Adams, *Org. Geochem.* **34** (2003) 1177
47. G. N. Gordzadze, *Thermolysis of organic substances in geochemical prospective explorations of oil and gas*, Institut geologii i razrabotki goryuchikh iskopaemikh, Moscow, 2002, p. 257 (in Russian)
48. A. G. Requejo, R. Sassen, T. McDonald, G. Denoux, M. C. Kennicutt, J. M. Brooks, *Org. Geochem.* **24** (1996) 1017
49. M. Šaban, B. Jovančićević, T. Glumičić, N. Dogović, *Rap. Comm. Mass Spectrom.* **4** (1990) 505
50. M. Šaban, B. Jovančićević, T. Glumičić, S. Saračević, *Org. Geochem.* **16** (1990) 477
51. A. K. Golovko, *Ph.D. Thesis*, University of Tomsk, Russia, 1997, p. 353 (in Russian)
52. K. Stojanović, B. Jovančićević, D. Vitorović, G. Pevneva, J. Golovko, A. Golovko, *Geochem. Inter.* **45** (2007) 781
53. M. Radke, H. Willsch, D. H. Welte, *Org. Geochem.* **10** (1986) 51
54. R. Ishiwatari, K. Fukushima, *Geochim. Cosmochim. Acta* **43** (1979) 1343.

Journal of the Serbian Chemical Society
JSCS@tmf.bg.ac.yu • www.shd.org.yu/JSCS

J. Serb. Chem. Soc. 72 (12) 1255–1263 (2007)
JSCS–3657

UDC 547.458.2+54.05:664.642:582.282.23
Original scientific paper

Preparation and studies on immobilized α-glucosidase from baker's yeast *Saccharomyces cerevisiae*

KHALED S. O. H. AHMED[1], NENAD B. MILOSAVIĆ[2*#], MILICA M. POPOVIĆ[1], RADIVOJE M. PRODANOVIĆ[1#], ZORICA D. KNEŽEVIĆ[3#] and RATKO M. JANKOV[1#]

[1]*Department of Biochemistry, Faculty of Chemistry, University of Belgrade, Studentski trg 12–16, 11000 Belgrade,* [2]*Department of Chemistry, Institute of Chemistry, Technology and Metallurgy, Njegoševa 12, 11001 Belgrade and* [3]*Department of Biochemical Engineering, Faculty of Technology and Metallurgy, University of Belgrade, Karnegijeva 4, 11000 Belgrade, Serbia*

(Received 10 July 2007)

Abstract: α-Glucosidase from *S. cerevisiae* was covalently immobilized onto Sepabeads EC-EA by the glutaraldehyde method. An analysis of the variables controlling the immobilization process is first presented and it is shown that the highest coupling of α-glucosidase occurred within 24 h. Also, a loading of 30 mg/g support proved to be effective, resulting in a rather high activity of around 45 U g^{-1} with a satisfactory degree of enzyme fixed. Both free and immobilized enzymes were then characterized by determining the activity profile as a function of pH, temperature and thermal stability. The obtained immobilized preparation showed the same optimum pH, but a higher optimum temperature compared with the soluble one. In addition, the immobilized enzyme treated at 45 ºC for 1 h still retained an activity of around 20 %, whereas the free enzyme completely lost its original activity under this condition. In conclusion, the developed immobilization procedure is quite simple, easily reproducible and provides a promising solution for the application of immobilized α-glucosidase.

Keywords: maltase, Sepabeads EC-EA, immobilization, stabilization.

INTRODUCTION

α-Glucosidase (EC 3.2.1.20) catalyzes not only the hydrolysis of α-glucoside linkages, but also the transglucosylation of α-glucosyl residues to various glucosyl co-substrates, resulting in the synthesis of new oligosaccharides, besides digestion, lysosomal catabolism of glycoconjugates and glycoprotein synthesis. Pompe disease is a genetic fetal muscle disorder caused by a deficiency of acid α-glucosidase, which results in glycogen accumulation in multiple tissues, with cardiac and muscular tissues being most seriously affected. One way of treating the disease is to employ α-glucosidase, *i.e.*, enzyme therapy.[1,2]

* Corresponding author. E-mail: nenadmil@chem.bg.ac.yu
# Serbian Chemical Society member.
doi: 10.2298/JSC0712255A

The yeast *Saccharomyces cerevisiae* synthesizes a maltose inducible and glucose repressible α-glucosidase or maltase. This intracellular enzyme is a monomer of 63,000 Da and has been purified to homogeneity and characterized.[3]

The concept of immobilizing proteins and enzymes to insoluble supports has been the subject of considerable research for over 30 years and, consequently, many different methodologies and a vast range of applications have been suggested. The aims often included such factors as: the reuse or better use of enzymes, especially if they are scarce or expensive, better quality products as there should be little enzyme in the product requiring inactivation or downstream purification, the production of biosensors, flow-through analytical devices, or the development of continuous manufacturing processes. Although large tonnages of immobilized enzymes are employed industrially, for example in the production of various syrups from starch,[4] and several smaller-scale industrial applications, the introduction of such biocatalysts has been disappointingly slow.

It is well known that multipoint attachment may promote an increased rigidity in immobilized enzymes.[5] This rigidity makes them more resistant to small conformational changes induced by heat, organic solvents, denaturing agents, *etc*. Multipoint attachment was mainly involved to explain the observed stabilization of randomly prepared derivatives and was considered less in developing strategies to obtain optimally stabilized immobilized systems.[6]

For the industrial application of enzymes acting on water-soluble substrates, such as carbohydrates, an effective immobilization method is required to facilitate the continuous processing and reuse of the biocatalyst.[7,8] In this context, the employment of available carriers for covalent immobilization of enzymes is of great interest. Sepabeads EC is a polymethacrylate-based carrier for enzyme immobilization.[9] Sepabeads EC-EA is an aminated support having ethylenediamine groups with a high reactive group density. Compared with other acrylic polymers, Sepabeads EC-EA possess a high mechanical stability and do not swell in water. In addition, the polymer is non-toxic, non-immunogenic and non-antigenic. Furthermore, the raw materials applied for the production of these supports are included in the EU list of resins allowed for the processing of food stuffs.[10]

In this work, α-glucosidase from *Saccharomyces cerevisiae* was immobilized on Sepabeads EC-EA and the conditions for immobilization and characterization of the immobilized enzyme were studied in detail. The first aim was to determine the optimal immobilization conditions, such as enzyme–support contact time and initial enzyme amount in the attachment solution, with respect to enzyme loading, catalytic activity and coupling yields (enzyme and activity). A comparative study between free and immobilized enzymes was then undertaken in terms of pH, temperature and thermal stability.

EXPERIMENTAL

Material

α-Glucosidase, isolated from baker's yeast by a slightly modified, previously published procedure,[11] showed a single band on SDS–gel electrophoresis, with an approx. molecular weight of 63 kDa. Its specific activity was 80 U mg^{-1} proteins and the K_M for 4-nitrophenyl α-D-glucopyranoside was 0.2 mM. All other chemicals were from Merck, Germany. Sepabeads EC-EA was kindly provided by Resindion S. R. L. (Mitsubishi Chemical Corporation, Milan, Italy). *p*-Nitrophenyl α-D-glucopyranoside (α-*p*NpG) was purchased from Fluka Chemie AG. All other reagents and solvents were of the highest available purity and used as purchased from Sigma.

Standard activity assay

The activity of soluble and immobilized α-glucosidase preparations were determined using sucrose as the substrate. The activity of soluble enzyme was measured at a substrate concentration of 10 % (w/v) sucrose in 50 mM sodium phosphate buffer, pH 7.0 at 25 ºC. One unit of enzyme activity was defined as 1 μmol glucose produced per minute under the above reaction conditions. Glucose was determined by the dinitrosalicylic acid reagent.[12]

Immobilization of α-glucosidase

The immobilization procedure consisted of two main steps: glutaraldehyde activation of the polymer and enzyme coupling to the polymer. Glutaraldehyde reacts with the amino groups of Sepabeads EC-EA, and the amino groups of the enzyme are then coupled to the carrier *via* the free carbonyl groups of the dialdehyde bound to the supports. Activation of polymer was performed by incubation of the polymer with 2.5 % (w/v) glutaraldehyde solution buffered at pH 7 (sodium phosphate buffer, 100 mM) for two hours at room temperature in the dark with occasional stirring. Subsequently, the polymer was incubated overnight with different amounts of enzyme (from 5 to 50 mg/g dry polymer) in sodium phosphate buffer, pH 7.0 at 4 ºC. After binding, any unbound enzyme was removed by washing several times with 1 M NaCl in 50 mM sodium phosphate buffer pH 7.0 and with buffer alone (the washing solutions were combined and stored for activity and determination of proteins) and stored at 4 ºC in 50 mM sodium phosphate buffer pH 7.0 until use.

Time-course of immobilization

A total of 0.5 g of support was suspended in 50 ml of enzyme solution (protein concentration 1 mg ml^{-1}) in sodium phosphate pH 7.0, 50 mM at 25 ºC. Periodically, samples of the supernatants were withdrawn and analyzed for enzyme activity.

Determination of proteins

Soluble protein was determined by the Bradford method,[13] using bovine serum albumin as the protein standard.

Effects of pH and temperature on α-glucosidase activity

The effect of temperature on the specific activity of the immobilized and soluble preparations was determined by incubation of the biocatalysts at a temperature ranging from 25 to 90 ºC with 10 % (w/v) sucrose in 50 mM sodium phosphate buffer pH 7.0. The specific activity at 30 ºC for the soluble and 40 ºC for the immobilized form was arbitrarily set as 100 % relative activity.

The optimal pH was determined with 10 % (w/v) sucrose in 50 mM sodium citrate phosphate buffer of pH values varying from 3 to 9 at 25 ºC. The specific activity value obtained at pH 6 for the soluble and 7 for immobilized form was taken as 100 % relative activity.

Enzyme inactivation experiments

Enzyme preparations (soluble and immobilized preparations) were incubated at pH 7.0 and 45 ºC. Periodically, samples were withdrawn and their remaining activities were assayed as des-

cribed above. The residual activity of α-glucosidase was expressed as the percentage of the initial activity for a given incubation time.

Kinetic deactivation model

Thermal deactivation kinetics of free and immobilized enzymes was studied based on a single step, first-order deactivation mechanism, having the final state of the enzyme, E_d, with or without residual activity:

$$\alpha E \xrightarrow{k} E_d \quad (1)$$

where E and E_d are the initial and final state of the enzyme, respectively; k is the first-order deactivation rate coefficient; α is the ratio of the specific activity of the E and E_d enzyme states. This mechanism leads to a model, where the residual enzyme activity at time t can be determined from the following equation:

$$A(t) = A_1 e^{-kt} + A_2 \quad (2)$$

$$A(t) = (100 - \alpha) e^{-kt} + \alpha \quad (3)$$

In the proposed kinetic model, the adjustable parameters are the rate coefficient, k, and the residual activity of the enzyme, α, which were determined by the least-squares fit to the experimental data using MAT-LAB software.

RESULTS AND DISCUSSION

For this immobilization study, a commercially available polymer, Sepabeads EC-EA was employed. The particle diameter, specific pore volumes and other parameters for the employed polymer are presented in Table I.

TABLE I. Physicochemical characteristics of Sepabeads EC-EA

	Active group	Functional group density mmol g^{-1} wet	Particle size range µm	Density g ml^{-1}	Pore diameter peak nm	pH stability range
Sephabeads EC-EA	Ethylendiamino	0.6	150–300	>1.1	>30	0–14

Time-course of α-glucosidase immobilization on Sepabeads EC-EA

The influence of the duration of the coupling was analyzed by measuring the activity of enzyme in the supernatant at various times, as described in the experimental section. The kinetic plot of enzyme coupling is presented in Fig. 1. It seems that during the first 20 h of coupling, around 25 % of the amount of initial enzyme was immobilized. After this initial phase, the rate of enzyme immobilization decreased and gradually ceased after about 24 h. After 20 h, only an addition 10 % of the initial enzyme activity was immobilized. Thus, an enzyme–support contact time of 24 h was considered to be optimal for the immobilization of α-glucosidase on Sepabeads EC-EA under the employed conditions (pH 7.0, 25 °C).

Effects of the amount of enzyme on the enzyme loading and activity coupling yield

An attempt was made to achieve the binding of high levels of enzyme with a high retention of hydrolytic activity. The influence of the amount of α-glucosi-

dase in the attachment solution in the range of 2.5–100 mg of enzyme per gram of dry support was studied. In each experiment, 0.05 g of support particles was immersed in a certain volume of enzyme solution. The aim was to determine an efficient relationship between the enzyme and the support. The results are presented in Fig. 2.

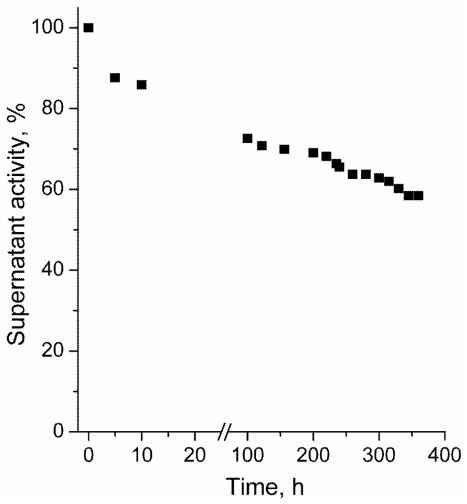

Fig. 1. Kinetics of α-glucosidase immobilization on Sepabeads EC-EA at 25 ºC and pH 7.0.

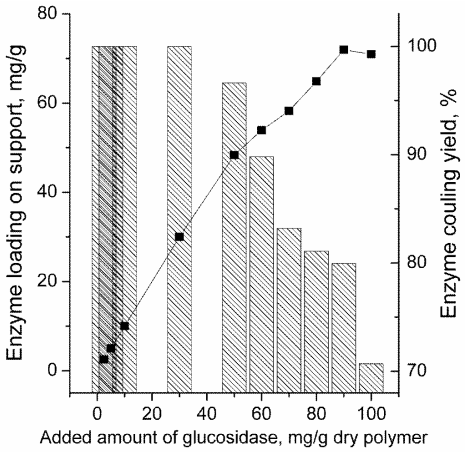

Fig. 2. Effects of the initial amount of α-glucosidase in the attachment solution on the enzyme coupling yield.

It is apparent from Fig. 2 that the enzyme loading on Sephabeads EC-EA initially increased rapidly with increasing amount of α-glucosidase but leveled off at about 70 mg/g. The enzyme coupling yield was in the range of 70–100 %. However, it is apparent from Fig. 3 that the activity yield is inversely related to the amount of enzyme bound. For example, increasing the α-glucosidase loading from 2.5 to 72 mg/g support resulted in a decrease in the activity yield from 96.9 to 13.11 %, possibly due to the close packing of the enzyme on the support surface, which could limit access of the substrate to the enzyme, required for the hydrolysis reaction. It is generally acknowledged that the catalytic efficiency of immobilization processes decreases when the enzyme loading exceeds a certain value and an optimum activity should be selected.[14,15] The loading of 30 mg/g support seems to be most appropriate for use, resulting in an activity yield of 30 % with satisfactory degree of bound enzyme. The present activity of the immobilized enzyme was higher than in a previously published study, where the immobilized α-glucosidase had an activity ranging from 44.8–80.7 U g^{-1}, depending of characteristics of the macroporous support.[16]

Dependence of the catalytic activity on pH and temperature

Both the soluble and immobilized form of α-glucosidase were the most active in the pH range 6–7 (Fig. 4). After immobilization, the optimal pH did not

change when compared with the pH profile of the soluble enzyme; the presented results are very similar to those previously published.[17]

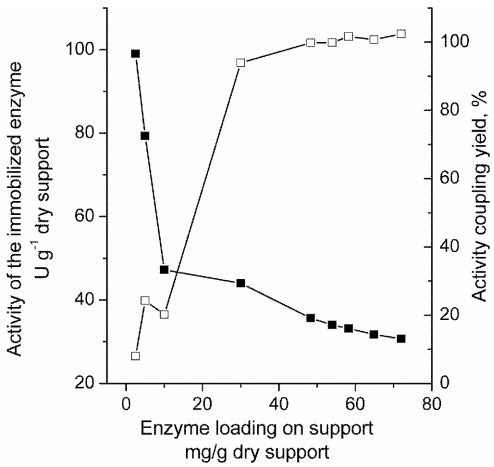

Fig. 3. Effect of enzyme loading on the activity of the biocatalysts and the activity coupling yield. The symbols represent the activity of the immobilized α-glucosidase (□) and the activity coupling yield (■).

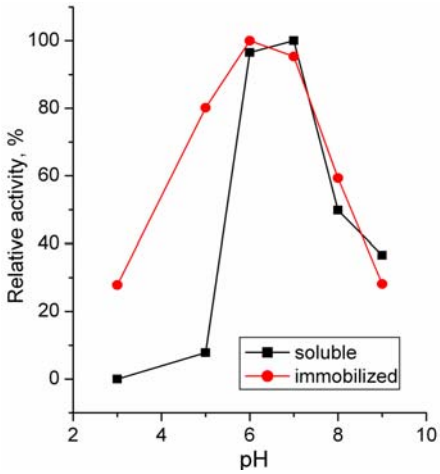

Fig. 4. Dependence of the relative activity of soluble and immobilized on Sephabeads EC-EA α-glucosidase from *S. cerevisiae* on pH (temperature 25 °C, 10 % (w/v) sucrose as substrate).

Temperature dependencies of the activities of the two forms of α-glucosidase, soluble and immobilized, are presented in Fig. 5. It appears that the optimal reaction temperature shifted from 30 °C for soluble α-glucosidase to almost 40 °C for the immobilized enzyme, suggesting a significantly better thermal stability of the immobilized enzyme.

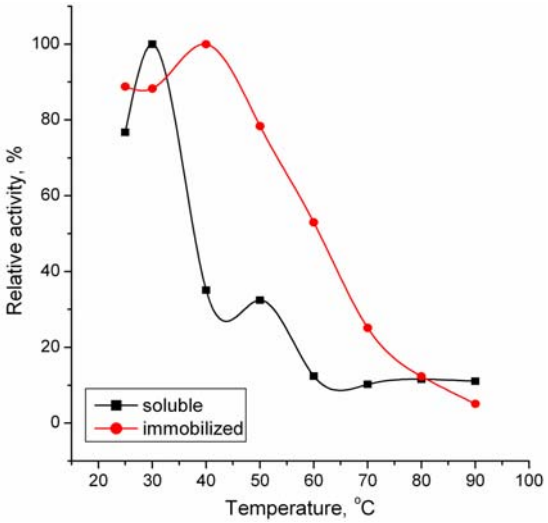

Fig. 5. Dependence of the relative activity of soluble and on Sephabeads EC-EA immobilized α-glucosidase from *S. cerevisiae* on temperature (pH 7.0, 10 % (w/v) sucrose as substrate).

Effect of immobilization on the thermal stability of the enzyme

An important consideration when evaluating an immobilized enzyme system is the reported enzyme deactivation. Moreover, for the design and operation of an enzyme reactor, a proper kinetic deactivation model and kinetic parameters are required. Therefore, the thermal stability of the immobilized enzyme was studied at 45 °C in an aqueous medium (50 mM sodium phosphate buffer, pH 7.0) and compared with that of the free enzyme.

The kinetic deactivation profiles at 45 °C for the free and immobilized enzyme are presented in Fig. 6. In order to interpret and analyze the obtained experimental results, the model based on a single step, first-order degradation kinetics was fitted to the deactivation curves (Eq. 3). The points on the graph are experimental data and the solid lines represent the best fits of the predictions of the theoretical model. The results show that immobilization of the enzyme on Sepabeads EC-EA offers a high degree of thermoprotection. For example, immobilized enzyme treated at 45 °C for 1 h still retained activity of around 20 %, whereas the free enzyme lost its original activity completely under this condition. This fact is of real significance in commercial applications.

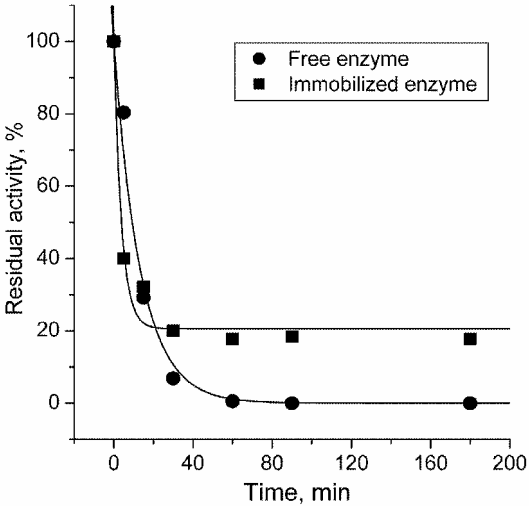

Fig. 6. Thermal deactivation of free (●) and immobilized enzyme (■) at 45 °C. The lines represent the best fits of the single step, first-order kinetic deactivation model. The initial activities were taken as 100 %.

It also seems that first order enzyme degradation kinetics fits the experimental data well for both soluble and immobilized enzymes, suggesting that the biocatalysts lose their activity in only one step at the tested temperature. The best-fit values of the deactivation rate constant, k, half life, $t_{1/2}$, and the residual activity of the final state enzyme, α, are listed in Table II. It appears that the free enzyme is more thermostable than the immobilized one, deduced from the k and $t_{1/2}$ values. However, immobilization enabled the enzyme to attain a final state, E_d, with a significant residual activity, while the final state of the free

enzyme was completely deactivated ($\alpha = 0$). Thus, the shape of the curve obtained for the immobilized enzyme showed that, after a first phase of rapid inactivation, the residual activity of the immobilized enzyme reached a defined plateau, yielding a stable enzyme form with a residual activity of around 20.56 % ($\alpha = 20.56$ %), indicating an improvement in the thermal stability of the enzyme upon immobilization.

TABLE II. Best-fit parameters of the first-order kinetic model (Eq. 3)

Biocatalyst	t / °C	k / min^{-1}	A_1	α (A_2)	$t_{1/2}$ / min
Free enzyme	45	0.075	100	0	9.24
Immobilized enzyme		0.260	79.08	20.56	3.79

CONCLUSION

To summarize, although Sepabeads EC-EA is known to be a good support for enzyme immobilization, its potential for α-glucosidase immobilization has not been fully explored. In the present study, the conditions for immobilization of α-glucosidase, the time course of immobilization and the amount of added enzyme were optimized. To prevent enzyme inactivation, an approach is presented for the stable covalent immobilization of α-glucosidase from *S. cerevisiae* on an amino-containing support (Sepabeads EC-EA) with a high retention of activity. The immobilized enzyme showed greater thermostability than the soluble one; after incubation of the enzymes at 45 °C for 1 h, the soluble form showed no activity but the immobilized enzyme retained a residual activity of around 20.56 %. Further work is in progress on the application of immobilized α-glucosidase for the continuous synthesis of various physiologically active compounds.

Acknowledgments. The authors thank Resindion S. R. L. (Mitsubishi Chemical Corporation, Milan, Italy) for the gift of the Sepabeads samples. Also, the authors are grateful for the financial support of the Ministry of Science of Serbia (Project No. 142020).

И З В О Д

ДОБИЈАЊЕ И ПРОУЧАВАЊЕ ИМОБИЛИЗАЦИЈЕ α-ГЛУКОЗИДАЗЕ ИЗ ПЕКАРСКОГ КВАСЦА *Saccharomyces cerevisiae*

KHALED S. O. H. AHMED[1], НЕНАД Б. МИЛОСАВИЋ[2], МИЛИЦА М. ПОПОВИЋ[1], РАДИВОЈЕ М. ПРОДАНОВИЋ[1],ЗОРИЦА Д. КНЕЖЕВИЋ[3] и РАТКО.М.ЈАНКОВ[1]

[1]Хемијски факултет, Универзитет у Београду, Студентски трг 12–16, 11000 Београд, [2]Центар за хемију, Институт за хемију, технологију и металургију, Његошева 12, 11001 Београд и [3]Технолошко–металуршки факултет, Универзитет у Београду, Карнегијева 4, 11000 Београд

Малтаза из *S. cerevisiae* је ковалентно имобилизована на Sepabeads EC-EA након активације носача раствором глутаралдехида. Испитивањем кинетике имобилизације утврђено је да се 25 % ензима имобилизује након 24 часа. Имобилизована α-глукозидаза има исти pH оптимум као и растворни ензим, док је оптимална температура за активност имобилизованог ензима увећана за 10 °C у поређењу са растворним ензимом. Када се упореде заостале активности растворне и имобилизоване форме α-глукозидазе, након инкубације од 1 h на

45 °C растворни ензим не показује активност док имобилизована форма задржава око 20 % почетне активности. Имобилизована форма ензима задржава 20 % почетне активности чак и после 3 h инкубације на 45 °C.

(Примљено 10. јула 2007)

REFERENCES

1. T. Kikuchi, H. Wen Yang, M. Pennybacker, N. Ichihara, M. Mizutani, J. L. K. Van Hove, Y.–T. Chen, *J. Clin. Invest.* **101** (1998) 827
2. K. Umapathysivam, A. Whitt, C. Bindloss, M. Ravenscroft, P. Meike, *Clin. Chem.* **46** (2000) 1318
3. R. Needleman, H. J. Federoff, T. Eccieshall, B. Buchferer, J. Marmur, *Biochemistry* **17** (1978) 4657
4. N. Milosavić, R. Prodanović, S. Jovanović, I. Novaković, Z. Vujčić, *J. Serb. Chem. Soc.* **70** (2005) 713
5. A. Klibanov, *Anal. Biochem.* **93** (1978) l
6. R. Prodanović, M. Simić, Z. Vujčić, *J. Serb. Chem. Soc*. **68** (2003) 819
7. A. Gomez de Segura, M. Alcalde, F. Plou, M. Remaud–Simeon, P. Monsan, A. Ballesteros, *Biocatal. Biotransform.* **21** (2003) 325
8. M. Martin, F. Plou, M. Alcalde, A. Ballesteros, *J. Mol. Catal. B: Enzym.* **21** (2003) 299
9. C. Mateo, O. Abian, G. Fernandez–Lorente, J. Pedroche, R. Fernandez–Lafuente, J. M. Guisan, A. Tam, M. Daminati, *Biotechnol. Prog.* **18** (2000) 629
10. Resolution AP (97)1. *On ion exchange and adsorbent resins used in the processing of foodstuffs* (adopted by the EU Committee of Ministers on September 30, 1997)
11. R. Prodanović, N. Milosavić, Z. Vujčić, in *Proceedings of 42nd Meeting of the Serbian Chemical Society*, Belgrade, Serbia, 2004, p. 142
12. G. Miller, *Anal. Chem.* **31** (1959) 426
13. M. Bradford, *Anal.Biochem.* **72** (1976) 248
14. Z. Knežević, N. Milosavić, D. Bezbradica, Ž, Jakovljević, R. Prodanović, *Biochem. Engin. J*. **30** (2006) 269
15. N. Milosavić, R. Prodanović, S. Jovanović, Z. Vujčić, *Enzyme Microb. Technol.* **40** (2007) 1422
16. R. Prodanović, N. Milosavić, S. Jovanović, T. Ćirković–Veličković, Z. Vujčić, R. Jankov, *J. Serb. Chem. Soc*. **71** (2006) 339
17. A. Dincer, B. Okutucu, F. Zihnioglu, A. Telefoncu, *Prep. Biochem. Biotechol*. **35** (2005) 103.

Journal of the Serbian Chemical Society
JSCS@tmf.bg.ac.yu • www.shd.org.yu/JSCS

J. Serb. Chem. Soc. 72 (12) 1265–1269 (2007) UDC 547.913.2/.5+547.565.2+537.363:615.277
JSCS–3658 *Original scientific paper*

Interactions of the anti-tumor sesquiterpene hydroquinone avarol with DNA *in vitro*

MIROSLAVA VUJČIĆ[1#], SRĐAN TUFEGDŽIĆ[1#], ZORAN VUJČIĆ[2#], MIROSLAV J. GAŠIĆ[1#] and DUŠAN SLADIĆ[2*#]

[1]*Institute of Chemistry, Technology and Metallurgy, Department of Chemistry, Njegoševa 12, 11000 Belgrade and* [2]*Faculty of Chemistry, University of Belgrade, Studentski trg 16, 11000 Belgrade, Serbia*

(Received 6 August 2007)

Abstract: Changes in electrophoresis pattern after interaction of supercoiled plasmid pBR322 DNA with avarol was studied at a micromolar concentration of reactants under mild reaction conditions. Interactions of avarol with linear high-molecular CT-DNA at millimolar concentrations were analyzed by electrophoresis and UV spectrophotometry. It was observed that avarol is capable of quenching ethidium bromide fluorescence in DNA bands. An increase in the absorbance of DNA was detected. The results indicate the binding of avarol to DNA and/or modification of nucleotide bases.

Keywords: avarol, hydroquinone, anti-tumor activity, pBR322 DNA, calf thymus DNA.

INTRODUCTION

DNA is the presumed intracellular target for a variety of quite structurally diverse low molecular weight ligands. A number of DNA-reactive synthetic and natural products or their derivatives have chemical, biological and medical significance as potential artificial gene regulators or clinically important chemotherapeutic agents. Low molecular weight ligands recognize and interact with DNA in different ways, including 1) DNA strand cleavage, 2) non-covalent association with the minor groove of DNA, 3) intercalation between DNA base pairs, 4) alkylation of a component nucleotide and 5) a combination of various effects.[1] Avarol is a marine sesquiterpenoid hydroquinone, isolated from the marine sponge *Dysidea avara*.[2] It was shown that avarol (Fig. 1) and the corresponding quinone avarone possess interesting activities towards DNA *in vivo*.[3–6] The aim of this study was to investigate the interactions of avarol with DNA *in vitro*. The possibility of avarol to induce DNA cleavage was measured by determining the

Serbian Chemical Society member.
* Corresponding author. E-mail: dsladic@chem.bg.ac.yu
doi: 10.2298/JSC0712265V

ability of the hydroquinone to transform the naturally occurring, covalently closed circular supercoiled form of plasmid pBR322 DNA to the open circular, relaxed form. The efficiency of the interaction of avarol with plasmid DNA was monitored by agarose gel electrophoresis experiments. Furthermore, the possibility of avarol of intercalating DNA molecules was investigated by UV spectral measurements of calf thymus DNA in presence of avarol. The obtained results might shed light on the mechanism of the anti-tumor activity of avarol.

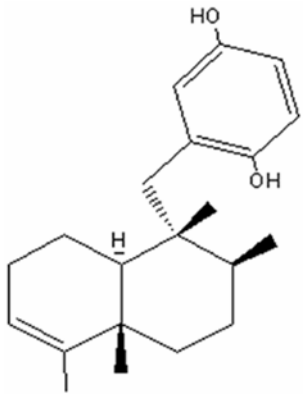

Fig. 1. Structure of avarol.

EXPERIMENTAL

Chemicals

Avarol was isolated from the sponge *Dysidea avara*, collected in the Bay of Kotor (Montenegro), as previously described.[2] Plasmid pBR322 from *Escherichia coli* RRI (containing more than 80 % supercoiled DNA) was purchased from Sigma–Aldrich, USA. Calf thymus DNA (lyophilized, highly polymerized) was obtained from Serva, Heidelberg. Agarose was purchased from Pharmacia-Biotech (GE Healthcare). All buffer solutions were prepared in deionized water and filtered through 0.2 μm filters (Nalgene, USA).

Interaction of avarol with plasmid pBR322

Avarol was dissolved in DMSO (0.01g ml^{-1}). Plasmid DNA (0.5 μg) was mixed with various amounts of avarol, so that the final concentrations of avarol were 10 μM, 20 μM and 30 μM, in 20 μl of the reaction mixture containing TAE buffer pH 8.24 (40 mM Tris-acetate, 1 mM EDTA, pH 8.0), or in 20 μl of the reaction mixture containing bicarbonate buffer (40 mM, pH 8.4). The contents were immediately analyzed by electrophoresis or incubated for 2 h at 37 °C with vortexing from time to time. The reaction was terminated by adding 5 μl of loading buffer (0.25 % bromophenol blue, 0.25 % xylene cyanol FF and 30 % glycerol in water). The samples were subjected to electrophoresis on 1 % agarose gel prepared in TAE buffer. The electrophoresis was performed at a constant voltage (80 V) for about 1.5 h (until bromophenol blue had passed through 75 % of the gel) in TAE buffer. After electrophoresis, the gel was stained for 30 min by soaking in an aqueous ethidium bromide solution (2 μl of 10 % (w/v) ethidium bromide in 40 ml of water). The gel was then destained for 5 min by keeping it in sterile distilled water. The stained gel was illuminated under a UV transilluminator Vilber–Lourmat (France) at 312 nm and photographed with a Panasonic DMC-LZ5 Lumix Digital Camera.

Interaction of avarol with calf thymus DNA

Calf thymus DNA (CT-DNA) was dissolved in 20 mM Tris-HCl pH 7.5/20 mM NaCl overnight at 4 °C. DNA concentration was adjusted with buffer to 5 mg ml^{-1}. This stock solution was stored at 4 °C and was stable for several days. A solution of calf thymus DNA in water gave a ratio of UV absorbance at 260 and 280 nm, A_{260}/A_{280} of 1.89–2.01, indicating that DNA was sufficiently free of protein. The concentration of DNA was measured by measuring the absorbance of DNA-containing solution at 260 nm. One optical unit corresponds to 50 μg ml^{-1} of double stranded DNA (based on the known molar absorption coefficient value of 6600 $M^{-1}cm^{-1}$).[7] 2.5 μl of stock solution of CT-DNA in 497.5 μl of TAE or bicarbonate buffer were incubated at 37 °C for 2 h, vortexing from time to time, with 10, 20 and 30 μl of an ethanolic solution of avarol (175 mg ml^{-1}), corresponding to final avarol concentrations of 11, 22 and 33 mM, respectively). Subsequently, the samples were cooled to 4 °C and centrifuged at 12000 rpm. 400 μl of the supernatant were used for measurements of absorbance on a UV Cintra 40 UV/Visible spectrometer. 10 μl of the supernatants were analyzed by electrophoresis on a 1 % agarose gel as described above.

RESULTS AND DISCUSSION

It was previously shown that incubation of pBR322 DNA with avarol caused a conversion of fully supercoiled DNA to nicked, circular molecules only in an oxygen atmosphere.[3] In this work pBR322 was incubated with avarol in air (milder reaction conditions). The electrophoresis pattern of the interaction of different concentrations of avarol with plasmid pBR322 DNA is shown in Fig. 2. No effects were observed immediately upon addition of avarol to the plasmid, regardless of the concentrations of avarol, as shown in Fig. 2A, lanes 1−4. After 2 h of reaction at 37 °C, no relaxation of supercoiled DNA was detected (Fig. 2A, B). These results differ from the previous ones obtained in an oxygen atmosphere but are in accordance with those obtained in nitrogen atmosphere.[3] It is likely that the amount of oxygen in air is insufficient for the process of DNA nicking by oxygen radicals to be detected. Some hydroquinone antioxidants also did not show damage to DNA unless the generation of semiquinone and hydroxyl radicals was additionally stimulated.[8] However, a dose-dependent quenching of the fluorescence of ethidium bromide was observed, as shown in Fig. 2B, lanes 1−4. The intensity of the bands diminished with increasing amount of avarol, indicating changes in the DNA molecules. This capability of avarol to interfere with the intercalation of ethidium bromide in supercoiled DNA was more pronounced in the bicarbonate than in the TAE buffer system (Fig. 2C).

Analysis of interaction of avarol with linear, high-molecular calf thymus DNA (CT-DNA) resulted in almost complete quenching of fluorescence in both buffer systems (Fig. 3). The nature of the observed DNA damage by avarol was investigated by DNA absorbance measurements. The absorption spectrum of CT-DNA was recorded in the absence and presence of increasing amounts of avarol. Typical sets of absorption spectra obtained in TAE and in bicarbonate buffers are shown in Fig. 4. An increasing quantity of avarol induced a hypochromic effect. The effect was again more pronounced in bicarbonate buffer. This hypochro-

mism can be ascribed to intercalative binding of avarol to the DNA helix.[9] Since avarol has only one planar ring, this type of binding should be weak, but the binding could be enhanced by positioning the sesquiterpene part of the molecule in the minor groove. Another possible cause of hypochromism could be modification of guanine and thymine residues, as was shown previously for some hydroquinones.[10]

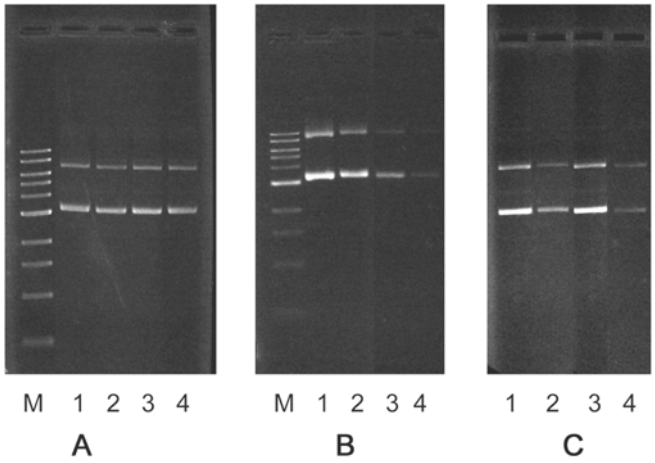

Fig. 2. Agarose gel electrophoresis of pBR322 after treatment with 0, 10, 20 and 30 μM of avarol (lanes 1, 2, 3, 4, respectively) at the beginning of the reaction – Panel A, and after 2 h at 37 °C – panel B. Panel C – Lanes 1 and 3 are pBR322 in TAE and bicarbonate buffer, respectively, without avarol; lanes 2 and 4 are pBR322 after treatment with 10 mM avarol in TAE and bicarbonate buffer, respectively. M – marker DNA.

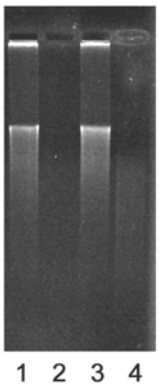

Fig. 3. Agarose gel electrophoresis of CT-DNA in TAE and in bicarbonate buffer without avarol (lanes 1 and 3, respectively) and after treatment with 10 mM avarol in TAE and in bicarbonate buffer (lanes 2 and 4, respectively).

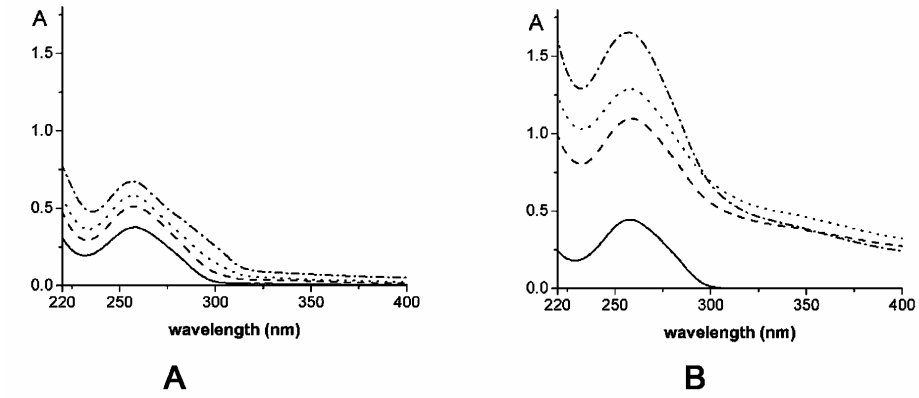

Fig. 4. Absorption spectra of CT-DNA in the absence (―) and presence of 11 (╍), 22 (┈), and 33 mM (┅) avarol. The absorption measurements were performed in TAE (panel A) and bicarbonate buffer (panel B).

CONCLUSIONS

Taken together, these results suggest that avarol possesses some DNA-damaging activity *in vitro*. The absence of changes in the electrophoresis pattern of circular plasmid DNA revealed that micromolar concentrations of the reactants under mild reaction conditions did not induce a relaxation of the supercoiled molecule. However, a quenching of the fluorescence of the ethidium bromide–DNA complex was observed. Interaction of avarol with linear high-molecular CT-DNA at millimolar concentrations gave, in addition to quenching the electrophoresis bands, an increase in the absorbance of DNA. The obtained results suggest that the mechanism of interaction of avarol with DNA under these reaction conditions *in vitro* may be similar, regardless of the source of DNA. These interactions could include binding to DNA as well as damage to nucleotide bases. These effects could be responsible for the pronounced anti-tumor activity of avarol.

Acknowledgements. The authors are grateful to the Ministry of Science of the Republic of Serbia for financial support (Grant 142026).

И З В О Д

ИНТЕРАКЦИЈЕ АНТИТУМОРСКОГ СЕСКВИТЕРПЕНСКОГ ХИДРОХИНОНА АВАРОЛА СА DNA *IN VITRO*

МИРОСЛАВА ВУЈЧИЋ[1], СРЂАН ТУФЕГЏИЋ[1], ЗОРАН ВУЈЧИЋ[2], МИРОСЛАВ Ј. ГАШИЋ[1] и ДУШАН СЛАДИЋ[2]

[1]ИХТМ, Центар за хемију, Београд и [2]Хемијски факултет, Универзитет у Београду, Београд

Проучаване су промене електрофоретског понашања DNA после интеракција суперхеликоидалног плазмида pBR322 с аваролом при микромоларним концентрацијама реактаната под благим реакционим условима. Интеракције аварола са линеарном високомолекулском CT-DNA при милимоларним концентрацијама анализиране су електрофорезом и UV спектрофотометријом. Уочено је да је аварол у стању да гаси флуоресценцију етидијум-бромида у тракама које потичу од DNA. Детектован је пораст апсорбанције DNA. Резултати указују на везивање аварона за DNA и/или модификацију нуклеотидних база.

(Примљено 6. августа 2007)

REFERENCES

1. J. A. Mountzouris, L. H. Hurley, in *Bioorganic Chemistry: Nucleic Acids*, S. M. Hecht, Ed., Oxford University Press, New York, 1996, p. 288
2. W. E. G. Müller, R. K. Zahn, M. J. Gašić, N. Dogović, A. Maidhof, C. Becker, B. Diehl–Seifert, E. Eich, *Comp. Biochem. Physiol.* **80C** (1985) 47
3. W. E. G. Müller, D. Sladić, R. K. Zahn, K. H. Bässler, N. Dogović, H. Gerner, H.C. Schröder, M. J. Gašić, *Cancer Res.* **47** (1987) 6565
4. M. J. Gašić, *J. Serb. Chem. Soc.* **53** (1988) 229
5. D. Sladić, M. J. Gašić, *J. Serb. Chem. Soc.* **59** (1994) 915
6. D. Sladić, M. J. Gašić, *Molecules* **11** (2006) 1
7. M. E. Reichmann, S. A. Rice, C. A. Thomas, P. Doty, *J. Am. Chem. Soc.* **76** (1954) 3047
8. T. Okubo, F. Nagai, K. Ushiyama, I. Kano, *Toxicol. Lett.* **90** (1997) 11
9. P. B. Arimondo, B. Baldeyrou, W. Laine, C. Bal, F. A. Alphonse, S. Routier, G. Coudert, J. Y. Merour, P. Colson, C. Houssier, C. Bailly, *Chem. Biol. Interact.* **138** (2001) 59
10. K. Hirakawa, S. Oikawa, Y. Hiraku, I. Hirosawa, S. Kawanishi, *Chem. Res. Toxicol.* **15** (2002) 76.

Journal of the Serbian Chemical Society
JSCS@tmf.bg.ac.yu • www.shd.org.yu/JSCS

J. Serb. Chem. Soc. 72 (12) 1271–1274 (2007) UDC **Gerardia savaglia*:639.61/.62:547.567:547.96
JSCS–3659 *Short communication*

SHORT COMMUNICATION

Chemical modification of the lectin of the marine coral *Gerardia savaglia* by marine quinone avarone

IVANA PAJIĆ[1], ZORAN VUJČIĆ[1#], MIROSLAVA VUJČIĆ[2#], IRENA NOVAKOVIĆ[2#], DUŠAN SLADIĆ[1#] and MIROSLAV J. GAŠIĆ[2*#]

[1]*Faculty of Chemistry, University of Belgrade, Studentski trg 16, 11000 Belgrade and* [2]*Center for Chemistry – ICTM, Njegoševa 12, 11000 Belgrade, Serbia*

(Received 3 August 2007)

Abstract: The quinone avarone, isolated from the marine sponge *Dysidea avara*, possesses the ability to chemically modify proteins. In this work, modification of lectin isolated from the coral *Gerardia savaglia* by avarone was examined. The techniques used for studying the modification were: SDS PAGE, isoelectric focusing and hemagglutination testing. The results of the SDS PAGE indicate dimerization of the protein. A shift of the pI toward lower value occurs upon modification. The change of the hemagglutination activity of the protein confirms that chemical modification of *G. savaglia* lectin by avarone changes its ability to interact with the membrane of erythrocytes.

Keywords: avarone, quinone, *Gerardia savaglia* lectin, covalent modification.

INTRODUCTION

Lectins are (glyco)proteins of plant or animal origin possessing an ability to specifically bind carbohydrate moieties. Such properties make them useful tools for the isolation and characterization of polysaccharides and glucoconjugates,[1,2] as well as in biomedical research.[3–5] Marine organisms are rich sources of lectins.[6,7] One of them, *Gerardia savaglia* lectin (GSL), was isolated from Adriatic sea coral and partially characterized.[8] This mannose specific lectin showed hemagglutinating activity toward human and some animal red blood cells, moderate mitogenic activity and a feature to bind glycoproteins present in the nuclei from CV-1 monkey kidney cells. A sesquiterpenoid hydroquinone avarol was isolated from the Mediterranean sponge *Dysidea avara* and oxidized to quinone avarone.[9,10]

In this work, the ability of avarone to chemically modify proteins, previously examined in case of some enzymes,[11,12] was tested. The significance of this study lies especially in the fact that modification of a marine lectin by a compound

Serbian Chemical Society member.
* Corresponding author. E-mail: mjgasic@chem.bg.ac.yu
doi: 10.2298/JSC0712271P

from the marine environment has been investigated, so that the results might give insight into marine ecological relations.

The chemical modification of GSL by avarone was studied by hemagglutination testing, SDS PAGE and isoelectric focusing.

EXPERIMENTAL

Avarol was isolated from the extract of the sponge *Dysidea avara*, collected in the Bay of Kotor (Montenegro) and oxidized to avarone with silver oxide.[10]

Gerardia savaglia lectin was isolated from crude coral extract in a pure form by affinity and gel chromatography.[8] The activity of the isolated lectin was examined by hemagglutination testing.[13]

Modification of *Gerardia savaglia* lectin was performed in 20 % EtOH. The final volume was 3.75 ml and the final concentrations of the lectin and avarone were 1 mg/ml and 0.5 mg/ml, respectively. The pH value of the mixture was adjusted to 8.5 with $NaHCO_3$. The reaction was performed at r.t. for 48 h with stirring. Subsequently, the mixture was centrifuged at 14000 rpm and the pellet was washed three times with ethanol. The pellet was then resuspended in 50 mM acetate buffer, pH 5.5 and prepared for hemagglutination testing, SDS PAGE and isoelectrofocusing.

Hemagglutination testing was performed on sheep erythrocytes.[13]

SDS PAGE was performed under reducing conditions. The molecular masses of the denatured protein samples were determined on 10 % polyacrylamide gel using molecular markers of 14.4 kD, 18 kD, 29 kD, 45 kD and 66 kD.[14]

Isoelectrofocusing was performed on 7.5 % polyacrylamide gel under non-reducing conditions with an ampholite range from 3−10 and a calibration pI kit.[15]

RESULTS AND DISCUSSION

After mixing avarone and the lectin solution, a change of color of the reaction mixture from light yellow to violet and pellet formation were visible after approximately 24 h.

The protein modification was examined by SDS PAGE. Reaction of avarone and *Gerardia savaglia* lectin gave a visible band at 30 kD (Fig. 1), which suggests dimerization of the protein (molecular mass of the monomer is 14.8 kD). Isolelectricfocusing showed four bands at pH values 8.7, 8.5, 8.3 and 7.3, indicating a shift of the pI value of the protein to lower pI values upon modification (Fig. 2). These results suggest that the side chains of basic amino acids, such as lysine amino groups, are involved in the reaction of the protein and the quinone.

The specific hemagglutinating activity of the resuspended pellet towards sheep erythrocytes was about 10-fold lower (160 hemagglutination units (HU)/mg protein) than the activity of the unmodified lectin (1706 HU/mg), which confirms the involvement of the same amino acid residues in the protein polymerization and interaction with the membrane of the erythrocytes. The identity of the modified residues remains to be determined. At present, there is no conclusive evidence whether the modification occurs in the binding site or in other regions resulting in a conformational change and concomitant decrease in activity.

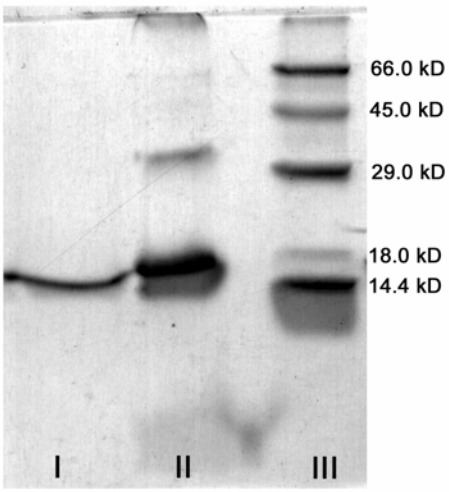

Fig. 1. SDS PAGE electrophoregram. I: Unmodified *G. savaglia* lectin. II: Modified *G. savaglia* lectin. III: Molecular weight markers.

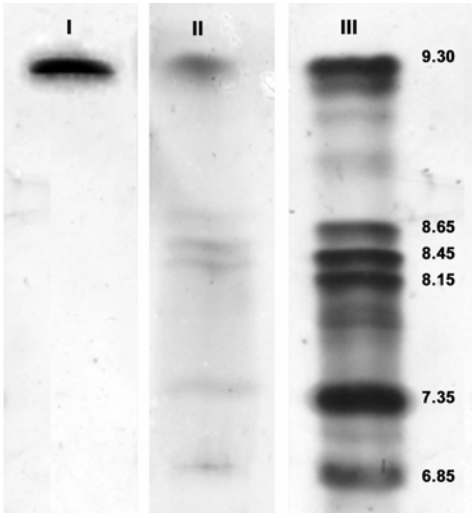

Fig. 2. Isoelectrofocusing gel. I: Unmodified *G. savaglia* lectin. II: Modified *G. savaglia* lectin. III: pI calibration kit markers. For clarity, only the region in which modified bands occur is shown.

CONCLUSIONS

The results presented in this work lead to the conclusion that avarone could chemically modify *Gerardia savaglia* lectin and that this modification altered its characteristics and biological activity.

The biological functions of lectins, especially those isolated from marine organisms, are still not completely understood. Marine lectins are involved in cell recognition and aggregation and in the process of the elimination of foreign organisms.[16,17] Although additional evidence is necessary, the obtained results could indicate covalent modification of the lectins as a possible manner of action in these processes, essential for the survival of these sedentary organisms. On the other hand, since compounds similar to avarone are present in algae,[18,19] ingestion of these algae could impair the interactions in which lectins are involved in the coral, so that a toxic effect to the animal could occur.

Acknowledgement. This work was partially supported by the Ministry of Science of the Republic of Serbia (Project No. 142026).

И З В О Д

ХЕМИЈСКЕ МОДИФИКАЦИЈЕ ЛЕКТИНА МОРСКОГ КОРАЛА *Gerardia savaglia* МОРСКИМ ХИНОНОМ АВАРОНОМ

ИВАНА ПАЈИЋ[1], ЗОРАН ВУЈЧИЋ[1], МИРОСЛАВА ВУЈЧИЋ[2], ИРЕНА НОВАКОВИЋ[2], ДУШАН СЛАДИЋ[1] и МИРОСЛАВ Ј. ГАШИЋ[1]

[1]*Хемијски факултет, Универзитет у Београду, Студентски трг 16, п. пр. 158, 11001 Београд и* [2]*ИХТМ – Центар за хемију, Његошева 12, п. пр. 473, 11001 Београд*

Аварон, хинон изолован из морског сунђера *Dysidea avara*, поседује способност да хемијски модификује протеине. У овом раду испитивана је модификација лектина изолованог из корала *Gerardia savaglia* авароном. Технике за праћење хемијске модификације биле су: SDS PAGE, изоелектрично фокусирање и хемаглутинациони тест. Резултати SDS PAGE упућују на димеризацију протеина. Долази до померања pI вредности протеина. Промена хемаглутинационе активности *G. savaglia* лектина авароном утицала је на његову способност интеракције са мембраном еритроцита.

(Примљено 3. августа 2007)

REFERENCES

1. H. Harada, M. Kamei, S. Yui, F. Koyama, *J. Chromtogr.* **355** (1986) 291
2. E. D. Green, R. M. Brodbeck, J. U. Baenziger, *J. Biol. Chem.* **262** (1987) 12030
3. L. Krogerus, L. C. Anderson, *Cancer* **66** (1990) 1802
4. U. Schumacher, E. Adam, S. A. Brooks, A. J. Leathem, *J. Histochem. Cytochem.* **43** (1995) 275
5. M. Oprić, S. Poznanović, Z. Kljajić, D. Sladić, G. Pupić, B. Perunović, M. J., Gašić, *Eur. J. Histochem.* **40** (1996) 211
6. R. M. Moura, A. F. S. Querioz, J. M. S. L. L. Fook, A. S. F. Dias, N. K. V. Monteiro, J. K. C. Ribeiro, G. E. E. D. Moura, L. L. P. Macedo, J. M. Santos, M. P. Sales, *Comp. Biochem. Physiol. A* **145** (2006) 517
7. P. A. Lukyanov, O. V. Chernikov, S. S. Kobelev, I. V. Chikalovets, V. I. Molchanova, W. Li, *Russ. J. Bioorg. Chem.* **33** (2007) 161
8. Z. Kljajić, H. C. Schröder, M. Rottmann, M. Čuperlović, M. Movsesian, G. Uhlenbruck, M. J. Gašić, R. K.Zahn, W. E. G. Müller, *Eur. J. Biochem.* **169** (1987) 97
9. T. Božić, *M. Sc. Thesis*, University of Belgrade (2002)
10. L. Minale, R. Riccio, G. Sodano, *Tetrahedron Lett.* **37** (1974) 3401
11. I. Novaković, Z. Vujčić, T. Božić, N. Božić, N. Milosavić, D. Sladić, *J. Serb. Chem. Soc.* **68** (2003) 243
12. D. Sladić, I. Novaković, Z. Vujčić, T. Božić, N. Božić, D. Milić, B. Šolaja, M. J. Gašić, *J. Serb. Chem. Soc.* **69** (2004) 901
13. I. Pajić, Z. Kljajić, N. Dogović, D. Sladić, Z. Juranić, M. J. Gašić, *Comp. Biochem. Physiol. C* **132** (2002) 213
14. U. K. Laemmli, *Nature* **227** (1970) 689
15. P. G. Righetti, *Isoelectrofocusing: Theory, Methodology and Applications*, Elsevier Biomedical Press, Amsterdam, 1983, p. 148
16. B. Diehl–Seifert, G. Uhlenbruck, M. Geisert, R. K. Zahn, W. E. G. Müller, *Eur. J. Biochem.* **147** (1985) 517
17. C. Wagner–Hüllsmann, N. Bachinski, B. Diehl–Seifert, B. Blumbach, R. Steffen, Z. Pancer, W. E. G. Mueller, *Glycoliology.* **6** (1996) 785
18. K. Kurata, K. Taniguchi, M. Suzuki, *Phytochemistry* **41** (1996) 749
19. L. Tziveleka, D. Abatis, K. Paulus, R. Bauer, C. Vagias, V, Roussis, *Chem. Biodiversity* **2** (2005) 901.

Journal of the Serbian Chemical Society
JSCS@tmf.bg.ac.yu • www.shd.org.yu/JSCS

J. Serb. Chem. Soc. 72 (12) 1275–1280 (2007) UDC 547.913.2/.5+547.473:543.062:543.422.25
JSCS–3660 *Short communication*

SHORT COMMUNICATION

Quantitative analysis of sesquiterpene lactone cnicin in seven *Centaurea* species wild-growing in Serbia and Montenegro using ^{1}H-NMR spectroscopy

VELE TEŠEVIĆ[1*#], SLOBODAN MILOSAVLJEVIĆ[1#], VLATKA VAJS[2#], PEDJA JANAĆKOVIĆ[3], IRIS ĐORĐEVIĆ[4], MILKA JADRANIN[2#] and IVAN VUČKOVIĆ[2]

[1]*Faculty of Chemistry, University of Belgrade, Studentski trg 12–16, P.O. Box 158, 11001 Belgrade,* [2]*Institute of Chemistry, Technology and Metallurgy, Njegoševa 12, 11001 Belgrade,* [3]*Faculty of Biology, University of Belgrade, Studentski trg 12–16, 11001 Belgrade and* [4]*Faculty for Veterinary Medicine, University of Belgrade, Bulevar Oslobođenja 18, 11000 Belgrade, Serbia*

(Received 2 March 2007)

Abstract: ^{1}H-NMR spectroscopy was applied for the quantitative analysis of cnicin, a bioactive germacranolide type sesquiterpene lactone, in the aerial parts of seven wild-growing *Centaurea* species collected in Serbia and Montenegro. The analysis was performed by comparison of the integral of the one-proton signal of cnicin (H-13, δ 5.75) with that of the two-proton singlet (δ 6.98) of 2,6-*bis*(1,1-dimethylethyl)-4-methylphenol (BHT), used as the internal standard. Cnicin, within the concentration range 1.06–6.12 mg/g, calculated per weight of the fresh plant material was detected in six species, the exception being *C. salonitana*. This method allows the rapid and simple quantification of cnicin without any pre-purification step.

Keywords: ^{1}H-NMR, *Centaurea*, cnicin, BHT.

INTRODUCTION

Centaurea, the largest genus of the family Compositae (Asteraceae), is represented with about 40 species in Serbia and Montenegro and has been the subject of many chemical investigations, which have led to the isolation of various types of compounds, such as sesquiterpene lactones,[1–5] acetylenes,[5–7] flavonoids[5,8] and lignans.[3–5] Many of the *Centaurea* species are known for their anti-diabetic, anti-diarrhetic, anti-rheumatic, anti-inflammatory, cholagog, choleretic, digestive, stomachic, diuretic, emenagogue, astringent, hypotensive, anti-pyretic, cytotoxic and antibacterial effects, and are used single or mixed.[9–11]

One of the first biologically active compounds to be isolated from the genus *Centaurea* was cnicin (C, Fig. 1), a sesquiterpene lactone of the germacranolide

* Corresponding author. E-mail: vtesevic@chem.bg.ac.yu
# Serbian Chemical Society member.
doi: 10.2298/JSC0712275T

type, known for a long time (since 1837) as the main "bitter" ingredient in blessed thistle, *Cnicus benedictus.*[12,13] Cnicin has been reported as a constituent of several species of the *Centaurea* genus,[14] such as *C. diffusa* (0.81 %),[15] *C. squarrosa* (0.8 %),[16] *C. affinis* (0.46 %),[3] *C. stoebe* (0.45 %),[17] *C. derventana* (0.2 %),[1] *C. nicaensis* (0.19 %),[18] *C. bruguierana* (0.16 %)[19] and *C. calcitrapa* (0.06 %).[20] Cnicin could be found in the glandular epithelial trichomes of the leaves and, to a lesser extent, the shoots of knapweeds and it finds its way into the soil *via* leaching or litter.[21] This compound has broad effects on other taxa (allelopathic effect). Various bioassays of cnicin revealed antibiotic, antifungal, phytotoxic, and anti-herbivore properties.[14,22,23] Additionally, it has been shown to be auto-toxic to knapweeds themselves.[21] Spotted (*C. maculata*), diffuse (*C. diffusa*) and Russian knapweeds (*C. repens*) all produce cnicin at fairly high levels.[24] Cnicin is used as a bitter tonic and the bitterness value is approximately 1,500.[25] The bitterness of these compounds stimulates digestive activity, including the flow of saliva and secretion of gastric juice, which leads to improved appetite and digestion.

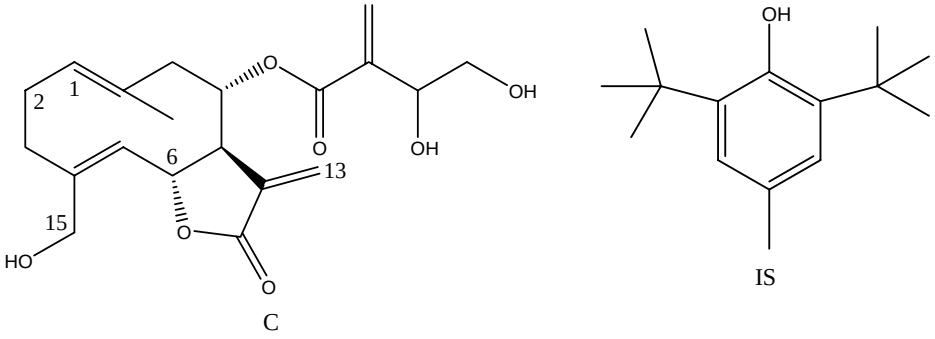

Fig. 1. Structure of cnicin (C) and BHT (IS).

Hitherto, various methods for the analysis of sesquiterpene lactones (SLs) in complex mixtures have been reported.[26] Most of them involve chromatographic techniques, such as GC and HPLC, or a combination of these with spectrometric methods, such as GC–MS, HPLC–MS and/or NMR. Since SLs are not volatile compounds and many of them are thermolabile, HPLC seems to be more suitable than GC. However, the lack of a specific and strong absorbing UV chromophore in SLs makes sensitivity a problem when conventional HPLC–UV detection is used. The chromatographic analysis usually requires tedious clean-up procedures, evaluation of suitable elution conditions, preparation of calibration curves for quantifications, and in some cases derivatization in order to enhance sensitivity and to remove compounds which interfere with the detection of the analyte.

Representing the method of choice in structure determination of natural products, NMR spectroscopy is mainly used qualitatively, although is generally accepted as a quantitative tool. The decisive advantage of NMR spectroscopy for

quantitative analysis over chromatographic methods is due to the fact that the preparation of the sample is much simpler. Nowadays, due to the enhanced sensitivity and introduction of the new pulse sequences, NMR spectroscopy (especially ^{1}H-NMR) is becoming a routine quantitative method in natural products laboratories. There are numerous examples of the application of quantitative ^{1}H-NMR in the analysis of different natural products, such as cannabinoids from *Cannabis sativa*,[27] terpene trilactones in *Ginkgo biloba*,[28,29] ephedrine alkaloids, the composition of *Ephedra* species,[30,31] camptothecin derivatives in *Nothapodytes foetida*[32] and parthenolide in feverfew products[33] and in the aerial parts of *Tanacetum larvatum*.[34]

In this paper, a survey of the cnicin content in seven wild-growing *Centaurea* species from Serbia and Montenegro measured using ^{1}H-NMR spectroscopy is reported.

EXPERIMENTAL

Plant material

The studied species and collection data are listed in Table I.

TABLE I. The studied *Centaurea* species, collection data and the average content of cnicin in the aerial parts (estimated recovery of cnicin: 95.51±2.2 %)

Species	Collection data[a]	Content, mg/g fresh plant ±*S.D.*
C. affinis Friv.	Vlasina lake, SE Serbia, July 2001 (CAf06072001)	6.12±0.15
C. arenaria Bieb. ex Willd.	New Belgrade, Serbia, June 2001 (CAr18062001)	1.06±0.06
C. cuneifolia S. S.	Progorelica, C. Serbia, June 2001 (Ccu11062001)	2.08±0.15
C. glaberima Tausch.	Kotor, Montenegro, June 2003 (Cgl29062003)	5.48±0.21
C. splendens L.	Mt. Orjen, Montenegro, June 2001 (CSpl3062001)	4.12±0.03
C. stoebe L.	Sićevo, SE Serbia, September 1998 (CSt391998)	2.61±0.06
C. salonitana Vis.	Niševac, SE Serbia, July 2001 (CS18072001)	Not detected

[a]Voucher specimens deposited at the Herbarium, Faculty of Biology, University of Belgrade – Herbarium Code BEOU

Sample preparation

An aliquot (1 g) of fresh aerial parts of the studied *Centaurea* species (cut into small pieces) was ultrasonicated, after addition of 1 ml (2.4 mg/ml) of BHT (IS, Fig. 1), with 25 ml of Et_2O at room temperature for 30 min. The extraction was repeated three times. The combined extracts were filtered and evaporated to dryness *in vacuo*. The residues were dissolved in 1 ml of $CDCl_3$ (99.9 %) and used for ^{1}H-NMR measurements. All results are based on triplicate measurements.

Recovery test of cnicin

A standard solution containing 1.87 mg of cnicin in Et_2O (1 ml) was spiked onto 1 g of filter paper disks (5891 white, Schleicher & Schuell GmbH, Kassel, Germany) cut into circles of *ca.* 1.0 cm

diameter, placed in an extraction vessel and dried at room temperature for 24 h. The NMR samples were prepared using the same procedures as above. The sample preparation and NMR measurements were carried out in triplicate.

^{1}H-NMR analysis

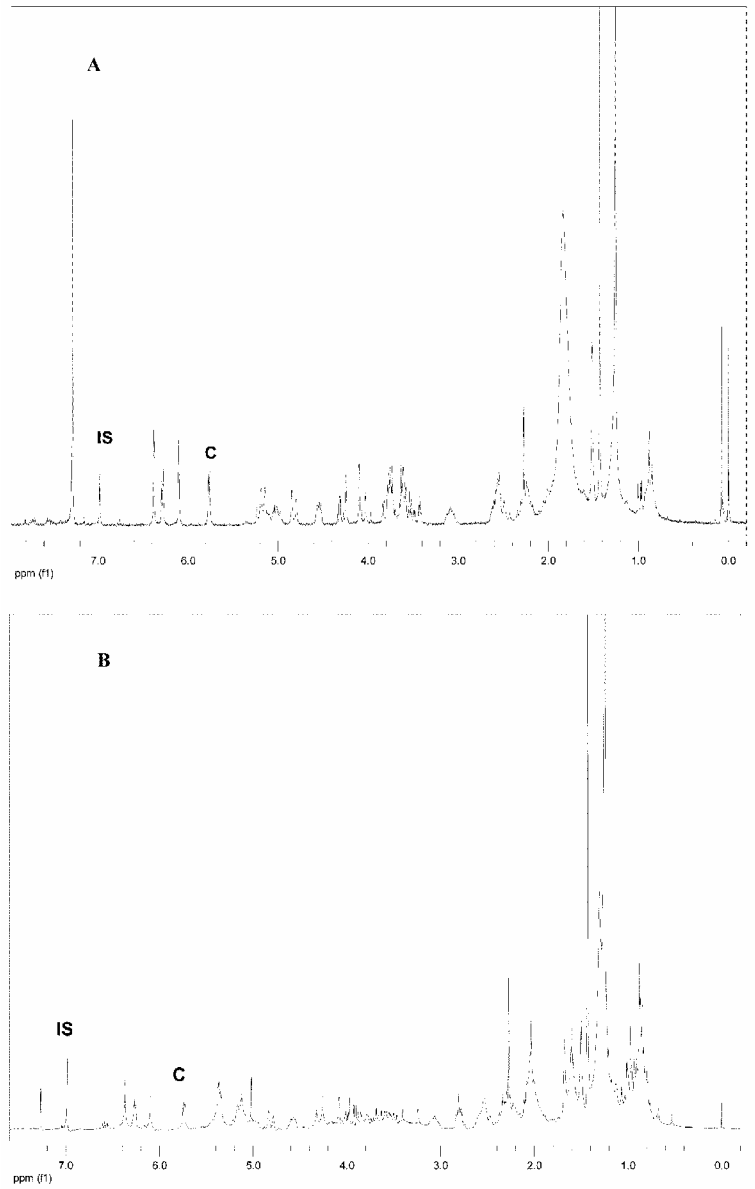

Fig. 2. ^{1}H-NMR spectra (200 MHz) in $CDCl_3$ of: cnicin + internal standard from the recovery experiment (A) and extract from *C. affinis* + internal standard (B). IS: the signal of H-3/5 from internal standard (BHT) and C: the signal of H-13 from cnicin.

The ^{1}H-NMR (200 MHz) spectra (in $CDCl_3$) were recorded using a Varian GEMINI 2000 spectrometer. For each sample, 100 scans were recorded with the following parameters: 0.187 Hz/point; spectral width, 3005.5 Hz; pulse width, 20 μs; relaxation delay, 4 s. For quantitative analysis, peak area was used and the start and end points of the integration of each peak were selected manually. The quantitative results were based on the integrals of the one-proton signal of cnicin (H-13, δ 5.75), not overlapped with other signals (see Fig. 2), and the two-proton singlet (δ 6.98) of 2,6-*bis*(1,1-dimethylethyl)-4-methylphenol (BHT), used as the internal standard (I_C and I_S, respectively), using the following equation:

$$\text{Cnicin (mg/g)} = (I_C \times M_C \times G_S)/[(I_S/2) \times M_S \times G]$$

where M_C and M_S are the molar masses of cnicin and the standard, respectively, while G and G_S are the weighed masses of the sample (g) and standard (mg), respectively.

RESULTS AND DISCUSSION

The results of the quantification of cnicin in the studied *Centaurea* species are given in Table I. The content of cnicin in six of them varied within the range 1.06–6.12 mg/g of fresh plant material, whereas cnicin was not detected in *C. salonitana*. It was demonstrated that using an appropriate choice of experimental conditions, ^{1}H-NMR spectroscopy is a suitable tool for the quantitative determination of cnicin in crude extracts. The results obtained by the ^{1}H-NMR method were found to be sufficiently accurate, with a standard deviation of between 0.03 and 0.21. The application of the ^{1}H-NMR method enabled the quantification of cnicin in a much shorter time than that required by the conventional chromatographic methods. *C. affinis*, *C. glaberima* and *C. splendens*, with a content of cnicin in the range of about 4–6 mg/g could be regarded as new sources of this valuable compound.

Acknowledgments. This research was supported by grant from the Ministry of Science of Serbia (Project No. 142053).

ИЗВОД

КВАНТИТАТИВНА АНАЛИЗА СЕСКВИТЕРПЕНСКОГ ЛАКТОНА КНИЦИНА У СЕДАМ САМОНИКЛИХ БИЉНИХ ВРСТА РОДА *Centaurea*, КОЈЕ РАСТУ У СРБИЈИ И ЦРНОЈ ГОРИ, КОРИШЋЕЊЕМ ^{1}H-NMR

ВЕЛЕ ТЕШЕВИЋ[1], СЛОБОДАН МИЛОСАВЉЕВИЋ[1], ВЛАТКА ВАЈС[2], ПЕЂА ЈАНАЋКОВИЋ[3], ИРИС ЂОРЂЕВИЋ[4], МИЛКА ЈАДРАНИН[2] и ИВАН ВУЧКОВИЋ[2]

[1]Хемијски факултет, Универзитет у Београду, Студентски трг 12–16, 11000 Београд, [2]Институт за хемију, технологију и металургију, Његошева 12, 11000 Београд, [3]Биолошки факултет, Универзитет у Београду, Студентски трг 12–16, 11000 Београд и [4]Факултет ветеринарске медицине, Универзитет у Београду, Булевар Ослобођења 18, 11000 Београд

^{1}H-NMR спектрометрија је примењена за квантитативну анализу кницина, биоактивног сесквитерпенског лактона германкранолидног типа, у надземном делу седам самониклих биљних врста рода *Centaurea* сакупљених у Србији и Црној Гори. Анализа је извршена поређењем интеграла сигнала једног протона кницина (H-13, δ 5.75) са синглетом који потиче од два протона (δ 6.98) интерног стандарда, 2,6-бис(1,1-диметилетил)-4-метилфенола (БХТ). Кницин је детектован у свим врстама, осим у *C. salonitana*, у концентрацијама у опсегу од 1,06 до 6,12 mg/g, рачунато на масу свежег биљног материјала. Овај метод омогућава брзу и једноставну квантификацију кницина без претходног пречишћавања.

(Примљено 2. марта 2007)

REFERENCES

1. V. Tešević, V. Vajs, P. Janaćković, N. Todorović, D. Đoković, P. Marin, S. Milosavljević, *Planta med.* **64** (1998) 488
2. V. Vajs, N. Todorović, M. Ristić, V. Tešević, B. Todorović, P. Janaćković, P. Marin, S. Milosavljević, *Phytochemistry* **52** (1999) 383
3. P. Janaćković, V. Tešević, S. Milosavljević, V. Vajs, P. D. Marin, *Biochem. System. Ecol.* **32** (2004) 355
4. V. Tešević, V. Vajs, N. Todorović, D. Đoković, P. Marin, S. Milosavljević, *J. Serb. Chem. Soc.* **63** (1998) 131
5. M. Kaıj-A-Kamb, M. Amoros, L. Girre, *Pharm. Acta Helv*. **67** (1992) 178
6. V. Tešević, D. Đoković, V. Vajs, P. Marin, S. Milosavljević, *J. Serb. Chem. Soc.* **59** (1994) 979
7. V. Tešević, S. Milosavljević, V. Vajs, P. Janaćković, M. Popsavin, *Biochem. System. Ecol.* **31** (2003) 89
8. D. P. Hollis, *Anal. Chem*. **35** (1963) 1682
9. G. Nowak, M. Holub, M. Budesinsky, *Acta Soc. Bot. Pol.* **58** (1989) 95
10. L. P. Christensen, J. Lam, *Phytochemistry* **29** (1990) 2753
11. L. P. Christensen, J. Lam, *Phytochemistry* **30** (1991) 3289
12. N. G Bissett, *Herbal drugs and phytopharmaceuticals*, MedPharm CRC Press, Stuttgart, 1994, p. 566
13. G. Schneider, I. Lachner, *Planta Med.* **53** (1987) 247
14. R.G. Kelsey and L. J. Locken, *J. Chem. Ecol.* **13** (1987) 19
15. A. M. Fortuna, E. C. de Riscala, C. A. N. Catala´n, T. E. Gedris, W. Herz, *Biochem. System. Ecol.* **30** (2002) 8
16. Sh. Z. Isamukhamedova, E. K. Dobronravova, T. T. Shakirov, *Khim. Prir. Soedin.* **3** (1977) 418
17. S. Huneck, J. Jakupovic, A. Schuster, *Planta Med*. **52** (1986) 398
18. M. Bruno, M. Pia Paternostro, T. Gedris, W. Herz, *Phytochemistry* **41** (1996) 335
19. A. Rustaiyan, A. Niknejad, Y. Aynechi, *Planta Med*. **44** (1982) 185
20. J. Jakupovič, Y. Jia, V. P. Pathack, F. Bolman, R. M. King, *Planta Med*. **5** (1986) 399
21. H. Skaltsa, D. Lazari, C. Panagouleas, E. Georgiadou, B. Garcia, M. Sokovic, *Phytochemistry* **55** (2000) 903
22. L. J. Locken, R. G. Kelsey, *Biochem. System. Ecol.* **15** (1987) 313
23. I. H. Landau, M. Scharer, P. I. Ward, *J. Chem. Ecol.* **20** (1994) 929
24. U. Holzgrabe, R. Deubner, C. Schollmayer, B. Waibel, *J. Pharm. Biomed. Anal.* **38** (2005) 806
25. http://en.wikipedia.org/wiki/Cnicin (21October, 2007)
26. I. Merfort, *J. Chromatogr. A* **967** (2002) 115, and references therein
27. A. Hazekamp, Y. H. Choi, R. Verpoorte, *Chem. Pharm. Bull.* **52** (2004) 718
28. C. Y. Li, C. H. Lin, C. C. Wu, K. H. Lee, T. S. Wu, *J. Agric. Food Chem.* **52** (2004) 3721
29. Y. H. Choi, H. K. Choi, A. Hazekamp, P. Bermejo, Y. Schilder, C. Erkelens, R. Verpoorte, *Chem. Pharm. Bull.* **51** (2003) 158
30. H. K. Kim, Y. H. Choi, W. T Chang, R. Verpoorte, *Chem. Pharm. Bull.* **51** (2003)1382
31. H. K. Kim, Y. H. Choi, C. Erkelens, A. W. M. Lefeber, R. Verpoorte, *Chem. Pharm. Bull.* **53** (2005) 105
32. C. Y. Li, C. H. Lin, T. S. Wu, *Chem. Pharm. Bull*. **53** (2005) 347
33. S. Heptinstall, D. V. C. Awang, B. A. Dawson, D. Kindack, D. W. Knight, J. May, *J. Pharm. Pharmacol*. **44** (1992) 391
34. I. Aljančić, V. Vajs, V. Bulatović, N. Menković, S. Milosavljević, *Biochem. System. Ecol.* **29** (2001) 655.

Journal of the Serbian Chemical Society
JSCS@tmf.bg.ac.yu • www.shd.org.yu/JSCS

J. Serb. Chem. Soc. 72 (12) 1281–1293 (2007)
JSCS–3661

UDC 546.732.004.12:548.7:547.772:548.73
Original scientific paper

Transition metal complexes with pyrazole based ligands. Part 27. Structural and thermal characterization of cobalt(II) halide and pseudohalide complexes with 4-acetyl-3-amino-5-methylpyrazole

VUKADIN M. LEOVAC[1*#], ZORAN D.TOMIĆ[2], KATALIN MÉSZÁROS SZÉCSÉNYI[1#], LJILJANA S. JOVANOVIĆ[1#] and MILAN D. JOKSOVIĆ[3]

[1]University of Novi Sad, Faculty of Sciences, Department of Chemistry, Trg D. Obradovića 3, 21000 Novi Sad, [2]"Vinča" Institute of Nuclear Sciences, Laboratory of Theoretical Physics and Condensed Matter Physics, P.O. Box 522, 11001 Belgrade and [3]Faculty of Sciences, University of Kragujevac, R. Domanovića 12, 34000 Kragujevac, Serbia

(Received 2 August 2007)

Abstract: The crystal and molecular structures of four tetrahedral structurally similar $[Co(aamp)_2X_2]$ complexes (aamp = 4-acetyl-3-amino-5-methylpyrazole, X = Cl, Br, I and NCS) were determined by X-ray diffraction analysis and are discussed in detail. It was found that the different capacity of the ligand X (NCS *vs*. Cl, Br, I) for the formation of non-bonding contacts influence the mode of molecular association in the solid state. The complexes were characterized by UV–Vis spectroscopy. The first step of the thermal decomposition of the compounds was checked and is discussed in the view of the IR spectrum of the intermediate isolated from $[Co(aamp)_2Br_2]$ by the quasi-isothermal technique.

Keywords: Cobalt(II) complexes, 4-acetyl-3-amino-5-methylpyrazole, crystal structure, electronic spectra, quasi-isothermal TA.

INTRODUCTION

Our interest in complexes with pyrazole based ligands has lasted more than a decade, due to their attractive physicochemical characteristics. Many pyrazole derivatives and their transition metal complexes exhibit biological activity, *e.g.*, derivatives of 3-aminopyrazole show anti-protozoal and cytotoxic activity.[1] Some of them are involved in enzymatic reactions.[2–4] Other 3-aminopyrazole derivatives may be used as anti-tumor agents *via* their inhibitory activity on cyclin-dependent kinase.[5–7] In order to gain a better understanding of the conditions affecting the formation of complexes, it was intended to obtain compounds in the form of single crystals with a tailored structure, by changing the experimental

* Corresponding author. E-mail: vule@ih.ns.ac.yu
# Serbian Chemical Society member.
doi: 10.2298/JSC0712281L

conditions step by step. For instance, at small pyrazole molecules, the type and position of the substituents, the solvent or the temperature of the reaction mixture, as well as the central atoms and their corresponding anions were changed.[8–11] With the title ligand, 4-acetyl-3-amino-5-methylpyrazole, compounds,[12,13] including the title compounds,[14,15] have already been prepared. However, more than ten years ago there was no the possibility to determine the crystal structure of the microcrystalline title compounds. Also, the determination of their thermal decomposition was limited by the sensitivity of the available thermobalances. Now, with up-to-date equipment, it is possible to refine earlier results. Thus, in this paper, the crystal and molecular structure of $[Co(aamp)_2X_2]$ complexes (aamp = 4-acetyl-3-amino-5-methylpyrazole, X = Cl, Br, I and NCS) are reported. The discussion includes an analysis of the different potentials of X and aamp for intermolecular interactions and how they affect the association of the molecules in the solid state. On the basis of new thermal measurements, the interpretation of the first decomposition step of the compounds is also revised.

EXPERIMENTAL

Single crystals suitable for X-ray structure determination were obtained with the synthetic procedure described earlier,[14] but using more dilute solutions. Some of the physico-chemical characteristics of these compounds have been described previously.[14] In the following text the compounds $[Co(aamp)_2X_2]$ with X = Cl, Br, I and NCS are marked as **1**, **2**, **3** and **4**, respectively.

The electronic spectra for 2×10^{-3}–3×10^{-3} mol dm^{-3} methanolic solutions of the complexes were recorded on a Secomam spectrophotometer (Anthelie 2, advanced, for the spectral range 220––900 nm) and on an FTIR instrument (NEXUS 670 FTIR, for the range 900–1400 nm).

Conductivity measurements in 1×10^{-3} mol dm^{-3} methanolic solutions of the complexes, after mild heating to complete dissolution, were performed on a digital conductivity meter, Jenway 4010.

Thermal measurements were performed using a TA Instruments SDT Q600 thermogravimetric analyzer, at a heating rate of 20 K min^{-1} in a dynamic air atmosphere (100 cm^3 min^{-1}). About 3 mg of the sample was placed in an alumina sample holder. As the reference for the DSC measurements, an identical empty alumina pan was used. For the isolation of the intermediate of the bromide compound, the SWI (quasi-isothermal[16]) mode was applied.

Crystal structure determination

The data were collected on a Bruker AXS SMART diffractometer, using MoKα radiation. The crystal structure was solved by direct methods using SIR92 software[17] and refined using the Oxford Crystals suite.[18] All non-hydrogen atoms were refined anisotropically. The hydrogen atoms were positioned geometrically at the calculated positions and allowed to ride on their parent atoms. The geometrical analysis was performed using PLATON.[19] The basic crystallographic data and structure refinement parameters are summarized in Table I.

A full list of the crystal data and refinement of **1**–**4** is deposited at the Cambridge Crystallographic Data Centre, CCDC, numbers: 655847, 655849, 655848 and 655850, respectively. They can be obtained free of charge from the Cambridge Crystallographic Data Centre *via* www.ccdc.cam.ac.uk/datarequest/cif; by post: Cambridge Crystallographic Data Centre, 12 Union Road, Cambridge CB2 1EZ, UK; by fax: +44-1223-336-033 or by e-mail: deposit@ccdc.camac.uk.

TABLE I. Selected crystallographic data and structure refinement parameters for **1**–**4**

	1	**2**	**3**	**4**
Empirical formula	$C_{12}H_{18}Cl_2CoN_6O_2$	$C_{12}H_{18}Br_2CoN_6O_2$	$C_{12}H_{18}CoI_2N_6O_2$	$C_{14}H_{18}CoN_8O_2S_2$
Formula weight	408.15	497.06	591.06	453.41
Temperature, K	293	293	293	293
Wavelength, Å	0.71073	0.71073	0.71073	0.71073
Crystal system	Monoclinic	Monoclinic	Triclinic	Monoclinic
Space group	C2/*c*	C2/*c*	P-1	P*c*
a / Å	18.785(2)	19.023(1)	8.1680(5)	9.1209 (17)
b / Å	8.498(1)	8.7846(6)	10.9704(7)	7.7106 (15)
c / Å	13.952(2)	13.998(1)	11.0852(7)	14.183 (3)
α / °	90	90	97.793(1)	90
β / °	131.156(2)	131.697(2)	98.213(1)	100.800 (8)
γ / °	90	90	108.925(1)	90
Volume, Å^3	1677	1746	912	980
Z	4	4	2	2
D_c / mg m^{-3}	1.617	1.890	2.152	1.537
F(000)	836	980	562	466
θ range, °	3.9–30.0	2.7–34.4	1.9–30.0	2.3–30.0
Reflections collected	11174	5659	12085	3142
Independent reflections	2423	3249	5277	2968
$N_{ref.}$ [$I > 2\sigma(I)$]	1741	2267	4273	2679
$N_{par.}$	105	141	208	244
GOF (F^2)	1.00	0.87	0.93	0.93
R [$I > 2\sigma(I)$]	0.0673	0.0324	0.0378	0.037
wR (all data)	0.1673	0.0685	0.0971	0.093

RESULTS AND DISCUSSION

Molecular and crystal structures

In all four complexes, the aamp ligand is bound to the metal through the N2 nitrogen of the pyrazole ring as a neutral monodentate ligand. The pair of X anions completes the distorted tetrahedral coordination, with the ambidentate NCS bound to Co(II) in **4** through the N atom. In the crystal structure of **1** and **2,** Co(II) resides on a twofold rotation axis. The perspective view of the complexes **2** and **4**, together with the atom numbering scheme are shown in Figs. 1 and 2. Selected bond angles and bond distances are given in Tables II and III. Comparison with the related structures[12] reveals no unexpected differences in the metric parameters of the title compounds. In complexes **1**–**3,** the anion ligands participate in hydrogen bonds with one of the amino hydrogens, while the other

amino hydrogen is weakly bound to the acetyl–O. Both hydrogen bonds are intramolecular, which indicates that X plays no significant role in the association of the molecules in the crystal structure. The dotted lines in Figs. 1 and 2 depict the weak intramolecular hydrogen bonds. In **4**, only one aamp ligand shows a similar spatial relation with X, with the amine hydrogen atoms involved in weak hydrogen bonds with the acetyl–O and the thiocyanato–N (Fig. 2, Table IV). In the same complex, the second pyrazole ligand exists in its other tautomeric form, *i.e.*, as 4-acetyl-5-amino-3-methylpyrazole. To the best of our knowledge, this is the first example of the isolation of the specified tautomer of this ligand. The difference is visualized in Fig. 3, where part of **4** is overlaid compound **2**.

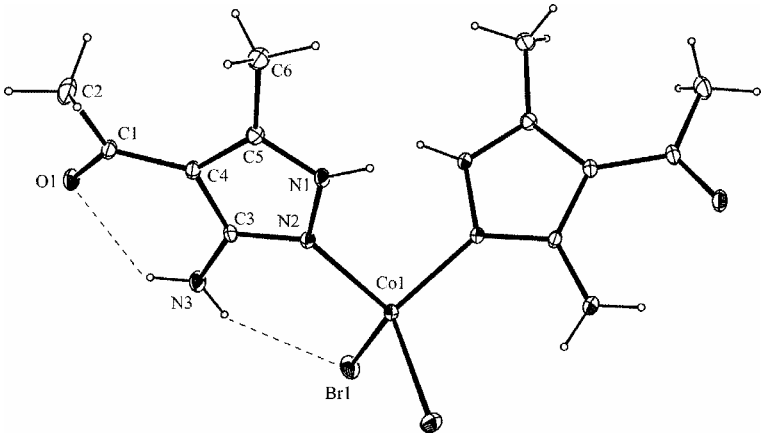

Fig. 1. The molecular unit and atom numbering scheme of $[Co(aamp)_2Br_2]$.

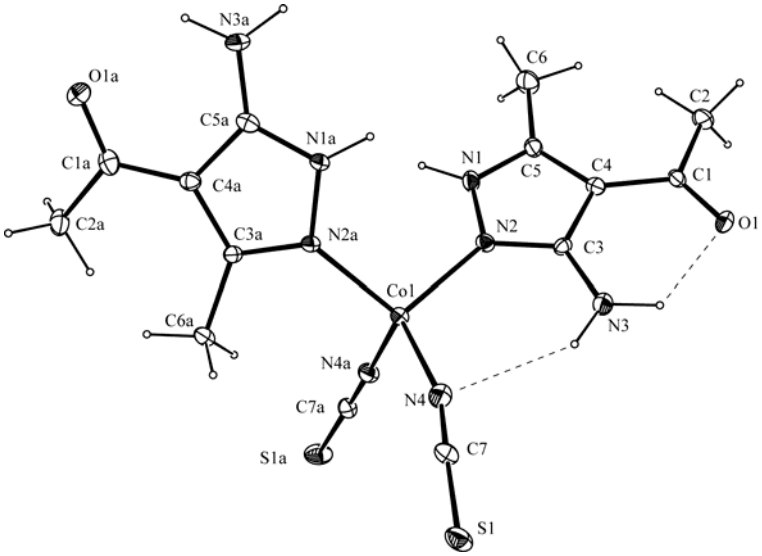

Fig. 2. Molecular structure and atom numbering scheme of $[Co(aamp)_2(NCS)_2]$.

TABLE II. Selected bond distances (Å) for **1**–**4**

	1	**2**	**3**	**4**
N1−N2	1.374(5)	1.386(3)	1.381(5)/1.376(5)	1.376(6)/1.392(6)
N2−C3	1.338(7)	1.348(4)	1.344(5)/1.343(5)	1.332(6)/1.352(6)
N1−C5	1.320(7)	1.326(5)	1.331(5)/1.340(5)	1.327(6)/1.341(6)
C3−C4	1.417(7)	1.420(4)	1.417(5)/1.441(5)	1.442(6)/1.421(6)
C4−C5	1.393(7)	1.406(4)	1.408(5)/1.389(6)	1.399(6)/1.412(6)
C3−N3	1.360(6)	1.346(3)	1.355(6)/1.342(5)	1.357(6)/1.343(6)
C4−C1	1.449(8)	1.443(4)	1.450(5)/1.445(5)	1.446(6)/1.445(6)
C5−C6	1.495(7)	1.484(4)	1.479(6)/1.489(6)	1.495(7)/1.494(6)
C1−C2	1.501(9)	1.502(5)	1.508(7)/1.502(6)	1.520(7)/1.515(6)
C1−O1	1.239(5)	1.240(3)	1.236(5)/1.238(5)	1.230(7)/1.249(6)
Co−N2	2.006(4)	2.002(3)	2.005(3)/2.004(3)	2.000(4)/2.007(4)
Co−X	2.247(2)	2.3840(5)	2.5964(6)/2.5682(6)	1.959(5)/1.950(4)

TABLE III. Bond angles (°) subtended at Co(II). Symmetry codes: i = 1 – *x*, *y*, –1/2–*z*; ii = 2 – *x*, *y*, 3/2 – *z*

1		**2**	
Cl2−Co1−N2	117.1(1)	Br1-Co1-N2	109.98(6)
Cl2−Co1−Cl2^{i}	108.3(6)	Br1-Co1-Br1^{ii}	105.67(2)
Cl2−Co1−N2^{i}	108.5(1)	Br1-Co1-N2^{ii}	116.77(7)
Cl2i−Co1−N2	108.5(1)	Br1^{ii} -Co1-N2	116.77(7)
N2−Co1−N2^{i}	97.4(2)	N2-Co1-N2^{ii}	98.1(1)
Cl2i−Co1−N2^{i}	117.1(1)	Br1^{ii}-Co1-N2^{ii}	109.98(6)
3		**4**	
I1−Co1−I2	111.04(2)	N2−Co1−N1a	104.7(2)
I1−Co1−N2	111.5(1)	N2−Co1−N4	109.6(2)
I1−Co1−N2a	110.3(1)	N2−Co1−N4a	108.6(2)
I2−Co1−N2	108.54(9)	N1a−Co1−N4	115.7(2)
I2−Co1−N2a	112.2(1)	N1a−Co1−N4a	110.5(2)
N2−Co1−N2a	103.0(1)	N4−Co1−N4a	107.6(2)

TABLE IV. Geometry of intermolecular hydrogen bonds. Symmetry codes: i = 1/2+*x*,1/2–*y*,1/2+*z*; ii = 1/2+*x*,3/2–*y*,1/2+*z*; iii = 2–*x*,2–*y*,2–*z*; iv = 1–*x*,1–*y*,1–*z*; v = *x*, –1–*y*,1/2+*z*

Compound	D–H···A	H···A (Å)	D–H···A (º)
1	N1−H11···O1^{i}	1.85	176
2	N1−H6···O1^{ii}	1.94	176
3	N1a−H11···O1^{iii}	1.80	169
	N1−H22··· O1a^{iv}	1.86	166
4	N1−H111···O1^{v}	1.81	154

The chemical similarity of compounds **1**–**3** reflects itself not only in the similar molecular structure of the three complexes (Table II), but also in their similar mode of molecular association in the crystal structure. The common motif responsible for the association of the molecules in the solid state is the N−H···O hydrogen bond formed between N1 of one molecule and the acetyl–O from the neighboring molecule. The geometrical parameters relevant for these interactions

are given in Table IV. This hydrogen bond leads to the formation of molecular chains (see Fig. 4). As Fig. 4 depicts, two neighboring molecules are connected by a pair of N–H···O hydrogen bonds. In the crystal structures of complexes **1**–**3**, the closest Co(II)···Co(II) distances are 9.02, 9.00 and 8.1 Å, respectively. In **4**, the Co(II) atoms are placed closer, at a distance of 7.63 Å. The arrangement of the molecular chains into the crystal structure in **1**–**3** is governed by weak van der Waals forces. For the sake of clarity, the hydrogen atoms which are not involved in hydrogen bonds are omitted in Fig. 4. The association of the molecules in **4** in the solid state (Fig. 5) also involves the N−H···O hydrogen bond of the same type as in **1**–**3**. However, in contrast to compounds **1**–**3**, only one of the pyrazole ligands, the one with the similar spatial relation towards X, is involved in such an interaction. The other aamp ligand is oriented so that the acetyl–O is placed at a distance 3.03 Å from the S atom of the neighboring molecule. This is 0.29 Å closer than a sum of the van der Waals radius of the S and O atoms.[20] This can be an indication for an interaction between these atoms. The role of S···O contact in the association of molecules is less investigated. However, recent results reveal its role in intermolecular interactions.[21] In the crystal structure of **4**, this contact leads to the association of two molecular chains (Fig. 5).

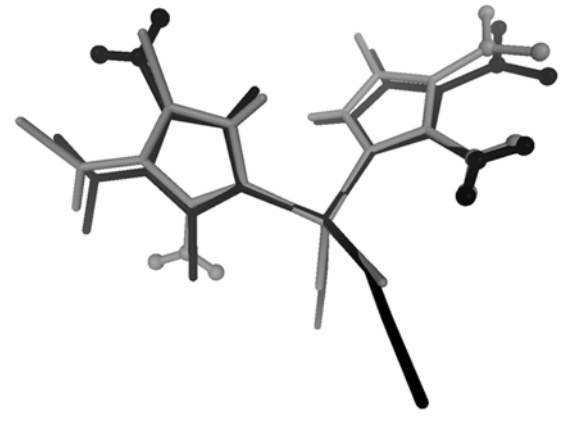

Fig. 3. Overlay of $[Co(aamp)_2(NCS)_2]$ (dark) and $[Co(aamp)_2Br_2]$ (grey) showing (left) the different orientation of the NH_2 groups (depicted as balls). Methyl hydrogens are excluded for clarity.

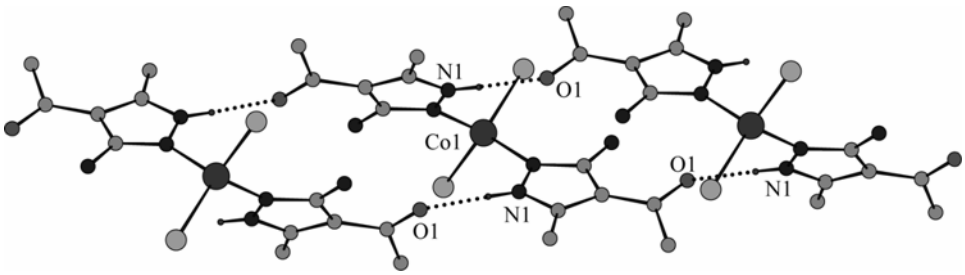

Fig. 4. Perspective view of the chain structure in $[Co(aamp)_2Br_2]$.

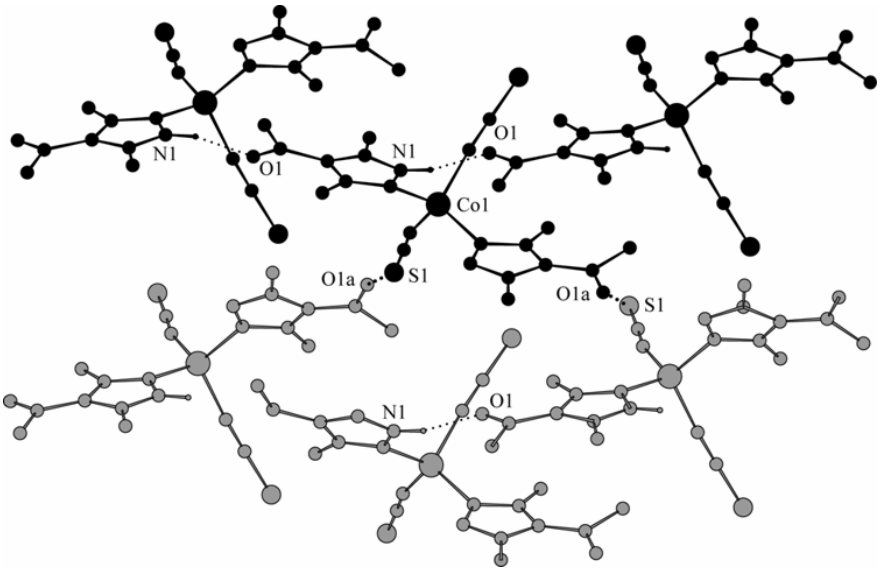

Fig. 5. Part of the crystal structure of $[Co(aamp)_2(NCS)_2]$ showing the formation of the molecular chain driven by the hydrogen bonds and association of two chains (depicted in black and grey) governed by S···O interactions.

Conductometric and electronic spectral data

Due to the low solubility of the compounds in cold methanol, the solutions had to be mildly heated for a short time before running the UV–Vis spectra. During dissolution, the initially turquoise solutions became pink, and remained stable for days. This change of color suggests a change in the configuration from tetrahedral to octahedral, by inclusion of solvent molecules in the Co(II) coordination sphere, accompanied by the partial or complete substitution of the X ligands with solvent molecules (Table V). Namely, as can be seen from the molar conductometric data, the most stable in this respect is the NCS complex, the Λ_M of which is below the range for electrolytes of the 1:1 type (80–115 S cm^2 mol^{-1}), while the least stable is **1**, the Λ_M of which is close to that for 2:1 electrolytes (160–220 S cm^2 mol^{-1}).[22]

TABLE V. Conductometric (Λ_M) and UV–Vis (λ_{max}) spectral data of the complexes in MeOH. *sh* – Shoulder, *bp* – broad peak

Complex	Λ_M / S cm^2 mol^{-1}	λ_{max} / nm(ε / dm^3 mol^{-1} cm^{-1})
$[Co(aamp)_2Cl_2]$	111	241(12300), 282(10900), 482(6), 523(8), ~650*sh*(1), ~1010*bp*(2)
$[Co(aamp)_2Br_2]$	125	241(11700), 282(11400), 522(9), 647(2), ~1030 *bp*(3)
$[Co(aamp)_2I_2]$	157	< 231, 282(9500), 518(8), ~667*sh*(1), 930–1030, *bp*(9)
$[Co(aamp)_2(NCS)_2]$	50	240(11800), 282(10600), 488(21), 520(28), 620*sh*(5), ~910(2), 1048(5)

The electronic spectra of the complexes in methanol (Table V) display several types of characteristic absorption bands. Generally, the two highest energy absorptions of the complexes are similar to those of the ligand itself [(λ_{max}, nm, 240 (ε, $dm^3\ mol^{-1}\ cm^{-1}$, 6280) and 283 (5600)[23]]. These bands are well defined and are due to intraligand transitions. Since π(ligand) $\rightarrow$ Co(II) electron transfers are also expected in this range ($\approx$ 280 nm),[24] the only slightly changed appearance and λ_{max} position of the band at 282 nm if compared to that of the ligand are the consequence of their weak intensity. In addition, the minor shifts in λ_{max} of both bands in the spectra of the complexes with respect to those of the ligand suggest a very loose covalency between the pyrazole ligand and Co(II).

No separate CT bands, due to X and Co(II) electron transfer were observed which, considering also the conductivity data, can be proof of their partial substitution by solvent molecule in coordination with Co(II). The pink color of all the complexes in methanol and the recorded spectra for d–d interactions suggest a pseudo-octahedral geometry. For this type of high-spin d^7 complexes, three basic electron transitions occur at the levels $^4T_{2g} \leftarrow {}^4T_{1g}$ (ν_1), $^4A_{2g} \leftarrow {}^4T_{1g}$ (ν_2) and $^4T_{1g}$ (P) $\leftarrow {}^4T_{1g}$ (ν_3).[25] A typical shape of a d–d band around ν_3 consists of a low energy shoulder and a weak, high energy absorption, as a consequence of, probably, spin–orbital coupling. The first absorption band located in the near IR range is very weak and in certain complexes rather broad (in **3** 100 nm), suggesting an apparent degeneracy of this level. The other transitions due presumably to trigonal distortion, which are located in the UV range, are probably either masked by strong intraligand transitions or positioned out of the available range. Hence, as can be seen from the data of the spectra of most complexes, only two separate bands (ν_1 and ν_3) are observed, which can be explained in the following way. First, $^4A_{2g} \leftarrow {}^4T_{1g}$ (ν_2) is a two-electron transition[25] and, therefore, relatively weak in intensity. Second, ν_2 and ν_3 are very close, which does not permit a precise determination of the weaker one, ν_2.

Thermal analysis

Simultaneous TG–DSC curves were recorded only up to 620 K, *i.e.*, only to obtain the first decomposition step. Namely, in a previous paper,[15] the thermal decomposition was described in detail. The sample masses used for the TA measurements in 1996 were about 100 mg and the heating rate was 10 K min^{-1}. All compounds showed a continuous decomposition, with a clearly separated first step. With the new up-to-date equipment, it seemed promising to isolate an intermediate and to characterize more closely the processes that might be involved in the decomposition. The TG curves are presented in Fig. 6.

The thermal stability increases in the following order **4** < **3** < **2** ~ **1**, as was found in a previous study.[15] However, at a higher heating rate and with a significantly lower sample mass, the thermal decomposition showed a completely

different pattern, with a much smaller mass decrease in the first step. In the case of **2**, the TG change at 560 K dropped almost to zero (see Fig. 6). The use of the quasi-isothermal (SWI) measurement mode allowed the preparation of an intermediate (Fig. 7). The mass loss corresponds to the departure of a molecule with a relative molar mass of about 39, which is much less than one HBr molecule, as was presumed earlier.[15] The FTIR spectrum of the intermediate, compared to that of the original compound is presented in Fig. 8. As can be seen, the most obvious feature of the spectra refers to demethylation of the complex (different CH_3 stretches in the range of 3000–2850 cm^{-1}, the absence of a strong CH_3 asymmetric def. + pyrazole skeleton stretch at 1492 cm^{-1} and that at 960 cm^{-1} related to C–C stretch + CH_3 rock[9]). The different bands in the 3450–2850 cm^{-1} range may also refer to the loss of an amine group. A very intensive CO stretch at 1624 cm^{-1} in the spectrum of the intermediate is still present, but shifted to a lower frequency (1600 cm^{-1}). This means that the departure of the acetyl group is excluded. Thus, the most probable decomposition mechanism may include the departure of both CH_2- and NH-groups. Obtained under the same conditions from **3**, the departing fragments have equal relative molar masses suggesting a similar decomposition pattern. However, the much higher mass loss ($M_r \approx 45$) for the chloride complex suggests a different decomposition route. This supposition is also supported by the different shape of the DTG curve of **1**. In the case of **4**, there is no way to explain the decomposition since it was not possible to isolate any intermediate. To suggest a probable decomposition mechanism, measurements using coupled TA–MS or TA–IR instruments would be necessary.[26,27]

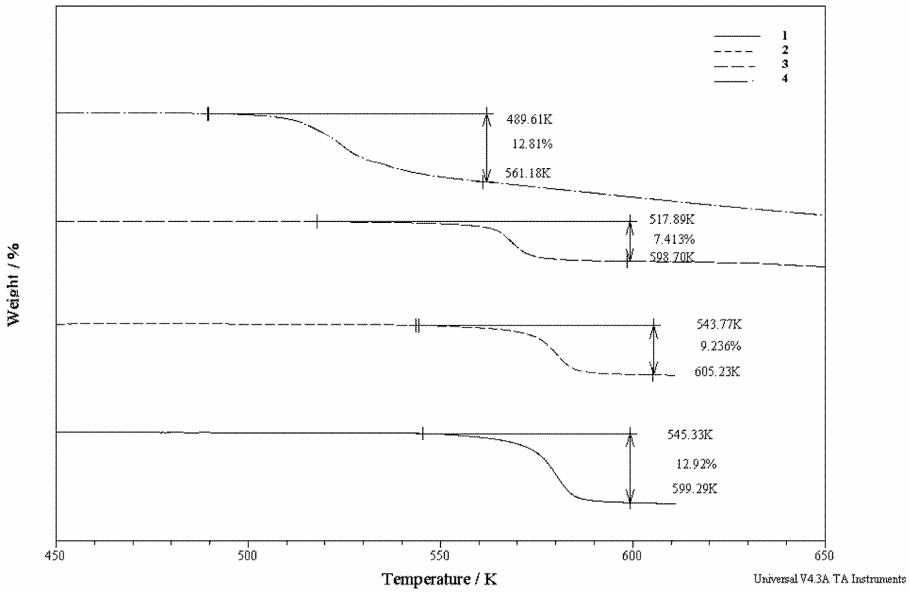

Fig. 6. The first TG-step of the decomposition of **1**–**4**.

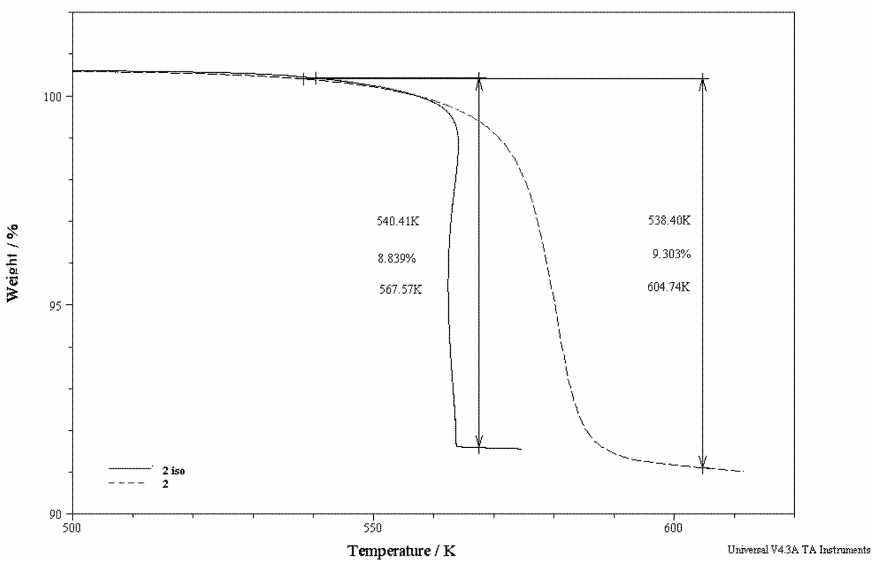

Fig. 7. SWI curve of **2** (—) compared with the corresponding TG (--) curve at a heating rate of 10 K min^{-1}.

The DSC curves (Fig. 9) of the complexes for the first decomposition step give different molar enthalpy changes, ranging from 36 kJ mol^{-1} (**3**) to 25 kJ mol^{-1} for (**2**). As these values show no regularity, they cannot be used for interpretation of the processes. The peak temperatures for **1**–**4** are 582.8, 582.5, 570.2 and 524.7 K, respectively. No melting of the compounds during the first decomposition step was observed. The blue color of **2** changed to deep (almost black) blue for its intermediate.

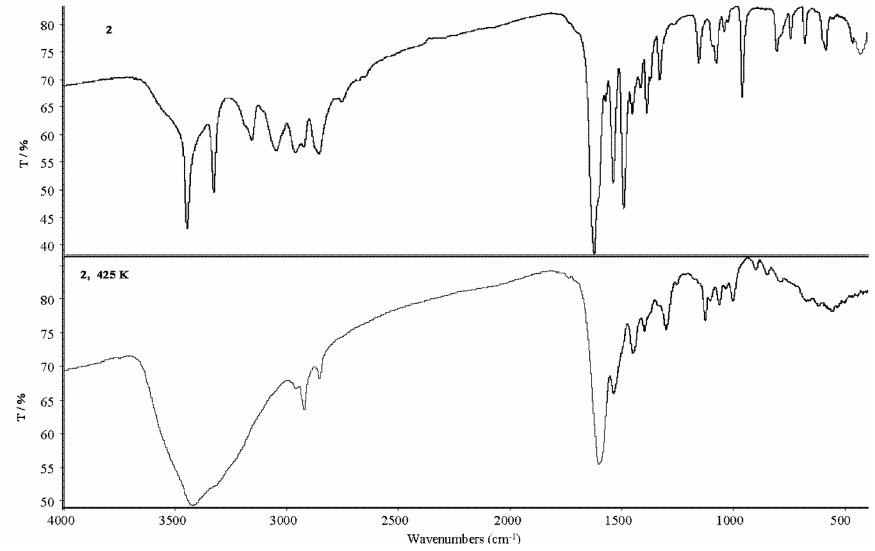

Fig. 8. FTIR spectrum of **2** and the corresponding spectrum of the intermediate at 425 K.

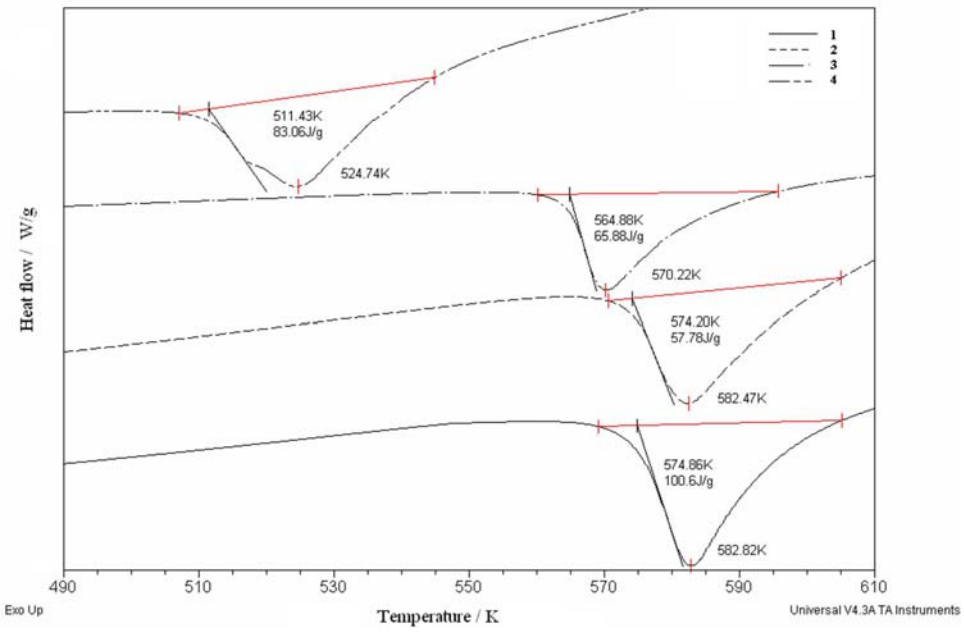

Fig. 9. DSC curves of complexes **1**–**4**.

Acknowledgement. The work was financed in part by the Ministry of Science of the Republic of Serbia (Grant No. 142028) and the Provincial Secretariat for Science and Technological Development of Vojvodina. K. M. Sz. thanks the Ministry for the donated SDT Q600, TA Instruments. The authors would like to thank Ivana Radosavljević–Evans (Dept. of Chemistry, University of Durham, UK) for solving the crystal structures.

И З В О Д

КОМПЛЕКСИ ПРЕЛАЗНИХ МЕТАЛА СА ЛИГАНДИМА ЗАСНОВАНИМ НА ПИРАЗОЛУ. ДЕО 27. СТРУКТУРНА И ТЕРМИЧКА КАРАКТЕРИЗАЦИЈА КОБАЛТ (II) ХАЛОГЕНИДНИХ И ПСЕУДОХАЛОГЕНИДНИХ КОМПЛЕКСА СА 4-АЦЕТИЛ-3-АМИНО-5-МЕТИЛПИРАЗОЛОМ

ВУКАДИН М. ЛЕОВАЦ[1], ЗОРАН Д. ТОМИЋ[2], KATALIN MÉSZÁROS SZÉCSÉNYI[1], ЉИЉАНА С. ЈОВАНОВИЋ[1] и МИЛАН Д. ЈОКСОВИЋ[3]

[1]Департман за хемију, Природно–математички факултет, Универзитет у Новом Саду, Трг Д. Обрадовића 3, 21000 Нови Сад, [2]Институт за нуклеарне науке "Винча", Лабораторија за теоријску физику и физику кондензоване материје, п. пр. 522, 11001 Београд и [3]Природно–математички факултет, Универзитет у Крагујевцу, Р. Домановића 12, 34000 Крагујевац

Дифракцијом X-зрака са монокристала одређене су кристалне и молекулске структуре четири врло слична тетраедарска комплекса кобалта (II) опште формуле $[Co(aamp)_2X_2]$ (aamp = = 4-ацетил-3-амино-5-метилпиразол, X = Cl, Br, I, NCS). Утврђено је да разлике у својствима анјонских лиганада (NCS у односу на Cl, Br и I) утичу на начин груписања молекула у чврстом стању. Комплекси су окарактерисани UV–Vis спектроскопијом и методама термичке анализе, уз интерпретацију првог ступња термичког разлагања.

(Примљено 2. августа 2007)

REFERENCES

1. N. R. Sperandeo, R. Brun, *ChemBioChem.* **4** (2003) 69
2. D. R. Compton, S. Sheng, K. E. Carlson, N. A. Rebacz, I. Y. Lee, B. S. Katzenellenbogen, J. A. Katzenellenbogen, *J. Med. Chem.* **47** (2004) 5872
3. M. Suzuki, H. Iwasaki, Y. Fujikawa, M. Sakashita, M. Kitahara, R. Sakoda, *Bioorg. Med. Chem. Lett.* **11** (2001) 1285
4. M. E. Fraley, R. S. Rubino, W. F. Hoffman, S. R. Hambaugh, K. A. Thomas, *Bioorg. Med. Chem. Lett.* **12** (2002) 3537
5. S. Samanta, B. Debnath, A. Basu, S. Gayen, K. Srikanth, T. Jha, *Eur. J. Med. Chem.* **41** (2006) 1190
6. P. Pevarello, M. G. Brasca, R. Amici, P. Orsini, G. Traquandi, L.Corti, C. Piutti, P. Sansonna, M. Villa, B. S. Pierce, M. Pulici, P. Giordano, K. Martina, E. L. Fritzen, R. A. Nugent, E. Casale, A. Cameron, M. Ciomei, F. Roletto, A. Isacchi, G. P. Fogliatto, E. Pesenti, W. Pastori, A. Marsiglio, K. L. Leach, P. M. Clare, F. Fiorentini, M. Varasi, A. Vulpetti, M. A. Warpehoski, *J. Med. Chem.* **47** (2004) 3367
7. P. Pevarello, D. Fancelli, A. Vulpetti, R. Amici, M. Villa, V. Pittalà, P. Vianello, A. Cameron, M. Ciomei, C. Mercurio, J. R. Bischoff, F. Roletto, M. Varasi, M. G. Brasca, *Bioorg. Med. Chem. Lett.* **16** (2006) 1084
8. K. Mészáros Szécsényi, V. M. Leovac, A. Kovács, G. Pokol, Ž. Jaćimović, *J. Therm. Anal. Cal.* **85** (2006) 289
9. K. Mészáros Szécsényi, V. M. Leovac, V. I. Češljević, A. Kovács, G. Pokol, Gy. Argay, A. Kálmán, G. A. Bogdanović, Ž. K. Jaćimović, A. Spasojević–de Biré, *Inorg. Chim. Acta* **353** (2003) 253
10. A. Kovács, D. Nemcsok, G. Pokol, K. Mészáros Szécsényi, V. M. Leovac, Ž. K. Jaćimović, I. Radosavljević–Evans, J. A. K. Howard, Z. D. Tomić, G. Giester, *New J. Chem.* **29** (2005) 833
11. A. Kovács, K. Mészáros Szécsényi, V. M. Leovac, Z. D. Tomić, G. Pokol, *J. Organomet. Chem.* **692** (2007) 2582
12. A. Hergold–Brundić, B. Kaitner, B. Kamenar, V. M. Leovac, E. Z. Ivegeš, N. Juranić, *Inorg. Chim. Acta* **188** (1991) 151
13. V. Yu. Kukushkin, E. A. Aleksandrova, V. M. Leovac, E. Z. Ivegeš, V. K. Konovalov, *Polyhedron* **11** (1992) 2691
14. V. M. Leovac, E. Z. Ivegeš, V. I. Češljević, A. F. Petrović, D. M. Petrović, D. Poleti, *J. Serb. Chem. Soc.* **61** (1996) 551
15. A. F. Petrović, S. R. Lukić, D. M. Petrović, E. Z. Ivegeš, V. M. Leovac, *J. Therm. Anal.* **47** (1996) 879
16. J. Paulik, F. Paulik, *Simultaneous Thermoanalytical Examinations by Means of the Derivatograph*, *Comprehensive Analytical Chemistry*, Vol. XII, Thermal Analysis, W. W. Wendlandt, Adv. Ed., Elsevier, Amsterdam, Oxford, New York, 1981, p. 47
17. A. Altomare, G. Cascarano, C. Giacovazzo, A. Guagliardi, M.C. Burla, G. Polidori, M. Camalli, J. *Appl. Crystallogr.* **27** (1994) 435
18. P. W. Betteridge, J. R. Carruthers, R. I. Cooper, K. Prout, D. J. Watkin, *J. Appl. Crystallogr.* **36** (2003) 1487
19. L. Spek, *PLATON-99, Molecular Geometry Program*, University of Utrecht, The Netherlands, 1999
20. A. Bondi, *J. Phys. Chem.* **68** (1964) 441
21. Y. Nagao, S. Miyamoto, M. Miyamoto, H. Takeshige, K. Hayashi, S. Sano, M. Shiro, K. Yamaguchi, Y. Sei, *J. Am. Chem. Soc.* **128** (2006) 9722
22. W. J. Geary, *Coord. Chem. Rev.* **7** (1971) 81
23. V. M. Leovac, Z. D. Tomić, A. Kovács, M. D. Joksović. Lj. S. Jovanović, K. Mészáros Szécsényi, *J. Organomet. Chem.* (2007), doi: 10.1016/j.organchem.2007.10.018

24. J. P. Jesson, S. Trofimenko, D. R. Eaton, *J. Am. Chem. Soc.* **89** (1967) 3148
25. A. B. P. Lever, *Inorganic Electronic Spectroscopy, Part 1*, 2nd Ed., Elsevier, Amsterdam, 1967 (Russian translation)
26. D. Czakis–Sulikowska, J. Radwańska–Doczekalska, A Czylkowska, A. Markiewicz, A. Broniarczyk, *J. Therm. Anal. Cal.* **86** (2006) 327
27. J. Madarász, G. Pokol, *J. Therm. Anal.* **88** (2007) 329.

Journal of the Serbian Chemical Society
JSCS@tmf.bg.ac.yu • www.shd.org.yu/JSCS

J. Serb. Chem. Soc. 72 (12) 1295–1308 (2007)
JSCS–3662

UDC 546.732+547.64:66.087.3
Original scientific paper

High-spin binuclear Co(II) complexes with a pendant octaazamaclocycle and carboxylates

G. VUČKOVIĆ[1]*[#], S. B. TANASKOVIĆ[2#], Z. M. MIODRAGOVIĆ[1#] and V. STANIĆ[1]

[1]*Faculty of Chemistry, University of Belgrade, P.O. Box 158, 11001 Belgrade and* [2]*Faculty of Pharmacy, University of Belgrade, Vojvode Stepe 450, 11001 Belgrade, Serbia*

(Received 24 September 2007)

Abstract: Three new binuclear Co(II) mixed-ligand complexes with *N,N′,N″,N‴*-tetrakis(2-pyridylmethyl)-1,4,8,11-tetraazacyclotetradecane (tpmc) and mono- or dicarboxylate ligands were prepared and some of their physical properties were determined. The general formulas: $[Co_2(HCOO)_2tpmc](ClO_4)_2{\cdot}4H_2O$, $[Co_2(CH_3COO)_2tpmc](ClO_4)_2$ and $[Co_2(tpht)tpmc](ClO_4)_2{\cdot}4H_2O$ ($tphtH_2$ = terephthalic acid) were proposed on the basis of elemental analyses (C,H,N) and molar conductivity. UV/Vis absorption and IR spectra, magnetic and CV measurements were used to study their geometries and properties. For the monocarboxylate complexes, an *exo* coordination of Co(II) with four nitrogens from tpmc and bis-bidentate bonded $HCOO^-/CH_3COO^-$ in the *trans* position is assumed. Tpmc adopts the chair conformation. For the dicarboxylate complex, it is supposed that a terephthalate dianion, as well as methylene chains from cyclam bridge two Co(II) atoms, while tpmc is in the boat conformation. The complexes were stable against chemical and electrochemical oxidation of Co(II) to Co(III). The data are compared with those for the previously published Cu(II) complexes containing the corresponding ligands and mutual similarities or differences were considered. Finally, some antibacterial activity of the complexes was found.

Keywords: Co(II) mixed-ligand complexes, *N,N′,N″,N‴*-tetrakis(2-pyridylmethyl)--1,4,8,11-tetraazacyclotetradecane, acetate, formate, terephthalate.

INTRODUCTION

Magnetic interactions between paramagnetic ions in bi- or polynuclear complexes containing bridged ligands have been the subject of numerous investigations, in order to obtain information for the design of inorganic–organic materials and active sites in functional biological substances.[1,2] A large number of mono-, bi- and tetranuclear mixed-ligand complexes containing pendant macrocycle *N,N′,N″,N‴*-tetrakis(2-pyridylmethyl)-1,4,8,11-tetraazacyclotetradecane (tpmc) (Fig. 1)[3] and one or two additional ligands of various type have hitherto been described. Most of them were Cu(II) and some of them Co(II) complexes.[3–16] In bi- and te-

* Corresponding author. E-mail: gordanav@chem.bg.ac.yu
[#] Serbian Chemical Society member.
doi: 10.2298/JSC0712295V

tranuclear complexes, depending on the number, sort and size of the donor atoms of the additional ligands, the central metal atom and the reaction conditions, different modes of macrocyclic conformations were found (Scheme 1). The macrocyclic ligand adopts a boat conformation when the additional ligand is bonded in a bridged manner (Schemes 1a and 1d) and a chair conformation when two other ligands are independently bonded in the *trans* position (Schemes 1b and 1c). The latter situation was observed in the case of voluminous additional ligands or if an excess of this ligand was added during preparation. The majority of Co(II) complexes with tpmc were stable against oxidation by air oxygen and toward hydrolysis.[4–6] This unexpected property is ascribed to the hydrophobic environment formed by macrocycle around the metal ion. However, by chemical oxidation of μ-carbonato or μ-α-aminoisobutyrato binuclear Co(II)tpmc complexes using H_2O_2, mixed-valence Co(2)/Co(3) complexes were formed.[5,6]

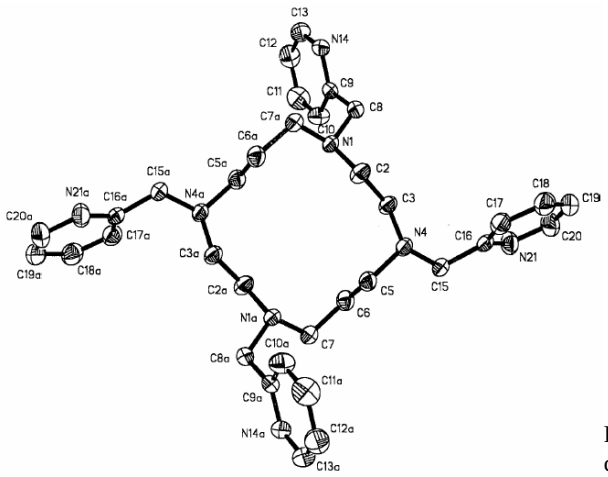

Fig. 1. Structure of the octaazamacrocyclic ligand tpmc.

A carboxylate group as a bridged ligand is present in several metalloenzymes. Due to the various coordination modes of mono- or polycarboxylato ligands and, consequently, the diversity of the possible geometries, the study of magnetic interactions in such complexes is very attractive. In a series of octahedral Co(II) complexes with the general formula $[Co_2(\mu\text{-}CH_3CO_2)Z_2(\mu\text{-}A)]^+$, (Z = *N*,*N*′,*N*″-trimethyl-1,4,7-triazacyclononane; A = OH^-, Cl^-, Br^-) weak antiferromagnetic interactions were found due to three factors: (1) smaller orbital contribution to the overall magnetic moment, (2) intermolecular antiferromagnetic and/or (3) intramolecular magnetic coupling between the Co(II) ions.[17]

In last two decades, complexes with mono- or dicarboxylato ligands, both aliphatic and aromatic, were intensively studied. In binuclear Co(II) complexes of the general formula $[Co_2(Y)tpmc]^{3+}$, HY = glycine, (*S*)-alanine, (*S*)-α-aminobutyric acid, α-aminoisobutyric acid, β-aminoisobutyric acid, β-aminobutyric acid

and (*S*)-phenylalanine, the aminocarboxylate anions are coordinated through the COO^- group.[5,6,14] The results of electronic spectroscopy, as well as magnetic measurements, corresponded to high-spin, pentacoordinated Co(II) complexes with a square pyramidal geometry. The IR spectroscopic data suggested that in the case of all the complexes both oxygen atoms of the carboxylato groups participate in the coordination. The value $\Delta\nu$ decrease in the row (*S*)-alanine > > glycine > β-aminobutyric acid > α-aminoisobutyric acid > β-aminoisobutyric acid > (*S*)-α-aminobutyric acid, indicating the diminution of the bond strength in the same order. For the complex with (*S*)-phenylalanine, it was supposed that hexa-coordination and bis(bidentate)-bridged coordination occured.

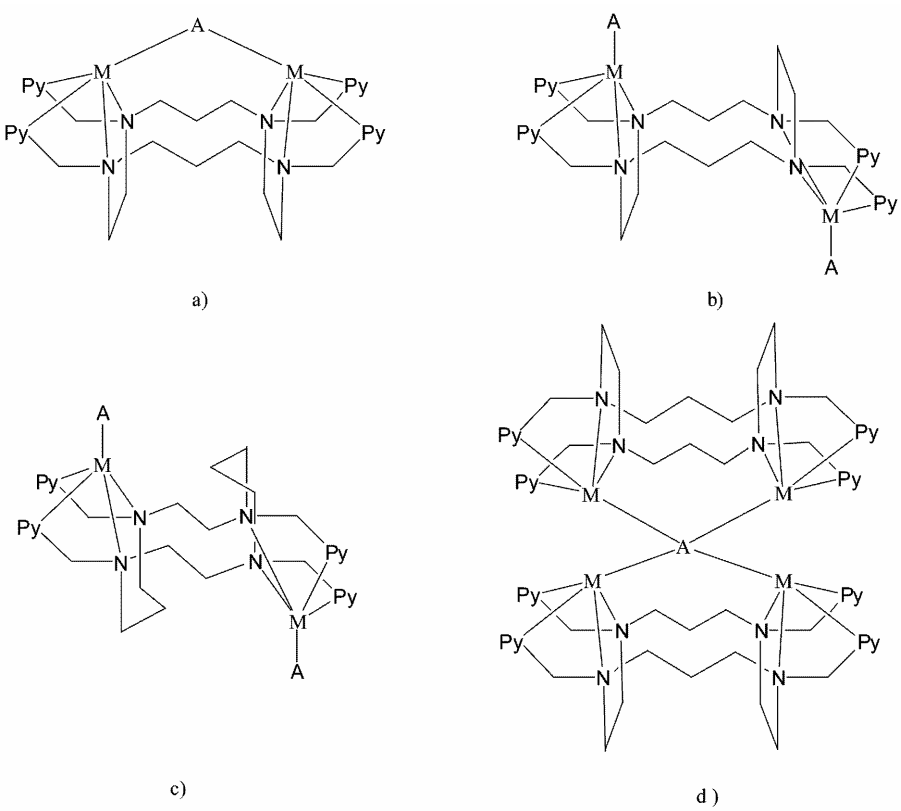

Scheme 1. Simplified coordination modes found in: a), b) c) dinuclear complexes, M = Co(II) and Cu(II); d) tetranuclear complexes, M = Cu(II) with aliphatic/aromatic carboxylates (A).

In addition, Co(II) or Cu(II) tpmc complexes with dicarboxylates (oxalate, malonate and the dianion of bicyclo[2.2.1]-hept-5-en-*endo*-2,3-*cis*-dicarboxylate) were also described.[7–9] According to X-ray analysis, in the $[Co(ox)tpmc](ClO_4)_2 \cdot 3H_2O$ complex, the geometry of 4N and 2O ligators around both Co(II) centres was distorted octahedral.[8] The oxalate dianion is bonded asymmetrically: two O atoms

from different carboxylic groups are coordinated to two different Co(II) ions; the third oxygen is simultaneously bonded to both Co ions and the last remained uncoordinated. The ν(C=O) band at 1670 cm^{-1} observed in the IR spectrum of the complex confirmed that one O atom remained uncoordinated. The electronic spectrum is consistent with octahedral high-spin Co(II) complexes. The variation of the μ_{eff} values from 0.78–4.66 μ_B/Co in the temperature range 4.2–292 K suggests the existence of weak antiferromagnetic interactions.

On the contrary, the absence of a free carbonyl group band in the IR spectrum of $[Co_2(mal)tpmc](ClO_4)_2$ (mal = the dianion of malonic acid) suggests that all O atoms of the carboxylate ligand are included in the coordination.[9] The UV/Vis spectrum of $[Co_2(\mu\text{-L})tpmc](ClO_4)_2{\cdot}CH_3CN$[7] (L= the dianion of the above-mentioned bicyclic ligand) is typical for high-spin Co(II) complexes of low symmetry. Based on IR and UV/Vis spectroscopic data, it was concluded that in a series of bi- or tetranuclear Cu(II) tpmc complexes with mono- ($HCOO^-$, CH_3COO^-, $C_6H_5COO^-$) or dicarboxylato (hydrogenphthalate, isophthalate and terephthalate) bridged ligand, with the CuN_4O chromophore, all the carboxylate oxygen atoms participated in coordination.[10–12] Preliminary X-ray analysis of $[Cu_4ipht(tpmc)_2](ClO_4)_6$ (ipht = the isophthalate dianion) confirmed that the aromatic carboxylato ligand connected two $[Cu_2(tpmc)]^{2+}$ units, engaging both COO^- groups (Fig. 2).[11] The complex $[Cu_2(HCOO)tpmc][Cu_2(CH_3COO)tpmc](ClO_4)_6{\cdot}6H_2O$ contained two different binuclear cations in the same crystal lattice.[15] Based on X-ray analysis, μ-O,O' coordination of formate/acetate anions were found. In the complexes $[Co_2(baib)(C_6H_5COO)_3]^+$ and $[Co_2(bhmp)(C_6H_5COO)_2]^+$ (baib = 1,3-bis[(2-dimethylaminoethyl)iminomethyl]benzene, bhmp = 2,6-bis[bis(2-hydroxyethyl)aminomethyl]-4-methylphenol), containing the μ-bonded $C_6H_5COO^-$ ligand, weak antiferromagnetic interactions were observed.[18,19] In the complex $[Cu_2(tpht)(bpy)_2(H_2O)_2](ClO_4)_2$ (bpy = 2,2'-bipyridine), strong antiferromagnetic interactions of an intermolecular nature are found.[20] A series of binuclear complexes of the general formula $[Co_2(tpht)A'_4](ClO_4)_2$; A' = phen, bpy and substituted bpy, with bridged terephthalate was also published.[21] In the coordination polymer $[\{Co_3(\mu\text{-tpht})_2(\mu\text{-OH})_2(phen)_2\}_n]$ (phen = phenanthroline), the trimer unit contains two carboxylate and two hydroxo bridges.[22] X-ray structural analysis confirmed that the geometry around Co(I) is square planar, while it is square pyramidal around Co(II) and Co(III). In the interval 300–41 K, ferromagnetic, but in the range 41–4 K, antiferromagnetic types of interactions were found.

Substituents on the phenyl group of aromatic dicarboxylato ligands could influence the intensity of the magnetic interactions in polynuclear complexes. For instance, in the series of the complexes $[Co_2(tcpht)(A)_4]^{2+}$, (tcpht = tetrachlorophthalate; A = phen, 5-nitro–phen or bpy), magnetic measurements were studied in the interval 77–300 K.[23] Antiferromagnetic spin-interchanges were found between the Co(II) ions. It is considered that they could be a result of the influence

of the phthalate group and/or the chloro substituents on it. Namely, the four Cl atoms with their negative inductive effect caused a decrease of electronic density in the bridge and thus of the strength of the electron−electron interactions, lowering the energetic level of the bridged orbitals and thus increasing the difference in energy between the orbitals of the metal and the bridge. The final effect was delocalization of the metal orbitals towards the O atom from the bridge and a decrease of the antiferromagnetic interactions.

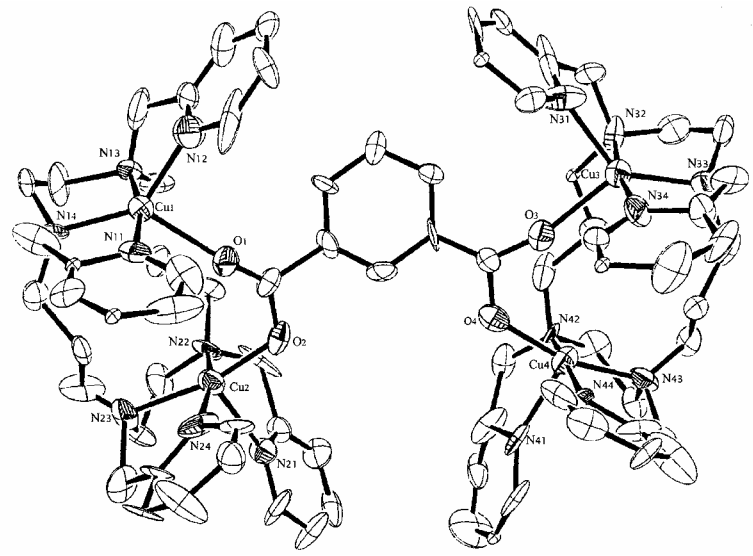

Fig. 2. Structure of the complex cation $[Cu_4ipht(tpmc)_2]^{6+}$.

EXPERIMENTAL

Synthesis

The ligand *N,N',N'',N'''*-tetrakis-(2-pyridylmethyl)-1,4,8,11-tetraazacyclotetradecane (tpmc) and $Co(ClO_4)_2 \cdot 6H_2O$ were prepared according to described procedures.[3,24] Piperidine terephthalate was isolated by the reaction of the total neutralization of terephthalic acid with piperidine.[25] This facilitates the solubility of the obtained salt and thus the coordination of terephthalate. The other chemicals used were commercial products of *p.a.* grade of purity and were used without further purification. CAUTION! Perchlorate salts of metal complexes with organic ligands are potentially explosive and should be handled with extreme caution!

*$[Co_2(HCOO)_2tpmc](ClO_4)_2 \cdot 4H_2O$ (**1**)*: To a solution of $Co(ClO_4)_2 \cdot 6H_2O$ (50 mg ; 0.137 mmol) in 2.0 cm^3 of CH_3OH, a solution of HCOONa (7 mg ; 0.103 mmol) in 0.2 cm^3 H_2O and 2 drops of conc. HCOOH were added. The reaction mixture was stirred and refluxed for 1 h on a water bath (≈ 70 °C), followed by the addition of a tpmc (38 mg; 0.067 mmol) suspension in 3 cm^3 of CH_3OH. The reaction was prolonged for a further 1.5 h and then the mixture was concentrated by heating at 70 °C to about 1/2 of its initial volume, covered with parafilm and left at room temperature until crystals deposited. The deep purple microcrystals were separated by suction, washed properly with several portions of cold CH_3OH and dried in a desiccator above silica gel. Yield: 48 mg (70 %). Anal. Calcd. for $Co_2C_{36}H_{54}O_{16}N_8Cl_2$: C, 41.43; H, 5.22; N, 10.74. Found: C, 41.46; H, 4.89; N, 10.77.

*[$Co_2(CH_3COO)_2$tpmc]$(ClO_4)_2$ (**2**)*: $Co(CH_3COO)_2 \cdot 4H_2O$ (34.5 mg; 0.112 mmol) was dissolved in 3.5 cm^3 of the mixture CH_3OH/H_2O (6:1; v/v) and a suspension of tpmc (38 mg; 0.067 mmol) in 3.0 cm^3 of CH_3OH was added. The purple reaction mixture was stirred at room temperature for 1h. When 0.5 cm^3 of a saturated aqueous solution of $NaClO_4$ was added, deep purple crystals appeared. The stirring was continued for the following 2 h. The further procedure was the same as for complex **1**. Yield: 52 mg (77 %). Anal. Calcd. for $Co_2C_{38}H_{50}O_{12}N_8Cl_2$: C, 45.66; H, 5.04; N, 11.20. Found: C, 45.41; H, 5.14; N, 10.91.

*[Co_2(tpht)tpmc]$(ClO_4)_2 \cdot 4H_2O$ (**3**)*: A **s**uspension of tpmc (38 mg, 0.067 mmol) in 3.0 cm^3 of CH_3OH was mixed with a solution of $Co(ClO_4)_2 \cdot 6H_2O$ (50 mg, 0.137 mmol) in 3.0 cm^3 of CH_3OH. The deep purple reaction mixture was stirred at room temperature for 1 h, and then a solution of piperidine terephthalate (34 mg, 0.105 mmol) in 4 cm^3 of CH_3OH was added and the stirring prolonged for the following 2 h. The further procedure was the same as for complexes **1** and **2**. Yield: 60 mg (79 %). Anal. Calcd. for $Co_2C_{42}H_{56}O_{16}N_8Cl_2$: C, 44.77; H, 5.10; N, 9.95. Found C, 45.02; H, 5.09; N, 9.87.

All three complexes were stable up to 250 °C (check with hot plate equipped with microscope). Some of the physical properties of the complexes are presented in Table I.

TABLE I. Values of molar electrical conductivity (type of electrolyte) in CH_3CN and solubility data of the complexes

Cmpd.	Λ_M / S cm^2 mol^{-1} at 25 °C	Solubility
1	276[a](1:2)	CH_3CN, DMF, CH_3OH, H_2O
2	217[a](1:2)	CH_3CN, H_2O, sparingly in DMF, CH_3OH, C_2H_5OH, DMSO
3	–	CH_3CN/H_2O (1:1, v/v), sparingly in DMF, CH_3CN, DMSO, insoluble in CH_3OH, H_2O

[a]Literature ranges: 120–160 S mol^{-1} cm^2 and 220–300 S mol^{-1} cm^2 for 1:1 and 1:2 type of electrolytes, respectively[26]

Methods and applied instruments

Elemental analysis **(**C, H, N) was performed by standard micromethods in the Centre for Instrumental Analysis of the Faculty of Chemistry, University of Belgrade.

The UV/Vis spectra of complexes (1×10^{-3} mol dm^{-3}) **1** and **2** were recorded in CH_3CN and of complex **3** in a CH_3CN/H_2O (1:1, v/v) mixture using a GBC UV/Vis 911 A spectrophotometer.

The IR spectra (KBr disk technique) were recorded on Perkin–Elmer FTIR 31725X spectrophotometer in the range 400–4000 cm^{-1}.

The molar conductivity of complexes **1** and **2** (see Table I) was determined in CH_3CN solution (1×10^{-3} mol dm^{-3}) at 25±2 °C with a Hanna Instruments HI 8820N conductometer**.** Complex **3** was not sufficiently soluble in common solvents and hence its conductivity was not determined.

Magnetic measurements were performed at room temperature (25±2 °C) on a magnetic balance, MSB-MKI, Sherwood Scientific Ltd., England. The data are corrected for diamagnetic susceptibilities using the Pascal's constants.[28]

Cyclic voltammetry (CV)

The electrochemical measurements were performed at room temperature (20±2 °C) using a Metrohm 797 apparatus in a standard three-electrode cell: Pt as the auxiliary electrode, standard Ag/AgCl as the reference and a glassy carbon electrode as the working one. The concentration of the solutions was $\approx 5\times10^{-4}$ mol dm^{-3}. The measurements were performed on 30 cm^3 of the complex solution in CH_3CN (complexes **1** and **2**) and in a mixture CH_3CN–H_2O (1:1, v/v) (complex **3**). The scan rate was 50 mV s^{-1}, in the potential interval from −1.0 to 1.0 V. Oxygen was removed from the system by bubbling N_2.

Biological activity

The biological activity of the simple Co(II) salt, solvent, ligands and the complexes was preliminary tested by the diffusion method through an agar plate. Nutrition, agar (powder) Tripton „Torlak'', was prepared by mixing agar (23.5 g) in water (100 cm^3) and, after 15 min, careful heating up to boiling until the agar had completely dissolved. After sterilization for 15 min in an autoclave at 120 °C, the nutrition was poured into Petri plates and inoculated with microorganisms from a physiological solution. The paper disks (1 cm in diameter) were previously sterilized using a UV lamp. The complexes were tested against the following strains of microorganisms: *Bacillus subtilis*, *Escherichia coli* ATCC 25923, *Bacillus cereus*, *Pseudomonas aeruginosa* and *Aspergillus niger*. 60 μl (concentration of $\approx 5\times10^{-4}$ mol dm^{-3}) of the complex solution or one crystal of the complex (if it was sparingly soluble) were put on the paper discs. The Petri plates were left for 48 hours thermostated at 28 °C and then the diameters of the inhibition zone were measured if microbiological activity was detected.

RESULTS AND DISCUSSION

The type and yields of the complexes described in this paper depended on the various factors: temperature, rate and the order of the added reactants, solvent, pH values on which mono-/dicarboxylic acid is neutralized and pH value of the reaction mixture. Co(II) perchlorate in the presence of tpmc always forms the very stable violet μ-OH^- binuclear complex $[Co_2(OH)tpmc](ClO_4)_3$ as a by-product. In a more basic medium, the formation of this product is favoured, while in more acidic medium the carboxylate ligand is protonated causing a decrease in its donor properties. However, the optimal conditions favoured the formation of the complexes **1** and **2** in good yield. In addition, aromatic carboxylic acids have a tendency to form polymeric Co(II) complexes, especially at elevated temperatures. Therefore, the synthesis with terephthalate was performed at room temperature.

The isolated complexes were microcrystalline compounds, of purple or dark purple colour. Their solubility in common solvents is given in Table I. The results of elemental analysis suggested binuclear complexes in all cases. The values of the molar conductivities for complexes **1** and **2** (Table I) corresponded to a 1:2 type of electrolyte.[26] The absorption maxima and intensities of peaks in the Vis spectra of the complexes **1**–**6** (Table II)[27] were similar and corresponded to d–d transitions in high-spin Co(II) complexes of low symmetry.[28] The ε values for complex **2** containing CH_3COO^- are larger than those for the complex **1** containing $HCOO^-$ (Table II). This is in accordance with the enhanced asymmetry in complex **2**, due to the stronger steric repulsion between tpmc pyridyl groups and the CH_3 groups of the acetate, than with the H from the formate ions in complex **1**. CT bands in the UV spectra of all the complexes were in the range 240–280 nm (ε = 6000–7100 $dm^3\ mol^{-1}\ cm^{-1}$). Interpretation of the electronic spectra of Co(II) complexes is usually complicated and the magnetic measurements are additional criterions for the assumption of the coordination geometry, although the variety of the possible magnetic interactions could be problematic.[29]

The values of μ_{eff}/Co at room temperature were in the range 4.57–5.08 μ_B, which confirmed the high-spin state of the cobalt(II) and weak magnetic interactions. Similar values were found earlier for some familiar complexes (Table II).

TABLE II. Vis spectral data and magnetic moment values of the synthesized and relevant described complexes

Complex	Maxima and shoulders (*sh*) λ_{max} / nm (ε / $dm^3mol^{-1}cm^{-1}$)	μ_{eff} per Co, μ_B (25 °C)
$[Co_2(HCOO)_2tpmc](ClO_4)_2 \cdot 4H_2O$ (**1**)	448(56); 521(67); 552(63)[b]	4.57
$[Co_2(CH_3COO)_2tpmc](ClO_4)_2$ (**2**)	480(60)*sh*; 504(70)*sh*; 527(73)[b]	5.01
$[Co_2(C_6H_5COO)_2tpmc](ClO_4)_2 \cdot 3H_2O$[a] (**6**)	479(66)*sh*; 516(75)[c]	4.81
$[Co_2(pht)tpmc](ClO_4)_2 \cdot 2H_2O$[a] (**4**)	487(74)*sh*; 523(86)[c]	4.74
$[Co_2(ipht)tpmc](ClO_4)_2 \cdot 4H_2O$[a] (**5**)	485(89)*sh*; 508(94)[c]	5.01
$[Co_2(tpht)tpmc](ClO_4)_2 \cdot 4H_2O$ (**3**)	485(100)*sh*; 508(106)[d]	5.08

[a]Literature data[27]. Solvents used: [b]CH_3CN; [c]DMF; [d]mixture CH_3CN–H_2O (1:1; v/v)

In the IR spectra of complexes **1**–**3**, some common characteristic bands were observed: at 3590–3220 cm^{-1} broad and strong, arising from ν(O–H) of the crystal H_2O molecules in the complexes; at ≈ 1610 cm^{-1} strong, sharp, assigned to the valence skeletal vibrations of the pyridine ring; at ≈ 1100 cm^{-1} broad, the strongest band, and at ≈ 630 cm^{-1} medium, sharp, due to the $\nu(ClO_4^-)$ and $\delta(ClO_4^-)$ of uncoordinated ClO_4^-, respectively.[30] The positions of the bands due to asymmetrical (ν_a) and symmetrical (ν_s) skeletal vibrations of carboxylic groups in the spectra of complexes and their corresponding alkaline salts are presented in Table III, together with the $\Delta\nu$ values (equal to ν_a–ν_s). Contrary to aliphatic μ-aminocarboxylato Co(II)tpmc complexes,[4,5] for which the positions of ν_a and ν_s are shifted to lower frequencies upon coordination and, consequently, the $\Delta\nu$ values in the spectra of the complexes are higher than those for the corresponding salts, for all complexes (**1**–**6**), ν_s is shifted towards higher frequencies and considerably lower $\Delta\nu$ values were observed. This is ascribed to coordination number 5 for the first type and 6 for the latter complexes. In the new complexes (**1**–**3**), the $\Delta\nu$ values were lower than those of the related alkaline salts were. The shift of ν_a(OCO) towards lower and ν_s(OCO) towards higher frequencies compared with the corresponding alkaline salts could be the consequence of the participation of the COO^- group in coordination through both oxygen atoms or due to the participation of the uncoordinated carboxylic O atom in hydrogen bond formation. In the complexes, hydrogen bond formation is slightly more difficult than in the alkaline salts, due to steric protection originating from the macrocyclic and carboxylate ligand. For complexes **1** and **3**, containing crystal H_2O, there is an enhanced possibility for hydrogen bond formation. The results suggest that the mono-/dicarboxylato ligands are bonded as chelates, while in complexes **4**–**6** as chelates and bridges.[27] The $\Delta\nu$ values of the complexes decrease with the strength of the Co(II)–O bonds, in the order: μ-formate (121 cm^{-1}) > μ-benzoate (113 cm^{-1}) > > μ-acetate (99 cm^{-1}) or μ-phthalate (120 cm^{-1}) > μ-*iso*phthalate (113 cm^{-1}) > > μ-terephthalate (106 cm^{-1}), respectively. Moreover, the strength of this bond parallels the strength of the monocarboxylic acids (Table IV) in complexes **1**–**3**.

However, when aromatic dicarboxylates are coordinated, besides their pH values, the mutual interactions between carboxylic groups (inductive, resonance, steric effects and the chelate ring size), as well as the hard–soft relations[29,31] of the ligands and metallic centres have a large influence. Finally, the rest of the molecule also contributes to overall geometry and deviations of some bond distances. The methyl group in the hard base CH_3COO^- with its (+)-inductive effect makes it softer than $HCOO^-$. On a contrary, the phenyl group in $C_6H_5COO^-$ has a weak (–)-inductive effect, but a positive resonance effect, being a harder base than acetate and softer than formate. In Co(II)/Cu(II)-tpmc complexes, the central atoms are chelate bonded with hard bases, N atoms from the pendant ligand, which increases their hardness. The Co(II)–O strength is also a result of a type of inductive effect, the position of the COO^- group at the aromatic ring and the mode of carboxylate bonding. The COOH group has a (–)- while COO^- a (+)-inductive effect. A coordinated COO^- group has a (–)-inductive effect which decreases dramatically with distance. Thus, when two coordinated COO^- are 1,2-positioned, the ligand is harder than in the case of 1,3- or 1,4-positioned ones, causing a stronger Co(II)–O bond. Some simplified carboxylate coordination modes are presented in Schemes 3b–3g. In addition, asymmetrical modes are possible, causing distortion of the octahedral and non-equal Co(II)–O bonds in the same molecule. This is obvious for complex **3**, the IR spectra of which distinguished themselves from those of the other complexes in exhibiting multiple ν_a and ν_s COO^- bands.

TABLE III. Position of the bands of the asymmetric (ν_a), and symmetric (ν_s) stretching vibrations of the carboxylic group and values of $\Delta\nu$ (ν_a–ν_s) in the IR spectra of the alkaline salts of the carboxylic acids and the related complexes (*s* = strong; *m* = medium intensity)

Cmpd.	ν_a / cm^{-1}	ν_s / cm^{-1}	$\Delta\nu$ / cm^{-1}
HCOONa	1567*s*	1366*m*	201
$[Co_2(HCOO)_2tpmc](ClO_4)_2\cdot 4H_2O$ (**1**)	1565*s*	1445*m*	120
CH_3COONa	1578*s*	1414*m*	164
$[Co_2(CH_3COO)_2tpmc](ClO_4)_2$ (**2**)	1549*s*	1450*m*	99
Na_2tpht	1561;	1400*m*	161
$[Co_2(tpht)tpmc](ClO_4)_2\cdot 4H_2O$ (**3**)	1550*s*	1444*m*	
	1509*s*	1403*m*	
	1529[a]	1424[a]	106
K_2pht[b]	1563*s*	1384*m*	179
$[Co_2(pht)tpmc](ClO_4)_2\cdot 2H_2O$ (**4**)	1544*s*	1423*m*	121
Na_2ipht[b]	1564*s*	1395*m*	169
$[Co_2(ipht)tpmc](ClO_4)_2\cdot 4H_2O$ (**5**)	1538*s*	1425*m*	113
C_6H_5COONa[b]	1580*s*	1413*m*	167
$[Co_2(C_6H_5COO)_2tpmc](ClO_4)_2\cdot 3H_2O$ (**6**)	1533*s*	1420*m*	113

[a]calculated as the average value of two bands; [b]data taken from the literature[27]

All three complexes are stable to oxidation in the open atmosphere, both in the solid state and in solution. This was confirmed by their time independent Vis spectra recorded after bubbling O_2 through solutions of the complexes.

TABLE IV. pK_a values of the aliphatic and aromatic mono-/dicarboxylic acids

p*K* Values	Formic acid	Acetic acid	Benzoic acid	Phthalic acid	Isophthalic acid	Terephthalic acid
pK_1	3.75	4.75	4.19	2.91	2.30	3.45
pK_2	–	–	–	5.13	4.66	4.45

The electrochemical behaviour of complexes **1**–**3** was studied in the potential range from 1 to −1 V (scan speed of 50 mV s^{-1}). The CV diagrams of the compounds were practically the same as that of the supporting electrolyte, confirming their great electrochemical stability under the studied conditions. The peaks remained unchanged on repeated cycling, as well as on holding the potential at − 1 and 1 V. Such properties give the possibility of the application of these complexes as catalysts.

It is known that HCOOH, CH_3COOH, C_6H_5COOH, and their salts are preservatives in the alimentary industry, while benzenedicarboxylic acids are poisons for microorganisms. Preliminary testing of the microbiological activity of the new complexes, together with familiar Co(II)tpmc complexes recently described,[27] against some Gram(+) and Gram(–)-bacteria and mould was performed in order to check if their activity is modified on coordination. Data for both tests described in the Experimental are presented in Table V. The solvent (CH_3CN), tpmc, the previously tested $Co(ClO_4)_2{\cdot}6H_2O$, the alkaline salts of pht, ipht and tpht, and the complexes **4**) and **5** were inactive. Complexes **1**–**3** and **6** exhibited antimicrobial activity towards particular strains, and C_6H_5COOH in all studied cases. Complexes **1**, **2** and **6** gave positive result only when applied in the solid state, providing for their high concentration on dissolution in the nutrition agar. The activity of complexes **1** and **2** is not ascribed to the carboxylato ligands themselves, as their concentration in the applied crystals was too small. The same is supposed for complex **6**, as the concentration of benzoate produced by its dissociation in the used aliquot is negligible. In spite of the fact that the tpht ligand was inactive, complex **3** containing this ligand was active.

Based on all the afore said, the most probable coordination geometry of the complex cations of **1** and **2** is presented in Scheme 2 (as already proposed for the benzoate analogue) and for the complex cation of **3** in Schemes 3g or 3f. The geometry in Scheme 3f has enhanced strain due to the longer Co···Co distance and, thus, much weaker Co(II)–O bonds.

When Co(II) and Cu(II)tpmc related complexes with: $HCOO^-$, CH_3COO^-, $C_6H_5COO^-$, dianions of: pht, ipht or tpht[11,27] ligands are mutually compared, it can be concluded that in no case was the same composition obtained. This is the result of specific properties of these metal ions (different electronic configurations, size of the ionic diameter, tendency to form 5- or 6-coordinated species, *etc*.), as well as the changed experimental conditions which were necessary to apply in

each case. With one $HCOO^-$ or CH_3COO^- ligand, Cu(II)tpmc formed five-coordinated bridged binuclear complexes, but in the case of Co(II) *bis*(bidentate), six-coordination of two such ligands was favoured. For $[Co_2(pht)tpmc]^{2+}$, pht was μ-bonded (Schemes 3b or 3c), while in the corresponding Cu(II) complex, $Hpht^-$ was a bridged ligand, engaging only one COO^- group. Co(II) formed binuclear complexes with ipht (Scheme 3d or 3e) and tpht (Scheme 3g and less probable 3f) when tpmc was present. On the contrary, Cu(II) complexes with the same ligands were tetranuclear ones in which four metallic centres were bridged with one dicarboxylate (Scheme 1d). These conclusions were supported by X-ray analyses of Cu(II)tpmc complexes with $ipht^{2-}$ and recently with $C_6H_5COO^-$.[11,32]

TABLE V. Results of the antimicrobial activity of the tested complexes, ligands and solvents

Cmpd.	*B. subtilis*	*B. cereus*	*E. coli*	*P. aeruginosa*	*A. niger*
	Gram(+) bacteria		Gram(–) bacteria		mould
Crystal of $[Co_2(HCOO)_2tpmc](ClO_4)_2 \cdot 4H_2O$ (**1**)	–	++	+	Not tested	–
Crystal of $[Co_2(CH_3COO)_2tpmc](ClO_4)_2$ (**2**)	–	+++	–	Not tested	–
C_6H_5COOH	+	+	+	+	+
$[Co_2(C_6H_5COO)_2tpmc](ClO_4)_2 \cdot 3H_2O$[a] (**6**)	–	+	+++	+	+
KHpht	–	–	–	–	–
K_2pht	–	–	–	–	–
$[Co_2(pht)tpmc](ClO_4)_2 \cdot 2H_2O$[a] (**4**)	–	–	–	–	–
H_2ipht	–	–	–	–	–
$[Co_2(ipht)tpmc](ClO_4)_2 \cdot 4H_2O$[a] (**5**)	–	–	–	–	–
H_2tpht	–	–	–	Not tested	–
Crystal of $[Co_2(tpht)tpmc](ClO_4)_2 \cdot 4H_2O$ (**3**)	–	+++	+	Not tested	–
Tpmc	–	–	–	–	–
CH_3CN	–	–	–	–	–

[a]Described complexes[27]; **(+)** antimicrobial activity with a diameter of the inhibition zone up to 10 mm; **(++)** antimicrobial activity with a diameter of the inhibition zone up to 30 mm**, (+++)** antimicrobial activity with a diameter of the inhibition zone larger than 30 mm; **(–)** antimicrobial activity was not detected

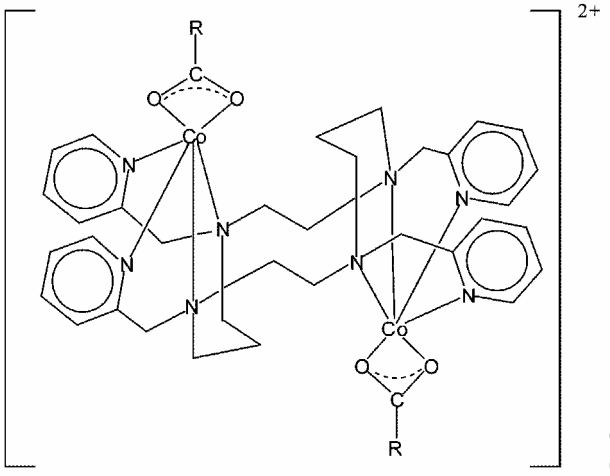

Scheme 2. Simplified structure of the complex cations of the complexes **1** (R = H) and **2** (R = CH_3).

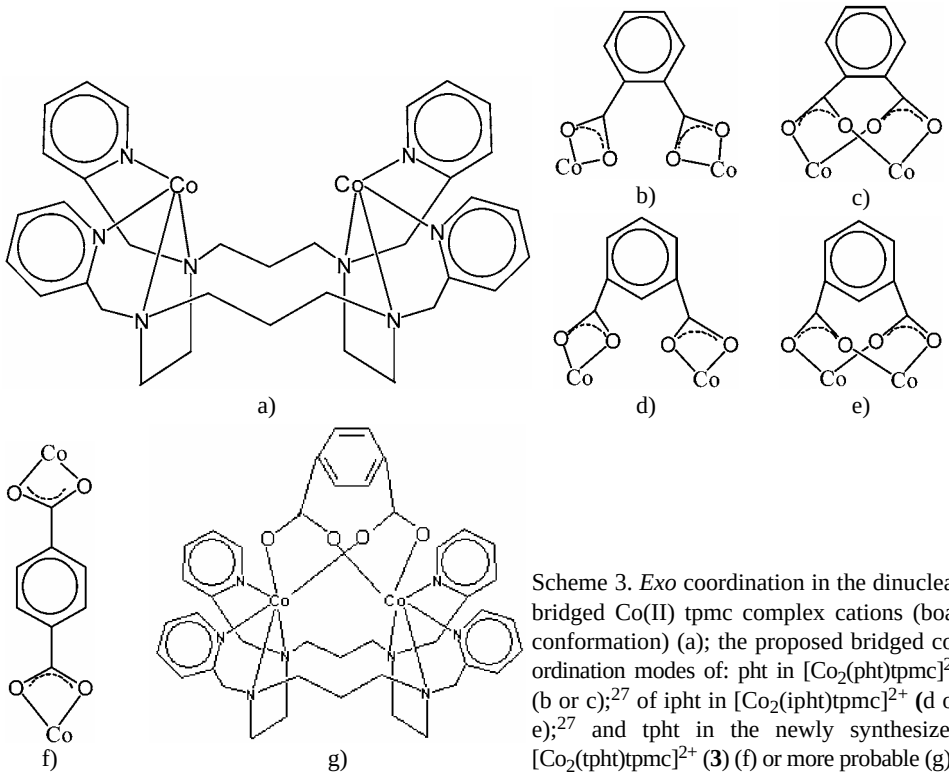

Scheme 3. *Exo* coordination in the dinuclear bridged Co(II) tpmc complex cations (boat conformation) (a); the proposed bridged coordination modes of: pht in $[Co_2(pht)tpmc]^{2+}$ (b or c);[27] of ipht in $[Co_2(ipht)tpmc]^{2+}$ **(**d or e);[27] and tpht in the newly synthesized $[Co_2(tpht)tpmc]^{2+}$ (**3**) (f) or more probable (g).

CONCLUSIONS

Three novel Co(II) complexes with pendant octaazamacrocyclic ligand *N*,*N*′,*N*″,*N*‴-tetrakis(2-pyridylmethyl)-1,4,8,11-tetraazacyclotetradecane (tpmc) and mono- ($HCOO^-$/CH_3COO^-) or dicarboxylate ligands (terephthalate dianion) were prepared, characterized by some physical properties and valuable methods and techniques (elemental analyses, molar electrical conductivity, spectroscopic data, magnetic measurements, cyclic voltammetry), and compared with the already described Co(II)/Cu(II) analogues. All complexes were binuclear and cationic. For Co(II)tpmc complexes containing two $HCOO^-$/CH_3COO^- ligands, bis(bidentate) coordination of the additional ligands in the *trans* position for each metal and the chair conformation of tpmc is predicted, while for the multidonor terephthalate dianion μ-O,O,O',O' coordination is supposed.

Acknowledgements. We gratefully acknowledge the financial support of the Ministry of Science (Project No. 142028) of the Republic of Serbia and Dr. Gordana Gojgić–Cvijović for the microbiological screening.

И З В О Д

ВИСОКОСПИНСКИ Co(II) КОМПЛЕКСИ СА ПЕНДАНТНИМ ОКТААЗАМАКРОЦИКЛОМ И КАРБОКСИЛАТИМА

Г. ВУЧКОВИЋ[1], С. Б. ТАНАСКОВИЋ[2], З. М. МИОДРАГОВИЋ[1] и В. СТАНИЋ[1]

[1]Хемијски факултет, Универзитет у Београду, п. пр. 158, 11001 Београд и [2]Фармацеутски факултет, Универзитет у Београду, Војводе Степе 450, 11000 Београд

Добијена су три нова динуклеарна Co(II) мешовито-лигандна комплекса са *N,N′,N″,N‴*-тетракис(2-пиридилметил)-1,4,8,11-тетраазациклотетрадеканом (tpmc) и моно- или дикарбоксилато лигандима и одређена су нека њихова физичка својства. Опште формуле: $[Co_2(HCOO)_2tpmc](ClO_4)_2\cdot 4H_2O$, $[Co_2(CH_3COO)_2tpmc](ClO_4)_2$ и $[Co_2(tpht)tpmc](ClO_4)_2\cdot 4H_2O$ ($tphtH_2$ = терефтална киселина) предложене су на основу резултата анализе (C,H,N) и мерења моларне електричне проводљивости. UV/Vis и IR спектри, магнетна и CV мерења коришћена су за проучавање геометрије и особина ових једињења. За монокарбоксилатне комплексе предложена је *exo* координација Co(II) са четири азотова атома tpmc-а и бис-бидентатно везаним $HCOO^-/CH_3COO^-$) у *trans* положају. Tpmc заузима конформацију столице. Претпостављено је да терефталатни дианјон, као и метиленске групе циклама премошћују два атома Co(II), а tpmc је у конформацији лађе. Комплекси су стабилни према хемијској и електрохемијској оксидацији Co(II) у Co(III). Подаци су упоређени са раније објављеним Cu(II) комплексима који садрже одговарајуће лиганде и разматране су међусобне сличности и разлике. Најзад, утврђена је извесна антимикробна активност комплекса.

(Примљено 24. септембра 2007)

REFERENCES

1. J. Mroziński, *Coord. Chem. Rev*. **249** (2005) 2534
2. J. A. Cowan, *Inorganic Biochemistry*, 2nd Ed., Wiley-VCH, New York, 1997, Chs. IV and V
3. S. Chandrasekhar, W. L. Waltz, L. Prasad, J. W. Quail, *Can. J. Chem.* **75** (1997) 1363
4. G. Vučković, D. Opsenica, S. P. Sovilj, D. Poleti, M. Avramov–Ivić, *J. Coord. Chem.* **42** (1997) 241
5. G. Vučković, D. Opsenica, S. P. Sovilj, D. Poleti, *J. Coord. Chem.* **47** (1999) 331
6. H. Harada, M. Kodera, G. Vučković, N. Matsumoto, S. Kida, *Inorg. Chem.* **30 (**1991) 1190
7. Z. M. Miodragović, G. Vučković, V. M. Leovac, V. M. Buzash, *Synth. React. Inorg. Met. – Org. Chem.* **30** (2000) 57
8. S. P. Sovilj, G. Vučković, K. B. Babić–Samardžija, N. Matsumoto, V. M. Jovanović, J. Mroziński, *Synth. React. Inorg. Met. – Org. Chem.* **29** (1999) 785
9. Z. M. Miodragović, G. Vučković, S. P. Sovilj, D. D. Manojlović, M. J. Malinar, *J. Serb. Chem. Soc*. **63** (1998) 781
10. E. Asato, H. Toftlund, S. Kida, M. Mikuriya, K. S. Murray, *Inorg. Chim. Acta* **165** (1989) 207
11. G. Vučković, M. Antonijević, D. Poleti, *J. Serb. Chem. Soc.* **67** (2002) 677
12. Z. M. Miodragović, G. Vučković, V. M. Leovac, *J. Serb. Chem. Soc*. **66** (2001) 597
13. G. Vučković, Z. M. Miodragović, S. Tanasković, *J. Serb. Chem. Soc*. **69** (2004) 17
14. Z. M. Miodragović, G. Vučković, M. Antonijević, in *Proceedings of 5th International Conference on Fundamental and Applied Aspects of Physical Chemistry*, *Physical Chemistry*, (2000), L8-P, p. 646
15. G. A. Bogdanović, Z. M. Miodragović, G. Vučković, R. Marković, A. Spasojević–de Biré, *Synth. React. Inorg. Met. – Org. Chem.* **31** (2001) 1189

16. G. Vučković, M. Antonijević–Nikolić, M. Korabik, J. Mroziński, D. D. Manojlović, G. Gojgić–Cvijović, N. Matsumoto, *Polish. J. Chem.* **79** (2005) 679
17. P. Chaudhuri, J. Querbach, K. Weighardt, *J. Chem. Soc. Dalton Trans.* (1990) 271
18. Md. J. Hossain, H. Sakiyama, *Inorg. Chim. Acta* **338** (2002) 255
19. Md. J. Hossain, M. Yamasaki, M. Mikuriya, A. Kuribayashi, H. Sakiyama, *Inorg. Chem.* **41** (2002) 4058
20. E. G. Bakalbassis, J. Mroziński, C. A. Tsipis, *Inorg. Chem.* **24** (1985) 4231
21. Sh. L. Ma, D. Zh. Liao, Z. H. Jiang, Sh. P. Yan, F. Ch. Xue, G. L. Wang, *Synth. React. Inorg. Met. – Org. Chem.* **23** (1993) 239
22. J. Zhang, X.–L. Zhao, P. Cheng, J.–Q. Xu, X. Tang, X.–B. Cui, W. Xu, T.–G. Wang, *Bull. Chem. Soc. Jpn.* **76** (2003) 1179
23. X.–R. Sun, P. Cheng, J.–Z. Cui, D.–Z. Liao, Z.–H. Jiang, S.–P. Yan, G.–L. Wang, *Transition Met. Chem.* **22** (1997) 65
24. V. A. Kiss and Z. M. Gerendas, *Phys. Chem.* **A180** (1937) 117
25. M. Verdaguer, J. Gouteron, S. Jeannin, Y. Jeannin, O. Kahn, *Inorg. Chem.* **23** (1984) 4291
26. J. W. Geary, *Coord. Chem. Rev.* **7** (1971) 79
27. G. Vučković, V. Stanić, S. P. Sovilj, M. Antonijević–Nikolić, J. Mroziński, *J. Serb. Chem. Soc.* **70** (2005) 1121
28. B. P. Lever, *Inorganic Electronic Spectroscopy*, 2nd Ed., Elsevier, Amsterdam, 1984, pp. 480 and 505
29. F. A. Cotton, G. Wilkinson, C. A. Murillo, M. Bochmann, *Advanced Inorganic Chemistry*, 6th Ed., Wiley, New York, 1999, p. 815
30. K. Nakamoto, *Infrared and Raman Spectra of Inorganic and Coordination Compounds*, *Part B*, 5th Ed., Wiley, New York, 1997, pp. 54 and 83
31. D. F. Shrivier, P. W. Atkins, *Inorganic Chemistry*, 3rd Ed., Oxford University Press, Oxford, New York, 1999, p. 168
32. G. Vučković, M. Antonijević–Nikolić, T. Lis, J. Mroziński, M. Korabik, D. D. Radanović, *J. Mol. Struct.* (2007), doi: 10.1016/j.molstruc.2007.02.028.

Journal of the Serbian Chemical Society
JSCS@tmf.bg.ac.yu • www.shd.org.yu/JSCS

J. Serb. Chem. Soc. 72 (12) 1309–1319 (2007) UDC 546.39+546.141:544.4:54–44:66.092–977
JSCS–3663 *Original scientific paper*

A kinetic study of the thermal degradation of cetyltrimethylammonium bromide inside the mesoporous SBA-3 molecular sieve

DJORDJE STOJAKOVIĆ[1]*, NEVENKA RAJIĆ[1], MAJA MRAK[2] and VENČESLAV KAUČIČ[3]

[1]*Faculty of Technology and Metallurgy, University of Belgrade, 11000 Belgrade, Serbia,* [2]*Jožef Štefan Institute, Jamova 39, 1000 Ljubljana and* [3]*National Institute of Chemistry, Hajdrihova 19, 1000 Ljubljana, Slovenia*

(Received 12 June 2007)

Abstract: The thermal degradation of cetyltrimethylammonium bromide (CTMAB) inside the mesoporous SBA-3 was studied under non-isothermal conditions. There are two distinct and complex kinetic processes which partly overlap, each consisting of one dominant and three minor individual processes. The two dominant processes can be described by the Sestak–Berggren model. The main decomposition step (the first dominant process) involves the overcoming of weak interactions between CTMAB and the silica network and proceeds with a lower E_a value (116±2 kJ mol^{-1}) than the second dominant process (153±5 kJ mol^{-1}), which can be explained by the size reduction of the pore openings due to the contraction of the SBA-3 unit cell caused by the removal of CTMAB.

Keywords: NPK method, non-isothermal kinetics, open-framework, SBA-3, cetyltrimethylammonium bromide (CTMAB).

INTRODUCTION

Microporous inorganic solids having pore diameters less than 2 nm and mesoporous inorganic solids with pore diameters ranging from 2 to 50 nm are of great industrial importance since they exhibit unique catalytic and sorption properties. This is mainly caused by their large internal surface area.

Microporous solids are generally prepared under hydrothermal conditions using different amines and/or quaternary amine salts which play a crucial structure-directing role.[1] Mesoporous materials are usually obtained by a liquid-crystal template mechanism (LCT) using mostly alkyltrimethylammonium surfactants. In the LCT mechanism, the inorganic phase occupies the continuous water (solvent) region to create inorganic walls between ordered surfactant micelles.[2]

* Corresponding author. E-mail: stojakovic@tmf.bg.ac.yu
doi: 10.2298/JSC0712309S

The as-synthesized mesoporous solid contains more than 50 % organic material by weight and is in effect an organic-inorganic composite.

An efficient removal of the organic component from the as-synthesized solid in order to access the internal free space is an important step in the final preparation of the porous materials. Recently, kinetic studies of the removal of cetyltrimethylammonium bromide (CTMAB) from MCM-41 and MCM-48 siliceous materials have been reported.[3,4] Both solids belong to the type having cubic mesostructured frameworks. It was found that the activation energy for the removal of CTMAB species from MCM-41 is rather high, having a value of 166±8.2 kJ mol^{-1}.[3] The removal of CTMAB from MCM-48 proceeds with an even higher activation energy (178±8.5 kJ mol^{-1}).[4]

In this study, the thermal removal of CTMAB from SBA-3 solid was examined. The latter is mesoporous silica having a pore size ranging from 2.2 to 2.5 nm.[5] In contrast to the syntheses of MCM-41 and MCM-48, which are performed in alkaline conditions, the preparation of SBA-3 proceeds in a strongly acidic solution below the isoelectric point of silica. During the polymerization process, the protons bound to silica species are eliminated, leaving the inorganic phase of the SBA-3 product electrically neutral. In contrast, the MCM materials obtained under alkaline conditions have a negatively charged silica network.[6] As the SBA-3 network is electrically neutral, it is to be expected that the main factor in the removal of CTMAB from SBA-3 would involve the overcoming of the framework–surfactant non-bonded interactions.

The kinetics of the thermal removal (decomposition) of CTMAB has been studied by the non-parametric kinetics (NPK) method of Serra *et al.*[7–9] The NPK method has been applied in recent years for the kinetic analysis of thermal degradation in a variety of chemical systems, *e.g.*, bis-urethanes,[10] transition metal carboxylates,[11] alkaline metal phosphates[12] and glutamates,[13] alkaline metal and alkaline-earth metal benzoates,[13] and a 3-D zincophosphate containing occluded ammonium species.[14]

EXPERIMENTAL

Synthesis

Cetyltrimethylammonium bromide (CTMAB, Aldrich) and tetraethyl orthosilicate (TEOS, Aldrich, 98 wt. %) were used as the surfactant and the silica source, respectively. The following molar composition of reactants was used: SiO_2:4.9HCl:0.24CTMAB:147H_2O. The CTMAB was dissolved in dilute hydrochloric acid (≈ 1.8 mol dm^{-3}) and then TEOS was added. The resulting mixture was stirred for about 2 h at room temperature and then aged without stirring for the next 72 h. The resultant white solid (SBA-3) was washed with deionized water and dried at 60 °C overnight. The mesostructure of SBA-3[5] was confirmed by the powder X-ray diffraction method [three diffractions at 2θ = 2.7, 4.7 and 5.3° are evident in the XRD pattern (recorded using CuKα radiation)]. The scanning electron micrograph (Fig. 1) reveals particles with a shape resembling interconnected snail shells.

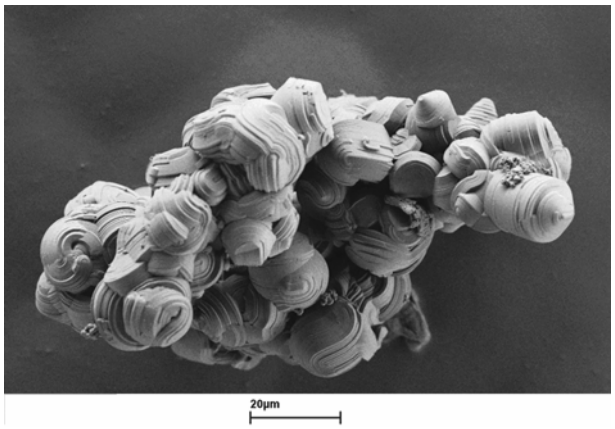

Fig. 1. SEM microphotograph of the as-synthesized SBA-3.

Instrumentation

The thermal decomposition measurements were performed using a SDT Q-600 simultaneous DSC–TGA instrument (TA Instruments). The samples (mass approx. 10 mg) were heated in a standard 90 µl alumina sample pan. All experiments were carried out under dynamic air at a flow rate of 0.1 dm^3 min^{-1}. Non-isothermal measurements were conducted at heating rates of 3, 6, 9, 12, and 16 K min^{-1}. Five experiments were performed at each heating rate.

RESULTS AND DISCUSSION

The TG and DTG curves for SBA-3 in the 300–1050 K range are shown in Fig. 2. The profiles of TG–DTA curves do not significantly differ from those of the MCM materials.[3,4,6] There are three main weight losses, two of them being sharp and distinct. The first loss (40 %) occurs in the 470–593 K range and it is centered at 519 K. The second weight loss (7.5 %, centered at 620 K) occurs in the 593–665 K range. The third loss (8.5 %) is rather diffuse-looking since it proceeds over a broad temperature range (670–950 K). The overall mass loss amounts to about 56 %, which is in accordance with the C,H,N-analysis of SBA-3.

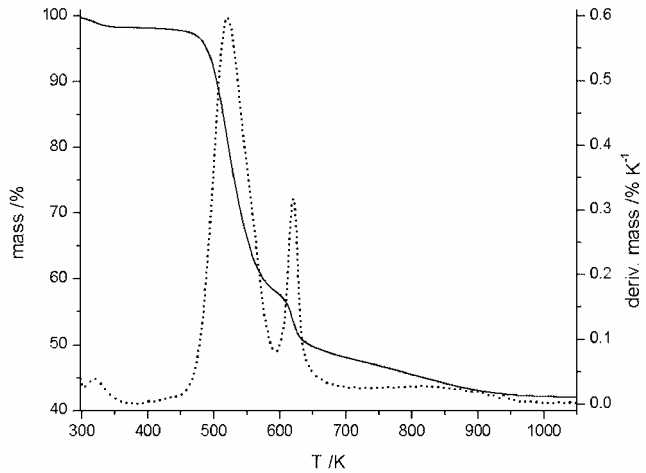

Fig. 2. TG/DTG curves for SBA-3 (TG: solid line; DTG: dotted line).

The first and second weight losses correspond to the decomposition of the surfactant, whereas the third loss can be attributed to the oxidative removal of residual carbonaceous species and the condensation of the remaining silanol groups.[3,4,6]

Kinetics of CTMAB decomposition during the thermal treatment of SBA-3

The decomposition of CTMAB during thermal treatment of SBA-3 was studied in an oxidative atmosphere under non-isothermal conditions. The measurements were performed at five different heating rates (β): 3, 6, 9, 12 and 16 K min^{-1}. The degrees of conversion, α, *vs.* the absolute temperature, *T*, thermogravimetry curves are shown in Fig. 3 and the corresponding reaction rates are shown in Fig. 4.

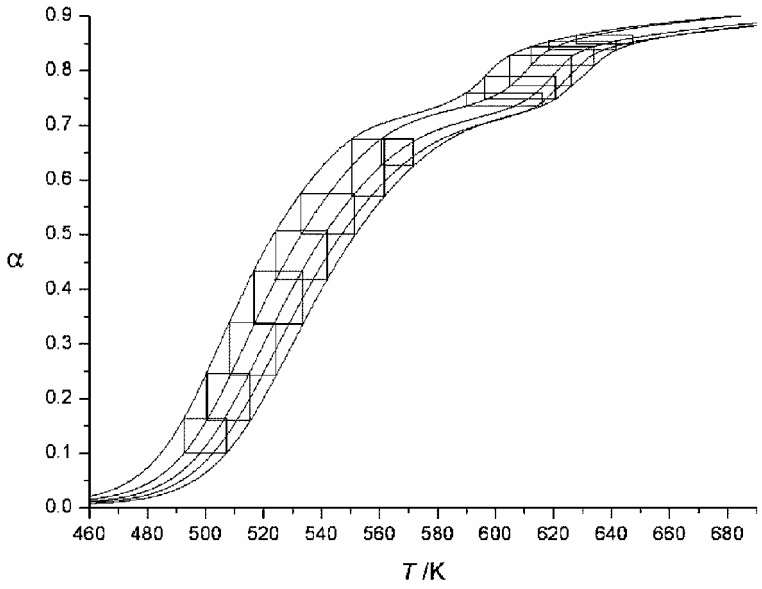

Fig. 3. Experimental curves for the decomposition of CTMAB in SBA-3 at different heating rates (from left to right: 3, 6, 9, 12 and 16 °C min^{-1}). The rectangles show the submatrices selected for the NPK analysis.

The kinetics of the decomposition of CTMAB were examined by the NPK method.[7–9,15] This method for the analysis of non-isothermal thermogravimetry data is based on the usual assumption that the reaction rate can be expressed as the product of two independent functions, $f(\alpha)$ and $h(T)$, where $f(\alpha)$ accounts for the kinetic model while $h(T)$ is a temperature-dependent function, usually the Arrhenius equation:

$$h(T) = k = A \exp(-E_a/RT)$$

The reaction rates, $\mathrm{d}\alpha/\mathrm{d}t$, measured from several experiments at different heating rates, can be expressed as a three-dimensional surface determined by the temperature and the degree of conversion. This surface can be organized as an ($n \times m$)

matrix *A*, in which the rows correspond to different degrees of conversion, from α_1 to α_n, while the columns correspond to different temperatures, from T_1 to T_m.

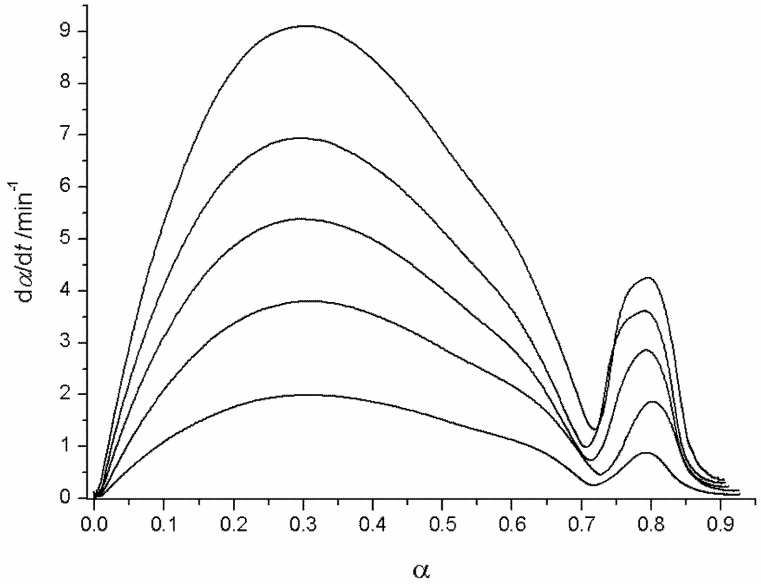

Fig. 4. Experimental reaction rates *vs.* the degree of conversion for the decomposition of CTMAB in SBA-3 at different heating rates (from bottom to top: 3, 6, 9, 12 and 16 °C min^{-1}).

The reaction rate, *i.e.*, the matrix *A*, can be expressed as the product of two vectors:

$$A = fh^T$$

where

$$f^T = [f(\alpha_1)\ f(\alpha_2)\ f(\alpha_3)\cdots f(\alpha_n)]$$
$$h^T = [h(T_1)\ h(T_2)\ h(T_3)\cdots h(T_m)]$$

In the next step of the NPK method, the matrix *A* is decomposed in order to obtain the vectors *f* and *h*. This is done by the mathematical procedure known as the singular value decomposition (SVD). From the vectors *f* and *h*, plots of $f(\alpha)$ against α and of $h(T)$ against T are readily available and the nature of the functions $f(\alpha)$ and $h(T)$ can be examined. This is a model-free method since it yields the temperature dependence of the reaction rate without having to make any prior assumptions about the kinetic model.

In actual practice, it is not possible to experimentally obtain all the elements of the matrix *A* for a sufficient range of alpha values and temperatures. Therefore, the α *vs.* T curves are divided into partly overlapping submatrices. SVD is then applied to each submatrix; if q submatrices were formed, the SVD on each of them will yield q matrices U_i and V_i as well as q singular value vectors s_i,

respectively. Finally, from the vectors u_i and v_i of the individual matrices U_i and V_i, the continuous vectors u and v can be obtained.[8,16,17] The results contained in the vector u are proportional to the function of conversion, $f(\alpha)$, and those in the vector $\boldsymbol{v}$ are proportional to the function of temperature, $h(T)$.

Fig. 4 confirms the observation stated in referring to Fig. 2, namely that the decomposition of CTMAB occurs in two distinct and fairly well separated main processes. The first one (process I) takes place approximately in the α range of 0.0–0.78, and the second one (process II) in the α range 0.67–0.9; there is a partial overlap of the two processes in the α region 0.67–0.78. The third mass loss (very broad) visible in Fig. 2 lies in the α region ranging from about 0.86 to 1 and it partly overlaps with process II. The NPK analysis was performed separately for process I and process II in the appropriate α regions. The third process could not be kinetically analyzed due to the large breadth of its temperature range.

Process I

The NPK treatment of the thermogravimetry data yielded 8 submatrices in the alpha range 0.1–0.68 and the temperature range of 493–572 K (Fig. 3); a total of 32 different alpha values and 28 different temperatures were used for the construction of the 8 submatrices. After SVD had been applied on each submatrix, the resulting s_i vectors contained in all 8 cases one dominant value and three smaller values. In particular, for the first six submatrices, the dominant value in each individual s_i accounts for more than 96 % of the sum of the values of this vector, whereas the other three values amount to approximately 2 %, 1 %, and 0.1 %, respectively. For the seventh and eighth submatrix, the dominant value accounts for about 93 %, and the other three for 5.4, 1.4, and 0.2 %, respectively. This indicates that in the 493–572 K temperature range there is one dominant kinetic process (process I-1), accompanied by three minor processes (processes I-2, I-3 and I-4).

Further kinetic analysis of process I was performed only for the dominant process I-1. The remaining three minor processes were not examined for the following reason. When more than one kinetic process is present, the individual vectors u for each process are in effect some linear combination of the corresponding true "kinetic vectors".[18] In the same manner, the individual vectors v are also the result of a linear combination. These linear combinations can be broken down only if the kinetic model for each of the processes is known. If these models are not known, it seems meaningful to analyze vectors u and v only for the process which is markedly predominant (provided one exists). Namely, in such circumstances one can reasonably assume that the vectors u and v of the dominant process should not differ significantly from the "kinetic vectors", whereas the corresponding vectors of the minor processes will be heavily influenced by the linear combination.

The kinetic analysis for the process I-1 proceeded as follows. From the vectors u_i and v_i of the individual matrices U_i and V_i the continuous vectors for the process I-1, u_1 and v_1, were compiled. Fig. 5 shows the plot of the $f(\alpha)$ values from the vector u_1 *vs.* α. The α_I scale in Fig. 5 was obtained by rescaling the experimental α range (0.0–0.78) which fully encompasses process I into an α range of 0.0–1.0. The $f(\alpha)$ values were examined against various known kinetic models, but the vector u_1 could not be satisfactorily fitted in most of them (R^2 of the fits being invariably < 0.9). Only the Sestak–Berggren model[19] yielded acceptable fits, the best fit (Fig. 5) being obtained with the two parameter Sestak–Berggren Eq. (1). The obtained parameters are $m = -0.157 \pm 0.006$ and $n = 1.98 \pm 0.03$, with $R^2 = 0.997$.

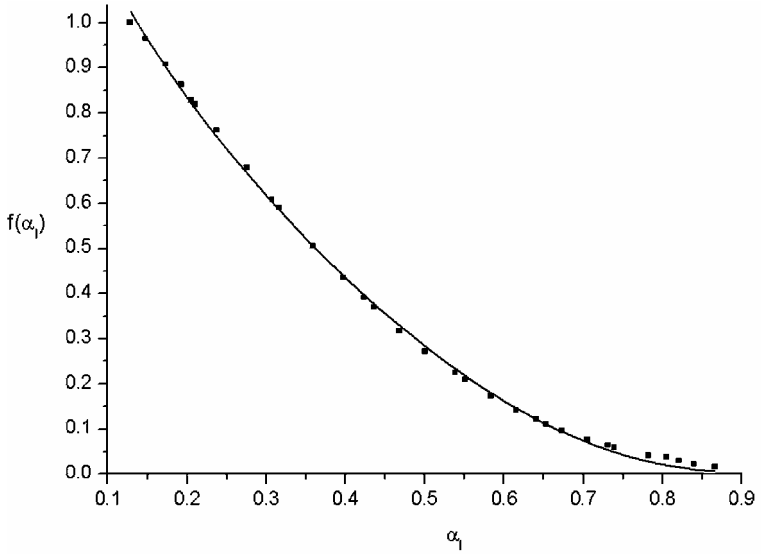

Fig 5. A plot of $f(\alpha)$ [normalized within (0,1)] *vs.* the rescaled degree of conversion for the process I-1: dark squares are the experimental points, while the line is the fit obtained by Eq. (2).

$$f(\alpha) = \alpha^m(1-\alpha)^n \quad (1)$$

$$f(\alpha) = \alpha^{-0.157}(1-\alpha)^{1.98} \quad (2)$$

It is worth noticing that the resulting Eq. (2) is a valid kinetic expression in the sense that it fulfils two boundary conditions[20] which a function must satisfy in order to consistently represent a given kinetic model. The two conditions are:

$$\lim_{\alpha \to 0} g(\alpha) = 0$$

and

$$\lim_{\alpha \to 1} g(\alpha) = \infty$$

where $g(\alpha)$ is the integrated form of $f(\alpha)$.

The plot of the ln [*h(T)*] values from the compiled vector v_1 *vs.* 1/*T* is shown in Fig. 6. The slope of the straight line (R = 0.997) gives the activation energy as E_a = 116±2 kJ mol^{-1}. From the intercept, the value of (5.6±2)×10^{12} min^{-1} is obtained and it essentially represents the Arrhenius pre-exponential constant A, somewhat modified by constants arising from scaling.[16]

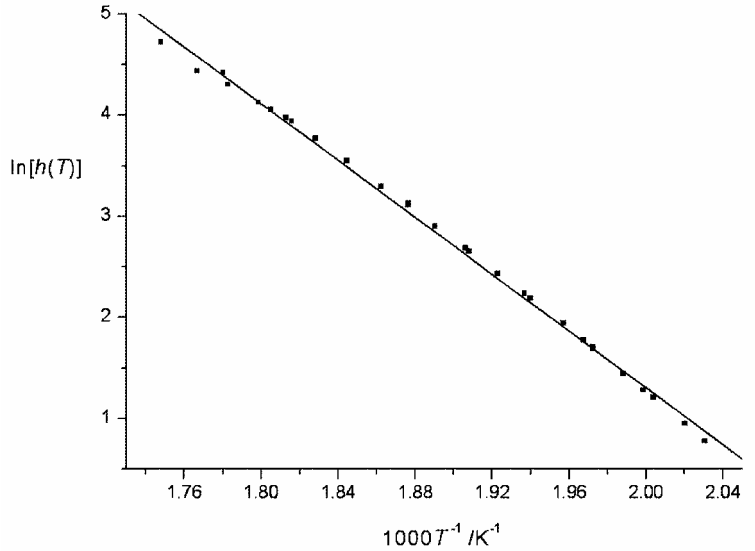

Fig. 6. An Arrhenius plot of ln [*h(T)*] *vs.* 1/*T* for the process I-1: the squares are the experimental points and the straight line is the best fit.

The relatively low E_a value for the process I-1 reflects the fact that a major factor influencing the removal of CTMAB from siliceous networks is the strength of the CTMAB-framework interactions. The framework–surfactant interactions in SBA-3 are not very strong since the inorganic framework is electrically neutral.

The obtained E_a value for process I-1 can be compared with the E_a values of 166 and 178 kJ mol^{-1}found for the thermal removal of CTMAB from MCM-41 and MCM-48 materials, respectively.[3,4] It is not surprising that these two values are higher than the E_a value obtained for SBA-3 since the mesoporous network of the MCM materials is based on stronger cooperative electrostatic interactions between negatively charged oligomeric silicate species and positively charged $CTMA^+$ ions.[21] The relatively weak intermolecular-type interactions in the SBA-3 framework allow CTMAB to be removed more easily than from MCM materials and this is essentially reflected in the corresponding activation energies.

Process II

The NPK treatment of the thermogravimetry data yielded 6 submatrices in the alpha range of 0.73–0.86 and the temperature range of 593–648 K (Fig. 3); a

total of 25 different alpha values and 24 different temperatures were used for the construction of 6 submatrices. After SVD had been applied on each submatrix, the resulting s_i vectors contained in all 6 cases one dominant value and three smaller values. In particular, for the first four submatrices the dominant value in each individual s_i accounts for more than 92 % of the sum of values of this vector, whereas the other three values amount to approximately 4, 2.5 and 0.2 %, respectively. For the fifth and sixth submatrix, the dominant value accounts for about 84 % and the other three for 11, 4 and 0.9 %, respectively. This indicates that there is one major kinetic process (process II-1), together with three minor processes (processes II-2, II-3 and II-4) in the 588–648 K temperature range.

For the same reason as given for process I, further kinetic analysis of process II was performed only for process II-1, in an analogous manner as for process I-1.

The plot of the $f(\alpha)$ values from the vector u_1 *vs.* α is shown in Fig. 7. The α_{II} scale in Fig. 7 was obtained by rescaling the experimental α range of 0.66–0.9 (which essentially encompasses the entire process II) into an α range of 0.0–1.0. The $f(\alpha)$ values for process II-1 could be satisfactorily fitted only with the empirical three-parameter Sestak–Berggren Eq. (3); which gives a fit having R^2 = = 0.994, with the parameters m = −116±0.9, n = 55±0.4 and p = 116±0.8.

$$f(\alpha) = \alpha^m (1-\alpha)^n (-\ln(1-\alpha))^p \tag{3}$$

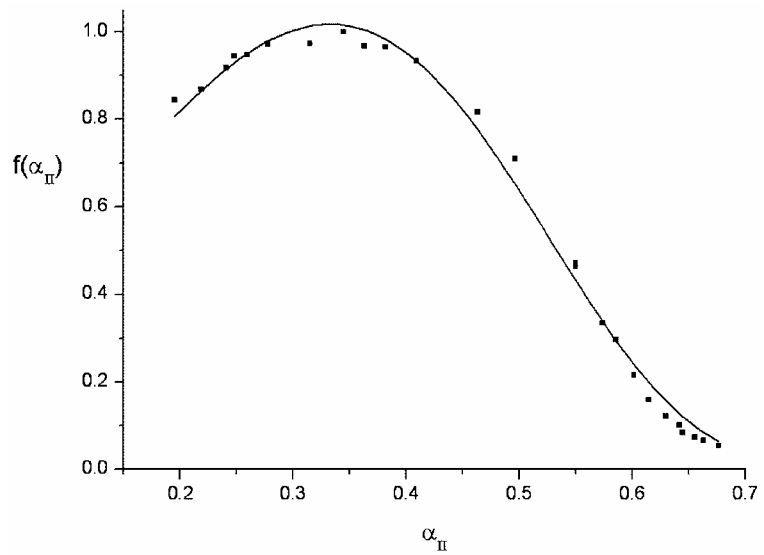

Fig 7. A plot of $f(\alpha)$ [normalized within (0,1)] *vs.* the rescaled degree of conversion for the process II-1: dark squares are the experimental points and the line is the fit obtained by Eq. (1).

The plot of the ln[$h(T)$] values from the compiled vector v_1 *vs.* 1/T is shown in Fig. 8. The slope of the straight line (R = 0.989) gives the activation energy as E_a = 153±5 kJ mol^{-1}. From the intercept, the Arrhenius pre-exponential constant A is found to be (2.3±2)×10^{13} min^{-1}.

The finding that the E_a of the process II-1 is higher than that for the process I-1 could be explained by the fact that the removal of CTMAB from SBA-3 causes a significant contraction of the unit cell of the remaining siliceous material (a contraction of approx. 18 %).[6] After the bulk of the CTMAB has been decomposed by the first process, the ensuing contraction of the unit cell renders the removal of the remaining parts of surfactant more difficult due to the reduced size of the pore openings.

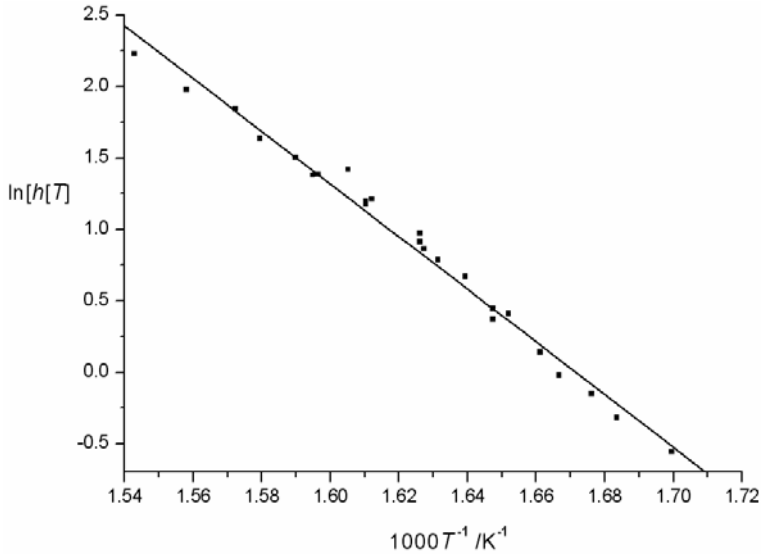

Fig. 8. An Arrhenius plot of ln [$h(T)$] *vs.* 1/T for the process II-1: the squares are the experimental points and the straight line is the best fit.

CONCLUSIONS

The removal of CTMAB from mesostructured SBA-3 was studied under non-isothermal conditions. There are two distinct and complex kinetic processes which partly overlap, each consisting of one dominant and three minor individual processes. Both the dominant processes can be described by the Sestak–Berggren model. The main decomposition step (the first dominant process) proceeds with a rather low E_a value for this type of system, due to weak intermolecular-type interactions between CTMAB and the silica network. The second decomposition step (the second dominant process) has a higher E_a value than the first one, indicating that it is primarily controlled by the size of the pore openings.

The non-parametric kinetics method proved helpful in the separate analyzes of the partly overlapping processes.

Acknowledgements. This work was supported by the bilateral project “By rational synthesis towards smart materials” financed by the Serbian Ministry of Science and the Slovenian Ministry of Higher Education Science and Technology. The authors also wish to thank Mr. Alen Kljajić for the preparation of the SBA-3 material.

И З В О Д

КИНЕТИЧКО ИЗУЧАВАЊЕ ТЕРМИЧКОГ РАЗЛАГАЊА ЦЕТИЛТРИМЕТИЛАМОНИЈУМ−БРОМИДА УНУТАР МЕЗОПОРОЗНОГ МОЛЕКУЛСКОГ СИТА SBA-3

ЂОРЂЕ СТОЈАКОВИЋ[1], НЕВЕНКА РАЈИЋ[1], MAJA MRAK[2] и VENČESLAV KAUČIČ[3]

[1]Технолошко–металуршки факултет, Универзитет у Београду, 11000 Београд, Србија, [2]Jožef Štefan Institute, Jamova 39, 1000 Ljubljana и [3]National Institute of Chemistry, Hajdrihova 19, 1000 Ljubljana, Slovenia

Изучавано је термичко разлагање под неизотермским условима цетилтриметиламонијум-бромида (CTMAB) унутар мезопорозног SBA-3. Постоје два разговетна и сложена кинетичка процеса који се делимично преклапају, при чему се оба састоје од по једног преовлађујућег и три споредна индивидуална процеса. Два преовлађујућа процеса могу се описати помоћу Шестак–Бергреновог модела. У главном ступњу разлагања (у првом преовлађујућем процесу) бивају надвладане слабе интеракције између CTMAB и решетке силицијум-диоксида, и тај ступањ се одвија уз мању вредност E_a (116±2 kJ mol^{-1}). Другом преовлађујућем процесу одговара већа вредност E_a (153±5 kJ mol^{-1}) него првом процесу, што се може објаснити смањењем величине отвора пора услед контракције јединичне ћелије SBA-3 изазване уклањањем цетилтриметиламонијум-бромида.

(Примљено 12. јуна 2007)

REFERENCES

1. N. Rajić, *J. Serb. Chem. Soc*. **70** (2005) 371
2. C. T. Kresge, M. E. Leonowicz, W. J. Roth, J. C. Vartuli, J. S. Beck, *Nature* **359** (1992) 710
3. M. J. B. Souza, A. O. S. Silva, J. M. F. B. Aquino, V. J. Fernandes Jr., A. S. Araujo, *J. Thermal Anal. Cal*. **75** (2004) 693
4. M. J. B. Souza, A. O. S. Silva, J. M. F. B. Aquino, V. J. Fernandes Jr., A. S. Araujo, *J. Thermal Anal. Cal*. **79** (2005) 493
5. F. Chen, S. Shen, X. –J. Xu, R. Xu, F. Kooli, *Microporous Mesoporous Mater*. **79** (2005) 85
6. F. Kleitz, W. Schmidt, F. Schuth, *Microporous Mesoporous Mater*. **65** (2003) 1
7. R. Serra, R. Nomen, J. Sempere, *J. Therm. Anal. Cal*. **52** (1998) 933
8. R. Serra, R. Nomen, J. Sempere, *Thermochim. Acta* **316** (1998) 37
9. J. Sempere, R. Nomen, R. Serra, *J. Therm. Anal. Cal*. **56** (1999) 843
10. T. Vlase, G. Vlase, N. Doca, C. Bolcu, *J. Therm. Anal. Cal*. **80** (2005) 59
11. T. Vlase, G. Vlase, A. Chiriac, N. Doca, *J. Therm. Anal. Cal*. **80** (2005) 87
12. T. Vlase, G. Vlase, N. Doca, *J. Therm. Anal. Cal*. **80** (2005) 207
13. T. Vlase, G. Vlase, N. Doca, *J. Therm. Anal. Cal*. **80** (2005) 425
14. Dj. Stojakovic, N. Rajic, N. Zabukovec Logar, V. Kaucic, *Thermochim. Acta* **449** (2006) 42
15. M. E. Brown, M. Maciejewski, S. Vyazovkin, R. Nomen, J. Sempere, A. Burnham, J. Opfermann, R. Strey, H. L. Anderson, A. Kemmler, R. Keuleers, J. Janssens, H. O. Desseyn, C.-R.. Li, T. B. Tang, B. Roduit, J. Malek, T. Mitsuhashi, *Thermochim. Acta* **355** (2000) 125
16. J. D. Sewry, M. E. Brown, *Thermochim. Acta* **390** (2002) 217
17. J. Sempere, R. Nomen, R. Serra, J. Soravilla, *Thermochim. Acta* **388** (2002) 407
18. J. Sempere, R. Nomen, *EU01-18 – Non-Parametric Kinetics (NPK) – Can it be used in Reaction Calorimetry?, 10th RXE User Forum Europe*, Lucerne, Switzerland, November 2001, http://us.mt.com/mt/appEdStyle/wr_RXEForum_EU01_18_Editorial-Generic_1117531464103.jsp, (April 16, 2007)
19. J. Sestak, G. Berggren, *Thermochim. Acta* **3** (1971) 1
20. J. Malek, J. M. Criado, J. Sestak, J. Militky, *Thermochim. Acta* **153** (1989) 429
21. R. Zana, J. Frasch, M. Soulard, B. Lebeau, J. Patarin, *Langmuir* **15** (1999) 2603.

Journal of the Serbian Chemical Society
JSCS@tmf.bg.ac.yu • www.shd.org.yu/JSCS

J. Serb. Chem. Soc. 72 (12) 1321–1327 (2007)
JSCS–3664

UDC 519.17–124+519.177:577.11
Original scientific paper

Relating Estrada index with spectral radius

IVAN GUTMAN[1*#], SLAVKO RADENKOVIĆ[1#], BORIS FURTULA[1], TOUFIK MANSOUR[2] and MATTHIAS SCHORK[3]

[1]*Faculty of Science, University of Kragujevac, P. O. Box 60, 34000 Kragujevac, Serbia,*
[2]*Department of Mathematics, University of Haifa, 31905 Haifa, Israel and*
[3]*Camillo–Sitte–Weg 25, 60488 Frankfurt, Germany*

(Received 3 July 2007)

Abstract: The Estrada index *EE* is a recently proposed molecular structure-descriptor, used in the modeling of certain features of the 3D structure of organic molecules, in particular of the degree of folding of proteins and other long-chain biopolymers. The Estrada index is computed from the spectrum of the molecular graph. Therefore, finding its relation with the spectral radius r (= the greatest graph eigenvalue) is of interest, especially because the structure-dependency of r is relatively well understood. In this work, the basic characteristics of the relation between *EE* and r, which turned out to be much more complicated than initially anticipated, was determined.

Keywords: molecular graph, Estrada index, spectral radius, graph spectrum.

INTRODUCTION

The Cuban–Spanish scholar Ernesto Estrada designed in the year 2000 a new structure descriptor,[1] capable of representing certain features of the 3D structure of organic molecules, especially those of biochemical importance. Eventually, this structure descriptor was named the Estrada index, and is usually denoted by *EE*. It could be shown[2,3] that the *EE* is particularly suitable for characterizing the degree of folding of proteins and similar long-chain biopolymers. More recently, several other applications of the Estrada index were reported,[4–7] which are, however, of lesser chemical relevance.

As the Estrada index is, in a relatively simple manner, computed from the spectrum of the corresponding molecular graph, efforts have been made to use the powerful mathematical apparatus of graph spectral theory[8] for determining the dependence of the *EE* on molecular structure. The hitherto obtained results are available in the literature.[9–12]

* Corresponding author. E-mail: gutman@kg.ac.yu
# Serbian Chemical Society member.
doi: 10.2298/JSC0712321G

Let λ_1, λ_2,…, λ_n be the eigenvalues of the molecular graph G (which in biochemical applications[1–3] may possess weighted edges).[8,13] These eigenvalues form the spectrum of G and will be labeled as $\lambda_1 \geq \lambda_2 \geq \cdots \geq \lambda_n$.

The greatest graph eigenvalue λ_1 has the property $\lambda_1 \geq |\lambda_k|$, $k = 2,3,\ldots,n$, and is therefore referred to as the spectral radius of the graph G. In what follows, λ_1 is denoted by r.

The spectral radius has been much investigated in graph spectral theory[8,14] and its dependence on the structure of the underlying graph is relatively well understood. This, in particular, applies to molecular graphs.[15,16]

The Estrada index is defined as:[1–7,9–12]

$$EE = \sum_{k=1}^{n} e^{\lambda_k} + \sum_{k=2}^{n} e^{\lambda_k} \qquad (1)$$

Thus EE is equal to the sum of terms of the form e^x, where $x = \lambda_k$, $k = 1,2,\ldots,n$, of which the greatest is e^r. Therefore it is plausible to expect that there is a relation (or, at least, a correlation) between the Estrada index and the spectral radius. However, this relation is not simple, as seen from the example shown in Fig. 1. The fact that the data points in Fig. 1 are grouped on several (almost) horizontal lines indicates that, in addition to the spectral radius, EE depends in a lesser manner on structural factors other than r.

In the subsequent section we elaborate an approach aimed at revealing the fine details of the structure-dependence of the EE is elaborated.

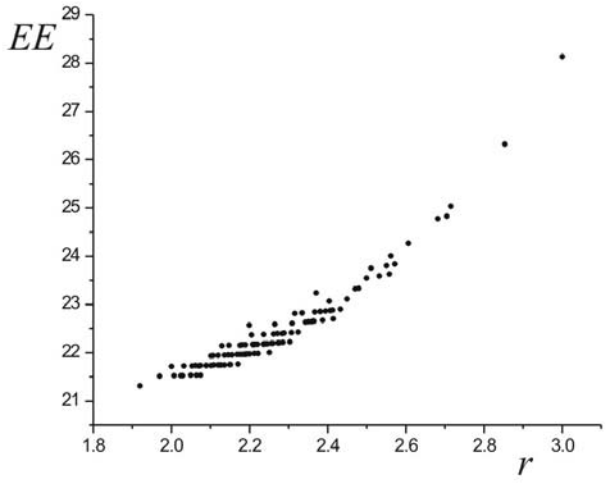

Fig. 1. The Estrada index (EE) of 10-vertex trees, plotted *versus* the spectral radius (r). There is an apparent (curvilinear) correlation between the data points. However, numerous data points lie on almost horizontal lines, indicating that factors other than r also influence the value of EE. In the case of benzenoid and acyclic molecules, the main among these "less important" factors have been identified.[10,11]

A POWER-SERIES-EXPANSION APPROACH

Formula (1) can be rewritten as:

$$EE = e^r \sum_{k=1}^{n} e^{\lambda_k - r}$$

and then, in view of the arguments outlined in the preceding section, it may be expect that the "less important" structural details influencing the value of the Estrada index are contained in the term $\sum_{k=1}^{n} e^{\lambda_k - r}$. Expanding $e^{\lambda_k - r}$ into a power series, one obtains:

$$EE = e^r \sum_{h=0}^{\infty} F_h \tag{2}$$

where

$$F_h = \sum_{k=1}^{n} \frac{(\lambda_k - r)^h}{h!} = \sum_{j=0}^{h} \frac{(-1)^{h-j}}{j!(h-j)!} r^{h-j} M_j$$

with M_j denoting the j-th spectral moment:

$$M_j = \sum_{k=1}^{n} \lambda_k^j$$

The structure dependences of the first few spectral moments of molecular graphs are known.[17–24] For instance:

$$M_0 = n;\ M_1 = 0;\ M_2 = 2m;\ M_3 = 6t$$

where n, m, and t stand, respectively, for the number of vertices, edges, and triangles. For benzenoid molecules, $M_4 = 18m - 12n$, whereas for acyclic molecular graphs, $M_4 = 2Zg - 2n + 2$, where Zg is the Zagreb index, the sum of the squares of the vertex degrees.[17,25–27] It is worth noting that for alternant hydrocarbons (*e.g.*, for acyclic and benzenoid systems), $M_j = 0$ whenever j is odd.

In view of this, the summation on the right-hand side of (2) is truncated, arriving at a series of approximate expressions for the Estrada index, *viz.*

$$EE(p) = e^r \sum_{h=0}^{2p} F_h\,,\ \ p = 1,2,\ldots \tag{3}$$

If so, then $EE(p)$ will depend on the spectral radius r and on the first $2p$ spectral moments (of which many are equal to zero).

It was previously shown that in the case of alkanes, $EE(2)$ is a monotonically increasing function of the variable r and it was concluded that alkanes with maximal EE value will be those possessing maximal spectral radius.[12] The latter alkanes were earlier characterized by Simić and Tošić,[16] who established that these correspond to the so-called Volkmann trees.[28,29] In a study[12] it was (erroneously) assumed that $EE \approx EE(2)$. To obtain the correct conclusion (concerning Volkmann trees), it was sufficient that there is a positive correlation between EE and $EE(2)$. That this is indeed the case can be seen from Fig. 2.

Numerical testing revealed that for the first few values of p, in particular for $p = 2$, the approximation $EE \approx EE(p)$ is highly inaccurate and should not have

been used. In the subsequent section, this matter is clarified and it is also shown that for any value of p, $p \geq 2$, there is a reasonably good, yet non-linear, correlation between EE and EE(p).

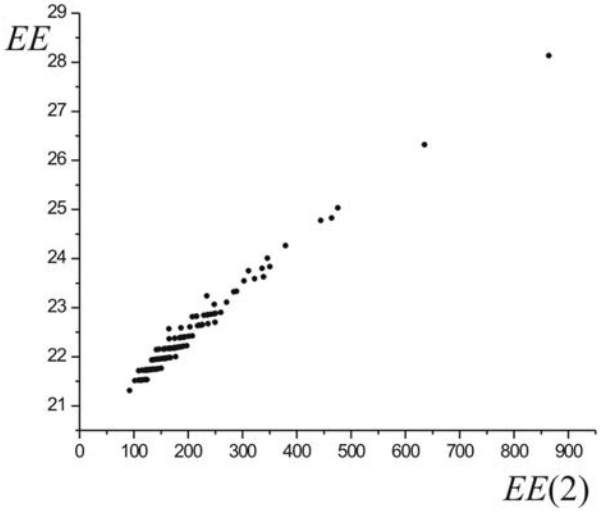

Fig. 2. The Estrada indexes (EE) of 10-vertex trees, plotted *versus* the approximate formula $EE(2)$, *cf.* Eq. (3). The correlation coefficient is equal to 0.993.

NUMERICAL WORK

The accuracy of the approximation $EE \approx EE(p)$ was tested for the first few values of the parameter p. Some characteristic results of this kind, pertaining to trees with 8, 10 and 12 vertices (23, 106 and 551 trees, respectively) are given in Table I.

TABLE I. Average relative errors (ARE) and maximal observed errors (MRE) in % of the approximations $EE \approx EE(p)$, $p = 1,2,\ldots,7$, for 8-, 10- and 12-vertex trees. Recall that there are 23, 106, and 551 such trees, respectively.

p	n					
	8		10		12	
	ARE	MRE	ARE	MRE	ARE	MRE
1	739.36	1426.1	886.83	2327.2	935.76	5092.9
2	617.94	1545.1	792.43	2969.7	1004.33	3506.9
3	281.47	1006.5	387.25	2391.5	475.01	4824.5
4	81.84	410.6	122.53	1245.3	56.42	3044.4
5	16.56	110.2	27.55	430.6	36.90	1287.2
6	2.47	20.7	4.46	104.3	6.67	382.2
7	0.28	2.9	0.63	18.6	0.97	83.5

The data in Table I clearly show that the approximation $EE \approx EE(p)$ is highly inaccurate and that only for very large values of p, say $p > 5$, are some more-or-less satisfactory results obtained. In other words, the expressions $EE(p)$ cannot be used for approximating the Estrada index. This is the bad news.

The good news is that the quantities *EE* and *EE*(*p*) are reasonably well correlated. The correlation between *EE* and *EE*(2) is essentially linear, as can be seen from Fig. 2. For greater values of the parameter *p*, the correlation becomes pronouncedly curvilinear. Two typical examples are shown in Figs. 3 and 4.

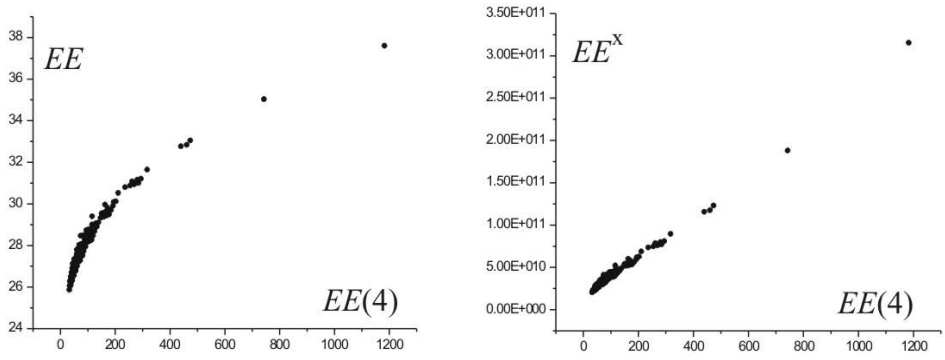

(a) (b)

Fig. 3. (a) The Estrada index (*EE*) of 12-vertex trees, plotted *versus* the approximate formula *EE*(4). (b) Linearization of the correlation is achieved by plotting EE^x *vs.* *EE*(4), for $x = 7.3$; the correlation coefficient is 0.995.

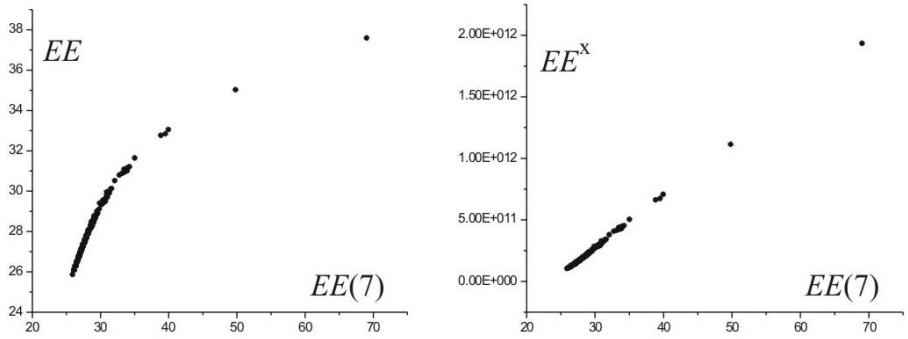

(a) (b)

Fig. 4. Same data as in Fig. 3 for $p = 7$ and $x = 7.8$; correlation coefficient = 0.9995.

The curvature of the *EE*–*EE*(*p*) correlation is best eliminated by plotting EE^x *versus* *EE*(*p*), for some appropriately chosen value of *x*. This value depends both on *p* and on the sample for which it is determined. For instance, for the sample consisting of 10-vertex trees and for $p = 7$, *x* has the value 5.6, in which case, the correlation coefficient for EE^x *vs.* *EE*(*p*) is as high as 0.9997. Two further examples are given in Figs. 3 and 4.

CONCLUSIONS

The expressions *EE*(*p*), given by Eq. (3), provide unacceptably inaccurate approximations for the Estrada index. Only for large values of the parameter *p*

(namely, for $p > 5$) does the approximation $EE \approx EE(p)$ have an average error below 10 %. However, for such large values of p the usage of the formula $EE(p)$ would be impractical and inferior to the direct (exact) calculation of EE from its definition.

On the other hand, for any $p \geq 2$, a reasonably good correlation exists between the Estrada index and $EE(p)$. This correlation is curvilinear, except for $p = 2$ when it is linear (see Fig. 2). Thus, the Estrada index is (in a statistical sense) a monotonically increasing function of the expressions $EE(p)$, $p = 2,3,\ldots..$ As a consequence, if $EE(p)$ is a monotonically increasing function of some variable (say, of the spectral radius r, as in the case of trees and $p = 2$), then is (in a statistical sense) also the Estrada index.

In summary: the present analysis confirms the validity of the conclusion drawn in a previous work[12] that the n-vertex Volkmann tree[28,29] has the greatest Estrada index among all n-vertex chemical trees. More generally: our analysis implies that it is justified to use $EE(2)$ and $EE(3)$ in the study of the structure dependence of the Estrada index. In other words – the structural features on which $EE(2)$ and $EE(3)$ depend (*i.e.*, on which the first few spectral moments depend, which all are known[17–24]) are to a great extent those on which the Estrada index depends. Therefore the employment of the expressions $EE(2)$ and $EE(3)$ enables the finer details of the structure dependency of the Estrada index to be resolved. This task has already been accomplished for benzenoid molecules[10] (using $EE(3)$) and alkanes[11,12] (using $EE(2)$), and now it can be achieved for any other class of molecules for which there is a chemical interest.

И З В О Д

ВЕЗА ЕСТРАДИНОГ ИНДЕКСА И СПЕКТРАЛНОГ РАДИЈУСА

ИВАН ГУТМАН[1], СЛАВКО РАДЕНКОВИЋ[1], БОРИС ФУРТУЛА[1], TOUFIK MANSOUR[2] и MATTHIAS SCHORK[3]

[1]Природно–математички факултет Универзитета у Крагујевцу, Србија, [2]Department of Mathematics, University of Haifa, 31905 Haifa, Israel и [3]Camillo–Sitte–Weg 25, 60488 Frankfurt, Germany

Естрадин индекс EE је један недавно предложени молекулски структурни дескриптор, који је примењен при моделирању извесних тродимензионалних структурних карактеристика органских молекула, нарочито степена савијања протеина и других биополимера дугачког ланца. Естрадин индекс се израчунава из спектра молекулског графа. Због тога је од интереса налажење релације између EE и спекралног радијуса r (= највеће сопствене вредности). Ово тим пре што је зависност r од молекулске структуре релативно добро истражена. У раду су одређене основне карактеристике релације између EE и r, која се показала много сложенијом него што се претпостављало.

(Примљено 3. јула 2007)

REFERENCES

1. E. Estrada, *Chem. Phys. Lett.* **319** (2000) 713
2. E. Estrada, *Bioinformatics* **18** (2002) 697

3. E. Estrada, *Proteins* **54** (2004) 727
4. E. Estrada, J. A. Rodríguez–Velázquez, *Phys. Rev.* **E71** (2005) 056103
5. E. Estrada, J. A. Rodríguez–Velázquez, *Phys. Rev.* **E 72** (2005) 046105
6. E. Estrada, J. A. Rodríguez–Velázquez, M. Randić, *Int. J. Quantum Chem.* **106** (2006) 823
7. E. Estrada, *Phys. Rev.* E75 (2007) 016103
8. D. Cvetković, M. Doob, H. Sachs, *Spectra of Graphs – Theory and Application*, Academic Press, New York, 1980; 2nd revised ed., Barth, Heidelberg, 1995
9. I. Gutman, E. Estrada, J. A. Rodríguez–Velázquez, *Croat. Chem. Acta* **80** (2007) 151
10. I. Gutman, S. Radenković, *Z. Naturforsch.* **62a** (2007) 254
11. I. Gutman, B. Furtula, B. Glišić, V. Marković, A. Vesel, *Indian J Chem.* **46** (2007) 723
12. I. Gutman, B. Furtula, V. Marković, B. Glišić, *Z. Naturforsch.* **62a** (2007) 495
13. I. Gutman, O. E. Polansky, *Mathematical Concepts in Organic Chemistry*, Springer–Verlag, Berlin, 1986.
14. D. Cvetković, P. Rowlinson, *Lin. Multilin. Algebra* **28** (1990) 3
15. I. Gutman, D. Vidović, *Theor. Chem. Acc.* **108** (2002) 98
16. S. K. Simić, D. V. Tošić, *MATCH Commun. Math. Comput. Chem*. **54** (2005) 351
17. I. Gutman, B. Ruščić, N. Trinajstić, C. F. Wilcox, *J. Chem. Phys*. **62** (1975) 3399
18. G. G. Hall, *Theor. Chim. Acta* **70** (1986) 323
19. I. Gutman, *J. Math. Chem.* **1** (1987) 123
20. S. Marković, I. Gutman, *J. Mol. Struct. (Theochem.)* **235** (1991) 81
21. S. Marković, *Theor. Chim. Acta* **81** (1992) 237
22. S. Marković, A. Stajković, *Theor. Chem. Acc*. **96** (1997) 256
23. S. Markovic, *J. Chem. Inf. Comput. Sci*. **39** (1999) 654
24. S. Marković, Z. Marković, R. I. McCrindle, *J. Chem. Inf. Comput. Sci*. **41** (2001) 112
25. B. Zhou, I. Gutman, *MATCH Commun. Math. Comput. Chem*. **55** (2005) 233
26. B. Liu, I.Gutman, *MATCH Commun. Math. Comput. Chem*. **55** (2006) 439
27. B. Zhou, D. Stevanović, *MATCH Commun. Math. Comput. Chem.* **56** (2006) 571
28. M. Fischermann, A. Hoffmann, D. Rautenbach, L. Székely, L. Volkmann, *Discr. Appl. Math*. **122** (2002) 127
29. M. Fischermann, I. Gutman, A. Hoffmann, D. Rautenbach, D. Vidović, L. Volkmann, *Z. Naturforsch.* **57a** (2002) 49.

Journal of the Serbian Chemical Society
JSCS@tmf.bg.ac.yu • www.shd.org.yu/JSCS

J. Serb. Chem. Soc. 72 (12) 1329–1341 (2007) UDC 532.74+519.6+519.218.7:541.124.7+537.872
JSCS–3665 *Original scientific paper*

Are the program packages for molecular structure calculations really black boxes?

ANA MRAKOVIĆ, MILICA DRVENDŽIJA, ALEKSANDRA SAMOLOV, MILENA PETKOVIĆ[#] and MILJENKO PERIĆ*

Faculty of Physical Chemistry, University of Belgrade, P. O. Box 137, 11000 Belgrade, Serbia

(Received 26 September 2007)

Abstract: In this communication it is shown that the widely held opinion that compact program packages for quantum–mechanical calculations of molecular structure can safely be used as black boxes is completely wrong. In order to illustrate this, the results of computations of equilibrium bond lengths, vibrational frequencies and dissociation energies for all homonuclear diatomic molecules involving the atoms from the first two rows of the Periodic Table, performed using the Gaussian program package are presented. It is demonstrated that the sensible use of the program requires a solid knowledge of quantum chemistry.

Keywords: mlecular structure calculations, Gaussian, dssociation energy.

INTRODUCTION

Some thirty years ago, when the senior author of this paper began working in the field of quantum chemistry and his coworkers were not yet born, no compact program packages for performing molecular structure calculations were avaiable. More precisely, several scientists had developed their own algorithms for solving approximately the electronic Schrödinger equation but even for the members of their working groups the use of these programs was impossible without deep knowledge of quantum chemistry, group theory, linear algebra and related topics. As a rule, any step beyond the computation of equilibrium geometries, vertical electronic spectra and potential energy surfaces (*e.g.*, consideration of nuclear dynamics, spin-orbit or non-adiabatic couplings) was connected with the necessity of inventing new methods and writing by oneself the corresponding computer programs. In the meantime considerable progress has been achieved and now several complete program packages for molecular structure calculations, such as Gaussian, MOLPRO, MOLCAS and TURBOMOL, developed by a number of experts in quantum chemistry, can be provided and, thanks to the corresponding more or less detailed manuals, employed by a broad class of users. A

[#] Serbian Chemical Society member.
* Corresponding author. E-mail: peric@ffh.bg.ac.yu
doi: 10.2298/JSC0712329M

consequence of this development is that nowadays many chemists, without profound knowledge of quantum mechanics, can (or at least believe they are able to) carry out quantum–chemical computations to support or explain their experimental results. The goal of the present study is to show that the "blind" use of these program packages and uncritical belief in the reliability of the results produced by them can be very dangerous.

COMPUTATION OF STRUCTURE PARAMETERS FOR DIATOMIC HOMONUCLEAR MOLECULES INVOLVING THE ATOMS FROM THE FIRST AND SECOND ROW OF THE PERIODIC TABLE, BY MEANS OF THE GAUSSIAN PROGRAM PACKAGE

The primary goal of the present study was not to achieve the best possible numerical results obtainable with the Gaussian program package[1] but instead to discuss the results of typical results and their accuracy. Presented here are the equilibrium bond lengths, harmonic vibrational frequencies and the dissociation energies for all homonuclar diatomic (neutral) molecules involving the atoms from the first two rows of the Periodic Table, obtained by means of the restricted Hartree–Fock (RHF) formalism, density functional theory (DFT) and, in the case of the H_2 molecule, using the configuration interaction (CI) approach. The atomic orbital (AO) basis 6−311+G(d,p) and the B3LYP functional were employed. The results are presented in Table I. They are compared with the corresponding experimental findings taken from Ref. 2.

TABLE I. Equilibrium bond lengths (r_e), harmonic vibrational frequencies (ω) and dissociation energies (D_0^0) for homonuclear diatomic molecules involving the atoms from the first two rows of the Periodic Table, obtained by means of the Gaussian program package (RHF, DFT) and derived from experimental data (exp.).[2] The symbol "–" means that the experimental or theoretical result is missing – the latter because the energy of the isolated atoms was not computed to be higher than that of the molecule and/or the potential curve did not converge to a constant value at the dissociation limit (actually at the internuclear distance of 20 Å).

Molecule	*GS*	El. conf.	Method	r_e / Å	ω / cm^{-1}	D_0^0 / eV	D_0^0 / eV $2E_{at} - E_{mol}$
H_2	$^1\Sigma_g^+$	$(1\sigma_g)^2$	RHF	0.735	4595	10.80	3.340
			DFT	0.744	4421	7.400	4.500
			exp.	0.741	4401	4.478	4.478
He_2	$^1\Sigma_g^+$	$(1\sigma_g)^2(1\sigma_u)^2$	RHF	3.368	13	–	–
			DFT	4.668	9.0	–	–
			exp.	2.970[a]	–	0.00090[a]	0.0090[a]
Li_2	$^1\Sigma_g^+$	$[He_2](2\sigma_g)^2$	RHF	2.785	337	–	0.15
			DFT	2.705	343	1.67	0.88
			exp.	2.673	351	1.04	1.04
Be_2	$^1\Sigma_g^+$	$[He_2](2\sigma_g)^2(2\sigma_u)^2$	RHF	1.810	921	–	–
			DFT	2.491	285	0.17	0.17
			exp.	–	–	–	–
B_2	$^3\Sigma_g^-$	$[Be_2](1\pi_u)^2$	RHF	1.639	942	–	0.80
			DFT	1.616	1002	2.52	2.52
			exp.	1.590	1051	3.00	3.00

TABLE I. Continued

Molecule	*GS*	El. conf.	Method	r_e / Å	ω / cm^{-1}	D_0^0 / eV	D_0^0 / eV $2E_{at} - E_{mol}$
C_2	$^1\Sigma_g^+$	$[Be_2](1\pi_u)^4$	RHF	1.245	1907	–	0.29
			DFT	1.252	1868	10.0	4.98
			exp.	1.242	1854	6.21	6.21
C_2	$^1\Sigma_g^+$	$[Be_2](1\pi_u)^4$	RHF	1.245	1907	–	0.29
			DFT	1.252	1868	10.0	4.98
			exp.	1.242	1854	6.21	6.21
N_2	$^1\Sigma_g^+$	$[Be_2](1\pi_u)^4(3\sigma_g)^2$	RHF	1.071	2735	32.10	4.830
			DFT	1.096	2445	18.02	9.600
			exp.	1.098	2359	9.759	9.759
O_2	$^3\Sigma_g^-$	$[Be_2](1\pi_u)^4(3\sigma_g)^2$ $(1\pi_g)^2$	RHF	1.152	2025	20.43	0.980
			DFT	1.206	1634	10.19	5.09
			exp.	1.208	1580	5.115	5.12
F_2	$^1\Sigma_g^+$	$[Be_2](1\pi_u)^4(3\sigma_g)^2$ $(1\pi_g)^4$	RHF	1.329	1225	–	–
			DFT	1.409	982.0	5.230	1.32
			exp.	1.412	916.6	1.602	1.60
Ne_2	$^1\Sigma_g^+$	$[Be_2](1\pi_u)^4(3\sigma_g)^2$ $(1\pi_g)^4(3\sigma_u)^2$	RHF	3.3	28	–	–
			DFT	3.1	39	–	–
			exp.	3.1	14[b]	0.00202[b]	0.00202[b]

[a]Derived from electron scattering experiments; [b]uncertain results

Before going into the qualitative analysis of the results shown in Table I, some trends should be noted. The equilibrium bond lengths are generally quite reasonably computed by both the HF and DFT approach, with the DFT results being superior in most cases. In the case of the noble-gas molecules He_2 and Ne_2, as well as for Be_2, the reliability of both the theoretical and experimental results is questionable. The same trends are found for the harmonic vibrational frequencies, except in the case of H_2, B_2, N_2, O_2 and F_2, for which the HF results are inaccurate. The dissociation energies were computed in two different ways: a) as the energy difference between the dissociation limit of the molecular potential energy curve and the zeroth vibrational level and b) as the difference between the energy of the isolated atoms in their ground states and that of the molecule in its equilibrium geometry, corrected by the zero-point vibrational energy. The first set of results is generally in very bad agreement with the experimental data in both the HF and DFT calculations. The HF results obtained by applying the second approach are again poor (they are close to those generated in the HF calculations employing saturated AO basis sets[3]), while their DFT counterparts are (except for C_2 and F_2) in reasonable agreement with the experimental values.

INTERPRETATION OF THE RESULTS OF COMPUTATIONS

Correlation energy error

As seen by inspection of Table I, the most serious computation errors for the molecules considered in the present study concern their dissociation energies. In this and the following subsection, explanations of the reasons for this are given.[4,5]

The HF energy of the ground electronic state of N_2 at its equilibrium geometry is computed to be −2965.19 eV. This value is very close to the HF limit (*i.e.*, to the HF energy obtained using an infinitely large basis set) of −2965.62 eV and simultaneously 99.5 % of the exact non-relativistic energy, −2980.58 eV. For the SCF energy of a nitrogen atom, a value of −1480.10 is obtained; the HF limit is −1480.22, and the exact energy −1485.39 eV. Thus, the energy of the atom is calculated with a relative error of only 0.35 %. In spite of this, the HF dissociation energy obtained as $E(2N) - E(N_2)$, 5.00 eV (or 4.83 eV if the energy of the zeroth vibrational level is taken into account) is only about 50 % of the experimental value (E_{dis} = 9.90 eV). The problem is namely that the experiments give information not about the total energies but about the energy differences and the latter are unfortunately only a very small part (say 1 %) of the total energy. Thus, an error of 1 % in the total energy can cause a huge error (say 50 %) in the energy difference actually measured. Moreover, if the dissociation energy is defined as the energy difference between the dissociation limit of the potential energy curve and its minimum, the HF value becomes as large as 32.10 eV!

The reasons for such an inaccuracy of the computed dissociation energies lie in the nature of the HF approach. First, this method assumes the total electronic wave function as an (anti-symmetric) product of individual one-electron wave functions (spin-orbitals) and as such it is not capable of taking properly into account the correlation of electronic motions; the real mutual interaction of individual electrons is simulated by an interaction of one particular electron with the mean field produced by all the other ones. This approximation works well as long as the electrons are far away from one another. However, when two electrons build a molecular orbital (MO), *i.e.*, when they form a chemical bond, they are found close to each other and the HF philosophy, which allows them to be arbitrarily close to each other, becomes unrealistic. The quantitative measure of this effect is the “dynamical correlation error”, being of different magnitude for different atoms and molecules, but also for different electronic states of the same molecular or atomic system. The electronic configuration of the nitrogen molecule at its equilibrium geometry represents a “closed shell” system (see Table I); the ground state of the nitrogen atom is, on the other hand, $1s^2\ 2s^2\ 2p^3$ ($^4S_{3/2}$), *i.e.*, two nitrogen atoms involve six open shells. This means that the dissociation of N_2 into two N atoms is characterized by the breaking of three bonds and this causes extremely different correlation errors when calculating these systems in the framework of the HF approach.

Another, usually even more serious, drawback of the HF method is a consequence of representing the electronic wave function by a Slater determinant corresponding to a particular electronic configuration. The closed-shell Slater determinant, reasonably approximating the electronic wave function not far from the equilibrium geometry, is totally inadequate for describing two open-shell

nitrogen atoms in their ground states. The closed-shell determinant employed leads thus into a "wrong" (much higher energy) dissociation channel.

The DFT energy at the equilibrium geometry of N_2 is computed to be −2981.12, *i.e.*, −2980.97 eV, with the zero-point vibrational energy correction. Thus the calculation error is only 0.01 %. For the energy of an isolated nitrogen atom the applied DFT approach gives −1485.68 eV (error of 0.02 %). A consequence of this improved accuracy, when compared with the HF treatment, is the dissociation energy $E(2N) - E(N_2) = 9.75$ (9.60) eV, which is in close agreement with the experimental value. The high accuracy of the DFT results in this case is a consequence of the fact that this method properly accounts for the correlation of the electronic motions. Note that the DFT results for absolute energies are in the present case slightly below the exact results; this may occur because the DFT (as opposed to the HF method) is not a completely variational approach. However, if the dissociation energy is computed as the difference between the asymptotic energy of the potential curve for N_2 and its minimum, the wrong value of 18.17 (18.02) eV is obtained. This means that the DFT method does not eliminate the "non-dynamical correlation error".

Dissociation of the hydrogen molecule

In this subsection, the problem of non-dynamic correlation is discussed on the example of the hydrogen molecule. The non-relativistic electronic Hamiltonian (involving also the nuclear repulsion term) for the hydrogen molecules can be written in the form (atomic units, $m_e \equiv 1$, $e \equiv 1$, $\hbar \equiv 1$, are used throughout this paper):

$$H = h_1 + h_2 + h_{12} + \frac{1}{r_{AB}} \tag{1}$$

where

$$\begin{aligned} h_1 &= -\frac{1}{2}\Delta_1 - \frac{1}{r_{A1}} - \frac{1}{r_{B1}}, \\ h_2 &= -\frac{1}{2}\Delta_2 - \frac{1}{r_{A2}} - \frac{1}{r_{B2}}, \\ h_{12} &= \frac{1}{r_{12}}. \end{aligned} \tag{2}$$

The nuclei are denoted by A and B and the electrons by 1 and 2. h_1 and h_2 are one-electron operators, while h_{12} is a two-electron operator. The Hamiltonian partitioned in such a form is adjusted to molecular orbital approaches, such as HF (and also DFT in its practical applications). For the discussion to follow, one can restrict oneself to the use of the minimal basis of AOs for the representation of the MOs; thus it is assumed that:

$$\psi_1 = \frac{1}{\sqrt{2(1+S)}}(s_A + s_B) \equiv \sigma_g ,$$
$$\psi_2 = \frac{1}{\sqrt{2(1-S)}}(s_A - s_B) \equiv \sigma_u , \tag{3}$$

where Ψ_1 and Ψ_2 are the MOs, s_A and s_B the 1*s* AOs centered on the nuclei *A* and *B*, respectively, and

$$S \equiv \langle s_A | s_A \rangle \equiv \int s_A^* s_B d\vec{r} \tag{4}$$

is the overlap integral. According to the Pauli principle, the two electrons of the hydrogen molecule can be distributed in six ways among the MOs σ_g and σ_u, resulting in six approximate total electronic functions in form of the Slater determinants:

$$\Phi_1 = \frac{1}{\sqrt{2}}\begin{vmatrix} \sigma_g\alpha(1) & \sigma_g\beta(1) \\ \sigma_g\alpha(2) & \sigma_g\beta(2) \end{vmatrix} = \sigma_g(1)\sigma_g(2)\frac{1}{\sqrt{2}}[\alpha(1)\beta(2) - \beta(1)\alpha(2)] \equiv {}^1\Sigma_g^+ ,$$
$$\Phi_2 = \frac{1}{\sqrt{2}}\begin{vmatrix} \sigma_g\alpha(1) & \sigma_u\alpha(1) \\ \sigma_g\alpha(2) & \sigma_u\alpha(2) \end{vmatrix} = \frac{1}{\sqrt{2}}[\sigma_g(1)\sigma_u(2) - \sigma_u(1)\sigma_g(2)]\alpha(1)\alpha(2) \equiv {}^3\Sigma_u^+(M_S = 1),$$
$$\Phi'_3 = \frac{1}{\sqrt{2}}\begin{vmatrix} \sigma_g\alpha(1) & \sigma_u\beta(1) \\ \sigma_g\alpha(2) & \sigma_u\beta(2) \end{vmatrix} = \frac{1}{\sqrt{2}}[\sigma_g(1)\alpha(1)\sigma_u(2)\beta(2) - \sigma_u(1)\beta(1)\sigma_g(2)\alpha(2)],$$
$$\Phi'_4 = \frac{1}{\sqrt{2}}\begin{vmatrix} \sigma_g\beta(1) & \sigma_u\alpha(1) \\ \sigma_g\beta(2) & \sigma_u\alpha(2) \end{vmatrix} = \frac{1}{\sqrt{2}}[\sigma_g(1)\beta(1)\sigma_u(2)\alpha(2) - \sigma_u(1)\alpha(1)\sigma_g(2)\beta(2)], \tag{5}$$
$$\Phi_5 = \frac{1}{\sqrt{2}}\begin{vmatrix} \sigma_g\beta(1) & \sigma_u\beta(1) \\ \sigma_g\beta(2) & \sigma_u\beta(2) \end{vmatrix} = \frac{1}{\sqrt{2}}[\sigma_g(1)\sigma_u(2) - \sigma_u(1)\sigma_g(2)]\beta(1)\beta(2) \equiv {}^3\Sigma_u^+(M_S = -1),$$
$$\Phi_6 = \frac{1}{\sqrt{2}}\begin{vmatrix} \sigma_u\alpha(1) & \sigma_u\beta(1) \\ \sigma_u\alpha(2) & \sigma_u\beta(2) \end{vmatrix} = \sigma_u(1)\sigma_u(2)\frac{1}{\sqrt{2}}[\alpha(1)\beta(2) - \beta(1)\alpha(2)] \equiv 2{}^1\Sigma_g^+ .$$

α and β represent the spin Eigen functions of individual electrons. As indicated in Eq. (5), the Slater determinants Φ_1, Φ_2, Φ_5 and Φ_6 are automatically Eigen functions of the total orbital and spin angular momenta; Φ'_3 and Φ'_4 are not, but these are their linear combinations,

$$\Phi_3 \equiv \frac{1}{\sqrt{2}}(\Phi'_3 + \Phi'_4) = \frac{1}{\sqrt{2}}[\sigma_g(1)\sigma_u(2) - \sigma_u(1)\sigma_g(2)]\frac{1}{\sqrt{2}}[\alpha(1)\beta(2) + \beta(1)\alpha(2)] \equiv {}^3\Sigma_u^+(M_S = 0),$$
$$\Phi_4 \equiv \frac{1}{\sqrt{2}}(\Phi'_3 - \Phi'_4) = \frac{1}{\sqrt{2}}[\sigma_g(1)\sigma_u(2) + \sigma_u(1)\sigma_g(2)]\frac{1}{\sqrt{2}}[\alpha(1)\beta(2) - \beta(1)\alpha(2)] \equiv {}^1\Sigma_u^+ . \tag{6}$$

In the vicinity of its equilibrium geometry, the ground electronic state of the hydrogen molecule is approximately described by the wave function Φ_1, corresponding to the doubly populated lower-energy MO, σ_g. Since the Hamiltonian does not involve the spin coordinates, the energy of this state is given by:

$$\langle E_1 \rangle = \langle \Phi_1 | H | \Phi_1 \rangle = \langle \sigma_g(1)\sigma_g(2) | h_1 + h_2 + h_{12} + \frac{1}{r_{AB}} | \sigma_g(1)\sigma_g(2) \rangle = 2h_g + J_{gg} + \frac{1}{r_{AB}}, \quad (7)$$

where

$$\begin{aligned} h_g &\equiv \langle \sigma_g(1) | h_1 | \sigma_g(1) \rangle = \langle \sigma_g(2) | h_2 | \sigma_g(2) \rangle, \\ J_{gg} &\equiv \langle \sigma_g(1)\sigma_g(2) | h_{12} | \sigma_g(1)\sigma_g(2) \rangle. \end{aligned} \quad (8)$$

The lowest-lying excited state is $1^3\Sigma_u^+$, corresponding to the wave functions Φ_1, Φ_2 and Φ_5. Its energy is:

$$\begin{aligned} &\langle E_{2,3,5} \rangle = \langle \Phi_2 | H | \Phi_2 \rangle = \langle \Phi_3 | H | \Phi_3 \rangle = \langle \Phi_5 | H | \Phi_5 \rangle \\ &= \frac{1}{2} \langle \sigma_g(1)\sigma_u(2) - \sigma_u(1)\sigma_g(2) | h_1 + h_2 + h_{12} + \frac{1}{r_{AB}} | \sigma_g(1)\sigma_u(2) - \sigma_u(1)\sigma_g(2) \rangle \\ &= h_g + h_u + J_{gu} - K_{gu} + \frac{1}{r_{AB}}, \end{aligned} \quad (9)$$

with

$$\begin{aligned} h_u &\equiv \langle \sigma_u(1) | h_1 | \sigma_u(1) \rangle = \langle \sigma_u(2) | h_2 | \sigma_u(2) \rangle, \\ J_{gu} &\equiv \langle \sigma_g(1)\sigma_u(2) | h_{12} | \sigma_g(1)\sigma_u(2) \rangle = J_{ug}, \\ K_{gu} &\equiv \langle \sigma_g(1)\sigma_u(2) | h_{12} | \sigma_u(1)\sigma_g(2) \rangle = K_{ug}. \end{aligned} \quad (10)$$

The second excited state is $1^1\Sigma_u^+$ with the energy:

$$\begin{aligned} &\langle E_4 \rangle = \langle \Phi_4 | H | \Phi_4 \rangle = \frac{1}{2} \langle \sigma_g(1)\sigma_u(2) + \sigma_u(1)\sigma_g(2) | h_1 + h_2 + h_{12} + \frac{1}{r_{AB}} | \sigma_g(1)\sigma_u(2) + \sigma_u(1)\sigma_g(2) \rangle \\ &= h_g + h_u + J_{gu} + K_{gu} + \frac{1}{r_{AB}}, \end{aligned} \quad (11)$$

and, finally, the third excited state corresponds to Φ_6 and has the energy:

$$\langle E_6 \rangle = \langle \Phi_6 | H | \Phi_6 \rangle = \langle \sigma_u(1)\sigma_u(2) | h_1 + h_2 + h_{12} + \frac{1}{r_{AB}} | \sigma_u(1)\sigma_u(2) \rangle = 2h_u + J_{uu} + \frac{1}{r_{AB}}, \quad (12)$$

where J_{uu} is defined analogously to J_{gg}.

In order to estimate the energy of the states in question in the dissociation limit ($r_{AB} \to \infty$),the energy formulae (7), (9), (11) and (12) are now presented in terms of the AOs. It is first found that:

$$h_g = \langle \sigma_g(\mu) | h_\mu | \sigma_g(\mu) \rangle = \frac{1}{2(1+S)} \langle s_A(\mu) + s_B(\mu) | h_\mu | s_A(\mu) + s_B(\mu) \rangle = \frac{1}{1+S}(h_{AA} + h_{AB}), \quad (13)$$

with

$$\begin{aligned} h_{AA} &\equiv \langle s_A(\mu) | h_\mu | s_A(\mu) \rangle = \langle s_B(\mu) | h_\mu | s_B(\mu) \rangle \equiv h_{BB}, \\ h_{AB} &\equiv \langle s_A(\mu) | h_\mu | s_B(\mu) \rangle \end{aligned} \quad (14)$$

and μ taking the values 1 and 2. In the same way one obtains:

$$\begin{aligned}
h_u &= \langle \sigma_u(\mu) | h_\mu | \sigma_u(\mu) \rangle = \frac{1}{1-S}(h_{AA} - h_{AB}), \\
J_{gg} &= \frac{1}{2(1+S)^2}\left[J_{AA} + J_{AB} + 2K_{AB} + 4(AB\|AA)\right], \\
J_{uu} &= \frac{1}{2(1-S)^2}\left[J_{AA} + J_{AB} + 2K_{AB} - 4(AB\|AA)\right], \\
J_{gu} &= \frac{1}{2(1-S^2)}\left[J_{AA} + J_{AB} - 2K_{AB}\right], \\
K_{gu} &= \frac{1}{2(1-S^2)}\left[J_{AA} - J_{AB}\right].
\end{aligned} \tag{15}$$

In Eq. (15), the notation:

$$\begin{aligned}
J_{AA} &\equiv \langle s_A(1)s_A(2) | h_{12} | s_A(1)s_A(2) \rangle = \langle s_B(1)s_B(2) | h_{12} | s_B(1)s_B(2) \rangle \equiv J_{BB}, \\
J_{AB} &\equiv \langle s_A(1)s_B(2) | h_{12} | s_A(1)s_B(2) \rangle = J_{BA}, \\
K_{AB} &\equiv \langle s_A(1)s_B(2) | h_{12} | s_B(1)s_A(2) \rangle = K_{BA}, \\
(AB\|AA) &\equiv \langle s_A(1)s_B(2) | h_{12} | s_A(1)s_A(2) \rangle = (AB\|BB).
\end{aligned} \tag{16}$$

is introduced.

At $r_{AB} \to \infty$, all the *S*, h_{AB}, J_{AB}, K_{AB} and $(AB\|BB)$ tend to zero, whereas J_{AA} takes the value denoted by J_{AA}^{∞}; consequently h_g and h_u become equal to the energy of an isolated hydrogen atom, E_H, and $J_{gg}, J_{uu}, J_{gu}, K_{gu} \to J_{AA}^{\infty}/2$. Thus the dissociation limits of the energy formulae (7), (9), (11) and (12) are:

$$\begin{aligned}
\langle E_1 \rangle^{\infty} &= 2E_H + \frac{1}{2}J_{AA}^{\infty} \equiv H_{11}^{\infty}({}^1\Sigma_g^+), \\
\langle E_{2,3,5} \rangle^{\infty} &= 2E_H \equiv E^{\infty}({}^3\Sigma_u^+), \\
\langle E_4 \rangle^{\infty} &= 2E_H + J_{AA}^{\infty} \equiv E^{\infty}({}^1\Sigma_u^+), \\
\langle E_6 \rangle^{\infty} &= 2E_H + \frac{1}{2}J_{AA}^{\infty} \equiv H_{66}^{\infty}({}^1\Sigma_g^+).
\end{aligned} \tag{17}$$

It can be seen that at $r_{AB} \to \infty$, the two states of the same spin and spatial symmetry, ${}^1\Sigma_g^+$, have the same energy, in contrast to the situation around the equilibrium geometry, where they are clearly separated from each other. Therefore, at very large internuclear distances, the interaction of these two species cannot be neglected. Thus, in order to obtain the correct dissociation channels for the states of ${}^1\Sigma_g^+$ symmetry one has to apply the configuration interaction approach, *i.e.*, to solve the system of equations:

$$\begin{pmatrix} \langle \Phi_1 | H | \Phi_1 \rangle^\infty - E^\infty & \langle \Phi_1 | H | \Phi_6 \rangle^\infty \\ \langle \Phi_6 | H | \Phi_1 \rangle^\infty & \langle \Phi_6 | H | \Phi_6 \rangle^\infty - E^\infty \end{pmatrix} \begin{pmatrix} c_1^\infty \\ c_2^\infty \end{pmatrix} \equiv \begin{pmatrix} H_{11}^\infty - E & H_{16}^\infty \\ H_{16}^\infty & H_{66}^\infty - E \end{pmatrix} \begin{pmatrix} c_1^\infty \\ c_2^\infty \end{pmatrix} = 0, \quad (18)$$

where

$$\langle \Phi_1 | H | \Phi_6 \rangle^\infty = \left(J_{gu} \right)^\infty = \frac{1}{2} J_{AA}^\infty. \quad (19)$$

One obtains:

$$\begin{aligned} E_1^\infty ({}^1\Sigma_g^+) &= H_{11}^\infty - H_{16}^\infty = 2E_H, \\ E_2^\infty ({}^1\Sigma_g^+) &= H_{11}^\infty + H_{16}^\infty = 2E_H + J_{AA}^\infty. \end{aligned} \quad (20)$$

Therefore, in the dissociation limit, the lower state of ${}^1\Sigma_g^+$ symmetry runs into the same dissociation channel as the ${}^3\Sigma_u^+$ species, while the $2{}^1\Sigma_g^+$ states dissociates into the same products as the $1{}^1\Sigma_u^+$ state.

Let us inspect the form of the approximate wave functions for the two ${}^1\Sigma_g^+$ species considered. The spatial parts of the functions Φ_1 and Φ_6 are

$$\begin{aligned} \Phi_1: \quad \sigma_g(1)\sigma_g(2) &= \frac{1}{2(1+S)} \left[s_A(1)s_B(2) + s_B(1)s_A(2) + s_A(1)s_A(2) + s_B(1)s_B(2) \right] \propto \Psi_{VB} + \Psi_{ion}, \\ \Phi_6: \quad \sigma_u(1)\sigma_u(2) &= \frac{1}{2(1-S)} \left[-s_A(1)s_B(2) - s_B(1)s_A(2) + s_A(1)s_A(2) + s_B(1)s_B(2) \right] \propto -\Psi_{VB} + \Psi_{ion}, \end{aligned} \quad (21)$$

where

$$\begin{aligned} \Psi_{VB} &= N \left[s_A(1)s_B(2) + s_B(1)s_A(2) \right], \\ \Psi_{ion} &= N \left[s_A(1)s_A(2) + s_B(1)s_B(2) \right]. \end{aligned} \quad (22)$$

Thus, both of these wave functions correspond to the dissociation scheme according to which the dissociation into the ions ($H^+ + H^-$) is equally probable as that into neutral atoms (H + H), with the consequence that the energy of the dissociation channel is:

$$E^\infty(\Phi_1) = E^\infty(\Phi_6) = \frac{1}{2} \left[(E_H + E_H) + (E_{H^+} + E_{H^-}) \right] = E_H + \frac{1}{2} E_{H^-}, \quad (23)$$

The wave functions corresponding to the asymptotic energies $E_1^\infty({}^1\Sigma_g^+)$ and $E_2^\infty({}^1\Sigma_g^+)$ are:

$$\begin{aligned} \Psi_1^\infty({}^1\Sigma_g^+) &= \frac{1}{\sqrt{2}}(\Phi_1 - \Phi_6) = \frac{1}{\sqrt{2}} \left[s_A(1)s_B(2) + s_B(1)s_A(2) \right] \frac{1}{\sqrt{2}} \left[\alpha(1)\beta(2) - \beta(1)\alpha(2) \right], \\ \Psi_2^\infty({}^1\Sigma_g^+) &= \frac{1}{\sqrt{2}}(\Phi_1 + \Phi_6) = \frac{1}{\sqrt{2}} \left[s_A(1)s_A(2) + s_B(1)s_B(2) \right] \frac{1}{\sqrt{2}} \left[\alpha(1)\beta(2) - \beta(1)\alpha(2) \right]. \end{aligned} \quad (24)$$

The first of the wave functions (24) describes the dissociation of H_2 into H + H, and the second one corresponds to the dissociation into the higher-energy channel involving H^+ and H^- ions.

Thus, it can be concluded that the configuration interaction treatment (or some alternative approach which accounts for both the dynamic and non-dynamic correlation energy) is inevitable for the correct dissociative behavior of the ground electronic state of H_2 to be obtained. In other words, the one-determinant approaches, such as HF or DFT, unavoidably lead to erroneous dissociation energy if it is computed as the difference between the asymptotic ($r_{AB} \to \infty$) energy and the energy at the equilibrium geometry (see Fig. 1).

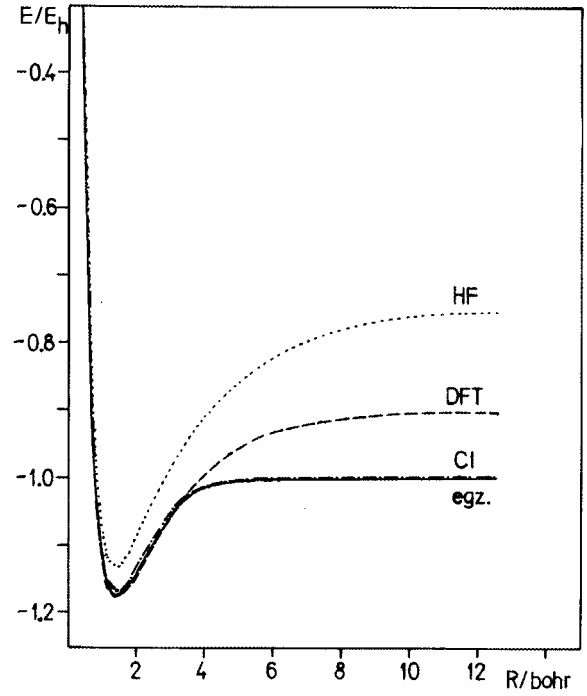

Fig.1. Potential energy curves for the H_2 molecule computed by means of the HF, DFT and CI method and the exact potential energy curve as obtained by Kolos and Wolniewicz.[6]

Towards larger molecules

In the two preceding subsections, some of the problems which arise by using compact program packages, such as Gaussian, for the calculation of molecular structure parameters were pointed out. There, as examples, only very small molecules built up of very light atoms and only the molecular (in majority of cases closed-shell) ground electronic states were considered as examples. When handling larger systems and/or excited electronic states, a number of additional problems have to be solved. Several of them will now be mentioned.

A typical quantum–mechanical task is to find the equilibrium geometry and the corresponding structure parameters of a large molecule (*i.e.*, a molecule composed of many atoms).The first problem which is encountered is the choice of the initial molecular geometry at which the calculation should commence. Theoretically, an *ab initio* quantum–mechanical approach does not require any infor-

mation about the molecule considered except of the number of its electrons and the number, the charges (and possibly masses) of its nuclei. However, in praxis some initial geometry has to be given. The program packages being considered normally incorporate some subroutines, such as *e.g.*, MOLDEN, which more or less automatically guess a reasonable initial geometry, but all the problems cannot be solved in this way. A molecule of say 100 atoms has a potential energy surface depending on 294 nuclear coordinates. It is to be expected that such a potential surface has a large number of local minima and the optimization of the molecular geometry is usually technically completed when one of these minima is attained. The local minimum which is found is to a great extent prejudiced by the choice of the initial geometry, *i.e.*, there is usually no guarantee that the global minimum of the potential surface, *i.e.*, the real equilibrium geometry, has been obtained. Another question is the physical/chemical meaning of local minima and the global minimum of a many-dimensional potential surface; how to interpret the results if there are several minima separated by very high or extremely low potential barriers?

Another difficult problem is the choice of the optimal approach and technical parameters (*e.g.*, AO bases, one-electron based functions in post-HF calculations, DFT functionals) for the system considered. As already mentioned, the HF and DFT approaches are usually not appropriate for calculating excited electronic states and the employment of methods accounting for the electron correlation more properly (Configuration Interaction, Coupled Cluster) is often not feasible for large molecules. Reliable computation of some structure parameters, such as hyperfine coupling constants, requires the use of special (typically compact) AO based functions; on the other hand, in the handling of negative ions and particularly a Rydberg electronic state, a standard AO basis must be augmented by several diffuse basis functions. By the choice of the method and the corresponding technical parameters, a fine balance between the desired accuracy of the final results and the computational requirements has to be achieved.

Special care is necessary when interpreting the obtained numbers. We mention only several questions which have to be answered: Does the computed property depend on the choice of the coordinate system (such as, *e.g.*, the dipole moment of an ion or the components of the hyperfine tensor)? Do the results depend on the choice of the subgroup of the actual point group of the molecule, employed in calculations? Why the components of a spatially degenerate electronic state of a linear molecule are sometimes computed to have different energy? Are the computed harmonic vibrational frequencies reliable? The answer to the last question necessitates knowledge of the manner in which the program computes them – by use of the second derivatives of the energy at equilibrium, energy gradients or in some other way. What is the reason for obtaining different values for two components of the bending vibrations in a spatially degenerate

electronic stale of a linear molecule? Which results are physically/chemically justified and not simply artifacts?

CONCLUSIONS

The general conclusion which follows from the preceding analysis is that the employment of the available compact program packages for calculating molecular structure parameters and particularly the interpretation of results of such calculations requires a profound knowledge of chemistry, quantum mechanics, molecular dynamics and related topics. Although written by the experts in the field and accompanied with detailed manuals, these programs are by no means easy to handle. In order to obtain reliable results and to understand them, the user is often forced to obtain insight into the structure of the programs and underlying quantum–chemical methods, which cannot be learnt solely by studying the instructions for their use.

Acknowledgements. The authors acknowledge the Ministry of Science of Serbia for their financial support (Project No. 142055).

И З В О Д

ДА ЛИ СУ ПРОГРАМСКИ ПАКЕТИ ЗА РАЧУНАЊЕ СТРУКТУРЕ МОЛЕКУЛА ЗАИСТА “ЦРНЕ КУТИЈЕ”?

АНА МРАКОВИЋ, МИЛИЦА ДРВЕНЏИЈА, АЛЕКСАНДРА САМОЛОВ, МИЛЕНА ПЕТКОВИЋ и МИЉЕНКО ПЕРИЋ

Факултет за физичку хемију, Универзитет у Београду, п. пр. 137, 11000 Београд

У овом раду показујемо да је широко распрострањено мишљење да се компактни програмски пакети за квантномеханичко рачунање структуре молекула могу безбрижно користити као “црне кутије” потпуно погрешно. Да бисмо то илустровали, приказујемо резултате рачунања дужине веза, вибрационих фреквенција и енергија дисоцијације за све хомонуклеарне двоатомске молекуле који укључују атоме из прве две периоде Периодног система, добијене помоћу програмског пакета Gaussian. Показано је да разумно коришћење програма претпоставља солидно познавање квантне хемије.

(Примљено 26. септембра 2007)

REFERENCES

1. Gaussian 03, Revision B.02, M. J. Frisch, G. W. Trucks, H. B. Schlegel, G. E. Scuseria, M. A. Robb, J. R. Cheeseman, J. A. Montgomery Jr., T. Vreven, K. N. Kudin, J. C. Burant, J. M. Millam, S. S. Iyengar, J. Tomasi, V. Barone, B. Mennucci, M. Cossi, G. Scalmani, N. Rega, G. A. Petersson, H. Nakatsuji, M. Hada, M. Ehara, K. Toyota, R. Fukuda, J. Hasegawa, M. Ishida, T. Nakajima, Y. Honda, O. Kitao, H. Nakai, M. Klene, X. Li, J. E. Knox, H. P. Hratchian, J. B. Cross, C. Adamo, J. Jaramillo, R. Gomperts, R. E. Stratmann, O. Yazyev, A. J. Austin, R. Cammi, C. Pomelli, J. W. Ochterski, P. Y. Ayala, K. Morokuma, G. A. Voth, P. Salvador, J. J. Dannenberg, V. G. Zakrzewski, S. Dapprich, A. D. Daniels, M. C. Strain, O. Farkas, D. K. Malick, A. D. Rabuck, K. Raghavachari, J. B. Foresman, J. V. Ortiz, Q. Cui, A. G. Baboul, S. Clifford, J. Cioslowski, B. B. Stefanov, G. Liu, A. Liashenko, P. Piskorz, I. Komaromi, R. L. Martin, D. J. Fox, T. Keith, M. A. Al-Laham, C. Y. Peng, A. Nanayakkara,

M. Challacombe, P. M. W. Gill, B. Johnson, W. Chen, M. W. Wong, C. Gonzalez, J. A. Pople, Gaussian, Inc., Pittsburgh PA, 2003
2. K. P. Huber, G. Herzberg, *Molecular Spectra and Molecular Structure IV. Constants of Diatomic Molecules*, Van Nostrand Reinhold Company, 1979
3. W. Kutzelnigg, *Einführung in die theoretische Chemie*, Verlag Chemie, Weinheim, 1975
4. A. Szabo, N. S. Ostlund, *Modern Quantum Chemistry*, Macmillan, New York, 1982
5. F. L. Pilar, *Elementary Quantum Chemistry*, McGraw-Hill, New York, 1968
6. W. Kolos, L. Wolniewicz, *J. Chem. Phys*. **49** (1968) 404.

Journal of the Serbian Chemical Society
JSCS@tmf.bg.ac.yu • www.shd.org.yu/JSCS

J. Serb. Chem. Soc. 72 (12) 1343–1350 (2007)
JSCS–3666

UDC 519.17–124+539.124+537.872
Original scientific paper

Total π-electron energy and Laplacian energy: How far the analogy goes?

SLAVKO RADENKOVIĆ[#] and IVAN GUTMAN*[#]

Faculty of Science, University of Kragujevac, P.O. Box 60, 34000 Kragujevac, Serbia

(Received 23 July 2007)

Abstract: The Laplacian energy *LE* is a newly introduced molecular-graph-based analog of the total π-electron energy *E*. It is shown that *LE* and *E* have a similar structure-dependency only when molecules of different sizes are compared, when a good linear correlation between them exists. Within classes of isomers, *LE* and *E* are either not correlated at all or (as in the case of acyclic systems) are inversely proportional. The acyclic graphs and molecular graphs having the greatest and smallest *LE* values (determined in this work) differ significantly from those (previously known) having the greatest and smallest *E* values.

Keywords: Laplacian energy, graph energy, total π-electron energy.

INTRODUCTION

The total π-electron energy *E*, as calculated within the Hückel molecular orbital (HMO) model, is one of the most thoroughly studied quantum–chemical characteristics of large polycyclic conjugated molecules. Details on the theory and applications of *E* can be found in the literature[1–3] and in the references cited therein. It was recognized a long time ago that the various π-electron descriptors of the HMO model, including *E*, can be calculated from the eigenvalues λ_1, λ_2, …, λ_n of the underlying molecular graph.[4,5] In particular, in the case of alternant hydrocarbons:

$$E = \sum_{i=1}^{n} |\lambda_i| \qquad (1)$$

where, as usual,[1,2,4,5] *E* is expressed in the units of the HMO carbon–carbon resonance integral β.

Formula (1) served as a motivation for the definition of the so-called graph energy. Namely, whereas within the HMO model *E* is meaningful only in the case of a restricted class of molecular graphs,[5] the right-hand side of (1) is a well-de-

[#] Serbian Chemical Society member.
* Corresponding author. E-mail: gutman@kg.ac.yu
doi: 10.2298/JSC0712343R

fined quantity for all graphs. In view of this, the energy of a graph (also denoted by E) is defined as the sum of the absolute values of all eigenvalues of this graph, and this definition extends to all graphs. This seemingly insignificant change in the interpretation of Eq. (1) resulted in a great expansion of research in this area and has advanced the theory of total π-electron energy greatly; for details see the reviews[1,6] and some of the most recent publications dealing with graph energy.[7–14]

By Eq. (1), the graph energy is defined in terms of the graph eigenvalues λ_1, λ_2, …, λ_n. Recall that these are just the eigenvalues of the adjacency matrix.[15] In graph spectral theory, the eigenvalues of several other matrices have been studied, of which the Laplacian matrix attracted the greatest attention in both mathematics[15] and chemistry.[16–21] In view of this, a Laplacian analog of E has recently been conceived,[22] defined as:

$$LE = \sum_{i=1}^{n} \left| \mu_i - \frac{2m}{n} \right| \qquad (2)$$

where μ_1, μ_2, …, μ_n are the Laplacian eigenvalues, m is the number of edges and n the number of vertices of the underlying graph. At the first glance, the forms of the right-hand sides of Eqs. (1) and (2) are different. However, both are special cases of the general expression:

$$\sum_{i=1}^{n} \left| x_i - \bar{x} \right|$$

where $\bar{x}$ is the average value of the eigenvalues x_1, x_2, …, x_n. Indeed,[1–18] $\lambda = 0$ whereas $\mu = 2m/n$.

Both in the first paper[22] on the Laplacian energy and in two consecutive papers[23,24] it could be shown that several mathematical properties of LE are fully analogous (or even identical) to properties of E. However, with regard to some other properties, LE and E differ significantly. Hitherto, no detailed numerical testing of the relation between LE and E has been reported. The aim of this work is to contribute towards filling this gap.

RELATION BETWEEN ENERGY AND LAPLACIAN ENERGY IN BENZENOID AND ACYCLIC SYSTEMS

It is known that the main parameters determining the value of the total π-electron energy E are n (= the number of carbon atoms, *i.e.*, the number of vertices of the molecular graph) and m (= the number of carbon–carbon bonds, *i.e.*, the number of edges of the molecular graph).[1,2,25,26] In order to test if, in the case of molecular graphs, the same parameters also influence the value of the Laplacian energy, E and LE have been correlated for benzenoid molecules (Fig. 1) and acyclic systems (Fig. 2). In Fig. 1, the standard set[1,26] of 106 Kekuléan benzenoids from the book[27] is employed. Figure 2 shows the correlation between E and LE for the set consisting of all n-vertex trees with n between 2 and 14, for which

$n_0 = 0$. Here n_0 stands for the number of zero eigenvalues, which in the HMO model are equal to the number of non-bonding molecular orbitals. The choice $n_0 = 0$ was made because earlier studies[28–30] revealed that the energy of trees is significantly influenced by the value of n_0, whereas *LE* was found to be practically independent of this value.

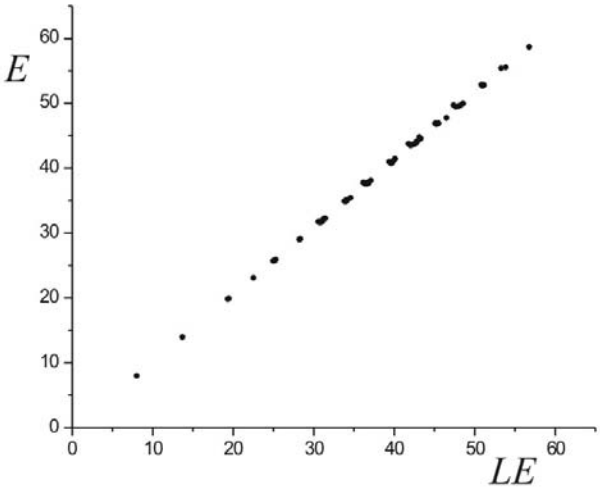

Fig. 1. The Laplacian energy (*LE*) of Kekuléan benzenoid molecules *versus* the respective total π-electron energy (*E*). The data set is taken from the book[27] and consists of 106 benzenoids of various sizes. The regression line reads $LE = (1.043\pm0.002)E - (0.42\pm0.08)$ and the correlation coefficient is 0.9998. For details, see the text.

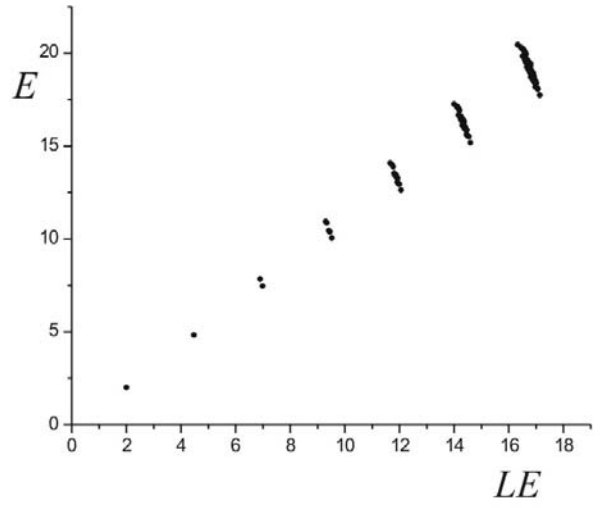

Fig. 2. The Laplacian energy (*LE*) of trees without zero eigenvalues ($n_0 = 0$) *versus* the respective *E* value. The data set consists of all 253 such systems with *n* vertices, $2 \leq n \leq 14$. Recall that from the requirement $n_0 = 0$ follows that *n* must be even.[15] The regression line reads $LE = (1.14\pm0.02)E - (0.0\pm0.3)$ and the correlation coefficient is 0.969. For details, see the text.

From Figs. 1 and 2, it can be seen that a very good linear correlation exists between *LE* and *E*, which means that the gross part of both the total π-electron energy and the Laplacian energy are determined by the parameters *n* and *m*. Furthermore, both *LE* and *E* depend on *n* and *m* in essentially the same way. As the (*n*,*m*)-dependence of *E* is well understood,[1,2,31] it may be said that the (*n*,*m*)-dependence of the Laplacian energy is also known.

RELATION BETWEEN ENERGY AND LAPLACIAN ENERGY IN SETS OF ISOMERS

Many graph-based molecular structure descriptors have the property that their value is mainly determined by the parameters *n* and *m.* In order to envisage the finer details of their structure-dependence, the standard procedure is to examine their behavior within sets of molecular graphs with equal *n* and *m*, *i.e.*, within sets of isomers.

In Figs. 1 and 2, isomers correspond to points that lie very near to each other. In Fig. 1, the spread of these points cannot be seen at all, implying that in the case of benzenoid molecules, structural details other than *n* and *m* have a very small influence on the values of *E* and *LE*. In the case of acyclic systems, this influence is somewhat stronger and the deviation of the data-points from the regression line is easily recognized.

Various sets of benzenoid isomers were examined and in all cases it was found that their Laplacian energies and total π-electron energies are completely unrelated. A characteristic example is shown in Fig. 3.

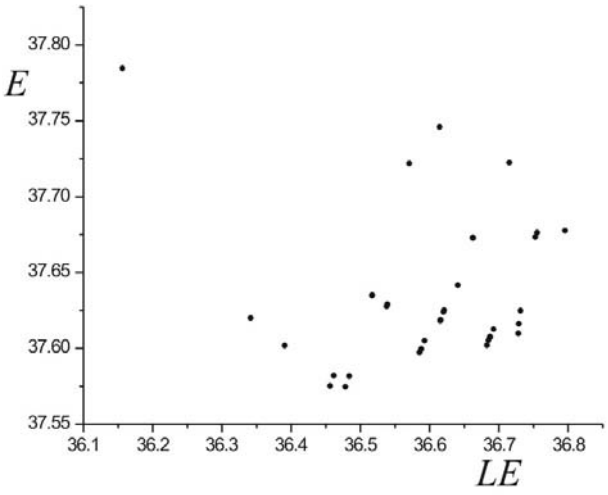

Fig. 3. The Laplacian energy *versus* the total π-electron energy for the set of all 36 (isomeric) catacondensed benzenoids with 6 hexagons, all having the formula $C_{26}H_{16}$. There is no correlation.

The fact that in the case of trees an inverse correlation between *LE* and *E* exists has already seen from Fig. 2. In Fig. 2, the group of near-lying data-points corresponds to a fixed value of *n* and, since for trees $m = n–1$, also to a fixed value of *m*. Note that all trees with odd number of vertices have the property $n_0 > 0$, and therefore for all acyclic systems shown in Fig. 2, the parameter *n* is even.

A detailed examination showed that for acyclic isomers with a fixed value of n_0, the (*LE*,*E*) data-points are linearly correlated. A characteristic example is shown in Fig. 4.

The finding that the slopes of the (*LE*,*E*) regression lines are negative is remarkable and (for the authors of this paper) was fully unexpected. It implies that within sets of acyclic isomers, the structural factors which increase the total π-ele-

ctron energy decrease the Laplacian energy, and *vice versa*. It has been known for a long time[32,33] that the extent of branching is the main such structural factor which decreases *E*. As a consequence of this, the more branched an acyclic system is, the greater will be its Laplacian energy. Thus, as far as the effect of branching is concerned, *E* and *LE* exhibit a different and opposite structure-dependence. Further consequences of this finding are outlined in the subsequent section.

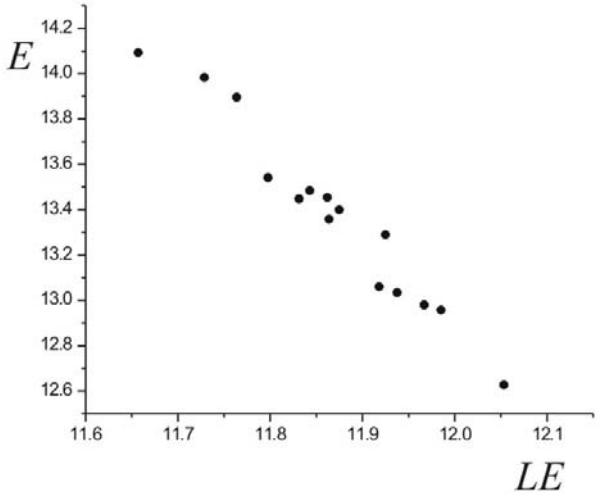

Fig. 4. The Laplacian energy *versus E* for the set consisting of all 10-vertex trees without zero eigenvalues (a total of 15); these graphs pertain to (isomeric) acyclic conjugated hydrocarbons with formula $C_{10}H_{12}$. As a kind of surprise, there is a decreasing linear correlation between *LE* and *E*, implying that acyclic isomers with large *E* have small *LE* and *vice versa*. The correlation coefficient is −0.980.

TREES AND CHEMICAL TREES WITH GREATEST AND SMALLEST LAPLACIAN ENERGY

In graph theory, a connected acyclic graph is called a "tree". A "chemical tree" is a tree in which no vertex has degree greater than 4. A "path" is a tree in which no vertex has degree greater than 2. A "star" is a tree in which all but one of the vertices are of degree 1. An *n*-vertex path and an *n*-vertex star will be denoted by P_n and S_n, respectively, see Fig. 5.

It is known[34] that among all *n*-vertex trees, P_n and S_n have, respectively, the greatest and smallest energy, that is:

$$E(P_n) < E(T_n) < E(S_n) \tag{3}$$

where T_n is any *n*-vertex tree different from P_n and S_n.

It was found now (by means of a computer-aided systematic search of all trees with *n* up to 17) that a relation opposite to (3) holds for the Laplacian energy, *viz.*:

$$LE(P_n) > LE(T_n) > LE(S_n) \tag{4}$$

In view of the Relations (3) and (4), one arrives at:

Rule 1. Among the *n*-vertex trees, the star S_n has the greatest Laplacian energy. In contrast with this, the star has the smallest energy.[34] Rule 1 holds for all $n \geq 4$, and in a trivial manner also for $n = 1,2,3$.

Rule 2. Among the n-vertex trees, the path P_n has the smallest Laplacian energy. In contrast with this, the path has the greatest energy.[34] Rule 2 holds for all $n \geq 4$, and in a trivial manner also for $n = 1,2,3$.

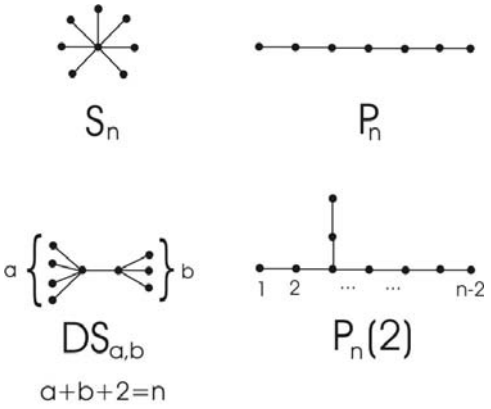

Fig. 5. Trees with extreme Laplacian energy; for details, see the text.

The trees with the second-maximal, third-maximal, and fourth-maximal Laplacian energy have also been determined. Let $DS_{a,b}$ be a "double star" with $a+b+2$ vertices, depicted in Fig. 5. Then one obtains:

Rule 3. If n is even, $n \geq 4$, then among the n-vertex trees, the double star $DS_{a,b}$ with parameters $a = (n-2)/2$, $b = (n-2)/2$ has the second-greatest Laplacian energy. If n is odd, $n \geq 5$, then among the n-vertex trees, the double star $DS_{a,b}$ with parameters $a = (n-1)/2$, $b = (n-3)/2$ has the second-greatest Laplacian energy.

Rule 4. If n is even, $n \geq 6$, then among the n-vertex trees, the double star $DS_{a,b}$ with parameters $a = n/2$, $b = (n-4)/2$ has the third-greatest Laplacian energy. If n is odd, $n \geq 7$, then among the n-vertex trees, the double star $DS_{a,b}$ with parameters $a = (n+1)/2$, $b = (n-5)/2$ has the third-greatest Laplacian energy.

Rule 5. If n is even, $n \geq 8$, then among the n-vertex trees, the double star $DS_{a,b}$ with parameters $a = (n+2)/2$, $b = (n-6)/2$ has the fourth-greatest Laplacian energy. If n is odd, $n \geq 9$, then among the n-vertex trees, the double star $DS_{a,b}$ with parameters $a = (n+3)/2$, $b = (n-7)/2$ has the fourth-greatest Laplacian energy.

Note that the trees described in Rules 3–5 are different from those with the second-minimal, third-minimal, and fourth-minimal energy.[34] On the other hand, the tree with the second-minimal Laplacian energy coincides with the tree with the second-maximal energy:

Rule 6. Among the n-vertex trees, the graph $P_n(2)$, the structure of which is depicted in Fig. 5, has the second-smallest Laplacian energy. In contrast with this, the same tree has the second-greatest energy.[34] Rule 6 holds for $n \geq 13$.

The trees specified in Rules 2 and 6 are molecular graphs. Therefore, these rules also automatically determine the chemical trees with the minimal and second-minimal Laplacian energy. A search for chemical trees with maximal Laplacian energy lead to another unexpected finding:

Rule 7. Among the n-vertex chemical trees, the trees the structure of which is depicted in Fig. 6 have the greatest Laplacian energy. Rule 7 holds for all $k \geq 2$, that is for $n \geq 6$ if $n = 3k$, for $n \geq 7$ if $n = 3k+1$ and for $n \geq 8$ if $n = 3k+2$.

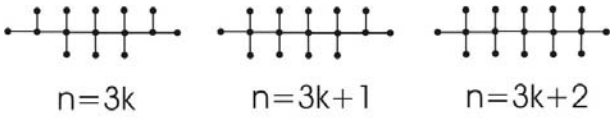

Fig. 6. Chemical trees with the greatest Laplacian energy; for details, see the text.

One should note that the chemical trees shown in Fig.6 with the maximal-Laplacian-energy are different from those having minimal energy.[35]

CONCLUDING REMARKS

The results outlined in the preceding sections reveal some quite unusual features of the relation between the Laplacian energy *LE* and the total π-electron energy (or graph energy) *E*. Whereas both *LE* and *E* have the same (*n*,*m*)-dependence (as seen from the good linear correlations shown in Figs. 1 and 2), this analogy breaks down when classes of isomers are considered, having equal (*n*,*m*). Then the correlation between *LE* and *E* may be completely lost (*cf.* Fig. 3) or an inverse correlation is found (*cf.* Fig. 4). In the case of trees, this inverse behavior of *LE* and *E* is best manifested in Rules 1 and 2 (and also in Rule 6). However, such an inverse analogy between *LE* and *E* is not generally obeyed, as seen in Rules 3, 4, 5, and 7.

In summary, the Laplacian energy and the total π-electron energy were found to be only weakly related. In other words: the analogy between *LE* and *E* does not go very far. This implies that the Laplacian energy depends on molecular structure in a manner that is different, but not completely different, from the (nowadays well understood[1,2]) structure-dependence of the total π-electron energy. Elucidation of the details of these differences remains a task for the future.

И З В О Д

УКУПНА π-ЕЛЕКТРОНСКА ЕНЕРГИЈА И ЛАПЛАСОВА ЕНЕРГИЈА: ДОКЛЕ ИДЕ АНАЛОГИЈА?

СЛАВКО РАДЕНКОВИЋ и ИВАН ГУТМАН

Природно-математички факултет Универзитета у Крагујевцу

Лапласова енергија *LE* је недавно уведен, на молекулском графу заснован, аналог укупне π-електронске енергије *E*. У раду је показано да *LE* и *E* имају сличне особине само када се упоређују молекули различитих величина, када међу њима постоји добра линеарна корелација. Унутар класа изомера, *LE* и *E* или уопште нису корелирани или су (као што је случај код ацикличних система) инверзно пропорционални. Ациклични графови и молекулски графови са највећим и најмањим *LE* вредностима (одређени у овом раду) битно се разликују од (раније познатих) ацикличних графова са највећим и најмањим *E* вредностима.

(Примљено 23. јула 2007)

REFERENCES

1. I. Gutman, *Topics Curr. Chem.* **162** (1992) 29
2. I. Gutman, *J. Serb. Chem. Soc.* **70** (2005) 441
3. M. Perić, I. Gutman, J. Radić–Perić, *J. Serb. Chem. Soc*. **71** (2006) 771
4. A. Graovac, I. Gutman, N. Trinajstić, *Topological Approach to the Chemistry of Conjugated Molecules*, Springer–Verlag, Berlin, 1977
5. I. Gutman, O. E. Polansky, *Mathematical Concepts in Organic Chemistry*, Springer–Verlag, Berlin, 1986
6. I. Gutman, *Chemical graph theory – The mathematical connection*, in: *Advances in Quantum Chemistry 51*, J. R. Sabin, and E. J. Brändas, Eds., Elsevier, Amsterdam, 2006, p. 125
7. W. Lin, X. Guo, H. Li, *MATCH Commun. Math. Comput. Chem.* **54** (2005) 363
8. F. Li, B. Zhou, *MATCH Commun. Math. Comput. Chem.* **54** (2005) 379
9. A. Yu, M. Lu, F. Tian, *MATCH Commun. Math. Comput. Chem.* **53** (2005) 441
10. W. Yan, L. Ye, *MATCH Commun. Math. Comput. Chem.* **53** (2005) 449
11. G. Indulal, A. Vijayakumar, *MATCH Commun. Math. Comput. Chem.* **55** (2006) 83
12. B. Zhou, *MATCH Commun. Math. Comput. Chem.* **55** (2006) 91
13. A. Chen, A. Chang, W. C. Shiu, *MATCH Commun. Math. Comput. Chem.* **55** (2006) 95
14. J. A. de la Peña, L. Mendoza, *MATCH Commun. Math. Comput. Chem.* **56** (2006) 113
15. D. Cvetković, M. Doob, H. Sachs, *Spectra of Graphs – Theory and Application*, Academic Press, New York, 1980
16. B. Mohar, *Stud. Phys. Theor. Chem.* **63** (1989) 1
17. N. Trinajstić, D. Babić, S. Nikolić, D. Plavšić, D. Amić, Z. Mihalić, *J. Chem. Inf. Comput. Sci.* **34** (1994) 368
18. I. Gutman, S. L. Lee, C. H. Chu, Y. L. Luo, *Indian J. Chem.* **33A** (1994) 603
19. I. Gutman, D. Vidović, D. Stevanović, *J. Serb. Chem. Soc*. **67** (2002) 407
20. I. Gutman, *J. Serb. Chem. Soc.* **68** (2003) 949
21. W. Xiao, I. Gutman, *Theor. Chem. Acc.* **110** (2003) 284
22. I. Gutman, B. Zhou, *Lin. Algebra Appl.* **414** (2006) 29
23. B. Zhou, I. Gutman, *MATCH Commun. Math. Comput. Chem.* **57** (2007) 211
24. I. Gutman, N. M. M. de Abreu, C. T. M. Vinagre, A. S. Bonifácio, S. Radenković, *MATCH Commun. Math. Comput. Chem.* **59** (2008), in press
25. I. Gutman, S. Marković, A. Vesović, E. Estrada, *J. Serb. Chem. Soc*. **63** (1998) 639
26. I. Gutman, T. Soldatović, *J. Serb. Chem. Soc*. **66** (2001) 101
27. R. Zahradnik, J. Pancir, *HMO Energy Characteristics*, Plenum Press, New York, 1970
28. I. Gutman, N. Cmiljanović, S. Milosavljević, S. Radenković, *Chem. Phys. Lett.* **383** (2004) 171
29. I. Gutman, N. Cmiljanović, S. Milosavljević, S. Radenković, *Monatsh. Chem.* **135** (2004) 765
30. I. Gutman, D. Stevanović, S. Radenković, S. Milosavljević, N. Cmiljanović, *J. Serb. Chem. Soc.* **69** (2004) 777
31. I. Gutman, T. Soldatović, *MATCH Commun. Math. Comput. Chem*. **44** (2001) 169
32. I. Gutman, B. Ruščić, N. Trinajstić, C. F. Wilcox, *J. Chem. Phys*. **62** (1975) 3399
33. I. Gutman, *J. Math. Chem*. **1** (1987) 123
34. I. Gutman, *Theor. Chim. Acta* **45** (1977) 79
35. M. Fischermann, I. Gutman, A. Hoffmann, D. Rautenbach, D. Vidović, L. Volkmann, *Z. Naturforsch*. **57a** (2002) 49.

Journal of the Serbian Chemical Society
JSCS@tmf.bg.ac.yu • www.shd.org.yu/JSCS

J. Serb. Chem. Soc. 72 (12) 1351–1362 (2007) UDC 661.183.6:544.354–128.4:549.632:544.344
JSCS–3667 *Original scientific paper*

Thermally induced conversion of Mg^{2+} cation exchanged LTA, FAU, GIS and SOD zeolites: syntheses and characterization of γ-cordierite, a new $Mg_2Al_4Si_5O_{18}$ polymorph

RADOVAN DIMITRIJEVIĆ[1] and VERA DONDUR[2*#]

[1]*Faculty of Mining and Geology, Department of Crystallography, University of Belgrade, Djušina 7, 11000 Belgrade and* [2]*Faculty of Physical Chemistry, Akademski trg 16, University of Belgrade, Serbia*

(Received 26 September 2007)

Abstract: The thermal behaviours of fully Mg^{2+} cation exchanged LTA, FAU (X and Y species), GIS and SOD zeolites were investigated in the temperature range from ambient to 1400 °C. The initial zeolite frameworks collapsed into amorphous intermediate substances after air heating between 800–850 °C. Prolonged annealing of these products above 850 °C induced recrystallization into sapphirine-like phases (Mg–LTA and Mg–FAU_x zeolites) and μ-cordierite (Mg–FAU_y and Mg–GIS zeolites) phases. These phases were unstable during further temperature/time treatment and between 1000–1100 °C they polymorphously transformed into γ-cordierite, a new $Mg_2Al_4Si_5O_{18}$ polymorph. γ-Cordierite was formed as a transformation product from the investigated zeolite precursors, except for the Mg–SOD zeolite. Structurally the γ-cordierite phase is a modulated, Mg-stuffed derivative of cristobalite with the approximate composition $Mg_2Al_4Si_5O_{18}$, which precedes the appearance of α-cordierite. The orthorhombic unit cell dimensions calculated from X-ray powder diffraction pattern are: a = 16.387(7) Å, b = 8.835(4) Å, c = 7.853(3) Å. γ-Cordierite has a narrow range of temperature stability (1100–1200 °C) and during prolonged temperature/time treatment, it is polymorphously transformed to the α-cordierite phase.

Keywords: Mg^{2+} cation exchanged zeolites, thermal conversion, γ-cordierite new polymorph, phase stability.

INTRODUCTION

Due to a wide range of suitable dielectric and thermomechanical properties, earth-alkaline aluminosilicate-based ceramics have attracted a great deal of attention in recent years as alternative substrate materials to the conventionally used corundum (α-alumina). Of ceramic compounds such as: celsian and hexacelsian ($BaAl_2Si_2O_8$), anorthite ($CaAl_2Si_2O_8$), Sr–feldspar ($SrAl_2Si_2O_8$) and α-cordierite ($Mg_2Al_4Si_5O_{18}$), the last offers the best combination of all these properties.[1,2]

* Corresponding author. E-mail: edondur@ffh.bg.ac.yu
# Serbian Chemical Society member.
doi: 10.2298/JSC0712351D

The crystal structure[3] of high-temperature α-cordierite form is characterized by hexagonal symmetry and a disordered distribution of Al and Si cations in a tetrahedral framework.[4] This form is metastable and under prolonged temperature/time annealing treatment,[5] it is polymorphously transformed into the ordered orthorhombic β-cordierite form.[6–8] The α-cordierite phase is conventionally prepared by melting the appropriate oxides and quenching to form a glass of the desired composition. The glass is subsequently crystallized in α-cordierite by controlled heat treatment. However, this process is usually preceded by primary crystallization of the μ-cordierite phase, which is the third $Mg_2Al_4Si_5O_{18}$ polymorph in the three-component phase $MgO–Al_2O_3–SiO_2$ (MAS) system.[9] The μ-cordierite phase is a metastable Mg-stuffed derivative[10] of the β-quartz structure,[11,12] which would be topotactically transformed into the α-cordierite phase by prolonged heating, Fig. 1.

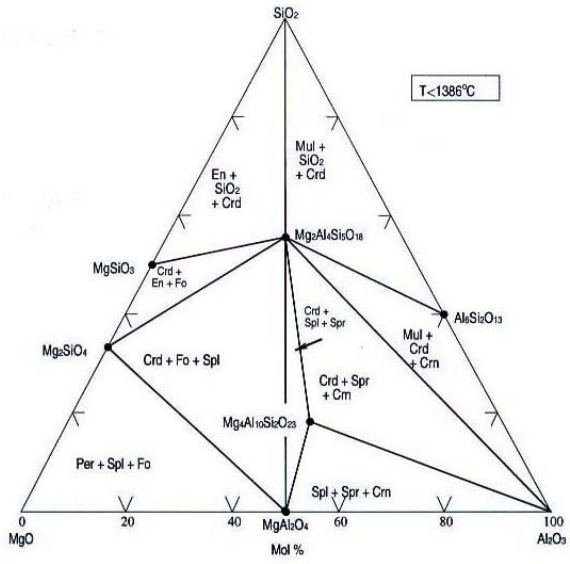

Fig. 1. Constitutional data for $MgO–Al_2O_3–SiO_2$ (MAS) ternary phase system.[9] Abbreviations: Crd – cordierite; Spl – spinel, Spr – sapphirine; Mul – mulite; En – enstatite; Fo – forsterite.

Due to the growing interest for the syntheses of α-cordierite, several publiccations[13–16] and patents,[17,18] dealing with the zeolite conversion route firstly proposed by Breck,[19] appeared recently. By this method of synthesis, which include the thermal conversion of cation exchanged zeolites, all the above-mentioned compounds were also prepared.[20–23] Moreover, several new aluminosilicate phases, such as: Ag-carnegieite,[24] γ-eucryptite,[25–27] δ-eucryptite,[28] $CsAlSiO_4$–ANA[29] and $KAlSiO_4$–ANA[30] were synthesized. Therefore, the discussed zeolite conversion route could be considered as a powerful method for the investigation of aluminosilicate phase systems.

The work presented here is a continuation of previous[21,22] studies on thermally induced phase conversions of sodium LTA, FAU, GIS, SOD[31] and other syn-

thetic zeolites, exchanged with alkaline earth elements. In this study, interest was focused on the titled zeolites, synthesis conditions and preliminary characterization of a new $Mg_2Al_4Si_5O_{18}$ phase, hitherto unrecognised in the other experiments.

EXPERIMENTAL

The initial sodium zeolites LTA (Si/Al = 1.00) and FAU (13X specie; Si/Al = 1.34 and SK-40 specie; Si/Al = 2.40; X and Y species, respectively) were manufactured by Union Carbide Co., whereas GIS (P specie; Si/Al = 1.38) and SOD (Si/Al = 1.00) zeolites were self-prepared. Near fully cation exchanged Mg^{2+} forms of these zeolites were obtained after several successive exchanges from aqueous 0.5 M solutions of $MgSO_4 \cdot H_2O$.

The chemical composition of the samples was analysed by atomic absorption spectrophotometry, using a Perkin Elmer 380 instrument.

The prepared Mg^{2+} cation exchanged forms of LTA, FAU, GIS and SOD zeolites were air-heated in a Carbolite CTF 15/75 electric furnace using a programmed temperature/time regime in the range from 700–1400 °C for 1–6 hours. Thermally induced structural conversions of the Mg^{2+} cation exchanged zeolites were followed on the calcined samples by the X-ray powder diffraction (XRPD) technique, after cooling to room temperature.

The XRPD patterns were obtained on a Phillips, PW-1710 automated diffractometer, using a Cu tube operated at 40 kV and 35 mA. The instrument was equipped with a diffracted beam curved graphite monochromator and a Xe-filled proportional counter. Diffraction data were collected in the 2θ angle range 4–70°, counting for 0.25 and 2.50 seconds at 0.02 steps. A fixed 1° divergence and 0.1 mm receiving slits were used. The trial and error indexing program Dicvol[32] and a program for the refinement of the cell dimensions Lsucrip[33] were used.

Investigations of the crystal morphology of the synthesized phases were performed by scanning electron microscopy (SEM), using a Jeol 840A instrument. The investigated samples were gold sputtered in a JFC 1100 ion sputter.

RESULTS

The results of the chemical analyses of the Mg^{2+} cation exchanged zeolites are presented in Table I. It is evident from the results that near complete $Mg^{2+} \rightarrow 2Na^+$ exchange was achieved for LTA, GIS and SOD zeolites, whereas for the species of FAU zeolite, the cation exchange was incomplete.

TABLE I. Chemical analyses of the initial Mg^{2+} cation exchanged zeolites: LTA, FAU, GIS and SOD, used as precursors for thermal conversion

Initial zeolite	Si/Al Ratios	Chemical analyses
Mg–LTA	1.00	$(0.988MgO \cdot 0.012Na_2O) \cdot Al_2O_3 \cdot 2.00SiO_2$
$Mg–FAU_{(X)}$	1.34	$(0.976MgO \cdot 0.024Na_2O) \cdot Al_2O_3 \cdot 2.48SiO_2$
$Mg–FAU_{(Y)}$	2.40	$(0.970MgO \cdot 0.030Na_2O) \cdot Al_2O_3 \cdot 4.80SiO_2$
$Mg–GIS_{(P)}$	1.38	$(0.991MgO \cdot 0.009Na_2O) \cdot Al_2O_3 \cdot 2.76SiO_2$
Mg–SOD	1.00	$(0.994MgO \cdot 0.006Na_2O) \cdot Al_2O_3 \cdot 2.00SiO_2$

The phase transformations of so-prepared zeolite precursors as a function of temperature are presented in Figs. 2–6. The thermally induced conversion processes could be summarized as follows: The aluminosilicate frameworks of the initial Mg^{2+} cation exchanged zeolites (Figs. 2–6, curves a), became unstable with increasing temperature and commenced to collapse between 700–850 °C,

when intermediate amorphous products were formed, (Figs. 2–6, curves b). Further annealing at about 900 °C led to the recrystallization of the amorphous products into Mg-aluminosilicates: sapphirine-like compounds (Figs. 2 and 3, curves c) and μ-cordierite (Figs. 4 and 5, curves c). These Mg-aluminosilicate phases were unstable during the prolonged temperature/time heat treatment and at about 1100 °C they recrystallized by complex polymorphic transformation processes to the same new phase, named γ-cordierite (Figs. 2–5, curves d). The behaviour of the Mg–SOD zeolite precursor (Fig. 6, curve a–e) was an exception, with the final conversion leading to a spinel phase and amorphous silica (Fig. 6, curve e).

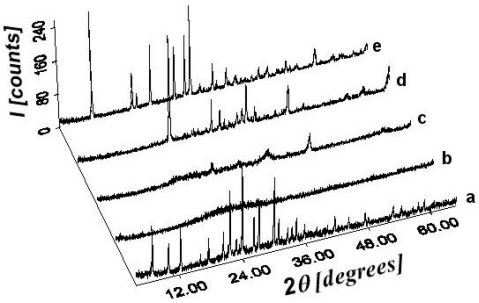

Fig. 2. XRPD Patterns of the phases synthesized in the process of thermally induced conversion of Mg^{2+} cation exchanged LTA zeolite: a) initial Mg–LTA zeolite (specie A, Si/Al = 1.00), 25 °C; b) amorphous intermediate substance, 800 °C, 1 h; c) sapphirine-like phase, 1030 °C, 2 h; d) γ-cordierite$_{LTA}$ phase, 1100 °C, 4 h; e) α-cordierite$_{LTA}$ phase, 1350 °C, 2 h.

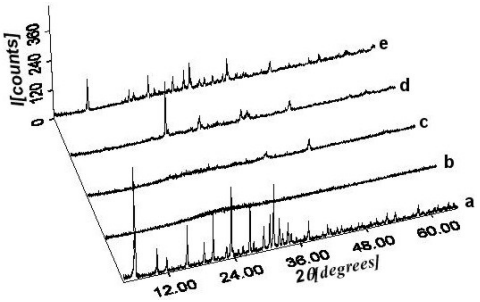

Fig. 3. XRPD Patterns of the phases synthesized in the process of thermally induced conversion of Mg^{2+} cation exchanged FAU (specie X) zeolite: a) initial Mg–FAU$_{(X)}$ zeolite (Si/Al = = 1.24), 25 °C; b) amorphous intermediate substance, 820 °C, 1 h; c) sapphirine-like phase, 1030 °C, 3 h; d) γ-cordierite$_{FAU(X)}$ phase, 1100 °C, 1 h; e) α-cordierite$_{FAU(X)}$ phase, 1350 °C, 2 h.

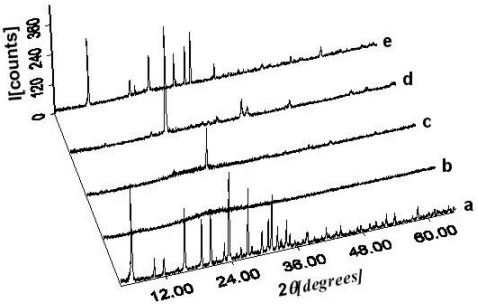

Fig. 4. XRPD Patterns of the phases synthesized in the process of thermally induced conversion of Mg^{2+} cation exchanged FAU (specie Y) zeolite: a) initial Mg–FAU$_{(Y)}$ zeolite (Si/Al = 2.40), 25 °C; b) amorphous intermediate substance, 850 °C, 1 h; c) μ-cordierite$_{FAU(Y)}$ phase, 1000 °C, 1 h; d) γ-cordierite$_{FAU(Y)}$ phase, 1150 °C, 3 h; e) α-cordierite$_{FAU(Y)}$ phase, 1350 °C, 2 h.

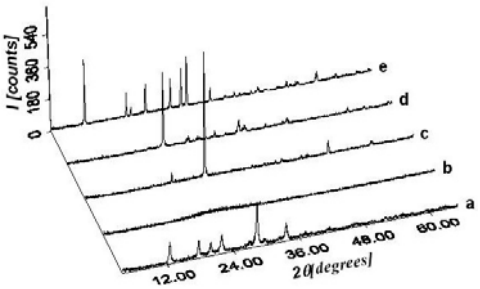

Fig. 5. XRPD Patterns of the phases synthesized in the process of thermally induced conversion of Mg^{2+} cation exchanged GIS (specie P) zeolite: a) initial Mg–GIS$_{(P)}$ zeolite (Si/Al = 1.38), 25 °C; b) amorphous intermediate substance, 820 °C, 1 h; c) μ-cordierite$_{GIS}$ phase, 900 °C, 1 h; d) γ-cordierite$_{GIS}$ phase, 1100 °C, 3 h; e) α-cordierite$_{GIS}$ phase, 1350 °C, 2 h.

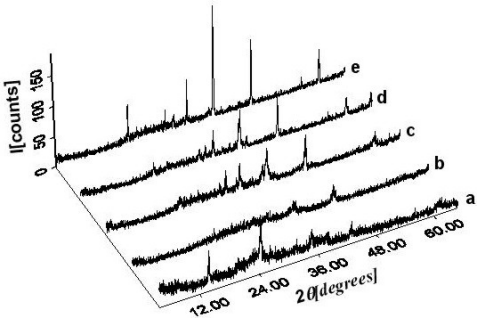

Fig. 6. XRPD Patterns of phases synthesized in the process of thermally induced conversion of Mg^{2+} cation exchanged SOD zeolite: a) initial Mg–SOD zeolite (Si/Al = 1.00), 25 °C; b) amorphous intermediate substance and low crystallized spinel, 850 °C, 1 h; c) amorphous intermediate substance and low crystallized spinel, 1000 °C, 1 h; d) well crystallized spinel and amorphous substance, 1200 °C, 2 h; e) excellently crystallized spinel and amorphous substance, 1350 °C, 2 h.

An example of the XRPD patterns for the novel γ-cordierite phase synthesized from Mg–GIS zeolite precursor is presented in Table II, whereas the unit cell dimensions are given in Table III. This newly synthesized Mg–aluminosilicate phase has a narrow interval of temperature stability (around 100–150 °C, Fig.7a and 7b), after which prolonged heating induced its conversion to α-cordierite (Figs. 2–5, curves e, and Fig. 8b) in all cases investigated. The final products synthesized at around 1350 °C, except for the quantitatively dominant α-cordierite phase, contained some traces of spinel, mullite and quartz phases.

TABLE II. XRPD Data for γ-cordierite$_{GIS(P)}$ polymorph synthesized by thermal decomposition of Mg–GIS$_{(P)}$ zeolite at 1100 °C for 4 hours

I/I_0, %	h	k	l	d_{obs} / Å	d_{calc} / Å
100	4	0	0	4.1013	4.0968
1	2	1	2	3.2846	3.2866
3	3	0	2	3.1928	3.1882
3	3	1	2	3.0020	2.9989
	4	2	0	–	3.0039
1	2	3	0	2.7742	2.7714
1	4	1	2	2.6969	2.6992
2	6	0	1	2.5808	2.5796
13	0	1	3	2.5122	2.5097
5	3	3	1	2.4606	2.4616
2	0	3	2	2.3560	2.3559
3	3	4	0	2.0484	2.0477
	8	0	0	–	2.0484
1	1	1	4	1.9029	1.9034
	2	3	3	–	1.9029
1	3	3	3	1.8417	1.8419
1	4	0	4	1.7704	1.7704
3	1	3	4	1.6258	1.6254
2	9	3	0	1.5491	1.5487
1	7	4	2	1.4864	1.4869
3	0	6	1	1.4471	1.4473
	4	1	5	–	1.4467
5	7	2	4	1.4232	1.4239

TABLE III. Unit cell dimensions of γ-cordierite$_{GIS(P)}$ phase and some cristobalite stuffed derivatives

Compound	a / Å	b / Å	c / Å	α / °	β / °	γ / °
γ-Cordierite$_{GIS(P)}$	16.387(7)	8.835(4)	7.853(3)	90.00	90.00	90.00
Ag–Carnegieite[24]	5.023(3)	5.074(3)	16.982(9)	98.30	81.62	119.20
Carnegieite[47]	10.261(1)	14.030(2)	5.1566(6)	90.00	90.00	90.00
γ-Eucryptite[26]	8.299(1)	5.0365(8)	8.263(1)	90.00	107.42	90.00

Due to the complexity of the system and the overlapping of the synthesized phases, the results of temperature/time transformation (TTT) processes are presented schematically in Figs. 7a and 7b. An analysis of the XRPD, SEM and TTT results, lead to the conclusion that the α-cordierite phase was obtained by different and complex transformation routes, whereas the γ-cordierite phase always proceeded to α-cordierite.

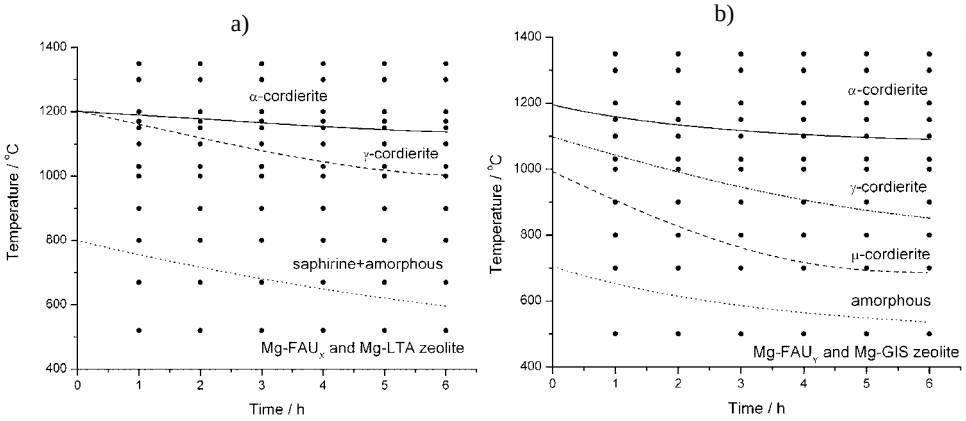

Fig. 7. A time-temperature-transformation (TTT) diagram for the cordierite polymorphs synthesized in the process of the thermally induced conversion of synthetic: a) Mg–LTA (Si/Al = 1.00) and Mg–FAU$_{(X)}$ (Si/Al = 1.24) zeolites; b) Mg-FAU$_{(Y)}$ (Si/Al = 2.40) and Mg–GIS$_{(P)}$ (Si/Al = 1.38) zeolites.

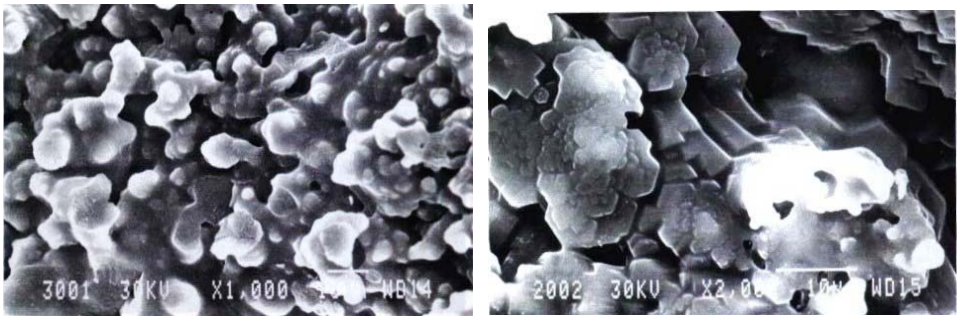

a) b)

Fig. 8. Selected characteristic SEM morphologies of cordierite polymorphs synthesized in the process of thermally induced conversion of Mg–GIS$_{(P)}$ zeolite: a) γ-cordierite$_{GIS(P)}$ phase morphology (rounded grains), 1100 °C, 3 h; b) α-cordierite$_{GIS(P)}$ phase morphology (hexagonal crystals), 1350 °C, 2 h.

DISCUSSION

The results obtained from the thermal investigation of Mg^{2+} cation exchanged zeolites confirmed the known transformation route to more densely packed structures *via* an amorphous[22] intermediary substance. Unlike the direct conversion of zeolite,[34,35] the amorphous synthesis route could be roughly divided into three different stages.

The initial step of the transformation correspond to changes in the frameworks of the Mg^{2+} cation exchanged zeolites, which occurs in the temperature range between ambient and temperatures where their collapse commences. These changes are generally connected with dehydration processes on the zeolite frameworks. All the investigated initial Mg^{2+} cation exchanged zeolites (Figs. 2–6, curves a) passed through this stage before the collapse of their frameworks.

Immediately after the collapse of their frameworks, the second step of the transformations commences. This is characterized by the formation of amorphous substances which retain such properties during the following 100–150 °C temperature rise (Figs. 2–5, curves b). The amorphous matter obtained after the collapse of the Mg–GIS zeolite is an exception, having amorphous characteristics in the range between 450–850 °C. Here it is important to emphasize that the so-prepared intermediate substances are dimensionally probably nanostructured,[22] *i.e.*, they consist of the relicts of different tetrahedral secondary building units,[31] which were the elements of the preceding zeolite frameworks. Although we do not have direct experimental evidence for the structural evolution of these amorphous matters in the above-mentioned temperature ranges, this could be deduced by comparing the initial zeolite structures with framework topologies with phases which recrystallized from the amorphous substances during prolonged heating. Moreover, it seems that the amorphous substances formed from the investigated Mg-zeolites as precursors possess some preferred characteristics not observed in the corresponding glasses obtained by classical melting/devitrification routes. As a proof for the validity of this assumption, the syntheses of Ag–carnegieite,[24] γ-eucryptite[25,26] and kaliophilite,[30] a new aluminosilicates prepared only by discussed method, can be cited. Another argument for the structural evolution of the amorphous intermediate substances lies in the particular segregation at the end of second stage, resulting in the recrystallization of the two-phase mixture. Such examples were observed earlier for Li–LTA,[25] Cs–LTA[29] and Ca–LTA[22] zeolite precursors, *i.e.*, their thermal conversions. Recently published results on $BaAl_2Si_2O_8$[36] and $NaAlSiO_4$[37] amorphous precursors prepared from LTA zeolites by the discussed route, confirmed the pest assumptions concerning its special characteristics.

The recrystallization of the intermediate amorphous substance simultaneously indicates the processes connected to the final step of the thermally induced conversion of the zeolites. This stage is mostly characterized by the crystalli-

zation of newly formed phase(s) and its polymorphous transformation to a more stable phase, because of prolonged heating. However, during this step of the transformations, characterized by high temperature/time conditions, solid state reactions are probable and phase formation processes could not be excluded.

In the case of Mg^{2+} cation exchanged zeolite precursors, the final step commences with the recrystallization of the intermediate amorphous substances into sapphirine-like (Figs. 2 and 3, curves c) and μ-cordierite phases (Figs.4 and 5, curves c), respectively. It is easily to conclude from Table I and Figs.7a and 7b, that the recrystallization of the intermediate amorphous substance is dependent on the Si/Al ratio. When this ratios is closer to unity (Mg–LTA; zeolite A and Mg–FAU; zeolite X) the TTT processes proceeded in the formation of a sapphirine-like (Fig. 7a) phase whereas the siliceous samples (Mg–FAU; zeolite Y and Mg–GIS; zeolite P) gave the μ-cordierite phase (Fig. 7b). The extension "like" is used due to the confusion concerning the sapphirine composition and its structural relation[38] to spinel, clinopyroxene and α-cordierite phases. Sapphirine is ideally $Mg_4Al_8Si_2O_{20}$, *i.e.*, clearly different from the stoichiometry of α-cordierite, but these phases are neighbours in the MAS phase system, separated by a common border (Fig. 1). Therefore, it seems probably that the sapphirine-like phases obtained in the present experiments have compositions closer to α-cordierite than to sapphirine. The polymorphous inversion between sapphirine-like and α-cordierite phases over an intermediate γ-cordierite phase was observed for the first time, confirming also their compositional similarities.

The initial crystallization of μ-cordierite from siliceous amorphous substances originating from $Mg–FAU_{(Y)}$ and $Mg–GIS_{(P)}$ zeolites is not surprising. It has been known for a long time that μ-cordierite precedes the crystallization of the α-cordierite phase in the MAS system, especially in the case of preheated glasses[11,12]. The fact that metastable μ-cordierite is the first crystallization product is in keeping with many such transformations. Metastable phases generally nucleate more readily than the equilibrium product, a fact that has been confirmed in many investigations of the MAS system.[39–43] However, the present results obtained for $Mg–FAU_{(Y)}$ and $Mg–GIS_{(P)}$ zeolite shows that the polymorphous transformation μ-cordierite $\rightarrow$ α-cordierite has an alternative route *via* the intermediate γ-cordierite phase according to scheme (1):

$$\mu\text{-cordierite} \rightarrow \gamma\text{-cordierite} \rightarrow \alpha\text{-cordierite} \qquad (1)$$

which was recognized for the first time in this study.

The synthesized sapphirine-like and μ-cordierite phase are unstable during prolonged heating. Therefore, at appropriate temperatures, these phases will polymorphously transform into the same phase, namely γ-cordierite, as discussed previously (Figs. 2–5, curves d and Figs. 7a and 7b). The XRPD pattern for γ-cordierite, Table II, could not be identified within the Mg-aluminosilicate phases deposited in the JCPDS file. However, the observed γ-cordierite patterns are si-

milar to low-cristobalite (file card No. 39-1425). The powder patterns of the synthesized γ-cordierites (Fig. 9, curves a–d) are also very similar to carnegieite,[44,45] γ-eucryptite[26] and Ag–carnegieite[24] (Fig. 9, curves e–g) patterns. Structurally these phases belong to the stuffed[10,46] derivatives of cristobalite. These were obtained by the same zeolite preparation route, as was the γ-cordierite phase. Moreover, the temperature induced structural inversions known for silica polymorphs[10,46] have counterpart behaviours in the case of silica stuffed derivative pairs such as: γ-eucryptite → β-eucryptite,[25,26] α-eucryptite → β-eucryptite[27] and low--carnegieite → nepheline → high-carnegieite.[44–48] According to this discussion and the reconstructive polymorphous inversion observed in μ-cordierite → γ-cordierite in the cases of Mg–$FAU_{(Y)}$ and Mg–$GIS_{(P)}$ zeolite, it is believed that the synthesized γ-cordierite is structurally a Mg-stuffed derivative of cristobalite. The minor differences in the calculated unit cell dimensions of the synthesized γ-cordierites suggest their probable non-stoichiometric composition inherited from parent zeolite, *i.e.*, sapphirine or μ-cordierite phases. From the crystallochemical aspect, the γ-cordierite phase is in terms of stoichiometry very similar to $Mg_2Al_4Si_5O_{18}$, *i.e.*, α-cordierite. According to preceding discussion, it is obvious that the γ-cordierite phase is situated in the MAS phase diagram, Fig. 1, in the field of α-cordierite in the border regions towards the sapphirine and tridymite/cristobalite (Mg-stuffed aluminosilicate derivatives) regions, due to their complex conversion relationships. Thus, the composition of γ-cordierite corresponds closely to those known for μ-cordierite[12,13] and α-cordierite phases. Finally, it should be emphasized that the results presented for the γ-cordierite phase are rather preliminary. Due to the strong susceptibility to modulation of its crystal lattice, the XRPD structure determinations as well as other investigations on pure γ-cordierite are in progress and will be published separately.

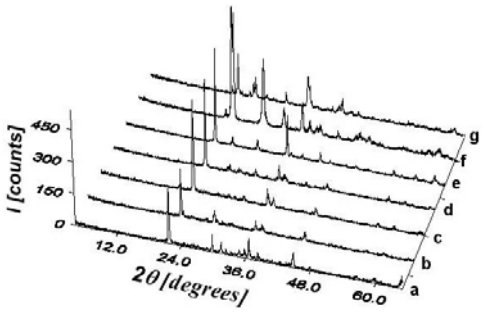

Fig. 9. XRPD Patterns of various cristobalite stuffed derivative phases synthesized by the thermally induced conversion route: a) γ-cordierite$_{LTA}$ phase, 1100 °C, 4 h; b) γ-cordierite$_{FAU(X)}$ phase, 1100 °C, 1 h; c) γ-cordierite$_{FAU(Y)}$ phase, 1150 °C, 3 h; d) γ-cordierite$_{GIS}$ phase, 1100 °C, 3 h; e) low-carnegieite phase;[45] f) γ-eucryptite phase;[26] g) Ag–carnegieite phase.[24]

The synthesized γ-cordierite phases are characterized by a narrow temperature/time stability range (Figs. 7a and 7b). With further annealing, the metastable γ-cordierite phases polymorphously convert, by reconstructive transformation, to more stable α-cordierite phases (Figs. 2–5, curves e and Fig. 8). Their frameworks are characterized by Si/Al disorder, which was tested by measuring the

$\Delta 2\theta$ distortion indices[49] and ^{27}Si-MAS–NMR spectroscopy[8], the results of which will also be published separately.

CONCLUSIONS

The employment of the XRPD and SEM techniques, enabled the time/temperature induced structural changes and complex solid state conversion of different Mg^{2+} cation exchanged zeolites, *i.e.*, LTA, FAU, GIS and SOD structural types, to be followed. Detailed phase analysis revealed very complex conversion processes (polymorphous transformations and reactions in the solid state), which finally led to the formation of α-cordierite phases. All the investigated Mg–zeolite transformation processes were characterized by the formation of the same, structurally metastable Mg-stuffed derivative of cristobalite, with the approximate composition $Mg_2Al_4Si_5O_{18}$. Due to its close polymorphous relationships with the known cristobalite structure and the μ- and α-cordierite phases, the recognized Mg-stuffed derivative phase is named γ-cordierite.

Acknowledgements. The authors are grateful to the Serbian Republic Research Fund for support (project No.142055). We are grateful to Professor I. Krstanovic for his constructive discussion. We are indebted to Professor M. Mitrovic for the SEM images and Mrs. I. Soten for technical assistance.

И З В О Д

ТЕРМАЛНО ИНДУКОВАНА КОНВЕРЗИЈА Mg^{2+} КАТЈОНСКИ ИЗМЕЊЕНИХ ЗЕОЛИТА ТИПА LTA, FAU, GIS И SOD; СИНТЕЗА И КАРАКТЕРИЗАЦИЈА γ-КОРДИЈЕРИТА НОВОГ $Mg_2Al_4Si_5O_{18}$ ПОЛИМОРФА

РАДОВАН ДИМИТРИЈЕВИЋ[1] и ВЕРА ДОНДУР[2]

[1]Рударско–геолошки факултет, Катедра за кристалографију, Универзитет у Београду, Ђушина 7, 11000 Београд и [2]Факултет за физичку хемију, Универзитет у Београду, Академски Трг 16, 11000 Београд

Термално индукована фазна конверзија Mg^{2+} катјонски измењених форми синтетичких зеолита типа: LTA, FAU (X и Y форма), GIS и SOD, испитивана је у температурном интервалу од 25–1400 °C. Полазне зеолитске алумосиликатне мреже стабилне су до око 700 °C, када започиње њихово рушење у аморфну супстанцу. Овај процес завршен је између 800 и 850 °C. Продужено загревање ових продуката изнад 850 °C, индукује рекристализацију аморфних продуката у фазу сличну сафирину (Mg–LTA и MG–$FAU_{(X)}$ зеолити) и μ-кордијерит (Mg–$FAU_{(Y)}$ и Mg–GIS зеолити). Рекристалисане фазе су нестабилне у току продуженог третмана температура/време, и између 1000 и 1100 °C, долази до њихове структурне трансформације у γ-кордијерит, нови кордијеритски полиморф. Са структурног аспекта γ-кордијерит представља попуњени дериватив кристобалита приближног састава $Mg_2Al_4Si_5O_{18}$ за који је из Ro-дифракционих мерења одређена ромбична јединична ћелија: a = 16.387(7) Å, b = 8.835(4) Å, c = 7.853(3) Å. γ-Кордијерит има узан опсег температурне стабилности (1100––1200 °C) и у продуженом третману температура/време структурно се трансформише у α-кордијерит, у свим испитиваним случајевима осим Mg–SOD зеолита, када се као крајњи продукт трансформације добија оксид спинел.

(Примљено 26. септембра 2007)

REFERENCES

1. R. Tummala, *Adv. Ceram*. **26** (1989) 3
2. R. Tummala, *J. Amer. Ceram. Soc*. **74** (1991) 895
3. G. Gibbs, *Amer. Mineral*. **51** (1966) 1068
4. A. Putnis, E. Salje, S. Redfern, C. Fyfe, H. Strobl, *Phys. Chem. Minerals* **14** (1987) 446
5. A. Putnis, D. Bish, *Amer. Mineral*. **68** (1983) 60
6. E. Meagher, G. Gibbs, *Canad. Mineral*. **15** (1977) 43
7. A. Putnis, C. Fyfe, G. Gobbi, *Phys. Chem. Minerals* **12** (1985) 211
8. C. Fyfe, G. Gobbi, A. Putnis, *J. Am. Chem. Soc*. **108** (1986) 3218
9. R. Smart, F. Glasser, *J. Mater. Sci*. **11** (1976) 1459
10. M. Buerger, *Amer. Mineral*. **89** (1954) 600
11. W. Schreyer, J. Schairer, *Z. Kristallogr*. **116** (1961) 60
12. H. Schulz, W. Hoffmann, G. Muchow, *Z. Kristallogr*. **134** (1971) 1
13. M. Subramanian, D. Corbin, U. Chowdry, *Bull. Mater. Sci*. **16** (1993) 665
14. M. Subramanian, D. Corbin, U. Chowdry, *Adv. Ceram.* **26** (1989) 239
15. G. Sankar, P. Wright, S. Natarajan, J. Thomas, G. Neville-Greaves, A. Dent, B. Dobson, C. Ramsdale, R. Jones, *J. Phys. Chem*. **97** (1993) 9550
16. B. Rudinger, R. Fischer, *Eur. J. Mineral*. **9** (1997) 1257
17. U. Chowdry, D. Corbin, M. Subramanian, *US Patent* 4,814,303 (1989)
18. R. Bedard, E. Flanigen, *US Patent* 4,980,323 (1990)
19. D. Breck, *Zeolite Molecular Sieves: Structure, Chemistry and Use*, Wiley, New York, 1974, p. 494
20. B. Hoghooghi, J. McKittrick, C. Butler, E. Helsel, O. Lopez, *Mat. Res. Soc. Symp. Proc*. **346** (1994) 493
21. V. Dondur, R. Dimitrijević, A. Kremenović, U. Mioč, R. Srejić, M. Tomasević–Čanović, in: *Adv. Sci. Technol. 3, Part B*., P. Vincenzini, Ed., Techna, Faenza, Italy, 1995, p. 687
22. R. Dimitrijević, V. Dondur, A. Kremenović, *Zeolites* **16** (1996) 294
23. J. Parise, D. Corbin, M. Subramanian, *Mat. Res. Bull*. **24** (1989) 303
24. N. Petranović, R. Dimitrijević, *Thermochim. Acta*, **84** (1985) 227
25. V. Dondur, R. Dimitrijević, *J. Solid State Chem*. **63** (1986) 46
26. R. Dimitrijević, V. Dondur, N. Petranović, *J. Serb. Chem. Soc*. **60** (1995) 1057
27. P. Norby, *Zeolites* **10** (1990) 193
28. J. Newsam, *J. Phys. Chem*. **92** (1988) 445
29. R. Dimitrijević, V. Dondur, N. Petranović, *J. Solid State Chem*. **95** (1991) 335
30. R. Dimitrijević, V. Dondur, *J. Solid State Chem*. **115** (1995) 214
31. W. Meier, D. Olson, in: *Atlas of Zeolite Structure Types*, Structure Commission of the IZA, Juris, Zurich, 1978, p. 56
32. A. Boutlif, D. Louer, *J. Appl. Cryst*. **24** (1991) 987
33. R. Garwey, *Powder Diffrac*. **1** (1986) 114
34. J. Richardson, J. Smith, J. Pluth, *J. Phys. Chem*. **94** (1990) 3365
35. S. Cartlidge, W. Meier, *Zeolites* **4** (1984) 218
36. J. Djordjević, V. Dondur, R. Dimitrijević, A. Kremenović, *Phys. Chem. Chem. Phys.* **3** (2001) 1560
37. G. Greaves, F. Meneau, G. Sankar, *Nucl. Instr. Met. Phys. Res. B* **199** (2003) 98
38. J. Barbier, B. Hyde, *Acta Cryst. B*. **44** (1988) 373
39. M. Tosić, R. Dimitrijević, M. Tomasević-Čanović, G. Djurković, *Sci. Sintering* **27** (1995) 199
40. I. Janković–Častvan, S. Lazarević, D. Tanasković, A. Orlović, R. Petrović, Dj. Janaćković, *Ceram. Internat*. **33** (2007) 1263
41. M. Karkhanavala, F. Hummel, *J. Am. Ceram. Soc*. **36** (1953) 389
42. D. Bridge, D. Holland, P. McMillan, *Glass Technol*. **26** (1985) 286

43. H. Wand, G. Fischman, H. Herman, *J. Mater. Sci*. **24** (1989) 811
44. R. Dimitrijević, V. Dondur, P. Vulić, S. Marković, S. Macura, *J. Phys. Chem. Solids* **65** (2004) 1623
45. S. Marković, V. Dondur, R. Dimitrijević, *J. Mol. Struct.* **654** (2003) 223
46. D. Palmer, *Rev. Mineral.* **29** (1994) 83
47. J. Thompson, R. Withers, A. Whittaker, R. Traill, J. Fitzgerald, *J. Solid State Chem*. **104** (1993) 59
48. A. Berger, T. Samsonova, L. Yakovlev, *Izv. Akad. Nauk. SSSR, ser. Himiceskaya* **10** (1971) 2129
49. A. Miyashiro, T. Iiyama, M. Yamasaki, T. Miyashiro, *Amer. J. Sci*. **253** (1955) 185.

Journal of the Serbian Chemical Society
JSCS@tmf.bg.ac.yu • www.shd.org.yu/JSCS

J. Serb. Chem. Soc. 72 (12) 1363–1367 (2007)
JSCS–3668

UDC 536.7+519.6+519.233:541.183
Short communication

SHORT COMMUNICATION

A consideration of the correct calculation of thermodynamic parameters of adsorption

SLOBODAN K. MILONJIĆ*#

The Vinča Institute of Nuclear Sciences, P.O. Box 522, 11001 Belgrade, Serbia

(Received 9 October 2007)

Abstract: The Langmuir and Freundlich isotherm equations have been widely used for interpreting various adsorption processes. There are, however, many serious mistakes in the literature in determination or calculation of thermodynamic parameters, especially in the determination of the change in the free energy of adsorption using Langmuir, Freundlich and Henry constants. Many authors used these constants for the determination of ΔG expressed instead of dimensionless in some concentration units (for example: l mol^{-1}, l g^{-1}, ml mg^{-1}, *etc.*).

Keywords: adsorption, thermodynamic parameters, correct calculation.

INTRODUCTION

Sorption occurring at a liquid or gaseous phase/solid surface interface plays an important role in many processes.[1,2] The sorption is a general term that comprises adsorption processes which occur at a solid/solution interface, as well as those in which a solute (molecule or ion) penetrates the bulk of a sorbent phase. The sorption of solutes by a solid phase is based on forces acting between the sorbent and the sorbate. These forces can be classified as van der Waals, Coulomb and Lewis acid–base interactions and range over many orders of magnitude.

The sorption of various ions or molecules plays a significant role in a wide variety of natural, synthetic, inorganic, biological, and technological processes, and is also of major theoretical interest. There are many studies of adsorption from solution by various solid adsorbents.

Different adsorption mechanisms may be found by studying the dependence of adsorption on various variables (pH, concentration of solutes, ionic strengths, and the type and topology of surfaces), and by interpreting the parameters of the determined adsorption isotherms. Also, thermodynamic parameters of adsorption from solutions provide a great deal of information concerning the type and mechanism of the adsorption process.

* E-mail: smiloni@vin.bg.ac.yu
# Serbian Chemical Society member.
doi: 10.2298/JSC0712363M

The correct calculation of thermodynamic parameters, especially the change of the free energy of adsorption at a solid/liquid interface is the subject of this paper.

ADSORPTION ISOTHERM EQUATIONS AND THERMODYNAMIC PARAMETERS

There are several types of adsorption from solutions isotherms.[3] Langmuir and Freundlich isotherms are the most commonly used models, since they can be applied to a wide range of adsorbate concentrations. The general form of the Langmuir[4] equation for adsorption from solution is:

$$q_e = q_{max} \frac{K_L c_e}{1 + K_L c_e} \tag{1}$$

where q_e is the amount of adsorbate adsorbed on the adsorbent at equilibrium (mol g^{-1}), q_{max} is the maximum adsorption capacity corresponding to a complete monolayer coverage on the adsorbent surface (mol g^{-1}), K_L is the Langmuir constant (dm^3 mol^{-1}), and c_e is the concentration of adsorbate at equilibrium (mol dm^{-3}). The values of q_{max} and K_L can be evaluated from the slope and the intercept of the linear form of the Langmuir equation:

$$\frac{c_e}{q_e} = \frac{1}{q_{max} K_L} + \frac{c_e}{q_{max}} \tag{2}$$

The Freundlich[5] equation is a semi-empirical one employed to describe heterogeneous systems:

$$q_e = K_F c_e^{1/n} \tag{3}$$

where K_F is the Freundlich constant (dm^3 g^{-1}) and $1/n$ is the heterogeneity factor. The value of K_F and n can be evaluated from the intercept of the slope of the linear form of the Freundlich equation:

$$\ln q_e = \ln K_F + (1/n) \ln c_e \tag{4}$$

The free energy change, ΔG, of adsorption is given by:

$$\Delta G = -RT \ln K \tag{5}$$

where R is the universal gas constant (8.314 J mol^{-1} K^{-1}), T is the temperature (K), and K is the equilibrium constant.

It is well known that the unit for ΔG is J mol^{-1}. Since the unit for the term RT is also J mol^{-1}, the equilibrium constant K in Eq. (5) must be dimensionless.

Very often, the calculation of the free energy change of adsorption applying Eq. (5), as found in the literature, is erroneous. Namely, many authors when calculating ΔG use numerical values for K given in various units (l mol^{-1}, l g^{-1}, ml mg^{-1}, *etc.*). As a consequence, the calculated values for the free energy change and the entropy change, ΔS, of adsorption are incorrect. In order to obtain a correct value of ΔG, the K value in Eq. (5) must be dimensionless.

If adsorption was investigated from an aqueous solution and if K is given in dm^3 mol^{-1}, then K can be easily recalculated as dimensionless by multiplying it

by 55.5 (number of moles of water per liter of solution). Accordingly, the correct ΔG value can be obtained from:

$$\Delta G = -RT \ln (55.5K) \quad (6)$$

The term $55.5K$ ($dm^3\ mol^{-1}\ mol\ dm^{-3}$) is dimensionless. In the case when K is given in $dm^3\ g^{-1}$, similar to above, K can be easily recalculated to become dimensionless by multiplying it by 1000 (1 dm^3 = 1000 ml (or g, since the solution density is $\approx 1\ g\ ml^{-1}$)).

SOME RECENT LITERATURE DATA AND DISCUSSION

Some examples of erroneous calculations of ΔG and ΔS values of various adsorption processes found in the literature are given below.

Recently, Gardea–Torresdey and co-workers presented a detailed thermodynamic and isotherm study of the biosorption of Cd(II), Cr(III), and Cr(VI) by saltbush (*Atriplex conescens*) biomass.[6] In the Conclusions, the authors wrote, "The Gibbs free energy values show that, though the biosorption was spontaneous for Cr(III) and Cd(II), the adsorption of Cr(III) was privileged compared to that of Cd(II), and that the biosorption of Cr(VI) was non-spontaneous." The authors came to such an erroneous conclusion on the basis of the values of ΔG calculated using Eq. (5). The biosorption equilibrium constants, K_c, for the binding data of Cd(II), Cr(III), and Cr(VI) by saltbush leaves biomass were calculated either from the intercept of the Khan and Singh plot[7] ($\ln (q_e/C_e)$ *versus* q_e, Fig. 3 in Ref. 6) or from the slope of the q_e *versus* c_e curve (Eq. [6], and Fig. 4 in Ref. 6). The calculated K_c values, in both cases, are expressed in $l\ g^{-1}$. The calculated K_c values are presented in Table I (Table 2 in Ref. 6). Accordingly, the values of ΔG (calculated using Eq. [5]) and K_c (expressed in $l\ g^{-1}$), given in Table I are incorrect.

TABLE I. Thermodynamic parameters for biosorption of Cd(II), Cr(III) and Cr(VI) on saltbush biomass at 24±2 °C[6]

Metal	Khan and Singh		q_e *versus* c_e plot	
	K_c / l g^{-1}	ΔG / kJ mol^{-1}	K_c / l g^{-1}	ΔG / kJ mol^{-1}
Cd(II)	1.334	–0.7121	1.380	–0.7957
Cr(III)	3.934	–3.3837	13.522	–6.4340
Cr(VI)	0.095	5.8075	0.251	3.4160

By multiplying these K_c values by 1000, dimensionless K_c values were obtained (Table II) and these values were used to recalculate the ΔG values, according to $\Delta G = -RT \ln 1000K_c$, also given in Table II. It is evident from the Table II that the recalculated ΔG values are negative for all investigated metal ions. This indicates that the sorption of Cd(II), Cr(III) and Cr(VI) on saltbush biomass is a spontaneous process.

Similarly, erroneous calculations of ΔG and ΔS values of various ions/molecules on various sorbents were published recently.[8–17] As a consequence of such

incorrect calculations, many erroneous conclusions, very often contradictory to the experimentally obtained results, were drawn.

TABLE II. The recalculated K_c and ΔG values for the biosorption of Cd(II), Cr(III) and Cr(VI) on saltbush biomass at 24±2 °C

Metal	Khan and Singh		q_e *versus* c_e plot	
	K_c	ΔG / kJ mol^{-1}	K_c	ΔG / kJ mol^{-1}
Cd(II)	1334	–17.77	1380	–17.85
Cr(III)	3934	–20.44	13522	–23.49
Cr(VI)	95	–11.24	251	13.64

In addition to these incorrect calculations, there are many erroneous methodical approaches in a large number of papers devoted to adsorption from solutions.

It is well known that the adsorption of metal ions is strongly dependent on the solution pH. Also, during the adsorption experiment there is a change in pH. For one adsorption isotherm, the solution pH should be constant. Also, the equilibrium solution pH, instead of initial one, should be given. The same is valid for adsorbate concentrations. Very often, some authors erroneously present the adsorbed amount of ions as a function of the initial instead of the equilibrium ion concentration. It is known that polyvalent metal ions hydrolyze in aqueous solutions. The degree of hydrolysis of a metal ion is affected by its type and concentration, solution pH, and temperature. Depending on these parameters, various hydrolytic species can exist in aqueous solutions. Very often, the authors neglect this phenomenon.

CONCLUSIONS

Several examples of various adsorption processes taken from the literature were examined. As shown, the calculated ΔG and ΔS values reported in these papers are incorrect. A correct calculation of the named thermodynamic parameters is suggested. Also, some serious mistakes made during adsorption experiments or interpretations of the obtained data are given. This paper can help all researchers working in the adsorption area, and especially those who may not be familiar with the subject.

Acknowledgement: The author is grateful to the Ministry of Science of the Republic of Serbia for financial support (Project No. 142004).

И З В О Д

НЕКА РАЗМАТРАЊА О ПРАВИЛНОМ ИЗРАЧУНАВАЊУ ТЕРМОДИНАМИЧКИХ ПАРАМЕТАРА ПРОЦЕСА АДСОРПЦИЈЕ

СЛОБОДАН К. МИЛОЊИЋ

Институт за нуклеарне науке "Винча", п. пр. 522, 11001 Београд

Ленгмирова и Фројндлихова адсорпциона изотерма широко се користе за интерпретацију различитих адсорпционих процеса. Међутим, постоје многе озбиљне грешке у литера-

тури при одређивању или израчунавању термодинамичких параметара, нарочито при израчунавању промене слободне енергије адсорпције из вредности Ленгмуирових, Фројндлихових и Хенријевих константи. Многи аутори користе бројчане вредности ових константи, за израчунавање ΔG, изражене у неким концентрационим јединицама (нпр. у: l mol^{-1}, l g^{-1}, ml mg^{-1}, итд.) уместо као бездимензионе величине.

(Примљено 9. октобра 2007)

REFERENCES

1. W. Stumm, *Chemistry of Solid–Water Interface*, Wiley – Interscience, New York, 1992, p. 428
2. *Adsorption on New and Modified Inorganic Sorbents*, A. Dabrowski, V. A. Tertykh, Eds., *Studies in Surface Science and Catalysis*, Vol. 99, Elservier, Amsterdam, 1996, p. 944
3. C. H. Giles, D. Smith, A. Huitson, *J. Colloid Interface Sci*. **47** (1974) 755
4. I. Langmuir, *J. Am. Chem. Soc*. **40** (1918) 1316
5. H. M. F. Freundlich, *Z. Phys. Chem. (Leipzig)* **57**A (1906) 385
6. M. F. Sawalha, J. R. Peralta–Videa, J. Romero–González, J. L. Gardea–Torresdey, *J. Colloid Interface Sci.* **300** (2006) 100
7. J. Romero–González, J. R. Peralta–Videa, E. Rodriguez, S. L. Ramirez, J. L. Gardea–Torresdey, *J. Chem. Thermodyn*. **37** (2005) 343
8. N. Sakkayawong, P. Thiravetyan, W. Nakbanpote, *J. Colloid Interface Sci*. **286** (2005) 36
9. M. Mouflih, A. Aklil, S. Sebti, *J. Hazard. Mater*. B**119** (2005) 183
10. M. Erdem, A. Ozverdi, *Sep. Purif. Technol*. **51** (2006) 240
11. Y. Liu, *Colloids Surf. A* **274** (2006) 34
12. R. Rakhshaee, M. Khosravi, M. T. Ganji, *J. Hazard. Mater. B* **134** (2006) 120
13. A. R. Cestari, E. F. S. Vieira, I. A. de Oliveira, R. E. Bruns, *J. Hazard. Mater*. **143** (2007) 8
14. B. H. Hameed, A. A. Ahmad, N. Aziz, *Chem. Eng. J.* **133** (2007) 195
15. C.–H. Weng, C.–Z. Tsai, S.–H. Chu, Y. C. Sharma, *Sep. Purif. Technol*. **54** (2007) 187
16. S. Kubilay, R. Gürkan, A. Savran, T. Sahan, *Adsorption* **13** (2007) 41
17. A. Sari, M. Soylak, *J. Serb. Chem. Soc*. **72** (2007) 485.

Journal of the Serbian Chemical Society
JSCS@tmf.bg.ac.yu • www.shd.org.yu/JSCS

J. Serb. Chem. Soc. 72 (12) 1369–1381 (2007)
JSCS–3669

UDC 546.56:536.5+66.087+532.612
Original scientific paper

Effect of temperature on the electrodeposition of disperse copper deposits

NEBOJŠA D. NIKOLIĆ[1#], LJUBICA J. PAVLOVIĆ[1#], MIOMIR G. PAVLOVIĆ[1#] and KONSTANTIN I. POPOV[1,2*#]

[1]*ICTM – Institute of Electrochemistry, University of Belgrade, Njegoševa 12, P. O. Box 473, 11001 Belgrade and* [2]*Faculty of Technology and Metallurgy, University of Belgrade, Karnegijeva 4, P. O. Box 3503, 11001 Belgrade, Serbia*

(Received 27 July 2007)

Abstract: The effect of temperature on the electrodeposition of copper at overpotentials belonging to the plateau of the limiting diffusion current density and higher was examined by the determination of the average current efficiency of hydrogen evolution and by scanning electron microscopic (SEM) analysis of the morphology of the formed copper deposits. Increasing the temperature of the solution led to a shift of both the beginning and the end of the plateau of the limiting diffusion current density towards lower electrodeposition overpotentials. Also, higher temperatures led to the formation of morphological forms of copper deposits characteristic for electrodeposition of copper at some higher overpotentials. The unexpected trend in the development of copper structures electrodeposited at an overpotential of 800 mV is discussed in terms of the effect of temperature on the viscosity and surface tension of the electroplating solution.

Keywords: electrodeposition, copper, hydrogen evolution, temperature, viscosity, surface tension.

INTRODUCTION

The open and porous structures of copper deposits with extremely high surface areas suitable for used as electrodes in electrochemical devices, such as fuel cells and chemical sensors, can be obtained by both galvanostatic[1] and potentiostatic[2] processes of electrodeposition. These copper structures obtained in the potentiostatic regime are denoted as honeycomb-like ones[3,4] and the phenomenology of their formation has been described in detail in the literature.[5] The main characteristics of this type of structure are holes or craters formed primarily due to the attachment hydrogen bubbles with agglomerates of copper grains between them.[3–6]

The critical conditions which must be fulfilled in order to obtain honeycomb-like copper structures were also determined.[2] It was shown that these stru-

#Serbian Chemical Society member.
* Corresponding author. E-mail: kosta@tmf.bg.ac.yu
doi: 10.2298/JSC0712369N

ctures can be formed by electrodeposition from solutions with lower concentrations of Cu(II) ions (0.15 M $CuSO_4$ and even less in 0.50 M H_2SO_4) at overpotentials outside the plateau of the limiting diffusion current density, (potential at which hydrogen evolution was vigorous enough to change the hydrodynamic conditions in the near-electrode layer). The quantity of evolved hydrogen leading to a change of hydrodynamic conditions corresponds to an average current efficiency of hydrogen evolution of 10.0 %. The critical conditions were determined by the examination of the effect of different concentrations of copper(II) ions and overpotentials of electrodeposition on the processes of copper electrodeposition.[2,3]

The possibility of practical application of the honeycomb-like structure requires the knowledge of the effect of all parameters of electrolysis which can be of the significance for the formation of this type of structure. Except the concentration of copper(II) ions and the overpotential of the electrodeposition, electrolysis parameters of significance for the formation of honeycomb-like copper structures are primarily the temperature of electrolysis and the concentration of the supporting electrolyte (H_2SO_4). The aim of this study was to examine the effect of temperature on the electrodeposition of copper at high overpotentials.

EXPERIMENTAL

Copper was potentiostatically deposited from 0.15 M $CuSO_4$ + 0.50 M H_2SO_4 in an open cell and at temperatures of 14.0±0.5, 35.0±0.5 and 50.0±0.5 °C. Doubly distilled water and analytical grade chemicals were used for the preparation of the solutions for the electrodeposition of copper. The reference and counter electrodes were of pure copper.

Copper electrodeposition onto cylindrical copper cathodes were performed at overpotentials of 550, 650 and 800 mV. The cathodes were prepared in the following way: the cylindrical copper electrodes were first covered with a thin copper film by a 2 min electrodeposition at an appropriate overpotential using the same copper plating solution which was later used for electrodeposition at the desired overpotential. The overpotentials at which copper was electrodeposited for 2 min were: 250, 200 and 125 mV at temperatures of 14.0±0.5, 35.0±0.5 and 50.0±0.5 °C, respectively. This manner of preparation of the copper cathodes was applied in order to obtain a uniform copper surface before electrodeposition at the desired overpotentials.

SEM Microphotographs corresponding to morphologies of copper deposits electrodeposited with a quantity of the electricity of 10.0 mA h cm^{-2} were obtained with a model JEOL T20 scanning electron microscope (SEM).

The procedure for the determination of the average current efficiency of hydrogen evolution has already been given.[2,3]

The viscosity of 0.15 M $CuSO_4$ in 0.50 M H_2SO_4 at the given temperatures was determined using an Ostwald viscometer, while the surface tension of the same electroplating solution at the examined temperatures was determined by the drop-weight method.

RESULTS AND DISCUSSION

The polarization curves for the electrodeposition of copper from 0.15 M $CuSO_4$ in 0.50 M H_2SO_4 at temperatures of 14.0±0.5, 35.0±0.5 and 50.0±0.5 °C are given in Fig. 1. The way of the determination of the length of the plateau of the limiting diffusion current density is also shown in Fig. 1. It can be seen from

Fig. 1 that increasing the temperature leads to an increase of the limiting diffusion current density, as well as to a shift of both the beginning and the end of the plateau of the limiting diffusion current density towards lower electrodeposition overpotentials. This can be explained in the following manner:

In the well-known Nernst limiting current density equation:

$$j_L = nFDc_0/\delta \tag{1}$$

where nF is the number of Faradays per mole of consumed ions, c_0 is concentration of Cu(II) ions, D is the diffusion coefficient and δ the thickness of the diffusion layer, a change of the temperature of the solution affects both D and δ. Changes of these variables are affected by the well-known fact concerning the change of the viscosity of a solution[7] with changing temperature.

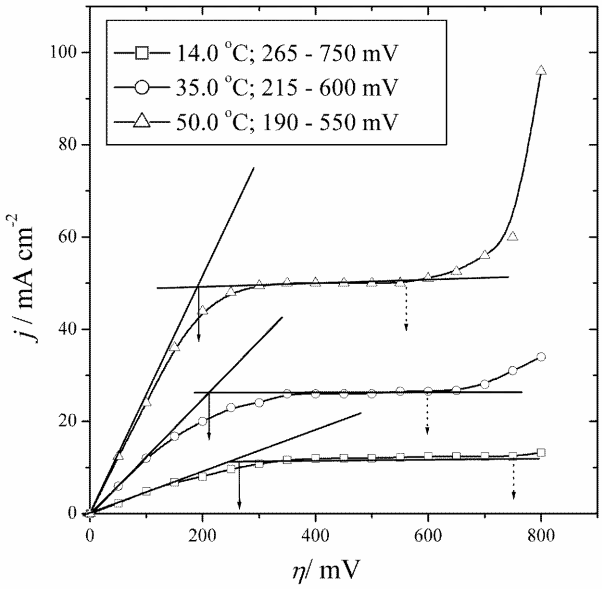

Fig. 1. Polarization curves for the electrodeposition of copper from 0.15 M $CuSO_4$ in 0.50 M H_2SO_4 at temperatures of 14.0±0.5, 35.0±0.5 and 50.0±0.5 °C.

On the other hand, it is a well known fact that the critical overpotential for the initiation of dendritic growth, η_I, is given by Eq. (2):

$$\eta_I = b_c \log \frac{4 j_L}{j_0} \tag{2}$$

being close to the beginning of the limiting diffusion current density plateau.[8]

Furthermore, it is known that the equation of a general polarization curve for sufficiently large overpotentials is given by Eq. (3):[9]

$$j = \frac{j_0 f_c}{1 + \frac{j_0 f_c}{j_L}} \tag{3}$$

and

$$f_c = 10^{(\eta / b_c)} \tag{4}$$

In the above Equations, j, j_0 and j_L are the current density, exchange current density and limiting diffusion current density, respectively, b_c is the cathodic Tafel slope and η is the overpotential.

The cathodic current density and the overpotential are taken as positive values for the sake of simplicity. Assuming that the ohmic drop[10] can be neglected for the deposition from 0.15 M $CuSO_4$ in 0.50 M H_2SO_4, the values of j_0 can be estimated as follows. If

$$j = 0.5 j_L \tag{5}$$

Equation (3) can be re-written in the form:

$$j_0 = \frac{j_L}{f_{c,1/2}} \tag{6}$$

where $f_{c,1/2}$ corresponds to the overpotential $\eta_{1/2}$ measured for $j = 0.5 j_L$.

Using the data from the diagrams presented in Fig. 1 and Eqs. (2) and (4–6), the critical overpotentials for the initiation of dendritic growth, η_I, are calculated and presented in Table I. The values of the overpotentials corresponding to the beginning of the limiting diffusion current density plateau, $\eta_{b,p}$ are also presented in Table I. Although both values of overpotentials are estimated values, they illustrate well in a qualitative way the change with increasing temperature.

TABLE I. The values of the calculated critical overpotentials of dendritic growth initiation, η_I, and the estimated values of the overpotentials corresponding to the beginning of the plateau of the limiting diffusion current density, $\eta_{b,p}$, as a function of the temperature of electrodeposition

Temperature, °C	$\eta_{I,calculated}$ / mV	$\eta_{b,p,estimated}$ / mV
14.0±0.5	205	265
35.0±0.5	185	215
50.0±0.5	177	190

It is clear from Fig. 1 that an overpotential of 550 mV belongs to the plateau of the limiting diffusion current density at all analyzed temperatures. An overpotential of 650 mV belongs to the plateau of the limiting diffusion current density only at a temperature of 14.0±0.5 °C. This overpotential is about 50 mV outside the plateau at a temperature of 35.0±0.5 °C and about 100 mV outside at a temperature of 50.0±0.5 °C. Finally, an overpotential of 800 mV is outside the plateau of the limiting diffusion current density at all temperatures.

The dependences of the overall currents of electrodeposition and the volumes of evolved hydrogen on electrodeposition time are shown in Fig. 2, from which increasing electrodeposition currents with increasing temperature can be observed at all overpotentials. At an overpotential of 550 mV, hydrogen evolu-

tion was detected only at a temperature of 50.0 °C when several hydrogen bubbles were registered by visual observation. Unfortunately, this hydrogen evolution was below the sensitivity of measurement technique. On the other hand, at overpotentials of 650 and 800 mV, hydrogen evolution was detected at all temperatures. Increasing the temperature increased the quantity of evolved hydrogen and decreased the time required for the solution to become supersaturated (Figs. 2b and 2c).

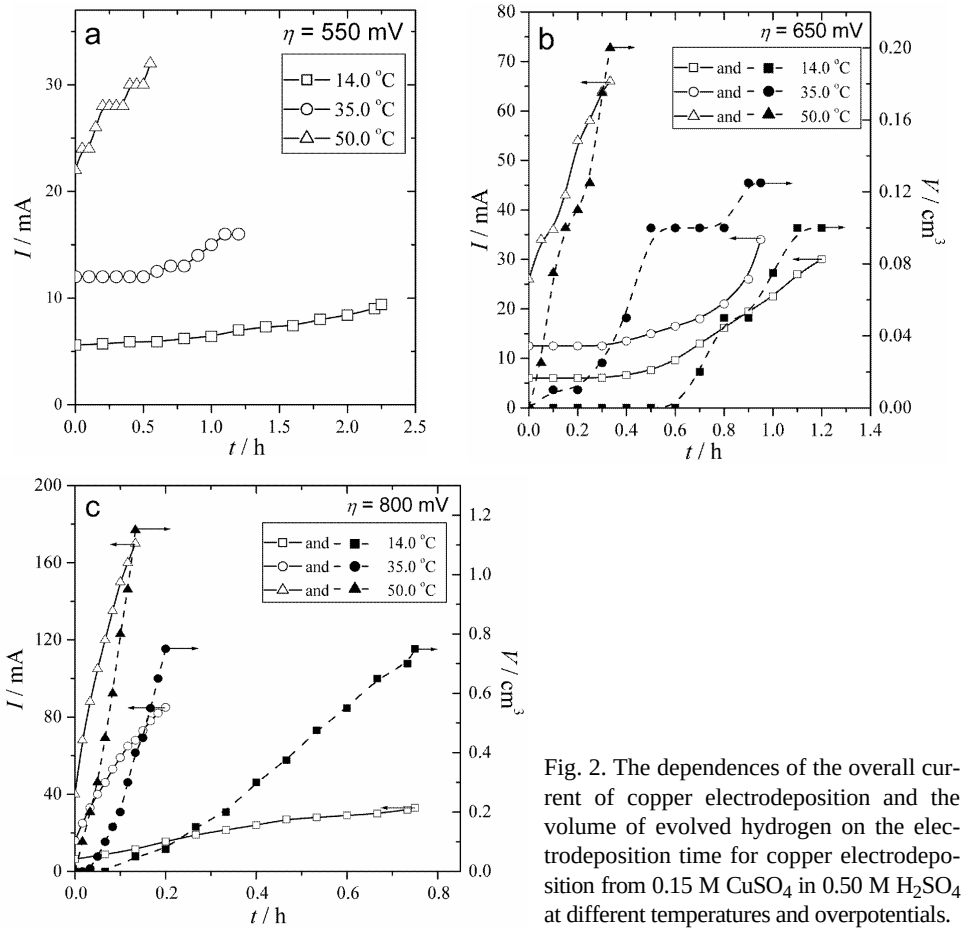

Fig. 2. The dependences of the overall current of copper electrodeposition and the volume of evolved hydrogen on the electrodeposition time for copper electrodeposition from 0.15 M $CuSO_4$ in 0.50 M H_2SO_4 at different temperatures and overpotentials.

The average current efficiencies for hydrogen evolution reaction, $\eta_{av}(H_2)$ at overpotentials of 650 and 800 mV, derived from the diagrams shown in Figs. 2b and 2c, respectively, are plotted as functions of the quantity of electricity, Q, in Fig. 3. These values are also summarized in Table II, which also includes the values of the average current efficiencies of a hydrogen evolution of 0.0 % obtained at an overpotential of 550 mV. It can be clearly seen from Fig. 3 and Table II that the electrodeposition processes at overpotentials of 650 and 800 mV are accom-

panied by increases of the average current efficiencies of hydrogen evolution with increasing temperature, causing a shift of the end of the limiting diffusion current density plateau toward lower values of the overpotential. This is due to the increased rate of hydrogen evolution with increasing temperature. In totality, three groups of the average current efficiencies of hydrogen evolution are of significance in the investigation of the effect of temperature on the electrodeposition of copper at high overpotentials.

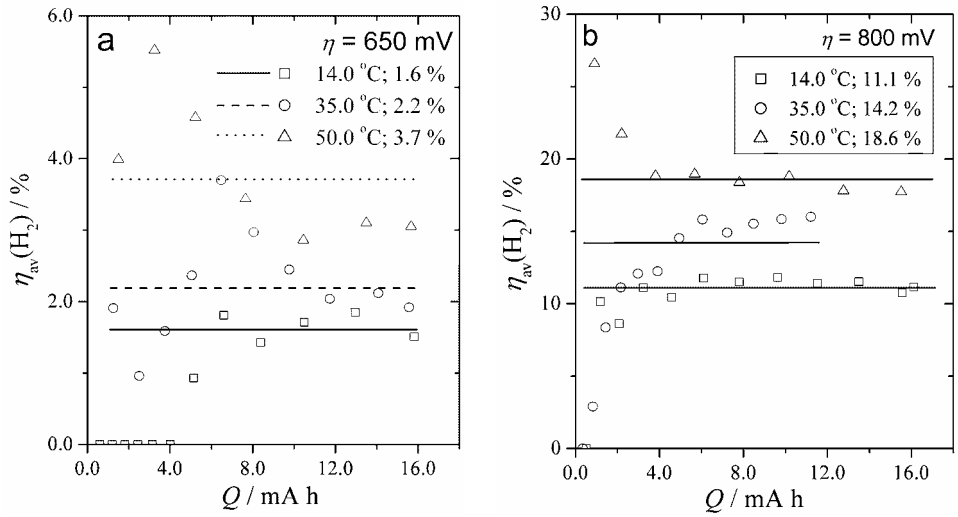

Fig. 3. The dependences of the average current efficiencies for the hydrogen evolution reaction on the quantity of used electricity, for copper electrodeposition from 0.15 M $CuSO_4$ in 0.50 M H_2SO_4 at different temperatures and overpotentials of 650 mV and 800 mV.

TABLE II. The values of the average current efficiencies of hydrogen evolution, $\eta_{av}(H_2)$, in the dependence on the temperature of electrodeposition at different overpotentials

Temperature, °C	$\eta_{av}(H_2)$ / %		
	550 mV	650 mV	800 mV
14.0±0.5	0	1.6	11.1
35.0±0.5	0	2.2	14.2
50.0±0.5	0	3.7	18.6

The first group is characterized by electrodeposition of copper at an overpotential of 550 mV, (potential at which there is no hydrogen evolution or hydrogen evolution was below the sensitivity of the measurement technique).

The second group is characterized by processes of electrodeposition at an overpotential of 650 mV (potential at which the average current efficiencies of hydrogen evolution were below the critical value of the average current efficiency of hydrogen evolution of 10.0 %, leading to a change of the hydrodynamic conditions in the near-electrode layer).

Finally, the third group includes electrodeposition processes at 800 mV, which are accompanied by an average current efficiency of hydrogen evolution above the critical value of 10.0 % required for a change of hydrodynamic conditions in the near-electrode layer. The quantities of evolved hydrogen corresponding to the average current efficiencies of hydrogen evolution above 10.0 % are only one of the ways to change the hydrodynamic conditions in the near-electrode layer. For example, a change of the hydrodynamic conditions can be realized under imposed magnetic fields (magnetohydrodynamic effects).[11–14]

The morphologies of the copper deposits electrodeposited at an overpotential of 550 mV are shown in Fig. 4. The copper deposit obtained at a temperature of 14.0 °C had a cauliflower-like structure (Fig. 4a). Spherical diffusion zones inside the linear diffusion layer of the macroelectrode were formed around the cauliflower particles (Fig. 4b). The copper deposit obtained at a temperature of 35.0 °C was a mixture of cauliflower-like (Fig. 4c) and dendritic forms (Fig. 4d). A mixture of cauliflower-like and dendritic forms was also obtained by electrodeposition at a temperature of 50.0 °C (Figs. 4e and 4f).

The size of the cauliflower-like particles did not change with increasing temperature, but the size of the sub-particles constituting the cauliflower-like forms decreased with increasing temperature of electrodeposition. The decrease of the size of sub-particles with increasing temperature can be explained by the well-known dependence of the nucleation rate on temperature,[15] which was derived by Volmer and Weber.[16]

The morphologies of the copper deposits obtained at an overpotential of 650 mV are shown in Fig. 5, from which the strong effect of temperature on the electrodeposition of copper at an overpotential of 650 mV can immediately be clearly seen. Very branched copper dendrites were formed during electrodeposition at a temperature of 14.0 °C (Fig. 5a). They were constructed of corncob-like elements (Fig. 5b). This is in accordance with the position of an overpotential of 650 mV in the limiting diffusion current density plateau. Dendritic forms were obtained during electrodeposition at a temperature of 35.0 °C (Fig. 5c) but holes, the origin of which was attached hydrogen bubbles, were also formed (the part in the circle in Fig. 5d). The increased hydrogen evolution at a temperature of 50.0 °C compared to that at 35.0 °C led to a change of the shape of the copper dendrites, which become similar to cauliflower-like forms (Fig. 5e) or, probably, degenerated dendrites were formed. Also, the holes formed due to the attachment of hydrogen bubbles can be observed in this copper deposit (Fig. 5f). These facts were unexpected because the current efficiency of the hydrogen evolution reaction was lower than 10.0 %, but it can be explained by the findings of Vogt and Balzer.[17] They showed that the bubble coverage of an electrode surface increased with temperature more than linearly. In addition, Krenz[18] observed an increase in bubble coverage of about 50 % as the temperature was raised from 25 to 50 °C.

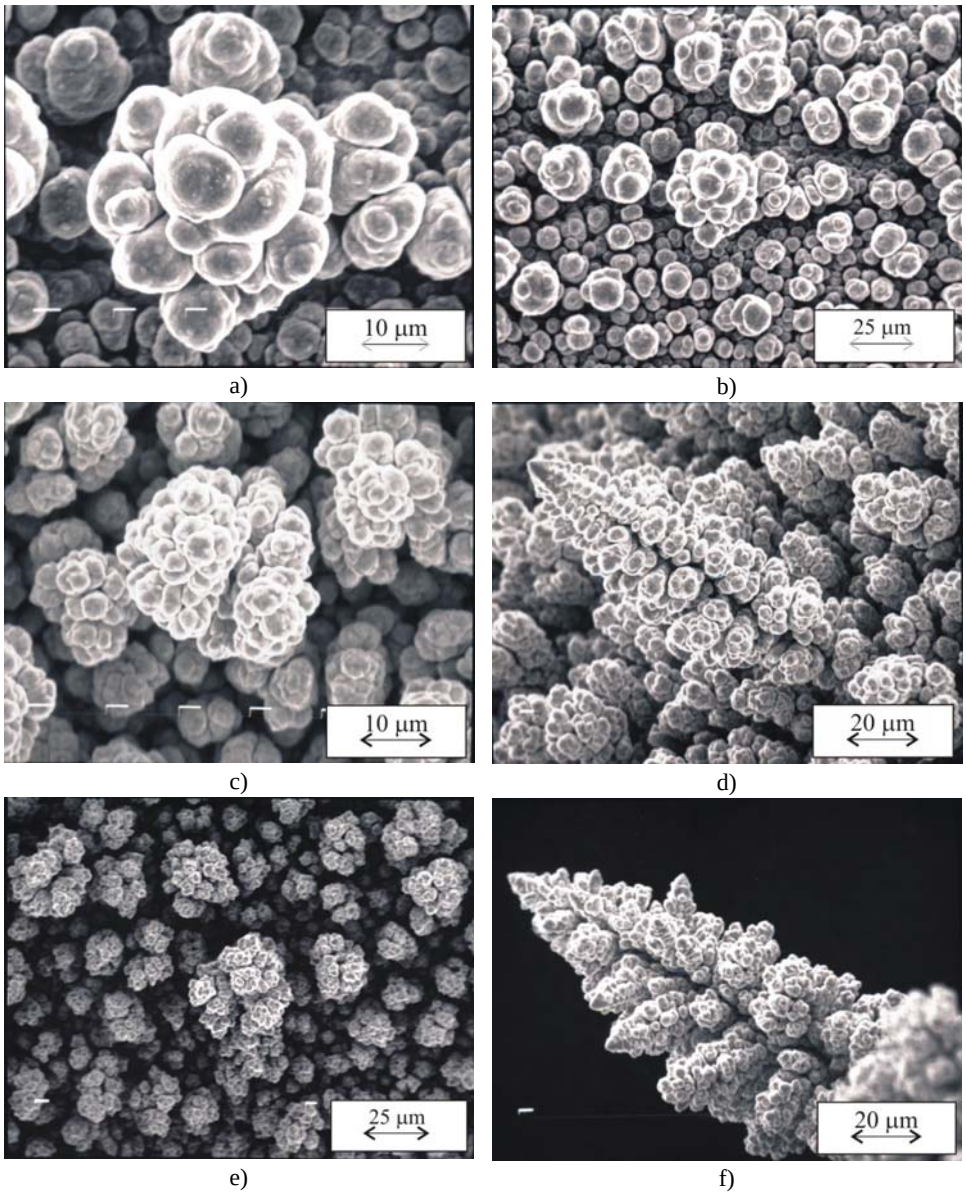

Fig. 4. Morphologies of copper deposits electrodeposited at an overpotential of 550 mV at temperatures of: a) and b) 14.0±0.5, c) and d) 35.0±0.5 and e) and f) 50.0±0.5 °C.

The morphologies of the copper deposits electrodeposited at an overpotential of 800 mV are shown in Fig. 6, from which the strong effect of evolved hydrogen on the morphologies of copper deposits is visible. Very porous structures, holes formed due to the attachment hydrogen bubbles, cauliflower-like forms and the

absence of dendritic forms were the main characteristics of copper deposits obtained at this overpotential. A decreased number of holes per mm^2 surface area of the copper electrodes and the increased diameter of the holes with increasing temperature can be observed from Fig. 6. Also, the portion of the copper structure consisting of dispersed agglomerates of copper grains, among which irregular channels were formed, increased with increasing temperature of the solution.

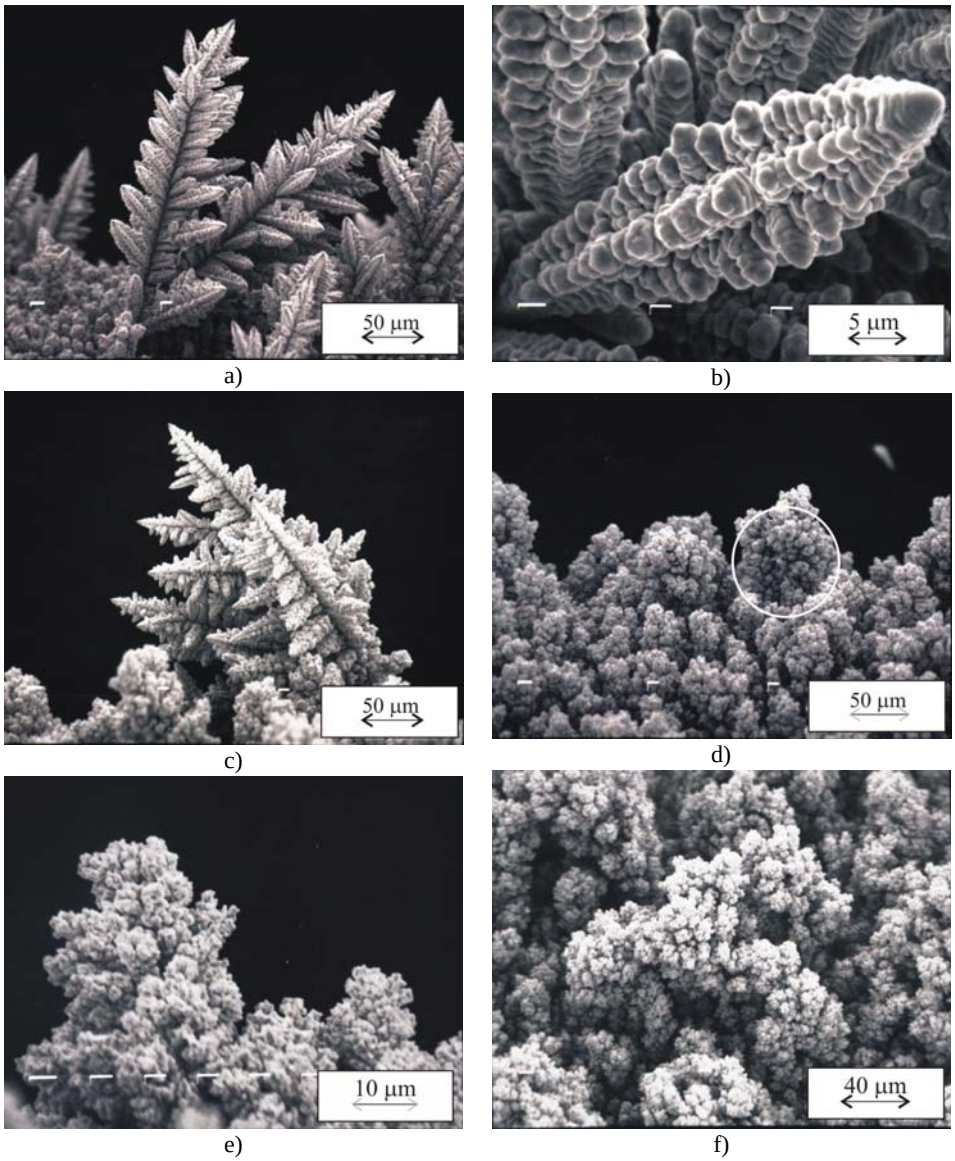

Fig. 5. Morphologies of copper deposits electrodeposited at an overpotential of 650 mV at temperatures of: a) and b) 14.0±0.5, c) and d) 35.0±0.5 and e) and f) 50.0±0.5 °C.

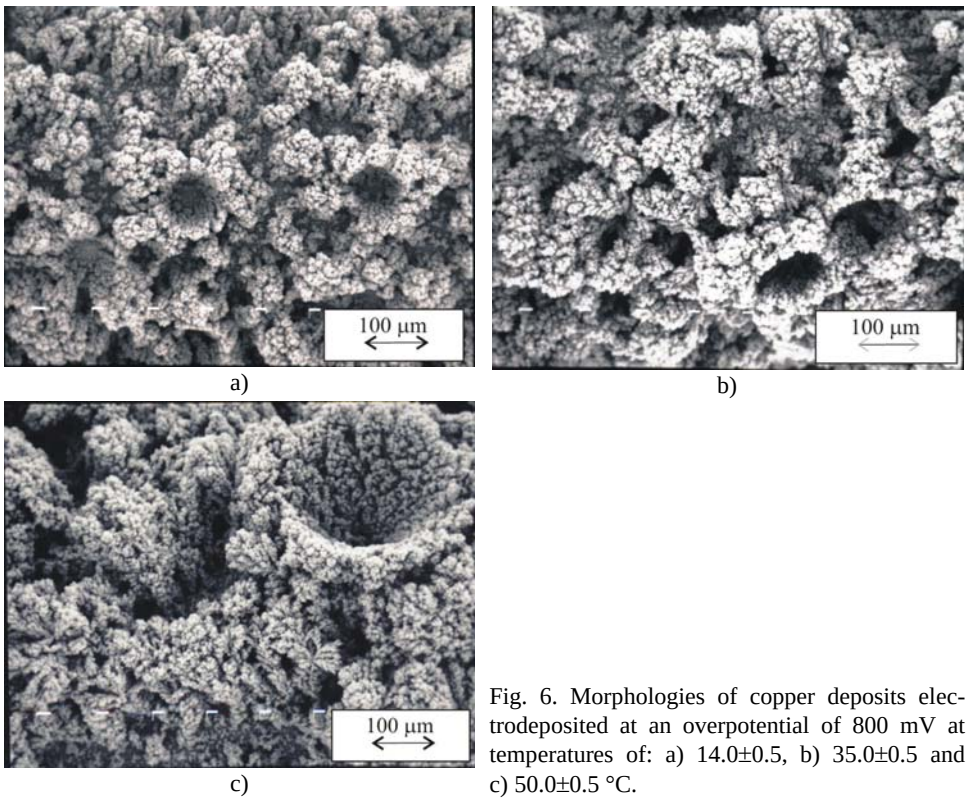

Fig. 6. Morphologies of copper deposits electrodeposited at an overpotential of 800 mV at temperatures of: a) 14.0±0.5, b) 35.0±0.5 and c) 50.0±0.5 °C.

Firstly, it is necessary to note that the decrease of the number of holes per mm^2 surface area of the copper electrode with intensification of hydrogen evolution was very surprising. It is opposed to our recently published results[2–4] when it was shown that intensification of hydrogen evolution reaction leads to an increase of the number of holes. Thus, the unexpected development of the copper structures with intensification of the hydrogen evolution reaction clearly highlights the necessity to take into consideration the effect of temperature on some properties of electroplating solution, as well as the already mentioned increased bubble coverage with the increasing temperature. The properties of an electrolyte of importance in metal electrodeposition processes which are affected by a change of temperature are the viscosity[7] and surface tension of the electrolyte.[17]

The values of the viscosity and surface tension of a copper solution containing 0.15 M $CuSO_4$ in 0.50 M H_2SO_4 at the examined temperatures are given in Table III. As expected, both the viscosity and the surface tension of this solution decrease with increasing temperature. The decrease of the surface tension of the solution lowers the break-off diameter of hydrogen bubbles from the electrode surface,[17] while the decreased viscosity of the solution probably facilitates the

transport of the detached hydrogen bubbles through the interior of the deposit, thus forming a channel structure through it. A typical channel structure formed at an overpotential of 800 mV at a temperature of 50.0 °C is shown in Fig. 7a, while the top view of this deposit shows that very disperse cauliflower-like agglomerates of copper grains were surrounded by irregular channels (Fig. 7b).

TABLE III. The values of the viscosity, ν, and surface tension, γ, of a copper solution containing 0.15 M $CuSO_4$ in 0.50 M H_2SO_4 at different temperatures

Temperature, °C	ν / 10^{-6} m^2 s^{-1}	γ / J m^{-2}
14.0±0.5	1.17	103.2
35.0±0.5	0.832	82.0
50.0±0.5	0.637	71.8

Hence, increasing the temperature led to a redistribution of evolved hydrogen from those creating a honeycomb-like structure (holes formed due to the attachment hydrogen bubbles with cauliflower-like agglomerates of copper grains between them) to those making a copper structure with the dominant presence of cauliflower-like forms and irregular channels between them. This increase of the portion of channel structure to the overall structure of the deposit in relation to the portion of holes to the overall structure is probably due to changes of the properties of the electroplating solution, caused by the dependences of the viscosity and surface tension of solution on temperature. As result of this, the formation of holes becomes less possible and hence large holes appear only due to the edge effect, as can be clearly seen from Fig. 6c. It is obvious that the probability of the formation of the nucleus of such a structure decreases with lowering of the break-off diameter of the bubbles.

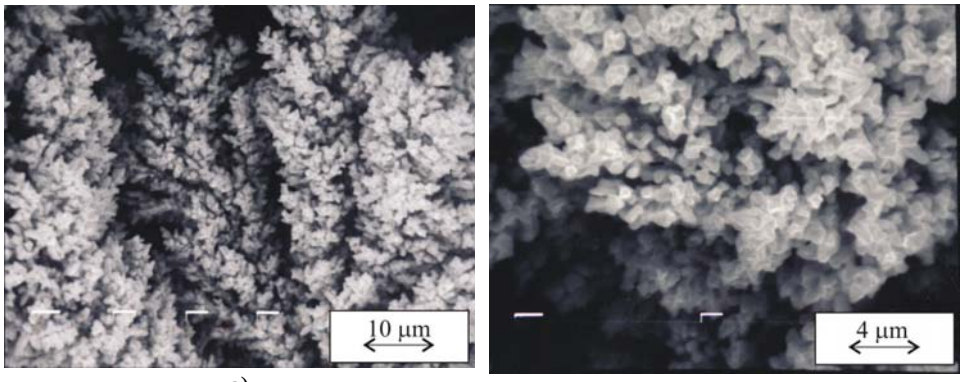

a) b)

Fig. 7. Morphologies of copper deposits electrodeposited at an overpotential of 800 mV at a temperature of 50.0±0.5 °C.

Also, it is necessary to note that increasing the temperature led to the formation of morphological forms of copper deposits characteristic for electrodeposi-

tion at higher overpotentials, probably because of the increase of bubble coverage with increasing temperature. The effect of temperature was opposite to those observed with increasing the concentration of copper(II) ions,[2] when increasing concentration of Cu(II) ions led to a formation of morphological forms of copper deposits characteristic for electrodeposition at lower overpotentials.[2]

From the point of view of the formation of copper structures suitable for electrodes in electrochemical devices, such as fuel cells and sensors, this means that increasing the temperature has a negative effect on the formation of such structures.

CONCLUSIONS

Electrodeposition of copper from 0.15 M $CuSO_4$ in 0.50 M H_2SO_4 at overpotentials belonging to the limiting diffusion current density and at higher ones was analyzed. The average current efficiencies of hydrogen evolution were determined at electrodeposition overpotentials of 550, 650 and 800 mV, and at temperatures of 14.0±0.5, 35.0±0.5 and 50.0±0.5 °C. The morphologies of the copper deposits obtained under the same electrodeposition conditions were examined by the scanning electron microscopy (SEM) technique.

Increasing the temperature led to an increase of the average current efficiencies of hydrogen evolution during electrodeposition of copper at overpotentials of 650 and 800 mV.

The morphological forms of the copper deposits obtained at overpotentials of 550 and 650 mV became similar to those obtained at some higher overpotentials. A very interesting and unexpected case was observed during copper electrodeposition at 800 mV. The intensification of the hydrogen evolution reaction caused by increasing temperature, opposite to expectation, led to a decrease of the number of holes per mm^2 surface area of the copper electrode. This decrease of the number of holes is ascribed to the effect of the temperature on both the viscosity and surface tension of the solution. The increase of a temperature led to a redistribution of evolved hydrogen from those creating holes to those favoring the formation of channel structures through the interior of the deposit.

Acknowledgement. The work was supported by the Ministry of Science of the Republic of Serbia under the research project: “Deposition of ultrafine powders of metals and alloys and nanostructured surfaces by electrochemical techniques” (Project No. 142032G).

И З В О Д

УТИЦАЈ ТЕМПЕРАТУРЕ НА ЕЛЕКТРОХЕМИЈСКО ТАЛОЖЕЊЕ ДИСПЕРЗНИХ ТАЛОГА БАКРА

НЕБОЈША Д. НИКОЛИЋ[1], ЉУБИЦА Ј. ПАВЛОВИЋ[1], МИОМИР Г. ПАВЛОВИЋ[1] и КОНСТАНТИН И. ПОПОВ[1,2]

[1]*ИХТМ – Центар за електрохемију, Универзитет у Београду, Његошева 12, 11000 Београд и*
[2]*Технолошко–металуршки факултет, Универзитет у Београду, Карнегијева 4, 11000 Београд*

Утицај температуре на електрохемијско таложење бакра на пренапетостима које припадају платоима граничне дифузионе густине струје, као и на вишим пренапетостима је ис-

питан одређивањем средњег искоришћења струје реакције издвајања водоника и анализом морфологија талога бакра техником скенирајуће електронске микроскопије. Повећање температуре раствора довело је до померања и почетка и краја платоа граничне дифузионе густине струје ка нижим пренапетостима. Такође, повећање температуре довело је до формирања морфолошких форми талога бакра карактеристичних за електрохемијско таложење на неким вишим пренапетостима. Неочекивани тренд у развоју структура бакра добијених на пренапетости од 800 mV је био дискутован на основу утицаја температуре на вискозност и површински напон раствора за електрохемијско таложење бакра.

(Примљено 27. јула 2007)

REFERENCES

1. H.–C. Shin, J. Dong, M. Liu, *Adv. Mater*. **15** (2003) 1610
2. N. D. Nikolić, K. I. Popov, Lj. J. Pavlović, M. G. Pavlović, *Sensors* **7** (2007) 1
3. N. D. Nikolić, K. I. Popov, Lj. J. Pavlović, M. G. Pavlović, *J. Electroanal. Chem.* **588** (2006) 88
4. N. D. Nikolić, K. I. Popov, Lj. J. Pavlović, M. G. Pavlović, *Surf. Coat. Technol.* **201** (2006) 560
5. N. D. Nikolić, K. I. Popov, Lj. J. Pavlović, M. G. Pavlović, *J. Solid State Electrochem.* **11** (2007) 667
6. N. D. Nikolić, Lj. J. Pavlović, M. G. Pavlović, K. I. Popov, *Electrochim. Acta* **52** (2007) 8096
7. A. Amadi, D. R. Gabe, M. Goodenough, *J. Appl. Electrochem.* **21** (1991) 1114
8. K. I. Popov, M. D. Maksimović, J. D. Trnjančev, M. G. Pavlović, *J. Appl. Electrochem.* **11** (1981) 239
9. K. I. Popov, S. S. Djokić, B. N. Grgur, *Fundamental Aspects of Electrometallurgy*, Kluwer Academic/Plenum Publishers, New York, 2002, p. 18
10. J. O'M. Bockris, A. K. N. Reddy, M. Gamboa–Aldeco, *Modern Electrochemistry 2A*, 2nd Ed., Kluwer Academic/Plenum Press, New York, 2000, p. 1107
11. N. D. Nikolić, *J. Serb. Chem. Soc.* **70** (2005) 785
12. N. D. Nikolić, *J. Serb. Chem. Soc.* **70** (2005) 1213
13. N. D. Nikolić, *J. Serb. Chem. Soc.* **71** (2006) 1083
14. N. D. Nikolić, *J. Serb. Chem. Soc.* **72** (2007) 787
15. E. Budevski, G. Staikov, W. J. Lorenz, *Electrochemical Phase Formation and Growth, An Introduction to the Initial Stages of Metal Deposition*, VCH Weinheim, New York, 1996, p. 163
16. M. Volmer, A. Weber, *Z. Physik. Chem.* **119** (1926) 277
17. H. Vogt, R. J. Balzer, *Electrochim. Acta* **50** (2005) 2073
18. M. Krenz, *Dissertation A*, Humboldt Universität, Berlin, 1984.

Journal of the Serbian Chemical Society
JSCS@tmf.bg.ac.yu • www.shd.org.yu/JSCS

J. Serb. Chem. Soc. 72 (12) 1383–1392 (2007) UDC 539.61:547–311+667.6:669.5–034:620.193
JSCS–3670 *Original scientific paper*

Adhesion of epoxy cataphoretic coatings on Zn alloys

JELENA B. BAJAT[1]*#, VESNA B. MIŠKOVIĆ–STANKOVIĆ[1#] and DRAGUTIN M. DRAŽIĆ[2#]

[1]*Faculty of Technology and Metallurgy, University of Belgrade, Karnegijeva 4, P.O. Box 35-03, 11120 Belgrade and* [2]*ICTM – IEC, P.O. Box 815, 11001 Belgrade, Serbia*

(Received 22 January 2007)

Abstract: One of the most important factors in corrosion prevention by protective coatings is the loss of coating adhesion under environmental influence. In this work, the adhesion of epoxy cataphoretic coatings was examined on steel and steel modified by Zn–Fe and Zn–Co alloys. The dry and wet adhesions of epoxy primers were measured by the direct pull-off standardized procedure, as well as indirectly by the NMP test. The corrosion stability of the coated samples was investigated by electrochemical impedance spectroscopy. It was shown that under dry testing conditions all the samples exhibited very good adhesion. However, different trends of adhesion loss of different protective systems during exposure to a corrosive agent (3 % NaCl solution) were observed. The lowest adhesion values were obtained for epoxy coating on the steel substrate. The change in adhesion of the epoxy coating on steel modified by Zn–Co alloy during immersion in 3 % NaCl solution for 24 days was the smallest of all the investigated samples. Electrochemical impedance measurements in 3 % NaCl solution confirmed the good protective properties of this protective system, *i.e.*, greater values of pore resistance were obtained.

Keywords: adhesion, Zn–Fe alloy, Zn–Co alloy, epoxy coating, electrochemical impedance spectroscopy.

INTRODUCTION

The most important properties of a protective coating are the anticorrosive action and the adhesion to the substrate.[1–4] Thus, the determination of adhesion is often used when characterizing protective properties of organic coatings on a metal substrate. In principle, paint adhesion can be improved by providing a substrate with a pre-treatment layer, followed by the application of a corrosion-inhibiting primer and a topcoat paint. One of the frequently used steel pre-treatments is electrochemical deposition of Zn alloys,[5–8] especially in the automotive industry, because of the increased requirements for coatings with longer service life, as well as being good replacements of toxic cadmium coatings.[9]

* Corresponding author. E-mail: jela@tmf.bg.ac.yu
# Serbian Chemical Society member.
doi: 10.2298/JSC0712383B

In this work, different methods were used to determine if and to what extent the adhesion of epoxy coatings depends on the modification of a steel substrate with zinc alloys. In addition, the results of the various methods (pull-off test, NMP test and EIS) were compared to determine whether they showed the same tendency.

EXPERIMENTAL

Electrodeposition of Zn alloys

The steel panels (40 mm×40 mm×0.25 mm employed for the adhesion pull-off measurements and 14 mm×14 mm×0.25 mm for the NMP test) were pretreated by mechanical cleaning (polishing successively with emery papers of the following grades: 280, 360, 800 and 1000) and then degreased in a saturated solution of sodium hydroxide in ethanol, pickled with a 1:1 hydrochloric acid solution for 30 s and finally rinsed with distilled water.

Zn–Fe Alloys were deposited galvanostatically at 4.0 A dm^{-2} on a steel panel at 25 °C from an alkaline bath: 0.09 mol dm^{-3} $ZnSO_4$, 0.01 mol dm^{-3} $FeSO_4$, 0.01 mol dm^{-3} ascorbic acid, ≈ 0.2 mol dm^{-3} triethanolamine, 30 g dm^{-3} Na_2SO_4 and 80 g dm^{-3} NaOH (pH ≈ 14).[10] Zn–Co Alloys were deposited galvanostatically at 5.0 A dm^{-2} on a steel panel from a chloride bath[11] at 25 °C: 80 g dm^{-3} $ZnCl_2$, 16 g dm^{-3} $CoCl_2{\cdot}6H_2O$, 25 g dm^{-3} H_3BO_3 and 210 g dm^{-3} KCl.

The employed electrolytes were prepared using p.a. chemicals (Merck, Aldrich, and Fluka) and double distilled water. The thickness of the Zn alloys was 10 μm.

Surface roughness

The surface roughness of the steel surface, Zn–Fe and Zn–Co alloys, as substrates for the deposition of an epoxy coating, was determined by a TR-200 handheld roughness tester.

Electrodeposition of epoxy coatings

Epoxy (pigmented) coatings were electrodeposited from an epoxy resin emulsion modified by amine and isocyanate on steel and a steel surface previously modified by Zn–Fe and Zn–Co alloy, using the constant voltage method (CATOLAC emulsion 543.052, produced by PPG). The resin concentration in the electrodeposition bath was a 10 wt. % solid dispersion in water at pH 5.7; the temperature was 26 °C and the applied voltage was 250 V.[12] After coating for 3 min, the coatings were rinsed with distilled water and cured at 180 °C for 30 min. The film thickness, determined by a Fischer Dualscope-Mpor, was 17±1 μm.

Adhesion measurements

The adhesion strength of the epoxy coatings on the metal substrates was determined by two methods: by the direct pull-off standardized procedure and by determining the NMPRT (*N*-methylpyrrolidone retention time).

Pull-off test

The adhesion strength of the epoxy coatings on steel and steel modified by Zn–Fe and Zn–Co alloys was determined by an Erichsen Adhesionmaster 513 MC/525 MC. The adhesion measurements were performed prior to exposure to 3 % NaCl solution (“dry” adhesion), as well as at certain time intervals during exposure to a 3 % NaCl solution at room temperature for a period of 24 days (“wet” adhesion).

For each type of protective system, five samples were tested and the average value of these measurements was taken. For all measurements only the ones with adhesive failure were taken into account.

NMP Test

The employed *N*-methylpyrrolidone (NMP) was of p.a. purity. In the NMP delamination test[13] panels of 2 cm^2 area were immersed in NMP at 60 °C. The paint always delaminated from the edges inwards. The time when the paint had completely delaminated was recorded. The experiment

was performed five times per panel and the average value was calculated as the NMPRT (NMP retention time, or the time for the paint film to delaminate completely from the substrate) for a particular primer–metal combination. Each panel was always treated in a fresh solvent.

Electrochemical impedance spectroscopy (EIS)

For the a.c. impedance measurements, the coated samples were exposed to 3 % NaCl in distilled water for 24 days. A three-electrode cell arrangement was employed for the experiments. The working electrode was a coated sample situated in a special Teflon holder. The counter electrode was a platinum mesh with a surface area considerably greater than that of the working electrode. The reference electrode was a saturated calomel electrode (SCE). The a.c. impedance data were obtained at the open-circuit potential using a PAR 273 potentiostat and PAR 5301 lock-in amplifier. The impedance measurements were performed over a frequency range of 100 kHz to 10 mHz using a 5 mV amplitude sinusoidal voltage. The impedance spectra were analyzed using a suitable fitting procedure.[14]

RESULTS AND DISCUSSION

Adhesion measurements

Adhesion is based on the chemical and physical forces between the top side of the metal substrate and the under side of the paint which covers the metal surface. To understand more about the forces between these two phases, *i.e.,* the metal substrate and the paint film, these forces should be measured. Two different adhesion tests were applied in order to gain some insight as to what kind of substrate would provide the best adhesion and for a more fundamental reason, to show how a surface roughness along with the surface wetability affect the adhesion as well as the corrosion resistance of protective systems.

NMP Test

NMP is a highly polar solvent and it is capable of forming strong hydrogen bonds, allowing it to rapidly diffuse into organic coating and causing extensive swelling.[13] Due to the swelling, shear stresses are imposed at the metal/coating interface. These shear stresses are, in most cases, relaxed by delamination of the coating. Thus longer the time until delamination, the better is the adhesion. The time for the paint film to delaminate completely and intact from the substrate, defined as NMP retention time (NMPRT), was recorded.

NMP Adhesion tests were performed initially before exposure to 3 % NaCl, *i.e.,* on the dry films, and the results are presented in Table I.

The highest NMP retention time (NMPRT) was obtained for the epoxy coating on steel modified by Zn–Co alloy. For epoxy coating on steel modified by Zn–Fe alloy, the delamination time was slightly shorter. These results point to higher initial adhesions of the epoxy coating on steel modified by Zn alloys as compared to the bare steel substrate.

Pull-off measurements

Wet adhesion, or the adhesion of a coating which is exposed to moisture, water or a corrosive agent, is very important because in the presence of moisture

the conditions can be simulated which occur in practical conditions.[4] For this reason, it is important to also know the adhesion strengths of protective systems which are exposed to a corrosive media.

TABLE I. NMPRT Values for epoxy coatings on steel and steel modified by Zn–Fe and Zn–Co alloys before exposure to 3 % NaCl

Substrate	NMPRT / min
Steel	3.0
Steel + Zn–Fe alloy	4.7
Steel + Zn–Co alloy	6.3

The pull-off results of the change of adhesion strength with time of immersion in NaCl solution for epoxy coatings on different substrates are shown in Fig. 1.

A general trend of decreasing adhesion strength with increasing exposure time was observed for all samples. The best performance was obtained for the epoxy coatings on steel modified by Zn–Co alloy, throughout the whole investigated time. The lowest values for both dry and wet adhesion were obtained for the epoxy coating on the steel substrate. Initially, during the first few days, the values of the adhesion strengths for epoxy coating on steel modified by Zn–Fe and Zn–Co alloy were very similar. However, after about 7 days, the adhesion strength of the epoxy coating on steel modified by Zn–Fe alloy drops sharply, whereas that of the epoxy coating on steel modified by Zn–Co alloy decreases only slowly, indicating a more stable protective system during exposure to a corrosive agent.

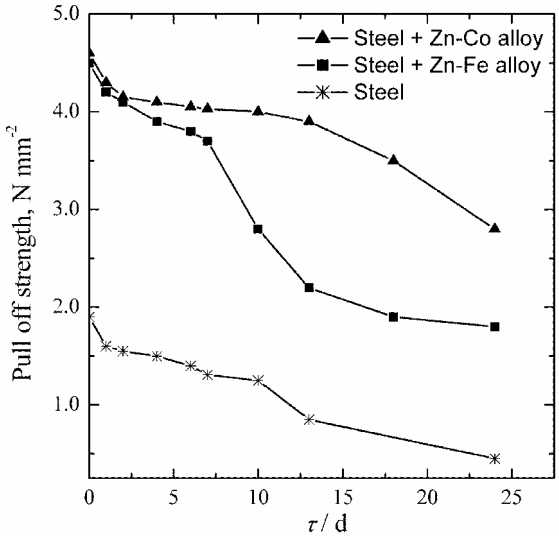

Fig. 1. The pull-off strength for epoxy coatings on steel and steel modified by Zn–Co and Zn–Fe alloys during exposure to 3 % NaCl solution.

The reductions of adhesion after one day of exposure to the corrosive agent and after the whole investigated time period are shown in Table II. Of all the protective systems investigated in this work, the smallest reduction of adhesion

was obtained for the epoxy coating on steel modified by Zn–Co alloy. After one day of exposure, the reduction of adhesion was very similar for epoxy coatings on both Zn alloys, but after 24 days of exposure to 3 % NaCl, the reduction of adhesion for epoxy coating on Zn–Co alloy was significantly lower (40 %) as compared to Zn–Fe alloy (60 %).

TABLE II. Dry and wet adhesion (in N mm^{-2}) and percentage of adhesion reduction after one day and 24 days of exposure to 3 % NaCl

		Substrate		
		Steel	Steel + Zn–Fe alloy	Steel + Zn–Co alloy
Dry adhesion		1.9	4.5	4.6
Wet adhesion	one day	1.6	4.2	4.3
	24 days	0.45	1.8	2.8
Adhesion reduction	one day	15.8	6.7	6.5
	24 days	76.3	60	40

The obtained initial values of adhesion strength (dry adhesion, Table II) compare very well with the results obtained using the NMP test (Table I), where it was also shown that the lowest adhesion was obtained for the epoxy coating on the steel substrate.

Surface roughness and wetability

Theoretically, for optimal adhesion, it would be important for the polymer solution to fully penetrate into the pores of the surface layer. Penetration of the polymer solution into the pores on a rough surface, *i.e.*, surface wetability by the polymer solution, depends on the contact angle and the shape of the pores. If these are favorable, which means greater surface roughness and smaller contact angle, *i.e.*, better wetability, a significant penetration may occur at equilibrium.

The values of surface roughness, R_a, on the steel substrate and the steel modified by electrochemically deposited Zn–Co and Zn–Fe alloys are given in Table III. Contact angle, φ, between the polymer solution and the different substrates was determined by the drop test and the results are also given in Table III.

TABLE III. The values of surface roughness, R_a, and contact angle, φ, for epoxy coatings on steel and steel modified by Zn–Co and Zn–Fe alloys

	Substrate		
	Steel	Steel + Zn–Fe alloy	Steel + Zn–Co alloy
R_a / μm	0.250	1.77	0.913
φ / °	45	10	Complete

The high value of surface roughness for the steel modified by Zn–Co alloy and the complete wetability by the epoxy emulsion could explain the good initial adhesion of this protective system. On the other hand, the large contact angle on

the steel surface, indicating the poor wetability of this substrate, together with the smallest surface roughness result in poor bonding of the epoxy emulsion with the steel surface and, as a consequence, the smallest adhesion was obtained for this protective system (Tables I and II, Fig. 1). A higher value of R_a but also a larger φ, results in almost the same value of dry adhesion (Table II).

The better adhesion of the epoxy coating on steel modified by Zn alloys compared to the same epoxy coating on steel can be explained as follows. Namely, it is well known the metal surfaces are generally covered with oxides and contain some hydrated polar groups, which is favorable in respect to bonding to an organic coating. In order to wet the surface and bond to the metallic substrate, polar primers require an oxide layer. It is well known that hot-dip galvanized steel, *i.e.,* Zn coatings, and Zn alloy coatings form zinc oxide and zinc hydroxide on their surfaces immediately after galvanizing. The results shown in Fig. 1 and Tables I and II indicate that bonds between the epoxy coating used in this work and zinc oxide and/or zinc hydroxide are stronger than the ones formed with iron oxides, which normally cover a steel surface.

Electrochemical properties

The Nyquist plots for the impedance of the epoxy coatings electrodeposited on steel and steel modified by Zn–Co and Zn–Fe alloys on the first day (after 2 hours) and after 8 days of exposure to 3 % NaCl are shown in Figs. 2 and 3, respectively. It can be seen from Figs. 2 and 3 that the epoxy coating on steel modified by Zn–Co alloy has larger values of the pore resistance than the epoxy coating on steel and steel modified by Zn–Fe alloy.

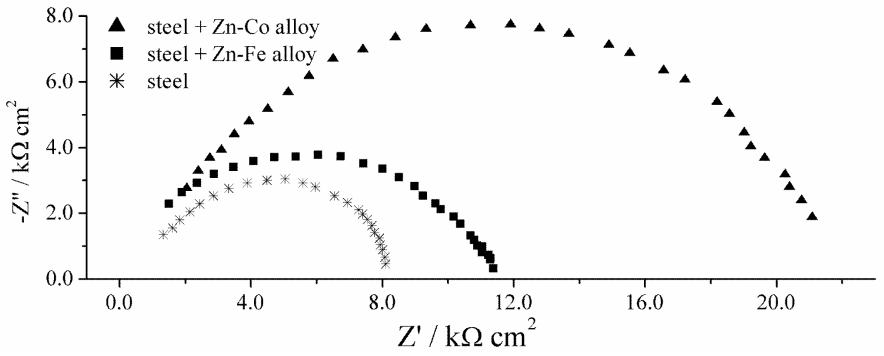

Fig. 2. Nyquist plots for epoxy coatings on steel and steel modified by Zn–Co and Zn–Fe alloys, on the first day of exposure to 3 % NaCl.

A general equivalent electrical circuit model for the behavior of polymer-coated metal in corrosive environments was used (Fig. 4),[15,16] where R_Ω is the electrolyte resistance, R_p is the coating pore resistance, C_c is the coating capacitance, R_{ct} is the charge transfer resistance and CPE is a constant phase element,

which represents all the frequency-dependent electrochemical phenomena, namely the double-layer capacitance and diffusion processes. The fitting of experimental data obtained using the procedure elaborated by Boukamp[14] enabled the determination of the pore resistance, R_p for the films formed on steel and steel modified by Zn alloys. The values of pore resistance for different protective systems, as a function of time of exposure to 3 % NaCl, are given in Table IV.

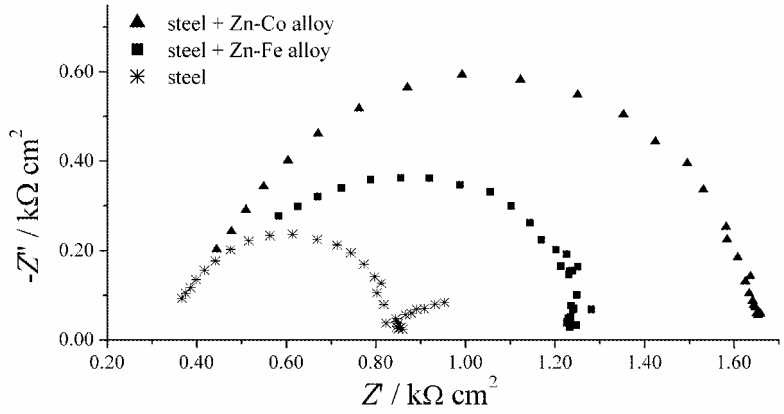

Fig. 3. Nyquist plots for epoxy coatings on steel and steel modified by Zn–Co and Zn–Fe alloys, after 8 days of exposure to 3 % NaCl.

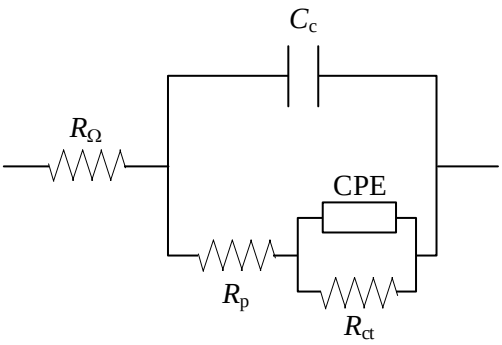

Fig. 4. Equivalent electrical circuit of a polymer-coated metal.

It can be seen that the values of the pore resistance for the epoxy coating on steel modified by Zn–Co alloy are larger compared to the epoxy coating on steel and steel modified by Zn–Fe alloy, indicating again the good corrosion stability of this protective system. This result is in good agreement with the adhesion measurements (Fig. 1, Tables I and II), where it was shown that this protective system had the highest adhesion values.

The smaller values of the pore resistance for the epoxy coating on Zn–Fe alloy as compared to the epoxy coating on Zn–Co alloy can be explained by local heating of the Zn–Fe cathode during the deposition of the epoxy coating, which could cause cratering of the epoxy coating. Namely, it is well known that a zinc

and zinc alloy-plated cathode attain higher temperatures during deposition as compared to a steel cathode, with a tendency for some erratic temperature variation, caused by local film ruptures (cratering).[17] Such a local heating of the cathode during the deposition process causes the formation of different structure of electrodeposited epoxy coating on zinc and zinc alloy-plated cathode as compared to the steel substrate, where local heating is significantly lower.[17,18] The results of Schoff[19,20] indicate that there is a greater tendency to crater over Zn–Fe alloy than over galvanized steel, Zn–Ni alloy and steel.

TABLE IV. The values of pore resistance, R_p, for epoxy coatings on steel and steel modified by Zn–Fe and Zn–Co alloy, during exposure to 3 % NaCl

Substrate	R_p / Ω cm^2		
	1st day	After 8 days	After 24 days
Steel	4365	316	250
Steel + Zn–Fe alloy	7586	562	282
Steel + Zn–Co alloy	13183	891	350

Another reason for the smaller values of the pore resistance for the epoxy coating on Zn–Fe alloy is blistering, since in the case of organic coatings on Zn–Fe alloys the presence of blisters is possible.[21] In the case of the investigated epoxy coating on Zn–Fe alloy, blisters were visible after about one week of exposure to 3 % NaCl. It was shown that the corrosion products in the protective system Zn–Fe alloy/organic coating consist of Fe_3O_4,[21] which probably lift the organic coating from the substrate and cause blister formation underneath. The more porous an organic coating is, the more easily will an electrolyte penetrate it, thus reaching the metal substrate below, *i.e.*, Zn–Fe alloy. Consequently, corrosion process will occur sooner and adhesion of the epoxy coating to the alloy substrate will be weakened. For this reason, a sharp decrease in the adhesion of the epoxy coating on Zn–Fe alloy occurs after 7 days of exposure to 3 % NaCl solution (Fig. 1).

The third reason of increased corrosion stability of epoxy coating on steel modified by Zn–Co alloy as compared to epoxy coating on steel modified by Zn–Fe alloy is the greater corrosion stability of Co as compared to Fe. Namely, the corrosion rate of pure Co in sea water is ten times slower then corrosion rate of pure Fe under the same conditions.[22] Since the amount of both Co and Fe in the alloys was ≈ 1.2 wt. %,[23] the amount of Co and Fe in the alloy is not the determining factor of the corrosion stability of an alloy, but rather the stability of the element itself.

All these results indicate a greater corrosion stability of the protective system based on the epoxy coating on steel modified by Zn–Co alloy.

CONCLUSIONS

Using EIS, pull-off adhesion measurements and the NMP test, the corrosion stability of an epoxy coating on steel and steel modified by electrodeposited Zn–Co

and Zn–Fe alloys were monitored during exposure to 3 % NaCl. It was shown that the substrate has a large influence on the corrosion resistance and adhesion strength of the protective systems based on an epoxy coating. The increased adhesion strength and higher values of the pore resistance for the epoxy coating on steel modified by Zn–Co alloy compared to the epoxy coating on steel and steel modified by Zn–Fe alloy indicate its higher corrosion stability.

The Zn–Co deposit on steel increased both the dry and wet adhesion strength of the epoxy coating. The overall increase in wet adhesion for this sample was maintained throughout the whole investigated time period.

The EIS results correlate well with the adhesion values obtained with both the pull-off and NMP test. The largest values of pore resistance were obtained for the epoxy coating on steel modified by Zn–Co alloy, then for the epoxy coating on steel modified by Zn–Fe alloy and the lowest values for the epoxy coating on steel. The adhesion strength decreased in the same manner.

Acknowledgement. This research was financed by the Ministry of Science of the Republic of Serbia, contract No. 142061.

ИЗВОД

АДХЕЗИЈА ЕПОКСИДНИХ КАТАФОРЕТСКИХ ПРЕВЛАКА НА ЛЕГУРАМА ЦИНКА

ЈЕЛЕНА Б. БАЈАТ[1], ВЕСНА Б. МИШКОВИЋ–СТАНКОВИЋ[1] и ДРАГУТИН М. ДРАЖИЋ[2]

[1]Технолошко–металуршки факултет, Универзитет у Београду, п. пр. 3503, 11120 Београд и [2]ИХТМ–Центар за електрохемију, п. пр. 815, Београд

Један од најважнијих фактора у заштити од корозије органским превлакама је губитак адхезије органских превлака под утицајем корозионе средине. У овом раду проучавана је адхезија епоксидних катафоретских превлака на челику и челику модификованом легурама Zn–Fe и Zn–Co. Испитиване су тзв. сува и мокра адхезија стандардним pull-off поступком, као и NMP тестом. Корозиона стабилност свих узорака је испитивана спектроскопијом електрохемијске импеданције. Сви узорци су имали добру почетну адхезију, међутим током деловања корозионог агенса (3 % NaCl) промена адхезије се значајно разликовала код различитих заштитних система. Најмање вредности адхезије су добијене у случају епоксидне превлаке на челику. Укупно смањење адхезије током 24 дана испитивања је најмање за епоксидну превлаку на челику модификованом Zn–Co легуром. Највеће вредности отпорности у порама епоксидне превлаке током целокупног испитиваног периода деловања корозионог агенса код превлаке на челику модификованом Zn–Co легуром такође указују на велику стабилност овог заштитног система.

(Примљено 22. јануара 2007)

REFERENCES

1. S. Gonzalez, V. Fox, R. M. Souto, *J. Adhesion Sci. Technol.* **18** (2004) 455
2. D. R. Moore, *Surface Coat. Int. B* **84** (2001) 243
3. C. I. Elsner, E. Cavalcanti, O. Ferraz, A. R. Di Sarli, *Prog. Org. Coat.* **48** (2003) 50
4. M. K. Harun, J. Marsh, S. B. Lyon, *Prog. Org. Coat.* **54** (2005) 317

5. R. Ramanauskas, R. Juskenas, A. Kalinicenko, L. F. Garfias-Mesias, *J. Solid State Electrochem.* **8** (2004) 416
6. N. Boshkov, K. Petrov, S. Vitkova, S. Nemska, G. Raichevsky, *Surface Coat. Technol.* **157** (2002) 171
7. N. Boshkov, K. Petrov, D. Kovacheva, S. Vitkova, S. Nemska,, *Electrochim. Acta* **51** (2005) 77
8. J. B. Bajat, A. B. Petrović, M. D. Maksimović, *J. Serb. Chem. Soc.* **70** (2005) 1427
9. R. Ramanauskas, L. Gudavicinte, L. Diaz–Ballote, P. Bartolo–Perez, P. Quintana, *Surface Coat. Technol.* **140** (2001) 109
10. V. Narasimhamurthy, B. S. Sheshadri, *J. Appl. Electrochem.* **26** (1996) 90
11. G. W. Loar, K. R. Romer, T. J. Aoe, *Plat. Surf. Fin.* **3** (1991) 74
12. J. B. Bajat, Z. Kačarević–Popović, V. B. Mišković–Stanković, M. D. Maksimović, *Prog. Org. Coat*. **39** (2000) 127
13. W. J. Van Ooij, R. A. Edwards, A. Sabata, J. Zappia, *J. Adhesion Sci. Technol.* **7** (1993) 897
14. B. Boukamp, *Sol. St. Ionics* **20** (1986) 31
15. J. B. Bajat, M. D. Maksimović, V. B.Mišković-Stanković, S. Zec, *J. Appl. Electrochem.* **31** (2001) 335
16. J. B. Bajat, V. B. Mišković–Stanković, *Prog. Org. Coat*. **49** (2004) 183
17. D. M. Dražić, N. M. Aćamović, O. D. Stojanović, *J. Coat. Technol*. **61** (1989) 27
18. N. M. Aćamović, D. M. Dražić, V. B. Mišković–Stanković, *Prog. Org. Coat*. **25** (1995) 293
19. C. K. Schoff, *J. Coat. Technol*. **62** (1990) 115
20. C. K. Schoff, H.–Y. Chen, *J. Oil Col. Chem. Assoc.* **69** (1985) 185
21. K. Nishimura, Y. Miyoshi, T. Hada, in *Proceedings of Symposium on Corrosion Protection by Organic Coatings*, M. W. Kendig, H. Leidheiser Jr., Eds., Vol. 87-2, Electrochemical Society, Pennington, N.J., 1987, p. 140
22. F. L. LaQue, H. R. Copson, *Corrosion Resistance of Metals and Alloys*, Reinhold Publishing Corporation, New York, USA, 1963, Ch. 2
23. J. B. Bajat, *PhD Thesis*, Faculty of Technology and Metallurgy, Belgrade, 2003 (in Serbian).

Journal of the Serbian Chemical Society
JSCS@tmf.bg.ac.yu • www.shd.org.yu/JSCS

J. Serb. Chem. Soc. 72 (12) 1393–1402 (2007)
JSCS–3671

UDC 544.773.42+546.82–31:620.197.5
Original scientific paper

Sol-gel prepared active ternary oxide coating on titanium in cathodic protection

VLADIMIR V. PANIĆ[1*#] and BRANISLAV Ž. NIKOLIĆ[2#]

[1]*ICTM – Center for Electrochemistry, Njegoševa 12, 11000 Belgrade and* [2]*Faculty of Technology and Metallurgy, University of Belgrade, Karnegijeva 4, P.O.Box 3503, 11120, Belgrade, Serbia*

(Received 24 July 2007)

Abstract: The characteristics of a ternary oxide coating, on titanium, which consisted of TiO_2, RuO_2 and IrO_2 in the molar ratio 0.6:0.3:0.1, calculated on the metal atom, were investigated for potential application for cathodic protection in a seawater environment. The oxide coatings on titanium were prepared by the sol-gel procedure from a mixture of inorganic oxide sols, which were obtained by forced hydrolysis of metal chlorides. The morphology of the coating was examined by scanning electron microscopy. The electrochemical properties of activated titanium anodes were investigated by cyclic voltammetry and polarization measurements in a H_2SO_4- and NaCl-containing electrolyte, as well as in seawater sampled on the Adriatic coast in Tivat, Montenegro. The anode stability during operation in seawater was investigated by the galvanostatic accelerated corrosion stability test. The morphology and electrochemical characteristics of the ternary coating are compared to that of a sol-gel-prepared binary $Ti_{0.6}Ru_{0.4}O_2$ coating. The activity of the ternary coating was similar to that of the binary $Ti_{0.6}Ru_{0.4}O_2$ coating in the investigated solutions. However, the stability in seawater is found to be considerably greater for the ternary coating.

Keywords: ruthenium-oxide-based coatings, sol-gel procedure, iridium oxide, cathodic protection, stability.

INTRODUCTION

Due to the good activity of RuO_2-based anodes for the chlorine evolution and oxygen reaction,[1–3] they are commercially widely applied in cathodic protection processes.[4]

The most often employed electrochemical protecting systems for steel constructions sunk in seawater include organic protective coatings and cathodic protection.[5,6] Although protection by sacrificial anodes is also an aspect of cathodic protection, the concept of impressed-current technology relates to the cathodic

* Corresponding author. E-mail: panic@ihtm.bg.ac.yu
# Serbian Chemical Society member.
doi: 10.2298/JSC0712393P

polarization of the species requiring protection, which are coupled to an anode over an appropriate power source. The protecting procedure by impressed current is one of most efficient since it allows highly automated control of the protection process. Also, it is desirable for the anode material to show high activity for the reactions which occur during protection in a given corrosion medium. In addition, cathodic protection process in seawater should also provide protection against overgrowth by biomaterials, which is realized by the use of anodes possessing a good activity for the chlorine evolution reaction.

Activated titanium anodes are commercially available for application in the cathodic protection of steel constructions in seawater, soil and concrete, as well as pipelines exposed to an aggressive environment.[4] Recently, investigations have considered alternative applications of ruthenium oxide in corrosion protection.[7–10] Darowicki and Janicki[8] improved the properties of a carbon/polyethylene/vinyl acetate composite material as an anode in cathodic protection by the addition of ruthenium oxide. The improvement was related to the increase in activity for the oxygen evolution reaction. Shibli *et al*.[9] increased the erosion stability of Al and Al–Zn sacrificial anodes and their anticorrosion characteristics in NaCl solution by activation of the surface with ruthenium oxide.

In addition to the commercially available activated titanium anodes named LIDA® and LIDA TSA™,[4] platinized titanium anodes (protection of ship hulls),[11] as well as Pb–Ag, Al–Zn and Fe–Si alloys (protection of offshore docks) are used for cathodic protection in seawater.[12–14] However, Ti/Pt anodes are expensive, while anodes made of alloys are of very limited service life due to side reactions of alloy dissolution. Anodes coated with RuO_2 also undergo degradation due to the electrochemical oxidation of Ru species. Since the products of oxidation are soluble, the anode coating is gradually enriched in insulating TiO_2, which leads to passivation of the anode surface. The anode activity for the oxygen evolution reaction, however, appears to play a key role in the process of anode degradation.[15–20] It is known that activated titanium anodes containing iridium oxide are more stable against passivation in the electrolysis of NaCl solutions than a binary RuO_2–TiO_2 coating.[16,21–24] This is due to the slower corrosion rate of IrO_2 with respect to RuO_2, especially when a considerable portion of the current is related to the oxygen evolution reaction.[25] For this reason, activated titanium anodes, commercially available for cathodic protection purposes, contain iridium oxide in small amounts, in addition to ruthenium and titanium oxide. It is to be mentioned that previous studies[18,19,26] postulated the higher activity for the chlorine and oxygen evolution reaction, as well as stability to passivation of $Ti_{0.6}Ru_{0.4}O_2$ coatings on titanium prepared by the sol-gel procedure, when compared to the coating prepared by the usual thermal decomposition of metal chlorides.[1,17] This effect was mostly due to the larger real surface area of the sol-gel prepared coating.

The aim of this work was to investigate the activity and stability of a ternary $Ti_{0.6}Ru_{0.3}Ir_{0.1}O_2$ coating on titanium, prepared by the sol-gel procedure, under

the conditions of the chlorine and oxygen evolution. The anode characteristics were investigated in NaCl and H_2SO_4 solutions as well as in seawater, and compared to the characteristics of a binary $Ti_{0.6}Ru_{0.4}O_2$ coating.

EXPERIMENTAL

Coating Preparation

Colloidal monodispersions of ruthenium, iridium and titanium oxide were obtained by the forced hydrolysis of metal chlorides in boiling 0.27 mol dm^{-3} HCl.[27] The dispersions of RuO_2, IrO_2 and TiO_2 (oxide sols) were formed during 46, 20 and 10 h (ageing times), respectively. These distinct ageing times were chosen to prepare the sols since coatings with the best electrochemical properties were formed from them.[18] The prepared oxide sols were mixed to form ternary or binary dispersions for the preparation of a coating with the desired composition of $Ti_{0.6}Ru_{0.3}Ir_{0.1}O_2$ or $Ti_{0.6}Ru_{0.4}O_2$. The dispersions were painted over Ti plates (1 cm×1 cm×0.89 mm), previously sand-blasted, degreased in saturated NaOH/ethanol solution and etched in hot 20 mass% HCl for 20 min. The coatings were applied in two layers, each converted into the gel phase at 90 ºC and annealed at 450 ºC, the first layer for 10 min and the second for 20 min, which developed the crystal structure of the oxide and provided good coating adhesion. The total coating mass was 1.0 mg cm^{-2} (calculated to the overall oxide).

Coating morphology

The microscopic appearance of the prepared coatings was examined before and after an accelerated stability test (AST) by scanning electron microscopy (SEM), using a JEOL microscope, model JSM-T20 (U_w = 20 kV).

Basic electrochemical properties

The capacitive behavior of the prepared anodes was investigated by cyclic voltammetry in 1.0 mol dm^{-3} H_2SO_4, 0.50 mol dm^{-3} NaCl and in mixtures of these two solutions, at room temperature and a sweep rate of 20 mV s^{-1}. A Pt plate electrode was used as the counter electrode, while the reference electrode was a SCE, and all potentials are referred to the SCE scale.

The polarization characteristics of the prepared oxide coatings, in the solutions used in the cyclic voltammetry measurements and additionally in seawater sampled in the harbor of Tivat, Montenegro, were registered by anodic linear sweep voltammetry at a scan rate of 0.50 mV s^{-1}. The electrochemical cell was the same as that used in the cyclic voltammetry measurements.

Anode stability

The stability of the prepared anodes was investigated in seawater by AST at a current density of 0.60 A cm^{-2} and a temperature of 16 ºC. The end of anode service life was seen as a sudden increase in potential, which is a measure of the anode stability to passivation under the given conditions.

RESULTS AND DISCUSSION

SEM microphotographs of the $Ti_{0.6}Ru_{0.3}Ir_{0.1}O_2$ and $Ti_{0.6}Ru_{0.4}O_2$ coatings prepared by the sol-gel procedure on titanium are shown in Fig. 1. The surfaces of the coating appear like “cracked mud” consisting of islands separated by cracks, with a uniform crack width independent of the coating composition. The island border zone appears brighter than the bulk of islands, which is usually assigned to edge segregation of titanium oxide.[17,28] This effect is more pronounced for $Ti_{0.6}Ru_{0.4}O_2$ than for $Ti_{0.6}Ru_{0.3}Ir_{0.1}O_2$ coating, which indicates more uniform composition (less pronounced TiO_2 edge segregation) of the ternary coating. How-

ever, the main difference in microscopic appearance between the binary and ternary coating should be addressed to the ubiquitous presence of sub-micron-sized spherical grains in the $Ti_{0.6}Ru_{0.3}Ir_{0.1}O_2$ coating (Fig. 1a), which occupy preferentially the hills of the coating (the coating is apparently not of uniform microthickness; the microphotograph in Fig. 1a was taken with a 45° incidence angle). The origin of grains could be assigned to the formation of a separate iridium oxide phase within the ternary coating, since the composition is the single qualitative difference between the binary and ternary coating.

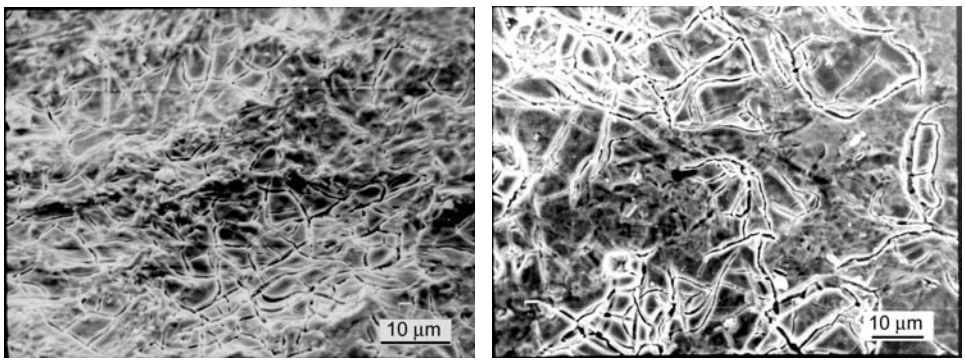

(a) (b)

Fig. 1. SEM Microphotographs of the surface of sol-gel prepared: (a) $Ti_{0.6}Ru_{0.3}Ir_{0.1}O_2$ and (b) $Ti_{0.6}Ru_{0.4}O_2$ coatings on titanium.

Cyclic voltammograms of the prepared anodes, registered in H_2SO_4, H_2SO_4/NaCl and NaCl electrolyte are shown in Fig. 2. The voltammetric curves are of the characteristic shape for RuO_2-based electrodes,[1,17,18,29] which demonstrates the almost pure capacitive behavior of the anodes within the potential region of electrolyte stability.[30] A broad reversible peak appears around the potential of 0.60 V in the proton-containing solutions (Figs. 2A and 2B), which is assigned to the solid state surface redox transition (SSSRT) of Ru with participation of protons.[29,30] The injection/ejection of protons involved in the following SSSRT[29] is seen at potentials below 0.10 V, which causes a pseudocapacitive energy storage (PCES) behavior of the coating in the potential region below 0.10 V (Figs. 2A and 2B). However, both capacitive features SSSRT and PCES are considerably suppressed in pure NaCl electrolyte (Fig. 2C), due to the lack of protons.

The capacitive behavior for the ternary and binary coating in the proton-containing electrolytes were similar (Figs. 2A and 2B). However, the voltammetric currents were lower in NaCl electrolyte for the ternary coating (Fig. 2C), due to the lower pseudocapacitive ability of IrO_2 with respect to RuO_2.[1,30,31]

The voltammogram in H_2SO_4 solution of the binary coating is more tilted due to a higher ohmic resistance (Fig. 2A). This could be caused by the more pronounced non-uniform composition of the binary coating, as seen in Fig. 1. The

coating parts with TiO_2 segregation (island edges) are regions with poor conductivity, since TiO_2 is known for its semi-conductive or insulating properties.[1] Through these regions, the current is carried preferentially by ions which fill the pores of the regions, making the total coating resistance dependent on the electrolyte resistance. As can be seen in Fig. 2B, the voltammograms are less tilted in H_2SO_4/NaCl solution, due to the higher ion concentration and, consequently, lower resistance.

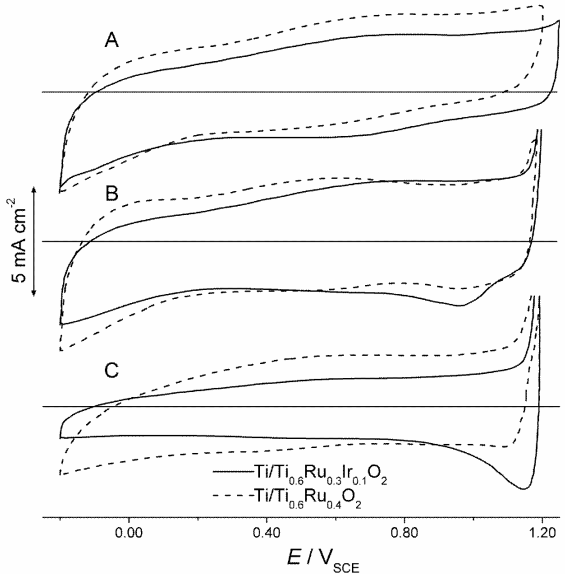

Fig. 2. Cyclic voltammograms of sol-gel prepared Ti/$Ti_{0.6}Ru_{0.3}Ir_{0.1}O_2$ and Ti/$Ti_{0.6}Ru_{0.4}O_2$ anodes registered in 1.0 mol dm^{-3} H_2SO_4 (A), 1.0 mol dm^{-3} H_2SO_4 + 0.50 mol dm^{-3} NaCl (B) and 0.50 mol dm^{-3} NaCl (C) at room temperature and sweep rate of 20 mV s^{-1}.

An increase in the anodic currents is seen in the voltammograms registered in Cl^--containing electrolytes at potentials more positive than 1.15 V (Figs. 2B and 2C), which corresponds to the onset of the chlorine evolution reaction (CER). The increase is followed by the appearance of a cathodic counterpart, assigned to the desorption of chlorine species,[32] at potentials increasing with increasing chloride concentration. The counterpart is more pronounced for the ternary coating. Since the CER commences on the ternary coating at even more positive potential than on the binary one, the more pronounced counterpart could be assigned to the larger surface area of the ternary coating available for chloride oxidation. It is known that IrO_2-containing coatings are more porous than those in which this oxide is not present.[21] Note that the larger surface area of the ternary coating is not visible in the capacitive region due to its already mentioned lower pseudocapacitive ability with respect to the binary coating.

The polarization curves registered in different solutions and in seawater for the Ti/$Ti_{0.6}Ru_{0.3}Ir_{0.1}O_2$ anode are shown in Fig. 3, while those of the Ti/$Ti_{0.6}Ru_{0.4}O_2$ anode are presented in Fig. 4.

The currents of oxygen evolution were registered at the most positive potentials in H_2SO_4 solution (curve 1, Figs. 3 and 4). The Tafel slopes are close to

60 mV, which is the usual value for this type of anodes.[33,34] When chloride ions were introduced into the H_2SO_4 solution, the Tafel plot for the chlorine evolution reaction was registered in the region of lower potentials (curve 2, Figs. 3 and 4). The slopes for both the ternary and binary coating are close to 35 mV, indicating the high activity of oxide coatings for this reaction.35 The slope in NaCl solution (curve 3) was almost doubled when compared to the H_2SO_4/NaCl solution. This is the consequence of the different reaction mechanisms. In acid chloride solution, protons are involved in the oxidation of the active sites, which makes the sites suitable for the adsorption of chlorine species.[36] The chlorine evolution reaction in such circumstances occurs at a lower overvoltage compared to the case in NaCl electrolyte.

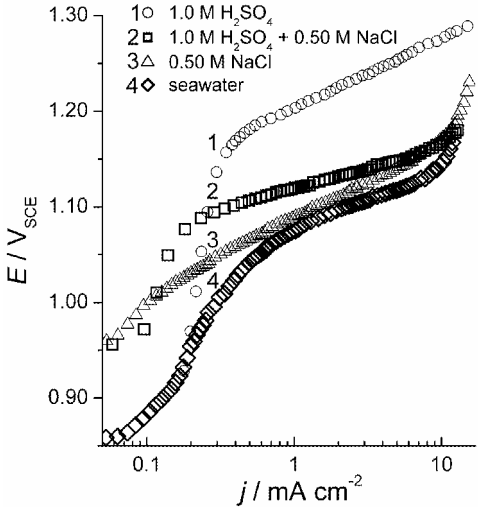

Fig. 3. Polarization curves for a $Ti/Ti_{0.6}Ru_{0.3}Ir_{0.1}O_2$ anode registered in different solutions and in seawater.

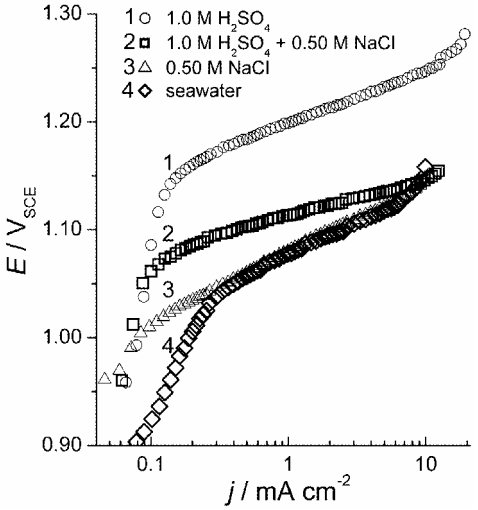

Fig. 4. Polarization curves for a $Ti/Ti_{0.6}Ru_{0.4}O_2$ anode registered in different solutions and in sea water.

The values of the current densities at potentials near the middle of the Tafel region, as registered in different solutions (Figs. 3 and 4), are given in Table I. Almost two times higher values were obtained for the binary coating in proton-containing solutions, while similar values for the binary and ternary coating were registered in NaCl solution and in seawater.

These results can be interpreted from two points of view: one is the dependence of the current on the real surface area and the other is the destruction rate of the oxide. It has already been mentioned in the discussion of the voltammetry results that the ternary coating should be more porous and of larger real surface area than the binary one. This makes the ternary coating more active at low overvoltages, as seen in Figs. 2B and 2C. It is seen also in the polarization curves from Figs. 3 and 4 that the currents were higher for the ternary coating up to

1.05 V_{SCE} and even up to 1.08 V_{SCE} in H_2SO_4/NaCl solution. However, evolved gas fills the coating pores at high overvoltages, which causes a reduction in the charge transfer availability of the coating surface. Since the ternary coating was more active at low overvoltage and particularly because of its more porous structure, the reduction in charge transfer availability should be more pronounced for the ternary than for binary coating. Also, this reduction is more evident in the solution favorable for oxygen evolution, due to the lower solubility of oxygen in comparison to chlorine.

TABLE I. Current densities at given potentials registered for $Ti/Ti_{0.6}Ru_{0.3}Ir_{0.1}O_2$ and $Ti/Ti_{0.6}Ru_{0.4}O_2$ anode in different solutions

Solution	E / V_{SCE}	j / mA cm^{-2}	
		$Ti/Ti_{0.6}Ru_{0.3}Ir_{0.1}O_2$	$Ti/Ti_{0.6}Ru_{0.3}Ir_{0.1}O_2$
1.0 mol dm^{-3} H_2SO_4	1.23	2.30	4.45
1.0 mol dm^{-3} H_2SO_4 + 0.50 mol dm^{-3} NaCl	1.13	1.73	3.02
0.50 mol dm^{-3} NaCl	1.10	1.86	2.00
Seawater	1.10	2.46	2.56

At higher overvoltages appreciable partial currents of the electrochemical dissolution of active oxide are to be expected.[15,22,23] It is known that the destruction rate and, consequently, the partial currents of dissolution in anodic polarization are lower for IrO_2 when compared to those of RuO_2.[22,23] This was registered as lower overall current densities at high overvoltages (Figs. 3 and 4).

The good activity of the prepared anodes in seawater is important for their application in cathodic protection. The AST results for both the ternary and binary coating are shown in Fig. 5 as the time dependence of the anode potential at a constant current density. Since IrO_2 is more stable during the simultaneous evolution of oxygen and chlorine, the durability of the ternary coating is longer than that of the binary coating.

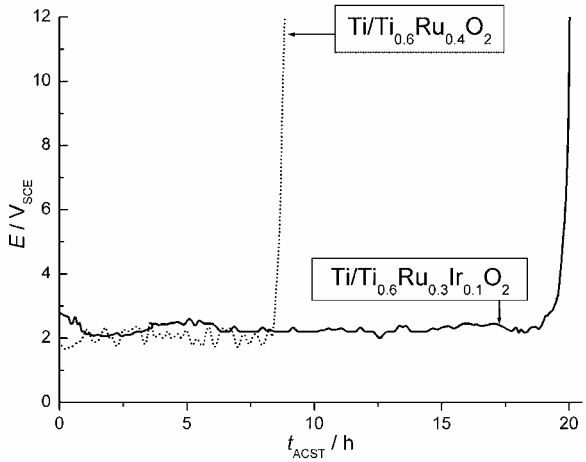

Fig. 5. Time dependences of the potential of a $Ti/Ti_{0.6}Ru_{0.3}Ir_{0.1}O_2$ and $Ti/Ti_{0.6}Ru_{0.4}O_2$ anode during the accelerated stability test in seawater at a current density of 0.60 A cm^{-2}.

A tentative explanation for considerably larger stability of the ternary coating could be as follows. The reactions of RuO_2 dissolution and oxygen evolution precede in parallel.[15] The mechanism for RuO_2 dissolution could be:

$$RuO_2 + H_2O \rightarrow RuO_2{-}OH + H^+ + e^- \quad (1)$$

$$RuO_2{-}OH \rightleftharpoons RuO_3 + H^+ + e^- \quad (2)$$

$$RuO_3 + H_2O \rightleftharpoons RuO_3{-}OH + H^+ + e^- \quad (3)$$

$$RuO_3{-}OH \rightleftharpoons RuO_4 + H^+ + e^- \quad (4)$$

while for oxygen evolution reaction proposed mechanism[15] suggests that steps (3) and (4) should be replaced by:

$$2RuO_3 \rightleftharpoons 2RuO_2 + O_2 \quad (5)$$

The steps (1) and (2) are the same for the two reactions, with the formation of $RuO_2{-}OH$, step (1), as the rate-determining step. The species in the subsequent steps (3)–(5) decompose giving either oxygen or RuO_4, which is soluble in acid solutions. However, when IrO_2 is present in the coating, oxygen evolution occurs mainly at the IrO_2 active sites. This hinders the decomposition reactions on the RuO_2 active sites and considerably extends the service life of the coating.

The effect of selective coating dissolution can be seen on SEM microphotographs given in Fig. 6, which illustrates the typical appearance of the ternary and binary coating after AST. Fig. 6a illustrates the appearance of the ternary coating along the hills at which the segregation if IrO_2 was seen on the freshly prepared coating (Fig. 1a). Complete depletion of the active material can be seen in the valleys of the coating, while it is retained to a great extent on the hills. This supports the conclusion that IrO_2 grains suppress the corrosion of the active material, while RuO_2-rich regions corrode faster. On the other hand, the binary coating corrodes uniformly, with depleted regions appearing from place to place.

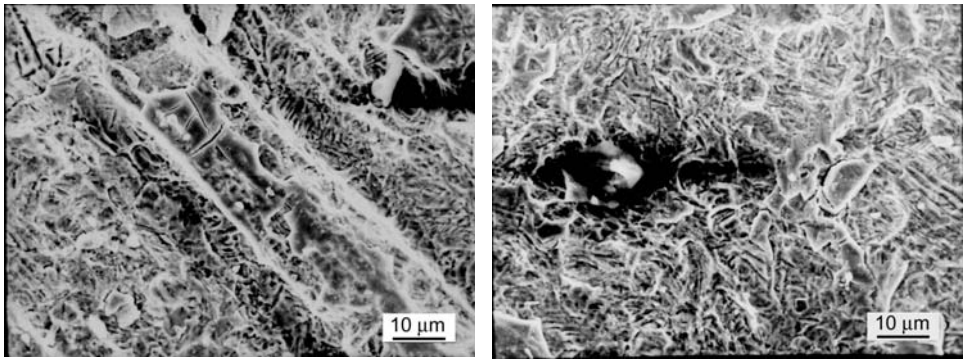

(a) (b)

Fig. 6. SEM Microphotographs of the surface of sol-gel prepared: a) $Ti_{0.6}Ru_{0.3}Ir_{0.1}O_2$ and b) $Ti_{0.6}Ru_{0.4}O_2$ coatings on titanium taken after the accelerated corrosion stability test.

CONCLUSIONS

The properties of sol-gel prepared ternary $Ti_{0.6}Ru_{0.3}Ir_{0.1}O_2$ and binary $Ti_{0.6}Ru_{0.4}O_2$ coatings on titanium with respect to their possible application for cathodic protection in seawater environments were investigated by scanning electron microscopy, cyclic voltammetry, polarization measurements and accelerated stability test in H_2SO_4 and NaCl solutions as well as in seawater.

The microscopic appearance of the ternary coating indicates segregation of IrO_2 in the sub-micron grains in the region of the hills in the coating.

Cyclic voltammetry investigations showed similar capacitive behavior of the ternary and binary coating, while the ternary coating seemed to be more active for chlorine evolution.

The polarization characteristics of the prepared coatings indicated similar activity of the ternary and binary coating in H_2SO_4, H_2SO_4/NaCl and NaCl solutions, while the partial currents related to the dissolution of the active material of the ternary coating was less pronounced than in the case of the binary coating at high overvoltages.

The results of an accelerated stability test of the prepared coatings showed that the ternary coating was considerably more stable during exploitation in seawater than the binary one, which is the consequence of the greater stability of IrO_2 under vigorous oxygen and chlorine evolution in comparison to RuO_2. This fact makes the ternary coating a better candidate as the anode in real applications.

Acknowledgement. This work was financially supported by the Ministry of science of the Republic of Serbia, Contract No. 142061B.

ИЗВОД

АКТИВНА ОКСИДНА ПРЕВЛАКА НА ТИТАНУ ДОБИЈЕНА СОЛ-ГЕЛ ПОСТУПКОМ КАО АНОДА ЗА КАТОДНУ ЗАШТИТУ У МОРСКОЈ ВОДИ

ВЛАДИМИР ПАНИЋ[1] и БРАНИСЛАВ НИКОЛИЋ[2]

[1]ИХТМ – Центар за електрохемију, Његошева 12, п. пр. 815, 11000 Београд и [2]Технолошко–металуршки факултет, Карнегијева 4, п.пр. 35-03, 11122 Београд

Карактеристике тројне оксидне превлаке на титану, која се састоји од TiO_2, RuO_2 и IrO_2 у молском односу 0.6:0.3:0.1 рачунато на атом метала, испитиване су са циљем потенцијалне примене за катодну заштиту у морској води. Оксидна превлака на титану формирана је сол-гел поступком из смеше неорганских оксидних солова, који су добијени форсираном хидролизом хлорида метала. Морфологија превлаке је испитивана скенирајућом електронском микроскопијом, док су електрохемијска својства активираних титанких анода испитивана методом цикличне волтаметрије и поларизационим мерењима у растворима H_2SO_4, NaCl и у реалним условима, у морској води узоркованој из Јадранског мора (Тиват, Црна Гора). Стабилност аноде током рада у морској води испитивана је галваностатски, убрзаним тестом стабилности. Добијене превлаке упоређене су са двојном $Ti_{0,6}Ru_{0,4}O_2$ превлаком, у погледу морфологије и електрохемиских карактеристика. Показано је да су тројна и двојна превлака сличне активности у испитиваним растворима. Међутим, у морској води стабилност тројне превлаке је знатно већа.

(Примљено 24. јула 2007)

REFERENCES

1. S. Trasatti, W. O'Grady in: *Advances in Electrochemistry and Electrochemical Engineering*, H. Gerisher, C. W. Tobias, Eds., Wiley, New York, 1981, p. 177
2. S. Trasatti, in *Interfacial Electrochemistry – Theory, Experiment and Applications*, A. Wieckowski, Ed., Marcel Dekker Inc., New York, 1999, p. 769
3. A. Cornell, F. Herlitz, in *Proceedings of the 4th Kurt Schwabe Corrosion Symposium*, Helsinki, Finland, *Proceedings*, (2004), p. 326
4. De Nora elettrodi network, http://www.lidaproducts.com (23.07.2007)
5. S. Eliassen, *Corr. Eng. Sci. Technol.* **39** (2004) 31
6. J.-L. Pey, *Anti-Corr. Methods Mater.* **44** (1997) 94
7. D. Tao, G. L. Chen, B. K. Parekh, *Minerals Eng.* **18** (2005) 481
8. K. Darowicki, S. Janicki, *Corr. Sci.* **41** (1999) 1165
9. S. M. A. Shibli, V. S. Gireesh, S. George, *Corr. Sci.* **46** (2004) 819
10. D. H. Kroon, L. M. Ernes, *Mater. Performance* **46** (2007) 26
11. A. O. Akomah, J. S. Dahele, D. J. Tighe-Ford, *British Corr. J.* **37** (2002) 114
12. J. Morgan, *Cathodic Protection*, 2nd Ed., NACE International, Houston TX., 1987
13. W. von Beaeckmann, W. Schwenk, W. Prinz, *Handbook of Cathodic Corrosion Protection*, Elsevier, Amsterdam, 1997
14. M. A. Kazraef, *J. Corr. Sci. Eng.* **9** (2006) 1
15. Lj. M. Gajić-Krstajić, T. Lj. Trišović, N. V. Krstajić, *Corr. Sci.* **46** (2004) 65
16. G. N. Martelli, R. Ornelas, G. Faita, *Electrochim. Acta* **39** (1994) 1551
17. V. Jovanović, A. Dekanski, P. Despotov, B. Nikolić, R. Atanasoski, *J. Electroanal. Chem.* **339** (1992) 147
18. V. Panić, A. Dekanski, S. Milonjić, R. Atanasoski, B. Nikolić, *Electrochim. Acta* **46** (2000) 415
19. V. Panić, A. Dekanski, V. B. Mišković–Stanković, S. Milonjić, B. Nikolić, *J. Electroanal. Chem.* **579** (2005) 67
20. F. Beck, *Electrochim. Acta* **34** (1992) 811
21. J.-M. Hu, J.-Q. Zhang, C.-N. Cao, *Inter. J. Hydrogen Ener.* **29** (2004) 791
22. V. V. Gorodetskii, V. A. Neburchilov, V. I. Alyab'eva, *Russ. J. Electrochem.* **41** (2005) 1111
23. V. I. Eberil', E. A. Novikov, A. F. Mazanko, *Russ. J. Electrochem.* **37** (2001) 1054
24. T.-X. Cai, H. Chen, H. Ju, L.-N. Lu, *Corr. Potection* **27** (2006) 522
25. M. G. Pavlović, A. B. Dekanski, *J. Solid State Electrochem.* **1** (1997) 208
26. V. Panić, A. Dekanski, S. Milonjić, V. B. Mišković–Stanković, B. Nikolić, *J. Serb. Chem. Soc.* **71** (2006) 1173
27. V. Panić, A. Dekanski, S. Milonjić, R. Atanasoski, B. Nikolić, *Colloids Surf. A* **157** (1999) 269
28. K. Komeyama, S. Shohji, S. Onoue, K. Nishimura, K. Yahikozawa, Y. Takasu, *J. Electrochem. Soc.* **140** (1993) 1034
29. S. Ardizzone, S. Trasatti, *Adv. Colloid Interface Sci.* **64** (1996) 173
30. B. Conway, *Electrochemical Supercapacitors – Scientific Fundamentals and Technological Applications*, Plenum Publishers, New York, 1999
31. S. Trasatti, *Electrochim. Acta* **36** (1991) 225
32. L. Tomcsányi, A. de Battisti, G. Hirschberg, K. Varga, J. Liszi, *Electrochim. Acta* **44** (1999) 2463
33. G. Lodi, E. Sivieri, A. De Battisti, S. Trasatti, J. *Appl. Electrochem.* **8** (1978) 135
34. C.-C. Chang, T.-C. Wen, *J. Appl. Electrochem.* **27** (1997) 355
35. L. Krishtalik, *Electrochim. Acta* **26** (1981) 329
36. J. L. Fernández, M. R. G. de Chialvo, A. C. Chialvo, *Electrochim. Acta* **47** (2002) 1129.

Journal of the Serbian Chemical Society
JSCS@tmf.bg.ac.yu • www.shd.org.yu/JSCS

J. Serb. Chem. Soc. 72 (12) 1403–1418 (2007) UDC 546.57'82–31+544.4.004.12:66.094.1:66.087+546.57
JSCS–3672 *Original scientific paper*

Tailoring the morphology and electrocatalytic properties of electrochemically formed Ag/TiO_2 composite deposits on titanium surfaces

S. V. MENTUS[1*#], I. BOŠKOVIĆ[2], J. M. PJEŠČIĆ[2], V. GRUDIĆ[2] and Ž. BOGDANOV[3]

[1]*Faculty of Physical Chemistry, University of Belgrade, Studentski trg 16, 11000 Belgrade, Serbia,* [2]*Faculty of Metallurgy and Technology, Podgorica University, 81000 Podgorica, Montenegro and* [3]*Vinča Institute of Nuclear Sciences, 11001 Belgrade, Serbia*

(Received 14 May 2007)

Abstract: Three different forms of Ag/TiO_2 composite layers, which have whisker-, dot- and island-like distribution of silver were obtained on a mechanically polished titanium surface by adjusting the conditions of silver deposition from an aqueous $AgNO_3$ solution. The deposit morphology was the result of both the program of electrode polarization and the template action of the simultaneously formed TiO_2 layer. The catalytic activity of the composite layers toward the oxygen reduction reaction was studied in aqueous 0.1 M NaOH solutions and found to be a function of both the surface loading of silver and the type of silver distribution within the Ag/TiO_2 composite layers. The reaction path of oxygen reduction on the composite layers was found to be always a $4e^-$ one, characteristic otherwise of polycrystalline silver electrodes.

Keywords: metal/oxide composite electrocatalysts, oxygen reduction reaction, rotating disc electrode, silver electrodeposition, titanium dioxide film.

INTRODUCTION

Heterogeneous systems consisting of small metal particles dispersed on electronic conductor, semiconductor and ionic conductor supports, display a number of interesting properties of both fundamental and applicative significance. By dispersing catalytically active metal over a high-surface-area support, its utilization may be enhanced simply based on the increase of the real surface area on which an electrochemical process, otherwise heterogeneous in nature, occurs. Metal–semiconductor heterogeneous systems are of significant interest in optics, electrophysics, catalysis, *etc.*[1] On going to nano-dispersions, quite new effects, characteristic of individual atoms, may also be experienced. For instance, Ng *et al.*[2] investigated the particular electrochemical behaviour of nano-dispersed sil-

* Corresponding author. E-mail: slavko@ffh.bg.ac.yu
# Serbian Chemical Society member.
doi: 10.2298/JSC0712403M

ver on carbon black, manifested as both a cathodic shift of the equilibrium potential and an aggravated anodic dissolution.

Polycrystalline silver shows a high catalytic effectiveness in electrochemical oxygen reduction in alkaline solutions.[3] McIntyre *et al.*[4] evidenced a four-electron reduction mechanism of oxygen reduction on all silver crystallographic planes in alkaline solutions. Following this knowledge, Hacker *et al.*[5] and Yang *et al.*[6,7] investigated the oxygen reduction reaction in alkaline solutions using nano-dispersed silver supported by carbon nano-fibres[5] and carbon black.[6,7] Chatenet *et al.* compared the catalytic effectiveness of carbon-supported silver[8] and bimetallic silver-platinum[9] catalysts with that of pure bulk platinum. Carbon supported silver was proposed to replace carbon supported platinum as the cathode material in fuel cells, metal–air batteries[10] and electrolysers for chlorine production.[11]

High surface area is not a unique benefit of supported metal catalysts in electrocatalysis. Another one may be the so-called strong metal–support interaction (SMSI), which enhances the catalytic effectiveness of a catalytically active metal. This effect was observed in systems of noble metals supported by reducible VIII group metal oxides, primarily TiO_2.[12–19]

The metal oxide films were synthesized preferably by thermal decomposition of thermodegradable compounds of titanium and catalytically active metals. Beer,[20] for instance, applied a RuO_2 coating on a Ti surface by thermal decomposition of $RuCl_3$. Haruta *et al.*[16–18,21] evidenced high catalytic effectiveness of a nano-Au/TiO_2 composite catalyst for CO oxidation at low temperatures, although each of the components alone is catalytically ineffective. This finding was given as an example of the SMSI effect. These authors prepared the catalyst by precipitation of Au(III)-hydroxide onto TiO_2 powder, with the subsequent reduction of the Au hydroxide by heating in a hydrogen atmosphere. Burrows *et al.*,[22] Kuhn *et al.*,[23] Kalinovski *et al.*[24] and Erenberg *et al.*[25] synthesized RuO_2–TiO_2 and RuO_2–TiO_2–IrO_2 layers on a Ti surface, known as effective composite catalysts in the oxidation of chloride. Some papers describe electrochemical procedures to deposit catalytically active metal on titanium. For instance, Vuković *et al.*[26–28] deposited noble metals and their alloys on a titanium surface galvanostatically and obtained very developed deposits. Mentus[29] deposited a Pt/TiO_2 layer potentiodynamically and outlined the template action of TiO_2. Emery *et al.*[30] studied the kinetics of cathodically induced nucleation of copper on nickel and tantalum surfaces.

Proceeding from the fact that bulk silver[3,4] and silver dispersed on a carbon support[5–8] are effective catalysts for the reduction of oxygen in alkaline solutions and that the electrochemical deposition of metals on a titanium surface provides highly developed surfaces,[26–29] an electrochemically formed Ag/TiO_2 composite was selected for detailed study. In continuation of a previous study of this composite formed by a definite program of potentiodynamic polarization,[31] and bear-

ing in mind the possible template action of a TiO_2 layer,[29] an attempt was made to enlarge the possibilities to control both the morphology and the catalytic effectiveness of electrochemically formed layers, by expanding the modes of silver deposition. In both deaerated and oxygen-saturated aqueous 0.1 M NaOH solution, the electrochemical behaviour of the obtained Ag/TiO_2 composite layers was examined and compared to that of a bulk polycrystalline silver electrode.

EXPERIMENTAL

The electrochemical cell was a double-walled thermostated glass cell, with the electrodes and gas inlet tube immersed through tight, machined orifices on the plastic top cover. The working electrode support was a rod of titanium 3 mm in diameter, pressed into a PTFE insulating cylinder, being the detachable part of a rotating electrode. The reference electrode was a commercial Beckman saturated calomel electrode (SCE). The counter electrode was a platinum foil. The reference electrode was separated from the bulk electrolyte by a Luggin capillary filled with the investigated electrolyte.

The solutions were made from Merck or Aldrich p.a. chemicals and redistilled water, which were either deaerated by an argon stream or oxygen-saturated by flowing gaseous oxygen. The purity of the gases was 99.999 vol. %.

The dc measurements were performed using a PAR Model 273 Potentiostat/Galvanostat. The rotation speed of the working electrode was controlled by a Beckman rotating electrode device. The electrolyte temperature was always kept at 25 °C.

To prepare the working electrode for electrochemical investigations, the exposed, disk-shaped Ti surface was dry-cleaned with emery paper No. 1200, and plated with silver from a dilute aqueous x M $AgNO_3$ + 0.1 M $KClO_4$ solution, either at a constant potential of −0.4 V *vs*. SCE, or by potentiodynamic cycling. Simultaneously, a TiO_2 layer was grown either spontaneously, by corrosion[32] or because of potentiodynamic polarization.

The microphotographs of the composite Ag/TiO_2 layers were taken by scanning electron microscope, Jeol JSM-840A.

RESULTS AND DISCUSSION

Cyclic voltammetry of freshly polished titanium in aqueous $AgNO_3$ solutions and the modes of formation Ag/TiO_2 composite layers

As a valve metal, under usual conditions, titanium is covered by a spontaneously formed semi-conductive oxide layer, which permits electrochemical reduction reactions[33] and suppresses oxidation ones.[34] If formed by anodic oxidation, the thickness of the oxide layer is closely related to the final anodic potential.[32] Electrochemical deposition of any metal on a titanium surface is always influenced by either the spontaneous or electrochemical formation of TiO_2, diminishing the adherence or directing the sites of preferential electrodeposition.[29] In order to test the conditions of silver deposition from the solution 1.76×10^{-2} M $AgNO_3$ in 0.1 M $KClO_4$ as supporting electrolyte, cyclic voltammograms of a freshly polished titanium electrode were recorded in this solution. The potential interval used, *i.e.*, between −0.4 and 0.8 V, as shown in Fig. 1, covers the range of cathodic deposition and anodic dissolution. The first scan reflects both silver

nuclei formation and growth of a TiO_2 layer. Since TiO_2 formation was completed within the first anodic sweep, usually not more than three polarization cycles were required to achieve voltammograms of reproducible shape. The voltammograms in Fig. 1 indicate that the reversible potential of a silver electrode in this solution is 0.35 V *vs.* SCE. Bearing in mind that TiO_2 does not permit anodic processes on its surface, the pronounced current of anodic dissolution shown in Fig. 1 evidences that most of the deposited silver is in electronic contact with the titanium support. Good contact, providing for both good anodic dissolution and reproducible voltammograms, may be achieved if the starting potential is as close as possible to the open circuit potential of metallic titanium, which is below −1 V in neutral aqueous solutions. Such a negative starting potential may enable silver nuclei to form on almost bare metal surface. Higher starting potentials cause an instantaneous growth of TiO_2, the thickness of which is closely correlated to the highest value of the anodic potential.[31,32] The study of Emery *et al.*[30] illustrates the consequences of the formation of such an oxide interlayer. These authors studied copper deposition on tantalum, starting the potentiodynamic polarization from the anodic side of the potential interval they studied. In such a manner, they formed an oxide layer prior to the commencement of electrocrystallisation of copper. In the case of the formation of this oxide layer, copper was easily deposited cathodically and accumulated in each polarization cycle, however, the anodic dissolution was almost completely blocked. In addition, Poroshkov *et al.*[1] reported a significant asymmetry between the current consumptions for the cathodic and anodic processes, in favour of the cathodic process, during silver deposition and dissolution on an anodised Ti surface.

The first type of Ag/TiO_2 deposit, labelled in this study as composite layer type I, presented in Fig. 2, was prepared by immersing a freshly polished titanium surface in solution 1.7×10^{-2} M $AgNO_3$ + 0.1 M $KClO_4$, and instantaneously subjecting it to a constant potential of −0.4 V *vs.* SCE. According to the voltammograms in Fig. 1, this potential corresponds to the limiting diffusion current of silver deposition from an unstirred solution. However, this potential allows the instantaneous formation of a TiO_2 film, about 1 nm thick. It is reasonable to expect that various imperfections caused by mechanical polishing and chemical impurities result in non-uniformity in the thickness of the layer in its initial stage of development, whereby nucleation of silver is favoured at the sites covered with a thinner TiO_2 layer. This causes a non-uniform surface coverage, *i.e.*, favoured sites of silver crystals development or, in other words, a template effect of the TiO_2 layer. During 30 s of silver deposition, the current increased almost linearly from 0 up to 1.4 mA cm^{-2}. According to the Faraday law, it is easy to calculate that the number of coulombs consumed in this procedure generates a surface loading by silver of 24 μg cm^{-2}. After this constant potential treatment, one potentiodynamic sweep in the same solution was performed with a ver-

tex anodic potential of 0.3 V, in order to thicken the TiO_2 layer on the silver-free fraction of the titanium surface. The vertex anodic potential was limited in this case to 0.3 V, since, as Fig. 1 shows, at higher potentials anodic dissolution of the deposit may occur.

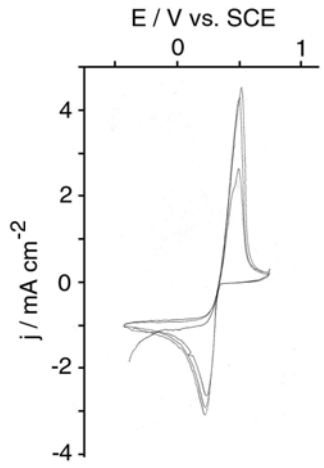

Fig. 1. The cyclovoltammograms of a Ti electrode in 1.76×10^{-2} M $AgNO_3$ + 0.1 M $KClO_4$ recorded between −0.4 and 0.8 V at a scan rate of 50 mV s^{-1}, with E_1 = −0.4 V and E_2 = 0.8 V, and $E_3 = E_1$ = −0.4 V *vs.* SCE.

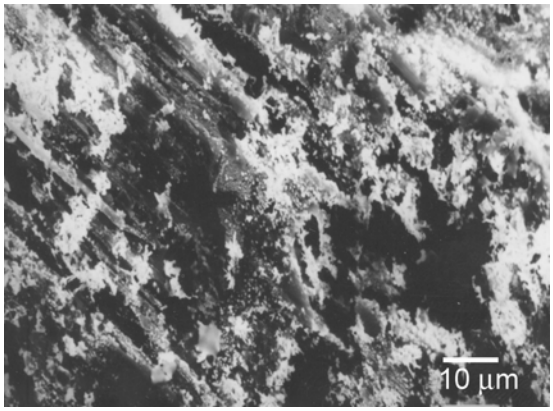

Fig. 2. The SEM microphotograph of a titanium surface with silver cathodically deposited at a constant potential of −0.4 V *vs.* SCE during 30 s (Ag/TiO_2, type I).

An SEM photograph of the Ag/TiO_2 surface with potentiostatically deposited silver is shown in Fig. 2. Since the back-scattered electron mode was used, the parts of surface rich in the heavier element, in this case Ag, appear highlighted. Along the surface, a number of randomly distributed silver dots, as well as cotton-like flecks composed of numerous branched silver nano-whiskers may be observed.

The type II composite layer was obtained when a freshly polished Ti electrode in a more dilute 1.74×10^{-3} M $AgNO_3$ + 0.1 M $KClO_4$ solution, was subjected to the potentiodynamic polarization program shown in Fig. 3. In this case, compared to Fig. 1, the polarization program emphasizes both the potential of cathodic deposition and that of anodic dissolution. However, the average time of deposition was longer than the average time of dissolution. Based on the voltammetric curves shown in Fig. 1, the working electrode type II was prepared starting the polarization sweep at –1 V *vs.* SCE, and sweeping the potential within the limits −0.8 and 0.5 V at a rate of 50 mV s^{-1}

The vertex cathodic potential of −0.4 V *vs.* SCE in the program shown in Fig. 3 corresponds, according to Fig. 1, to silver deposition under diffusion limi-

tation, when, as Fig. 2 shows, silver is able to deposit in the form of branched whiskers. However, at vertex anodic potentials of the potentiodynamic sweeps, (0.5 V), massive anodic dissolution occurs, whereby whiskers are primarily removed. However, under potentiodynamic conditions at the chosen vertex anodic potential, anodic dissolution is incomplete and each polarization cycle leaves a new portion of silver. As a result, a rather regular, dot-like, silver deposit imbedded in the TiO_2 layer appears. The mean diameter may be regulated by the number of polarization cycles. The deposit formed after 8 polarization cycles is shown in Fig. 4. For this type of layer, the surface loading by silver may be determined from the distribution density and mean diameter of silver dots by assuming that they are hemispherical in shape.[31] For further comparison with other types of composite layer types, a layer with a silver loading of 6 μg cm^{-2} was used.

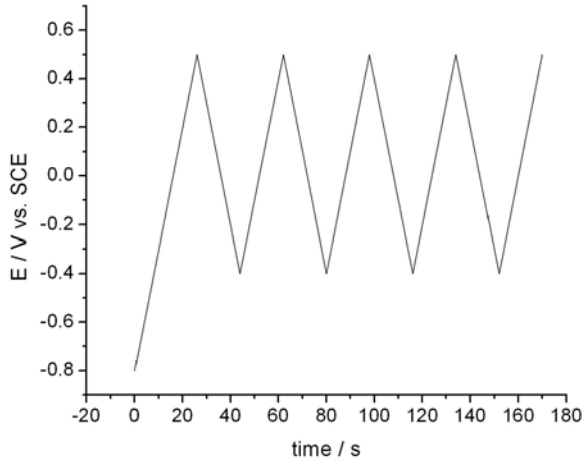

Fig. 3. The program of potentiodynamic polarization by which the Ag/TiO_2 deposit shown in Fig. 4 was obtained.

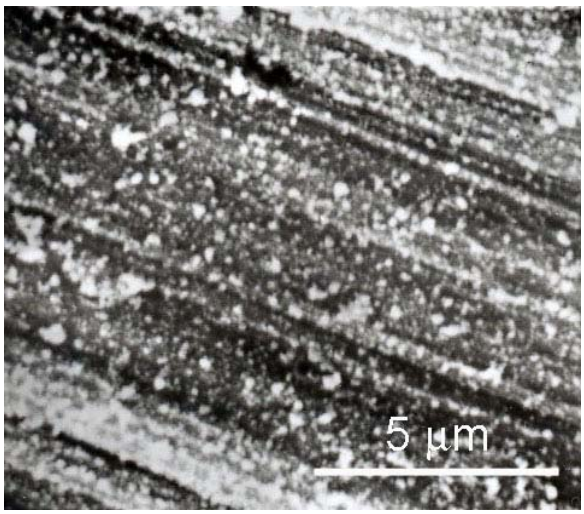

Fig. 4. The SEM microphotograph of a titanium surface upon potentiodynamic deposition of silver, using 8 cycles within the potential limits −0.4 and 0.5 V, at a scan rate 50 mV s^{-1} (Ag/TiO_2, type II).

If the polarization program shown in Fig. 5 is applied to a freshly polished titanium surface in 1.74×10^{-2} $AgNO_3$ + 0.1 M $KClO_4$, with vertex anodic potentials of at least 0.8 V, which provides for almost complete anodic dissolution of silver in each polarization cycle, a new type of deposit appears, labelled as composite layer type III. During each anodic sweep of the polarization cycle, according to Fig. 1, the whiskers grown above the TiO_2 layer during cathodic polarization are subjected to complete anodic dissolution. However, a part of the silver, most probably that screened by the TiO_2 layer growing during anodic polarization, remains protected from anodic dissolution and serves as the sites on which further cathodic deposition is favoured. This explanation is in accordance with the literature,[2] when a notable resistance towards anodic dissolution was reported for silver particles of nanometer dimensions on a graphite support. The SEM picture of the resulting Ag/TiO_2 composite surface is shown in Fig. 6. The silver is placed within randomly distributed micron-sized regions, visible as highlighted areas, integrated in the TiO_2 layer. The silver-rich islands are distributed relatively uniformly over the whole titanium surface and occupy about 50 % of the surface. Using a higher magnification, silver agglomerates approx. 50–150 nm in diameter may be distinguished within these silver-rich regions. The composite layer produced by the above described potentiodynamic procedure appears to be very adherent; namely, it cannot be striped by strong rubbing with filter paper. This is expectable, since during each polarization cycle when the potentials exceeds 0.4 V, the exposed part of silver deposit, namely that not captured by TiO_2, is removed by anodic dissolution.

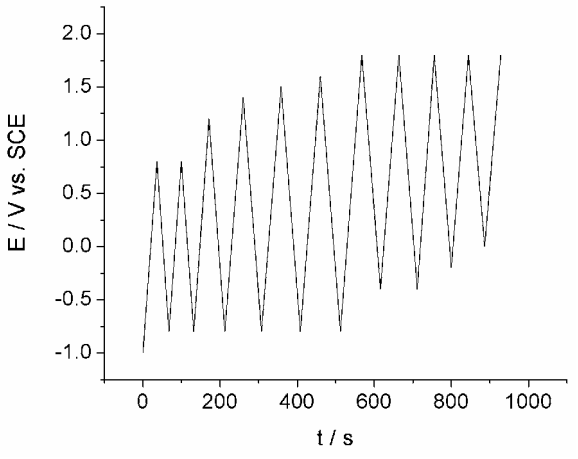

Fig. 5. The potential–time program used for the synthesis of the Ag/TiO_2 layer shown in Fig. 6.

The cyclic voltammograms of the Ag/TiO_2 composite layers in deaerated alkaline solutions

In alkaline solutions under anodic polarization, silver does not dissolve anodically but undergoes surface oxidation.[35–37] The redox processes in Ag/Ag_2O−AgO

systems in alkaline solutions present the fundamentals of silver–zinc alkaline batteries. Numerous papers published previously[35–41] were dedicated to the investigation of electrochemically induced changes on a silver surface in alkaline solutions. Oxidation was found to be a multi-stage process. In the region of surface oxidation, the two main anodic peaks, between 0 and 0.8 V *vs.* SCE correspond to the formation of Ag_2O and AgO, respectively, the first of which displays a fine structure. The majority of authors agree that the pre-peak which arises at about 0.1 V *vs.* SCE and precedes the formation of Ag_2O may be attributed to a phase transformation of adsorbed OH^- into an AgOH layer. The other two peaks, situated between 0.2 V and 0.4 V *vs.* SCE, are due to the formation of compact and porous Ag_2O layer, respectively.[40,41] Much more cathodic, between −0.5 and −0.8 V *vs.* SCE, at a substantially expanded current scale, a pair of peaks, which were attributed to the adsorption/desorption of OH^- ions[42] can be discerned. The presence of adsorbed OH^- ions was recently confirmed by XPS,[43,44] Raman spectroscopy[45] and by electron diffraction.[46]

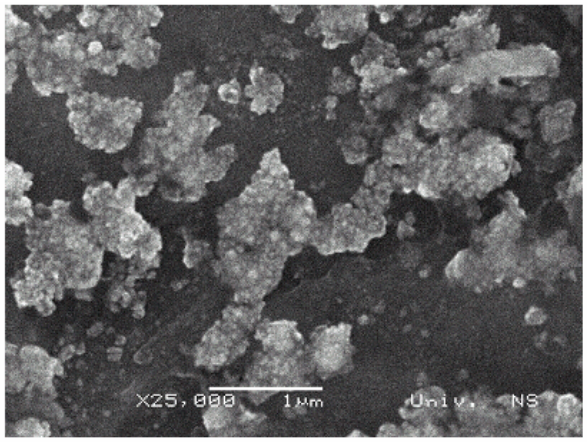

Fig. 6. SEM Microphotographs of Ag/TiO_2 (type III) surface.

To estimate the fraction of silver within the Ag/TiO_2 composite layer, which may be transformed into oxides, a titanium electrode covered by a Ag/TiO_2 layer in perchlorate solution was rinsed with distilled water, transferred into a 0.1 M NaOH solution, and then voltammograms were recorded in the potential range −1.0 to 0.9 V. These voltammograms are presented in Figs. 7 and 8, together with the voltammograms of a bulk polycrystalline silver electrode, which had been abraded in the same manner as the titanium one, supporting the Ag/TiO_2 layer.

The voltammogram of bulk polycrystalline silver (the second polarization cycle is presented) displays two well-known main anodic peaks. The second one of these two oxidation peaks, if a slow polarization rate is used, may be completely separated from the current of oxygen evolution.[38,42] However, in the present case these processes are somewhat merged. For this reason, the cathodic peaks appear to be more representative to estimate the charge consumed for the forma-

tion of surface oxides. In Fig. 7, for polycrystalline silver, the surface of the higher cathodic peak corresponds to a surface charge density of 129 mC cm^{-2}, which, assuming Ag_2O reduction corresponds to a further coverage by silver of 144 μg cm^{-2}. Other authors found that a charge of 130 mC cm^{-2} might be consumed for oxide formation,[20] which is very similar to the value found here. To estimate the thickness of a silver surface layer, expressed as the number of atomic layers, which participates in oxide formation, the number of atoms within one atomic layer has to be known. Horswell *et al.*[46] reported that the number of silver atoms per square centimeter for low-index planes of an Ag monocrystal amounts on average to 10^{15}. The above-mentioned value of 129 mC cm^{-2} corresponds to roughly 8×10^{17} silver atoms per square centimetre of geometric surface area. Thus, taking into account a roughness factor of between 1 and 3 for polycrystalline silver abraded with emery paper and bearing in mind the average number of atoms in one surface atomic layer,[46] it is reasonable to assume that several hundreds of atomic layers on the surface of a bulk silver electrode participate in metal oxide conversion reactions.

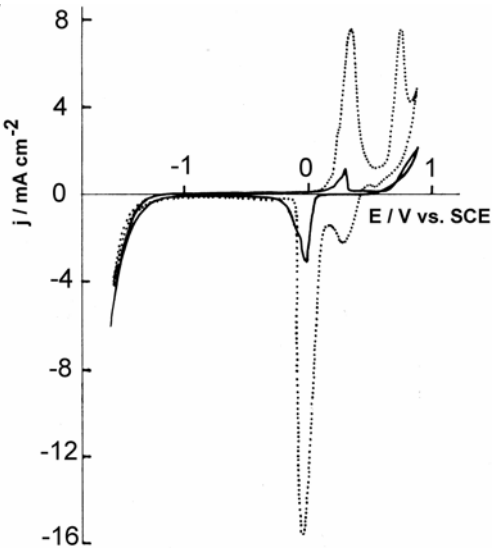

Fig 7. The voltammogram of an Ag/TiO_2 type I layer (full line) and the voltammogram (second scan) of bulk polycrystalline Ag (dotted line), recorded in 0.1 M NaOH between −1.6 and 0.9 V *vs.* SCE,at a scan rate 20 mV s^{-1}.

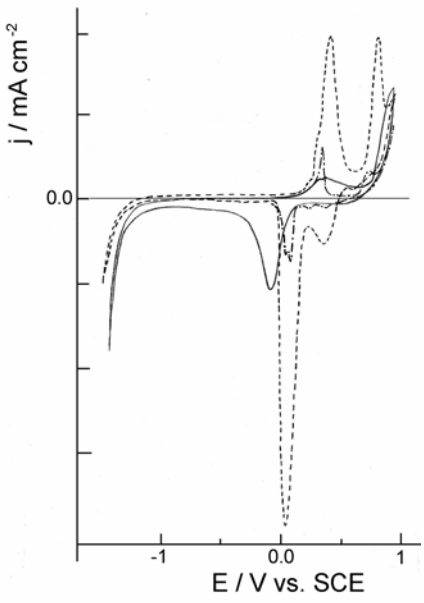

Fig. 8. The voltammograms of Ag/TiO_2 composite type II (full line) and type III (dash-dotted line), and the voltammogram of a bulk silver electrode in argon-purged 0.1 M NaOH, at a scan rate 20 mV s^{-1}. The unit of current density axis is 4.0, 0.4 and 1.0 mA cm^{-2}, for the bulk silver, composite layer type II and composite layer type III, respectively.

For Ag/TiO_2, type I layer, in Fig. 7, the surface area of the cathodic peak is about 5.4 times lower than that of an activated bulk silver electrode, and corresponds to a surface loading by silver of 25.7 μg cm^{-2}. Bearing in mind that a loading by silver of 24 μg cm^{-2} was calculated on the basis of the electricity consumed for the synthesis of this composite layer, it may be concluded that, within experimental error, the silver involved in the surface of an Ag/TiO_2 type I composite layer may be converted completely into oxide.

For Ag/TiO_2 type II and III layer, in Fig. 8, the charge density which corresponds to oxide reduction amounts to 4.9 and 3 mC cm^{-2}, respectively. The value 4.9 mC cm^{-2} corresponds to 5.4 μg cm^{-2}, which is reasonably close to the 6 μg cm^{-2} calculated based on the SEM picture (Fig. 4, top). Returning to the Ag/TiO_2 electrode type III, the value of 3 mC cm^{-2} for the main reduction peak corresponds to a silver loading of 3.4 μg cm^{-2}. This value is also far lower than that (130 mC cm^{-2}) consumed to oxidize the bulk silver surface and, therefore, it may be assumed that this is the silver loading responsible for the catalytic activity of this layer.

The voltammograms of the Ag/TiO_2 composite layers in oxygen-saturated alkaline solutions

Bulk polycrystalline platinum, carbon-supported platinum[47] and platinum alloys[48,49] display admirable catalytic activity towards the oxygen reduction reaction, ORR, in both acidic and alkaline solutions and thus present the unavoidable candidate for practical application in low temperature fuel cells. Many years ago, Tarasevich *et al.*[3] published that in alkaline solutions only, silver displays a catalytic activity for the ORR comparable to that of platinum. Based on this knowledge, some authors recently investigated the possibility of developing a carbon-supported silver catalyst for oxygen reduction in alkaline solutions.[5–9] The present study follows this trend using another type of supporting material, namely titania covered titanium, and a different electrochemical procedure of synthesis.

The voltammograms of the ORR on an Ag/TiO_2 rotating disc in 0.1 M NaOH oxygen-saturated solutions are presented in Fig. 9. According to Figs. 7 and 8, in the voltage region given in Fig. 9, the silver surface is free of silver oxide. However, in a part of this voltage region, namely that between −0.8 and 0.0 V, according to observations by very sensitive methods,[42–45] the silver is covered by adsorbed OH^- ions. The voltammograms in Fig. 9 indicate that the ORR proceeds easily on the composite surfaces under investigation and attains diffusion limitation over a large voltage interval. Mentus[31] published that the ORR also proceeds on anodic TiO_2 alone. However, in comparison to even extensively activated TiO_2,[50] a much lower overvoltage is required to run the ORR on Ag/TiO_2 than on pure TiO_2. It is thus certain that silver plays the main role in the acceleration of the ORR on Ag/TiO_2 composite layers.

The voltammograms from Fig. 9 were transformed into Tafel plots, which are shown in Fig. 10. The correction for the diffusion current consisted in the fac-

tor $j_l/(j_l-j)$, where j_l is the limiting diffusion current.[8,9] For the sake of comparison, the Tafel curves for the ORR on the surface of activated bulk polycrystalline silver is also presented.

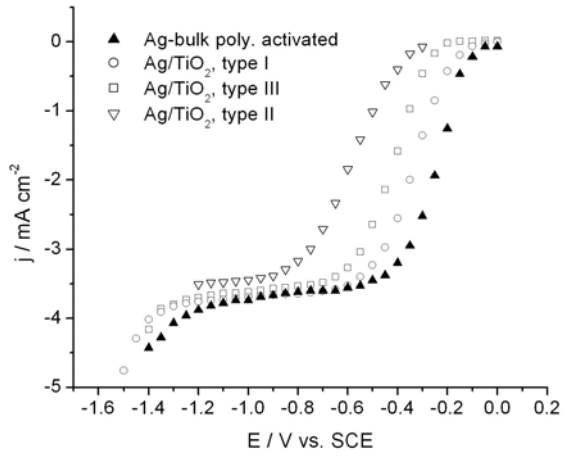

Fig. 9. The voltammograms of the oxygen reduction on various Ag/TiO_2 composite deposits on a rotating Ti disc electrode in oxygen saturated 0.1 M NaOH solutions, at a common rotation rate of 10 rps.

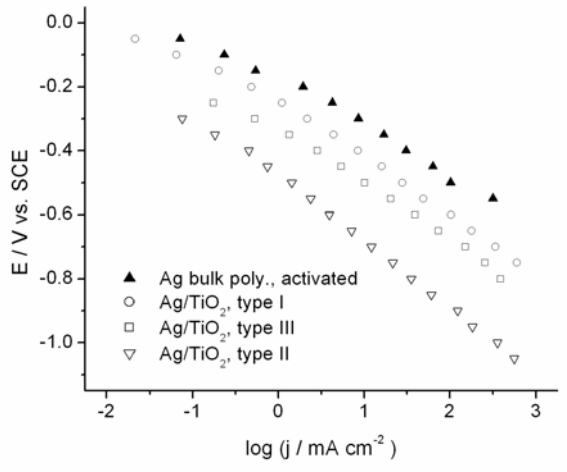

Fig. 10. Tafel plot of oxygen reduction on various Ag/TiO_2 composite deposits and bulk polycrystalline silver in oxygen-saturated aqueous 0.1 M NaOH solutions.

The Tafel slopes in Fig. 10 range between the lowest one of 100 mV for activated bulk silver (which is very similar to the slope found by Blizanac[51] for an Ag(100) surface in 0.1 M KOH) to the highest 200 mV per decade for the type II composite Ag/TiO_2 surface for higher current densities, cds. Assuming the rate controlling step is $O_2 + e^- = O_2^-$, the expected Tafel slope should amount to −60 mV per decade and such a slope was observed with platinum and some other noble metals in the low current density range.[52] However, usually a transition in slope from −60 to −120 mV per decade was observed on going from the low current density (lcd*)* towards the high current density *(*hcd*)* region. This transition was explained in terms of a transition from Temkin to Langmuir conditions caused by

a drop to zero in the surface coverage of adsorbed oxygen,[52] not in change in the nature of the rate determining step. Regarding silver, from both a previous[51] and this study, it seems that the low current density range of oxygen reduction, like that observed with a platinum electrode, is completely absent. A feature connected to the ORR on an Ag/TiO_2 surface is the larger Tafel slope in comparison to bulk silver. Thus, it seems that Ag/TiO_2 displays generally an averaged behaviour between that of pure silver and that of pure TiO_2. The same behaviour was evidenced elsewhere in the case of a Pt/TiO_2 catalyst, for low metal loadings.[53]

In alkaline solutions, the oxygen reduction reaction proceeds on different electrode materials usually as a direct, $4e^-$ reaction or as an indirect, $2e^-$ reaction,[58] whereby the latter one is accompanied and detectable by peroxide ion liberation from the electrode surface. A rotating disc–ring electrode presents a powerful tool to distinguish easily between these two reaction paths. Using the ring–disc method, Blizanac[51] evidenced that the oxygen reduction reaction for compact monocrystalline silver electrodes in alkaline solutions always proceeds through a $4e^-$ path. To prove the possible reaction path on the various Ag/TiO_2 composite layers, the results of rotating disc experiments were analysed using current–potential plots recorded at various rotation rates.

For a diffusion limited electrochemical reaction on rotating disc electrode, the current density follows the linear dependence on the square root of the rotation frequency, as predicted by the Levich equation:

$$j_l = 0.62nFD^{2/3}\nu^{-1/6}\omega^{1/2}c \tag{1}$$

This may be written in its shorter form:

$$j_l = B\omega^{1/2} \tag{1'}$$

where ν presents the kinematic viscosity, *i.e.*, the viscosity divided by density, and ω is the angular rotation frequency ($\omega = 2\pi f$, where f is the rotation frequency). The kinematic viscosities of the dilute perchlorate solutions used here are very close to that of water and thus may be taken to amount to 0.01 $cm^2\ s^{-1}$. The disc current density of any mixed activation–diffusion controlled process, at a fixed potential, follows the Koutecky–Levich (K–L) plot:[54]

$$\frac{1}{j} = \frac{1}{j_\infty} + \frac{1}{B\omega^{1/2}} \tag{2}$$

The meaning of B is visible from Eqs. (1) and (1'), while j_∞^{-1} is the intercept on the ordinate at infinite rotation frequency.

For dilute, oxygen-saturated solutions, B depends exclusively on the number of electrons, n, consumed per one oxygen molecule and for $n = 4$ amounts to 0.432 mA $cm^{-2}\ s^{1/2}$, while for $n = 2$, it is 0.216 mA $cm^{-2}\ s^{1/2}$.

The K–L slopes obtained for the studied composites are compared to that for a monocrystalline Ag(100) surface[51] in Fig. 11. In all cases observed in this study, as Fig. 11 shows, the K–L slopes were very close to that found with Ag(100) monocrystalline surface, which definitely corresponds to a $4e^-$ reaction path.[51] This is an expected result, since both Ag[51] and TiO_2,[50] support a $4e^-$ path in alkaline solutions.

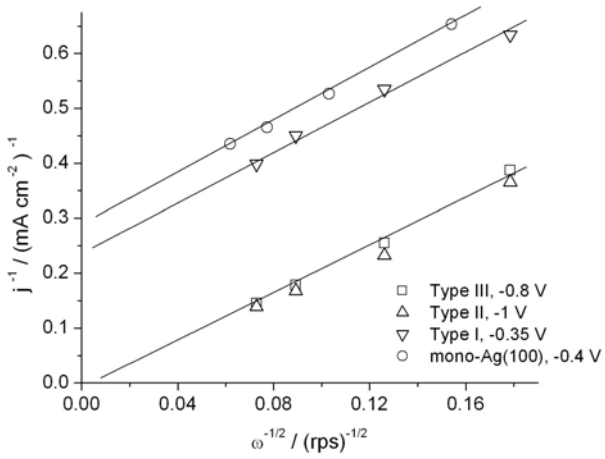

Fig. 11. Koutecky–Levich plot for the oxygen reduction reaction on different types of Ag/TiO_2 composite layers, compared to literature data for Ag(100) in 0.1 M NaOH.[51]

The value of the current density at a common overvoltage may be used as a measure of catalytic activity. For a fixed potential of −0.3 V *vs.* SCE, from Fig. 10, the current readings are 0.079, 0.50, 2.0 and 8.9 mA cm^{-2}, for composites with a silver loading 6.0, 3.4, 24 μg cm^{-2}, and activated bulk silver, respectively. The increase in catalytic activity follows generally the loading by silver. However, the inversion, appearing in the range of the lowest loadings, indicates also the influence of the mode of surface preparation. Namely better activity was observed with the composite layer in which a better degree of integration of silver into TiO_2 was achieved (Fig. 6 *vs.* Fig. 4). This inversion may be taken as evidence of a synergistic effect in the observed system.

It would be more exact to correlate the catalytic effectiveness to the number of surface silver atoms (*i.e.*, the real silver surface area), being a more fundamental parameter of catalysis than surface loading. However, to date, there is no reliable method for the determination of the real surface area of a silver electrode, such as that developed for platinum based on hydrogen electrosorption,[47] or that developed for gold based on oxygen electrosorption.[55] Namely, the amount of OH^- ions adsorbed on a silver surface in the potential range −0.8 to −0.5 V *vs.* SCE[44–46] does not achieve a plateau, characteristic of monolayer formation[46] and, with further anodic polarization, passes rather continuously into oxide formation, while the oxide formation itself is multilayer in nature.[39–41]

The fair catalytic activity of the Ag/TiO_2 layer at relatively small surface loadings of only 3.4–6 and 24 μg cm^{-2} may be the result of some combined effects connected to the dispersed structure of the silver deposit. Recently, several authors reported on the importance of disorder of the surface atoms or atom clusters as being essential for catalytic activity.[56–58] Namely, a surface layer often consists of atoms and clusters in metastable states, which are difficult to generate in a reproducible manner.[57,58] This concept of metastable surfaces may be interrelated to surface reconstructions.[59,60] Using both the thickness of anodic surface oxides and the dependence of voltammograms on the type of electrode pre-treatment (Figs. 7 and 8), as a measure of surface metastability, silver may be classified to metals the surface of which is easily transferred into metastable states. The developed morphology of silver within the Ag/TiO_2 composite layer allows a great number of disordered surface atoms, as well as a pronounced synergy.

CONCLUSIONS

Proceeding from the fact that a thin TiO_2 film, if formed on a Ti surface simultaneously with the cathodic formation of metal nuclei, may template metal nuclei distribution, the forms Ag/TiO_2 deposits obtained either by potentiostatic or potentiodynamic polarization of a freshly polished titanium surface in dilute aqueous solutions of silver nitrate were investigated. The SEM micrographs indicate that branchy silver whiskers crossing the TiO_2 layer were obtained by potentiostatic deposition, while dot-like and island-like silver deposits integrated in the TiO_2 layer were obtained by potentiodynamic polarization. By comparing the cyclic voltammograms of composite Ag/TiO_2 electrodes to a bulk Ag electrode in deaerated 0.1 M NaOH solution, it was concluded that all the silver in an Ag/TiO_2 layer could be converted to oxide. Consequently, cyclic voltammetry was used for coulometric determination of the surface loading by silver. The surface loading, determined in such a way, corresponded well to the one determined by other methods used, based either on the current consumption during potentiostatic deposition, or on SEM analysis.

The catalytic activity of Ag/TiO_2 layers toward oxygen reduction reaction was investigated in oxygen saturated alkaline 0.1 M NaOH. Fair electrocatalytic activity was evidenced for very small loadings of silver of the order 10^{-6} g cm^{-2}. As expected, the catalytic activity increases with increasing silver loading. A registered deviation of this rule evidenced the role of silver integration into TiO_2.

By the Koutecky–Levich analysis, a $4e^-$ reaction path of oxygen reduction, characteristic of bulk silver in alkaline solutions, was confirmed for all the studied Ag/TiO_2 composite layers.

Acknowledgements. One of the authors (S. M) is participant in the EU Project “Prometeas”, Contract No. ICA2-CT-2001-10037 and in the contract No. 142047 agreed with the Ministry of Science of the Republic of Serbia. The authors S. M, I. B, J. P. and V. G. are grateful to the Ministry of Education and Science of the Republic of Montenegro which supported this work through contract No. 05-1/2-1530/2005.

И З В О Д

ПОДЕШАВАЊЕ МОРФОЛОГИЈЕ И ЕЛЕКТРОКАТАЛИТИЧКИХ СВОЈСТАВА ЕЛЕКТРОХЕМИЈСКИ ФОРМИРАНОГ КОМПОЗИТНОГ СЛОЈА Ag/TiO_2 НА ПОВРШИНИ ТИТАНА

С. В. МЕНТУС[1], И. БОШКОВИЋ[2], Ј. М. ПЈЕШЧИЋ[2], В. ГРУДИЋ[2] и Ж. БОГДАНОВ[3]

[1]Факултет за физичку хемију, Универзитет у Београду, Студентски Трг 16, 11000 Београд, [2]Универзитет у Подгорици, Металуршко–технолошки факултет, 81000 Подгорица, Црна Гора и [3]Институт за нуклеарне науке "Винча", 11001 Београд

У воденом раствору $AgNO_3$, подешавајући услове издвајања сребра на површини механички полираног титана, добијене су три различите форме композитног слоја Ag/TiO_2, у којима депозит сребра има облик иглица, тачака и острвца. Морфологија депозита је резултат програма поларизације електроде и усмеравајућег (темплатног) дејства слоја TiO_2 који се формира паралелно са издвајањем сребра. Каталитичка активност композитних депозита према редукцији кисеоника испитивана је у воденом раствору 0,1 M NaOH. Показано је да она зависи од количине и типа дистрибуције сребра унутар слоја Ag/TiO_2. Независно од форме композита, реакциони пут редукције кисеоника је четвороелектронски, иначе карактеристичан за поликристално сребро у алкалном раствору.

(Примљено 14. маја 2007)

REFERENCES

1. V. P. Poroshkov, V. S. Gurin, *Surf. Sci.* **331−333** (1995) 1520
2. K. H. Ng, H. Liu, R. M. Penner, *Langmuir* **16** (2000) 4016
3. N. A. Shumilova, G. N. Zhutaeva, M. R. Tarasevich, *Electrochim. Acta* **11** (1967) 967
4. J. D. McIntyre, W. F. Peck, in: *The Physics and Chemistry of Electrocatalysis*, J. D. E. McIntyre, M. J. Weaver, E. Yeager, Eds., Pennington, N.Y, 1984, p. 102
5. V. Hacker, E. Wallöfer, W. Baumgartner, T. Schaffer, J. O. Besenhard, H. Schröttner, M. Schmid, *Electrochem.Commun.* **7** (2005) 377
6. Y.–F. Yang, Y.–H. Zhon, *J. Electroanal. Chem.* **397** (1995) 271
7. Y.–F. Yang, Y.–H. Zhon, *J. Electroanal. Chem.* **415** (1996) 143
8. M. Chatenet, L. Genies–Bultel, M. Aurousseau, R. Durand, F. Andolfatto, *J. Appl. Electrochem.* **32** (2002) 1131
9. M. Chatenet, M. Aurousseau, R. Durand, F. Andolfatto, *J. Electrochem. Soc.* **150** (2003) D47
10. S. Gamburzev, K. Petrov, A. J. Appleby, *Book of Abstracts*, in *Proceedings of Joint Meeting – – 200th Meeting of ECS, Inc., and 52nd Ann. Meeting of ISE*, San Francisco, California, 2001, Abst. No. 353
11. R. R. Adžić, J. X. Wang, *Electrochim. Acta* **45** (2000) 4203
12. S. J. Tauster, S. C. Fung, R. T. K. Baker, J. A. Horsley, *Science* **211** (1981) 1121
13. G. L. Haller, D. E. Resasco, *Adv. Catal.* **36** (1989) 173
14. B. C. Beard, P. N. Ross, *J. Electrochem. Soc.* **133** (1986) 1839
15. S. G. Neophytides, S. H. Zafeiratos, M. M. Jaksić, *J. Electrochem. Soc.* **150** (2003) E512
16. M. Haruta, S. Tsubota, T. Kobayashi, H. Kageyama, M. J. Genet, B. Delmon, *J. Catal.* **144** (1993) 175
17. G. R. Bamwenda, S. Tsubota, T. Nakamura, M. Haruta, *Catal. Lett.* **44** (1997) 83
18. M. Okumura, K. Tanaka, A. Ueda, M. Haruta, *Solid State Ionics* **95** (1997) 143
19. S. Trasatti, in: *Interfacial Electrochemistry, Theory, Experiment and Applications*, A. Wieckowski Ed., M. Dekker Inc., New York, 1999, p. 769

20. H. B. Beer, *J. Electrochem.Soc.* **127** (1980) 303C
21. S. Tsubota, D. A. H. Cunningham, Y. Baudo, M. Haruta, *Preparation of Catalysts* **6** (1995) 227
22. J. R. Burrows, J. H. Eutwisle, J. A. Harrison, *J. Electroanal. Chem*. **77** (1977) 21
23. A. T. Kuhn, C. J. Mortimer, *J. Electrochem. Soc*. **12** (1973) 231
24. E. A. Kalinovskii, R. V. Boudar, N. N. Meshkova, *Elektrokhimiya* **8** (1972) 1468
25. R. G. Erenberg, L. J. Krishtalik, V. J. Bystrov, *Elektrokhimiya* **8** (1972) 1740
26. D. Čukman, M. Vuković, *J. Electroanal. Chem.* **279** (1990) 273
27. D. Čukman, M. Vuković, M. Milun, *J. Electroanal. Chem.* **389** (1995) 209
28. M. Vuković, D. Marijan, D. Čukman, P. Pervan, M. Milun, *J. Mat. Sci*. **34** (1999) 869
29. S. Mentus, *Electrochim. Acta* **50** (2005) 3609
30. S. B. Emery, J. L. Hubbey, D. Roy, *J. Electroanal. Chem.* **568** (2004) 121
31. I. Bošković, S. V. Mentus, M. Pješčić, *Electrochim. Acta* **51** (2006) 2793
32. J. Pješčić, S. Mentus, N. Blagojević, *Mater. Corros.* **53** (2002) 44
33. R. M. Torresi, O. R. Camara, C. P. DePauli, M. C. Giordano, *Electrochim. Acta* **32** (1987) 1357
34. S. K. Poznyak, A. I. Kokorin, A. I. Kulak, *J. Electroanal. Chem*. **442** (1998) 99
35. B. V. Tilak, R. Perkins, H. A. Kozlowska, B. E. Conway, *Electrochim. Acta* **17** (1972) 1447
36. R. S. Perkins, B. V. Tilak, H. A. Kozlowska, *Electrochim. Acta* **17** (1972) 1471
37. J. M. M. Droog, P. T. Alderliesten, G. A. Bootsma, *J. Electroanal. Chem.* **99** (1979) 173
38. M. Hepel, M. Tomkiewicz, *J. Electrochem. Soc.* **131** (1984) 1288
39. M. L. Teijelo, J. R. Vilche, A. J. Arvia, *J. Appl. Electrochem.* **18** (1988) 691
40. B. M. Jović, V. D. Jović, G. R. Stafford, *Electrochem. Commun.* **1** (1999) 247
41. B. M. Jović, V. D. Jović, *J. Serb. Chem. Soc.* **69** (2004) 153
42. G.I. Lacconi, A.S. Gioda, V.A. Macagno, *Electrochim.Acta* **30** (1985) 211
43. D. Hecht, H.H. Strehblow, *J. Electroanal. Chem*. **440** (1997) 211
44. D. Lutzenkirchen–Hecht, H.H. Strehblow, *Electrochim. Acta* **43** (1998) 2957
45. E. R. Savinova, P. Kraft, B. Pettinger, K. Doblhofer, *J. Electroanal. Chem.* **430** (1997) 47
46. S. L. Horswell, A. L. N. Pinheiro, E. R. Savinova, M. Danckwerts, B. Pettinger, M.–S. Zei, G. Ertl, *Langmuir* **20** (2004) 10970
47. T. J. Schmidt, H. A. Gasteiger, G. D. Stab, P. M. Urban, D. M. Kolb and R. J. Behm, *J. Electrochem. Soc.* **95** (1998) 2354
48. A. L. N. Pinheiro, A. O. Neto, E. C. de Souza, J. Perez, V. A. Paganin, E. A. Ticianelli and E. R. Gonzales, *J. New Mat. Electrochem. Sys.* **6** (2003) 1
49. U. A. Paulus, A. Wokaun, G. G. Scherer, T. J. Schmidt, V. Stamenković, N. M. Marković, P. N. Ross, *Electrochim. Acta* **47** (2002) 3787
50. T. Clark, D. C. Johnson, *Electroanal.* **9** (1997) 273
51. B. Blizanac, *PhD Thesis*, Faculty of Physical Chemistry, Belgrade University, 2004 (in Serbian)
52. J. O'M. Bockris, S. U. M. Khan, *Surface Electrochemistry, A Molecular Level Approach*, Plenum Press, New York, London, 1993, p. 331
53. M. I. Rojas, M. J. Esplandiu, L. B. Avalle, E. P. M. Levia, V. A. Macagno, *Electrochim. Acta* **43** (1998) 1785
54. K. Tammeveski, T. Tenno, A. Rosental, P. Talonen, L.-S. Johansson, L. Niinistö, *J. Electrochem. Soc.* **146** (1999) 669
55. D. A. J. Rand, R. Woods, *J. Electroanal. Chem. Interf. Electrochem*. **31** (1971) 29
56. G. A. Somorjai, *Chem. Rev.* **96** (1996) 1223
57. M. S. Spencer, *Nature* **323** (1986) 685
58. L. D. Burke, *Gold Bull.* **37** (2004) 125
59. D. M. Kolb, *Prog. Surf. Sci.* **109** (1989) 51
60. A. Henglein, *Ber. Bunsenges. Phys. Chem.* **101** (1997) 1562.

Journal of the Serbian Chemical Society
JSCS@tmf.bg.ac.yu • www.shd.org.yu/JSCS

J. Serb. Chem. Soc. 72 (12) 1419–1425 (2007) UDC 66.094.3+544.6:547.261+547.263+544.478:621.352
JSCS–3673 *Short communication*

SHORT COMMUNICATION

Mixtures of methanol and 2-propanol as a potential fuel for direct alcohol fuel cells

S. LJ. GOJKOVIĆ[1*#], A. V. TRIPKOVIĆ[2#] and R. M. STEVANOVIĆ[2#]

[1]*Faculty of Technology and Metallurgy, University of Belgrade, Karnegijeva 4, P.O. Box 3503, 11120 Belgrade and* [2]*ICTM-Institute of Electrochemistry, University of Belgrade, Njegoševa 12, P.O.Box 473, 11000 Belgrade, Serbia*

(Received 30 May 2007)

Abstract: The electrochemical oxidation of methanol, 2-propanol, and their mixtures was investigated on a Pt/C thin film electrode in acid solution. It was confirmed that the oxidation of 2-propanol commences at less positive potentials than that of methanol and exhibits significantly higher oxidation current densities at low potentials. When both methanol and 2-propanol were present in the solution, the onset of the oxidation current was the same as for the oxidation of pure 2-propanol. Although both alcohols inhibit the oxidation reaction of each other to a certain extent, steady-state polarization measurements showed that their mixture provides higher current densities than single alcohols over the entire potential region from the hydrogen region to oxide formation on the Pt surface. This implies that the addition of 2-propanol into the fuel may extend the operational range of direct methanol fuel cells.

Keywords: electrochemical oxidation, 2-propanol, methanol, platinum supported catalyst, fuel cell.

INTRODUCTION

Solid polymer electrolyte fuel cells (SPEFC) which use directly alcohols as the fuel are promising power sources for portable electronic devices. Methanol has been considered as the best choice because it is readily available at low cost and has a high energy density. However, the kinetics of the methanol oxidation is slow and leads to high anodic overpotentials.[1–4] This essential drawback of direct methanol fuel cells (DMFC) induced extensive investigations of the electro-oxidation of other alcohols. Ethanol is an attractive alternative[5] because it is non-toxic and can be produced from biomass. Although the cleavage of a C–C bond is necessary to achieve complete oxidation of ethanol, the oxidation commences at less positive potentials than methanol oxidation,[6,7] yielding acetate and CO as the

* Corresponding author. E-mail: sgojkovic@tmf.bg.ac.yu
# Serbian Chemical Society member.
doi: 10.2298/JSC0712419G

adsorbates[8] and acetaldehyde, acetic acid, and CO_2 as the main products.[9] The oxidation of C_3 alcohols on Pt was also examined. It was revealed that the adsorbed intermediates and products depend on the position of the OH group in the molecule. Thus, during the oxidation of 1-propanol, adsorbates with one (*e.g.*, linearly bonded CO), two, and three C atoms were found and propionic acid and CO_2 were detected as the main products.[10,11] Oxidation of 2-propanol produced acetone and CO_2, but no adsorbed CO was found and all adsorbates retained three C-atoms.[10,12,13] When the onset potentials for oxidation of different alcohols were compared, the performance of 2-propanol was superior to that of methanol,[7] ethanol[7,14] and 1-propanol.[10] Also, several researchers conducted parallel studies on direct alcohol fuel cells with 2-propanol as the fuel (DPFC) and DMFC. Wang *et al.*[15] reported that a DPFC operating at 190 ºC with either 1- or 2-propanol showed a much worse performance than a DMFC. However, recent studies which were performed at 25 to 90 ºC concurred that the performance of the DPFC using 2-propanol was substantially higher than that of a DMFC at current densities lower than 100–200 mA cm^{-2}, while the DMFC was better at higher current densities.[16–19] Considering these facts, in this study an attempt was made to combine the good characteristics of both alcohols. The results of the electrochemical oxidation of mixtures of methanol and 2-propanol on carbon supported Pt nanoparticles are reported here.

EXPERIMENTAL

The catalyst used in the experiments was platinum supported on XC-72R high-area carbon (Pt/C). Platinum was deposited on the support by a modified ethylene glycol method. The details of the preparation were given elsewhere.[20] The Pt loading of the catalyst was 16.6 mass %.

The catalyst was applied to a gold substrate (5 mm diam.) in the form of a thin film.[21] Two milligrams of Pt/C was mixed with 1.0 ml of water and 50 µl of Nafion solution (5 mass %, Aldrich). The suspension was agitated in an ultrasonic bath for 60 min and 12.5 µl of it was placed on the gold electrode using a micro-pipette and left to dry over night. The amount of Pt on the electrode was 4.15 µg.

A standard glass cell was used with a Pt wire spiral as the counter electrode and a saturated calomel electrode as the reference electrode. All the potentials reported in this paper are expressed on the scale of the reversible hydrogen electrode (RHE). The electrolyte contained 0.1 M H_2SO_4 as the supporting electrolyte and various concentrations of methanol and 2-propanol. All solutions were prepared with high purity water (Millipore, 18 MΩ cm resistivity) and p.a. grade chemicals (Merck). The electrolyte was deaerated with high purity N_2. The cell was thermostated at 30.0 ºC. A Pine RDE4 Potentiostat and a Philips PM 8143 X-Y recorder were used in all experiments.

After immersing a Pt/C electrode in the supporting electrolyte, the potential was cycled between the H_2 and O_2 evolution regions at a rate of 50 mV s^{-1} until a steady-state voltammogram was obtained. Then in the positive-going sweep, the potential was held at 0.1 V *vs.* RHE, the alcohols were added into the electrolyte and sweep was continued at 50 mV s^{-1}. After attaining a steady-state curve for the oxidation of alcohol, the potential was again held at 0.1 V *vs.* RHE and a polarization curve was recorded at a slow sweep of 1 mV s^{-1}.

The real surface areas of the Pt electrocatalysts were determined using the hydrogen adsorption/desorption charge from the steady-state cyclic voltammograms in the supporting electrolyte

and assuming a charge of 210 μC cm^{-2} for a monolayer hydrogen adsorption. The anodic part of the voltammograms corresponding to hydrogen desorption was integrated and the double-layer charging current was subtracted. The average of fifteen experiments resulted in a specific surface area of 84.6±8.2 m^2 g^{-1}, which is the equivalent of a particle diameter of 3.3±0.3 nm (assuming that they were ideal spheres). Current densities for the oxidation of the alcohols were calculated per surface area determined for this particular thin film.

RESULTS AND DISCUSSION

The cyclic voltammogram of the Pt/C electrocatalyst, given in Fig. 1a, shows the usual characteristics of a Pt surface, except that current peaks for the adsorption/desorption of hydrogen are not as sharp and well-resolved as on a smooth Pt electrode. The hydrogen region is followed by a double layer charging current, adsorption of oxygen-containing species and their reduction.

The potentiodynamic polarization curves of the oxidation of 0.1 M methanol, 0.01 M 2-propanol, and their mixture are presented in Fig. 1b, while the same curves but with 0.1 M 2-propanol are presented in Fig. 1c. Methanol oxidation shows familiar features, *i.e.*, the onset of the reaction requires the complete desorption of adsorbed hydrogen atoms and the adsorption of OH particles, but the reaction slows down when the formation of Pt oxide commences. On the contrary, the oxidation of 2-propanol commences at the surface which is partially covered with adsorbed hydrogen and has no OH particles attached on it. The difference in the onset potentials of the oxidation of methanol and 2-propanol is caused by the different reaction mechanisms. Methanol adsorbs on the Pt surface dissociatively, CO_{ads} develops, and the oxidation reaction cannot begin until OH species are formed, either on Pt or on some other atoms in a case of a bi-metal catalyst (*e.g.*, Pt–Ru).[1–3] During the adsorption of 2-propanol, not one C–C bond is broken and there are no strongly adsorbed intermediates, such as CO_{ads}.[10,13] This implies that OH species are not necessary for the reaction, which was proven by experiments in which modification of the Pt surface by Ru did not influence the onset potential of 2-propanol oxidation.[11]

When both methanol and 2-propanol were present in the electrolyte, the oxidation current appeared at approximately the same potential as in the electrolyte containing only 2-propanol (Figs. 1b and 1c). It should be noted that the onset potential of the oxidation of the mixture is the same regardless of which alcohol was added first to the electrolyte. In the potential region before the maximum of the 2-propanol oxidation rate, the mixture with 0.01 M 2-propanol (Fig. 1b) exhibits slightly lower current densities than the solution containing only 2-propanol at the same concentration, while in the mixture containing 0.1 M 2-propanol (Fig. 1c), the current densities practically overlap with those obtained with the solution containing only 0.1 M 2-propanol. Oxidation of the first mixture shows that CO_{ads} originating from methanol adsorption slightly hinders the adsorption of 2-propanol, which is consistent with a coverage by CO_{ads} of about 0.2.[22] It seems that the oxidation of methanol is suppressed until the oxidation of 2-propanol reaches

its maximum, especially when the concentration of 2-propanol in the mixture was 0.1 M (Fig. 1c). This is probably due to adsorption of large 2-propanol molecules, which delays the adsorption of OH species necessary for the oxidation of CO_{ads} generated by the dissociation of methanol molecules.

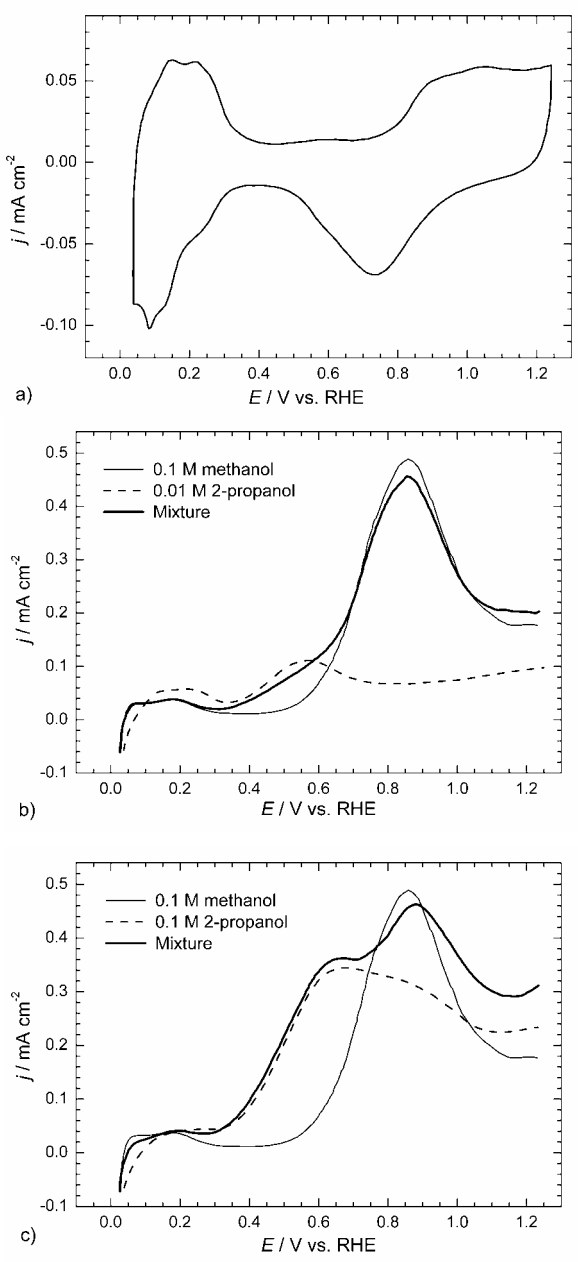

Fig. 1. a) Cyclic voltammogram of Pt/C electrocatalyst, b) potentiodynamic curves for the oxidation of 0.1 M methanol, 0.01 M 2-propanol and their mixture, and c) potentiodynamic curves for oxidation 0.1 M methanol, 0.1 M 2-propanol and their mixture. Supporting electrolyte 0.1 M H_2SO_4, temperature 30 ºC, scan rate 50 mV s^{-1}.

At the potentials more positive than 0.7 V, the oxidation current densities of the mixtures trace the methanol oxidation curve when the concentration of 2-propanol was low (Fig. 1b). At the high concentration of 2-propanol in the mixture (Fig. 1c), the potential of the maximum is shifted by about 30 mV with respect to pure methanol and the current densities are higher after the maximum, indicating a hindrance of the formation of Pt oxide in the presence of 2-propanol.

The applicability of the mixture of the alcohols as the fuel in a fuel cell was estimated from the steady-state polarization curves recorded at 1 mV s^{-1}. Since DMFCs with a Pt–Ru alloy as the anode electrocatalyst are the only direct alcohol fuel cells already in use, the oxidation of methanol and 2-propanol on the Pt/C electrocatalyst was compared with the oxidation of methanol on PtRu/C electrocatalysts (data taken from Ref. 23). All the currents are expressed as mass activities, *i.e.*, the current per mass of metal or alloy. The Tafel plots in Fig. 2 show the remarkably better performance of both pure 2-propanol and the mixtures, compared to methanol, at potentials up to about 0.6 V. At higher potentials, pure methanol and the mixtures are superior to 2-propanol. Therefore, only a mixture of methanol and 2-propanol can deliver a significant anodic current over the entire potential range from 0.2 to 0.8 V.

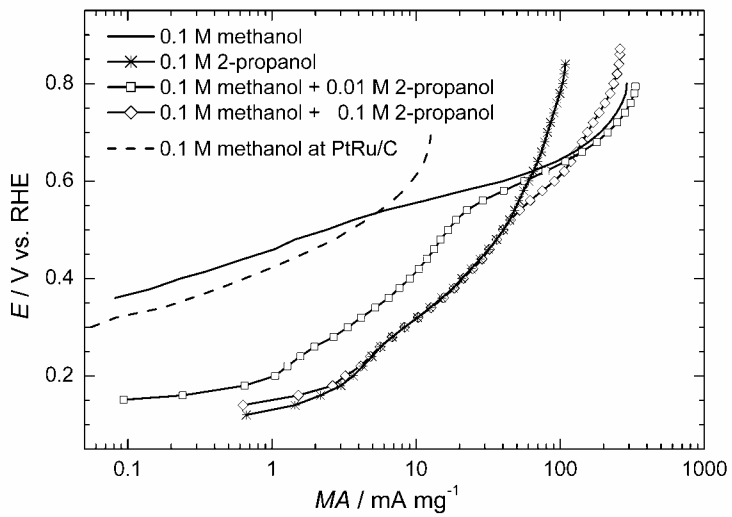

Fig.2. Polarization curves for the oxidation of 0.1 M methanol at Pt/C and PtRu/C catalysts, oxidation of 0.1 M 2-propanol and the oxidation of the mixtures of 0.1 M methanol with 0.1 and 0.01 M 2-propanol at a Pt/C catalyst. Supporting electrolyte 0.1 M H_2SO_4, temperature 30 ºC, scan rate 1 mV s^{-1}.

CONCLUSIONS

Investigation of the simultaneous oxidation of methanol and 2-propanol on a Pt/C electrocatalyst showed that 2-propanol exhibits significantly higher oxida-

tion current densities than methanol at low potentials, despite the fact that 2-propanol oxidizes incompletely, yielding acetone as the main product and only two electrons per molecule. When both alcohols are present in the electrolyte, methanol slightly suppresses the oxidation of 2-propanol, but only if the mixture contains a low concentration of 2-propanol. On the other hand, a high concentration of 2-propanol in the mixture delays OH adsorption and shifts the methanol oxidation towards more positive potentials. Although both alcohols inhibits the oxidation reaction of each other to a certain extent, steady-state polarization curves recorded at a slow sweep rate clearly showed that their mixture provides higher current densities than the single alcohols over the entire potential region from the hydrogen region to oxide formation on the Pt surface.

The results imply that a direct alcohol fuel cell operating with a mixture of methanol and 2-propanol should give higher voltages than a DMFC with a Pt–Ru anode. According to literature,[16-18] when pure 2-propanol was used as the fuel (DPFC), a rapid drop at high current densities was observed. With a mixture of methanol and 2-propanol, this failure should be overcome because methanol can take on the anodic reaction. This statement requires verification under fuel cell conditions.

Acknowledgement. This work was financially supported by the Ministry of Science of the Republic of Serbia, under Contact No. 142056.

И З В О Д

СМЕША МЕТАНОЛА И 2-ПРОПАНОЛА КАО ПОТЕНЦИЈАЛНО ГОРИВО У ГОРИВИМ СПРЕГОВИМА СА АЛКОХОЛОМ

С. Љ. ГОЈКОВИЋ[1], А. В. ТРИПКОВИЋ[2] и Р. М. СТЕВАНОВИЋ[2]

[1]*Технолошко–металуршки факултет, Карнегијева 4, 11000 Београд и*
[2]*ИХТМ – Центар за електрохемију, Његошева 12, 11000 Београд*

Испитивана је електрохемијска оксидација метанола, 2-пропанола и њихових смеша на танком филму Pt/C катализатора у киселој средини. Потврђено је да оксидација 2-пропанола почиње на мање позитивним потенцијалима него оксидација метанола и да даје знатно веће густине струја при нижим потенцијалима. Када су и метанол и 2-пропанол присутни у раствору, струја оксидације се појављује на истом потенцијалу као у случају чистог 2-пропанола. Мада оба алкохола инхибирају оксидацију оног другог у извесној мери, стационарма мерења су показала да њихова смеша даје веће густине струја од појединачних алкохола у целој области потенцијала од водоничне области па до формирања оксида на платини. То указује да се радни опсег горивог спрега са метанолом може повећати додатком 2-пропанола у гориво.

(Примљено 30. маја 2007)

REFERENCES

1. T. D. Jarvi, E. M. Stuve, in *Electrocatalysis*, J. Lipkowski, P. N. Ross Eds., Wiley, New York, 1998, p. 75
2. S. Wasmus, A. Küver, *J. Electroanal. Chem.* **461** (1999) 14

3. T. Iwasita, *Electrochim. Acta* **47** (2002) 3663
4. A. V. Tripković, S. Lj. Gojković, K. Dj. Popović, J. D. Lović, *J. Serb. Chem. Soc.* **71** (2006) 1333
5. S. Song, P. Tsiakaras, *Appl. Catal. B* **63** (2006) 187
6. C. Lamy, E. M. Belgsir, J.–M. Léger, *J. Appl. Electrochem.* **31** (2001) 799
7. C.–G. Lee, M. Umeda, I. Uchida, *J. Power Sources* **160** (2006) 78
8. M. H. Shao, R. R. Adzic, *Electrochim. Acta* **50** (2005) 2415
9. G. A. Camara, T. Iwasita, *J. Electroanal. Chem.* **578** (2005) 315
10. E. Pastor, S. Wasmus, T. Iwasita, M. C. Arévalo, S. Gonzáles, A. J. Arvia, *J. Electroanal. Chem.* **350** (1993) 97
11. I. de A. Rodrigues, J. P. de Souza, E. Pastor, F. C. Nart, *Langmuir* **13** (1997) 6829
12. S.–G. Sun, Y. Lin, *Electrochim. Acta* **44** (1998) 1153
13. E. Pastor, S. Gonzáles, A. J. Arvia, *J. Electroanal. Chem.* **395** (1995) 233
14. S. S. Gupta, J. Datta, *J. Chem. Sci.* **117** (2005) 337
15. J. Wang, S. Wasmus, R. F. Savinell, *J. Electrochem. Soc.* **142** (1995) 4218
16. Z. Qi, M. Hollett, A. Attia, A. Kaufman, *Electrochem. Solid-State Lett.* **5** (2002) A129
17. Z. Qi, A. Kaufman, *J. Power Sources* **112** (2002) 121
18. D. Cao, S. H. Bergens, *J. Power Sources* **124** (2003) 12
19. T. Kobayashi, J. Otomo, C. Wen, H. Takahashi, *J. Power Sources* **124** (2003) 34
20. B. M. Babić, Lj. M. Vračar, V. Radmilović, N. V. Krstajić, *Electrochim. Acta* **51** (2006) 3820
21. T. J. Schmidt, H. A. Gasteiger, R. J. Behm, *Electrochem. Commun.* **1** (1999) 1
22. S. Park, Y. Xie, M. J. Weaver, *Langmuir* **18** (2002) 5792
23. S. Lj. Gojković, T. R.Vidaković, D. R. Đurović, *Electrochim. Acta* **48** (2003) 3607.

Journal of the Serbian Chemical Society
JSCS@tmf.bg.ac.yu • www.shd.org.yu/JSCS

J. Serb. Chem. Soc. 72 (12) 1427–1436 (2007) UDC 544.6:615.33:541.135.5–034.21+541.135
JSCS–3674 *Original scientific paper*

A study of the electrochemical activity of some macrolide antibiotics on a gold electrode in a neutral electrolyte

M. L. AVRAMOV IVIĆ[1*#], S. D. PETROVIĆ[2,3#] and D. Ž. MIJIN[2#]

[1]*ICTM – Institute of Electrochemistry, University of Belgrade, Njegoševa 12, Belgrade*
[2]*Faculty of Technology and Metallurgy, University of Belgrade, Karnegijeva 4, Belgrade and* [3]*Hemofarm Group, Pharmaceutical and Chemical Industry, Vršac, Serbia*

(Received 8 October 2007)

Abstract: The aim of the present study is to present the different reactivity of azithromycin and clarithromycin (pure and commercial) at a gold electrode in neutral electrolyte using cyclic linear sweep voltammetry under the same experimental conditions. A gold electrode was successfully used for the electrochemical qualitative and quantitative determination of azithromycin dihydrate and azithromycin from capsules (Hemomycin®) and for the separation of azithromycin from one of the excipients, lactose monohydrate. The good catalytically activity of the gold electrode was employed only for the qualitative electrochemical determination of pure clarithromycin by appearance of one cathodic and four anodic reactions, which enabled structural changes in this molecule during electrochemical reactions to be studied. Commercial clarithromycin, Clathrocyn® was qualitative determined by one reproducible anodic reaction. The activity of one of the excipients, Avicel, observed as a cathodic peak at different potential from the cathodic peak obtained with pure clarithromicin was used for the determination of its presence in Clathrocyn® tablets. FTIR Analysis showed the apparent changes in structure of pure clarithromycin, as well as in the molecule of clarithromycin in Clathrocyn® tablets. HPLC Analysis showed a significant decrease in the concentration of azithromycin, Hemomycin® clarithromycin and Clathrocyn® after the electrochemical reactions.

Keywords: azithromycin, clarithromycin, gold electrode, cyclic voltammetry.

INTRODUCTION

Macrolide antibiotics are active on both gram-positive and, to a lesser extent, on gram-negative microorganisms. They exert their antimicrobial action by binding to the bacterial 50S ribosomal subunit and inhibiting ribosomal assembly and protein synthesis. Erythromycin is a natural compound metabolized by a strain of *Streptomyces erythreus.* As a broad-spectrum antibiotic, it has proved invaluable for the treatment of bacterial infections in patients with β-lactam hypersen-

* Corresponding author. E-mail: milka@tmf.bg.ac.yu
# Serbian Chemical Society member.
doi: 10.2298/JSC0712427A

sitivity. From this parent macrolide, several derivatives have been synthesized. Beckmann rearrangement of the 9-oxime followed by reduction and methylation gives azithromycin, which shows good activity against gram-negative bacteria, including *Haemophilus influenzae*. If the 6-hydroxy group is methylated, clarithromycin is obtained, which has an improved pharmacokinetic profile compared to the parent molecule. Azithromycin has a methylated nitrogen atom at position number nine on the macrolide lactone ring, and clarithromycin has a methyloxyl substitution at position number six of the macrolide ring (Fig. 1). These modifycations affect the biological potency of the molecules, with azithromycin having a stronger affinity for ribosome and affecting equally the 50S ribosomal assembly and protein elongation.[1,2] Clarithromycin also affects both processes but at a concentration 10 times higher than that of azithromycin, and erythromycin inhibits translation much more efficiently than the ribosomal assembly.[2]

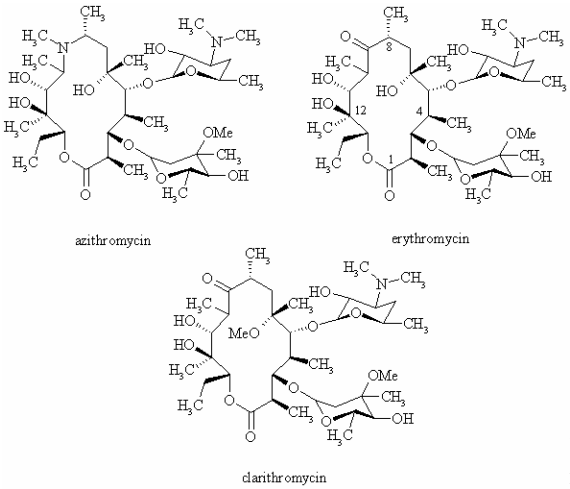

Fig. 1. Chemical structures of azithromycin, erythromycin and clarithromycin.

Azithromycin and clarithromycin present several clinical advantages over erythromycin, including better oral bioavailability, enhanced spectrum activity, higher tissue concentrations and improved tolerability.[3] Clarithromycin is widely used for the eradication of *Helicobacter pylori*, which causes gastritis and gastric ulcers.[4] Oral clarithromycin is used in combination with amoxicilin and lansoprazole or omeprazole (triple therapy) for the treatment of *Helicobacter pylori* infections and duodenal ulcers.[5–7] Quantitative methods using high performance liquid chromatography (HPLC) procedures for the analysis of azithromycin and clarithromycin have been widely applied.[8–11] Electrochemical methods for azithromycin determination are promising, being the cheaper and faster. Studies on the electrochemical oxidation and determination of azithromycin on glassy carbon and modified glassy carbon electrodes have been frequently published in the last few years. Hitherto, voltammetric determinations of azithromycin, including its determination in pharmaceutical dosage forms have been published.[12,13] In

the above-mentioned publications, the electrode material was usually glassy carbon, graphite and carbon paste or multi wall carbon nanotubes.

The aim of the present study is to present the different reactivity of azithromycin and clarithromycin (pure and commercial) in order to develop an electrochemical method for their qualitative and quantitative determination, as well as to separate or determine them in the presence of some excipient compounds in capsule (tablets) form. The macrolide antibiotics were examined at a gold electrode in neutral electrolyte using cyclic linear sweep voltammetry under the same experimental conditions. HPLC and FTIR spectroscopy were used for the analysis of the bulk electrolyte after the electrochemical reactions.

EXPERIMENTAL

Azithromycin dihydrate and clarithromycin, kindly provided by Hemofarm (Vršac, Serbia), were examined separately as pure substances, without further purification, in one set of electrochemical experiments. A comparative study was performed with capsulated azithromycin, marketed by Hemofarm as Hemomycin®, which except azithromycin contains the excipients: sodium lauryl sulfate, magnesium stearate, lactose monohydrate and corn starch. A comparative study was also performed with clarithromycin in tablet form, marketed by Hemofarm as Clathrocyn®, which in addition to pure clarithromycin contains the excipients: magnesium stearate, corn starch, Povidon 490, Avicel P401 and Prosolv SMC 90. The pure macrolide antibiotics and the content of the tablets (capsules) were added directly into the electrolytes in the concentrations given in detail in the Fig. captions. Before each measurement the electrolytes were purged with nitrogen for 20 minutes.

The $NaHCO_3$ used for the supporting electrolyte was of analytical grade (Merck). The solutions were prepared with 18 MΩ water. Standard equipment and a three electrode electrochemical cell were used for the cyclic voltammetry measurements, as previously described in detail.[14–18] Polycrystalline gold (surface area 0.500 cm^2), which served as the working electrode, was polished with diamond paste and cleaned with a mixture of 18 MΩ water and sulfuric acid. A platinum wire was used as the counter electrode and a saturated calomel electrode (SCE) as the reference electrode. All the potentials are given *vs.* SCE. The electrode surface was controlled by cyclic voltammetry before each experiment. Prior to the control of the electrode surface and before the addition of the macrolide antibiotics, the electrolyte was purged with nitrogen. All the experiments were performed at room temperature.

The pH of the electrolyte was measured using a PHM 93 reference pH meter, Radiometer, Copenhagen.

The characteristics of the HPLC instrument are as follows: HPLC Instrument GBC, pump LC 1120, UV VIS detector LC 1205, manual injector RHEODYNE 7725i, column Asahipak ODP-50 (250 mm×4 mm), stationary phase L21 (USP-a rigid, spherical styrene–divinyl benzene copolymer, 5 μm), mobile phase 0.002 M diammonium hydrogen phosphate, propanol-2, acetonitrile (pH 9.5, flow rate 1.0 $cm^3\ min^{-1}$), wave length 215 nm.

The IR spectra were obtained using a FTIR BOMEM MB 100 Hartmann Braun FTIR spectrometer. The samples were analyzed in the form of KBr pellets after removal of the liquid under high vacuum at low temperature.

RESULTS AND DISCUSSION

A polycrystalline gold electrode was selected as the optimal working electrode for the examination of pharmaceutical compounds because it is completely defined with an always reproducible cyclic voltammogram and consequently, all

the electrochemical reactions at this electrode can be attributed only to the studied molecule. In order to avoid the influence of organic molecules (with direct oxidation/reduction ability or adsorption ability at a gold electrode) arising from a solvent or a part of a buffer solution in the electrolyte and to obtain only the reactions of the pharmaceutical compounds, 0.05 M $NaHCO_3$ was selected as the supporting electrolyte.

Cyclic voltammetry investigations of pure azithromycine showed that the oxidative peak of pure azithromycin at 0.6 V in 0.05 M $NaHCO_3$ at a scan rate of 50 mV s^{-1} is a linear function of the concentration:[14]

$$i_{pa}\ (\text{mA cm}^{-2}) = 0.023\ (\pm 0.0043) + 0.110\ (\pm 0.0099)\ c\ (\text{mg cm}^{-3}),\ r = 0.9921 \quad (1)$$

Cyclic voltammograms presented in Fig. 2 show that for every investigated azithromycin dihydrate concentration only one very clear, wide and reproducible anodic peak was obtained in the concentration range 0.235–0.588 mg cm^{-3}. It is to be mentioned that that there is no cathodic activity of azithromycin.

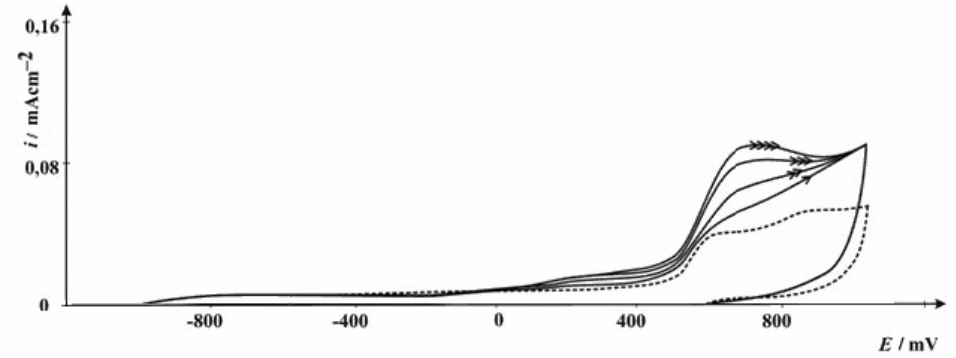

Fig. 2. Anodic part of the cyclic voltammogram of an Au electrode in 0.05 M $NaHCO_3$ (·····) and with the addition of 0.235, 0.353, 0.471 and 0.588 mg cm^{-3} pure azithromycin dihydrate (full line); the lowest concentration is assigned by one arrow andthe highest with four arrows. Sweep rate 50 mV s^{-1}.

The anodic part of the cyclic voltammograms obtained with azithromycin in capsule form, Hemomycin®, is presented in Fig. 3, from which it is obvious that two peaks appeared. The peak at 0.6 V, which is the oxidative peak of pure azithromycin is already observed in Fig. 2, but second peak at 0.4 V is the oxidative peak of the one excipient, lactose monohydrate. Sodium lauryl sulfate, magnesium stearate and corn starch are electrochemically totally inactive under the applied experimental conditions.[14] Using the anodic behavior of azithromycin in capsule, Hemomycin®, shown in Fig 3, an electrochemical method for the separation of azithromycin from lactose monohydrate at a gold electrode surface was developed. From the reproducible anodic peak at 0.4 V, lactose monohydrate is always recognized in the tested contents of capsule, which is important for the additional control of the contents of Hemomycin® capsules using a non time consuming and simple electrochemical method.

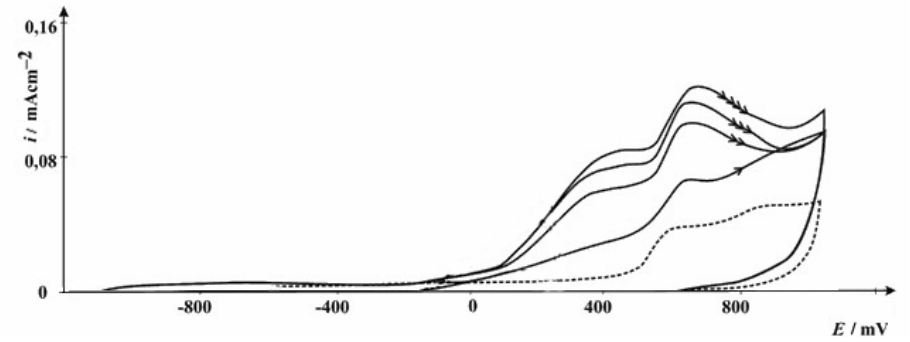

Fig. 3. Anodic part of the cyclic voltammogram of an Au electrode in 0.05 M $NaHCO_3$ (·····) and with addition of 0.235, 0.353, 0.471 and 0.588 mg cm^{-3} of Hemomycin® from capsules (full line), the lowest concentration is assigned by one arrow and highest with four arrows. Sweep rate 50 mV s^{-1}.

Each of the investigate concentrations of Hemomycin® gave a reproducible anodic oxidation peak and a linearity of the anodic peak current *vs.* concentration was obtained, as in the case of pure azithromycin. The linearity of the anodic peak current *vs.* concentration was obtained for lactose monohydrate in the investigated range of concentrations presented in Fig. 3, which opens the possibility for the development of a method for the quantitative detection of this compound.

HPLC Analysis of the bulk of electrolyte confirmed the data obtained by analysis of the peak current values concerning the correlation with the investigate concentrations for azithromycin and Hemomycin®.

Azithromycin has a methylated nitrogen atom at position nine on the macrolide lactone ring and clarithromycin has a methyloxyl substitution at position six of the macrolide ring (Fig. 1), which suggests possible different electrochemical activities of this two compounds.

The anodic part of the cyclic voltammogram of pure clarithromycin is presented in Fig. 4, from which it can be seen that in the anodic direction, a small, wide and reproducible anodic peak appears at −0.58 V.

Two reproducible anodic peaks were also observed at 0.10 V and at 0.33 V. In the region of AuO formation, a minor reproducible increase of the oxide peaks is seen. In this region the apparent activity of azithromycin (Fig. 2) can be used for its qualitative and quantitative determination. At –0.58 V in the anodic direction, azithromycin is not active and at 0.10 V and at 0.33 V, just a small increase of anodic currents is obvious, but there are no peaks (Fig. 2).

In Fig. 5 it is shown that a reproducible cathodic peak was obtained with clarithromycin at −0.61 V. However, with clarithromycin none of the observed peaks are proportional to the concentration of the antibiotic in the range of 0.110–0.625 mg cm^{-3}, which is in accordance with the conclusion that four reproducible anodic peaks and one cathodic peak only qualitatively determine clarithromycin.[15]

In order to get insight in the structural changes in the clarithromycin molecule during electrochemical reactions, electrochemical studies combined with the

analysis of the bulk electrolyte after the electrochemical reactions by FTIR spectroscopy and HPLC were performed.

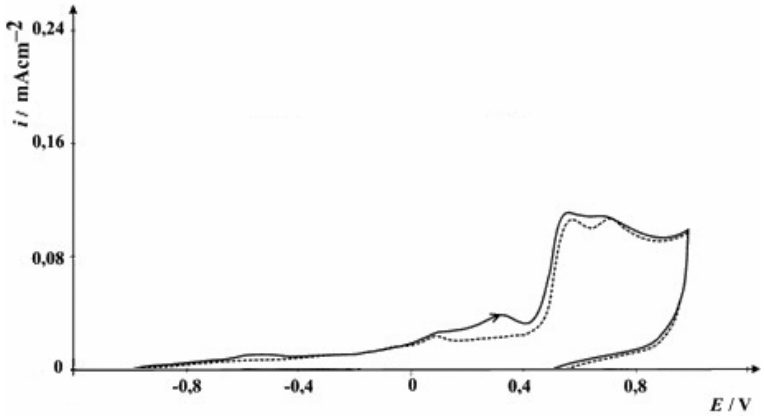

Fig. 4. Anodic part of the cyclic voltammogram of an Au electrode in 0.05 M $NaHCO_3$ (·····) and with the addition of 0.32 mg cm^{-3} of pure clarithromycin, (full line). Sweep rate 50 mV s^{-1}.

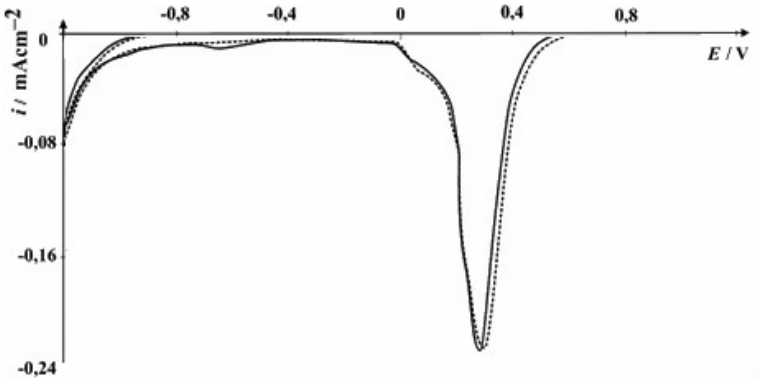

Fig. 5. Cathodic part of the cyclic voltammogram of an Au electrode in 0.05 M $NaHCO_3$ (·····) and with the addition of 0.32 mg cm^{-3} of pure clarithromycin, (full line). Sweep rate 50 mV s^{-1}.

The FTIR spectrum of pure clarithromycin and clarithromycin mixed with carbonates, both before the electrochemical experiment, served as reference for the further analysis. The observed changes in the molecule of clarithromycin were tracked with these data. The potential was held at selected values corresponding to all the observed current peaks (at −0.58 V, 0.10 V, 0.33 V and −0.61 V) for 4, 8 and 10 h and two samples of the electrolyte were analyzed by FTIR spectroscopy and HPLC. Significant changes in the molecular structure of clarithromycin were observed when the potential had been held at the potential of the cathodic peak observed in Fig. 5 (–0.61 V) for 4 h,[15] 8 and 10 h.

The FTIR spectrum reveals two obvious changes after holding the potential: the disappearance of the 1730 cm^{-1} peak corresponding to the carbonyl group vi-

bration of the lactone, and an intense reduction of the 1170 cm^{-1} peak, probably corresponding to the C–O vibration in the lactone, which implies changes in the ester bond of the lactone. The disappearance of the carbonyl band at 1690 cm^{-1} indicates a change in this group also. No absorptions were recorded in the 1000–1100 cm^{-1} range, which could be the result of changes in the ether and acetal bonds.[15] When the potential was held at the cathodic peak potential observed in Fig. 5 (–0.61 V) for 8 and 10 h, the FTIR spectrum showed the same changes.

The FTIR analysis did not reveal clear changes in the molecule structure after 4 and 10 h of holding the potential at 0.10V and at 0.33 V, except a minor reduction of the bands in the 1000–1100 cm^{-1} region.

Cyclic voltammogram investigation of clarithromycin in tablets, Clathrocyn®, indicated a different behavior from the pure antibiotic and that observed activities can be attributed to the excipient Prosolv, as an anodic peak at 0.33 V and to the excipient Avicel, as a cathodic peak at −0.90 V, which could be important for the electrochemical control of theirs contents in Clathrocyn®,[16] although a concentration dependency of commercial clarithromycin and Avicel was not observed.

The anodic part of the cyclic voltammogram of Clathrocyn® as presented in Fig. 6, shows only one reproducible and characteristic, sharp anodic peak in the potential region from 0.60 V to 0.80 V in the range of concentrations 0.110–0.725 mg cm^{-3}.

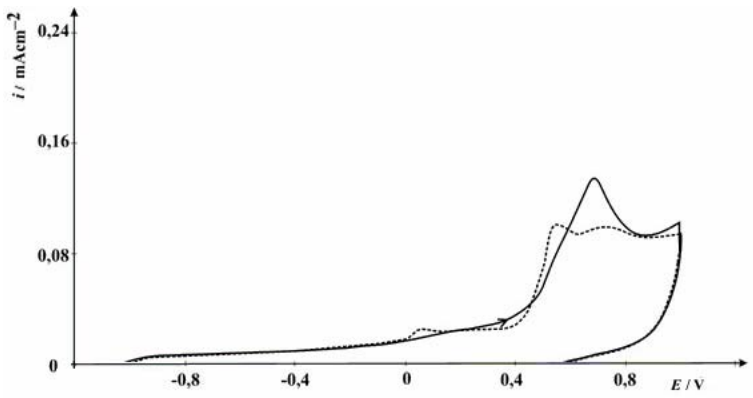

Fig. 6. Anodic part of the cyclic voltammogram of an Au electrode in 0.05 M $NaHCO_3$ (·····) and with addition of 0.56 mg cm^{-3} of Clathrocyn® (full line). Sweep rate: 50 mV s^{-1}.

In order to investigate the structural changes in the clarithromycin molecule in Clathrocyn® tablets caused by electrochemical processes, electrochemical studies combined with the analysis of the bulk electrolyte after the electrochemical reactions by Fourier transform infrared spectroscopy and high performance liquid chromatography were performed, similar to the investigation of pure clarithromycin.[16]

The FTIR spectrum of the bulk electrolyte after cycling the potential, in the range presented in Fig. 6 for 8 h shows: the disappearance of the peak at 1730 cm^{-1}

(carbonyl group of lactone) and the very small peak at 1170 cm^{-1} (C(O)−O−C vibrations of the lactone), indicating the disappearance of the lactone structure. Also, the reduction of intensity of the vibration band at 1695 cm^{-1} indicates changes of the carbonyl group at position 9 of the clarithromycin molecule in Clathrocyn® tablets. The same changes in the clarithromycin molecule in Clathrocyn® tablets were observed under the experimental conditions previously published.[16] As in the case of pure clarithromycin, this FTIR data combined with cyclic voltammetry can be helpful in the qualitative detection of the examined commercial clarithromycin.

HPLC Analysis of the bulk of electrolyte (the potential was held for 4 h at the 0.10 V and 0.70 V) showed a significant decrease (40 %) of the concentration of clarithromycin, both pure and commercial, as a consequence of the electrochemical reactions which had occurred.

Erithromycin was chosen as the macrolide antibiotic for the subject of the present studies because today it is the most safe antimicrobes drug and it was 162nd of the top 300 prescribed drugs in the year 2005 (which includes different drugs, for example, drugs for neoplastic action (20) (FDA)),[19] while azithromycin was 176th in the year 2005.[20] Cyclic voltammetry, HPLC and FTIR results with erithromycin suggest electrochemical activity similar to clarithromycin.[20]

CONCLUSIONS

In a conclusion, it should be pointed out that clarithromycin investigated under the same experimental conditions as azithromycin showed quite different behavior, which is attributed to the fact that azithromycin has a methylated nitrogen atom at position number nine on the macrolide lactone ring while clarithromycin has a methyloxyl substitution at position number six of the macrolide ring. It was shown that a gold electrode can be successfully employed for the qualitative and quantitative electrochemical determination of azithromycin dihydrate and azithromycin from capsules (Hemomycin®) and for the separation of azithromycin from lactose monohydrate. Lactose monohydrate can also be quantitatively determined.

The good catalytic activity of a gold electrode can be employed only for the qualitative electrochemical determination of pure clarithromycin by the appearance of the one cathodic and four anodic reactions, which enables structural changes in this molecule during electrochemical reactions to be studied. FTIR analysis showed significant structural changes in the clarithromycin molecule, *i.e.*, changes in the ester bond of the lactone and changes in the ether and acetal bonds. Clarithromycin in tablets, Clathrocyn®, is defined by one reproducible anodic peak and the activity of the excipient Avicel was used for the determination of its presence in Clathrocyn® tablets. FTIR analysis showed changes in the structure of the molecule indicating the disappearance of the lactone moiety and changes of carbonyl group at position 9. HPLC Analysis of the bulk elec-

trolyte showed a significant decrease in the concentration of all the examined macrolide antibiotics, as a consequence of the electrochemical reactions which had occurred.

Acknowledgments. The authors are grateful to the Ministry of Science of Serbia for financial support (project 142063).

И З В О Д

ПРОУЧАВАЊЕ ЕЛЕКТРОХЕМИЈСКЕ АКТИВНОСТИ НЕКИХ МАКРОЛИДНИХ АНТИБИОТИКА НА ЕЛЕКТРОДИ ОД ЗЛАТА У НЕУТРАЛНОМ ЕЛЕКТРОЛИТУ

М. Л. АВРАМОВ ИВИЋ[1], С. Д. ПЕТРОВИЋ[2,3] и Д. Ж. МИЈИН[2]

[1]ИХТМ – Центар за електрохемију, Његошева 12, Београд, [2]Технолошко–металуршки факултет, Карнегијева 4, Београд и [3]Хемофарм група, Фармацеутска и хемијска индустрија, Вршац

У раду су приказани резултати испитивања електрохемијске активности азитромицина и кларитромицина (чисте супстанце и комерцијалног фармацеутског производа) на електроди од злата у неутралном електролиту. HPLC и FTIR спектроскопија су коришћене за анализу електролита после електрохемијске реакције. Показано је да под истим експерименталним условима азитромицин и кларитромицин испољавају потпуно различито електрохемијско понашање условљено разликама у структури макролидног прстена. Максимална вредност висине јединог струјног врха оксидације чистог азитромицина и азитромицина у капсули Хемомицина® на 0,6 V у 0,05 M $NaHCO_3$ при 50 mV s^{-1} је линеарна функција концентрације у опсегу 0,235–0,588 mg cm^{-3} што је омогућило развијање методе за његово квалитативно и квантитативно одређивање. Развијена је и метода за сепарацију и квантитативно одређивање ексципиента, монохидрата лактозе. Квалитативно је одређен чист кларитромицин детекцијом репродуктивне четири анодне и једне катодне реакције док је кларитромицин у таблети, Clathrocyn®, квалитативно одређен једном репродуктивном анодном реакцијом. FTIR анализа је показала уочљиве промене у структури молекула кларитромицина. Такође су уочене и структурне промене после испитивања кларитромицина у таблети Клатроцина®. HPLC анализа је указала на значајно смањење концентрација азитромицина, Хемомицина®, кларитромицина и Клатроцина® у електролиту после електрохемијских реакција.

(Примљено 8. октобра 2007)

REFERENCES

1. R. C. Goldman, S. W. Fesik, C. C. Doran, *Antimicrob. Agents Chemother.* **34** (1990) 426
2. S. Mabe, J. Eller, W. S. Champney, *Curr. Microbiol.* **49** (2004) 248
3. J. M. Zuckerman, *Infect. Dis. Clin. North Am.* **18** (2004) 621
4. D. Y. Graham, A. R. Opekun, P. D. Klein, *J. Clin. Gastroenterol.* **16** (1993) 292
5. S. Khanal, B. S. Rao, Y. Sharma, G. M. Khan, R. Makaju, *Kathmandy Univ. J. Sci. Eng. Tech.* **1** (2005)
6. A. Saltermann, A. Perrent, S. Schmid, F. Eigenmann, R. Guller, K. B. Weber, J. Meier, P. Eichenberger, P. Komminote, *Swiss. Med. Weekly* **135** (2005) 327
7. W. Luman, *J. Royl. Coll. Physicians Edinburgh* **35** (2005) 45
8. J. Sastre–Torano, H. J. Guchelaar, *J. Chromatogr. B* **720** (1998) 89
9. C. Taninaka, H. Ohtani, E. Hanada, H. Kotaki, H. Sato, T. Iga, *J. Chromatogr. B* **738** (2000) 405
10. E. Wilms, H. Trumpie, W. Veenendaal, D. Touw, *J. Chromatogr. B* **814** (2005) 37
11. O. A. El–Moaty Farghaly, N. A. L. Mohamed, *Talanta* **62 (**2004**)** 531

12. B. Nigović, *Anal. Sci.* **20** (2004) 639
13. B. Nigović, B. Simunic, *J. Pharm. Biomed. Anal.* **32** (2003) 197
14. M. L. Avramov Ivić, S. D. Petrović, D. Ž. Mijin, P. M. Živković, I. M. Kosović, K. M. Drljević, M. B.Jovanović, *Electrochim. Acta* **51** (2006) 2407
15. M. L. Avramov Ivić, S. D. Petrović, V. Vonmoos, D. Ž. Mijin, P. M. Živković, K. M. Drljević, *Electrochem. Commun.* **9** (2007) 1643
16. M. L. Avramov Ivić, S. D. Petrović, V. Vonmoos, D. Ž. Mijin, P. M. Živković, K. M. Drljević, *Russ. J. Electrochem*., in press
17. V. M. Jovanović, M. Avramov–Ivić, S. D Petrović, *J. Serb. Chem. Soc.* **60** (1995) 879
18. G. A. Ragoisha, V. M. Jovanovic, M. A. Avramov–Ivic, R. T. Atanasoski, W. H. Smyrl., *J. Electroanal. Chem.* **319** (1991) 373
19. M. Avramov Ivić, S. D. Petrović, E. Kalman, T. Milosavljević, I. Reljin, B. Reljin, G. Bogdanović, V. Vit. Baltić, Z. Keresztes, *J. Serb. Chem. Soc.* **70** (2005) 823
20. M. Avramov Ivić, S. D. Petrović, D. Mijin, V. Radović, in preparation.

Journal of the Serbian Chemical Society
JSCS@tmf.bg.ac.yu • www.shd.org.yu/JSCS

J. Serb. Chem. Soc. 72 (12) 1437–1463 (2007) UDC 544.344+536.7.004.12:681.3.042/.043:536.658
JSCS–3675 *Review paper*

REVIEW PAPER

Modelling of volumetric properties of binary and ternary mixtures by CEOS, CEOS/G^E and empirical models

BOJAN D. DJORDJEVIĆ*#, SLOBODAN P. ŠERBANOVIĆ#, IVONA R. RADOVIĆ#, ALEKSANDAR Ž. TASIĆ and MIRJANA LJ. KIJEVČANIN#

Faculty of Technology and Metallurgy, University of Belgrade, Karnegijeva 4, P.O. Box 35-03, 11120 Belgrade, Serbia

(Received 15 August 2007)

Abstract: Although many cubic equations of state coupled with van der Waals-one fluid mixing rules including temperature dependent interaction parameters are sufficient for representing phase equilibria and excess properties (excess molar enthalpy H^E, excess molar volume V^E, *etc.*), difficulties appear in the correlation and prediction of thermodynamic properties of complex mixtures at various temperature and pressure ranges. Great progress has been made by a new approach based on CEOS/G^E models. This paper reviews the last six-year of progress achieved in modelling of the volumetric properties for complex binary and ternary systems of non-electrolytes by the CEOS and CEOS/G^E approaches. In addition, the vdW1 and TCBT models were used to estimate the excess molar volume V^E of ternary systems methanol + chloroform + benzene and 1-propanol + chloroform + benzene, as well as the corresponding binaries methanol + chloroform, chloroform + benzene, 1-propanol + chloroform and 1-propanol + benzene at 288.15–313.15 K and atmospheric pressure. Also, prediction of V^E for both ternaries by empirical models (Radojković, Kohler, Jackob–Fitzner, Colinet, Tsao–Smith, Toop, Scatchard, Rastogi) was performed.

Keywords: correlation, prediction, volumetric properties, cubic EOS mixing rules, empirical models, non-electrolyte multicomponent systems.

CONTENTS:

* Corresponding author. E-mail: bojan@tmf.bg.ac.yu
# Serbian Chemical Society member.
doi: 10.2298/JSC0712437D

1. INTRODUCTION

CEOS and CEOS/G^E models are widely applied for the representation of vapour–liquid equilibria, VLE, liquid–liquid equilibria, LLE, and other thermodynamic properties of mixtures required for synthesis, design of chemical plants, optimization and development of chemical, gas processing, petrochemical and other industries. Since the first van der Waals-one fluid mixing rule was introduced, continuous effort has been made on the development of new mixing rules. Recently, great advancement was achieved by using G^E mixing rules incorporated into CEOS equations.

The interest was focused on experimental measurements and thermodynamic modelling of mixtures containing various groups of organic compounds: alcohols, aromatics and alkyl chlorides, since they exhibit varying molecular interactions, resulting in specific deviations from ideal behaviour. In addition, these mixtures are important from a practical point of view, due to their diverse industrial applications and presence in main pollution generating industries and processes, causing air, water and soil contamination. Alcohols and aromatics are widely employed in a variety of industrial and consumer applications, such as perfumes, cosmetics, paint, varnish, drugs, fuel, explosives, fats, waxes, resin, plastics, rubber, detergents, DDT, *etc.* Chloroform is applied as a solvent in various industries, *e.g.*, in the extraction of penicillin and other antibiotics in the pharmaceutical industry, for pesticides, fats, oils, rubber, alkaloids, waxes, *etc.* In a mixture with alcohol or benzene, chloroform is widely used as an eluting system, such as, for medical purposes, in radiopharmacy, in chemical reactions, *etc.*; also, chloroform and benzene are very often contained in the wastewater of different industries as pollutants having cancerous features.

One part of the present work is a review of experimental investigations of the volumetric properties of binary and ternary systems, performed at atomspheric pressure using Anton Paar digital vibrating U-tube densimeters: DMA 55[1,2] and DMA 5000,[3–8] with a precision $\pm 1\times10^{-5}$ g cm^{-3} and $\pm 1\times10^{-6}$ g cm^{-3}, respectively. In both cases, the samples were prepared by weight using mass balances having a precision $\pm 1\times10^{-4}$ g. The experimental accuracy achieved by the DMA 55 densimeter was better than $\pm 3\times10^{-5}$ g cm^{-3}, while the uncertainty in the density measured by the DMA 5000 densimeter was about $\pm 1\times10^{-5}$ g cm^{-3} and the average uncertainty in the excess molar volume was estimated to be $\pm 3\times10^{-3}$ cm^3 mol^{-1}.

The other goal of this work was to provide a review of the obtained results in recent investigations performed by the CEOS and CEOS/G^E models on the evaluation of the volumetric properties of binary and ternary mixtures.[2–5,8–13] Also, for the ternary systems methanol + chloroform + benzene and 1-propanol + chloroform + benzene results of the prediction and correlation of V^E values obtained by these models are presented, bearing in mind that previously[6,7] only experi-

mental data were published. In addition, the prediction of V^E values for both ternaries was performed by frequently employed empirical models. Recently, published papers were connected to some advances in describing phase equilibria and excess properties using CEOS/G^E models.[9–13]

2. EVALUATION OF VOLUMETRIC PROPERTIES

2.1. Testing of CEOS and CEOS/G^E models

The ability of composition dependent CEOS (vdW1)[14] and CEOS/G^E mixing rules (Gupta–Rasmunsen–Fredenslund GRF[15] which incorporates the NRTL equation[16] as the G^E model) to correlate the V^E of non-electrolyte binary mixtures was investigated.[9] Very complex systems of diverse structure and complexity were selected: monocyclic ether + *n*-alkane, + 1-alcohol, + cyclohexane, + toluene. A relatively large number of data points (562) over the entire composition range and in the temperature interval 288.15–308.15 K were covered. The complexity of the chosen systems is characterized by their non-ideal behaviour, exhibiting an asymmetric shape of the V^E – composition relationship having very small or large excess volumes, *etc*. The mentioned data base allowed an analysis of several aspects of the properties of the mixtures: the increase/decrease in the number of the carbon atom chain of the alkane or alcohol series; in addition, diverse structures and complexity of the molecular interactions in the liquid mixtures were examined, which accounted for their ability to affect the V^E–composition behaviour. The influence of the applied mixing rule (CEOS or CEOS/G^E), as well as the influence of the incorporated temperature dependent interaction parameters, on the correlation of the V^E data was tested.[3–5,8]

The results of the investigation[9] lead to the following conclusions: (a) correlation of the data at a single isotherm can be successfully performed using the vdW1 or GRF models with no-temperature dependent parameters of the NRTL equation; (b) however, for the correlation in a temperature range, the obtained results indicate that incorporation of a more flexible mixing rule, which includes all temperature dependent interaction parameters, should be used.

Critical examination of the applicability of the cubic equations of state (CEOS) mixing rules to the representation of V^E data for systems containing dicyclic ethers with alkanes, alcohols and cyclohexane[10] represents a continuation of our effort expended in analyzing V^E data for mixtures of monocyclic ethers with various substances reported previously.[9] Twenty four highly non-ideal mixtures, consisting of 593 data points, were included. Sixteen binaries at 298.15 K and eight systems in the temperature range 288.15–308.15 K were analysed. The V^E––composition dependence for the binaries with dicyclic ethers, mentioned above, were correlated by the Peng–Robinson–Stryjek–Vera cubic equation of state (PRSV CEOS),[17] coupled with two different classes of mixing rules: (a) the composition dependent van der Waals (vdW1) one-fluid models[14] and (b) two types of

the excess free energy mixing rules (CEOS/G^E), the general form based on GRF,[15] as well as the mixing rule of Twu–Coon–Bluck–Tilton (TCBT).[18] Both rules were used with NRTL equation as the G^E model.

According to the obtained results, the following evidence were provided: (*i*) for the correlation of isothermal V^E data at 298.15 K using the CEOS mixing rules for the systems of dicyclic ethers with alcohols and cyclohexane, the use of temperature dependent parameters was not necessary; in addition, it was shown that the correlation of V^E data from a single isotherm can be successfully performed using the GRF model with no temperature dependent parameters in the NRTL equation; (*ii*) for correlation of V^E data of dicyclic ethers with alkanes in the temperature range 288.15–308.15 K, it was found that the use of the new TCBT model with no temperature dependent parameters was adequate. Alternatively, the GRF mixing rule with all temperature dependent parameters worked satisfactorily.

2.2. Binary systems

In this part of research,[1] the effort was directed toward the investigation of the excess molar volume (V^E) of the non-ideal behaviour of two binary mixtures containing alcohol and acetonitrile. The systems methanol + acetonitrile and ethanol + acetonitrile were treated. The density measurements for these systems were performed at 298.15 K and used for the determination of V^E over the entire composition range. During mixing with acetonitrile, which contains a proton acceptor group, a part of the alcohol will tend to dissociate and form other kinds of hydrogen bonds within the molecules. The nature of the mixture was investigated over the composition range. The composition dependence of mixtures was fitted by the Redlich–Kister (RK) polynomial equation.[19] It was shown that the V^E values for both systems are small and that they rise with increasing length of the alkyl chain in the alcohol.

The excess molar volume for the methanol + acetonitrile system is negative over the entire composition range, tending to be skewed toward mixtures rich in acetonitrile. This could be a consequence of the association between the nitrile group and the proton of the methanol hydroxyl group, outweighing the effect of dissociation of the alcohol molecules.

The V^E *vs.* composition curve for the system with ethanol has a S-shaped form; the V^E values are positive in the region of low alcohol concentration, and negative for mole fractions of ethanol higher than 0.35.

The TCBT model was used in an attempt to extend its applicability to the correlation of experimentally obtained V^E data,[11] as described in a previous paper (for the acetonitrile + methanol and acetonitrile + ethanol systems).[1] For the system acetonitrile + methanol, the best results of correlation were obtained by employing the TCBT-2, TCBT-3 and TCBT-5 models, having three, four and

five parameters, respectively. It was shown that improvement of the results by using TCBT-3 and TCBT-5 models was not achieved, comparing to those obtained by the TCBT-2 model. The acetonitrile + ethanol system exhibits S-shaped dependence of V^E on composition. It was shown that the models TCBT-2 and TCBT-3 gave similar results. In addition, the results of the correlation showed that a constant value for the parameter $\alpha_{ij} = 0.3$ should be used.

In conclusion, it can be noticed that, the TCBT models with binary interaction parameters of the vdW fluid gave exceptionally good results for the investtigated systems at 298.15 K.

The increased interest in the determination of excess molar volumes was the encouragement to continue work[9–11] on the improvement of the correlation of V^E. Experimental V^E data, calculated from density measurements of the systems methanol + benzene, ethanol + benzene, methanol + chlorobenzene and ethanol + chlorobenzene, at the temperatures 288.15, 293.15, 298.15, 303.15, 308.15 and 313.15 K were presented.[3] The data of the above-mentioned binaries, measured over the entire composition range at the specified temperatures were fitted to the RK equation, with the optimal number of adjustable parameters used according to the F-test.[20] It was observed that, in all cases, V^E increased with increasing temperature. The shape of the V^E–composition relationship can be explained qualitatively on the basis of the following opposite effects, predominant in a certain mole fraction region:[21,22] (a) positive values (in the alcohol lower region) are attributed to rupture or stretch of the hydrogen bonding of self-associated molecules of alcohol; (b) negative values are thought to be due to unlike specific interactions; (c) the geometric fitting of benzene or chlorobenzene into the remaining alcohol structure makes this effect negative to V^E. The magnitude and sign of V^E are a consequence of the contributions occurring in the investigated mixtures.

Correlation of the V^E data was performed using the PRSV CEOS coupled with the vdW1 and CEOS/G^E mixing rules introduced by Twu *et al.*[18] (TCBT). The NRTL equation was used as the G^E model. Modelling of the binary V^E data was performed based on two approaches: (a) the temperature independent and (b) temperature dependent vdW1 and TCBT mixing rules. Correlation of the V^E data by temperature independent PRSV CEOS models showed the following: (*i*) for the methanol + benzene system, the three parameter TCBT-3 model was superior; (*ii*) for the ethanol + benzene system, V^E correlation with the two and three parameter TCBT models gave better results than the vdW1-3 model; (*iii*) in the case of the methanol + chlorobenzene system, except for the best TCBT-3 model, all models gave errors which increased with increasing temperature. In addition, the vdW1-3 model can be treated as very satisfactory; (*iv*) for the ethanol + chlorobenzene system, the vdW1-3 and TCBT models functioned quite similar. Correlation of the V^E data by the temperature dependent PRSV CEOS models gave higher errors for the systems with benzene compared to those with chloro-

benzene, because of the S-shaped V^E curves and the considerably lower values of this property. In addition, it could be observed that the three parameter models for both kinds of systems gave better results.

Additional results, related to experimental volumetric determination and thermodynamic modelling based on some CEOS mixing rules for the correlation and prediction of V^E data and the limiting partial excess molar volumes ($\overline{V}_i^{E\infty}$) were also presented.[4] The aim of that investigation was to extend our previous work concerned with the measurements of V^E of methanol + chlorobenzene and ethanol + chlorobenzene[3] to mixtures of some other alcohols, namely 1-propanol, 1-butanol, 2-butanol, 2-methyl-2-propanol, or 1-pentanol, with chlorobenzene, at six temperatures, *i.e.*, 288.15, 293.15, 298.15, 303.15, 308.15 and 313.15 K. Also, density measurements for the 2-methyl-2-propanol + chlorobenzene system were performed at temperatures 303.15, 308.15, 313.15, 318.15 and 323.15 K, since the melting point of 2-methyl-2-propanol is about 298.15 K. All the investtigated systems (except 2-methyl-2-propanol + chlorobenzene system) exhibit S-shaped V^E–composition relationship (in the temperature range of interest for the present work); the system 2-methyl-2-propanol + chlorobenzene exhibited positive V^E values over the entire composition range at each isotherm. Excess molar volumes of the investigated binaries were fitted using the RK equation.

The dependence of V^E on both composition and temperature, for the mixtures studied, can be explained qualitatively as a balance between opposite effects.[4] In addition to aspects of the molecular interactions, mentioned above, the obtained results were theoretically discussed in terms of the chain length of the alcohols, degree of branching in the chain and relative position of the alkyl and OH group in the alcohol. As a consequence of increasing temperature, in general, hydrogen bonding becomes weaker; the molecular interaction energy is lower, leading to an increase of the distance between the molecules, causing the volume to increase. The results of this work show that an order of limiting partial excess molar volume ($\overline{V}_i^{E\infty}$) was established; for example at 298.15 K the following order was recognised: for $\overline{V}_1^{E\infty}$ – ethanol < 1-propanol < 1-butanol ≈ 1-pentanol, whereas for $\overline{V}_2^{E\infty}$ – ethanol > 1-propanol > 1-butanol > 1-pentanol. In addition, the influence of temperature variation on $\overline{V}_i^{E\infty}$ was described and discussed. In addition, the following order of increase of $\overline{V}_1^{E\infty}$ and $\overline{V}_2^{E\infty}$ for mixtures with branched alcohols was noted: primary < secondary < tertiary alcohols.

As mentioned previously,[4] thermodynamic modelling of the experimental V^E data was performed by the PRSV CEOS coupled with two types of mixing rules, vdW1 and TCBT. In both mixing rules, the parameters were used as temperature independent and as temperature dependent ones.

It was shown that for all treated cases, except for the 2-methyl-2-propanol + + chlorobenzene system, which exhibited positive V^E values, the form of the V^E–composition relationship was S-shaped.[4] Modelling of the experimental V^E

data by the mentioned thermodynamic method was applied to each binary system separately and corresponding instructions on the best approach for treating particular data sets was proposed.[4]

2.3. Ternary systems

Excess molar volume data of the ternary system ethanol + 2-butanone + benzene at 298.15 K, which were not available in the literature, were investtigated.[2] In addition, the corresponding binary V^E measurements[2] were compared to the data of other authors reported earlier.[23–27] The binary data were fitted to the RK equation, while for the ternary V^E data, the Nagata and Tamura expression (NT)[28] was employed.

The V^E data of all three binaries were correlated by the vdW and TCBT mixing rules coupled with the PRSV CEOS. For all systems, the best results were obtained by the three-parameter TCBT-3 model, except for the case of the ethanol + 2-butanone mixture, where the vdW1-3 model gave very good results. Prediction and correlation of the ternary V^E data were performed using the corresponding binary parameters. Inspection of the ternary predictions indicates that the use of the vdW1-1 and vdW1-2 models gave fair results, whereas those attained by the vdW1-3 model were very good. Ternary correlation by the TCBT mixing rules, which included a ternary contribution in the NRTL equation, could be estimated as acceptable and mutually very similar.

A systematic study of the excess molar volume for binaries and ternary systems of non-electrolytes was performed.[5] In this work, the densities for the ternary system ethanol + chloroform + benzene and the two corresponding binaries ethanol + chloroform and chloroform + benzene were measured. All these measurements were obtained at the temperatures 288.15, 293.15, 298.15, 303.15, 308.15 and 313.15 K. The related V^E data were obtained from the measured densities. As already was mentioned,[3] thermodynamic investigations of alcohol + aromatic systems are of great importance due to their broad industrial application, as well as because of the complex molecular interactions present in these mixtures. Also the influence of the third component, chloroform, on the interaction between the alcohol and aromatic hydrocarbon in the ternary system was studied.[5] The V^E of the binary mixtures were fitted by the RK equation and the ternary data with the NT equation, while the Radojković *et al.*[29] equation was used for the prediction of the ternary data. Correlation of the binary data was performed by the PRSV CEOS using selected mixing rules: (a) the composition dependent vdW1 and (b) the TCBT mixing rules. Prediction of V^E of the ternary system was performed by the same vdW1 and TCBT models. For the correlation of the ternary V^E data, only the TCBT mixing rules were employed. Inspection of the binary V^E data for ethanol + chloroform shows that the V^E–composition relationship exhibits S-shape curves; also, an increase of V^E with increasing temperature

(from 288.15 to 313.15 K) was found. For the system chloroform + benzene, positive values of V^E were observed over the entire composition range. The highest values were obtained at 288.15 K.

Factors influencing the behaviour of the excess molar volume have already been discussed in the literature for the binary systems ethanol + benzene[3] and ethanol + chloroform.[30] Particularly, in the case of the chloroform + benzene system, some influences can be mentioned as an explanation of the V^E–composition behaviour, for example: (a) the difference between van der Waals volumes[31] of the constituents, (b) the formation of a weak complex between benzene and chloroform[32,33] and (c) the presence of steric hindrance effects in the mixture. The behaviour of the V^E–composition relationship of the ternary system ethanol + chloroform + benzene, in the given temperature range, was discussed in detail.[5] The influence of various factors affecting molecular interactions in the mixture was analysed. It was observed that the highest interactions of the components were obtained when the composition was slightly shifted to a mixture rich in ethanol.

Modelling of the binary V^E data was performed for each isotherm separately over the whole temperature range. The results obtained employing the temperature independent PRSV CEOS models indicate that the three parameter models (vdW1-3 and TCBT-3), for both binaries were the best.

For the prediction of ternary V^E data at the investigated temperatures, the binary interaction parameters of the CEOS models, generated from binary data, were used. The obtained results show that the predictions corresponding to the vdW1-2, vdW1-3 and TCBT-2 models are qualitatively acceptable and approximate to those obtained by the Radojković *et al.*[29] equation. Correlation of the ternary V^E data was performed only by the TCBT model, which included a ternary contribution parameter in the NRTL equation. Fitting of these data could be regarded as fair and similar.

A continual effort to investigate the volumetric properties of binary and ternary mixtures containing different types of organic solvents frequently used in various industries was described.[6] Thermodynamic investigation of alcohols, chloroform and aromatics, either pure or in mixtures, is of considerable interest due to the complex molecular interactions present in these mixtures. Densities for the ternary system methanol + chloroform + benzene and for the binary system methanol + chloroform at 288.15, 293.15, 298.15, 303.15, 308.15 and 313.15 K and atmospheric pressure were measured.[6] From these measurements, the V^E data were calculated. The binary V^E data were fitted using the RK equation, while the NT equation was used for the ternary data. The root-mean-square deviation (RMSD) between the experimental binary data from those computed using the RK equation were 0.0028×10^{-6} m^3 mol^{-1} to 0.0034×10^{-6} m^3 mol^{-1}, whereas for the ternary system, it was in the range: 0.0035×10^{-6} m^3 mol^{-1} to 0.0040×10^{-6} m^3 mol^{-1}.

A further contribution to previous research of the volumetric properties of binary and ternary mixtures containing various alcohols, chloroform and benzene was of primary interest.[7] The density of the ternary system 1-propanol + chloroform + benzene, and the binaries 1-propanol + chloroform and 1-propanol + benzene at the temperatures of 288.15, 293.15, 298.15, 303.15, 308.15 and 313.15 K and atmospheric pressure were measured and used for the calculation of V^E data. The fitting equations for the correlation of binary and ternary V^E data used in the previously discussed work[6] were also employed here. The RMSD of the experimental data from those calculated from the fitting models lay in the ranges: for the 1-propanol + chloroform system, 0.0036 to 0.0038×10^{-6} m^3 mol^{-1}; for the system 1-propanol + benzene, 0.0033 to 0.0044×10^{-6} m^3 mol^{-1}, whereas the RMSD for the ternary system was in the range 0.0039 to 0.0045×10^{-6} m^3 mol^{-1}.

The density of the ternary mixture 1-butanol + chloroform + benzene and the binaries 1-butanol + chloroform and 1-butanol + benzene were measured at six temperatures in the interval 288.15–313.15 K.[8] The corresponding V^E values were calculated from these density measurements and fitted by the polynomial equations: (a) of the RK equation for the binary systems and (b) of the NT equation for the ternary system. Ternary prediction was performed by the equation of Radojković *et al*.[29] The dependence of V^E on composition for the system 1-butanol + chloroform at 288.15, 293.15, 298.15, 303.15, 308.15 and 313.15 K exhibits a S-shaped curve, with a positive maximum and negative minimum values of V^E. It was remarked that these values increase with increasing temperature. The V^E–composition relationships for the system 1-butanol + benzene show positive values that increase with increasing temperature. A qualitative explanation of the V^E–composition relationship could be given on the basis of the opposite contributions, predominating in certain mole fraction regions.[8] The magnitude and sign of V^E have been interpreted as resulting from the balance between these effects.

For the investigated ternary system, positive V^E were obtained over most of the composition field, except in the region in the vicinity to 1-butanol in binary mixture with chloroform, where the sign was negative. Maximum V^E values appear close to the binary chloroform + benzene border, suggesting that the unpacking effect, which is a result of complex formation of chloroform + benzene, and the disruptive effect on the self- associated molecules of 1-butanol are more dominant. In addition, an increase of the maximum values of V^E with increasing temperature was remarked, bringing about a diminishing of the negative V^E region. Also, the excess molar volume maximum is located approximately near the centre of the triangular diagram.

V^E Data were used to test the CEOS and CEOS/G^E models for their correlative and predictive abilities.[8] For the correlation of the binary data, PRSV CEOS coupled with temperature independent and temperature dependent mixing rules,

the composition dependent vdW1 and the TCBT models, were used. Correlation of the ternary V^E data was performed by employing the TCBT model, whereas for ternary prediction the vdW1 and TCBT models were used.

3. SIMULTANEOUS CORRELATION OF VLE, H^E AND c_p^E

Considering the fact that phase equilibria: vapour–liquid (VLE), liquid–liquid (LLE), gas solubility and excess properties: excess molar enthalpies (H^E), excess heat capacity (c_p^E), excess molar volume (V^E), *etc*., of liquid systems are of great importance for the design and operation of industrial processes, as well as the fundamental necessity for a better understanding of molecular interactions in fluid systems from the thermodynamic point of view, simultaneous correlation of two (VLE + H^E, VLE + c_p^E and H^E + c_p^E) and three properties (VLE + H^E + c_p^E) was carried out.[12] For this purpose, the corresponding data of diethers (1,4-dioxane and 1,3-dioxolane) with *n*-alkanes (heptane, octane, nonane and decane) were selected.

VLE and excess properties (H^E and c_p^E) for diether + *n*-alkane systems were simultaneously correlated,[13] employing the CEOS incorporating the activity coefficient model (CEOS/G^E). The approach of Kohler,[34] already used,[35–37] in the form of an empirical equation of the polynomial form, was applied[12] for the simultaneous correlation of the data of the above-mentioned systems. All the coefficients in the expression for the temperature dependent polynomial parameters were generated from the corresponding fits of VLE + H^E, VLE + c_p^E and H^E + + c_p^E or VLE + H^E + c_p^E data.

The calculation results obtained by the Kohler polynomial model were compared with those corresponding to the previously applied CEOS/G^E models (MHV1 and MHV2).[13]

The main results of the investigation on the simultaneous correlation of diverse thermodynamic properties by the Kohler polynomial equation (VLE + H^E, VLE + c_p^E and H^E + c_p^E) for the systems investigated gave very successful results, as was the case with the CEOS/G^E models. However, the correlation of three properties (VLE + H^E + c_p^E) showed that the Kohler model was more suitable than the CEOS/G^E models.

Finally, it can be concluded that the simultaneous correlation of three thermodynamic properties should be further investigated because of its importance from the theoretical and practical points of view.

4. MODELLING OF TERNARIES ALCOHOLS + CHLOROFORM + BENZENE

4.1. Correlation and prediction of V^E *by the vdW1 and TCBT models*

The general two-parameter cubic equation of state (CEOS) has the form:

$$P = \frac{RT}{V - b} - \frac{a(T)}{(V + ub)(V + wb)} \tag{1}$$

where P, T, V, and R denote pressure, temperature, molar volume and gas constant, respectively; the CEOS dependent constants u and w for the Peng–Robinson–Stryjek–Vera (PRSV) equation[17] applied here are: $u=1-\sqrt{2}$ and $w=1+\sqrt{2}$. For the pure substance, the energy a_i and co-volumen b_i parameters are determined as:

$$a_i(T) = 0.457235\frac{(RT_{ci})^2}{P_{ci}}[1+m_i(1-\sqrt{T_{ri}})]^2 \tag{2}$$

$$b_i = 0.077796\frac{RT_{ci}}{P_{ci}} \tag{3}$$

$$m_i = k_{0i} + k_{1i}(1+\sqrt{T_{ri}})(0.7-T_{ri}) \tag{4}$$

$$k_{0i} = 0.378893 + 1.4897153\omega_i - 0.1713848\omega_i^2 + 0.0196554\omega_i^3 \tag{5}$$

where T_{ci} and P_{ci} are the critical temperature and critical pressure of component i, respectively, T_{ri} denotes the reduced temperature, T/T_{ci}, ω_i is the acentric factor, and k_{1i} represents the pure substance adjustable parameter.[17]

For the determination of the a and b parameters of a mixture, two different types of mixing rules are used: vdW1 and TCBT.

The vdW1 mixing rule[14] is given by the following equations:

$$a = \sum_i \sum_j x_i x_j \left(a_i a_j\right)^{1/2}\left[1-k_{ij}+l_{ij}\left(x_i - x_j\right)\right] \tag{6}$$

$$b = \sum_i \sum_j x_i x_j \left(b_i b_j\right)^{1/2}\left(1-m_{ij}\right) \tag{7}$$

where k_{ij}, l_{ij} and m_{ij} are the binary interaction parameters.

The TCBT mixing rule[18] developed for no reference pressure conditions relates the excess molar Gibbs energy, G^E, with the excess molar Gibbs energy based on the van der Waals reference fluid (vdW), G^E_{vdW}, as:

$$\frac{G^E}{RT} - \frac{G^E_{vdW}}{RT} + \left(Z - Z_{vdW}\right) = \ln\left\{\left(\frac{V^*_{vdW}-1}{V^*-1}\right)\left(\frac{b_{vdW}}{b}\right)\right\} - \\ -\frac{1}{w-u}\left\{\frac{a^*}{b^*}\ln\left(\frac{V^*+w}{V^*+u}\right) - \frac{a^*_{vdW}}{b^*_{vdW}}\ln\left(\frac{V^*_{vdW}+w}{V^*_{vdW}+u}\right)\right\} \tag{8}$$

where G^E_{vdW} is calculated for the PRSV CEOS and $V^* = V/b = Z/b^*$ denotes the reduced liquid volume at the P and T of the mixture. The compressibility factors Z and Z_{vdW} are calculated from Eq. (1) expressed in the Z form. Bearing in mind that V^* does not have an explicit solution, an iterative technique is required for the calculation.

The parameters a_{vdW} and b_{vdW} are determined using Eqs. (6) and (7), while the reduced parameters a^*, b^*, a^*_{vdW} and b^*_{vdW} are obtained from the following equations:

$$a^* = Pa/R^2T^2 \qquad b^* = Pb/RT \tag{9}$$

In this paper, the NRTL equation was used as the G^E model:

$$\frac{G^E}{RT} = \sum_i x_i \frac{\sum_j x_j G_{ji}\tau_{ji}}{\sum_k x_k G_{ki}} \tag{10}$$

For a binary mixture, the following equations are incorporated

$$\begin{aligned} &G_{12} = \exp\left(-\alpha_{12}\tau_{12}\right) \quad G_{21} = \exp\left(-\alpha_{12}\tau_{21}\right) \\ &\tau_{12} = (g_{12} - g_{22})/RT = \Delta g_{12}/RT \quad \tau_{21} = (g_{21} - g_{11})/RT = \Delta g_{21}/RT \end{aligned} \tag{11}$$

and for a ternary mixture:

$$\tau'_{ij} = \tau_{ij} + \frac{\sum_{k=1}^{n} x_k \Delta g_{ijk}}{RT} \tag{12}$$

Δg_{12} and Δg_{21} are the binary energy parameters and Δg_{ijk} is the ternary contribution.

For the temperature range, temperature dependent parameters are used in the following manner:

$$Y = Y_1 + Y_2T \tag{13}$$

where $Y = k_{ij}$, l_{ij}, m_{ij}, Δg_{12} and Δg_{21}. The models used here for all calculations were obtained by applying sets of the corresponding equations as listed in the footnotes of the Tables I–IV. In order to obtain the model parameters or coefficients, the Marquardt optimisation technique[38] was used for the minimization of the objective function given by the equation:

$$OF = \frac{1}{n}\sum_{i=1}^{n}\left(\frac{V^E_{\exp} - V^E_{cal}}{V^E_{\exp}}\right)_i^2 \rightarrow \min \tag{14}$$

The results of the V^E calculation were assessed by the RMSD, defined by the equation:

$$\sigma = \left(\sum_{i=1}^{n}\left(V^E_{\exp,i} - V^E_{cal,i}\right)^2 \Big/ n\right)^{1/2} \tag{15}$$

and the percentage average absolute deviation PD(V^E):

$$PD(V^E) = \frac{100}{n}\sum_{i=1}^{n}\left|\frac{V^E_{\exp} - V^E_{cal}}{\left(V^E_{\exp}\right)_{\max}}\right|_i \tag{16}$$

In the present paper, modelling of the previously obtained experimental V^E data[6,7] for two ternary systems: methanol + chloroform + benzene and 1-propanol + chloroform + benzene and their binary constituents: methanol + chloroform, chloroform + benzene, 1-propanol + chloroform and 1-propanol + benzene, was performed by the PRSV CEOS, coupled with two types of mixing rules: vdW1 and TCBT mixing rules. According to the previously established procedure, the parameters in both mixing rules were employed as: (*i*) temperature independent (correlation at each temperature) or (*ii*) temperature dependent (correlation in the temperature range). The values of the model parameters, PD(V^E) and corresponding RMSD for each temperature separately, as well as in temperature range, are given in Tables I and II for the binary systems and in Tables III and IV for the ternary systems.

TABLE I. Correlation of the V^E data by the temperature independent PRSV CEOS models for the investigated binary systems at the temperatures 288.15 to 313.15 K and atmospheric pressure

	$k_{ij,1}$	$l_{ij,1}$	$m_{ij,1}$	$\Delta g_{12,1}$ J mol^{-1}	$\Delta g_{21,1}$ J mol^{-1}	PD(V^E) %	$\sigma\times10^6$ m^3 mol^{-1}
Methanol (1) + Chloroform (2)							
T = 288.15 K							
vdW1-2[a]	0.009327		–0.015852			10.54	0.01946
vdW1-3[b]	–0.038847	–0.007914	–0.023699			9.85	0.01836
TCBT-2[c]				$0.217463\cdot10^4$	$-0.756278\cdot10^3$	10.94	0.02069
TCBT-3[d]	0.100778			$0.521710\cdot10^4$	$0.127565\cdot10^4$	2.01	0.00402
T = 293.15 K							
vdW1-2	0.022390		–0.013519			11.00	0.02005
vdW1-3	–0.039467	–0.009997	–0.024002			9.89	0.01815
TCBT-2				$0.207827\cdot10^4$	$-0.726828\cdot10^3$	11.10	0.02067
TCBT-3	0.107533			$0.534685\cdot10^4$	$0.134597\cdot10^4$	2.13	0.00433
T = 298.15 K							
vdW1-2	0.035134		–0.011080			11.59	0.02093
vdW1-3	–0.039430	–0.011948	–0.024231			9.93	0.01795
TCBT-2				$0.193950\cdot10^4$	$-0.665477\cdot10^3$	11.31	0.02092
TCBT-3	0.109918			$0.531074\cdot10^4$	$0.131166\cdot10^4$	1.52	0.00308
T = 303.15 K							
vdW1-2	0.048135		–0.008427			12.45	0.02212
vdW1-3	–0.039532	–0.139192	–0.024516			9.99	0.01770
TCBT-2				$0.184834\cdot10^4$	$-0.633676\cdot10^3$	11.50	0.02078
TCBT-3	0.116340			$0.544517\cdot10^4$	$0.135931\cdot10^4$	3.34	0.00704
T = 308.15 K							
vdW1-2	0.061420		–0.005532			13.55	0.02371
vdW1-3	–0.040293	–0.016039	–0.024954			10.12	0.01737
TCBT-2				$0.175258\cdot10^4$	$-0.595395\cdot10^3$	11.70	0.02048
TCBT-3	0.120553			$0.543282\cdot10^4$	$0.137033\cdot10^4$	1.86	0.00372

TABLE I. Continued.

	$k_{ij,1}$	$l_{ij,1}$	$m_{ij,1}$	$\Delta g_{12,1}$ J mol^{-1}	$\Delta g_{21,1}$ J mol^{-1}	PD(V^E) %	$\sigma\times10^6$ m^3 mol^{-1}
				T = 313.15 K			
vdW1-2	0.073170		–0.002752			14.95	0.02563
vdW1-3	–0.040648	–0.017897	–0.025352			10.29	0.01704
TCBT-2				$0.163854\cdot10^4$	$-0.541875\cdot10^3$	12.00	0.02036
TCBT-3	0.121939			$0.536275\cdot10^4$	$0.130523\cdot10^4$	1.87	0.00364
				T = 288.15–313.15 K			
vdW1-2	0.021634		–0.013486			12.94	0.0238
vdW1-3	–0.003207	–0.009216	–0.017999			10.61	0.0194
TCBT-2				$0.163364\cdot10^4$	$-0.454764\cdot10^3$	25.34	0.0516
TCBT-3	–0.079651			$0.260148\cdot10^4$	$-0.332486\cdot10^4$	12.31	0.0227
				Chloroform (1) + Benzene (2)			
				T = 288.15 K			
vdW1-2	–0.064033		–0.017573			3.49	0.0076
vdW1-3	–0.008514	–0.004581	–0.008628			2.74	0.0060
TCBT-2				$0.147247\cdot10^3$	$0.751000\cdot10^5$	1.39	0.0039
TCBT-3	–0.009258			$-0.208918\cdot10^4$	$0.260580\cdot10^4$	1.25	0.0032
				T = 293.15 K			
vdW1-2	–0.057860		–0.016649			3.65	0.0076
vdW1-3	–0.007256	–0.004148	–0.008197			2.98	0.0062
TCBT-2				$0.135332\cdot10^3$	$0.771195\cdot10^5$	1.46	0.0038
TCBT-3	0.086805			$0.241585\cdot10^4$	$0.126727\cdot10^4$	1.38	0.0032
				T = 298.15 K			
vdW1-2	–0.052200		–0.015754			3.81	0.0074
vdW1-3	–0.007308	–0.003688	–0.007991			3.21	0.0063
TCBT-2				$0.123980\cdot10^3$	$0.791928\cdot10^5$	1.56	0.0037
TCBT-3	–0.010119			$-0.223158\cdot10^4$	$0.277009\cdot10^4$	1.41	0.0031
				T = 303.15 K			
vdW1-2	–0.047203		–0.014929			3.98	0.0073
vdW1-3	–0.006771	–0.003315	–0.007689			3.45	0.0063
TCBT-2				$0.112960\cdot10^3$	$0.811204\cdot10^5$	1.67	0.0036
TCBT-3	0.093752			$0.250866\cdot10^4$	$0.130924\cdot10^4$	1.48	0.0032
				T = 308.15 K			
vdW1-2	–0.042161		–0.014053			4.22	0.0073
vdW1-3	–0.006426	–0.002946	–0.007429			3.76	0.0065
TCBT-2				$0.103211\cdot10^3$	$0.834117\cdot10^5$	1.89	0.0037
TCBT-3	0.107109			$0.277853\cdot10^4$	$0.153623\cdot10^4$	1.49	0.0028
				T = 313.15			
vdW1-2	–0.038595		–0.013418			4.55	0.0086
vdW1-3	–0.005877	–0.002714	–0.007144			4.13	0.0069
TCBT-2				$0.936483\cdot10^2$	$0.852738\cdot10^5$	2.27	0.0043
TCBT-3	0.110792			$0.281775\cdot10^4$	$0.155558\cdot10^4$	1.57	0.0029

TABLE I. Continued.

	$k_{ij,1}$	$l_{ij,1}$	$m_{ij,1}$	$\Delta g_{12,1}$ J mol^{-1}	$\Delta g_{21,1}$ J mol^{-1}	PD(V^E) %	$\sigma\times10^6$ m^3 mol^{-1}
				T = 288.15–313.15 K			
vdW1-2	–0.043300		–0.014259			3.93	0.0078
vdW1-3	–0.039939	–0.001267	–0.013681			3.71	0.0072
TCBT-2				$-0.173424\cdot10^3$	$0.310596\cdot10^3$	11.27	0.0235
TCBT-3	–0.023914			$0.664817\cdot10^3$	$-0.124516\cdot10^4$	3.36	0.0067
				1-Propanol (1) + Chloroform (2)			
				T = 288.15 K			
vdW1-2	0.174217		0.024898			4.38	0.01036
vdW1-3	0.129286	–0.014223	0.017524			3.05	0.00702
TCBT-2				$-0.218026\cdot10^4$	$0.360541\cdot10^4$	8.01	0.01908
TCBT-3	–0.054472			$0.509984\cdot10^4$	$-0.429655\cdot10^4$	2.19	0.00587
				T = 293.15 K			
vdW1-2	0.173022		0.025272			4.87	0.01113
vdW1-3	–0.225282	–0.126330	–0.033387			1.97	0.00471
TCBT-2				$-0.219034\cdot10^4$	$0.359501\cdot10^4$	8.69	0.01969
TCBT-3	–0.069108			$0.326820\cdot10^6$	$-0.216475\cdot10^4$	2.67	0.00721
				T = 298.15 K			
vdW1-2	0.171632		0.025609			5.55	0.01186
vdW1-3	–0.223173	–0.122970	–0.034729			1.91	0.00431
TCBT-2				$-0.221130\cdot10^4$	$0.361135\cdot10^4$	9.32	0.01985
TCBT-3	–0.067705			$0.126275\cdot10^3$	$-0.218022\cdot10^4$	2.96	0.00708
				T = 303.15 K			
vdW1-2	0.170105		0.025914			6.40	0.01274
vdW1-3	–0.220424	–0.119406	–0.036028			1.81	0.00402
TCBT-2				$-0.219890\cdot10^4$	$0.356070\cdot10^4$	10.13	0.02085
TCBT-3	–0.065541			$0.304066\cdot10^3$	$-0.221137\cdot10^4$	3.47	0.00722
				T = 308.15 K			
vdW1-2	0.168101		0.026105			7.48	0.01370
vdW1-3	–0.215685	–0.115100	–0.037099			1.73	0.00375
TCBT-2				$-0.224538\cdot10^4$	$0.363529\cdot10^4$	10.59	0.01972
TCBT-3	–0.066717			$0.302224\cdot10^3$	$-0.220774\cdot10^4$	4.14	0.00782
				T = 313.15 K			
vdW1-2	0.166654		0.026414			7.42	0.01484
vdW1-3	–0.212065	–0.111441	–0.038326			1.51	0.00366
TCBT-2				$-0.225261\cdot10^4$	$0.362813\cdot10^4$	9.53	0.01992
TCBT-3	–0.072421			$0.126495\cdot10^3$	$-0.220248\cdot10^4$	4.21	0.00844
				T = 288.15–313.15 K			
vdW1-2	0.148321		0.021650			16.33	0.0325
vdW1-3	0.083043	–0.025685	0.010283			5.30	0.0107
TCBT-2				$-0.220178\cdot10^4$	$0.356811\cdot10^4$	15.05	0.0315
TCBT-3	–0.057814			$0.529087\cdot10^4$	$-0.443514\cdot10^4$	5.31	0.0111

TABLE I. Continued.

	$k_{ij,1}$	$l_{ij,1}$	$m_{ij,1}$	$\Delta g_{12,1}$ J mol^{-1}	$\Delta g_{21,1}$ J mol^{-1}	PD(V^E) %	$\sigma\times10^6$ m^3 mol^{-1}
1-Propanol (1) + Benzene (2)							
T = 288.15 K							
vdW1-2	0.099354		0.008781			6.56	0.00943
vdW1-3	–0.087552	–0.043591	–0.017779			3.11	0.00432
TCBT-2				$-0.330450\cdot10^3$	$0.116520\cdot10^4$	3.64	0.00528
TCBT-3	–0.007406			$-0.103855\cdot10^4$	$0.171633\cdot10^4$	3.47	0.00512
T = 293.15 K							
vdW1-2	0.102011		0.009528			6.74	0.01071
vdW1-3	–0.082157	–0.041959	–0.017690			3.15	0.00499
TCBT-2				$-0.412421\cdot10^3$	$0.123388\cdot10^4$	3.63	0.00594
TCBT-3	–0.010342			$-0.145386\cdot10^4$	$0.214933\cdot10^4$	3.46	0.00559
T = 298.15 K							
vdW1-2	0. 105052		0.010371			6.37	0.01109
vdW1-3	–0.079083	–0.040908	–0.017906			2.32	0.00447
TCBT-2				$-0.491062\cdot10^3$	$0.130171\cdot10^4$	2.69	0.00542
TCBT-3	–0.005818			$-0.106759\cdot10^4$	$0.178137\cdot10^4$	2.59	0.00502
T = 303.15 K							
vdW1-2	0.106924		0.011029			6.91	0.01345
vdW1-3	–0.063084	–0.036901	–0.016220			2.94	0.00610
TCBT-2				$-0.558168\cdot10^3$	$0.135830\cdot10^4$	3.13	0.00696
TCBT-3	–0.008956			$-0.145230\cdot10^4$	$0.216459\cdot10^4$	2.83	0.00623
T = 308.15 K							
vdW1-2	0.108334		0.011612			6.98	0.01508
vdW1-3	–0.059628	-0.035631	-0.016339			2.95	0.00689
TCBT-2				$-0.605775\cdot10^3$	$0.139267\cdot10^4$	3.06	0.00793
TCBT-3	–0.008339			$-0.147150\cdot10^4$	$0.219964\cdot10^4$	2.73	0.00676
T = 313.15 K							
vdW1-2	0.111750		0.012629			6.67	0.01631
vdW1-3	–0.058310	–0.035148	–0.016750			2.97	0.00744
TCBT-2				$-0.708732\cdot10^3$	$0.149942\cdot10^4$	3.12	0.00816
TCBT-3	–0.012342			$-0.192761\cdot10^4$	$0.271223\cdot10^4$	2.75	0.00709
T = 288.15–313.15 K							
vdW1-2	0.085992		0.007330			12.42	0.0212
vdW1-3	0.043469	–0.013948	0.000395			4.08	0.0079
TCBT-2				$-0.441345\cdot10^3$	$0.122594\cdot10^4$	20.85	0.0356
TCBT-3	–0.044303			$0.241384\cdot10^4$	$-0.273162\cdot10^4$	6.13	0.0113

[a]Eqs. (1)-(7), (13), l_{ij} = 0; [b]Eqs. (1)-(7), (13); [c]Eqs. (1)–(11), (13), $k_{ij} = l_{ij} = m_{ij} = 0$; α_{ij} = 0.3 (found by trial and error and set to 0.3 in all cases); [d]Eqs. (1)–(11), (13); $l_{ij} = m_{ij} = 0$; α_{ij} = 0.3.

Analysing the results obtained for the system methanol + chloroform by the temperature-independent PRSV CEOS models at each temperature, it is evident that only the three parameter TCBT-3 model worked very well, having errors near or below 2 %, while the results obtained by the two parameter vdW1-2 and TCBT-2 models and three parameter vdW1-3 model are unacceptable. The evident superiority of the TCBT-3 model in comparison with the TCBT-2 model, which is unable to fit the shape of the V^E–x_1 curve is illustrated in Fig. 1a. Over the entire range of temperature, the correlating results attained by all the temperature independent (Table I) or temperature dependent (Table II) models are unsatisfactory.

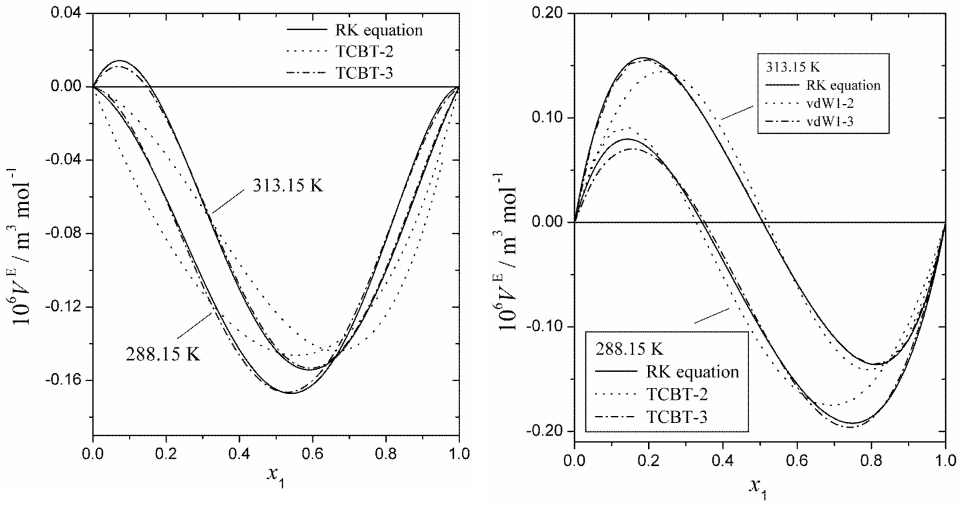

Fig. 1. Correlation of V^E data at 288.15 and 313.15 K by the vdW1 and TCBT models for the binary systems: a) methanol (1) + chloroform (2), b) 1-propanol (1) + chloroform (2). The various types of lines are reported in the legend.

TABLE II. Correlation of the V^E data by the temperature dependent PRSV CEOS models for the investigated binary systems at the temperature range 288.15–313.15 K and atmospheric pressure

	$k_{ij,1}, k_{ij,2}$	$l_{ij,1}, l_{ij,2}$	$m_{ij,1}, m_{ij,2}$	$\Delta g_{12,1}$ / J mol^{-1} $\Delta g_{12,2}$ / J mol^{-1}K^{-1}	$\Delta g_{12,1}$ / J mol^{-1} $\Delta g_{12,2}$ / J mol^{-1}K^{-1}	PD(V^E) %	$\sigma\times10^6$ m^3 mol^{-1}
Methanol (1) + Chloroform (2)							
vdW1-2[a]	–0.329138 0.001237		–0.093779 0.000280			12.40	0.0224
vdW1-3[b]	–0.201810 0.000540	0.086387 –0.000330	–0.036700 0.000041			10.02	0.0178
TCBT-2[c]				$0.234574\cdot10^4$ –4.24111	$-0.336333\cdot10^4$ $0.160156\cdot10^4$	20.75	0.0425
TCBT-3[d]	-0.028209			$0.539437\cdot10^4$ $0.209787\cdot10^4$	$-0.804127\cdot10^5$ $0.507668\cdot10^3$	12.82	0.0267

TABLE II. Continued.

	$k_{ij,1}, k_{ij,2}$	$l_{ij,1}, l_{ij,2}$	$m_{ij,1}, m_{ij,2}$	$\Delta g_{12,1}$ / J mol^{-1} $\Delta g_{12,2}$ / J mol^{-1}K^{-1}	$\Delta g_{12,1}$ / J mol^{-1} $\Delta g_{12,2}$ / J mol^{-1}K^{-1}	PD(V^E) %	$\sigma\times10^6$ m^3 mol^{-1}
Chloroform (1) + Benzene (2)							
vdW1-2	–0.222941 0.000576		–0.042765 0.000091			3.93	0.0075
vdW1-3	0.002189 –0.000030	–0.029164 0.000085	–0.018467 0.000035			3.38	0.0064
TCBT-2				$0.757263\cdot10^3$ –2.12153	$-0.458710\cdot10^5$ $0.419412\cdot10^3$	1.72	0.0039
TCBT-3	0.001067			$0.840710\cdot10^3$ –2.26987	$-0.476777\cdot10^5$ $0.427966\cdot10^3$	1.76	0.0039
1-Propanol (1) + Chloroform (2)							
vdW1-2	0.256907 –0.000287					6.02	0.0125
vdW1-3	5.297000 40.17777	1.487200 –0.005164	0.849304 –0.002861			4.89	0.0104
TCBT-2				$-0.626817\cdot10^3$ –5.39751	$0.169979\cdot10^4$ 6.59297	9.94	0.0196
TCBT-3	–0.071912			$-0.935801\cdot10^3$ $0.384292\cdot10^4$	$-0.462837\cdot10^4$ 8.09348	5.04	0.0109
1-Propanol (1) + Benzene (2)							
vdW1-2	–0.002183 0.000359		–0.028480 0.000130			6.74	0.0130
vdW1-3	–0.258366 0.000626	–0.103036 0.000214	–0.006209 –0.000036			2.96	0.0133
TCBT-2				$0.168836\cdot10^4$ –7.43558	$0.210817\cdot10^3$ 3.82951	3.89	0.0073
TCBT-3	–0.002192			$0.946773\cdot10^3$ –5.64250	$0.903744\cdot10^3$ 2.03577	3.98	0.0075

[a]Eqs. (1)–(7), (13), $l_{ij} = 0$; [b]Eqs. (1)–(7), (13); [c]Eqs. (1)–(11), (13), $k_{ij} = l_{ij} = m_{ij} = 0$; $\alpha_{ij} = 0.3$; [d]Eqs. (1)–(11), (13), $l_{ij} = m_{ij} = 0$; $\alpha_{ij} = 0.3$

For the system chloroform + benzene, it can be observed that when the correlation of the V^E data was performed at each temperature, the percentage deviations of the CEOS and CEOS/G^E models were somewhat higher when the temperature was higher. The two parameter vdW1-2 and TCBT-2 models worked very similar to the three parameter vdW1-3 and TCBT-3 models, respectively, with slightly higher errors. In the temperature range, except for TCBT-2, the applied CEOS and CEOS/G^E models gave relatively good results. It is evident from Table II that a significant improvement was achieved when the temperature dependent parameters were introduced only in the TCBT-2 model and partly in the TCBT-3 model, while for the vdW1 models, the errors were slightly better.

For the 1-propanol + chloroform system, it is noticeable that with increasing temperature, the errors incresed as well, except for the vdW1-3 model which be-

comes dominant at higher temperatures. The two parameter vdW1-2 and TCBT-2 models are not suitable at higher temperatures for the correlation of the V^E data for this system. A comparison between the experimental results (RK equation) and the correlating results obtained by the vdW1 and TCBT models at 288.15 and 313.15 K is shown in Fig. 1b. At 288.15 K, the V^E–x_1 curve obtained by the TCBT-2 model cannot satisfactorily describe the S-shape of the experimental values, especially in the extremities, while the TCBT-3 model is more successful. At 313.15 K, the dominance of the vdW1-3 over the vdW1-2 model is evident. In the range of temperature, three parameter models worked better than the two parameter models, but also unsatisfactorily, irrespective of whether temperature dependent parameters were used or not.

When the correlation of the V^E data was performed for 1-propanol + benzene system, at each temperature, relatively similar result around 3 % was obtained with vdW1-3, and both TCBT models, while two parameter vdW1-2 model gave some higher errors. In the temperature range, two parameter temperature independent vdW1-2 and TCBT-2 models worked considerably poorer than three parameter vdW1-3 and TCBT-3 models. Also, it is evident from Table II that considerable improvement was achieved by introducing temperature dependence in vdW1-2 and TCBT-2 models.

Prediction of V^E for the ternary systems methanol (1) + chloroform (2) + benzene (3) and 1-propanol (1) + chloroform (2) + benzene (3) at each temperature over the entire temperature range was performed using the CEOS and CEOS/G^E models, with the binary interaction parameters of these models generated from appropriate binary data. From Table III it is evident that, for both systems, the applied CEOS/G^E models are not suitable for this type of thermodynamic modelling. Much better, but still not acceptable results, were obtained by the vdW1-3 model, while only the simplest vdW1-2 model in the case of the 1-propanol (1) + chloroform (2) + benzene (3) system achieved good results. Correlation of ternary V^E data for these systems was performed using TCBT models adding the ternary contribution in the interaction parameters. Comparing the results obtained by the TCBT-2 and TCBT-3 models for both systems, it is evident that the TCBT-3 model worked slightly better at each temperature and in the temperature interval.

TABLE III. Prediction of V^E by the PRSV CEOS models for the investigated ternary systems

T / K	vdW1-2[a]		vdW1-3[b]		TCBT-2[c]		TCBT-3[d]	
	PD(V^E) %	$\sigma\times10^6$ $m^3\ mol^{-1}$	PD(V^E) %	$\sigma\times10^6$ $m^3\ mol^{-1}$	PD(V^E) %	$\sigma\times10^6$ $m^3\ mol^{-1}$	PD(V^E) %	$\sigma\times10^6$ $m^3\ mol^{-1}$
Methanol (1) + Chloroform (2) + Benzene (3)								
288.15	12.26	0.02609	14.49	0.03149	HV[g]	0.2618	HV	0.3111
293.15	13.19	0.02685	15.25	0.03178	HV	0.2597	73.91	0.1600
298.15	14.34	0.02825	16.06	0.03227	HV	0.2515	HV	0.3504

TABLE III. Continued.

T / K	vdW1-2[a]		vdW1-3[b]		TCBT-2[c]		TCBT-3[d]	
	PD(V^E) %	$\sigma\times10^6$ $m^3\,mol^{-1}$	PD(V^E) %	$\sigma\times10^6$ $m^3\,mol^{-1}$	PD(V^E) %	$\sigma\times10^6$ $m^3\,mol^{-1}$	PD(V^E) %	$\sigma\times10^6$ $m^3\,mol^{-1}$
Methanol (1) + Chloroform (2) + Benzene (3)								
303.15	15.73	0.03027	17.01	0.03309	HV	0.2483	91.40	0.1881
308.15	17.36	0.03290	17.79	0.03376	HV	0.2441	HV	0.2223
313.15	18.72	0.03494	18.54	0.03446	HV	0.2388	HV	0.2437
288.15––313.15[e]	15.88	0.0316	15.28	0.0305	–	–	16.95	0.0341
288.15––313.15[f]	15.22	0.0300	16.58	0.0329	56.89	0.01148	HV	1.0254
1-Propanol (1) + Chloroform (2) + Benzene (3)								
288.15	3.49	0.00928	18.37	0.05128	HV[g]	0.4008	92.68	0.2534
293.15	4.01	0.01043	23.35	0.06609	HV	0.4096	81.99	0.2215
298.15	4.43	0.01156	24.87	0.06925	HV	0.4215	76.88	0.2089
303.15	4.79	0.01268	24.23	0.06860	HV	0.4270	HV	0.3916
308.15	5.44	0.01441	23.72	0.06851	HV	0.4474	HV	0.4244
313.15	5.85	0.01590	23.35	0.06925	HV	0.4565	HV	0.5184
288.15––313.15[e]	9.06	0.0252	5.35	0.0150	25.72	0.0758	52.84	0.1464
288.15–313.15[f]	4.71	0.0127	15.99	0.0555	87.83	0.2196	71.70	0.1979

[a]Eqs. (1)–(7), (13), $l_{ij} = 0$; [b]Eqs. (1)–(7), (13); [c]Eqs. (1)–(11), (13), $k_{ij} = l_{ij} = m_{ij} = 0$; $\alpha_{ij} = 0.3$; [d]Eqs. (1)–(11), (13), $l_{ij} = m_{ij} = 0$; $\alpha_{ij} = 0.3$; [e]prediction of V^E using temperature independent binary parameters; [f]prediction of V^E using temperature dependent binary parameters; [g]High value

TABLE IV. Correlation of V^E by the PRSV CEOS models for the investigated ternary systems

	Δg_{123} / J mol^{-1} Δg_{132} / J mol^{-1}	Δg_{213} / J mol^{-1} Δg_{231} / J mol^{-1}	Δg_{312} / J mol^{-1} Δg_{321} / J mol^{-1}	PD(V^E) / %	$\sigma\times10^6$ $m^3\,mol^{-1}$
Methanol (1) + Chloroform (2) + Benzene (3)					
T = 288.15 K					
TCBT-2[a]	$-0.216001\cdot10^4$ $0.330521\cdot10^3$	$0.331983\cdot10^4$ $-0.305165\cdot10^4$	$-0.895245\cdot10^3$ $-0.685207\cdot10^5$	3.00	0.00757
TCBT-3[b]	$-0.181584\cdot10^4$ $-0.220503\cdot10^4$	$-0.486347\cdot10^3$ $0.246196\cdot10^4$	$-0.175874\cdot10^4$ $-0.112493\cdot10^4$	1.73	0.00423
T = 293.15 K					
TCBT-2	$-0.204943\cdot10^4$ $0.143604\cdot10^4$	$0.223202\cdot10^4$ $-0.227332\cdot10^4$	$-0.415594\cdot10^3$ $-0.698775\cdot10^5$	2.89	0.00722
TCBT-3	$0.371297\cdot10^4$ $0.235339\cdot10^4$	$0.269915\cdot10^4$ $0.185877\cdot10^4$	$-0.518535\cdot10^4$ $-0.169579\cdot10^4$	1.61	0.00384
T = 298.15 K					
TCBT-2	$-0.191181\cdot10^4$ $-0.396537\cdot10^3$	$0.152833\cdot10^4$ $-0.187830\cdot10^4$	$0.178648\cdot10^3$ $-0.715393\cdot10^5$	2.87	0.00707
TCBT-3	$-0.548621\cdot10^4$ $0.500719\cdot10^4$	$0.127889\cdot10^3$ $-0.510516\cdot10^4$	$-0.217509\cdot10^4$ $0.353247\cdot10^4$	1.57	0.00345

TABLE IV. Continued.

	Δg_{123} / J mol^{-1} Δg_{132} / J mol^{-1}	Δg_{213} / J mol^{-1} Δg_{231} / J mol^{-1}	Δg_{312} / J mol^{-1} Δg_{321} / J mol^{-1}	PD(V^E) / %	$\sigma\times10^6$ m^3 mol^{-1}
Methanol (1) + Chloroform (2) + Benzene (3)					
			T = 303.15 K		
TCBT-2	$-0.181260\cdot10^4$ $0.120825\cdot10^3$	$0.153214\cdot10^4$ $-0.214668\cdot10^4$	$0.245954\cdot10^3$ $-0.737614\cdot10^5$	3.00	0.00719
TCBT-3	$-0.690601\cdot10^4$ $0.800038\cdot10^3$	$-0.164110\cdot10^4$ $0.787850\cdot10^2$	$0.694574\cdot10^4$ $0.234458\cdot10^4$	1.57	0.00340
			T = 308.15 K		
TCBT-2	$-0.170755\cdot10^4$ $0.177365\cdot10^3$	$0.146794\cdot10^4$ $-0.221035\cdot10^4$	$0.362709\cdot10^3$ $-0.757075\cdot10^5$	3.17	0.00746
TCBT-3	$-0.733523\cdot10^4$ $0.543242\cdot10^3$	$-0.152677\cdot10^4$ $0.690292\cdot10^3$	$0.729489\cdot10^4$ $0.315206\cdot10^4$	1.85	0.00397
			T = 313.15 K		
TCBT-2	$-0.159713\cdot10^4$ $0.130813\cdot10^4$	$0.200236\cdot10^4$ $-0.271314\cdot10^4$	$-0.227257\cdot10^2$ $-0.785854\cdot10^5$	3.52	0.00793
TCBT-3	$-0.865464\cdot10^4$ $0.131091\cdot10^3$	$-0.146771\cdot10^4$ $0.218790\cdot10^4$	$0.931429\cdot10^4$ $0.433321\cdot10^4$	1.84	0.00399
			T = 288.15–313.15 K[c]		
TCBT-3	$-0.643200\cdot10^4$ $-0.147793\cdot10^4$	$-0.416194\cdot10^4$ $-0.508707\cdot10^4$	$0.925400\cdot10^4$ $0.831354\cdot10^4$	4.54	0.0110
			T = 288.15–313.15 K[d]		
TCBT-2	$-0.102981\cdot10^4$ $0.237608\cdot10^4$	$-0.112302\cdot10^4$ $-0.150594\cdot10^4$	$0.108598\cdot10^4$ $-0.687462\cdot10^5$	6.91	0.0159
TCBT-3	$-0.297640\cdot10^3$ $-0.156207\cdot10^4$	$0.860895\cdot10^5$ $0.112204\cdot10^4$	$0.112204\cdot10^4$ $0.942530\cdot10^5$	4.45	0.0110
1-Propanol (1) + Chloroform (2) + Benzene (3)					
			T = 288.15 K		
TCBT-2	$0.228110\cdot10^4$ $-0.144128\cdot10^3$	$-0.404970\cdot10^4$ $0.402080\cdot10^4$	$-0.805761\cdot10^3$ $-0.151393\cdot10^4$	3.09	0.00947
TCBT-3	$-0.537758\cdot10^4$ $-0.414362\cdot10^4$	$0.564205\cdot10^4$ $0.626995\cdot10^4$	$-0.694120\cdot10^4$ $-0.575803\cdot10^3$	1.78	0.00496
			T = 293.15 K		
TCBT-2	$0.220340\cdot10^4$ $-0.182405\cdot10^3$	$-0.361646\cdot10^4$ $0.406272\cdot10^4$	$-0.949869\cdot10^3$ $-0.102617\cdot10^5$	3.05	0.00926
TCBT-3	$0.821370\cdot10^4$ $-0.233635\cdot10^4$	$0.758260\cdot10^4$ $0.735235\cdot10^4$	$-0.500333\cdot10^4$ $-0.193503\cdot10^4$	1.43	0.00414
			T = 298.15		
TCBT-2	$0.226181\cdot10^4$ $-0.153375\cdot10^3$	$-0.379604\cdot10^4$ $0.408361\cdot10^4$	$-0.952405\cdot10^3$ $-0.323087\cdot10^4$	3.04	0.00943
TCBT-3	$0.838612\cdot10^4$ $-0.638441\cdot10^4$	$-0.305674\cdot10^4$ $0.745891\cdot10^4$	$0.357589\cdot10^4$ $-0.170838\cdot10^4$	1.70	0.00489

TABLE IV. Continued.

	Δg_{123} / J mol^{-1} Δg_{132} / J mol^{-1}	Δg_{213} / J mol^{-1} Δg_{231} / J mol^{-1}	Δg_{312} / J mol^{-1} Δg_{321} / J mol^{-1}	PD(V^E) / %	$\sigma\times10^6$ m^3 mol^{-1}
1-Propanol (1) + Chloroform (2) + Benzene (3)					
		T = 303.15 K			
TCBT-2	$0.229285\cdot10^4$ $-0.265356\cdot10^3$	$-0.396769\cdot10^4$ $0.420063\cdot10^4$	$-0.859157\cdot10^3$ $-0.121934\cdot10^5$	2.85	0.00909
TCBT-3	$-0.524865\cdot10^4$ $0.111767\cdot10^5$	$-0.311913\cdot10^4$ $-0.376340\cdot10^4$	$0.533207\cdot10^4$ $0.832227\cdot10^4$	1.69	0.00485
		T = 308.15 K			
TCBT-2	$0.233657\cdot10^4$ $-0.202952\cdot10^3$	$-0.393679\cdot10^4$ $0.420418\cdot10^4$	$-0.983846\cdot10^3$ $-0.907649\cdot10^4$	2.93	0.00924
TCBT-3	$-0.552509\cdot10^4$ $0.116962\cdot10^5$	$0.304273\cdot10^4$ $-0.402050\cdot10^4$	$0.519002\cdot10^4$ $0.887191\cdot10^4$	1.71	0.00515
		T = 313.15 K			
TCBT-2	$0.236775\cdot10^4$ $-0.277245\cdot10^3$	$-0.385129\cdot10^4$ $0.395861\cdot10^4$	$-0.830860\cdot10^3$ $0.861178\cdot10^2$	2.84	0.00937
TCBT-3	$-0.631254\cdot10^4$ $0.989397\cdot10^4$	$0.126667\cdot10^5$ $-0.115236\cdot10^5$	$-0.832791\cdot10^4$ $0.965200\cdot10^4$	1.80	0.00557
		T = 288.15–313.15 K[c]			
TCBT-2	$0.295533\cdot10^4$ $0.276140\cdot10^4$	$-0.306031\cdot10^4$ $0.246993\cdot10^4$	$-0.101354\cdot10^4$ $-0.537722\cdot10^4$	12.26	0.0344
TCBT-3	$-0.516953\cdot10^4$ $-0.495301\cdot10^4$	$0.823286\cdot10^4$ $0.836822\cdot10^4$	$-0.561513\cdot10^4$ $-0.692308\cdot10^3$	2.57	0.0077
		T = 288.15–313.15 K[d]			
TCBT-2	$0.244863\cdot10^4$ $0.589126\cdot10^2$	$-0.461499\cdot10^4$ $0.458958\cdot10^4$	$-0.125297\cdot10^4$ $0.940416\cdot10^5$	3.65	0.0107
TCBT-3	$0.928149\cdot10^4$ $0.145152\cdot10^4$	$0.523491\cdot10^4$ $-0.450387\cdot10^4$	$-0.197974\cdot10^4$ $0.568441\cdot10^5$	2.88	0.0085

[a]Eqs. (1)–(13), $k_{ij} = l_{ij} = m_{ij} = 0$, $\alpha_{ij} = 0.3$; [b]Eqs. (1)–(13), $l_{ij} = m_{ij} = 0$, $\alpha_{ij} = 0.3$; [c]correlation of V^E using prediction results obtained with temperature independent binary parameters; [d]correlation of V^E using prediction results obtained with temperature dependent binary parameters

4.2. Prediction of V^E *by empirical models*

An attractive alternative to the CEOS and CEOS/G^E models is the prediction of V^E for multicomponent systems performed by empirical equations existing in the literature.

Frequently used expressions for these models are as follows:

i) The Radojković *et al.* model[29]

$$V_{123}^E = V_{12}^E + V_{13}^E + V_{23}^E \tag{17}$$

in which the binary contributions V_{ij}^E are determined directly using the ternary mole fractions;

ii) The Kohler model[34]

$$V_{123}^E = \left(x_1 + x_2\right)^2 V_{12}^E(x_1^a, x_2^a) + \left(x_1 + x_3\right)^2 V_{13}^E(x_1^a, x_3^a) + \left(x_2 + x_3\right)^2 V_{23}^E(x_2^a, x_3^a) \quad (18)$$

Kohler's equation is symmetric, treating all binaries identically. The mole fractions in binary contributions are $x_i^a = 1 - x_j^a = x_i / \left(x_i + x_j\right)$;

iii) The Jacob–Fitzner model[39]

$$\begin{aligned} V_{123}^E = {} & x_1 x_2 \Big/ \left[\left(x_1 + x_3/2\right)\left(x_2 + x_3/2\right)\right] V_{12}^E(x_1^b, x_2^b) + \\ & + x_1 x_3 \Big/ \left[\left(x_1 + x_2/2\right)\left(x_3 + x_2/2\right)\right] V_{13}^E(x_1^b, x_3^b) + \\ & + x_2 x_3 \Big/ \left[\left(x_2 + x_1/2\right)\left(x_3 + x_1/2\right)\right] V_{23}^E(x_2^b, x_3^b) \end{aligned} \quad (19)$$

where $x_i^b = 1 - x_j^b = \left(1 + x_i - x_j\right)/2$;

iv) The Colinet model[40]

$$V_{123}^E = 0.5 \left\{ \begin{aligned} & \left[x_2/\left(1-x_1\right)\right] V^E(x_1, 1-x_1) + \left[x_1/\left(1-x_2\right)\right] V^E(1-x_2, x_2) + \\ & + \left[x_3/\left(1-x_1\right)\right] V^E(x_1, 1-x_1) + \left[x_1/\left(1-x_3\right)\right] V^E(1-x_3, x_3) + \\ & + \left[x_3/\left(1-x_2\right)\right] V^E(x_2, 1-x_2) + \left[x_2/\left(1-x_3\right)\right] V^E(1-x_3, x_3) \end{aligned} \right\} \quad (20)$$

v) The Tsao–Smith model[41]

$$V_{123}^E = \left[x_2/\left(1-x_1\right)\right] V_{12}^E(x_1^c, x_2^c) + \left[x_3/\left(1-x_1\right)\right] V_{13}^E(x_1^c, x_3^c) + \left(1-x_1\right) V_{23}^E(x_2^c, x_3^c) \quad (21)$$

Bearing in mind that this model is asymmetric, the binary contributions are evaluated in following manner:

a) $x_i^c = x_1$ and $x_j^c = 1 - x_i^c$ for binaries 1–2 and 1–3, and $x_2^c = 1 - x_3^c = x_2 / \left(x_2 + x_3\right)$ for binary 2–3 (option *a* in Table V)

b) $x_i^c = x_2$ and $x_j^c = 1 - x_i^c$ for binaries 2–1 and 2–3, and $x_1^c = 1 - x_3^c = x_1 / \left(x_1 + x_3\right)$ for binary 1–3 (option *b* in Table V)

c) $x_i^c = x_3$ and $x_j^c = 1 - x_i^c$ for binaries 3–1 and 3–2, and $x_1^c = 1 - x_2^c = x_1 / \left(x_1 + x_2\right)$ for binary 1–2 (option *c* in Table V)

vi) The Toop model[42]

$$V_{123}^E = \left[x_2/\left(1-x_1\right)\right] V_{12}^E(x_1^c, x_2^c) + \left[x_3/\left(1-x_1\right)\right] V_{13}^E(x_1^c, x_3^c) + \left(1-x_1\right)^2 V_{23}^E(x_2^c, x_3^c) \quad (22)$$

in which the binary mole fractions are computed as in the Tsao–Smith model (Eq. (21)).

vii) The Scatchard model[43]

$$V_{123}^E = \left[x_2/\left(1-x_1\right)\right] V_{12}^E(x_1^c, x_2^c) + \left[x_3/\left(1-x_1\right)\right] V_{13}^E(x_1^c, x_3^c) + V_{23}^E(x_2, x_3) \quad (23)$$

where x_i^c and x_j^c were computed as in the case of the Tsao-Smith model (Eq. (21)).

viii) The Rastogi model[44]

$$V_{123}^E = 0.5\left[\left(x_1 + x_2\right) V_{12}^E(x_1^a, x_2^a) + \left(x_1 + x_3\right) V_{13}^E(x_1^a, x_3^a) + \left(x_2 + x_3\right) V_{23}^E(x_2^a, x_3^a)\right] \quad (24)$$

where $x_i^a = 1 - x_j^a = x_i / \left(x_i + x_j\right)$.

TABLE V. Prediction of the V^E data by the empirical models for the investigated ternary systems

Model	$\sigma \times 10^6$ / m^3 mol^{-1}					
	Methanol (1) + Chloroform (2) +Benzene (3)					
	T / K					
	288.15	293.15	298.15	303.15	308.15	313.15
Radojković	0.0336	0.0340	0.0344	0.0350	0.0358	0.0363
Kohler	0.0309	0.0310	0.0312	0.0315	0.0320	0.0320
Jacob–Fitzner	0.0336	0.0340	0.0344	0.0350	0.0358	0.0363
Colinet	0.0294	0.0294	0.0296	0.0300	0.0305	0.0304
Tsao–Smith[a]	0.0078	0.0077	0.0078	0.0080	0.0083	0.0092
Tsao–Smith[b]	0.0318	0.0329	0.0339	0.0352	0.0365	0.0372
Tsao–Smith[c]	0.0516	0.0517	0.0519	0.0520	0.0520	0.0518
Toop[a]	0.0254	0.0242	0.0231	0.0219	0.0208	0.0194
Toop[b]	0.0311	0.0324	0.0338	0.0355	0.0375	0.0391
Toop[c]	0.0350	0.0354	0.0360	0.0366	0.0376	0.0379
Scatchard[a]	0.0256	0.0245	0.0234	0.0222	0.0211	0.0198
Scatchard[b]	0.0315	0.0328	0.0343	0.0362	0.0384	0.0402
Scatchard[c]	0.0373	0.0378	0.0385	0.0393	0.0405	0.0409
Rastogi	0.0528	0.0516	0.0506	0.0498	0.0493	0.0486
	1-Propanol (1) + Chloroform (2) + Benzene (3)					
Radojković	0.0302	0.0304	0.0312	0.0319	0.0326	0.0339
Kohler	0.0304	0.0303	0.0308	0.0310	0.0310	0.0321
Jacob-Fitzner	0.0302	0.0304	0.0312	0.0319	0.0326	0.0339
Colinet	0.0274	0.0275	0.0280	0.0282	0.0285	0.0294
Tsao–Smith[a]	0.0348	0.0349	0.0347	0.0350	0.0349	0.0354
Tsao–Smith[b]	0.0424	0.0417	0.0414	0.0408	0.0395	0.0394
Tsao–Smith[c]	0.0538	0.0524	0.0515	0.0501	0.0484	0.0476
Toop[a]	0.0159	0.0165	0.0171	0.0181	0.0187	0.0201
Toop[b]	0.0491	0.0501	0.0514	0.0526	0.0536	0.0554
Toop[c]	0.0409	0.0413	0.0424	0.0431	0.0437	0.0453
Scatchard[a]	0.0158	0.0163	0.0166	0.0176	0.0180	0.0192
Scatchard[b]	0.0531	0.0540	0.0555	0.0567	0.0580	0.0598
Scatchard[c]	0.0399	0.0408	0.0422	0.0433	0.0444	0.0465
Rastogi	0.0581	0.0585	0.0595	0.0610	0.0633	0.0660

[a]Methanol or 1-propanol is the asymmetric components; [b]chloroform is the asymmetric component; [c]benzene is the asymmetric component

As can be seen from Table V, the best results of V^E predictions for the system methanol + chloroform + benzene were obtained with the a-type Tsao–Smith Equation. This a-type asymmetric model assumes that component shown as first in the numbering (methanol) is the asymmetric component. This type is the most adequate, giving the best agreement with the experimental data for this system. In addition, two other asymmetric expressions, the a-type Toop and the a-type Scatchard Equation, produced lower RMSD and could be recommended. The Radojković, Kohler, Jacob–Fitzner, Colinet, b-type Tsao–Smith, b-type Toop and b-type Scatchard function satisfactorily, while the other models present clearly higher deviations and can not be recommended.

The best agreement with experimental V^E data for the system 1-propanol + + chloroform + benzene, as shown in Table V, was achieved by the asymmetric models: the a-type of Scatchard and the a-type of Toop, having in both cases 1-propanol as the asymmetric component. Satisfactory results were obtained using the symmetric models of Radojković, Kohler, Jacob–Fitzner and Colinet. All other asymmetric equations worked very poorly, whereas the worst predictions were obtained with the symmetric Rastogi model. It can be concluded that for both studied ternary systems, the majority of the examined predictive models gave adequate predictions of V^E from the data of their binary sub-systems.

Comparison of the results achieved by the empirical models and the CEOS and CEOS/G^E models leads to the following remarks: for the methanol + chloroform + benzene system, the results obtained by both CEOS models (vdW1-2 and vdW1-3) are of the same quality compared with those attained by the majority of the empirical models (an exception is the a-type Tsao–Smith model). For the 1-propanol + chloroform + benzene system, the vdW1-2 model worked signifycantly better than the vdW1-3 one and all empirical models. The applied CEOS/G^E models, as it was already mentioned, are not suitable for this type of estimations for the ternary systems examined here.

5. CONCLUSION

In the last decades, powerful thermodynamic models (G^E, CEOS, polynomials, *etc.*) have been developed. Firstly, the achievement was mainly directed to the correlation, prediction, cross prediction and simultaneous fitting of VLE, LLE, H^E, c_p^E, *etc.* However, until the employment of CEOS/G^E models, which are no longer limited to non-polar systems, the range of applicability could not be extended to very complex mixtures with polar components over wide ranges of pressure and temperature, including the critical region. This rapid progress was imposed by a specific behaviour of G^E on the CEOS model through its additional flexible mixing rules. The accurate results of the CEOS/G^E models, such as the TCBT-3 model, used in correlating and predicting V^E for diverse, strongly non-ideal systems over a large range of temperature, are very promising. In addition, the range of their applicability could be extended to other thermodynamic properties (H^E, c_p^E, *etc.*) and, as the most important, to mixtures which hitherto could not be successfully represented by CEOS. Based on the results of this study, it can be concluded that the CEOS/G^E mixing rules have an advantage over the vdW1-one fluid mixing rules for almost all the here investigated binary and ternary systems and in some cases the improvement was quite significant. The results obtained using the TCBT model with an insignificant change of parameters, generated from an individual isotherm, support the opinion that the influence of temperature on the CEOS/G^E parameters is reduced, enabling extrapolation over wider ranges of temperature. A number of the examined empirical models, especially some of the

asymmetric ones, such as Tsao–Smith, Toop and Scathhard, allowed adequate prediction of V^E of ternary mixtures from the data of binary subsystems. However, the reliability that most of the empirical polynomials employed exhibited suggests that no unique equation can represent the diverse types of complex systems.

Acknowledgement. This work was supported by a grant from the Research Fund of Ministry of Science of Serbia and the Faculty of Technology and Metallurgy, University of Belgrade (project No. 142064).

И З В О Д

МОДЕЛОВАЊЕ ВОЛУМЕТРИЈСКИХ СВОЈСТАВА БИНАРНИХ И ТЕРНЕРНИХ СМЕША ПОМОЋУ CEOS, CEOS/G^E И ЕМПИРИЈСКИХ МОДЕЛА

БОЈАН Д. ЂОРЂЕВИЋ, СЛОБОДАН П. ШЕРБАНОВИЋ, ИВОНА Р. РАДОВИЋ, АЛЕКСАНДАР Ж. ТАСИЋ И МИРЈАНА Љ. КИЈЕВЧАНИН

Технолошко–металуршки факултет, Универзитет у Београду, Карнегијева 4, 11000 Београд

Иако су правила мешања базирана на кубним једначинама стања и van der Waals-један флуид правилу мешања, која укључују температурно зависне параметре, довољна за прорачун равнотеже пара–течност и допунских својстава (допунска моларна енталпија H^E, допунска моларна запремина V^E, итд.), проблеми настају при корелисању и предсказивању термодинамичких својстава сложених смеша у различитим интервалима температуре и притиска. Велики напредак је остварен приступом базираном на CEOS/G^E моделима. Овај рад представља преглед доприноса у последњих шест година наше истраживачке групе у моделовању волуметријских својстава сложених бинарних и тернерних система неелектролита помоћу CEOS и CEOS/G^E приступа. Посебно, vdW1 и TCBT модели су примењени за израчунавање V^E података тернерних система метанол + хлороформ + бензен и 1-пропанол + хлороформ + бензен, као и одговарајућих бинарних система метанол + хлороформ, хлороформ + + бензен, 1-пропанол + хлороформ и 1-пропанол + бензен у интервалу температуре 288.15–313.15 K и на атмосферском притиску. Такође, извршено је и предсказивање V^E података за оба тернерна система емпиријским моделима (Radojković, Kohler, Jackob–Fitzner, Colinet, Tsao–Smith, Toop, Scatchard и Rastogi).

(Примљено 15. августа 2007)

REFERENCES

1. I. R. Grgurić, A. Ž. Tasić, B. D. Djordjević, M. Lj. Kijevčanin, S. P. Šerbanović, *J. Serb. Chem. Soc.* **67** (2002) 581
2. I. R. Grgurić, S. P. Šerbanović, M. Lj. Kijevčanin, A. Ž. Tasić, B. D. Djordjević, *Thermochim. Acta* **412** (2004) 25
3. S. P. Šerbanović, M. Lj. Kijevčanin, I. R. Radović, B. D. Djordjević, *Fluid Phase Equilib.* **239** (2006) 69
4. I. R. Radović, M. Lj. Kijevčanin, E. M. Djordjević, B. D. Djordjević, S. P. Šerbanović, *Fluid Phase Equilib.* in press
5. M. Lj. Kijevčanin, S. P. Šerbanović, I. R. Radović, B. D. Djordjević, A. Ž. Tasić, *Fluid Phase Equilib.* **251** (2007) 78
6. M. Lj. Kijevčanin, M. M. Djuriš, I. R. Radović, B. D. Djordjević, S. P. Šerbanović, *J. Chem. Eng. Data* **52** (2007) 1136
7. M. Lj. Kijevčanin, I. M. Purić, I. R. Radović, B. D. Djordjević, S. P. Šerbanović, *J. Chem. Eng. Data* **52** (2007) 2067

8. J. D. Smiljanić, M. Lj. Kijevčanin, B. D. Djordjević, D. K. Grozdanić, S. P. Šerbanović, *Int. J. Thermophys.*, in press
9. M. Lj. Kijevčanin, B. D. Djordjević, S. P. Šerbanović, I. R. Grgurić, A. Ž. Tasić, *Physic. Chem. Liquids* **42** (2004) 147
10. M. Lj. Kijevčanin, B. D. Djordjević, S. P. Šerbanović, I. R. Grgurić, A. Ž. Tasić, *Physic. Chem. Liquids* **44** (2006) 233
11. I. R. Grgurić, A. Ž. Tasić, B. D. Djordjević, M. Lj. Kijevčanin, S. P. Šerbanović, *J. Serb. Chem. Soc.* **68** (2003) 47
12. M. Lj. Kijevčanin, S. P. Šerbanović, I. R. Radović, B. D. Djordjević, A. Ž. Tasić, *J. Serb. Chem. Soc.* **71** (2006) 807
13. S. P. Šerbanović, I. R. Grgurić, M. Lj. Kijevčanin, A. Ž. Tasić, B. D. Djordjević, *Korean J. Chem. Eng.* **21** (2004) 858
14. Y. Adachi, H. Sugie, *Fluid Phase Equilib.* **23** (1986) 103
15. P. A. Gupta, P. Rasmussen, A. Fredenslund, *Ind. Eng. Chem. Fundam.* **25** (1986) 636
16. H. Renon, J.M. Prausnitz, *AIChE J.* **14** (1968) 135
17. R. Stryjek, J. H. Vera, *Can. J. Chem. Eng.* **64** (1986) 323
18. C. H. Twu, J. E. Coon, D. Bluck, B. Tilton, *Fluid Phase Equilib.* **158**–**160** (1999) 271
19. O. Redlich, A. Kister, *Ind. Eng. Chem.* **40** (1948) 345
20. P. R. Bevington, D. K. Robinson, *Data Reduction and Error Analysis for the Physical Sciences*, McGraw-Hill, Singapore, 1994
21. T. M. Letcher, J. A. Nevines, *J. Chem. Thermodyn.* **26** (1994) 697
22. R. Tanaka, S. Toyama, *J .Chem. Eng. Data* **42** (1997) 871
23. J.–P. E. Grolier, G. C. Benson, P. Picker, *J. Chem. Eng. Data* **20** (1975) 243
24. T. M. Letcher, J. A. Nevines, *J. Chem. Eng. Data* **40** (1995) 293
25. J. Inarrea, J. Valero, P. Perez, M. Gracia, C. G. Losa, *J. Chem. Thermodyn.* **20** (1988) 193
26. K. N. Marsh, C. Burfitt, *J. Chem. Thermodyn.* **7** (1975) 955
27. R. Malhotra, B. S. Mahl, Int. Data Ser. Sel. Data Mixtures Ser. A 1 (1991) 52
28. I. Nagata, K.Tamura, *J. Chem. Thermodyn.* **22** (1990) 279
29. N. Radojković, A. Tasić, D. Grozdanić, B. Djordjević, D. Malić, *J. Chem. Thermodyn.* **9** (1977) 349
30. P. P. Singh, B. R. Sharma, K. S. Sidhu, *Can. J. Chem*. **56** (1978) 2127
31. T. E. Daubert, R. P. Danner, *Physical and Thermodynamic Properties of Pure Chemicals; Data Compilation*, Hemisphere Publishing Corporation, New York, 1989
32. J.-P. E. Grolier, G. Roux–Desgranges, Z. S. Kooner, J. F. Smith, L. G. Hepler, *J. Solution Chem.* **16** (1987) 745
33. H. Nomura, S. Koda, Y. Miyahara, *J. Chem. Phys.* **65** (1976) 4339
34. F. Kohler, *Monatsh. Chem.* **91** (1960) 738
35. P. K. Talley, J. Sangster, C. W. Bale, A. D. Pelton, *Fluid Phase Equilib*. **85** (1993) 101
36. M. Dominguez–Perez, S. Freire, J. J. Llano, E. Rilo, L. Segade, O. Cabeza, E. Jimenez, *Fluid Phase Equilib*. **212** (2003) 331
37. A. Touriño, M. Hervello, V. Moreno, G. Marino, M. Iglesias, *J. Serb. Chem. Soc.* **69** (2004) 461
38. D. W. Marquardt, *J. Soc. Ind. Appl. Math*. **2** (1963) 431
39. K. T. Jakob, K. Fitzner, *Thermochim. Acta* **18** (1977) 197
40. C. Colinet, *Ph.D. Thesis*, University of Grenoble, France, 1967
41. C. C. Tsao, J. M. Smith, *Chem. Eng. Prog. Symp. Series* **49** (1953) 107
42. G. W. Toop, *Trans. TMS-AIME* **233** (1965) 850
43. G. Scatchard, L. B. Ticknor, J. R. Goates, E. R. McCartney, *J. Am. Chem. Soc.* **74** (1952) 3721
44. R. P. Rastogi, J. Nath, S. S. Das, *J. Chem. Eng. Data*, **22** (1977) 249.

Journal of the Serbian Chemical Society
JSCS@tmf.bg.ac.yu • www.shd.org.yu/JSCS

J. Serb. Chem. Soc. 72 (12) 1465–1475 (2007)
JSCS–3676

UDC 543:615.285+615.45:541.135.5–039.26
Original scientific paper

Determination of various insecticides and pharmaceuticals using differently modified glassy carbon electrodes

FERENC F. GAÁL[1,2*#], VALÉRIA J. GUZSVÁNY[1#] and LUKA J. BJELICA[1#]

[1]*Faculty of Sciences, Department of Chemistry, Trg D. Obradovića 3, 21000 Novi Sad and* [2]*Academy of Sciences and Arts of Vojvodina, Dunavska 37, 21000 Novi Sad, Serbia*

(Received 31 July 2007)

Abstract: The applicability of differently modified glassy carbon (GC) electrodes for direct or indirect determinations of various physiologically active compounds (insecticides and pharmaceuticals) in different formulations and some real samples was investigated. Samples of selected insecticides from the group of neonicotinoids with nitroguanidine (thiamethoxam and imidacloprid), cyanoimine (acetamiprid) and nitromethilene (nitenpyram) fragments, prepared in an appropriate manner, were determined by voltammetry on bare and surface-modified GC electrodes, while in the case of pharmaceuticals such as Trodon and Akineton, the chloride anion titration was followed using bare GC and phosphorus doped (P–GC) electrodes. The P–GC was also used to monitor the chloride content in the photocatalytic degradation of the (4-chloro-2-methylphenoxy)acetic acid herbicide. It was found that apart from the nature of the electrode material, the analyte and supporting electrolyte, as well as the pretreatment of the electrode surface essentially influences the applicability of the employed sensors.

Keywords: bismuth film electrode, tetradecane film electrode, phosphorus-doped glassy carbon, insecticides, pharmaceuticals, electroanalytical determinations.

INTRODUCTION

Of various electrode materials, glassy carbon (GC) is particularly useful because of its high electrical conductivity, impermeability to gases, high chemical resistance, reasonable mechanical and dimensional stability and widest potential range of all carbonaceous electrodes.[1] Although GC serves as a very good electrode material, many attempts have been made to improve its electrochemical properties by chemical modification. Surface modification comprises several methodologies, including 1) the addition of a variety of molecular catalysts and mediators to the electrode surface by adsorption, 2) covalent bonding of electroactive catalysts, 3) entrapment of metals within an affixed polymer film and 4) va-

* Corresponding author. E-mail: gaal@ih.ns.ac.yu
# Serbian Chemical Society member.
doi: 10.2298/JSC0712465G

por or electrodeposition of metals directly onto the electrode.[1,2] It is well known that GC is a convenient material for surface modification with metals, *e.g.*, mercury[3] and bismuth.[4] Although bulk bismuth electrodes were used in amperometric titration several decades ago,[5] this electrode has recently experienced its renaissance in voltammetric determinations.[6] Namely, apart from bulk bismuth electrodes, use is often made of its film, primarily aimed at replacing toxic Hg film.[7,8] Such films have been used in different types of anodic stripping analysis for trace level determination of a wide assortment of metal ions.[7–11] On the other hand, the application of bismuth and bismuth film electrodes (BiFEs) have been much less studied for the determination of organic compounds.[12,13]

Another approach, yielding homogeneously modified materials, involves the introduction of heteroatoms in the carbon precursor.[2,14–16] Such a homogeneous modification of GC is highly desirable because of the expectation that an electrode modified at the atomic level would exhibit efficient catalysis, high stability, and comparatively simple renewability. Hitherto, a number of elements have been used for GC doping, *e.g.*, nitrogen,[2] chlorine,[14] fluorine,[14] platinum,[2] lithium,[15] boron,[16] phosphorus,[16] *etc*.

It is generally accepted that the microstructure of the carbon material, cleanliness of the electrode surface and surface functional groups are important determinants of electrode reactivity and suitability for surface modification. It is also known that bare solid electrodes suffer from memory effects and, due to the inability to achieve surface renewal, surface regeneration is frequently required.[1,17] The strategies for surface renewal include polishing,[18] electrochemical activetion,[17,19] ultrasonic activation,[20] laser activation,[21] *etc*.

Cyclic voltammetry (CV) and differential pulse voltammetry (DPV) on bare or differently modified GC electrodes have proved to be suitable for the sensitive and selective determination of many pharmaceutical[22–24] and pesticide compounds.[25–27]

The aim of this work was to study the possibility of applying various GC-based electrodes, *i.e.*, two bare GC samples from different manufacturers, surface modified GC (bismuth film, BiFE, and tetradecan film, C14FE) and bulk-modified GC with phosphorus as dopant (P–GC) for direct or indirect determinations of various physiologically active compounds (insecticides and pharmaceuticals) in different formulations and some real samples.

EXPERIMENTAL

Reagents and solutions

All chemicals used were of the analytical reagent grade. The reference standards were: nitenpyram ($C_{11}H_{15}ClN_4O_2$), pestanal, purity 99.9 %, and (4-chloro-2-methylphenoxy)acetic acid, MCPA ($C_9H_9ClO_3$) (Riedel-de-Haën, Germany), purity 98.8 %, thiamethoxam ($C_8H_{10}ClN_5O_3S$), acetamiprid ($C_{10}H_{11}ClN_4$) and imidacloprid ($C_9H_{10}ClN_5O_2$) pestanals (Syngenta, Switzerland), purity > 99.7 %. The applied commercial formulation of acetamiprid was Volley (Nippon Soda, Japan). Primary stock solutions were prepared by dissolving each reference standard in doubly distilled wa-

ter or in buffer solutions at a concentration of 0.50 mg cm^{-3}. The contents of chloride were determined in the following pharmaceutical preparations: biperiden hydrochloride ($C_{21}H_{30}ClNO$) in Akineton tablets (Lek, Slovenia) and tramadol hydrochloride ($C_{16}H_{26}ClNO_2$) in Trodon capsules (Hemofarm, Serbia). Britton–Robinson buffer solutions were prepared from a 0.04 mol dm^{-3} stock solution of phosphoric (Merck, Germany), boric (Merck), and acetic (Merck) acids by adding 0.2 mol dm^{-3} sodium hydroxide (Merck) to the required pH.

Apparatus

Voltammetric measurements were performed on an Easyscan 5000 (Amel, Italy) instrument furnished with a software package for pulse techniques. The stand included a three-electrode system, a Radiometer saturated calomel electrode (SCE), a platinum ring auxiliary electrode and a GC (Sigri Electrographit, HTT 2400 °C, Sigri-GC and Amel, Amel-GC, HTT not stated), BiFE or C-14FE as working electrode.

The surface morphology of the bare GC and bismuth films was studied on a JEOL JSM-6460LV scanning electron microscope (SEM, Japan Electron Optics Laboratory, Japan). Energy dispersive spectroscopic (EDS) microanalysis was performed using an INCA microanalysis system (Oxford Instruments, United Kingdom).

The course of indirect controlled-current potentiometric titrations was monitored using P–GC and standard Sigri-GC electrodes. Both GC electrodes were in the form of rods (Ø 3 mm) and were mounted in Teflon holders. The P–GC was prepared by carbonizing a phenol–formaldehyde resin, containing 1 % w/w phosphorus added in the form of $(NH_4)_2HPO_4$, at 1000 °C.[28]

The microcomputer-aided[29] potentiometric (I = 1 μA) titrations were performed using a negatively polarized indicator electrode coupled to a Radiometer SCE *via* a double-junction salt bridge ([GC(–)|SCE(+)]). Comparative argentometric potentiometric titrations were performed with the aid of a silver wire electrode connected *via* a suitable SCE and an appropriate resistor, to ensure the zero-current regime. The titrant was added continuously by a Radiometer ABU 80 automatic piston burette at an optimum rate of 0.25 cm^3 min^{-1}.

Comparative high-performance liquid chromatography (HPLC) measurements were performed on an Agilent 1100 series liquid chromatograph (Agilent Technologies Inc., USA) using a Zorbax Eclipse XDB-C18 (4.6 mm×250 mm, 3.5 μm) column and a diode-array detector (DAD) for insecticide determination and a Shimadzu Class LC-10 chromatographic system with a Shimadzu, Japan UV/Vis, SPD-10A detector at 272 nm for Trodon analysis, according to the manufacturer's procedure.

All pH measurements were made on a digital pH meter (Radiometer, Netherlands) using a combined glass electrode (Metrohm, Switzerland).

Voltammetric investigations

The GC electrode, was polished with alumina powder (Buechler, USA) of different particle size (0.5 and 0.3 μm) suspended in doubly distilled water, using finally 0.3 μm grade on a polishing cloth, to attain a mirror fine finish. Afterwards, the GC electrode was washed in an ultrasonic bath with doubly distilled water to remove any residual polishing material. To attain a better functioning, the electrode was pretreated by *ex situ* potential cycling (10 cycles) with amplitude in the 0.4 to −1.9 V (*vs.* SCE) before each measurement. This was carried out in an aqueous solution of the same supporting electrolyte as in voltammetric experiments. In the case of the deposition of a bismuth film, the plating procedure was carried out *ex situ* in a still solution consisting of 0.02 M $Bi(NO_3)_3$, 1 M HCl and 0.5 M KBr[10] at −0.25 V for 60 s.[26] Subsequently, the BiFE was rinsed slightly with 1 M HCl. Before film deposition, the polished GC electrode was activated by *in situ* potential cycling in the plating solution from −0.40 to −1.2 V. To remove the film, a potential of 0.20 V was applied. The tetradecane film electrode was prepared by placing two drops of alkane

solution in hexane on a polished, ethanol-washed and dried Sigri-GC. The film was dried by manual rotation of the electrode. In all cases, the insecticides in the model systems and commercial formulations were measured in 10.0 cm^3 solution in the presence of Britton–Robinson buffer solution, after recording the baseline. For the real samples, the overall volume was 2.00 cm^3. All data were taken at ambient temperature.

Zero-current and controlled-current potentiometric titrations

An aliquot of the titrated solution was diluted with 5.00 cm^3 of doubly distilled water and the mixture was titrated with standard silver nitrate solution. The indicator electrode was P–GC or Sigri-GC. The titration end-point was determined using a computer program[29] for finding the intersection of the straight lines before and after the equivalence point in chloride determination. The procedure was the same in the zero-current regime with a silver indicator electrode. The titration end-point was determined using the mentioned computer program[29] for finding the maximum of the first derivative of the titration curves. In all cases the results were corrected for the blank (10^{-5} mol dm^{-3} solution of potassium nitrate). The procedures for comparative methods were as recommended by the manufacturer.

RESULTS AND DISCUSSION

Glassy carbon and surface-modified glassy carbon electrodes in insecticide analysis

As the nitroguanidine (imidacloprid and thiamethoxam), nitromethylene (nitenpyram) and cyanoimine (acetamiprid) neonicotinoid insecticides have functional groups reducible in a fairly negative potential range (from −0.5 to −2.0 V), *ex situ* potential cycling of the working electrode was employed to expand the potential window. It appeared that the electrochemically pretreated electrode had an about 150 mV more negative potential of hydrogen evolution than the polished electrode and the residual current was significantly higher in the case of the polished surface. The voltammograms recorded in the neonicotinoid model solutions with an *ex situ* pretreated electrode showed a two times more reproducible response (RSD between 2.5 and 3.1 %) than a wet-polished working electrode. The shape of obtained voltammograms was strongly dependent on pH, which can be explained by the significant role played by protons in the complex reduction mechanisms.[30] Since the Sigri-GC and Amel-GC electrodes had different residual currents in the range where the reduction peaks were observed, it appeared that the nature of the GC substrate influenced significantly the determination. By comparing the reduction signals of acetamiprid obtained with Amel-GC (Fig. 1A) and Sigri-GC (Fig. 1B), it can bee seen that the latter was two times more intensive, hence this electrode was used in its determination as the active component in the commercial formulation Volley by the standard addition method (Fig. 1C). The obtained results are in agreement with those of the manufacturer's declaration and the HPLC/DAD method. The advantage of the voltammetric method lies in the simplicity of the sample preparation and the speed of the determination of neonicotinoids (imidacloprid, thiamethoxam, nitenpyram and acetamiprid), although in a higher concentration range (from about 30 to 500 μg cm^{-3}).

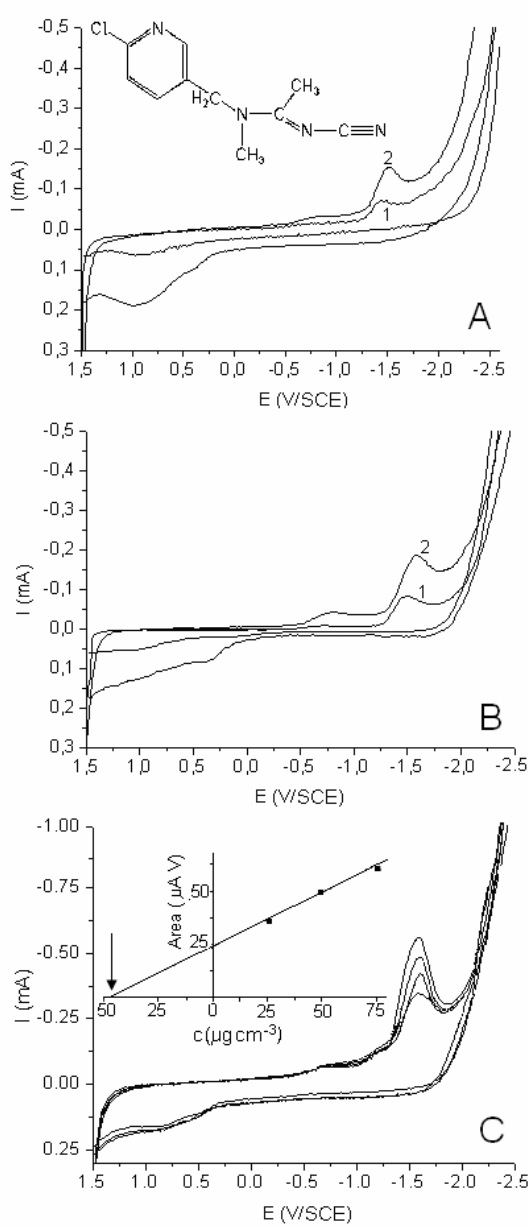

Fig. 1. Cyclic voltammograms of acetamiprid obtained with Amel-GC (A) and Sigri-GC (B) electrodes in Britton–Robinson buffer model solution pH 3.0 at a scan rate of: 1) 100 mV s^{-1} and 2) 500 mV s^{-1} and cyclic voltammograms of its commercial formulation Volley obtained by Sigri-GC (C) at pH 3.0 and 500 mV s^{-1}; the voltammograms recorded after standard addition of acetamiprid. The inset shows the corresponding calibration curve.

With the aim of improving the sensitivity and reproducibility of the determination, two different films, BiFE and C-14FE, were tested in the cathodic voltammetric analysis of thiamethoxam. In the case of an *ex situ* cathodic application, the BiFE should be removed from the plating solution, and, very often, immersed in a neutral or basic solution, which may passivate its surface. This ope-

ration yields a different distribution of the bismuth crystals, which certainly influences the nature of the sensing surface. In the present case, washing in 1 M HCl appeared to be a suitable procedure for the removal of the bismuth bromide complex without affecting the sensitivity of the surface. EDS analysis of the BiFE surface showed that, apart from 60 % of carbon and 20 % of bismuth, there was a significant amount of bromide, which was not observed after washing. After such a pretreatment, the electrode was subjected to electrochemical activation by potential cycling in the potential range from −0.40 V to −1.6 V in the supporting electrolyte. A comparison of the BiFE surfaces before and after potential cycling reveals a rearrangement of bismuth crystals (Fig. 2).

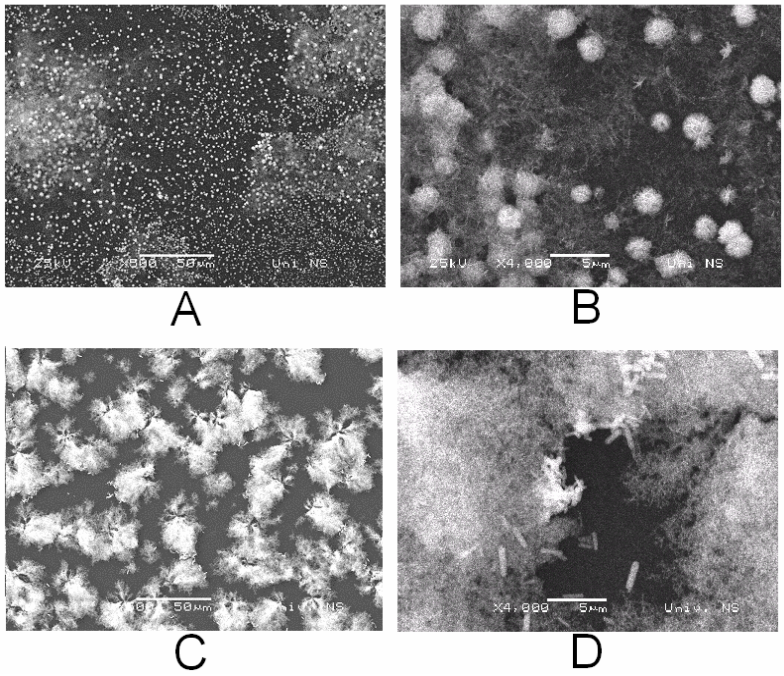

Fig. 2. SEM Morphology of the freshly electrodeposited (A, B) and electrochemically-conditioned BiFE (C, D) taken at two magnifications.

The cyclic volammograms obtained in the conditioning procedure also showed surface stabilization and a significant decrease of the background current after the first cycle (Fig. 3A), which is of a peculiar shape.[26] The electrode prepared in this manner, in combination with the highly sensitive DPV method under optimized conditions, appeared to be convenient for the determination of thiamethoxam in maize[26] and potato (Fig. 3B) samples.

In contrast to the BiFE, with the C-14FE potential cycling did not facilitate film adsorption. This may be explained by the fact that electrochemical conditioning yields a more hydrophilic GC electrode surface compared to the surface

prepared only by polishing. With *n*-alkane films, the hydrophobic interaction of the surface and the compound may favor film adsorption. A comparison of the cyclic voltammograms for thiamethoxam reduction on a C-14FE (Fig. 4, curve 1) and a bare Sigri-GC electrode (Fig. 4, curve 2) shows that the former electrode is advantageous over the latter one. Namely, the corresponding reduction peak is better defined and more symmetric, and the peak current is by 1.2 times higher. The application of the stripping step at 1.0 V and 60 s yielded an increase of the signal by 2.5 times, even at a thiamethoxam concentration of 0.08 mg cm^{-3}.

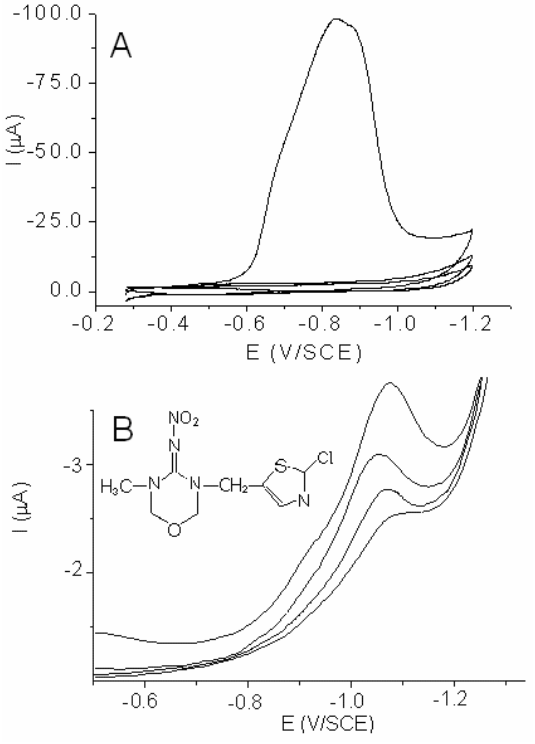

Fig. 3. Electrochemical conditioning of the BiFE surface by cyclic voltammetry (A) and the DPV determination of thiamethoxam on BiFE (B).

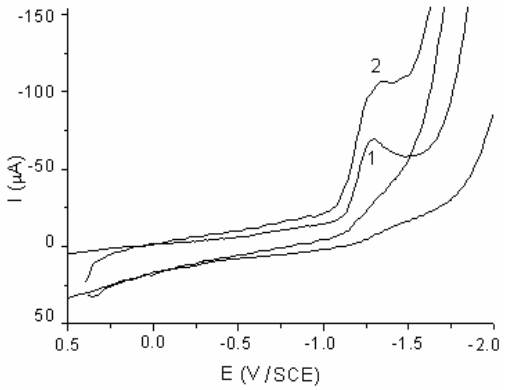

Figure 4. Cyclic voltammograms of thiamethoxam obtained on a C-14FE (1) and a bare Sigri-GC electrode (2).

On the basis of the above, it can be concluded that the different types of GC electrodes differed in their applicability for the determination of organic compounds with functional groups reducible in a fairly negative potential range. Furthermore, the above films in combination with a stripping step in the case of C-14FE and a pulse technique for BiFE lowered the limit of determination and improved the reproducibility.

Bulk-modified glassy carbon electrode in pharmaceutical analysis

In a previous study, it was shown that doping of GC with phosphorus yielded significant changes in the surface properties of the material in comparison to the undoped one and the Sigri-GC electrode. This material was applied as the sensor in the potentiometric argentometric controlled-current titrations of halides and compared with the performance of the Sigri-GC and Ag-wire electrodes. Generally, the P–GC electrode appeared to be suitable for the determination of halides in model systems, and also for the indirect determination of the active component of pharmaceutical preparations containing chlorine and bromine.[24,28] As can be seen from Fig. 5A, the shape of the curves recorded in the titration of chloride from Trodon capsules (curves 1 and 3) and the model solution of chloride (curves 2 and 4) was favorable in the case of using a P–GC electrode. Similar results were also obtained in the titration of chloride from Akineton tablets.

The experiments showed that the potentiometric response depended on the mode of polarization and nature of the analyte and supporting electrolyte. In addition, electrochemical conditioning of the P–GC surface also played an important role. Namely, it was observed that a negative polarization (1.0 V *vs.* SCE until the residual current decayed to about 5 μA) of GC in a 10^{-5} mol dm^{-3} potassium nitrate solution had a favorable effect on the shape of the titration curve. The starting potential of such an electrode was much more negative than in the case when the same electrode was pretreated by polishing. Such a treatment probably resulted in the reduction of oxygen functional groups, thus making the surface more sensitive to silver ions. This conditioning procedure was most favorable for functionalization of a P–GC electrode. It should be noticed that the negative polarization *in situ* did not result in any satisfactory results. Furthermore, the presence of acetate buffer (pH 4.5) in the model system improved the reproducibility even by three times (RSD 0.6 %). It can be supposed that similar buffer additives in the medicaments can have the same effect.

As can be seen from Fig. 5B, the method developed for the indirect determination of different pharmaceuticals was also applicable for monitoring of the chloride concentration during the photocatalytic degradation of the herbicide MCPA in the presence of TiO_2 catalyst. The obtained results are in agreement with literature data.[31] The advantage of a P–GC electrode over a silver electrode lies in the possibility of measuring 100 times lower concentrations of chloride, which is especially important with those systems where the solubility of the parent compound itself is low.

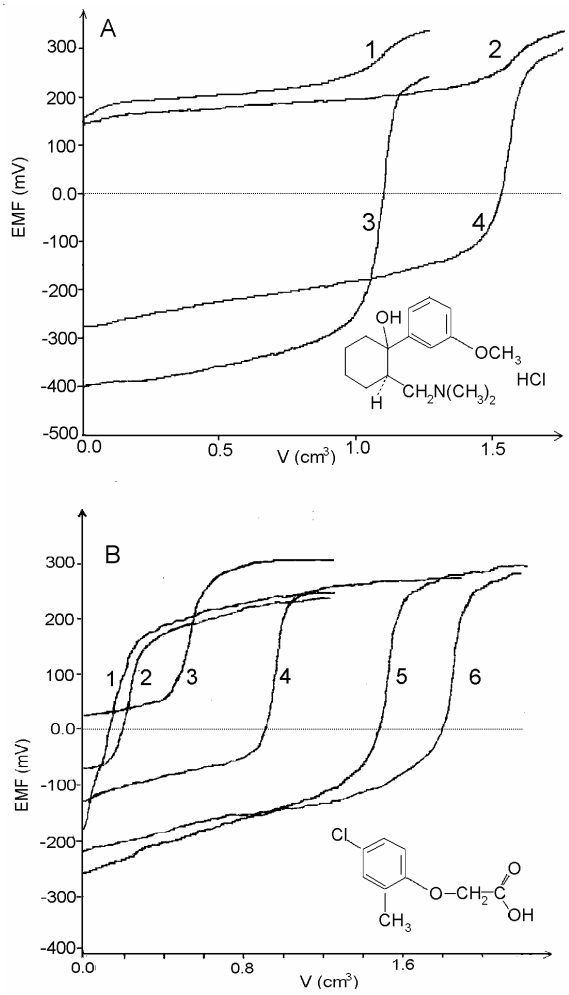

Fig. 5. Zero-current [Ag|SCE], (I = 0) (1,2) and controlled-current [P–GC(–)|SCE(+)], (I = 1 μA) potentiometric titration curves (3,4) of 4.65 mg of tramadol hydrochloride in Trodon capsules (A) and controlled-current [P–GC(–)|SCE(+)], (I = 1 μA) potentiometric titration curves of chloride with 1×10^{-2} mol dm^{-3} $AgNO_3$ obtained in the monitoring of the photocatalytic degradation of 2.7 mol m^{-3} MCPA in the presence of O_2/TiO_2 (B) in the following UV irradiation intervals: 1) 0; 2) 10; 3) 30; 4) 60; 5) 120 and 6) 180 min.

As can be seen from the above examples, various GC-based electrodes are applicable for the determination of different compounds. These methods do not require tedious pretreatment and involve a limited pre-separation procedure, which, consequently, reduces the cost of the analysis.

Acknowledgement. This study was supported by the Ministry of Science of the Republic of Serbia (Project: "Development of New and Improvement of the Existing Procedures for the Monitoring and Advancement of the Quality of the Environment", No. ON142029).

И З В О Д

ОДРЕЂИВАЊЕ РАЗНИХ ИНСЕКТИЦИДА И ФАРМАЦЕУТСКИХ ПРОИЗВОДА ПРИМЕНОМ РАЗЛИЧИТО МОДИФИКОВАНИХ ЕЛЕКТРОДА ОД СТАКЛАСТОГ УГЉЕНИКА

FERENC F. GAÁL[1,2], VALÉRIA J. GUZSVÁNY[1] И ЛУКА Ј. БЈЕЛИЦА[1]

[1]Природно–математички факултет, Департман за хемију, Трг Д. Обрадовића 3, 21000 Нови Сад и [2]Војвођанска академија наука и уметности, Дунавска 37, 21000 Нови Сад

Испитана је могућност примене различито модификованих електрода на бази стакластог угљеника за директно или индиректно одређивање физиолошки активних једињења (инсектицида и лекова) у различитим типовима узорака. Одабрани инсектициди из групе неоникотиноида са нитрогуанидинским (тиаметоксам и имидаклоприд), цијаноиминским (ацетамиприд) и нитрометиленским (нитенпирам) фрагментом су одређивани волтаметријски применом електрода на бази стакластог угљеника, које су биле са и без површинске модификације, док је у случају лекова (тродон и акинетон) титрација хлоридног анјона праћена електродама од стакластог угљеника (GC) и електродама допованим фосфором (P–GC). P–GC електрода је такође примењена за праћење садржаја хлорида у фотокаталитичкој деградацији хербицида (4-хлор-2-метилфенокси)сирћетне киселине. Нађено је да поред природе електродног материјала, аналита и основног електролита припрема електродне површине посебно утиче на применљивост коришћених сензора.

(Примљено 31. јула 2007)

REFERENCES

1. R. L. McCreery, in: *Electroanalytical Chemistry*, Dekker, New York, 1991, p. 221
2. N. L. Pocard, D. C. Alsmeyer, R. L. McCreery, T. X. Neenan, M. R. Callstrom, *J. Mater. Chem.* **2** (1992) 771
3. T. M. Florence, *Anal. Chim. Acta* **119** (1980) 217
4. J. Wang, J. Lu, S. B. Hočevar, P. A. M. Farias, B. Ogorevc, *Anal. Chem.* **72** (2000) 3218
5. M. S. Jovanović, F. F. Gaál, L. J. Bjelica, *Z. Anal. Chem.* **255** (1971) 277
6. M. Bučková, P. Gründler, U. G. Flechsig, *Electroanalysis* **17** (2005) 440
7. J. Wang, *Electroanalysis* **17** (2005) 1341
8. A. Economou, *Trends Anal. Chem.* **24** (2005) 334
9. K. Vytřas, I. Švancara, R. Metelka, *Electroanalysis* **14** (2002) 1359
10. A. Królicka, A. Bobrowski, *Electrochem. Commun.* **6** (2004) 99
11. S. B. Hočevar, B. Ogorevc, J. Wang, B. Pihlar, *Electroanalysis* **14** (2002) 1707
12. E. A. Hutton, B. Ogorevc, S. B. Hočevar, F. Weldon, M. R. Smyth, J. Wang, *Electrochem. Commun.* **3** (2001) 707
13. E. A. Hutton, B. Ogorevc, M. R. Smyth, *Electroanalysis* **16** (2004) 1616
14. H. D. Hutton, W. Huang, D. C. Alsmeyer, J. Kometani, R. L. McCreery, T. X. Neenan, M. R. Callstrom, *Chem. Mater*. **5** (1993) 1110
15. H. Maleki, C. D. Cojocaru, C. M. A. Brett, G. M. Jenkins, J. R. Selman, *J. Electrochem. Soc*. **145** (1998) 721
16. T. Đurkić, A. Perić, M. Laušević, A. Dekanski, O. Nešković, M. Veljković, Z. Laušević, *Carbon* **35** (1997) 1567
17. L. J. Bjelica, R. Parsons, R. M. Reeves, in: *Electrode Processes*, S. Bruckenstein, J. D. E. McIntyre, B. Miller, E. Yeager, Eds., The Electrochemical Society, Princeton, NJ, 1980, p. 190
18. G. N. Kamau, W. S. Willis, J. F. Rusling, *Anal. Chem*. **57** (1985) 545

19. T. Nagaoka, T. Fukunaga, T. Yoshino, I. Watanabe, T. Nakayama, S. Okazaki, *Anal. Chem*. **60** (1988) 2766
20. Q. Fulian, R. G. Compton, *Anal. Chem.* **72** (2000) 1830
21. P. Chen, R. L. McCreery, *Anal. Chem.* **68** (1996) 3958
22. B. Uslu, B. Doğan, S. A. Özkan, *Anal. Chim. Acta* **537** (2005) 307
23. M. R. Majidi, A. Jouyban, K. Asadpour–Zeynal, *J. Electroanal. Chem*. **589** (2006) 32
24. B. F. Abramović, V. J. Guzsvány, F. F. Gaál, *J. Pharm. Biomed. Anal*. **37** (2005) 265
25. V. J. Guzsvány, F. F. Gaál, L. J. Bjelica, Sz. N. Ökrész, *J. Serb. Chem. Soc*. **70** (2005) 735
26. V. Guzsvány, M. Kádár, F. Gaál, L. Bjelica, K. Tóth, *Electroanalysis* **18** (2006) 1363
27. D. C. Coomber, D. J. Tucker, A. M. Bond, *J. Electroanal Chem.* **452** (1998) 5
28. B. F. Abramović, L. J. Bjelica, F. F. Gaál, V. J. Guzsvány, Lj. S. Jovanović, *Electroanalysis* **15** (2003) 878
29. B. F. Abramović, S. D. Tepavčević, B. K. Abramović, F. F. Gaál, *Analyst* **121** (1996) 425
30. V. Guzsvány, M. Kádár, F. Gaál, K. Tóth, L. Bjelica, *Microchim. Acta* **154** (2006) 321
31. A. Topalov, B. Abramović, D. Molnár-Gábor, J. Csanádi, O. Arcson, *J. Photochem. Photobiol. A* **140** (2001) 249.

Journal of the Serbian Chemical Society
JSCS@tmf.bg.ac.yu • www.shd.org.yu/JSCS

J. Serb. Chem. Soc. 72 (12) 1477–1486 (2007) UDC 544.4+541.14+66.092.094:632.954+628
JSCS–3677 *Original scientific paper*

Photocatalytic removal of the herbicide clopyralid from water

BILJANA F. ABRAMOVIĆ[1*#], VESNA B. ANDERLUH[1#], DANIELA V. ŠOJIĆ[1#] and FERENC F. GAÁL[1,2#]

[1]*Faculty of Sciences, Department of Chemistry, Trg D. Obradovića 3, 21000 Novi Sad and* [2]*Academy of Sciences and Arts of Vojvodina, Dunavska 37, 21000 Novi Sad, Serbia*

(Received 20 July 2007)

Abstract: The stability of the herbicide clopyralid (3,6-dichloro-2-pyridinecarboxylic acid) was studied under different experimental conditions of pH, illumination and initial substrate concentration. It was found that in the pH interval from 1.0 to 9.0 in the presence/absence of daylight, clopyralid solutions were stable for at least a period of two months. The kinetics of the photocatalytic degradation of clopyralid in aqueous suspensions of TiO_2 (Degussa P25) under UV and visible light, as well as of direct photolysis using the same radiation sources, were also investigated. It was found that the rate of photocatalytic degradation in the presence of UV light was more than five times higher compared to direct photolysis, whereas in the presence of visible light, the corresponding rates of photocatalytic/photolytic degradation were much lower (more than 15 times). The reaction in the investigation concentration range is zero-order with respect to the degradation of the clopyralid pyridine moiety, with a reaction rate of 3.4×10^{-6} mol dm^{-3} min^{-1} and an adsorption coefficient of the substrate of 2.5×10^{4} dm^{3} mol^{-1}.

Keywords: clopyralid, photocatalytic degradation, TiO_2 Degussa P25, photolysis, water treatment.

INTRODUCTION

Clopyralid (3,6-dichloro-2-pyridinecarboxylic acid, CAS No. 1702-17-6, $C_6H_3Cl_2NO_2$, M_r = 192.00 g mol^{-1}) is a systemic herbicide from the chemical class of pyridine compounds, *i.e.*, pesticides of picolinic acid. It was registered by the U. S. Environmental Protection Agency (EPA) for the control of weeds and woody plants in lawns, turf, pastures, rights-of-way and various crops, such as wheat, barley and oats. This substance is absorbed by the leaves and the roots of the weed and moves rapidly through the plant. It affects plant cell respiration and growth. The acidic form of clopyralid[1] and especially three clopyralid salts, *i.e.*, triethylamine, triisopropylamine and monoethanolamine, are very soluble in wa-

* Corresponding author. E-mail: abramovic@ih.ns.ac.yu
# Serbian Chemical Society member.
doi: 10.2298/JSC0712477A

ter and very mobile in soil, thus having the potential to leach to ground water and contaminate surface water.[2] Clopyralid is formulated in the form of concentrated solutions. In Serbia it is commercially available as Lontrel 100, Pikogal, Piralid 100 and Hemoklop 100-SL, which contain 100 g dm^{-3} of clopyralid. It is also sold in combination with other herbicides, such as triclopyr, (4-chloro-2-methylphenoxy)acetic acid (MCPA) and (2,4-dichlorophenoxy)acetic acid (2,4-D).[3] Clopyralid is by its structure and mode of action similar to the herbicide picloram.[3]

Efficiency is certainly a very important characteristic of pesticides but their degradability is equally, if not more, important because of their potential to contaminate water courses. For this reason, special attention has recently been paid to the degradation of pesticides as a means of water decontamination. A promising way to perform the mineralization of this type of substance is the application of an advanced oxidation process (AOP). Heterogeneous photocatalysis with titanium dioxide as a semiconductor is one of the most popular treatment technologies for eliminating a number of pesticides from water based on AOPs, as can be seen from the large amount of information available in the literature.[4–10] Continuing on previously initiated investigations of the kinetics and mechanism of photocatalytic degradation of compounds which in their structures contain chlorinated pyridine moiety, such as 3-amino-2-chloropyridine and 2-amino-5-chloropyridine[11–13] as model compounds for pyridine containing pesticides, the aim of this work was to study the kinetics of the photocatalytic degradation of the herbicide clopyralid from the mentioned group of compounds. The kinetics of photocatalytic degradation under UV light was compared to that of direct photolysis, as well as to the kinetics under visible irradiation in the presence and absence of TiO_2. The effect of the initial concentration of pesticide was also investigated.

EXPERIMENTAL

Chemicals and solutions

All chemicals used in the investigation were of reagent grade and were used without further purification. Clopyralid, 99.4 %, PESTANAL®, analytical standard, was purchased from Riedel-de Haën. Britton–Robinson (BR) buffers were prepared using hydrochloric acid, 35 %, p.a., and phosphoric acid, 85 %, p.a., both purchased from Lachema, Neratovice; acetic acid, 99.5 %, p.a., from Polskie Odczynniki Chemiczne S. A., Gliwice; boric acid, 99.8 %, p. a., from Kemika, Zagreb; while sodium hydroxide, p.a., was purchased from ZorkaPharm, Šabac. All solutions were made using doubly distilled water. Acetonitrile, 99.8 % (J. T. Baker, Deventer) was used as a component of the mobile phase for HPLC analyses.

Stock solutions with 1.0 and 3.0 mol m^{-3} of clopyralid were prepared and protected from the sunlight. For the investigations of the influence of pH on the kinetics of photodegradation, 0.10 mol m^{-3} solutions of clopyralid were prepared by measuring 5.00 cm^3 of 1.0 mol m^{-3} stock solution into 50.00 cm^3 volumetric flasks. Then, 25.0 cm^3 of BR buffer of appropriate pH were added to each flask and the solutions were made up to mark with doubly distilled water. For the investigation of the effect of the initial clopyralid concentration, stock solutions were further diluted to prepare lower concentration solutions. Standard solutions for the construction of the calibration curves (3.1×10^{-3}–5.0×10^{-2} mol m^{-3}) for spectrophotometric and HPLC determinations were prepared by measuring the necessary volumes of stock solutions into 10.00 cm^3 volumetric flasks.

Degussa P25 TiO_2 (75 % anatase and 25 % rutile form, 50±15 $m^2 g^{-1}$, about 20 nm, non-porous) was used as the photocatalyst.

Photodegradation procedure

For the investigation of the stability of clopyralid solutions at various pH values, experiments were performed at 25±2 °C, either exposed to daylight or in the dark during the spring months of 2007.

The photocatalytic reaction was carried out in a cell (sample volume 20.0 cm^3, continuously flushed with O_2) made of Pyrex glass, with a plain window on which the light beam was focused, equipped with a magnetic stirring bar and a water circulating jacket. Aqueous suspensions of TiO_2 Degussa P25, containing 1.0 mol m^{-3} herbicide (except for the study of the effect of initial substrate concentration), were sonicated for 15 min before illumination, to make the particles of the photocatalyst uniform. The thus obtained suspension was thermostated at 40±1 °C in a stream of O_2 and then irradiated. Irradiation in the UV range was performed using a 125-W medium-pressure mercury lamp (Philips, HPL-N, emission bands in the UV region at 304, 314, 335 and 366 nm, with maximum emission at 366 nm), with an appropriate concave mirror. Irradiation in the visible range was performed using a 50-W halogen lamp (Philips) and a 400-nm cut-off filter. During irradiation, the mixture was stirred at a constant speed. All the experiments in the presence of photocatalyst were carried out using 2 mg cm^{-3} TiO_2.

Direct photolysis experiments were performed under the same conditions, but without catalyst addition.

Analytical procedure

For the spectrophotometric determination of the effect of pH on the stability of the clopyralid solutions under daylight and in the dark, 5.00 cm^3 aliquots of the samples were taken and diluted to 10.00 cm^3 with doubly distilled water. For the blank, 2.0 cm^3 aliquots of BR buffer of the appropriate pH value were taken and diluted to 10.00 cm^3 with doubly distilled water.

For the spectrophotometric monitoring of the degradation of the substrate, aliquots of 0.50 cm^3 of the reaction mixture were taken at regular time intervals, then 5.0 cm^3 of 0.1 mol dm^{-3} HCl were added, and the solution diluted to 10.00 cm^3 with doubly distilled water. The suspensions containing the photocatalyst were filtered through Millipore (Milex-GV, 0.22 μm) membrane filters and the spectra were recorded in the wavelength region from 200 to 400 nm on a Secomam Anthelie Advanced 2 spectrophotometer in 1 cm quartz cells. The kinetics of the degradation of the pyridine moiety was monitored at 225 nm.

For the HPLC determinations, the samples were prepared in the same way as for the spectrophotometric measurements. After that, 20 μl of the sample were injected and analyzed on an Agilent Technologies 1100 Series liquid chromatograph, with a UV/VIS DAD set at 225 nm and with an Eclyps XDB-C18 column (150 mm×4.6 mm, particle size 5 μm). The mobile phase (flow rate 1.0 cm^3 min^{-1}) was a mixture of acetonitrile and water acidified with 0.1 % phosphoric acid (3:7, v/v). For the 3D HPLC measurements of the potentially formed intermediates, 1.00 cm^3 aliquots of the reaction mixture were taken at regular time intervals without subsequent dilution.

RESULTS AND DISCUSSION

Since it was to be expected that the degradation of clopyralid would be accompanied by changes in pH, because of both the disappearance of clopyralid (p*K* 2.0)[1] and the formation of hydrochloric acid and, presumably, nitrate/ammonium (due to the presence of chlorine and nitrogen in the molecule), it was also necessary to investigate the effect of pH on the spectral pattern (Fig. 1). As can be seen, in the investigated pH range, certain changes in the shape of the spec-

trum occurred, and a spectrum with a well defined maximum at 225 nm was obtained at pH 1.0. Hence, this pH value was adjusted in the spectrophotometric monitoring of the kinetics of clopyralid photodegradation.

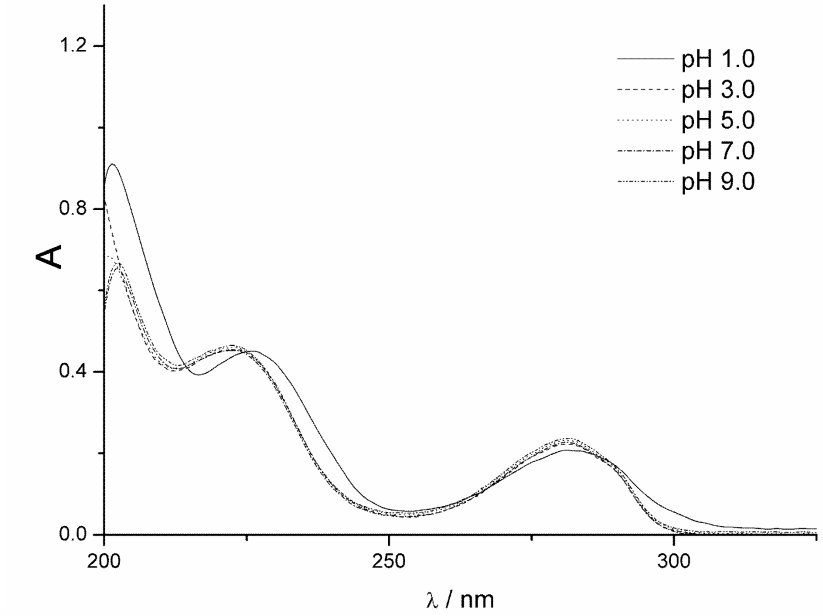

Fig. 1. The influence of pH on the shape of the absorption spectra of a 5×10^{-2} mol m^{-3} clopyralid solution.

To investigate the stability of clopyralid solution (0.10 mol m^{-3}) experiments were performed in the presence and absence of daylight in the pH interval 1.0–9.0 during the spring months of 2007. On the basis of the obtained results, it can be concluded that in none of the cases did degradation of the substrate occur in the period of two months, which indicates its stability under the given experimental conditions. This is an indicator of the even greater importance of studying the efficiency of the process of the photocatalytic degradation of clopyralid.

As can be seen from Fig. 1, the optimal wavelength for monitoring the kinetic of the photocatalytic degradation of clopyralid by the HPLC method was 225 nm. It was found that the peak with a retention time (t_r) at 3.2 min, corresponding to clopyralid, had disappeared completely after 240 minutes of illumination, indicating that in this period complete degradation of the parent compound had occurred (Fig. 2, curve 2). On the basis of these measurements, it was found that the reaction is of zero-order with $k_a = 4.61\times10^{-6}$ mol dm^{-3} min^{-1} (linear regression coefficient, $r = 0.997$). The kinetic curve obtained by the spectrophotometric monitoring of the photocatalytic degradation of clopyralid is shown in Fig. 2 (curve 1). The difference in the presented kinetic curves, *i.e.*, the lower rate

of degradation of clopyralid obtained by spectrophotometric monitoring (k_a = = 4.11×10^{-6} mol dm^{-3} min^{-1}; r = 0.998), suggests the presence of intermediates with a pyridine moiety, which absorbs at the same wavelength as the substrate. The small difference in the kinetic curves indicates a low concentration of the intermediates.

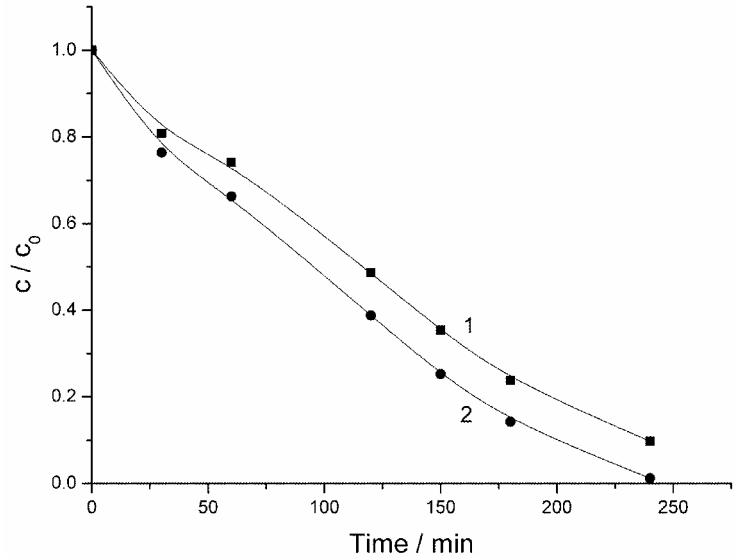

Fig. 2. Kinetics of the photocatalytic degradation of clopyralid (1.0 mol m^{-3}) in the presence of TiO_2 (2 mg cm^{-3}) under UV light: (1) spectrophotometry (λ = 225 nm); (2); HPLC (λ = 225 nm).

Since the concentration of intermediates during photodegradation was low, 3D chromatograms were recorded for aliquots of the reaction mixture without dilution. A 3D chromatogram taken after 180 min of irradiation is presented in Fig. 3, from which the presence of intermediates is visible. Similar chromatograms were also obtained for shorter irradiation times. On the basis of the spectra of the intermediates it can be supposed with great certainty that pyridine derivatives are in question. The formation of such a small number of these intermediates at low concentrations is a good indicator of the efficiency of the heterogeneous photocatalysis in the destruction of clopyralid.

To explore the photocatalytic activity of TiO_2 in the UV light region (Fig. 4, curve 4), the kinetics of degradation of clopyralid under UV light was compared to that under visible light (Fig. 4, curve 2). It can be said that the rate of clopyralid degradation in the former case was about 30 times higher (Table I).

To investigate the photodegradation efficiency of the catalyst, experiments were also performed under conditions of direct photolysis without TiO_2 using artificial UV radiation (Fig. 4, curve 3) and visible (Fig. 4, curve 1) light. The results of these experiments show that in this case too, clopyralid degradation occurred under UV irradiation, although at a significantly lower rate, *i.e.*, about five

times slower compared to photocatalytic degradation (Table I). Under the conditions of visible light, photolysis of the substrate was much slower. Therefore, the slower processes observed in both cases indicate that direct photolysis does not play a significant role in the overall photocatalytic degradation.

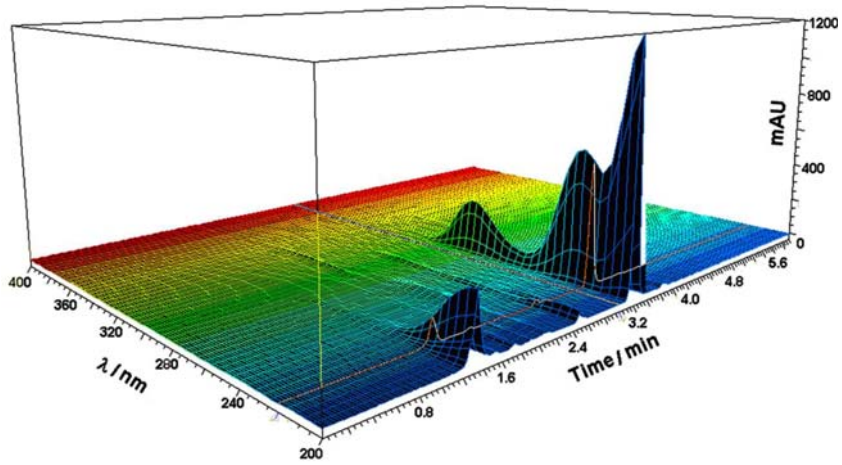

Fig. 3. The 3D chromatogram obtained after 180 min of photocatalytic degradation of clopyralid (1.0 mol m^{-3}) in the presence of TiO_2 (2 mg cm^{-3}) under UV light.

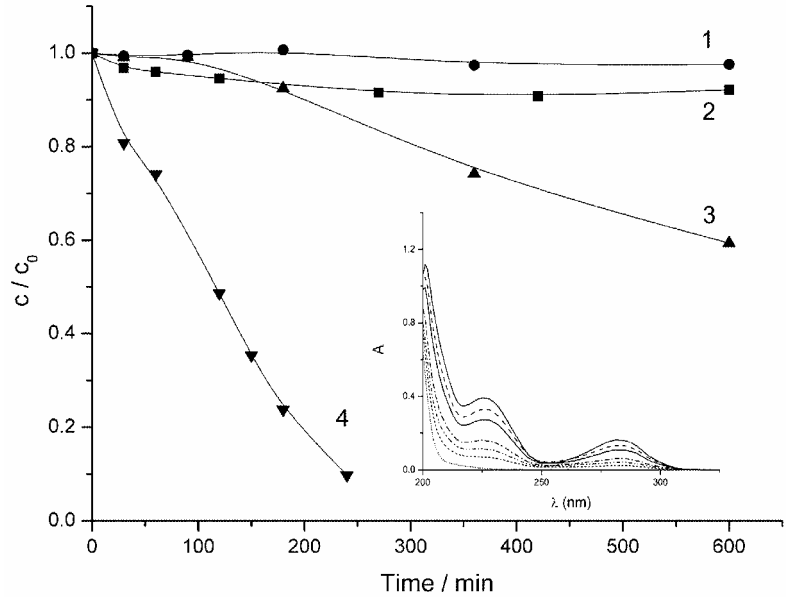

Fig. 4. Kinetic curves for the degradation of the pyridine moiety of clopyralid (1.0 mol m^{-3}) monitored by spectrophotometry: (1) direct photolysis, visible light; (2) TiO_2 (2 mg cm^{-3}), visible light; (3) direct photolysis, UV light; (4) TiO_2 (2 mg cm^{-3}), UV light. Insert represents the profiles of the UV spectrum during the photocatalytic degradation of clopyralid in the presence of TiO_2 under UV light.

TABLE I. Effect of various light sources on the degradation rate, R, of the pyridine moiety of clopyralid[a]

	$R\times10^6$ / mol dm^{-3} min^{-1}	
	Mercury lamp	Halogen lamp
TiO_2 Degussa P25	3.76[b]	0.13
Direct photolysis	0.68	0.04

[a]Degradation rate calculated for time period of 600 min, except [b]240 min

On comparing the obtained results with those obtained in a study of the efficiency of the photocatalytic degradation of mecoprop[14] under visible light, it can be concluded that the efficiency of clopyralid degradation is significantly lower. Namely, the efficiency of photocatalytic degradation of mecoprop under visible light was practically the same as in the direct photolysis by UV light, whereas with clopyralid, as already mentioned, the difference is very large (about five times, Fig. 4, curves 2 and 3). This confirms the supposition that the efficiency of TiO_2 as a photocatalyst under artificial visible light depends to a great extent of the type of substrate.[15]

The effect of the initial substrate concentration on the reaction kinetics was investigated in the concentration range 0.5–3.0 mol m^{-3} (Fig. 5). It was found that the substrate concentration decreased linearly with irradiation time, *i.e.*, the reaction was of zero-order (Table II), which is in agreement with the Langmuir–Hinshelwood (L–H) kinetic model.[16,17] Since the rate of photodegradation in the irradiated suspensions could be satisfactorily described by formal zero-order kinetics (the linear correlation coefficients varied in the range of 0.997–0.999, Table II), the kinetic behavior of clopyralid was subsequently characterized by the initial decomposition rates obtained by linear regression fits (by the least squares method with simple weighting) to the curves c(substrate) *vs.* t(irradiation). The slopes of these plots were used to calculate the k_a values (the apparent zero-order reaction rate constant). It is worthy of mention that a significant deviation from linearity was found only for high conversions (>80 %).

On the basis of the L–H kinetic model[17] transformed to Eq. (1):

$$t_{1/2} = \frac{0.693}{k_r K} + \frac{0.5c_0}{k_r} \quad (1)$$

where k_r is the reaction rate constant and K is the equilibrium adsorption constant of the substrate, a linear dependence (r = 0.986) of the half-life, $t_{1/2}$, against the initial substrate concentration, presented in the insert of Fig. 5, is obtained. The value for k_r determined from the line slope was 3.4×10^{-6} mol dm^{-3} min^{-1} and for K from the intercept 2.5×10^4 dm^3 mol^{-1}.

By comparing the results obtained for the photocatalytic degradation of clopyralid with those of the degradation of 3-amino-2-chloropyridine and 2-amino-5-chloropyridine,[11–13] as model compounds for pyridine-containing pesticides,

it can be concluded that there is a significant difference between them. Namely, the rate of photocatalytic degradation of the pyridine moiety of clopyralid is about two times slower. This difference in the degradation rate is probably a consequence of the different substituents on the pyridine moiety, which influence the kinetics of photocatalytic degradation.

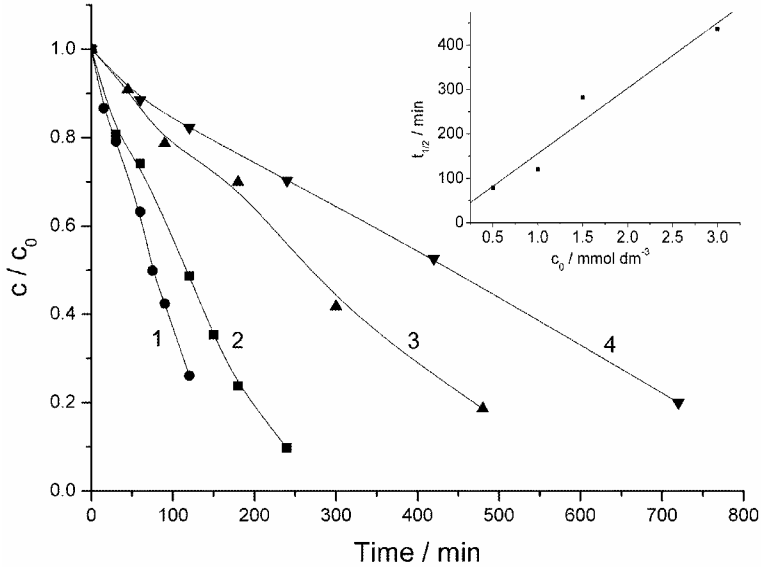

Fig. 5. Effect of the initial clopyralid concentration on its degradation in the presence of TiO_2 (2 mg cm^{-3}) under UV light: (1) 0.5; (2) 1.0; (3) 1.5; (4) 3.0. The inset represents the plot of $t_{1/2}$ against the initial clopyralid concentration.

TABLE II. Effect of the initial concentration, c_0, of clopyralid on the rate of photocatalytic degradation of the pyridine moiety with UV light

c_0 / mol m^{-3}	$k_a \times 10^6$ / mol dm^{-3} min^{-1}[a]	r	$t_{1/2}$ / min
0.5	3.04	0.999	78.6
1.0	4.11	0.998	120
1.5	2.55	0.997	282
3.0	3.21	0.999	436

[a]apparent zero-order rate constant

CONCLUSION

In the presence/absence of daylight at pH 1.0–9.0, clopyralid is stable for at least two months. The rate of photocatalytic degradation of clopyralid under UV light is about 30 times higher than that under visible light. A comparison of the results of the photocatalytic degradation of clopyralid in the presence of TiO_2 with those of direct photolysis obtained under the same irradiation with UV light shows that the substrate decomposition by direct photolysis is considerably slo-

wer (about five times). It was also found that the kinetics of the degradation of the parent substrate are of zero-order, with $k_a = 4.61\times10^{-6}$ mol dm^{-3} min^{-1} ($r = 0.997$). In the investigated concentration range, the reaction is of zero-order with respect to the degradation of the pyridine moiety clopyralid, with a reaction rate constant of 3.4×10^{-6} mol dm^{-3} min^{-1} and adsorption coefficient of the substrate of 2.5×10^{4} dm^{3} mol^{-1}.

Acknowledgments. The authors acknowledge the financial support of the European Community allocated by the European Agency for Reconstruction through the Ministry of International Economic Relations within the Neighboring Program Hungary–Serbia (Action entitled: Regional Water Resources Investigations in the Scope of Sustainable Development, Grant No. 04SER02/01/009) and the Ministry of Science of the Republic of Serbia (Project No. ON142029).

И З В О Д

ФОТОКАТАЛИТИЧКО УКЛАЊАЊЕ ХЕРБИЦИДА КЛОПИРАЛИДА ИЗ ВОДЕ

БИЉАНА Ф. АБРАМОВИЋ[1], ВЕСНА Б. АНДЕРЛУХ[1], ДАНИЕЛА В. ШОЈИЋ[1] и FERENC F. GAÁL[1,2]

[1]*Природно–математички факултет, Департман за хемију, Трг Д. Обрадовића 3, 21000 Нови Сад и*
[2]*Војвођанска академија наука и уметности, Дунавска 37, 21000 Нови Сад*

Испитана је стабилност хербицида клопиралида (3,6-дихлор-2-пиридинкарбоксилна киселина) при различитим експерименталним условима. При проучавању утицаја pH у интервалу од 1,0 до 9,0 у присуству и одсуству дневне светлости нађено је да је раствор клопиралида стабилан најмање у периоду од два месеца. Испитана је и кинетика фотокаталитичке разградње клопиралида у воденим суспензијама TiO_2 (Degussa P25) уз озрачивање UV и видљивом светлошћу, као и директне фотолизе применом истих извора зрачења. Нађено је да је брзина фотокаталитичке разградње у присуству UV светлости преко пет пута већа у поређењу са директном фотолизом, као и да је применом видљивог зрачења брзина разградње у оба случаја знатно нижа (преко 15 пута). При испитивању утицаја почетне концентрације клопиралида на брзину фоторазградње пиридинског прстена, нађено је да је реакција нултог реда са константом брзине од $3{,}4\times10^{-6}$ mol dm^{-3} min^{-1} и коефицијентом адсорпције супстрата $2{,}5\times10^{4}$ dm^{3} mol^{-1}.

(Примљено 20. јула 2007)

REFERENCES

1. *Dow AgroSciences*, Clopyralid a North American technical profile, July 1998, http:// //wric.ucdavis.edu/yst/manage/ClopTechProfile.pdf (July 15, 2007)
2. C. Cox, *Journal of pesticide reform*, **18** (Winter 1998) No 4 http://www.mindfully.org/ /Pesticide/Clopyralid.htm (July 15, 2007)
3. V. N. Mitić, *Pesticides in agriculture and forestry in Serbia and Montenegro*, Serbian Society for Plant Protection, Belgrade, 2004, p. 465 (in Serbian)
4. D. Chatterjee, S. Dasgupta, *J. Photochem. Photobiol. C* **6** (2005) 186
5. D. M. Blake, *Bibliography of Work on the Heterogeneous Photocatalytic Removal of Hazardous Compounds from Water and Air*, National Renewable Energy Laboratory, Golden, Colorado, 2001, http://www.nrel.gov/docs/fy02osti/31319.pdf (July 15, 2007)
6. S. Chiron, A. Fernandez–Alba, A. Rodriguez, E. Garcia–Calvo, *Wat. Res*. **34** (2000) 366
7. A. Fujishima, T. N. Rao, D. A. Tryk, *J. Photochem. Photobiol. C* **1** (2000) 1

8. U. Stafford, K. A. Gray, P. V. Kamat, *Chem. Rev.* **3** (1996) 77
9. M. R. Hoffmann, S. C. Martin, W. Choi, D. W. Bahnemann, *Chem. Rev.* **95** (1995) 69
10. O. Legrini, E. Oliveros, A. M. Braun, *Chem. Rev.* **93** (1993) 671
11. B. F. Abramović, V. B. Anderluh, A. S. Topalov, F. F. Gaál, *J. Serb. Chem. Soc.* **68** (2003) 961
12. B. F. Abramović, V. B. Anderluh, A. S. Topalov, F. F. Gaál, *APTEFF* **35** (2004) 79
13. B. F. Abramović, V. B. Anderluh, A. S. Topalov, F. F. Gaál, *Appl. Catal. B* **48** (2004) 213
14. B. F. Abramović, D. V. Šojić, V. B. Anderluh, *Acta Chim. Slov.* **54** (2007) 558
15. A. G. Agrios, K. A. Gray, E. Weitz, *Langmuir* **20** (2004) 5911
16. J. Theurich, M. Lindner, D. W. Bahnemann, *Langmuir* **12** (1996) 6368
17. H. Al–Ekabi, N. Serpone, *J. Phys. Chem.* **92** (1988) 5726.

Journal of the Serbian Chemical Society
JSCS@tmf.bg.ac.yu • www.shd.org.yu/JSCS

J. Serb. Chem. Soc. 72 (12) 1487–1492 (2007)
JSCS–3678

UDC 54.06+663.251:546.3:543.41
Original scientific paper

Multivariate data visualization methods based on elemental analysis of wines by atomic absorption spectrometry

SLAVICA RAŽIĆ[1*#], ĐURO ČOKEŠA[2#] and SNEŽANA SREMAC[2#]

[1]*Faculty of Pharmacy, Institute of Analytical Chemistry, Vojvode Stepe 450, 11211 Belgrade and* [2]*The Vinča Institute of Nuclear Sciences, P.O. Box 522, 11001 Belgrade, Serbia*

(Received 24 July 2007)

Abstract: The contents of five metals (Cu, Mn, Fe, Cd, and Pb) in several red and white wines originating from different regions of Serbia were determined by flame and graphite furnace atomic absorption spectrometry. The data were processed using chemometric techniques. Principal component and factor analysis were applied in order to highlight the relations between the elements and, after data reduction, three main factors controlling variability were identified. Application of hierarchical cluster analysis to the studied wines indicated differentiation of the samples belonging to different origins. No discrimination between red and white wines was found.

Keywords: principal component analysis, factor analysis, cluster analysis, metals, wines, classification.

INTRODUCTION

A number of articles have been published involving the analysis of metals in wines.[1–15] The interest of studying minor and trace metals in wines is due to their potential toxicity, some undesired phenomena (precipitation, *etc.*) which can arise, and the use of mineral profiles to determine the authenticity of wines.[4] Due to the fact that grape pressing and the skin maceration time can substantially affect the final concentrations of minerals in wine, quantification of some typical elements can help in the improvement of the manufacturing process. Since metals are not metabolized during the vinification and storage, they can be considered as good indicators for the identification of the origin of a wine. The most frequently analyzed metals are: K, Na, Fe, Zn, Rb, Ca, Mg, Mn, Cu, Cr, Co, Sb, Cs, Br, Al, Ba, As, Li and Ag.[6–9] However, by selecting some elements as key features, it is possible to use a far smaller number of variables to classify wines.[10–15]

Recently, chemometric analysis has received increasing attention in the analysis of wines.[8–22] A variety of multivariate methods based on diverse chemical

* Corresponding author. E-mail:snsn@sezampro.yu
# Serbian Chemical Society member.
doi: 10.2298/JSC0712487R

data were reported: principal component analysis (PCA), cluster analysis (CA) and discriminate analysis of the data from FAAS/FAES analysis,[8,12] proton and ^{13}C shifts measurements,[19] GC–MS,[20] ICP–OES,[11] ICP–MS[9,14] and SNIF–NMR results.[18,21] Furthermore, there were also reported PCA and CA from TXRF analysis,[13] K-nearest neighbors cluster analysis, canonical analysis, and soft independent modeling of class analogy (SIMCA) in GC and AAS analyses,[6,8,22] PCA and Kohonen artificial neural network (ANN) using SNIF–NMR and IRMS,[5,18] three-layer ANN using ICP–OES,[11] two-layer ANN using FAAS[12] and correlation between NIRS and AAS data by partial least squares regression (PLSR).

The objective of this study was to investigate the correlation among common trace metals in selected wine samples and to explore the possibility of wine classification by applying chemometrics.

EXPERIMENTAL

The samples of wines commonly found on the Serbian market: 1 – Kosovski cabernet (red), 2 – Kosovski riesling (white), 3 – Rubin burgundac (red), 4 – Rubin riesling (white), 5 – Džervin (red), 6 – Džervin riesling (white), 7 – Cabernet sauvignon (red) and 8 – Italian riesling (white), were supplied bottled. The origin of the grapes is as follows: southern Serbia (1 and 2), central Serbia (3 and 4), eastern Serbia (5 and 6) and northern Serbia (7 and 8).

A flame atomic absorption spectrometer (Perkin Elmer model 3100) was employed for the determination of Cu, Mn, and Fe, while Cd and Pb were determined by a graphite furnace atomic absorption spectrometer (Perkin Elmer model 4100zl). Analytical reagent grade chemicals, Merck standards (Darmstadt, Germany) and Milli-Q water were used. The metal concentrations were calculated using the standard addition method. The analytical procedures, described in detail elsewhere,[23-25] allowed the determination of the selected elements with no matrix effect of organic compounds. None of the wine samples analyzed in this work exceeded the EU's current limit value for heavy metals content of 100 ppm by weight.

The statistical analyses were performed by means of the Minitab 13.0 software package (Minitab Inc., USA).

RESULTS AND DISCUSSION

Multivariate analysis of wine was assessed without taking into account factors such as the type of wine. Some of the elements might be arise from the treatment (*i.e.*, Cu from the Bordeaux mixture), which will not be meaningful in the statistical evaluation unless the particular treatment is only used in one region. A data matrix was formed with 8 wine samples and 5 variables, the concentration of the several minor and trace metals. The average concentrations, standard deviations, minimum and maximum values of metals in the studied wines are presented in Table I. It can be seen that the examined metals are present in the following order of concentrations: Fe > Mn > Cu > Pb > Cd. The correlation matrix of the data on the minor and trace metals are given in Table II. The pairs Cu–Fe (0.786), Cd–Pb (0.696), and Mn–Pb (0.453) show the highest positive correlations. No significant correlations are observed between the other variables.

Principal component analysis (PCA) is a well-established multivariate technique in which data reduction is performed by transforming the data into ortho-

gonal components which are linear combinations of the original variables. The application of PCA to the data matrix of the wine analysis revealed that a total of three PCs accounted for 94 % of the total variance (Fig. 1).

TABLE I. Average content (mg l^{-1}, except for Cd μg l^{-1}) of minor and trace metals in the examined wine samples

Metal	Mean value	Standard deviation, *SD*	Minimum value	Maximun value
Cu	0.58	0.78	0.09	2.30
Mn	1.61	1.02	0.40	3.65
Fe	4.55	2.78	1.93	10.7
Cd	12.0	3.62	8.60	17.7
Pb	0.14	0.05	0.10	0.23

TABLE II. Correlation coefficients for the total samples (Pearson correlation)

	Cu	Mn	Fe	Cd
Mn	0.081 0.879[a]			
Fe	0.786 0.064[a]	0.172 0.745[a]		
Cd	–0.168 0.750[a]	–0.107 0.840[a]	0.045 0.933[a]	
Pb	–0.053 0.921[a]	0.453 0.367[a]	–0.094 0.860[a]	0.696 0.125[a]

[a]The significance level (*P* value)

Fig. 2 shows that Cd and Pb load highly into the first component whereas Cu and Fe are high in the second. A different behavior is noticed for Mn, for which both components are significant. The loading plot is related to the variables and shows their association with respect to the models. In this case, discrimination between the minor metals (Cu, Fe) and trace metals (Cd, Pb) is obvious.

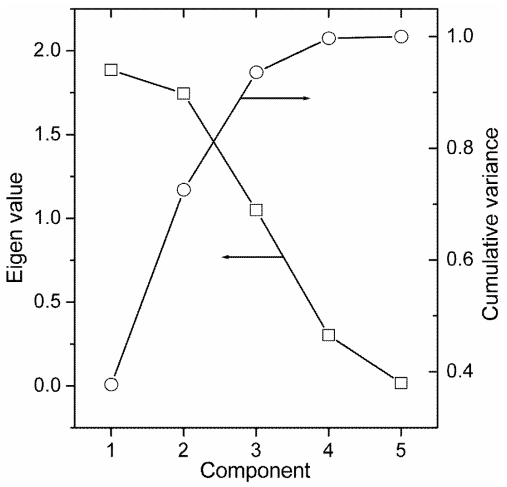

Fig. 1. Eigen analysis of the correlation matrix.

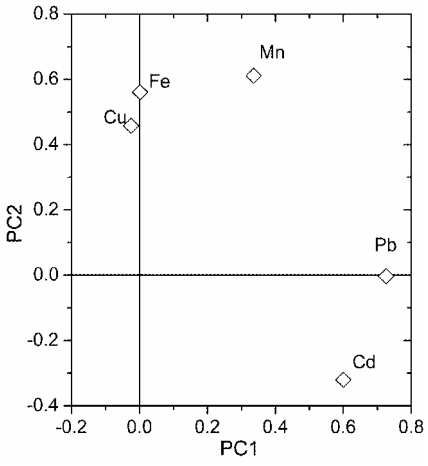

Fig. 2. Plot of the first two component weights of the variables.

In order to identify interrelated variables and make easier the visualization, the data were compressed to a few dimensions using factor analysis (FA). The number of significant factors was selected on the basis of the Kaiser criterion (eigenvalue > 1).[26] Three significant factors were extracted and varimax orthogonal rotation (Table III) enabled a better visualization of the latent structure of the database. Factor 1 has a high loading of Cu and Fe, while Pb and Cd contribute to Factor 2. Mn dominantly contributes to Factor 3. It can be supposed that Factor 1 is related to the influence of the wine making process on minor metals, while Factor 2 can be related to trace metal pollution. However, the fate of Mn in wines is defined by Factor 3, which indicates a different input of Mn.

TABLE III. Varimax rotated factor loadings

Variable	Factor 1	Factor 2	Factor 3
Cu	0.964	–0.099	0.011
Mn	0.075	0.035	0.997
Fe	0.916	0.031	0.103
Cd	–0.033	0.975	–0.137
Pb	–0.051	0.833	0.427

The provenance and authenticity of wines can be recognized on the basis of typical mineral and trace elements patterns by means of chemometric methods. The Cu and Fe content of wines originate from the grapes. It has been reported that up to 90 % of the Cu and up to 70 % of the Fe initially present in grape juice is eliminated during fermentation, mainly by yeast assimilation.[27] However, an excessive content of Cu and Fe in wines is the result of careless contact of wine, after fermentation and during aging or processing, with steel or Cu alloy surfaces. The wines containing an excess of 0.5 mg l^{-1} Cu or 10 mg l^{-1} Fe my be susceptible to clouding or sedimentation as well as flavor deterioration by the strong catalytic and oxidative properties of these cations. As wines with a Pb content of above 100 μg l^{-1} are considered to have been polluted by the material during the wine making process or storage,[17] for most of the studied wines a proximity to a busy road or a city was implied. In spite of Cd being generally associated to oil or fossil fuel combustion, the high value for Pb reveals that traffic exhaust gases were a more relevant source of Cd. The levels of Mn are of special interest, the great differences in the concentration for this metal in wines can be an indicator for the geographical classification of the samples.[10–12,15]

A hierarchical cluster analysis of the standardized variables using the Ward method[28] as an amalgamation rule and the squared Euclidean distance as a measure of the proximity between the samples was carried out. The dendrogram presenting the clustering of wines is shown in Fig. 3. A good separation of the Džervin wines from the Rubin ones and that originating from other regions was found,

while, on the other hand, the grouping of the Kosovo wines was not satisfactory. However, there seems to be no discernible differences among white and red wines.

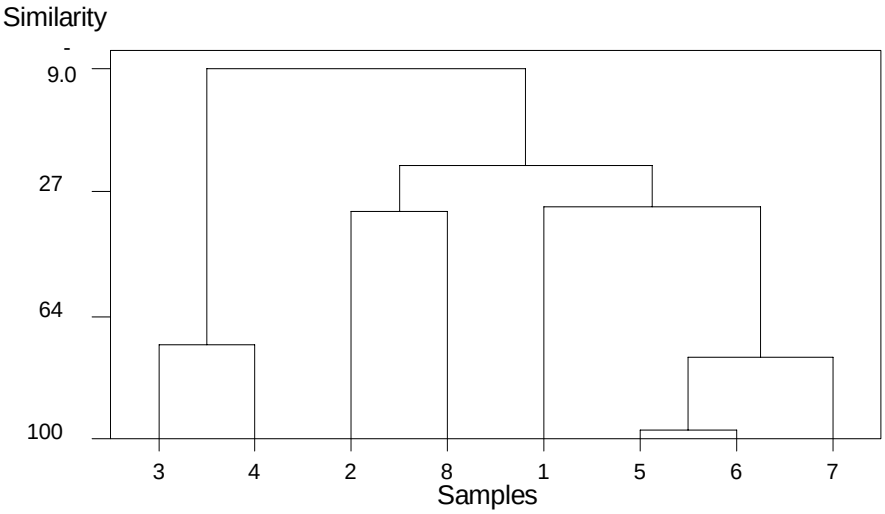

Fig. 3. Dendrogram of cluster analysis of wines.

CONCLUSION

The application of flame atomic absorption spectroscopy and graphite furnace atomic absorption spectrometry in conjunction with multivariate statistics gave good results in the characterization of wines. Principal component analysis reduced the dimensionality of the descriptor space to a total of three PCs. A differentiation between trace metals was obtained by means of factor analysis. Cadmium and Pb load highly into the first component, whereas Cu and Fe are high in the second. A different behavior was noticed for Mn, for which both components are significant. Hierarchical cluster analysis applied to study the results of the analysis of metals in wines seems to discriminate between samples belonging to different origins.

И З В О Д

МЕТОДЕ МУЛТИВАРИЈАНТНЕ ВИЗУАЛИЗАЦИЈЕ ПОДАТАКА БАЗИРАНЕ НА ЕЛЕМЕНТАЛНОЈ АНАЛИЗИ ВИНА АТОМСКОМ АПСОРПЦИОНОМ СПЕКТРОМЕТРИЈОМ

СЛАВИЦА РАЖИЋ[1], ЂУРО ЧОКЕША[2] И СНЕЖАНА СРЕМАЦ[2]

[1]Институт за аналитичку хемију, Фармацеутски факултет, Универзитет у Београду, п. пр. 146, 11211 Београд и [2]Институт за нуклеарне науке "Винча", п. пр. 522, 11522 Београд

Применом метода пламене атомске апсорпционе спектрометрије, као и атомске апсорпционе спектрометрије са електротермалном атомизацијом, одређиван је садржај пет метала (Cu, Mn, Fe, Cd и Pb) у узорцима неколико црвених и белих вина, из раличитих региона Србије. Резултати су обрађивани хемометријским методама. Примењена је анализа главних

компоненти, као и факторска анализа, у циљу разјашњавања односа између елемената. Након редукције података идентификована су три главна фактора који утичу на варијабилност. Кластерска анализа узорака вина наглашава диференцијацију узорака различитог порекла али не и раздвајање између црвених и белих вина.

(Примљено 24. јула 2007)

REFERENCES

1. M. J. Baxter, H. E. Crews, M. J. Dennis, I. Goodall, D. Anderson, *Food Chem.* **60** (1997) 443
2. A. Stroh, P. Bruckner, C. Volthof, *At. Spectrosc.* **15** (1994) 100
3. E. McCurdy, D. Potter, M. Medina, *Laboratory News* **9** (1992) 10
4. P. R. Arhurst, M. J. Dennis, *Food Authentication*, Chapman–Hall, London, UK, 1996
5. M. I. Guerrero, C. Herce–Pagliai, A. Cameán, A. M. Troncoso, G. Gonzaález, *Talanta* **45** (1997) 379
6. I. Moret, G. Scarponi, P. Cescon, *J. Agric. Food Chem.* **42** (1994) 1143
7. R. Seeber, G. Sferlazzo, R. Leardi, *J. Agric. Food Chem.* **39** (1991) 1764
8. S. Frias, J. E. Conde, J. J. Rodrigez–Bencomo, F. Garcia–Montelongo, J. P. Perez–Trujillo, *Talanta* **59** (2003) 335
9. P. Kment, M. Mihaljevič, V. Ettler, O. Šebek, L. Strand, L. Rohlova, *Food. Chem.* **91** (2005) 157
10. M. J. Latorre, C. Garcia–Jares, B. Medina, C. Herrero, *J. Agric. Food Chem.* **42** (1994) 1451
11. L. Xian–Sun, K. Danzer, G. Thiel, *Fresenius J. Anal. Chem.* **359** (1997) 143
12. E. A. Hernandez–Caraballo, R. M. Avila–Gomez, T. Capote, F. Rivas, A. G. Perez, *Talanta* **60** (2003) 1259
13. S. J. Haswell, A. D. Walmlsey, *J. Anal. At. Spectrom.* **13** (1998) 131
14. G. Thiel, G. Geisler, I. Blechschmidt, K. Danzer, *Anal. Bioanal. Chem.* **378** (2004) 1630
15. H. Yu, Y. Zhou, X. Fu, L. Xie, Y. Ying, *Eur. Food Res. Technol.* **225** (2007) 313
16. J. F. Hair, R. E. Anderson, R. L. Tatham, W. C. Black, *Multivariate Data Analysis*, 4th Ed., Prentice Hall, London, UK, 1995
17. I. S. Arvanitoyannis, M. N. Katsota, E. P. Psarra, E. H. Soufleros, S. Kallithraka, *Trends Food Sci. Technol.* **10** (1999) 321
18. I. J. Košir, M. Kocjančič, N. Ogrinc, J. Kidrič, *Anal. Chim. Acta* **429** (2001) 195
19. J. T. W. E. Vogels, A.C. Tas, F. van den Berg, J. van der Greef, *Chemometr. Intell. Lab.* **21** (1993) 249
20. J. Weber, M. Beeg, C. Bartzsch, K. H. Feller, D. García, M. Reichenbaecher, M. Danzer, *J. High Res. Chromatogr.* **22** (1999) 322.
21. G. J. Martin, C. Guillou, M. L. Martin, M. T. Cabanis, Y. Tep, J. Aerny, *J. Agric. Food Chem.* **36** (1988) 316
22. S. Rebolo, R.M. Peña, M. J. Latorre, S. García, A.M. Botana, C. Herrero, *Anal. Chim. Acta*, **417** (2000) 211
23. S. Ražić, M.Todorović, I.Holclajtner–Antunović, Z.Ilić, *Fresenius J. Anal. Chem.* **355** (1996) 274
24. S. Ražić, M. Todorović, I. Holclajtner–Antunović, M. Stoiljković, *Fresenius J. Anal. Chem.* **365** (1999) 367
25. M. Tripković, M. Todorović, I. Holclajtner–Antunović, S. Ražić, A. Kandić, D. Marković, *J. Serb. Chem. Soc.* **65** (2000) 323
26. H. F. Kaiser, *Educ. Psychol. Meas.* **20** (1960) 141
27. G. Thoukis, M. A. Amerine, *Am. J. Enol.* **7** (1956) 45
28. J. H. Ward, *J. Am. Stat. Assoc.* **58** (1963) 236.

Journal of the Serbian Chemical Society
JSCS@tmf.bg.ac.yu • www.shd.org.yu/JSCS

J. Serb. Chem. Soc. 72 (12) 1493–1506 (2007)
JSCS–3679

UDC 678.741.004.12:541.135.21:542.913
Original scientific paper

Properties of aliphatic hyperbranched polyesters in dilute solutions

JASNA VUKOVIĆ[1]*, MANFRED D. LECHNER[1#] and SLOBODAN JOVANOVIĆ[2#]

[1]*Institute for Chemistry, University of Osnabrueck, Barbarastraße 7, 49069 Osnabrueck, Germany and* [2]*Faculty of Technology and Metallurgy, University of Belgrade, Karnegijeva 4, 11120 Belgrade, Serbia*

(Received 20 August 2007)

Abstract: The results of an investigation of the influence of the synthesis procedure, number of pseudo generations and degree of branching of hydroxy-functional aliphatic hyperbranched polyesters (AHBP) on the values of limiting viscosity number, [η], hydrodynamic radius, R_η, molar mass and polydispersity index, Q, are presented in this paper. Two series of AHBP, synthesized from 2,2-bis(hydroxymethyl)propionic acid and di-trimethylolpropane using a pseudo-one-step and a one-step procedure were investigated. The obtained results show that the values of [η] and R_η for all examined samples are the highest in a 0.7 mass % solution of LiCl in *N*,*N*-dimethylacetamide (LiCl/DMAc), which indicates that this solvent is the best from the investigated ones. The values of [η] in *N*-methyl-2-pyrrolidinone (NMP) increased up to the sixth pseudo generation, after which a slight decrease occurred as the consequence of the presence of side-reaction products, formed during the synthesis. The appearance of these side-reaction products was also confirmed from the characteristic GPC chromatograms. For the samples of AHBP synthesized using the pseudo-one-step procedure, a good linear dependence between log [η] and log M_w was obtained up to the fifth pseudo generation, when LiCl/DMAc, NMP and DMAc were used as solvents. The values of the "shrinking" factor, g', were calculated for all investigated AHBPs.

Keywords: aliphatic hyperbranched polyesters, dilute solutions, limiting viscosity number, GPC.

INTRODUCTION

The scientific importance of dendritic polymers, *i.e.*, dendrimers (ideally branched) and hyperbranched polymers (non-ideally branched) has been proved over the last two decades through the significant number of publications.[1] The results obtained during investigation of the structure and properties of these specific polymers have made great contribution to their growing fields of applica-

* Corresponding author. E-mail: jasnav2002@yahoo.com
# Serbian Chemical Society member.
doi: 10.2298/JSC0712493V

tion.[2] Dendritic polymers are often used in solution and therefore special attention has been devoted to the research of their behaviour in dilute and concentrated solutions.[3–12] It was shown that these polymers have lower limiting viscosity number, [η], values than the analogue linear polymers of the same molar mass and chemical composition, due to the presence of highly branched macromolecules. In addition, the logarithm of the limiting viscosity number of linear polymers increases linearly with increasing logarithm of molar mass, while for dendrimers a maximum is usually observed in this relationship.[3–5] Beside experimental work, there are also different simulation methods which predict this behaviour of dendrimers in dilute solutions.[6] This specific behaviour of dendrimers in dilute solutions can be explained by the fact that their hydrodynamic radius linearly increases with increasing number of generation, *n*, while their molar mass grows as according to 2^n (the factor "2" comes from the assumed dendrimer functionality).

Concerning the dependence between log [η] and log *M* for hyperbranched polymers, different results can be found in the literature. Fréchet *et al.* suggested that [η] always increases with the molar mass but slower than for linear polymers.[7] However, the dependence log [η] = *f* (log *M*) of poly(amidoamine) hyperbranched polymers was shown to have the same trend as for dendrimers.[8] Published simulations of the behaviour of hyperbranched polymers in solution predict the presence of a maximum in the dependence between log [η] and log *M*, but this maximum comes at a higher number of generations than for the equivalent dendrimers and it disappears when the degree of branching is lower than 0.3.[9,10] On the other hand, for several hyperbranched polymers, this maximum was not observed.[1g,11]

In this study, the influence of the synthesis procedure (pseudo-one-step and one-step), number of pseudo generations and degree of branching of hydroxy-functional aliphatic hyperbranched polyesters (AHBP) synthesized from 2,2-*bis*(hydroxymethyl)propionic acid (*bis*-MPA) and di-trimethylolpropane (DiTMP) on the limiting viscosity number, dimensions of the macromolecules in solution, R_η, molar mass and polydispersity index, *Q*, was investigated. The obtained results are compared with appropriate experimental results presented in the literature.

EXPERIMENTAL

Materials

Two series of hydroxy-functional aliphatic hyperbranched polyesters were synthesized *via* an acid-catalyzed polyesterification reaction starting from *bis*-MPA (Aldrich), as the AB_2 monomer, and DiTMP (Fluka Chemika), as the tetrafunctional core molecule,[1h] methanesulphonic acid (Aldrich) was used as the catalyst. Samples of series I of the second (AHBP-2I), third (AHBP-3I), fourth (AHBP-4I), fifth (AHBP-5I), sixth (AHBP-6I), eighth (AHBP-8I) and tenth (AHBP-10I) pseudo generation were synthesized using a pseudo-one-step procedure. On the other hand, samples of series II of the fourth (AHBP-4II), sixth (AHBP-6II) and eighth (AHBP-8II) pseudo generation were synthesized using a one-step procedure. In this work, three commercially available AHBPs (Boltorn®) of the second (BH-2), third (BH-3) and fourth (BH-4) pseudo generation were also in-

vestigated. These AHBP were supplied by Perstorp (Specialty Chemicals AB, Sweden). According to the supplier's data, the commercial AHBPs were synthesized *via* a pseudo-one-step procedure from *bis*-MPA as monomer and a tetrafunctional ethoxylated pentaerythrytol (PP50) core. All other chemicals were obtained from Aldrich and used as received, without further purification.

Characterization

^{13}C-NMR spectra of the samples were recorded on a Bruker (250 MHz) NMR spectrometer at room temperature using deuterated dimethylsulfoxide (DMSO-d_6) as the solvent. The degree of branching (*DB*) was calculated from the values obtained by integration of the appropriate peaks, corresponding to the dendritic, linear and terminal units and using the equation developed by Fréchet:[13]

$$DB = (n_D + n_T)/(n_D + n_L + n_T) \quad (1)$$

where n_D, n_T and n_L represent the number of dendritic, terminal and linear units, respectively.

Vapour pressure osmometry (VPO) of the synthesized and commercial samples was performed using a Knauer vapour pressure osmometer. The measurements were realised in *N*,*N*-dimethylformamide as the solvent at 90 °C. Benzil was used for the calibration.

Determination of the molar mass distribution of the AHBPs was performed by the GPC technique using a Spectra-Physics chromatograph equipped with Rheodyne universal injector and Spectra-Physics differential refractometer as detector. The separation was achieved across a set of two gel columns (MZGPC columns) with porosities of 1000 Å. Tetrahydrofuran (THF) was used as the eluent at a nominal flow rate of 1.0 cm^3 min^{-1}. The quantity of injected polymer was 100 µl ($c \approx$ $\approx$ 20 g l^{-1}) and the measurements were performed at 25 °C. The molar mass characteristics of the polymers were calculated from a polystyrene calibration curve, constructed with narrow molar mass distribution polystyrene standards (Polymer Standards Service), using Chrom Gate 3.1.4 software (Knauer).

The viscosity measurements of dilute solutions of the AHBPs in different solvents were performed in an Ubbelohde capillary viscometer (Schott, capillary sizes O_a and I) using an automatic timer (Schott AVS 300), at 25±0.1 °C. The limiting viscosity number and Huggins constant, k_H, of the samples were determined graphically by extrapolation of the η_{sp}/c values (determined at five different concentrations) to infinite dilution using the Huggins equation.[14]

Seven samples of self-synthesized and Boltorn® hyperbranched polyesters (AHBP-3I, AHBP-4I, AHBP-6I, AHBP-8I, AHBP-10I, BH-3 and BH-4) were fractionated using the precipitation fractionation method[15] from a solvent/non-solvent (acetone/*n*-hexane) mixture to obtain three fractions of each sample. All obtained fractions were dried in a vacuum oven to remove the volatile materials.

RESULTS AND DISCUSSION

For all AHBP samples investigated in this work, the value of the number average molar mass was determined using vapour pressure osmometry, $(M_n)_{VPO}$, while the *DB* value was calculated according to Fréchet.[13] These values together with theoretical number of pseudo generation, n_{theor}, and theoretical molar mass, M_{theor}, are listed in Table I.

From the parameters listed in Table I, it can be seen that the molar mass, $(M_n)_{VPO}$, increased only up to the sixth pseudo generation and simultaneously was much lower than the theoretical value. The reason for this specific behaviour is the occurrence of side reactions during the synthesis of these polyesters.[1h] The extent of undesired reactions increased with increasing generation number. For all the investigated AHBPs, the values of the degree of branching slightly de-

creased with increasing theoretical number of pseudo generations. Moreover, for the samples of the second series AHBP-4II, AHBP-6II and AHBP-8II, the *DB* values were lower than for the corresponding samples of the first series, indicating a slight influence of the synthesis procedure on the degree of branching.

TABLE I. Values of the theoretical number of pseudo generation, n_{theor}, theoretical molar mass, M_{theor}, number average molar mass determined by VPO, $(M_n)_{VPO}$ and degree of branching, *DB*, of the investigated AHBPs

Sample	n_{theor}	M_{theor} / g mol^{-1}	$(M_n)_{VPO}$[a] / g mol^{-1}	*DB*
AHBP-2I	2	1642	–	0.47[a]
AHBP-3I	3	3498	2027	0.45[a]
AHBP-4I	4	7210	2819	0.44[a]
AHBP-5I	5	14634	3044	0.45[a]
AHBP-6I	6	29482	3575	0.43[a]
AHBP-8I	8	118570	3571	0.43[a]
AHBP-10I	10	474922	3552	0.42[a]
AHBP-4II	4	7210	5415	0.42[a]
AHBP-6II	6	29482	–	0.43[a]
AHBP-8II	8	118570	3284	0.37[a]
BH-2	2	1747	1343	0.43[b]
BH-3	3	3604	3081	0.42[b]
BH-4	4	7316	2716	0.40[b]

[a]Results for $(M_n)_{VPO}$, and *DB* are presented in Ref. 1h; [b]data of Luciani *et al.*[16]

Limiting viscosity number and hydrodynamic radius of the AHBP in different solvents

Since the polyesters investigated in this work had a large number of free OH groups, it is reasonable to expect that the macromolecules of AHBP in solution, similar to poly(vinyl alcohol), would connect with each other through the hydrogen bridges and form aggregates. Investigation of the properties of macromolecules in solution becomes much more difficult when spontaneous aggregate formation occurs. Žagar *et al.*[17] reported that samples of AHBP thermally pre-treated for 20 min at 140 °C do not form aggregates at room temperature in a 0.7 mass % solution of LiBr in N,N-dimethylacetamide (LiBr/DMAc) and in a mixture of tetrahydrofuran (THF) and CH_3OH (90:10 by volume) and that these solvents are therefore suitable for the investigation of the properties AHBPs in solution. Instead, LiBr/DMAc, a 0.7 mass % solution of LiCl in DMAc (LiCl/DMAc) was used for the determination of $[\eta]$ in this work. In addition to this solvent, viscosity measurements were also performed in *N*-methyl-2-pyrrolidone (NMP), *N*,*N*-dimethylacetamide (DMAc), THF and in a mixture THF/CH_3OH (90:10 by volume).

As examples of the determination of $[\eta]$, the dependences of η_{sp}/c *vs.* c for different AHBP of series I in NMP and for the sample AHBP-8I in the employed solvents are presented in Figs. 1a and 1b, respectively. Since a linear relationship

was obtained between η_{sp}/c and c in all the employed solvents, it can be concluded that no aggregation occurred in the investigated concentration range or that the shear stress which developed in the capillary of the viscosimeter was high enough to lead to the rupture of the intermolecular hydrogen bonds present in the aggregates formed in the static solution.

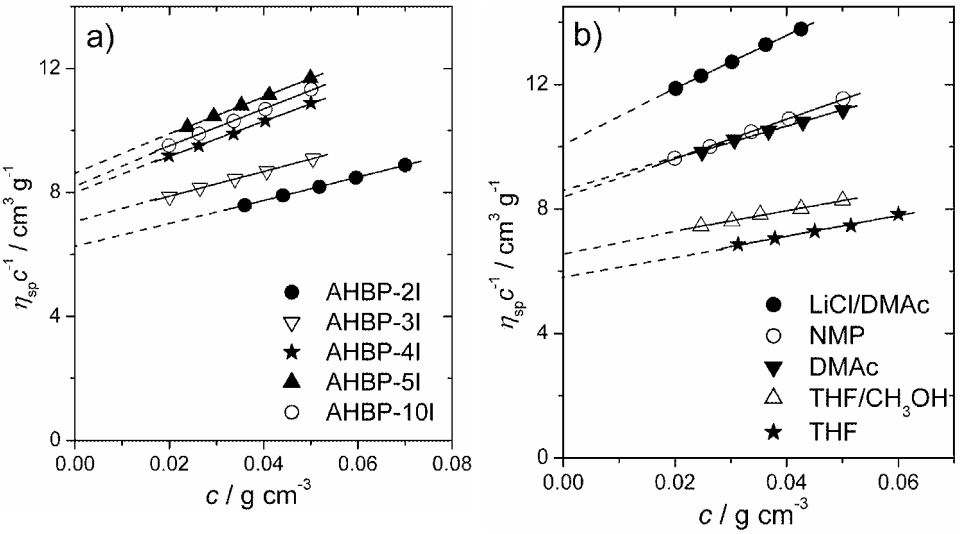

Fig 1. Dependence of η_{sp}/c versus c for a) different AHBPs in NMP and b) for the sample AHBP-8I in different solvents, at 25 °C.

The values of $[\eta]$ were determined for all the examined AHBPs in the mentioned solvents at 25 °C and they are listed in Table II. It should be mentioned that the samples of AHBP were not thermally pre-treated prior to the viscosity measurements.

The dependence of the $[\eta]$ values for the AHBPs from series I in LiCl/DMAc *vs.* $[\eta]$ of the same samples in NMP is presented in Fig. 2. As all the experimentally determined points fall on one linear plot, it can be concluded that value of $[\eta]$ in LiCl/DMAc and NMP for these AHBPs is independent of the number of pseudo generation, *i.e.*, of the molar mass. This indicates that AHBP samples were dissolved on the molecular level under applied experimental conditions and without thermal pre-treatment, *i.e.*, aggregation did not occur.

The value of $[\eta]$, as well as the value of the slope from the linear dependence $\eta_{sp}/c = f(c)$, presented in Fig. 1b, represent a measure of the solvent quality for the investigated polymer. According to these criteria, LiCl/DMAc is the best of the investigated solvents for AHBP, while the other solvents are ordered as follows:

$$[\eta]_{LiCl/DMAc} > [\eta]_{NMP} > [\eta]_{DMAc} > [\eta]_{THF/CH_3OH} > [\eta]_{THF} \quad (2)$$

TABLE II. Values of the limiting viscosity number, [η], of the AHBPs determined in different solvents at 25 °C

Sample	$[\eta]_{LiCl/DMAc}$ $cm^3\ g^{-1}$	$[\eta]_{NMP}$ $cm^3\ g^{-1}$	$[\eta]_{DMAc}$ $cm^3\ g^{-1}$	$[\eta]_{THF/CH_3OH}$ $cm^3\ g^{-1}$	$[\eta]_{THF}$ $cm^3\ g^{-1}$
AHBP-2I	6.8	6.2	6.4	–	4.0
AHBP-3I	7.9	7.1	6.5	–	4.8
AHBP-4I	9.9	8.0	7.0	6.4	5.6
AHBP-5I	10.8	8.7	7.8	6.4	5.4
AHBP-6I	11.0	8.9	8.3	6.5	5.9
AHBP-8I	10.2	8.3	8.6	6.6	5.8
AHBP-10I	10.0	8.3	8.2	6.4	–
AHBP-4II	–	8.0	–	–	–
AHBP-6II	–	9.2	–	–	–
AHBP-8II	–	9.3	–	–	–
BH-2	7.0	6.0	6.1	–	–
BH-3	9.2	7.4	–	5.5	–
BH-4	10.7	8.6	–	6.7	4.9

In good agreement with this order of solvents is also the solubility parameter, δ, 10^3 $(J\ m^{-3})^{0.5}$, which for AHBP have the value of 23.0 for LiCl/DMAc, while the solubility parameters for NMP, DMAc, THF/CH_3OH and THF are 23.1, 22.6, 19.7 and 18.6, respectively.[18] The improvement of the solubility of AHBP in the mixture LiCl/DMAc in comparison to pure DMAc is due to the influence of the Li^+ ions on the rupture, not only of intermolecular, but also intramolecular hydrogen bonds in the AHBP macromolecules, which further leads to the increase of their volume in solution and, consequently, to the increase of their [η] value.

From the slope of the linear dependence of η_{sp}/c *vs.* c for all investigated AHBPs in different solvents, the values of the Huggins constants, k_H, were determined. For the samples of the series I in LiCl/DMAc value of k_H is 0.65±0.15, in NMP 0.80±0.20, in DMAc 1.0±0.3 and in THF/CH_3OH 0.75±0.05. For AHBP of series II in NMP the value of k_H is 0.85±0.15. For the commercial AHBP, k_H is 0.55±0.05 in LiCl/DMAc and 0.80±0.02 in NMP and in the mixture THF/CH_3OH.

The determined values of k_H are different and therefore it is possible to use them for the calculation of [η] from the Huggins equation by determination of the specific viscosity, η_{sp}, for only one concentration of the solution, but only for the mentioned AHBP samples. For most linear polymers in good solvents, the value of k_H is 0.3–0.4 and is independent of the chemical composition of the polymer. Values of k_H for the examined AHBPs in various solvents are different from the values for linear polymers due to the specific molecular structure of the AHBPs and presence of a large number of end groups.

The dependence of [η] for AHBP in NMP *vs.* the theoretical number of pseudo generations is presented in Fig. 3. According to these results, an increase of

[η] up to the sixth pseudo generation can be observed for the samples of series I, after which the values of [η] slightly decrease. A similar observation was made for the AHBP of series II, while for the commercial samples, [η] continuously increased, since these samples were examined only from the second up to the fourth pseudo generation. This specific shape of the dependence presented in Fig. 3 for the samples of series I and II is not a consequence of the increase of the macromolecular packing density with increasing pseudo generation, as is predicted by different simulation methods of the behaviour of hyperbranched polymers in solution.[9,10] The break in the increase of the [η] value after the sixth pseudo generation in this case occurs due to the presence of side reaction products in these polymers, which prevent a further increase of the molar mass.[1h] Samples of the series II have somewhat higher values of [η] in NMP than the AHBPs from series I. This is probably a consequence of the slightly lower values of the degree of branching (Table I) and, therefore, higher amounts of linear branches present in the macromolecules of these samples, which further leads to an increase in [η]. On comparing the [η] values obtained in THF/CH_3OH for AHBPs from the fourth up to the tenth pseudo generation, it can be observed that [η] is practically constant, *i.e.*, it does not depend on the molar mass. These results indicate that THF/CH_3OH is a poor solvent, probably due to the fact that these AHBP were not thermally pre-treated, as was the case in other studies.[17,19]

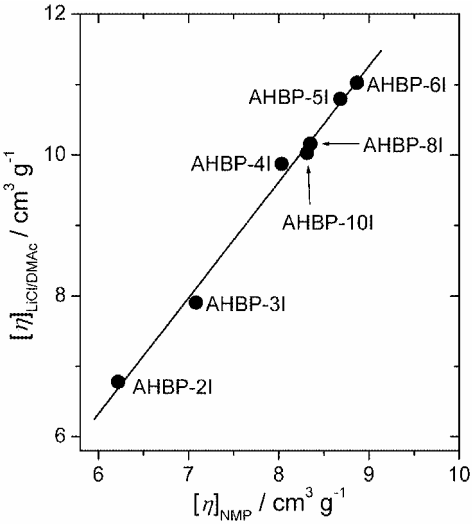

Fig. 2. Correlation of the limiting viscosity numbers determined for AHBP of the series I in LiCl/DMAc and in NMP.

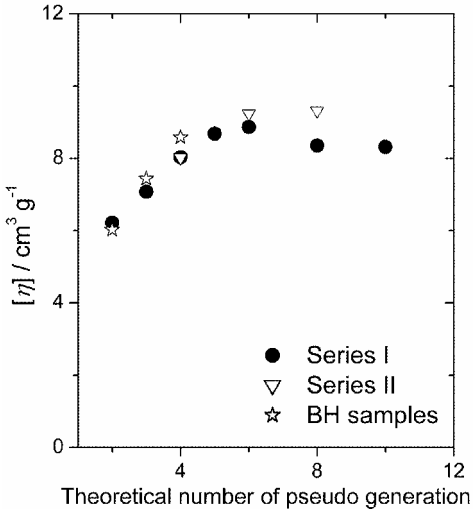

Fig. 3. Dependence of [η] for the AHBPs determined in NMP *vs.* the theoretical number of pseudo generations.

The dependences of log [η] *vs.* log M_w for AHBPs of series I from the second up to the sixth pseudo generation in LiCl/DMAc and NMP are presented in Fig. 4. The values of the weight average molar mass of the AHBPs were calculated from

the values of the polydispersity index, $Q = (M_w/M_n)_{GPC}$, determined by the GPC technique (Table V) and the corresponding values of the number average molar mass, $(M_n)_{VPO}$, determined from VPO measurements (Table I). Using the Kuhn–Mark–Houwink–Sakurada (KMHS) equation ($[\eta] = K_\eta M^a$) and the dependences presented in Fig. 4, the values of the exponent a and constant K_η for the investigated AHBPs in NMP and LiCl/DMAc were determined and given in Table III, in which are also given the corresponding values for the same samples in DMAc.

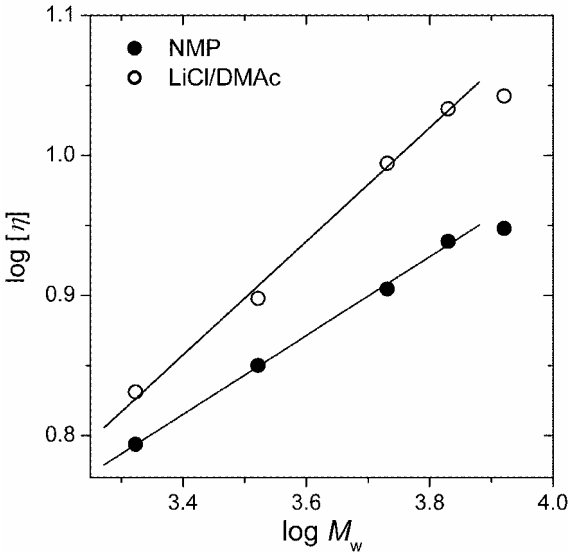

Fig. 4. Dependence of log $[\eta]$ *vs.* log M_w for the AHBPs of series I, obtained using the values of $[\eta]$ determined in NMP and LiCl/DMAc as solvents.

TABLE III. Values of the exponent a and constant K_η determined from the KMHS equation in different solvents at 25 °C for the investigated AHBPs

Sample group	LiCl/DMAc		NMP		DMAc	
	a	K_η	a	K_η	a	K_η
Series I	0.40	0.30	0.28	0.72	0.25	1.44

The results presented in Fig. 4 clearly show that there is a good linear relationship between log $[\eta]$ and log M_w up to the fifth pseudo generation and that for this region of molar masses, the parameters K_η and a can be used for the determination of molar mass by viscosimetry for samples synthesized in the same manner as the AHBP of series I. It has been already stated elsewhere that for branched polymers, a linear log $[\eta]$–log M relationship is only obtained for very narrow molar mass ranges.[20] The exponent a from the KMHS equation is also a measure of the solvent quality for some linear polymers. In good solvents, the value of a is usually between 0.60 and 0.85, while $a \leq 0.50$ is typical only for poor solvents.[20] The obtained values of the exponent a (Table III) are all lower than 0.50, which is a characteristic only for highly branched polymers in good solvents. The values of the exponent a increases with solvent quality. However,

the division of the solvents for hyperbranched polymers into good and poor according to the *a* values is not yet possible.

Hydrodynamic radius of macromolecules in solution, R_η, is connected with $[\eta]$ and the molar mass, M, through the Einstein equation:

$$R_\eta = (0.3[\eta]M\pi^{-1}N_A^{-1})^{1/3} \quad (3)$$

where N_A is Avogadro's number. By introducing the determined values of $[\eta]$ (Table II) and molar mass $(M_w)_{real}$, (Table V) into Eq. (3), the values of R_η for the investigated AHBPs in four different solvents were calculated and given in Table IV. From the results given in Table IV, it can be seen that the value of R_η of AHBPs depends on the solvent quality in the same manner as for linear polymers. However, due to the specific molecular structure of AHBPs this dependence is not as strong as for linear polymers. As was expected, the largest dimensions of these hyperbranched polyesters were obtained in LiCl/DMAc. The small values of R_η of AHBPs in solution, the large number of functional groups and, simultaneously, the low viscosity of their solutions provide the successful application of AHBPs for the production of special coatings, ink for the printers or drug carriers.[21]

TABLE IV. Values of the hydrodynamic radius, R_η, for the investigated AHBPs in LiCl/DMAc, NMP, DMAc and THF/CH_3OH at 25 °C

Sample	$(R_\eta)_{LiCl/DMAc}$ / nm	$(R_\eta)_{NMP}$ / nm	$(R_\eta)_{DMAc}$ / nm	$(R_\eta)_{THF/CH_3OH}$ / nm
AHBP-2I	1.3	1.3	1.3	/
AHBP-3I	1.6	1.5	1.5	/
AHBP-4I	2.0	1.9	1.8	1.8
AHBP-5I	2.3	2.2	2.0	1.9
AHBP-6I	2.4	2.3	2.2	2.0
AHBP-8I	2.3	2.2	2.2	2.0
AHBP-10I	2.2	2.0	2.0	1.9
AHBP-4II	–	2.4	–	–
AHBP-8II	–	2.2	–	–
BH-2	1.3	1.2	1.2	–
BH-3	2.1	1.9	–	1.7
BH-4	2.3	2.2	–	2.0

GPC Measurements

The determination of the molar mass distribution of the investigated AHBPs and three fractions of the sample AHBP-6I was performed by the GPC technique in the manner described in the Experimental. Linear polystyrene standards were employed for the calibration of the instrument, since adequate AHBP standards are not available. As branched macromolecules have a much lower hydrodynamic radius than the corresponding linear macromolecules of the same molar mass,

the obtained values of M_w and M_n can not be consider as correct. Therefore, the GPC chromatograms of the investigated AHBPs were used only for a comparison of the shape of their traces and to calculate the values of the polydispersity index, Q, as well as for the calculation of $(M_w)_{real}$.

As illustrations, the GPC chromatograms of the AHBPs of series I and the commercial samples are presented in Fig. 5a and 5b, respectively. From the obtained GPC results for all investigated AHBP, as well as for the three fractions of the sample AHBP-6I, the values of the molar masses $(M_w)_{GPC}$ and $(M_n)_{GPC}$ and the polydispersity index Q were calculated and are given in Table V.

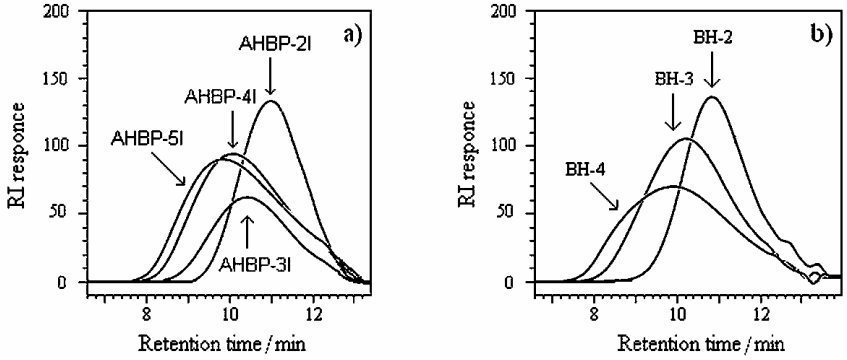

Fig. 5. GPC chromatograms of AHBPs a) synthesized by the pseudo-one-step procedure (samples of series I) and b) commercial AHBPs.

TABLE V. Values of the molar masses $(M_w)_{GPC}$ and $(M_n)_{GPC}$, polydispersity index, Q, $(M_w)_{real}$ and limiting viscosity number of the fractions determined in NMP, $[\eta]_F$, of the investigated hyperbranched polyesters and selected fractions

Sample	$(M_w)_{GPC}$ / g mol^{-1}	$(M_n)_{GPC}$ / g mol^{-1}	Q	$(M_w)_{real}$ / g mol^{-1}	$[\eta]_F$ / cm^3 g^{-1}
AHBP-2I	1041	749	1.39	–	–
AHBP-3I	1655	1008	1.64	3324	–
AHBP-4I	2238	1172	1.91	5384	–
AHBP-5I	2688	1213	2.22	6758	–
AHBP-6I	2993	1287	2.33	8330	–
F1	5581	2260	2.47	–	10.4
F2	3832	1973	1.94	–	8.7
F3	1080	771	1.40	–	6.5
AHBP-8I	2994	1348	2.22	7928	–
AHBP-10I	2111	1155	1.83	6500	–
AHBP-4II	2475	1189	2.08	11263	–
AHBP-6II	2912	1179	2.47	–	–
AHBP-8II	2674	1148	2.33	7652	–
BH-2	1120	782	1.43	1920	–
BH-3	2227	1147	1.94	5977	–
BH-4	3454	1242	2.78	7550	-

The results presented in Fig. 5 and Table V show that the GPC traces, *i.e.*, the molar mass distributions of the AHBPs, become broader with increasing theoretical number of generations, *i.e.*, up to the sixth pseudo generation. Only for the sample AHBP-2I was a symmetrical GPC profile obtained, while for the samples of higher generation number, a broad tail on the low molar mass side of the distribution can be observed. This specific shape of the GPC traces is a consequence of side reactions responsible for the formation of small molar mass AHBP molecules, the portion of which increases with increasing pseudo generation, during the main polycondensation reaction.[1h] The GPC chromatograms of the AHBPs synthesized by the one-step procedure have a similar profile as those synthesized by the pseudo-one-step procedure, but they also have slightly higher values of *Q*. This is in good agreement with the results presented by Hult *et al.*, who showed that the slow monomer addition method (pseudo-one-step procedure for the synthesis) could reduce the polydispersity of hyperbranched polyesters.[1a]

As it was expected, the molar mass averages determined by GPC using linear polystyrene standards for calibration are lower than the theoretical values and results obtained by VPO (Table I). The number average molar masses obtained by GPC and VPO measurements for the AHBP of series I are plotted in Fig. 6. It can be observed that a relatively good linear correlation between $(M_n)_{GPC}$ and $(M_n)_{VPO}$ for the samples from the third up to the eighth pseudo generation was obtained, which indicates that the ratio $(M_n)_{GPC}/(M_n)_{VPO}$ does not change with increasing molar mass. Assuming that determined values of *Q* are real, the values of the real weight average molar mass of the examined AHBPs, $(M_w)_{real}$, were calculated using the equation:

$$(M_w)_{real} = Q\,(M_n)_{VPO} \tag{4}$$

The co-calculated values of $(M_w)_{real}$ are also given in Table V. These values were used for the determination of the calibration diagram log $[\eta]$–log *M* and for the calculation of the "shrinking" factor, *g*', of the branched AHBP macromolecules.

Most of the self-synthesized samples were fractionated using the precipitation fractionation method to obtain three fractions in order to investigate in which manner the degree of branching changes with molar mass within one sample. According to the obtained values of the limiting viscosity number, $[\eta]_F$, (Table V), it was concluded that fractionation was successful. However, when the GPC method was used to re-fractionate the AHBP fractions, different results were obtained. As an illustration, the GPC traces of AHBP-6I and three fractions obtained by precipitation fractionation method are presented in Fig. 7. The corresponding values of $(M_w)_{GPC}$, $(M_n)_{GPC}$ and *Q* are given in Table V. From these results it can be observed that polydispersity increased from the third up to the first fraction, *i.e.*, that the molar mass distribution becomes broader with increasing degree of polymerization. However, the fact that value of *Q* for the first fraction is higher than for the parent sample indicates that fractionation under described experi-

mental conditions was not efficient. Therefore, the values of the degree of branching for the fractions of an AHBP cannot be accepted as correct and, conesquently, they are not presented in this work.

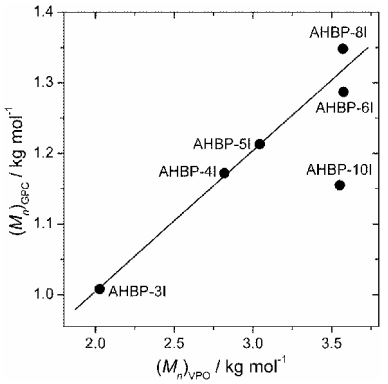

Fig. 6. Correlation of the number average molar mass obtained from GPC and VPO measurements for the AHBPs of series I.

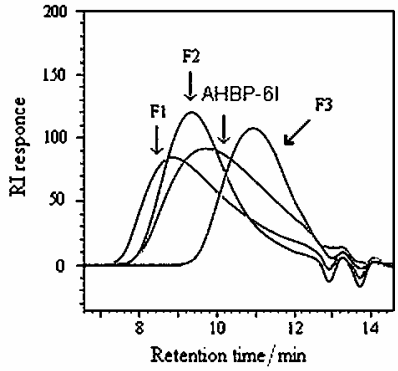

Fig. 7. GPC chromatograms of AHBP-6I and three fractions obtained by the precipitation fractionation method.

Using the results obtained by the GPC technique, the values of the "shrinking" factor, g', of the macromolecular coils of the examined AHBPs in relation to linear polymers of corresponding molar masses were calculated:

$$g' = [\eta]_{HBP}/[\eta]_L \quad (5)$$

where $[\eta]_{HBP}$ and $[\eta]_L$ represent the limiting viscosity numbers of the given hyperbranched polymer and its linear analogue, respectively. The calculation of shrinking factor was performed using the fact that the product of the limiting viscosity number and molar mass at a certain elution volume is always the same and independent of the polymer type.[22] Therefore, it can be written:

$$[\eta]_{HBP}M_{HBP} = [\eta]_L M_L \quad (6)$$

where M_{HBP} and M_L are the molar masses of the hyperbranched polyesters and the linear polymers (polystyrene) used for the calibration, respectively. From the Eq. (6), it follows that g' can be calculated as M_L/M_{HBP}. The values of M_L were calculated by determination of the retention time which corresponds to the position of the peak in the GPC traces of different AHBPs. Then these retention times were used to determine the molar masses of the corresponding polystyrene from the calibration curve. On the other hand, for M_{HBP}, the weight average molar mass $(M_w)_{real}$ was used (Table V). The determined values of g' for the AHBPs are listed in Table VI. As can be seen, the values of g' for all the AHBPs are between 0.27 and 0.57. Similar results were obtained for other hyperbranched polymers.[23]

TABLE VI. Values of the "shrinking" factor, g', for the investigated AHBPs

Sample	g'	Sample	g'
AHBP-2I	0.44	AHBP-10I	0.27
AHBP-3I	0.45	AHBP-8II	0.30
AHBP-4I	0.35	BH-2	0.57
AHBP-5I	0.34	BH-3	0.29
AHBP-6I	0.31	BH-4	0.31
AHBP-8I	0.32		

CONCLUSIONS

The results obtained in this study show that of the tested ones, the best solvent for the examined AHBPs is 0.7 mass % solution of LiCl in DMAc. In *N*-methyl-2-pyrrolidone, the values of $[\eta]$ increase up to the sixth pseudo generation. The slight decrease of $[\eta]$ for samples of a higher pseudo generation is the conesquence of the occurrence of side reactions during the synthesis of investigated AHBPs, which hindered a further increase of the molar mass. The values of $[\eta]$ for the AHBPs synthesized by the one-step procedure were slightly higher than those of the corresponding samples synthesized by the pseudo-one-step procedure, indicating a slight influence of the synthesis procedure on the behaviour of AHBPs in dilute solutions. The calculated values of the exponent a from the KMHS equation for the samples of series I in different solvents are lower than 0.50, because of the highly branched structure of these polymers. The values of the "shrinking" factor of the examined AHBPs are similar to those presented in the literature for other hyperbranched polymers.

ИЗВОД

СВОЈСТВА АЛИФАТСКИХ ХИПЕРРАЗГРАНАТИХ ПОЛИЕСТАРА У РАЗБЛАЖЕНИМ РАСТВОРИМА

ЈАСНА ВУКОВИЋ[1], MANFRED D. LECHNER[1] и СЛОБОДАН ЈОВАНОВИЋ[2]

[1]Institute for Chemistry, University of Osnabrueck, Barbarastraße 7, 49069 Osnabrueck, Germany и 2Технолошко–металуршки факултет, Универзитет у Београду, Карнегијева 4, 11120 Београд

У овом раду су приказани резултати добијени испитивањем утицаја процедуре за синтезу, броја псеудогенерације и степена гранања хидрокси-функционалних алифатских хиперразгранатих полиестара (AHBP) на вредност граничног вискозитетног броја, $[\eta]$, хидродинамичког радијуса, R_η, моларне масе и индекса полидисперзности, Q. Испитане су две серије AHBP, синтетисане од 2,2-бис(хидроксиметил)пропионске киселине и ди-триметилолпропана коришћењем "pseudo-one-step" и "one-step" процедуре. Добијени резултати показују да су вредности $[\eta]$ и R_η за све испитане узорке највеће у 0.7 % раствору LiCl у *N*,*N*-диметилацетамиду (LiCl/DMAc), што указује да је од коришћених овај растварач најбољи. Вредности $[\eta]$ у *N*-метил-2-пиролидону (NMP) расту до шесте псеудогенерације, након чега долази до благог опадања као последица присуства продуката споредних реакција насталих у току синтезе. Појава продуката споредних реакција је такође потврђена на основу карактеристичног облика GPC хроматограма. За узорке AHBP синтетисане "pseudo-one-step" процедуром добијена је добра линеарна зависност између log $[\eta]$ и log M_w до пете псеудогенера-

ције, када су као растварачи коришћени LiCl/DMAc, NMP и DMAc. Вредности степена контракције макромолекулског клупка, *g'*, су израчунате за све испитане узорке АНВР.

(Примљено 20. августа 2007)

REFERENCES

1. a) E. Malmström, M. Johansson, A. Hult, *Macromolecules* **28** (1995) 1698; b) M. L. Mansfield, L. I. Klushin, *J. Phys. Chem.* **96** (1992) 3994; c) L. J. Hobson, W. J. Feast, *Polymer* **40** (1999) 1279; d) M. Sun, Z. Bo, *J. Polym. Sci. A* **45** (2007) 111; e) M. Malkoch, H. Claesson, P. Löwenhielm, E. Malmström, A. Hult, *J. Polym. Sci. A* **42** (2004) 1758; f) V. Petkov, V. Parvanov, D. Tomalia, D. Swanson, D. Bergstrom, T. Vogt, *Solid State Commun.* **134** (2005) 671; g) D. Parker, W. J. Feast, *Macromolecules* **34** (2001) 2048; h) J. Vuković, M. D. Lechner, S. Jovanović, V. Vodnik, Unpublished results
2. a) M. Johansson, A. Hult, *J. Coat. Technol.* **67** (1995) 35; b) Y. Zhang, L. Wang, T. Wada, H. Sasabe, *Macromol. Chem. Phys.* **197** (1996) 667; c) T. Griebel , G. Maier, *Polym. Prepr. (Am. Chem. Soc., Div. Polym. Chem.)* **41** (2000) 89; d) M. Johansson, E. Malmström, A. Hult, *J. Polym. Sci. A* **31** (1993) 619; e) Y. H. Kim, O. W. Webster, *Macromolecules* **25** (1992) 5561; f) R. Esfand, D. A. Tomalia, *Drug Discovery Today* **6** (2001) 427; g) K. Uhrich, *Trends in Polym. Sci.* **5** (1997) 388; h) C.–Y. Hong, Y.–Z. You, D. Wu, Y. Liu, C.–Y. Pan, *Macromolecules* **38** (2005) 2606; i) E. Malmström, M. Johansson, A. Hult, *Macromol. Chem. Phys.* **197** (1996) 3199
3. D. A. Tomalia, A. M. Naylor, W. A. Goddard, *Angew. Chem. Int. Ed. Engl.* **29** (1990) 138
4. I. B. Rietveld, J. A. M. Smit, *Macromolecules* **32** (1999) 4608
5. T. H. Mourey, S. R. Turner, M. Rubinstein, J. M. J. Fréchet, C. J. Hawker, K. L. Wooley, *Macromolecules* **25** (1992) 2401
6. R. L. Lescanec, M. Muthukumar, *Macromolecules* **23** (1990) 2280
7. J. M. J. Fréchet, C. J. Hawker, I. Gitsov, J. W. Leon, *J. Macromol. Sci. Pure Appl. Chem.* **A33** (1996) 1399
8. L. J. Hobson, W. J. Feast, *Chem. Commun.* **21** (1997) 2067
9. A. H. Widmann, G. R. Davies, *J. Comput. Theor. Polym. Sci.* **8** (1998) 191
10. J. Aerts, *J. Comput. Theor. Polym. Sci.* **8** (1998) 49
11. S. R. Turner, B. I. Voit, T. H. Mourey, *Macromolecules* **26** (1993) 4617
12. J. Vuković, M. D. Lechner, S. Jovanović, *Macromol. Chem. Phys.* **208** (2007) 2321
13. C. J. Hawker, R. Lee, J. M. J. Fréchet, *J. Am. Chem. Soc.* **113** (1991) 4583
14. M. L. Huggins, *J. Am. Chem. Soc.* **64** (1942) 2716
15. D. Braun, H. Cherdron, W. Kern, *Praktikum der makromolekularen organischen Chemie* 3. Auflage, Hüthig, Heidelberg, (1979)
16. A. Luciani, C. J. G. Plummer, T. Nguyen, L. Garamszegi, J.–A. E. Månson, *J. Polym. Sci. B* **42** (2004) 1218
17. E. Žagar, M. Žigon, *J. Chromatogr. A* **1034** (2004) 77
18. J. Vuković, *M.Sc. Thesis*, Faculty of Technology and Metallurgy, University of Belgrade (2003) p. 53
19. E. Žagar, M. Žigon, *Macromolecules* **35** (2002) 9913
20. W.–M. Kulicke, C. Clasen, *Viscosimetry of Polymers and Polyelectrolytes*, Springer-Verlag, Berlin, Heidelberg, New York, 2004, p. 83
21. M. E. Mackay, G. Carmezini, *Chem. Mater.* **14** (2002) 819
22. E. Schröder, G. Müller, K.-F. Arndt, *Polymer characterization*, Hanser Publishers, Munich, Vienna, New York (1988)
23. K. Ishizu, D. Takahashi, H. Takeda, *Polymer* **41** (2000) 6081.

Journal of the Serbian Chemical Society
JSCS@tmf.bg.ac.yu • www.shd.org.yu/JSCS

J. Serb. Chem. Soc. 72 (12) 1507–1514 (2007)
JSCS–3680

UDC 678–13+66–96+544.35:543.422.25
Original scientific paper

Preparation and modification of itaconic anhydride–methyl methacrylate copolymers

MILOŠ B. MILOVANOVIĆ[1#], SNEŽANA S. TRIFUNOVIĆ[2#], LYNNE KATSIKAS[3] and IVANKA G. POPOVIĆ[3*#]

[1]*Institute of Chemistry, Technology and Metallurgy, University of Belgrade, Njegoševa 12, Belgrade,* [2]*Faculty of Chemistry, University of Belgrade, Studentski trg 12–16, Belgrade and* [3]*Faculty of Technology and Metallurgy, University of Belgrade, Karnegijeva 4, Belgrade, Serbia*

(Received 2 August 2007)

Abstract: The free radical copolymerisation of itaconic anhydride and methyl methacrylate in solution was studied at 60 °C. The copolymer composition was determined by ^{1}H-NMR spectroscopy and the obtained monomer reactivity ratios were calculated, $r_{ITA} = 1.35\pm0.11$; $r_{MMA} = 0.22\pm0.22$ (by the Fineman–Ross method) and $r_{ITA} = 1.27\pm0.38$; $r_{MMA} = 0.10\pm0.05$ (by the Mayo–Lewis method). The synthesised copolymers were modified by reaction with di-*n*-butyl amine. The copolymer composition after amidation was determined by elemental analysis *via* the nitrogen content. Amidation of the anhydride units in the copolymers with di-*n*-butyl amine resulted in complete conversion to itaconamic acid.

Keywords: copolymerisation, itaconic anhydride, methyl methacrylate, amidation, itaconamic acid.

INTRODUCTION

Copolymers containing both hydrophilic and hydrophobic segments (amphiphilic polymers) are drawing considerable attention because of their possible use in biological systems. *N*-Substituted itaconamic acids are strongly amphiphilic molecules. Homopolymers and copolymers obtained from such monomers may have wide applications. Various copolymer compositions can produce a very large number of different arrangements, producing materials of varying chemical and physical properties. Thus, the hydrophilicity of copolymers can be modified by changing the amount of incorporated itaconamic acid. Also, the alkyl side chain in these polymers can be varied, resulting in polymers with different side chain length, thus controlling the hydrophobicity.[1,2] However, poly(*N*-substituted itaconamic acid)s are difficult to obtain by direct polymerisation of their monomers and the preparation of itaconamic acids, by reaction of itaconic anhydride

Serbian Chemical Society member.
* Corresponding author. E-mail: ivanka@tmf.bg.ac.yu
doi: 10.2298/JSC0712507M

with amines, can be complicated.[3–5] Thus, the isomerisation of itaconic anhydride to citraconic anhydride occurs in the presence of amine. The rate of isomerisation depends on the amine base strength and solvent medium, with strong bases in a polar solvent resulting in a much faster isomerisation than weak bases in a non-polar solvent.[4] Also, the isolation and purification of the produced itaconamic acids can be difficult, particularly if they do not crystallise.[5]

Another convenient way of obtaining amphiphilic polymers is to functionalise polymers and copolymers. The modification of poly(itaconic anhydride) or its copolymers by different reactions (alcoholysis, hydrolysis, amidation) seems not to have been investigated extensively.[6–8] In the experiments presented in this paper, copolymers of itaconic anhydride and methyl methacrylate were modified by amidation with di-*n*-butyl amine. Hitherto, there have been no data reported on the amidation of such copolymers.

EXPERIMENTAL

Materials

Commercially available reagent grade chemicals were used for all the experimental work. Itaconic acid was supplied by Aldrich and used as received. Acetyl chloride and di-*n*-butyl amine (both obtained from Aldrich) were purified by distillation.

α,α'-Azobisisobutyronitrile (AIBN) was supplied by Aldrich and recrystallised from methanol.

Solvents used for the isolation, purification, reprecipitation and modification of the copolymers were dried over molecular sieves in order to minimise the hydrolysis of itaconic anhydride units in the copolymers.

Monomer and polymer preparation

Itaconic anhydride (ITA) was prepared by dehydrating itaconic acid with acetyl chloride following an improved previously reported procedure.[9] The crude itaconic anhydride was purified by several recrystallisations from chloroform. Anhydrous conditions were observed to minimise the hydrolysis of the anhydride to acid. White crystals with a melting point of 68−70 °C were obtained and the structure confirmed by ^{1}H-NMR and IR spectroscopy.

Methyl methacrylate (MMA) was washed with 10 % NaOH aqueous solution to remove inhibitor, washed with water to neutral, dried over calcium hydride and vacuum distilled.

Copolymers of itaconic anhydride and methyl methacrylate were prepared by the solution copolymerisation technique using AIBN as the initiator. A 100 ml three-necked flask equipped with a magnetic stirrer and condenser protected from moisture was used for the copolymerisations. The solution copolymerisations were performed under a nitrogen atmosphere using 2-butanone as the solvent. The desired amounts of itaconic anhydride and methyl methacrylate were dissolved in 2-butanone together with AIBN (0.25 mol %) in a three-necked flask. Nitrogen was bubbled for 15 minutes at room temperature through the solution before starting the polymerisation, while during the polymerisation the nitrogen stream was directed over the top of the condenser. A preheated water bath was employed to commence the polymerisations. The copolymerisations were performed at 60 °C for different times, depending on the composition of the monomer feed (Table I). The copolymers were precipitated in a ten-fold amount of methanol, redissolved in 2-butanone and reprecipitated twice in anhydrous diethyl ether. The copolymers were dried under vacuum at room temperature to remove the residual volatiles.

Amidation of the copolymers

A 50 ml three-necked flask, equipped with a magnetic stirrer, dropping funnel and condenser, protected from moisture, was used for the amidation reaction. A solution of freshly distilled di-*n*-butyl amine (1 g) in chloroform (10 ml) was added dropwise over 90 minutes to a well-stirred solution of a copolymer (0.2 g) in chloroform (15 ml) at 0 °C. The di-*n*-butyl amine was always in large excess to insure that the amidation went to completion. The reaction mixture was vigorously stirred for one day at room temperature. Only the copolymer from the feed composition of 2 mol % itaconic anhydride dissolved immediately in chloroform. The solubility of the copolymers in chloroform decreased with increasing amount of itaconic anhydride in the monomer feed. As the amidation reaction progressed, the copolymers dissolved, finally resulting in a colourless solution. The modified copolymers were precipitated in diethyl ether, dissolved in chloroform, reprecipitated into petroleum ether, and dried under vacuum to constant mass. White powdery polymers were obtained.

TABLE I. Preparation of ITA–MMA copolymers

Monomer feed, mol % ITA	Polymerisation time, min	Yield, wt %
2	45	3.14
6	50	2.48
11	60	1.85
20	105	1.62
30	240	2.27
40	360	6.41

Copolymer characterisation

The copolymers were characterised by ^{1}H-NMR spectrometry on a Varian GEMINI 200 instrument (200 MHz) using TMS as the internal standard and deuterochloroform and deuteroacetone as solvents for the modified and unmodified copolymers, respectively. Infrared spectra were obtained using a BOMEM, MB-Series FTIR spectrometer. The samples were recorded in KBr pellets. Elemental analysis measurements were performed using a Vario III CHNOS Elemental Analyzer, Elemental Analysen Systeme GmbH, to determine the nitrogen content in the copolymers.

The molar masses of the amidated copolymer samples were measured by gel permeation chromatography, GPC, at 30 ºC using a Waters 1500 Series instrument fitted with four analytical columns and an RI detector. Chloroform was used as the mobile phase at a flow rate of 1 ml min^{-1}. The columns were calibrated with narrow molar mass poly(methyl methacrylate) standards and the chromatograms were processed with Waters Breeze software. The molar masses of the unamidated copolymers and homopoly(itaconic anhydride) could not be measured by GPC due to lack of solubility in chloroform.

RESULTS AND DISCUSSION

Copolymers of itaconic anhydride and methyl methacrylate were obtained by free radical copolymerisation in 2-butanone using AIBN as initiator. The copolymer composition was determined by ^{1}H-NMR spectroscopy. The ratio of the signals at 3.65 ppm (associated with the hydrogen from the methylene group in the anhydride ring) and 3.57 ppm (associated with the hydrogen from the methyl ester group from methyl methacrylate) gave the copolymer composition. As these two peaks overlapped, they were deconvoluted using the PeakFit V.4 computer program. The determined copolymer compositions are given in Table II, from which it can be seen that the content if anhydride moieties was enriched in the copolymers with regard to the feed composition.

The monomer reactivity ratios for the copolymerisation of itaconic anhydride and methyl methacrylate determined by the Fineman and Ross method[10] are $r_{ITA} = 1.35 \pm 0.11$ and $r_{MMA} = 0.22 \pm 0.22$ and those calculated by the Mayo–Lewis method[11] are $r_{ITA} = 1.27 \pm 0.38$ and $r_{MMA} = 0.10 \pm 0.05$.

The free radical copolymerisation of itaconic anhydride–methyl methacrylate was previously reported by Cowie and co-workers,[12] who prepared copolymers by bulk copolymerisation at 70 °C. The values of the monomer reactivity ratios reported in this investigation, calculated by the Mayo–Lewis method, were $r_{ITA} = 0.99 \pm 0.40$ and $r_{MMA} = 0.18 \pm 0.07$. The monomer reactivity ratios for this system suggested that the copolymers were essentially statistical with little tendency towards alternation or the formation of long sequences of either type of monomer.

TABLE II. Composition of the prepared copolymers of methyl methacrylate and itaconic anhydride

mol % ITA in the monomer feed	mol % ITA in the copoymer
2	12.86
6	23.59
11	42.47
20	47.29
30	59.86
40	66.47

A comparison of the results of Cowie and co-workers with the data obtained in this study is shown in Fig. 1, from which it can be seen that the agreement between the two sets of results is good considering the present copolymers were prepared in solution at 60 °C, whereas those of Cowie *et al.* were prepared in bulk at 70 °C. Obviously, the polymerisation conditions did not play a great role in determining the polymer compositions.

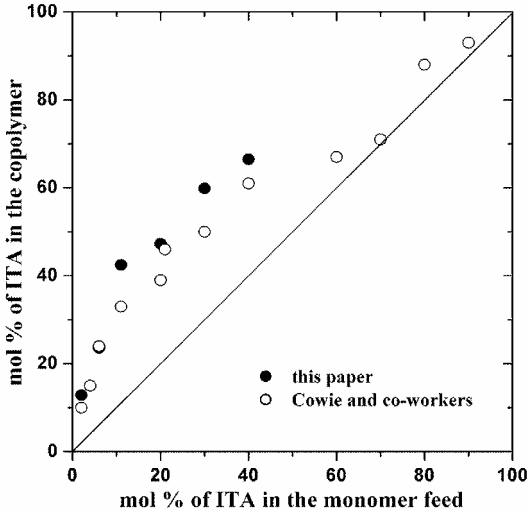

Fig. 1. Comparison of the compositions of ITA–MMA copolymers presented in this paper with the results of Cowie and co-workers.[12]

The copolymers of itaconic anhydride and methyl methacrylate were modified by amidation with di-*n*-butyl amine. The reaction between an amine and the itaconic anhydride units would be expected to yield two possible isomers (Scheme I).

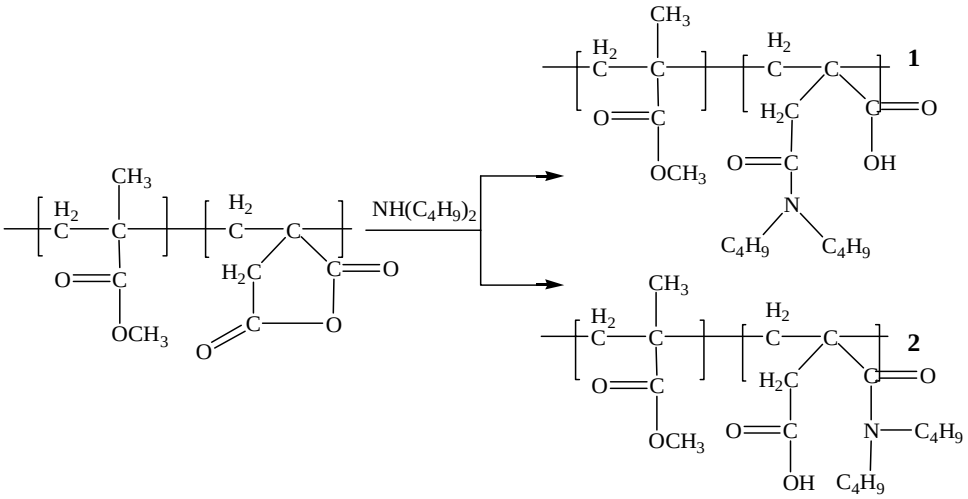

Scheme 1. The reaction between di-*n*-butyl amine and an itaconic anhydride moiety in ITA–MMA copolymers.

It has been reported[13] that ring opening in the reaction of itaconic anhydride monomer and amines gives only the product with structure 1, although Galanti and co-workers presented evidence that trace quantities of isomer 2 are also produced.[14] The presence of small amounts of conjugated amide isomers was also reported by Hartford and co-workers.[15] Accordingly, a similar yield ratio of the two isomers obtained as the result of the amidation of itaconic anhydride units in the copolymers of ITA–MMA could be expected.

The IR spectra of the unmodified copolymers show carbonyl absorptions of the anhydride group at 1856 (ν_{sym}) and 1785 cm^{-1} (ν_{asym}). These peaks are characteristic of cyclic anhydride indicating that the polymerisation did not disrupt the itaconic anhydride moieties. The peak of the ester at 1733 cm^{-1} originates from methyl methacrylate. A comparison of the IR spectra of the modified with the unmodified copolymers (Fig. 2), shows the absence of the peaks characteristic of the anhydride group, and the appearance of absorption of the carbonyl amide group at 1634 cm^{-1}, which suggests that the amidation reaction went to completion.[16]

^{1}H-NMR Spectroscopy confirmed the results of the IR analysis. The ^{1}H-NMR spectra of the ITA–MMA copolymer with 30 mol % of ITA in the monomer feed before and after amidation are shown in Fig. 3. Differences can be seen in the presence of peaks at 3.65 ppm (the hydrogen from the methylene group in the anhydride ring) and 3.59 ppm (the hydrogens from the methyl ester group from methyl methacrylate). The peak at 3.65 ppm disappeared after reaction with di-*n*-butyl amine, indicating that the amidation went to completion.

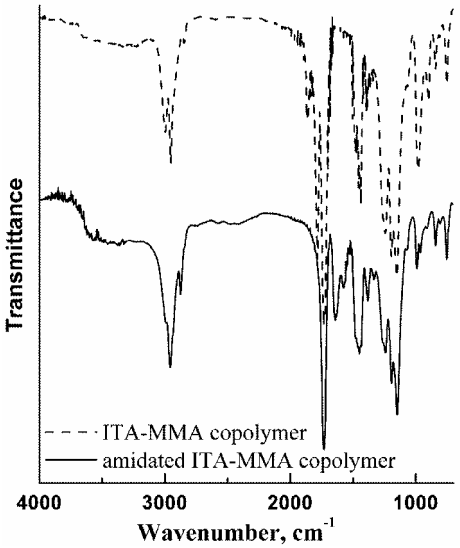

Fig. 2. IR Spectra of copolymer ITA–MMA with 6 mol % of ITA in the monomer feed before and after modification with di-*n*-butyl amine.

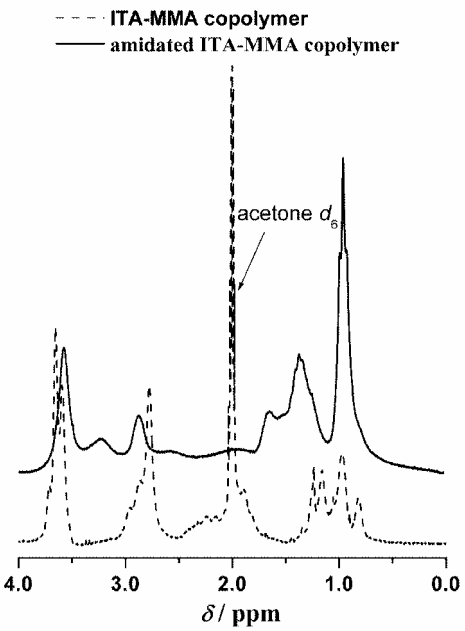

Fig. 3. ^{1}H-NMR Spectra of copolymer ITA–MMA with 30 mol % of ITA in the monomer feed before and after the reaction with di-*n*-butyl amine.

The compositions of the copolymers after modification by amidation with di-*n*-butyl amine were determined by elemental analysis *via* the nitrogen content in the copolymer. The molar percent of itaconamic acid in the obtained copolymers are given in Table II. It can be seen again that the amidation went to completion, which is in agreement with the results of ^{1}H-NMR and IR spectroscopy, and that the percent of amidation does not depend on the copolymer composition. A comparison of the copolymer compositions before and after modification is shown in Fig. 4.

The molar masses of the prepared copolymers after amidation were measured by GPC. The number average molar masses are plotted against the mol % of itaconic anhydride in Fig. 5, together with the polydispersity index.

As can be seen from Fig. 5, both the molar mass and the polydispersity of the resulting polymer decreased with increasing amount of itaconic acid in the monomer feed. Both facts could be consistent with the occurrence of chain transfer to monomer or additive in the monomer mixture. As the concentration of solvent was approximately constant in all polymerisations, one plausible explanation is that as well as being a comonomer, the itaconic anhydride could be a transfer agent (the chain transfer to methyl meythacrylate being very low[17]). It is well known that the chain transfer to monomer constant in the radical polymeri-

sation of di-*n*-alkyl itaconates is relatively high and two orders of magnitude higher than that of methyl methacrylate because of the presence of allylic hydrogens in the basic structure of itaconic acid-based monomers.[18]

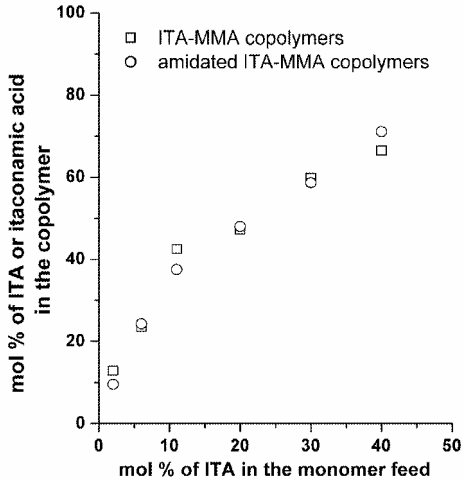

Fig. 4. Comparison of the compositions of ITA–MMA copolymers before and after amidation.

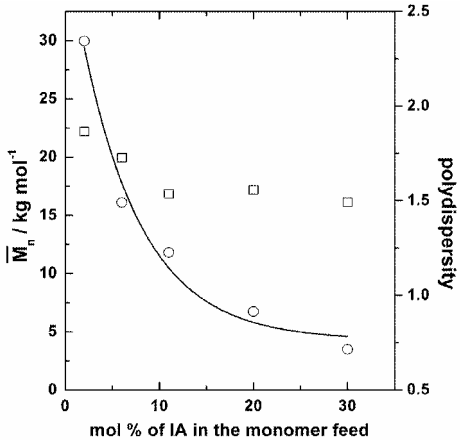

Fig. 5. Number average molar mass (○) and polydispersity (□) of the prepared copolymers as a function of the mol % itaconic acid in the monomer feed.

CONCLUSIONS

Copolymers of itaconic anhydride and methyl methacrylate were synthesised in solution at 60 °C. The determined monomer reactivity ratios are r_{ITA} = = 1.35±0.11; r_{MMA} = 0.22±0.22 (by the Fineman–Ross method) and r_{ITA} = 1.27± ±0.38; r_{MMA} = 0.10±0.05 (by the Mayo–Lewis method). The reactivity ratios are in agreement with literature values[12] for the copolymerisation of these monomers in bulk at 70 °C.

Chain transfer to itaconic anhydride occurred during the radical copolymerisations, limiting the molar masses of the polymers obtained from monomer feeds containing larger amounts of itaconic anhydride.

Amidation of the anhydride units in the copolymer with di-*n*-butyl amine gave itaconamic acid with complete conversion (confirmed by ^{1}H-NMR and IR spectroscopy and nitrogen analysis). The percent of amidation did not depend on the copolymer composition.

This method of modification of itaconic anhydride moieties in copolymers offers a convenient method of obtaining itaconamic acid-containing polymers without the difficulties generally experienced in the preparation of itaconamic acid monomers and in their direct polymerisation.

Acknowledgement. This investigation was financed by the Ministry of Science of Serbia through project No.142023.

И З В О Д

СИНТЕЗА И МОДИФИКАЦИЈА КОПОЛИМЕРА АНХИДРИДА ИТАКОНСКЕ КИСЕЛИНЕ И МЕТИЛ-МЕТАКРИЛАТА

МИЛОШ Б. МИЛОВАНОВИЋ[1], СНЕЖАНА С. ТРИФУНОВИЋ[2], LYNNE KATSIKAS[3] и ИВАНКА Г. ПОПОВИЋ[3]

[1]Институт за хемију, технологију и металургију, Универзитет у Београду, Његошева 12, Београд,
[2]Хемијски факултет, Универзитет у Београду, Студентски трг 12–16, Београд и
[3]Технолошко–металуршки факултет, Универзитет у Београду, Карнегијева 4, Београд

Испитивана је радикална кополимеризација анхидрида итаконске киселине и метил-метакрилата у раствору на 60 °C. Састав кополимера одређен је ^{1}H-NMR спектроскопијом и израчунати су односи реактивности мономера, r_{ITA} = 1.35±0.11; r_{MMA} = 0.22±0.22 (методом Фајнман–Рос) и r_{ITA} = 1.27±0.38; r_{MMA} = 0.10±0.05 (методом Мејо–Луис). Синтетизовани кополимери су модификовани реакцијом са дибутил-амином. Након амидације састав кополимера одређен је елементалном анализом на основу садржаја азота. Амидацијом анхидридних јединица у кополимерима дибутил-амином настале су комономерне јединице итаконамичне киселине.

(Примљено 2. августа 2007)

REFERENCES

1. T. Oishi, *Polym. J.* **12** (1980) 719
2. M. Urzua, A. Opazo, L. Gargallo, D. Radić, *Polym. Bull.* **40** (1998) 63
3. T. Otsu, H. Watanabe, J.–Z. Yang, M. Yoshioka, A. Matsumoto, *Makromol. Chem., Macromol. Symp*. **63** (1992) 87
4. A. V. Galanti, B. T. Keen, R. H. Pater, D. A. Scola, *J. Polym. Sci.* **26** (1981) 2243
5. T. M. Pyriadi, A. S. Berzinji, *Designed Monom. Polym.* **6** (2003) 115
6. K. Yokota, T. Hirabayashi, T. Takashima, *Makromol. Chem.* **176** (1975) 1197
7. W. Mormann, J. Ferbitz, *Eur. Polym. J.* **39** (2003) 489
8. T. Otsu, J.–Z. Yang, *Polym. Int* . **25** (1991) 245
9. A. V. Galanti, D. A. Scola, *J. Polym. Sci.* **19** (1981) 451
10. M. Fineman, S. D. Ross, *J. Polym. Sci.* **5** (1950) 259
11. F. Mayo, F. Lewis, *J. Am. Chem. Soc.* **66** (1944) 1594
12. A. F. Miles, J. M. G. Cowie, *Eur. Polym. J.* **27** (1991) 165
13. F. K. Beilstein, *Handbook of Organic Chemistry*, Vol. 17, Springer, Berlin, 1933, p. 442
14. A. V. Galanti. F. Liotta, B. T. Keen, D. A. Scola, *J. Polym. Sci*. **20** (1982) 233
15. S. L. Hartford, S. Subramanian, J. A. Parker, *J. Polym. Sci.* **16** (1978) 137
16. R. M. Silverstein, G. C. Bassler, T. C. Morrill, *Spectrometric Identification of Organic Compounds*, Wiley, New York, 1974
17. *Polymer Handbook*, J. Brandrup, E. H. Immergut, Eds., 3rd Ed., Wiley, New York, 1989, p. II/85
18. S. L. Tomić, J. M. Filipović, J. S. Veličković, L. Katsikas, I. G. Popović, *Macromol. Chem. Phys.* **200** (1999) 2421.

Journal of the Serbian Chemical Society
JSCS@tmf.bg.ac.yu • www.shd.org.yu/JSCS

J. Serb. Chem. Soc. 72 (12) 1515–1531 (2007)
JSCS–3681

UDC 678.048:542.913:678.742.004.12
Original scientific paper

The influence of antioxidant and post-synthetic treatment on the properties of biodegradable poly(butylene succinate)s modified with poly(propylene oxide)

DRAGANA PEPIĆ#, MARIJA RADOIČIĆ, MARIJA S. NIKOLIĆ# and JASNA DJONLAGIĆ*#

Faculty of Technology and Metallurgy, University of Belgrade, Karnegijeva 4, 11000 Belgrade, Serbia

(Received 31 July 2007)

Abstract: Novel poly(ester–ether)s based on poly(butylene succinate) (PBS) as the hard segments and 30 mass % of poly(propylene oxide) (PPO) as the soft segments were synthesized with varying amount of the antioxidant (*N,N'*-diphenyl-*p*-phenylenediamine, DPPD). The influences of the addition of DPPD and the impact of post-synthetic treatment by precipitation on the molecular structure, thermal and physical properties, as well as on the storage stability of the biodegradable aliphatic copolyesters, were investigated. The structure and composition of the copolymers were determined by means of ^{1}H-NMR spectroscopy. The molecular weight and polydispersity of the poly(ester–ether)s were evaluated from solution viscosity and GPC measurements. The thermal properties and stability were evaluated, respectively, by means of DSC and non-isothermal thermogravimetry in an inert nitrogen atmosphere. The biodegradability potential of the polymers was studied in hydrolytic and enzymatic degradation tests with *Candida cylindracea* lipase by monitoring the weight loss of polymer films after incubation. The weight losses of the samples increased with time and were in the range from 1 to 5 mass % after 4 weeks. GPC analysis confirmed that there were changes in the molecular weight of the copolyesters during both hydrolytic and enzymatic degradation tests, leading to the conclusion that the degradation mechanism of poly(butylene succinate)s modified with PPO occurred through surface erosion and bulk degradation.

Keywords: poly(ester–ether), poly(butylene succinate), poly(propylene oxide), biodegradable, antioxidant, enzymatic degradation.

INTRODUCTION

Due to their low cost, easy processing and resistance to degradation under environmental conditions, the use of synthetic polymeric materials has been growing progressively in the past few decades. However, environmental concerns about the waste resulting from these materials, especially those from short-term applications, has become the centre of attention in the last decade. Replacement

Serbian Chemical Society member.
* Corresponding author. E-mail: jasna@tmf.bg.ac.yu
doi: 10.2298/JSC0712515P

of the currently used bioresistant polymeric materials with biodegradable polymers is one of the solutions for global waste problems.[1,2] Only a few types of synthetic polymers can be considered as potential biodegradable materials, mainly ones with hydrolysable groups incorporated into the polymeric chain.[3,4] Aliphatic polyesters, with hydrolysable ester units within the polymeric chain are recognised as one of the most promising polymers for the development of ecologically friendly materials.[5,6] Intense interest in these polymers as degradable thermoplastic exists also for medical application, where there is a need for materials which will be eliminated after time-limited applications, for example in surgery and in formulations for controlled drug release.[7–9] The development of aliphatic polyesters as biodegradable materials has advanced to such a high level that some polymers belonging to this class have already found commercial application, such as poly(glycolic acid) (PGA), poly(L-lactic acid) (PLLA), poly(ε-caprolactone) (PLC) and different poly(hydroxyalkanoates).

The properties of aliphatic polyesters in terms of time-tunable degradability and mechanical properties can be further developed, usually by copolymerization, in order to fulfil different application demands. For some applications, elastomeric materials are more suitable than relatively hard ones, such as aliphatic crystalline polyesters. Biodegradable thermoset elastomers were synthesized from a star copolymers of ε-caprolactone and *D,L*-lactide and also from copolymers of poly(ethylene oxide) and citric acid.[10,11] All these formulations involve crosslinking during the final stage of thermoset preparation. One of the developed ways to obtain thermoplastic elastomers without chemical crosslinking is copolymerization with flexible polyethers.[12,13] In addition to altered mechanical properties, copolymerization with polyethers has the advantage of introducing hydrophilic groups, which render the so-obtained polymers more susceptible to biodegradation. Among different polyethers, poly(ethylene oxide), PEO, and poly(tetramethylene oxide), PTMO, were used to modify the properties of not only aliphatic, but also of aliphatic/aromatic polyesters. For example, PEO was used as the soft segments in a number of cases, *i.e.*, in combination with poly–(lactic acid), poly(butylene terephthalate), poly(butylene succinate) and poly(ε-caprolactone).[14–19] The less hydrophilic PTMO was also used as a constituent part of the soft segments in copolymerization with aromatic and aromatic/aliphatic polyesters.[20–22] In previous studies, it was shown that poly(butylene succinate), PBS, modified with flexible PEO segments has better biodegradability properties compared to PBS modified with PTMO, due to the increased hydrophilicity of the former.[16] However, the oxidative instability of poly(ester–ether)s with PEO is also much more pronounced in comparison to poly(ester–ether)s with PTMO. There has been a report on aliphatic polyesters with poly(propylene oxide) as a building part of the soft segments in biodegradable aliphatic copolyesters.[23] This study showed that the investigated poly(ester–ether)s with PPO had in some ins-

tances even better biodegradability profiles compared to the corresponding ones with PEO.

The main disadvantage of segmented polymers with polyethers as soft segments is their long-term instability under environmental conditions. The oxidative reactions of the ether bonds *via* a free-radical mechanism lead to chain scission and can be thermo-, photo- or γ-radiation initiated. Thus, some attempts to improve the oxidative instability during storage of polymers with PEO included the use of the antioxidant vitamin E as well as commercially available hindered phenols.[24] Hindered amines, such as *N*,*N*'-diphenyl-*p*-phenylenediamine, are also used as radical scavengers where oxidative reactions are expected to occur, such as in the rubber processing and in biomedical applications.[25,26]

In this work poly(ester–ether)s with PPO in the soft segments and poly(butylene succinate) as the hard segments were synthesized and their properties including biodegradability compared to those previous prepared copolymers based on PBS but with PEO or PTMO as the soft segments. Poly(propylene oxide), with a methyl group as a side-group in the repeating units, is a logical extension of our previous studies. The influence of the amount of antioxidant, *N*,*N*'-diphenyl-*p*-phenylenediamine, DPPD, on the long-term stability and overall properties, including biodegradability, was investigated. Since the stability of the polymers, as well as biodegradability depends on the form in which the polymers are stored, the influence of post-synthetic treatment through precipitation was also evaluated.

EXPERIMENTAL

Materials

Dimethyl succinate (Alfa AESAR, GC > 98 %) was used as received. α,ω-Hydroxyl terminated poly(propylene oxide), PPO, with a molecular weight of 1200 g mol^{-1}, (Fluka) was used as obtained. 1,4-Butanediol (MERCK) was purified by vacuum distillation. Titanium-tetrabutoxide, $Ti(OBu)_4$, (Aldrich) was used as a solution in dry *n*-butanol (1:9 v/v). The antioxidant *N*,*N*'-diphenyl–*p*-phenylendiamine, DPPD, (Bayer) was used as received. *Candida cylindracea* lipase was purchased from Sigma.

Synthesis of the polyesters

The aliphatic poly(ester–ether)s, PBSPPOs, were synthesized by a two step transesterification reaction in the bulk, starting from dimethyl succinate, 1,4-butanediol and 30 mass % of α,ω-hydroxyl-terminated poly(propylene oxide) (PPO, M_n = 1200 g mol^{-1}). The diol component was used in a 15 mol % excess over the dimethyl ester. A series of PBSPPOs without antioxidant and with 0.5 and 1 mass % of DPPD as the antioxidant were synthesized. As an example, the synthesis of a poly(ester–ether) without stabilizer, PBSPPO-0, is described. A three-necked laboratory reactor equipped with a condenser, nitrogen inlet tube, magnetic stirrer and thermometer was charged with 40.88 g (0.28 mol) of dimethyl succinate, 18.24 g (0.152 mol) of poly(propylene oxide) and 27.36 g (0.304 mol) of 1,4-butanediol. The reaction mixture was purged with nitrogen and the reaction was started by the introduction of 0.075 g (0.221 mmol) of $Ti(OBu)_4$, as catalyst. The reaction mixture was heated quickly to 150 °C and then gradually (1 °C min^{-1}) to the final reaction temperature of 220 °C. The methanol formed during the first stage was distilled off. The second phase of reaction was carried out with a second portion of catalyst (0.221 mmol), under vacuum ($p \approx 0.5$ mm Hg).

For the different composition of the reaction mixture and applied vacuum, different reaction times from 24 to 54 h were required in order to obtain polymers of high molecular weight. After completion of the reaction, the poly(ester–ether) was cooled in the reactor to room temperature under nitrogen. One portion of the poly(ester–ether) was precipitated from chloroform into methanol (PBSPPO-0-P) and dried under vacuum, while the rest was stored and used further without precipitation (PBSPPO-0). All the other polyesters were synthesized in the manner described above. The other two PBSPPOs in the series were synthesized with 0.5 mass % (PBSPPO-0.5) and 1 mass % (PBSPPO-1) of DPPD. The numbers in the abbreviations of poly(ester–ether)s indicate the mass percent of antioxidant, while for the precipitated samples, the letter P is used at the end of the abbreviation.

Characterization of the polyesters

^{1}H-NMR spectra were recorded in $CDCl_3$ solution with tetramethylsilane as the reference standard using a Varian-GEMINI-200 (200 MHz) instrument. The ^{1}H-NMR spectra of these polymers showed characteristic peaks: protons from the succinic acid appear at δ = 2.63 ppm, protons from the methylene group in the poly(propylene oxide) which were attached to the ether group at δ = = 3.52–3.62 ppm, and central and terminal protons from the 1,4-butanediol at δ = 1.64–1.77 ppm and δ = 4.09–4.12 ppm, respectively. Protons from the methylene group in poly(propylene oxide) which were attached to the ester group appear at δ = 4.09–4.30 ppm, and in the same region a signal from the terminal methylene protons in 1,4-butanediol appears. Protons from methylene group of the poly(propylene oxide) appear at δ = 3.41–3.45 ppm and the signal of the protons from the methyl group of the poly(propylene oxide) appear at δ = 1.15–1.25 ppm. The compositions of the polyesters were calculated from the relative intensities of the peaks characteristics for the succinic acid residue and for the protons from the side methyl groups of the poly(propylene oxide).

The viscosities of solutions of the polymers in chloroform were measured at 25 °C using an Ubbelohde viscometer. The intrinsic viscosity, [η], was calculated from these measurements.

Gel permeation chromatography (GPC) was performed using a Waters 2414 instrument at 30 °C, with four Styrogel columns and a refractive index detector. The columns cover a range of molar masses from 2500 g mol^{-1} to 1 million g mol^{-1}. Calibration was performed with poly(methyl methacrylate) standards. Chloroform was used as the eluent at a flow rate of 1 ml min^{-1}. The copolyesters were injected onto the column as 10 mg ml^{-1} solutions with a 200 μl loop. The number-average (M_n) and weight-average molecular weights (M_w) and polydispersity indexes were evaluated from these measurements using Waters Breeze software.

Differential scanning calorimetry (DSC) was performed using a TA Instruments SDT Q600 analyser under a nitrogen atmosphere in the temperature range from 30 to 160 °C at a heating and cooling rate of 10 °C min^{-1}. The polyester samples were scanned from 30 to 160 °C, then cooled to 30 °C and heated again to 160 °C. The melting temperatures were determined from the initial scan as the temperature of the maximum of the main endothermic peak in the DSC curves.

The TA Instruments SDT Q600 was also used for thermogravimetry. Non-isothermal experiments were performed in the temperature range 30–500 °C at a heating rate of 10 °C min^{-1}. The thermal stability of the poly(ester–ether)s was studied under a dynamic atmosphere of nitrogen (the flow rate was 100 cm^3 min^{-1}).

The moisture uptake of the poly(ester–ether)s was measured as the increase in the mass of polymer films, which were placed in a chamber above a saturated solution of K_2SO_4, giving a relative humidity of 97 %, for 7 days at room temperature.

Enzymatic and hydrolytic degradation tests were performed on poly(ester–ether)s films. The polymer films were obtained by hot pressing at 20 °C above the melting temperature. In addition, the films were stored at ambient temperature for at least three weeks before characterization in order to attain equilibrium crystallinity. The films (10×40 mm^2 and about 150 μm thick) were incubated in a phosphate buffer solution (pH ≈ 7.00) (hydrolytic degradation) or with 2 mg ml^{-1} li-

pase from *Candida cylindracea* (enzymatic degradation) in an incubator at 37 °C. The enzymatic and hydrolytic degradation tests of the poly(ester–ether)s films were run in duplicate. Every 7 days, the enzyme solution was replaced with a freshly prepared one. The films were removed either from the enzymatic or buffer solution after selected time intervals, washed with distilled water, and dried under vacuum at room temperature to constant weight. The extent of biodegradation was quantified as the percent weight loss of the polymeric films.

The surfaces of the samples were observed using an optical microscope "Carl Zeiss Jena" in reflected light before and after hydrolytic and enzymatic degradation, without any further mechanical treatment.

RESULTS AND DISCUSSION

Synthesis and stabilisation of poly(ester–ether)s

Aliphatic poly(ester–ether)s with poly(propylene oxide) as the soft segments and poly(butylene succinate) as the hard segments were synthesised with varied amount of the antioxidant *N,N*'-diphenyl-*p*-phenylenediamine (DPPD). In addition to the influence of the different amounts of antioxidant, the influence of post-synthetic treatment of the obtained polymers on the properties of the poly(ester–ether)s was also investigated.

All poly(ester–ether)s in the series with varying amount of DPPD and constant amount of the soft segments (5.5 mol % or 30 mass %) were synthesised according to the well-established transesterification reaction procedure for obtaining polyesters of high molecular weight.[16] Starting from dimethylsuccinate, 1,4-butanediol and poly(propylene oxide) (M_n = 1200 g mol^{-1}) and using a $Ti(OBu)_4$ as the catalyst, oligomeric chains were produced in the first phase of reaction under atmospheric pressure and nitrogen atmosphere. Thereafter, a vacuum was applied in order to produce chain extension and to obtain polymers of high molecular weight with the addition of the antioxidant DPPD. Longer reaction times for the second phase of the reaction, *i.e.*, polycondensation, were required compared to those for the homopolyester, PBS.[17] These results are in agreement with the fact that the reaction rate decreases due to the higher transesterification activation energy of dimethyl succinate and PPO compared to dimethyl succinate with 1,4-butanediol.[27,28]

The structure and composition of the synthesized poly(ester–ether)s were confirmed by ^{1}H-NMR spectroscopy (Fig. 1). Using the intensity ratio of the methylene protons peak from the succinic acid residue (signal a in Fig. 1) and the methyl protons peak from the side group in the poly(propylene oxide) units (signal g in Fig. 1), the mol and mass fraction of soft segments in the polymer chain were determined. As can be seen from the results presented in Table I in all cases, good agreement with the theoretical composition based on the feed composition was achieved. Thus, the presence of the antioxidant did not influence the composition of the synthesised poly(ester–ether)s. Secondly, in all three cases, the composition of the polymer chains was not altered through precipitation, indicating that the formation of the polymers during the course of the synthesis

was uniform, and that there was no preferential incorporation of either diol units; thus finally random copolymers were obtained.

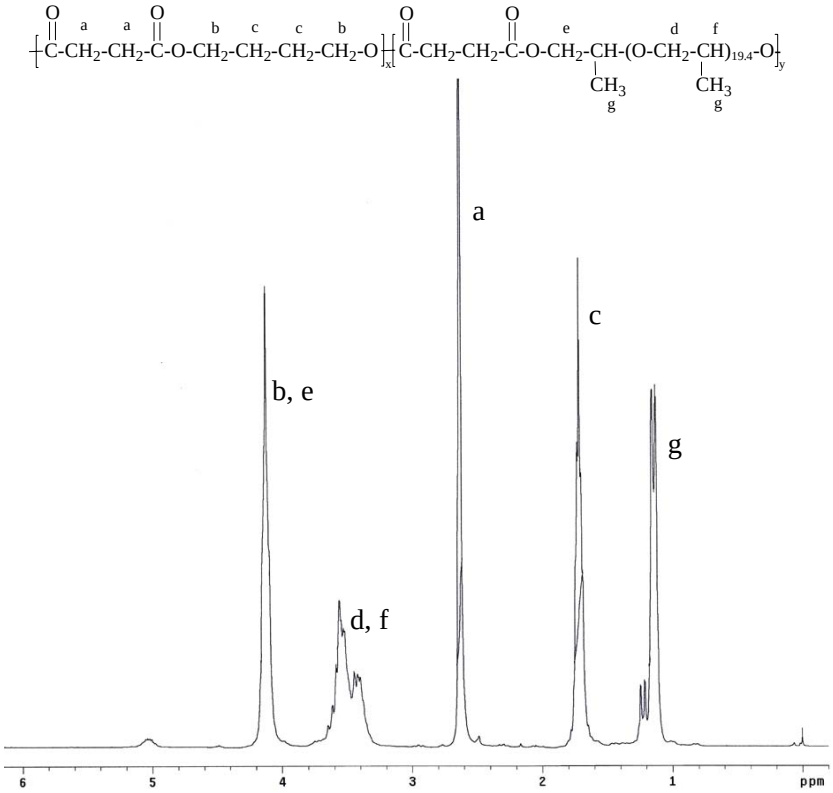

Fig. 1. ^{1}H-NMR spectrum of the poly(ester–ether) PBSPPO-0 in $CDCl_3$.

TABLE I. Composition of poly(ester–ether)s determined from the ^{1}H-NMR spectra

Polymer	Mass fraction of soft segments mass %		Mole fraction of soft segments mol %		L_n
	Theoretical	Experimental	Theoretical	Experimental	
PBSPPO-0	30	29.6	5.5	5.9	17.0
PBSPPO-0-P		29.3		5.4	18.4
PBSPPO-0.5		29.3		5.2	19.1
PBSPPO-0.5-P		29.2		5.2	19.3
PBSPPO-1		29.7		6.0	16.7
PBSPPO-1-P		29.8		6.2	16.2

Under the assumption that the length of the soft segment is one, and taking into account the fact that the copolymers are random, the average length of the hard poly(butylene succinate) segments was calculated from the mole fraction of PBS in the copolymer, using the formula:

$$L_n = \frac{1}{1 - x_{PBS}} - 1$$

The values are included in Table I. In previous studies on the biodegradebility of poly(ester–ether)s with PTMO as the soft segments, it was shown that there is an optimal hard segment length for promoting catalytic action of *Candida cylindracea* lipase,[22] which was also used in the present work. The compositions of the PBSPPOs in this study were designed to obtain poly(ester–ether)s with hard segments of 17 to 18 PBS units, in order to have the optimal catalytic action of the chosen enzyme. As can be seen from the data in Table I, the average sequence length of the PBS hard segments was between 16 and 19, depending on the molar fraction of the soft PPO segments, which varied from 5.5 to 6.2 mol %.

The results of characterisation in terms of the size of polymeric chain, *i.e.*, intrinsic viscosities and molecular weights obtained in GPC analysis, are summarised in Table II. The values of intrinsic viscosities of the synthesized copolyesters were from 78.9 to 101.5 $cm^3\ g^{-1}$. With increasing content of the antioxidant, the molecular weights of the synthesised poly(ester–ether) increased. While for the lower content of DPPD (0.5 %), only a moderate increase was observed, for the higher content of DPPD (1 %), the increase in molecular weight was much more pronounced. It can be concluded that some thermal degradation reactions occurred during the synthesis, although, under the chosen reaction conditions (vacuum at 220 °C), appreciable degradation of the polymers is not to be expected. These thermal degradation reactions could be efficiently prevented by the use of DPPD.

TABLE II. Intrinsic viscosity, molecular weights and molecular weight distribution of the synthesized poly(ester–ether)s

Polymer	$[\eta]^a$ / $cm^3\ g^{-1}$	$[\eta]^b$ / $cm^3\ g^{-1}$	$M_n{}^b$ / 10^4 g mol^{-1}	$M_w{}^b$ / 10^4 g mol^{-1}	$M_w/M_n{}^b$
PBSPPO-0	78.9	74.9	2.72	5.16	1.90
PBSPPO-0-P	82.6	13.8	0.49	0.92	1.88
PBSPPO-0.5	79.6	68.1	2.71	4.61	1.70
PBSPPO-0.5-P	84.2	77.1	2.69	4.67	1.74
PBSPPO-1	87.5	81.5	3.34	6.28	1.88
PBSPPO-1-P	101.5	94.0	3.17	5.72	1.81

[a]Determined for the as-prepared samples; [b]determined after 8 months of aging at room temperature

In this study, it was shown that relatively high-molecular weight poly(ester––ether)s based on PPO could be synthesized using a highly effective catalyst, *i.e.*, tetra-*n*-butyl-titanate, and the molecular weight increased with increasing content of antioxidant, as well as by precipitation leading to the elimination of low-molecular weight fractions. All the synthesized copolymers exhibited macromolecular behaviour and were suitable for the preparation of elastomeric, flexible and tough films by the melt-press method.

As can be seen from the values of the intrinsic viscosities after 8 months of aging, the poly(ester–ether)s are prone to degradation under ambient conditions, as shown in previous studies.[17,22] This can also be seen from GPC measurements which were made after 8 months of aging. This is especially the case for PBSPPO-0-P, which was precipitated after the synthesis. Probably, the reason is in addition to the absence of antioxidant, the morphology of the sample, which was in the form of a powder with a high surface to volume ratio. The results obtained for the samples with DPPD show that the oxidative degradation could be suppressed, although not completely prevented, even with the highest employed amount of DPPD. For complete prevention of the oxidative degradation of poly–(ester–ether)s, higher quantities than 1 mass % of DPPD are recommended.

Thermal properties of the poly(ester-ether)s

The thermal properties of poly(ester–ether)s were characterized by DSC analysis in terms of melting temperatures and enthalpies of melting. Poly(butylene succinate) homopolymer is a crystalline polyester with a melting temperature of 115–117 °C. The main disadvantage of the copolymers of this polyester is that the melting temperatures are usually decreased to below 100 °C. The composition of the poly(ester–ether) was chosen to be such as to obtain polymers with a melting temperature above 100 °C, which is important from the technical point of view. The melting temperatures of all the synthesized poly(ester–ether)s were in temperature region from 104 to 109 °C, irrespective of the presence of a heat stabiliser or post-synthetic treatment (Fig. 2 and Table III).

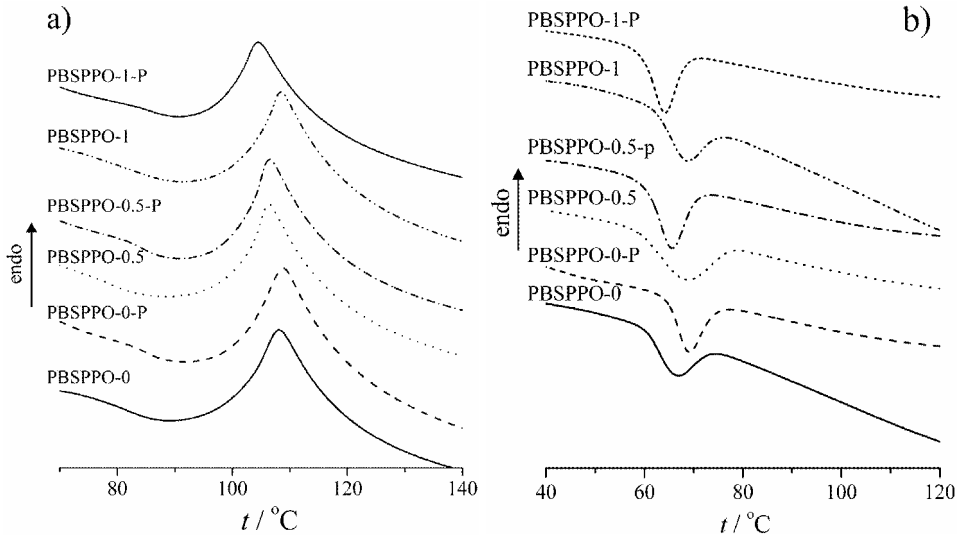

Fig. 2. DSC thermograms of the poly(ester–ether)s obtained in the initial heating scan (a) and subsequent cooling (b); heating and cooling rate 10 °C min^{-1}, nitrogen atmosphere.

TABLE III. Thermal properties of the poly(ester–ether)s

Polymer	T_{mI} / °C	ΔH_{mI} / J g^{-1}	T_{mII} / °C	ΔH_{mII} / J g^{-1}	T_c / °C	X_c[a] / %	x_{cPBS}[b] / %
PBSPPO-0	108.5	56.8	107.9	48.4	65.8	51.4	73.1
PBSPPO-0-P	109.5	60.3	109.2	51.7	68.9	54.6	77.2
PBSPPO-0.5	106.5	54.2	105.6	48.9	67.8	49.0	67.2
PBSPPO-0.5-P	106.7	55.2	106.0	53.9	65.3	49.9	68.9
PBSPPO-1	108.7	55.8	108.1	46.0	67.8	50.5	71.9
PBSPPO-1-P	104.8	45.9	104.7	41.2	64.0	41.5	58.6

[a]Determined as the ratio of the apparent to theoretically calculated enthalpy of melting for perfectly crystalline PBS; [b]degree of crystallinity of PBS, calculated using the experimentally determined mass fraction of PBS in the poly(ester–ether)s

The presence of the antioxidant and the thus obtained differences in the molecular weights of the samples did not have a significant influence on the melting temperatures. The post-synthetic treatment by precipitation, in which smaller molecular weight fractions were removed, also did not have a great impact on the melting temperatures, except in the case of the polyester with the highest content of DPPD. As the largest difference in the values of the intrinsic viscosities before and after precipitation was observed in the case of this poly(ester–ether), the differences in the melting temperatures can be ascribed to changes in the molecular weight and polydispersity between the treated and untreated sample.

Similar tendencies as those in the case of melting temperatures were observed for the enthalpies of melting, ΔH_m, and, consequently, the total degrees of crystallinity, x_c. The enthalpies of melting were used to calculate the total degrees of crystallinity as the ratio of the observed enthalpy to that theoretically calculated on the basis of the group contribution method,[29] of perfectly crystalline PBS (ΔH_m^0 = 110.5 J g^{-1}). The total degree of crystallinity of the poly(ester–ether)s was in the range from 41.5 to 54.6 %.

For the untreated samples obtained with different amount of DPPD, the differences in the degree of crystallinity were just a few percent, which were in the range of experimental error of the determination of the degree of crystallinity by the DSC method. For the samples which were precipitated, the degree of crystallinity decreased following the trend of increasing molecular weight in the series. Except for the sample with the highest content of DPPD, the degree of crystallinity of the other samples rose slightly after precipitation. As the lower molecular weight fractions were removed, the sample with a narrower molecular weight distribution forms a more uniform and perfect crystal structure with fewer defect, which can disturb crystalline growth and overall degree of crystallinity. In addition, all the investigated samples showed a single endothermic peak on heating, which is an indication of the perfection of the crystallite size distribution. The biggest change in the degree of crystallinity due to the post-synthetic treatment and in the opposite direction from the other PBSPPOs was observed for the

sample with 1 mass % of DPPD. The reason for the decrease of almost 10 % in the degree of crystallinity after precipitation for this sample is probably due to the high molecular weight of the precipitated sample, as judged from the value of the intrinsic viscosity. The enthalpies of melting for this sample remained very low also in the second DSC run, which indicates retarded crystallisation, probably due to the increased viscosity of this sample because of its high molecular weight. All the poly(ester–ether)s exhibited a total degree of crystallinity which were greatly reduced compared to usually observed values for pure PBS determined by DSC, which is around 80 %.[17,22] Since biodegradability depends strongly on the degree of crystallinity, as shown in a number of studies, the obtained poly(ester–ether)s should have improved biodegradability properties compared to PBS, while still maintaining optimal thermal properties.

The degree of crystallinity relative to the mass fraction of hard crystallisable PBS segments, x_{cPBS}, were in the range 58.6 to 77.2, which means that only 59 to 77 weight % of the PBS segments in the poly(ester–ether)s crystallized. From the values of x_{cPBS}, it is clear that the presence of the soft polyether segments disturbs the crystal growth of hard PBS segments. However, the presence of polyether in polymeric chains does not affect the rate of crystallisation compared to pure PBS. The supercooling ($\Delta T_h = T_m - T_c$), the difference between the melting and crystallisation temperature, which is an indicator of the rate of crystallisation, was around 40±2 °C, which is close to the value for pure PBS, which has a ΔT_h value of 38 °C and is considered to be a fast crystallising polymer.

Thermal stability of the poly(ester-ether)s

From the processing and application standpoint, as well as from the interest in chemical recycling, it is important to evaluate thermal stability of new polymeric materials. The poly(ester–ether)s were investigated by non-isothermal thermogravimetry (TG) in order to determine their thermal stability and degradation behaviour. All the poly(ester–ether)s showed a single peak in the differential thermogravimetry (DTG) curves, indicating that there is no difference in the mechanism of the degradation between the poly(ester–ether)s obtained in the presence of different contents of DPPD or between the samples which had undergone post-synthetic treatment by precipitation.

The temperatures at which the poly(ester–ether)s had lost 5 % of their initial mass, which is considered as the beginning of degradation, and the temperatures at the maximum degradation rate, as well as the residual mass at 450 °C are summarised in Table IV. As can be seen from the data presented in Table IV, there is slight difference in the thermal stability between polymers obtained in the presence of DPPD and without antioxidant, the later being more stable.

The only exception is the sample obtained with highest amount of DPPD and without any post-synthetic treatment. There were no differences observed in the

mass remaining at the end of degradation, showing that the differences observed could not be ascribed to the presence of the volatile DPPD, which was present in such a low content. Overall, the observed unexpected differences between poly(ester–ether)s obtained under different conditions could not be explained with the present available set of data. However, the differences between the samples are so small that the whole series can be compared with other polyesters intended for the same application. Poly(ester–ether)s based on PPO exhibit improved stability compared to almost all well known hydroxyalkanoic acid based polyesters, investigated in similar TG experiments.[30] The thermal stability of the poly(ester–ether)s modified with PPO is comparable to the most stable poly(hydroxylalkanoate)s, poly(δ-valerolactone) and poly(ε-caprolactone).

TABLE IV. $T_{5\%}$, T_d^{max} and residual mass at 450 °C obtained by thermogravimetry

Polymer	$T_{5\%}$ / °C	T_d^{max} / °C	Residue at 450 °C, mass %
PBSPPO-0	349.6	400.8	4.2
PBSPPO-0-P	349.9	401.4	2.5
PBSPPO-0.5	327.5	385.3	1.9
PBSPPO-0.5-P	328.3	382.6	3.5
PBSPPO-1	349.5	401.0	4.5
PBSPPO-1-P	336.6	384.1	2.4

Biodegradability tests

Hydrolytic degradation of the poly(ester–ether)s in phosphate buffer solution and in the presence of the lipase from *Candida cylindracea* on polymer films was followed by mass loss during degradation and changes in the molecular weight by GPC analysis, as well as by optical microscopy of the surface of the degraded and non-degraded samples. All samples were included in the study except for PBSPPO-0-P, which was to fragile due to oxidation that films of sufficient strength could not be obtained.

Among all other factors which can affect biodegradability through scission of hydrolysable bonds within a polymeric chain, hydrophilicity is the one which can greatly influence the rate and extent of degradation. With the introduction of polyether soft segments, the hydrophilicity of so obtained poly(ester–ether) is increased, and as shown in a number of studies, the biodegradability is thus improved.[21] Moisture-uptake tests were performed on the novel poly(ester–ether)s synthesized within the framework of this study in order to investigate the influence of the presence of the aromatic antioxidant, as well as the influence of post-synthetic treatment on the hydrophilicity of the obtained copolymers. The results obtained for moisture uptake of polymeric films after 7 days of incubation in an atmosphere of relative humidity 97 % are presented in the Fig. 3.

It is obvious that with increasing content of the aromatic, hydrophobic DPPD, the absorption of moisture was decreased for both the precipitated and unpreci-

pitated samples. A possible explanation is that the presence of the aromatic antioxidant renders the surface of the samples more hydrophobic, which results in a decreased moisture uptake with increasing content of DPPD. It is also apparent that the samples obtained from the poly(ester–ether)s which were precipitated absorbed more water than the untreated ones when the poly(ester–ether)s were synthesized in the presence of DPPD. Some of the DPPD was obviously lost during the precipitation procedure which resulted in the observed difference between the precipitated and unprecipitated samples. Compared to the poly(ester––ether)s containing poly(ethylene oxide) soft segments of comparable molecular weight to that of the PPO employed in this study, the presently investigated poly–(ester–ether)s were less hydrophilic and the differences within the series were smaller. Thus, the biodegradability cannot be mainly determined by the slightly increased hydrophilicity compared to PBS found in some of previous studies.[16,21]

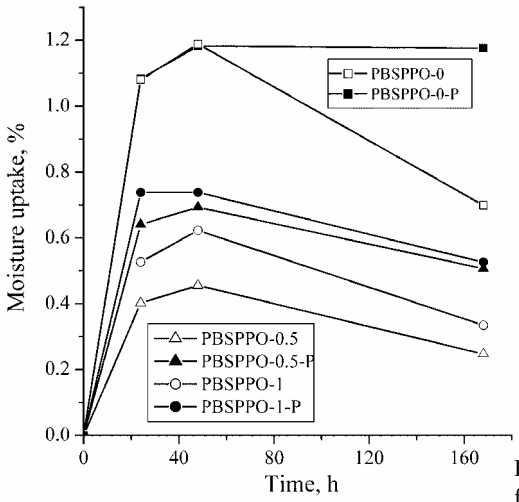

Fig. 3. Moisture uptake of the poly(ester–ether) films incubated in a 97 % humidity atmosphere.

The weight losses of the poly(ester–ether)s based on PPO in the hydrolytic tests increased with time and were from 1 to 5 mass % after 28 days. A mild catalytic activity of the lipase from *Candida cylindracea* was confirmed since in all cases the weight losses in the tests conducted with the enzyme were slightly higher than those observed in the tests performed in buffer solution without the enzyme. The weight losses of the poly(ester–ether) samples with different contents of antioxidant incubated in the enzyme buffer solution for 28 days are presented in Fig. 4. The highest weight losses are observed for the poly(ester–ether) obtained without the addition of the antioxidant, which is in agreement with the assessment of the hydrophilicity obtained in the moisture-uptake tests. Nevertheless, all samples showed similar rates of weight loss within the investigated timeframe, which were much higher compared to poly(butylene succinate) investigated in a similar manner in previous studies.[16,17,22] The same explanation which con-

nects the increased degradability of poly(ester–ether)s compared to PBS homopolyester of increased flexibility and decreased crystallinity for the copolymer also holds in this case. Since the degrees of crystallinity were similar for all samples and the hydrophilicity was not greatly affected by the presence of the hydrophobic DPPD, the degradation rates were, as expected, of a similar magnitude.

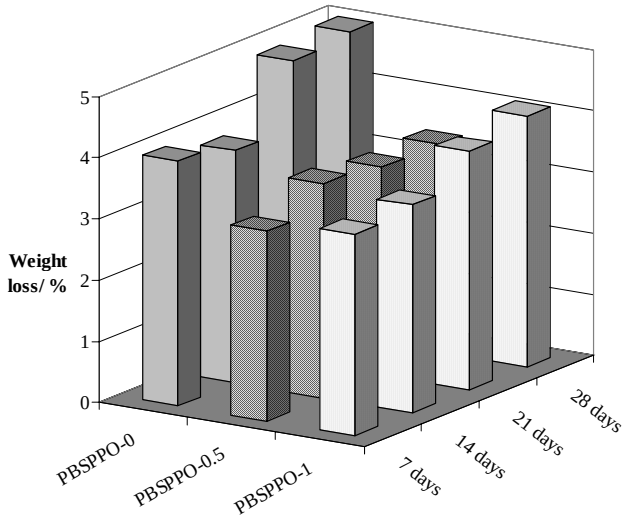

Fig. 4. Weight losses in the enzymatic degradation tests of the poly(ester–ether)s with different contents of DPPD.

The precipitated and unprecipitated samples were also compared for the poly(ester–ether)s obtained in the presence of the antioxidant DPPD (Fig. 5). While the post-synthetic treatment did not have any influence on the degradability of the samples with the lower content of DPPD, the poly(ester–ether) obtained with 1 % of DPPD exhibited a greatly reduced susceptibility toward degradation after precipitation, and was the least degradable sample of all the ones investigated. As can be seen from the values of the intrinsic viscosity, this sample showed the highest relative increase in molecular weight after precipitation. It can be concluded that in this case the biodegradability depended strongly on the molecular weight, since the degradability was greatly reduced after the lower molecular weight fractions had been removed.

The results obtained in GPC measurement before and after hydrolytic and enzymatic degradation tests on the samples incubated for 28 days show that the enzymatic degradation proceeds *via* bulk degradation of the polymeric films, since a decrease in molecular weight was observed after the degradation experiments (Fig. 6). This was not the case, however, when the weight losses were small, as in the case of PBSPPO-1-P, where no change in molecular weight was observed (Fig. 6b).

The structure of the surface of poly(ester–ether)s films was inspected by optical microscope before and after degradation. In all the samples, a spherulite

structure was clearly visible. The poly(ester–ether) with the highest amount of DPPD appeared to have spherulites of the smallest size of all the samples. There was no change in the structure observed for the precipitated samples in comparison to the unprecipitated ones. Upon incubation in buffer solution with or without the addition of the lipase, no visible cracks or holes were detected. Although the degradation proceeds *via* bulk degradation the extent of weight loss in the investigated timeframe was so small that no observable erosion could be detected. Representative images of the surface of the polymeric films before and after hydrolytic and enzymatic degradation are presented in Fig. 7.

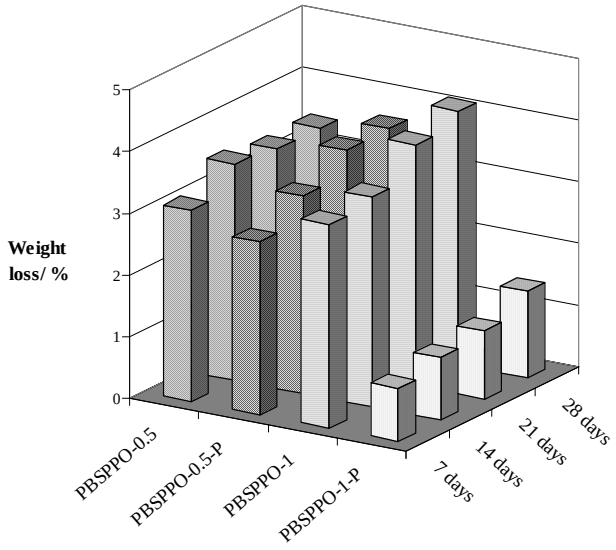

Fig. 5. Weight losses in the enzymatic degradation tests of unprecipitated and precipitated poly(ester–ether)s with different contents of DPPD.

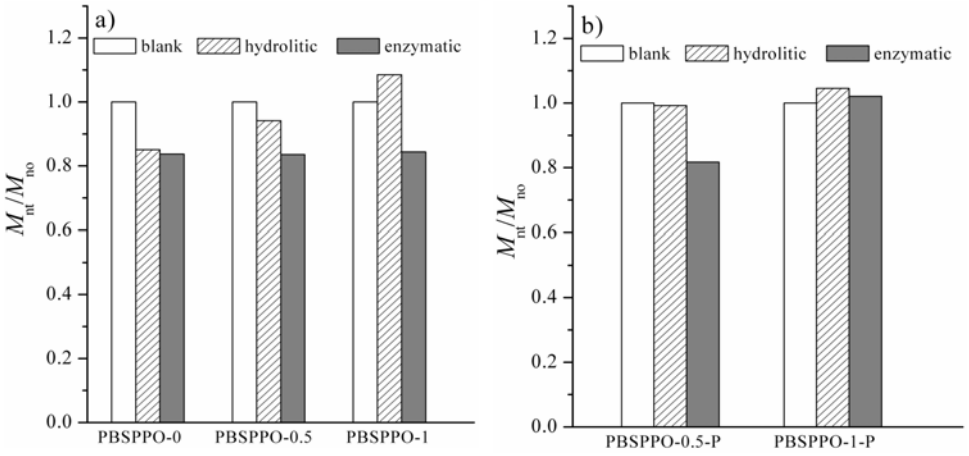

Fig. 6. Change in the number average molecular weight after 28 days of incubation (M_{nt}) in buffer solution (hydrolytic) or enzyme solution (enzymatic) relative to the initial number molecular weight, M_{no}; a) untreated samples, b) samples after precipitation.

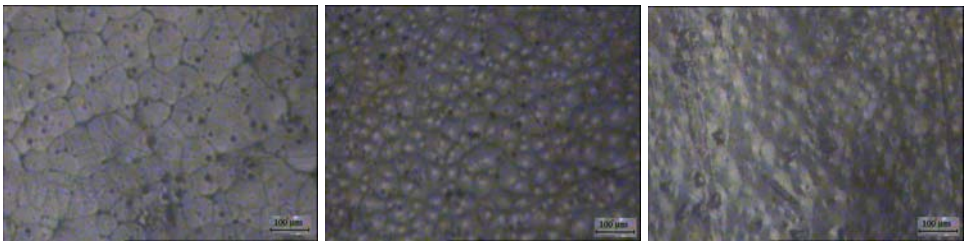

a b c

Fig. 7. Surface appearance of the poly(ester–ether) PBSPPO-0 before (a) and after hydrolytic (b) and enzymatic (c) degradation for 28 days.

CONCLUSIONS

High molecular weight poly(ether–ester)s based on poly(butylene succinate) as the hard segments and poly(propylene oxide) as the soft segments were successfully synthesized by a catalysed transesterification reaction in the melt. The number average molecular weights, M_n, of the copolyesters in the series were above 27000 g mol^{-1}, while the polydispersity index, M_w/M_n, was in the range 1.7 to 1.8. The molecular weights of synthesized copolyesters increased both in the presence of antioxidant (*N*,*N*'-diphenyl-*p*-phenylenediamine, DPPD) as well as by precipitation of the polymers. The oxidative degradation of poly(ester–ether)s based on PPO could be suppressed, although not completely prevented, even with highest amount of added antioxidant DPPD. For complete prevention of the oxidative degradation of the copolyesters, higher quantities of DPPD are recommended.

The melting temperatures of the poly(ether–ester)s based on PPO were lower than that of PBS but above 100 °C, which is important for their possible application. The copolymers exhibited macromolecular behaviour and were suitable for the preparation of flexible and tough films by the melt-press method. The total degree of crystallinity of the poly(ether–ester)s was in the range of 41 to 55 %, *i.e.*, lower than the degree of crystallinity of the homopolyester (PBS). The degree of crystallinity calculated with respect to the weight fraction of PBS segments (x_{cPBS}) in the poly(ether–ester)s indicated a decreasing tendency of crystallization of the hard segments with increasing molecular weight of the synthesized copolyesters.

Incubation in a buffer solution for 4 weeks resulted in mass losses from 1 to 5 %, depending on the content of antioxidant and post-synthetic treatment. Enzymatic degradation in the presence of lipase from *Candida cylindracea* was slightly increased compared to hydrolytic degradation. The enzymatic degradation showed that the introduction of the soft PPO segments into the polymer chains increased the degradability compared to PBS, showing the dependence of the amount of degradation on the chain structure, *i.e.*, molecular weight and hydrophilicity. GPC Analysis confirmed that there were changes in the molecular weight of the copolyesters during both hydrolytic and enzymatic degradation tests, leading to

the conclusion that the degradation mechanism of the poly(ester–ether)s based on PPO occurs through surface erosion and bulk degradation.

High molecular weight poly(ester–ether)s based on PBS and hydrophilic poly(propylene oxide) show promise as biodegradable elastomers, having satisfactory thermal and mechanical properties and simultaneously good biodegradability.

Acknowledgement. This work was financially supported by the Ministry of Science of the Republic of Serbia (Project No. 142023).

И З В О Д

УТИЦАЈ АНТИОКСИОДАНСА И НАЧИНА ИЗДВАЈАЊА ПОЛИМЕРА НА СВОЈСТВА БИОДЕГРАДАБИЛНИХ ПОЛИ(БУТИЛЕН СУКЦИНАТА) МОДИФИКОВАНИХ ПОЛИ(ПРОПИЛЕНОКСИДОМ)

ДРАГАНА ПЕПИЋ, МАРИЈА РАДОИЧИЋ, МАРИЈА С. НИКОЛИЋ и ЈАСНА ЂОНЛАГИЋ

Технолошко–металуршки факултет, Универзитет у Београду, Карнегијева 4, 11000 Београд

У оквиру овог рада синтетисани су нови поли(естар–етри) на бази поли(бутилен сукцината) (PBS) као тврдих сегмената и 30 масених % поли(пропиленоксида) (PPO) уграђених у меке сегменте, без и у присуству антиоксиданса *N,N′*-дифенил-*p*-фенилендиамина (DPPD). Изучавао се утицај антиоксиоданса DPPD као и начина издвајања полимера, односно преталожавања на структуру и величину молекула, термичка и физичка својства као и на стабилност биодеградабилних алифатских кополиестара. Структура и састав кополиестара су проверени ^{1}H-NMR спектроскопијом. Величина молекула и расподела величина молекула синтетисаних поли(естар–етара) су одређени вискозиметријом разблажених раствора и GPC анализом. Термичка својства и термичка стабилност поли(естар–етара) су анализирана DSC и неизотермском термогравиметријом у инертној атмосфери азота. Биодеградабилни потенцијал полимера је изучаван у огледима хидролотичке и ензимске деградације у присуству липазе *Candida cylindracea* пратећи промене у маси полимерних филмова током инкубације. Губици су расли са временом и после 4 недеље су били у опсегу од 1 до 5 масених %. GPC анализа је потврдила да постоје промене у моларној маси узорака и у огледима хидролитичке и ензимске деградације на основу чега се може закључити да се механизам деградације поли(естар–етара) на бази PPO одвија кроз ерозију површине и деградацију у маси.

(Примљено 31. јула 2007)

REFERENCES

1. J. S. Huang, *Biodegradable Polymers*, *Encyc. Polym. Sci. Eng.*, Wiley–Interscience, New York, 1985, vol. 2, p. 220
2. G. Kale, T. Kijchavengkul, R. Auras, M. Rubino, S. E. Selke, S. P. Singh, *Macromol. Biosci.* **7 (**2007) 255
3. R. Chandra, R. Rustgi, *Prog. Polym. Sci.* **23** (1998) 1273
4. M. Okada, *Prog. Polym. Sci.* **27** (2002) 87
5. K. Sudesh, H. Abe, Y. Doi, *Prog. Polym. Sci.* **25** (2000) 1503
6. M. Vert, *Biomacromolecules* **6** (2005) 538
7. A. Lendlein, R. Langer, *Science* **296** (2002) 1637
8. Z. Gan, T. F. Jim, M. Li, Z. Yuer, S. Wang, C. Wu, *Macromolecules* **32** (1999) 590
9. A. Mahmud, X. B. Xiong, A. Lavasanifar, *Macromolecules* **39** *(*2006) 9419
10. B. Amsden, S. Wang, U. Wyss, *Biomacromolecules* **5** (2004) 1399

11. T. Ding, Q. Liu, R. Shi, M.Tian, J. Yang, L. Zhang, *Polym. Deg. Stab.* **91** (2006) 733
12. G. Holden, *Elastomers Thermoplastic, Encyclopedia of polymer Science and Technology*, Wiley–Interscience, New York, 1986. vol 5, p. 416.
13. R. Saint–Loup, J.–J. Robin, *Macromol. Chem. Phys.* **206** (2005) 1190
14. S. M. Li, I. Rashkov, J. L. Espartero, N. Manolova, M. Vert, *Macromolecules* **27** (1996) 57
15. A. A. Deschamps, A. A. van Apeldoorn, H. Hayen, J. D. de Bruijn, U. Karst, D.W. Grijpma, J. Feijen, *Biomaterials* **25** (2004) 247
16. D. Jovanović, M. S. Nikolić, J. Djonlagić, *J. Serb. Chem. Soc.* **69** (2004) 1013
17. D. Pepic, E. Zagar, M. Zigon, A. Krzan, M. Kunaver, J. Djonlagic, submitted
18. D. Chen, H. Chen, J. Bei, S. Wang, *Polym. Int.* **49** (2000) 269
19. M.–H. Huang, S. Li, D. W. Hutmacher, J. Coudane, M. Vert, *J. Appl. Polym. Sci.* **102** (2006) 1681
20. Y. H. Park, C. G. Cho, *J. Appl. Polym. Sci.* **79** (2001) 2067
21. M. Nagata, T. Kiyotsukuri, S. Minami, N. Tsutsumi, W. Sakai, *Polym. Int.* **39** (1996) 83
22. D. Pepic, S. M. Nikolic, J. Djonlagic, *J. Appl. Polym. Sci.* **106** (2007) 1777
23. Y. Maeda, K. Sakai, A. Nakayama, I. Arvanitoyannis, N. Kawasaki, K. Hayashi, S. Aiba, N. Yamamoto, *J. Appl. Polym. Sci.* **68** (1998) 2095
24. A. A. Deschamps, D. W. Grijpma, J. Feijen, *Polymer* **42** (2001) 9335
25. Z. Cibulkova, P. Simona, P. Lehocky, J. Balko, *Polym. Deg. Stab.* **87** (2005) 479
26. S. M. Park, H. C. Jung, I. S. Koak, H. Y. Na, J. S. Woo, J. S. Jung, Y, K, Kim, *Pharmacol. Toxicol.* **92** (2003) 43
27. Y. Zhang, Z. Feng, Q. Feng, F. Cui, *Eur. Polym. J.* **40** (2004) 1297
28. J. Hsu, K. Y. Chio, *J. Appl. Polym. Sci.* **33** (1987) 329
29. D. W. Van Krevelen, *Properties of Polymers*, Elsevier, Amsterdam, 1990
30. H. Abe, *Macromol. Biosci.* **6** (2006) 469.

Journal of the Serbian Chemical Society
JSCS@tmf.bg.ac.yu • www.shd.org.yu/JSCS

J. Serb. Chem. Soc. 72 (12) 1533–1543 (2007)

Contents of Volume 72

NUMBER 1

NUMBER 2

NUMBER 12

Theoretical Chemistry

Physical Chemistry

Electrochemistry

Thermodynamics

Analytical Chemistry

Polymers

Journal of the Serbian Chemical Society
JSCS@tmf.bg.ac.yu • www.shd.org.yu/JSCS

J. Serb. Chem. Soc. 72 (12) 1545–1548 (2007)

Subject index

Journal of the Serbian Chemical Society
JSCS@tmf.bg.ac.yu • www.shd.org.yu/JSCS

J. Serb. Chem. Soc. 72 (12) 1549–1554 (2007)

Author index

End of Volume 72.

Journal of the Serbian Chemical Society
JSCS@tmf.bg.ac.yu • www.shd.org.yu/JSCS
www.shd.org.yu
J. Serb. Chem. Soc. Vol. 72, No. 12 (2007)

CONTENTS

ISSN 0352–5139
J. Serb. Chem. Soc. Vol. 72, No. 12 (2007)

CONTENTS. Continued

Published by the Serbian Chemical Society
Karnegijeva 4/III, 11120 Belgrade, Serbia
Printed by the Faculty of Technology and Metallurgy
Karnegijeva 4, P.O. Box 35-03, 11120 Belgrade, Serbia